

University of Texas at Arlington

MavMatrix

Civil Engineering Dissertations

Civil Engineering Department

2021

Evaluation of Surface Asphalt Mixes containing Recycled Asphalt Materials in North-East Texas using Accelerated Pavement Testing

Ana Maria Coca

Follow this and additional works at: https://mavmatrix.uta.edu/civilengineering_dissertations



Part of the [Civil Engineering Commons](#)

Recommended Citation

Coca, Ana Maria, "Evaluation of Surface Asphalt Mixes containing Recycled Asphalt Materials in North-East Texas using Accelerated Pavement Testing" (2021). *Civil Engineering Dissertations*. 314.
https://mavmatrix.uta.edu/civilengineering_dissertations/314

This Dissertation is brought to you for free and open access by the Civil Engineering Department at MavMatrix. It has been accepted for inclusion in Civil Engineering Dissertations by an authorized administrator of MavMatrix. For more information, please contact leah.mccurdy@uta.edu, erica.rousseau@uta.edu, vanessa.garrett@uta.edu.

EVALUATION OF SURFACE ASPHALT MIXES CONTAINING RECYCLED
ASPHALT MATERIALS IN NORTH-EAST TEXAS USING ACCELERATED
PAVEMENT TESTING

by

ANA MARIA COCA

DISSERTATION

Submitted in partial fulfillment of the requirements
for the degree of Doctor of Philosophy at
The University of Texas at Arlington
December 2021

Arlington, Texas

Supervising Committee:

Stefan Romanoschi, PhD, PE, Supervising Professor

Suyun Ham, PhD, PE

Xinbao Yu, PhD, PE

Stefan Dancila, PhD

Copyright © ANA MARIA COCA

All Rights Reserved



Acknowledgments

Completing this dissertation, I feel deeply indebted to many wonderful people who have greatly inspired and supported me during my doctoral studies at the University of Texas at Arlington.

First and foremost, I would like to express my deepest gratitude to my research supervisor, Dr. Stefan Romanoschi for providing me the opportunity to work on this research project. I would like to offer my sincere appreciation for his continuous support, patience, and motivation. From the beginning of the program to its completion, he devoted so much time and interest to help me succeed. I will not forget the long enlightening discussions with him at each stage of my Dissertation writing, which have led me to the final completion of this project. His broad knowledge, dedication and enthusiasm for research encouraged and motivated me throughout this challenging journey. I could not have imagined having a better mentor and for that I am heartfelt grateful.

Many thanks to my committee members Dr. Xinbao Yu, Dr. Ham, and Dr. Dancila for the valuable feedback, comments, and suggestions. I greatly appreciate their advice and their engineering approach.

My gratitude extends to the Texas Department of Transportation for the funding of this research project and to the Texas A&M Transportation Institute for providing help and expertise.

Thank you to all the students and colleagues involved in this research project for their work and dedication. Your help is much appreciated, and you all made my doctoral pursuit an enjoyable experience.

I am extremely thankful to Dr. Radu Andrei from the Technical University of Gheorghe Asachi, Iassy, Romania. Not only he instilled the passion for Pavement engineering, but he encouraged me to pursue further doctoral studies. For that, I will always be grateful.

My profound recognition goes to my parents, Constantin and Zenovia, my sister and brother-in-law, Lacramioara and Alexandru. To them, I owe all that I accomplished. Even though they are far away, they accompanied me in all the steps of this journey. Their love, uplifting support and continuous encouragement are immeasurable.

Finally, but not the least, I would like to express my gratitude to my love, Zack. His love and support lifted me when I was down and pushed me to reach my goal.

December 17th, 2021

Abstract

Evaluation of Surface Asphalt Mixes containing Recycled Asphalt Materials in North-East Texas
using Accelerated Pavement Testing

Ana Maria Coca, Ph.D.

The University of Texas at Arlington, 2021

Supervising professor: Stefan A Romanoschi, Ph.D., P.E.

Reclaimed asphalt pavement (RAP) and Reclaimed Asphalt Shingles (RAS) has proved to be an effective alternative to virgin materials in HMA production. Despite that recycling asphalt creates a cycle that optimizes the use of natural resources and sustains the pavement industry, State transportation departments have limited the maximum amount of RAP used in surface layers because of the variability concerns and lack of guidance provided. Even though at the moment, the United States recycles more RAP than Europe does in terms of percentage of the total RAP extracted from old pavements, it still lags Japan and other countries.

A special concern is the use of RAP and RAS in asphalt surface mixes and overlays, which are subjected while in service to higher stresses from the action of vehicle traffic and environment than the mixes in the lower layers. More effort and evaluation of field performance are necessary to develop guidance on best practices when using RAP for surface layers. Currently, Texas Department of Transportation (TxDOT) allows RAP to replace up to 20 percent of virgin binder in surface course mixes, and up to 40 percent of virgin binder in the underlying layers. Despite many efforts, past asphalt recycling projects showed mixed results in terms of performance, even

for mixes that fulfilled the requirements for maximum content of RAP/RAS and maximum percentage of recycled binder.

In response to this need, an accelerated pavement test project was sponsored by the Texas Department of Transportation. For this project, eight pavement test sections were built and tested under accelerated loading conditions with the Pavement Testing Machine (PTM).

The objectives of this research were to evaluate the field performance of the most commonly used mixes containing RAP/RAS in North-East Texas using Accelerated Pavement Testing (APT), to compare the results obtained from laboratory tests performed on the same mixes with the APT performance results and to evaluate the effect of artificial ageing of asphalt mixtures.

A series of laboratory tests was conducted to evaluate the resistance to rutting and fatigue cracking. The results obtained in the laboratory testing were correlated with the field performance measured by the APT experiment. Rutting is not a problem for Texas mixes, regardless the percent of recycled materials incorporated. Out of all the tests performed to evaluate the resistance to rutting, the Hamburg Wheel Track Test correlated the best with the field performance.

The addition of recycled materials increased the stiffness of the asphalt mix making it more prone to cracking. There was minimal or no correlations found between the laboratory cracking tests and the performance recorded by the APT.

Table of Contents

List of Figures

List of Tables

CHAPTER 1. INTRODUCTION	1
1.1 Introduction.....	1
1.2 Problem Statement	3
1.3 Research Objectives.....	4
CHAPTER 2. RECYCLED ASPHALT MIXTURES. RELATED RESEARCH.....	5
2.1 History of Recycling Asphalt.....	5
2.2 Characterization of Recycled Materials.....	11
2.3 Mix Design of RAP/RAS Asphalt Mixes	17
2.3.1 Current Mix Design Method for RAP/RAS mixtures	17
2.3.2 Balanced Mix Design	23
2.4 Laboratory Evaluation of Recycled Asphalt Mixtures	32
2.5 Field Performance of Recycled Asphalt Mixtures.....	42
2.5.1 APT Testing.....	43
2.5.2 Field Performance Studies in the United States.....	45
2.5.3 Field Performance Studies in Texas	50
2.6 Summary and Remarks	58
CHAPTER 3. PERFORMANCE OF FIELD SECTIONS AT APT FACILITY	60
3.1 Research Tools.....	60
3.1.1 APT Facility and PTM.....	60
3.1.2 Oxidation Chambers	63
3.2 Construction of Pavement Sections and Instrumentation	65
3.2.1 Construction of the top subgrade soil	67
3.2.2 Construction of the base layer.....	70
3.2.3 Strain gauge instrumentation	74

3.2.4 Construction of the HMA layers	78
3.3 Artificial Aging of Pavement Sections	90
3.4 APT Testing of Pavement Sections	98
3.4.1 Loading conditions.....	98
3.4.2 Temperature during APT testing	100
3.5 Rutting measurements.....	101
3.6 Deflection measurements.....	106
3.7 Cracking measurements	111
3.8 Strain measurements	124
CHAPTER 4. LABORATORY PERFORMANCE OF RAP MIXES	129
4.1 Evaluation of Rutting Resistance.....	131
4.1.1 Hamburg Wheel Track Test.....	131
4.1.2 Dynamic Modulus Test.....	136
4.1.3 IDEAL Rutting Test.....	143
4.1.4 Ranking of Rutting Tests and correlation with the Field Performance	150
4.2 Evaluation of Cracking Resistance	157
4.2.1 Texas Overlay Test	157
4.2.2 IDEAL-CT Test	164
4.2.3 Semicircular Bend Test.....	170
4.2.4 Ranking of Cracking Tests and correlation with the Field Performance....	150
CHAPTER 5. CONCLUSIONS AND RECOMMENDATIONS	184
REFERENCES	189
APPENDIX A	
A1. Mix design of the mixes	
A2. Laboratory results for the imported soil	
A3. Laboratory results for the flex base material	

A4. Photographs taken during the paving process

A5. Infrared camera temperature

A6. FWD Data

APPENDIX B

B1. Measured transverse profiles

B2. Excel VBA code

APPENDIX C

Overall pavement stiffness and central deflection recorded by the L-FWD

APPENDIX D

D1. Summary of the longitudinal and transverse strain signals

D2. Longitudinal and transverse strain signals – graph representation

APPENDIX E

Hamburg Wheel Track Test results

APPENDIX F

Dynamic Modulus Test results

APPENDIX G

IDEAL-CT Test results

APPENDIX H

SCB Test results

APPENDIX I

Mechanistic Design Check – FPS21

List of Figures

Figure 2.1 Historical Crude Oil Prices 1940-2020	5
Figure 2.2 Kansas DOT Monthly Computed Asphalt Material Index	10
Figure 2.3 Oil price developments in USD dollars	11
Figure 2.4 Blending chart for Method A	18
Figure 2.5 Blending chart for Method B	19
Figure 2.6 Graphical concept of $T_{c,s}$ and $T_{c,m}$	22
Figure 2.7 Proposed “Balanced” Mixture Design from Francis Hveem	24
Figure 2.8 Hamburg Wheel Tracking Test	25
Figure 2.9 Overlay Tester	25
Figure 2.10 Balanced Mix Design Approach	25
Figure 2.11 The Balanced Mixture Design Concept	27
Figure 2.12 The most predominant asphalt distresses across United States	29
Figure 2.13 Cracking tests	33
Figure 2.14 IDT strength test results for gravel mixtures-left and limestone mixtures-right	38
Figure 2.15 Overlay tester results	41
Figure 2.16 DCT fracture energy results	41
Figure 2.17 Pavement Testing Methods	44
Figure 2.18 NCAT Test Track – Alabama.....	44
Figure 2.19 I-40 Experimental sections. Existing pavement condition after 4” milling	51
Figure 2.20 Excellent condition of RAP/ RAS test sections on SH146, Houston	54
Figure 2.21 Reflective cracking of RAS test sections on US87, Amarillo	55
Figure 2.22 Reflective cracking development of RAS test sections on US87, Amarillo	55
Figure 3.1 Layout of the APTF – University of Texas at Arlington.....	60
Figure 3.2 Pavement Testing Machine	61
Figure 3.3 Schematic configuration of the PTM	62
Figure 3.4 Schematic configuration of the oxidation chamber	63
Figure 3.5 Construction of the oxidation chambers	64
Figure 3.6 Electrical box equipped with data logger	65
Figure 3.7 Layout of the experimental APT sections	66
Figure 3.8 Moisture-density curve for the subgrade soil	67
Figure 3.9 Placement of new subgrade soil	68
Figure 3.10 Compaction of new subgrade soil	68

Figure 3.11 Location of the nuclear density measurements.....	69
Figure 3.12 Moisture-density curve for the flex base material	70
Figure 3.13 Placement of flex base.....	71
Figure 3.14 Compaction of flex base -2 nd lift	71
Figure 3.15 Location of the nuclear density measurements.....	72
Figure 3.16 Spraying of Prime Coat on top of the flex base.....	73
Figure 3.17 Constructed base layer with Prime coat.....	74
Figure 3.18 Strain gauge, model PMFLS-60-50-2LTSC.....	74
Figure 3.19 Schematic layout of the in-pavement instrumentation	76
Figure 3.20 Strain gauges on Sections M	76
Figure 3.21 Longitudinal and Transverse Strain Gauges on Sections O and P	77
Figure 3.22 Instrumented sections M and N-ready to be paved	77
Figure 3.23 Thermocouples inside the PTM placed at surface, 0.5 in and 3 in depth	78
Figure 3.24 Sequence of Asphalt Mix Paving	79
Figure 3.25 Steel Roller Compacting the Pavement HMA Sections	79
Figure 3.26 The Infra-Red Camera Recording Pavement Construction Temperature	80
Figure 3.27 A Sample of Infra-Red Temperature Map captured during Section P Paving	80
Figure 3.28 Measuring Field Density Using the Nuclear Density Gauge.....	82
Figure 3.29 TTI extracting cores from Section S	83
Figure 3.30 GPR with 1.0 GHz Horn Antenna and GPR	85
Figure 3.31 GPR data display from the run over sections M and Q.....	85
Figure 3.32 Detailed dielectric and thickness data computed for the sections Q and M	86
Figure 3.33 HMA thickness for Lane M, N, O and P.....	87
Figure 3.34 HMA thickness for Lane Q, R, S and T	87
Figure 3.35 FWD testing on Section M	88
Figure 3.36 Location of the FWD testing, Section S and T.....	88
Figure 3.37 Small artificial aging box	90
Figure 3.38 Coring after 4 weeks of artificial aging	92
Figure 3.39 Extracted cores after 3 weeks of artificial aging	92
Figure 3.40 Oxidation chambers places on Lane Q and R.....	93
Figure 3.41 Thermal data recorded on Lane M.....	94
Figure 3.42 Thermal data recorded on Lane N.....	94
Figure 3.43 Thermal data recorded on Lane O	95
Figure 3.44 Thermal data recorded on Lane P.....	95

Figure 3.45 Thermal data recorded on Lane Q	96
Figure 3.46 Thermal data recorded on Lane R	96
Figure 3.47 Thermal data recorded on Lane S	97
Figure 3.48 Thermal data recorded on Lane T	97
Figure 3.49 PTM positioned on Lane Q and R	98
Figure 3.50 Lateral wander pattern followed by the PTM	99
Figure 3.51 Temperature recorded during APT testing on Section O and P	100
Figure 3.52 Main components of the transverse profiler	101
Figure 3.53 Example of transverse profile, Lane O-Profile 3	102
Figure 3.54 Progression of permanent deformation in Section M and N	103
Figure 3.55 Progression of permanent deformation in Section O and P	104
Figure 3.56 Progression of permanent deformation in Section S and T	104
Figure 3.57 Ranking of computed permanent deformation	105
Figure 3.58 Light Falling Weight Deflectometer measurements	106
Figure 3.59 Average central deflection for all sections	109
Figure 3.60 Average pavement stiffness for all sections	109
Figure 3.61 Ranking of the central deflection measured by L-FWD	111
Figure 3.62. Crack extent evaluation using a grid panel of squares	112
Figure 3.63 Cracking in section M after 200,000 passes	112
Figure 3.64 Cracking in section M after 300,000 passes	113
Figure 3.65 Cracking in section O after 200,000 passes	113
Figure 3.66 Cracking in section O after 300,000 passes	114
Figure 3.67 Cracking in section O after 300,000 passes	114
Figure 3.68 Cracking in section P after 100,000 passes	115
Figure 3.69 Cracking in section P after 200,000 passes	115
Figure 3.70 Cracking in section P after 300,000 passes	116
Figure 3.71 Cracking in section P after 350,000 passes	116
Figure 3.72 Cracking in section S after 46,000 passes	117
Figure 3.73 Cracking in section S after 57,000 passes	117
Figure 3.74 Cracking in section T after 46,000 passes	118
Figure 3.75 Cracking in section T after 57,000 passes	118
Figure 3.76 Cracking in section Q after 50,000 passes	119
Figure 3.776 Cracking in section Q after 60,000 passes	119
Figure 3.78 Cracking extent during APT loading	120

Figure 3.79 Surface cracking on lane M after 300,000 passes.....	121
Figure 3.80 Surface cracking on lane O after 350,000 passes	122
Figure 3.81 Surface cracking on lane P after 350,000 passes	122
Figure 3.82 Surface cracking on lane T (left) and S (right) after 57,000 passes	123
Figure 3.83 Wheel position during strain measurements	124
Figure 3.84 Typical strain signal observed	126
Figure 3.85 Example of longitudinal and transverse strain signal	128
Figure 4.1 Temperature data recorded during the artificial oxidation	130
Figure 4.2 Sequence of covering the core holes	130
Figure 4.3 Top view of test specimen configuration for the HWT device (Tex-242-F).....	131
Figure 4.4 Schematic rut depth measurement points	132
Figure 4.5 Cutting of the specimens and testing assembling in the HWT device	133
Figure 4.6 Average central rut depth for all sections	135
Figure 4.7 HWTT Rut Depths recorded for aged and unaged samples	135
Figure 4.8 Sample preparation for the Dynamic Modulus Test.....	137
Figure 4.9 Dynamic Modulus Results @15°C.....	139
Figure 4.10 Dynamic Modulus Results @20°C.....	139
Figure 4.11 Dynamic Modulus Results @25°C.....	140
Figure 4.12 Phase Angle values obtained from the Dynamic Modulus test @15°C	141
Figure 4.13 Phase Angle values obtained from the Dynamic Modulus test @20°C	141
Figure 4.14 Phase Angle values obtained from the Dynamic Modulus test @25°C	142
Figure 4.15. IDEAL RT test jig and sample showing shear planes caused by compression	144
Figure 4.16 IDEAL-RT Test setup and failed specimens	146
Figure 4.17 RT_{INDEX} values obtained on aged and unaged field cores	148
Figure 4.18 Correlation between HWT and Dynamic Modulus Test.....	149
Figure 4.19 Correlation between IDEAL RT and Dynamic Modulus Test	149
Figure 4.20 Correlation between IDEAL RT and HWT Test.....	150
Figure 4.21 Ranking of HWTT results	150
Figure 4.22 Rut depth measured on lane Q.....	152
Figure 4.23 Average permanent deformation (mm)	153
Figure 4.24 Ranking performance based on the Dynamic Modulus Test	154
Figure 4.25 Ranking performance based on the data from IDEAL-RT test	155
Figure 4.26 Ranking of laboratory tests vs. measured performance.....	155
Figure 4.27 Overlay Tester equipment	157

Figure 4.28 OT Sample preparation	159
Figure 4.29 CFE and CPR representation and calculation.....	160
Figure 4.30 Critical Fracture Energy for all mixes	162
Figure 4.31 Cracking Progression Rate for all mixes	162
Figure 4.32 CPR values obtained on aged and unaged field cores	164
Figure 4.33 Testing setup for the IDEAL-CT Test	166
Figure 4.34 Load versus displacement curve for IDEAL-CT.....	167
Figure 4.35 CT_{INDEX} before and after artificial aging.....	169
Figure 4.36 Variation of the CT_{INDEX} over aging period.....	170
Figure 4.37 SCB Test setup and failed specimens.....	173
Figure 4.38 Relationship between the CT_{INDEX} and FI-SCB.....	174
Figure 4.39 Relationship between the FI-SCB and Overlay Tester.....	175
Figure 4.40 Relationship between the CT_{INDEX} and Overlay Tester	175
Figure 4.41 Ranking of the CPR values -Overlay Test.....	176
Figure 4.42 Ranking of the CT_{INDEX} values -IDEAL-CT Test.....	176
Figure 4.43 Ranking of the FI values -SCB Test	177
Figure 4.44 FPS21-Mechanistic Design Check	178
Figure 4.45 Correlation between CPR and APT performance.....	181
Figure 4.46 Correlation between CT Index and APT performance	181
Figure 4.47 Correlation between FI-SCB and APT performance.....	182

List of Tables

Table 2.1 Early Central Plant Recycling Projects	7
Table 2.2 Trends in RAS-Bearing Mixtures	8
Table 2.3. The Maximum Allowable Amounts of Recycled Binder	13
Table 2.4 Asphalt Shingle Composition	15
Table 2.5 NCAT Survey results	27
Table 2.6 Construction of High RAP mixes	36
Table 2.7 Rejuvenators used	40
Table 2.8 Proposed mix performance testing	40
Table 2.9 Differences between fixed APT and Test Tracks	45
Table 2.10 Summary of Test Sections and Binder Test Data	46
Table 2.11 Performance comparison: Virgin vs. 30% RAP Mixes	48
Table 2.12 Experimental plan for each demonstration project	49
Table 2.13 Field RAP/RAS Test Sections and Observed Performance	52
Table 2.14. Experimental Pavement Structures	56
Table 3.1 HMA Mix Designs of the Pavement Structures.....	67
Table 3.2 Moisture-density curve for the subgrade soil.....	69
Table 3.3 Moisture-density curve for the flex base.....	73
Table 3.4 Tokyo Sokki PMFLS-60-50-2LTSC specifications	75
Table 3.5 Paving temperatures recorded behind the paver	81
Table 3.6 Compaction densities (pcf)	82
Table 3.7 QC test results performed on field cores.....	84
Table 3.8 Summary of deflection data from all sections after construction	89
Table 3.9 Summary of deflection data from the north section after artificial aging and 10 months after construction.....	89
Table 3.10 Binder extraction data	93
Table 3.11 Central deflection and the calculated overall pavement stiffness	108
Table 3.12. Asphalt layer thickness in the testing location.....	110
Table 3.13 Longitudinal and transverse strain signals recorded for Lane M and N	126
Table 3.14 Longitudinal strain signals recorded for Lane O and P	127
Table 3.15 Transverse strain signals recorded for Lane O and P.....	127
Table 4.1 Hamburg Wheel Test Requirements.....	132

Table 4.2 Sample dimensions and characteristics.....	134
Table 4.3 Air Voids of the Dynamic Modulus specimens	138
Table 4.4 Air Voids of the Ideal-RT specimens	145
Table 4.5 Load at 5mm deformation.....	147
Table 4.6 OT Sample Dimensions and AV%	158
Table 4.7 Overlay Tester Results	161
Table 4.8 IDEAL-CT Sample Dimensions and AV%	165
Table 4.9 IDEAL-CT Results	168
Table 4.10 FPS21 Inputs.....	179
Table 4.11 Adjustment of the APT fatigue performance based on k_2 calibration.....	180

CHAPTER 1. INTRODUCTION

1.1 Introduction

Over 90 percent of U.S. highways and paved roads are paved with hot mix asphalt (HMA). To provide a safe and reliable transportation of people and goods, these pavements require regular maintenance and periodic rehabilitation which demand a continuous supply of aggregate and asphalt binder. In the current economy, the fluctuating price of oil and implicitly of the bitumen and the more limited availability of aggregates, there is a renewed interest towards the use of recycled asphalt material in pavements. Increasing the percentage of recycled materials such as Reclaimed Asphalt Pavement (RAP) and Reclaimed Asphalt Shingles (RAS) in the new asphalt concrete mixtures has proved to have benefic environmental and economic results. According to the National Asphalt Paving Association (NAPA, 2019), some of the main advantages of recycling RAP and RAS are conservation of virgin binder and aggregates, reduced cost in the production of asphalt mixes due to binder and aggregate replacement, reduced cost of material disposal and reduced cost in the production of greenhouse gases and other emissions.

A typical asphalt mixture is composed by approximately 95% aggregates and 5% asphalt binder by weight. Starting the very first day of service and continuing ever after, the physical properties of the asphalt mixture change. As the asphalt binder ages, its viscosity increases, and the bitumen becomes stiffer and more brittle. This process is called aging and is a result of multiple factors: oxidation, volatilization, polymerization, syneresis and separation (Vallerga et al., 1957). Although the process is irreversible, the materials in a heavily aged pavement still have remarkably value. Through demolition and milling, the old pavement is transformed in Reclaimed Asphalt Pavement (RAP) and can be further reused in new asphalt mixtures. To embolden the use of

recycled asphalt materials in the construction of new asphalt mixes, the Federal Highway Administration recycling policy states that the same materials used to build the original highway system can be re-used to repair, reconstruct, and maintain the road network, (FHWA, 2003). Although using recycling materials in new asphalt mixtures is highly promoted, a major concern comes from the fact that their binder is stiff due to ageing from several years of service; stiffer bitumen increases the rutting resistance while it makes the asphalt mixture prone to cracking. To address this concern, numerous research studies proposed different mix design approaches (Epps et al., 1980; Newcomb et al., 1993; McDaniel & Anderson, 2001; Shah et al., 2007; Newcomb et al., 2007; West et al., 2013; and Zhou et al., 2013b). However, following these mix design methods has not always resulted in good performing mixtures, especially for mixtures used in wearing courses and overlays.

As mentioned before, RAP is created by the removal of an existing asphalt pavement during reconstruction or rehabilitation. The broken material is collected, crushed, screened, and deposited in stockpiles. When properly processed, RAP consists of high quality, well-graded aggregates coated by asphalt binder; it is commonly nicknamed as “black rock”. However, the high variability of RAP due to different RAP sources, the aged asphalt binder of RAP, the cost of demolition and milling processes and the lack of guidance for the design process of recycled mixes are some of the major obstructions that limit the use of RAP material to obtain high-quality recycled asphalt mixtures.

Recycled Asphalt Shingles (RAS) are another recycled material that has been used in the production of asphalt mixtures. RAS results from the removal of old asphalt shingles from damaged roofs (tear offs) or as waste from the manufacture of new asphalt shingles. Shingles are

typically composed of 25 to 30 percent asphalt cement, 40 to 60 percent hard aggregate and 3 to 12 percent fiber. Due to the high asphalt content, shingles can be recycled in asphalt mixes.

A special concern is the use of RAP and RAS in asphalt surface mixes and overlays, which are subjected while in service to higher stresses from the action of vehicle traffic and environment than the mixes in the lower layers are. Currently, the Texas Department of Transportation (TxDOT) allows RAP to replace up to 20 percent of virgin binder in surface course mixes, and up to 40 percent of virgin binder in the underlying layers. However, past TxDOT asphalt recycling projects showed mixed results in terms of performance, even for mixes that fulfilled the requirements for maximum content of RAP and maximum percentage of recycled binder. More effort and evaluation of field performance are necessary to develop guidance on best practices when using RAP for surface layers.

1.2 Problem Statement

While virgin material for pavement applications is depleting the resources, the volume of pavement material reclaimed from in-service pavements is increasing. Therefore, there is an increased interest in the use of reclaimed asphalt materials in the production of new asphalt mixes to reduce costs and preserve nonrenewable resources.

Despite many efforts, past asphalt recycling projects showed mixed results in terms of performance, even for mixes that fulfilled the requirements for maximum content of RAP/RAS and maximum percentage of recycled binder. More effort and evaluation of field performance is necessary to develop guidance on best practices when designing asphalt mixtures containing RAP/RAS for surface layers in Northeast Texas.

Laboratory performance evaluation is not completely reliable; their outcome is sometimes inconsistent, which raises doubts to the usefulness of the results. A validation of the laboratory

tests with field data is necessary and is expected to offer practical results that will have an immediate impact on the methodology currently used in designing surface courses containing RAP/RAP. For this purpose, accelerated pavement testing can provide fast and reliable results on the performance of recycled mixtures. Having a better performing recycled asphalt mixes will have a major positive impact on maintaining or extending the life of RAP asphalt pavements while protecting the environment and improving the safety and comfort of road users.

1.3 Research Objectives

The objectives of this research are to evaluate the field performance of the most commonly used mixes containing RAP/RAS in North-East Texas using Accelerated Pavement Testing (APT), to compare the results obtained from laboratory tests performed on the same mixes with the APT performance results and to evaluate the effect of artificial aging of asphalt.

CHAPTER 2. RECYCLED ASPHALT MIXTURES. LITERATURE REVIEW

2.1 History of Recycling Asphalt

Asphalt may be found in natural deposits or may be a refined product. Naturally occurring asphalt is usually specified by the term “crude bitumen” while the material obtained from the fractional distillation of crude oil is referred to as “refined bitumen”. The largest natural source of crude bitumen in the world is Pitch Lake, Venezuela, estimated to contain ten million tons of asphalt.

The increased demand of asphalt together with the limited availability of naturally occurring bitumen pushed the industry into using refined bitumen. The cost of refined bitumen is highly dependent upon the crude oil price. Figure 2.1 shows the history of crude oil prices between January 1940 and February 2020 based upon data from the Energy Information Administration, (MacroTrends,2021) where the gray bars represent recession periods.

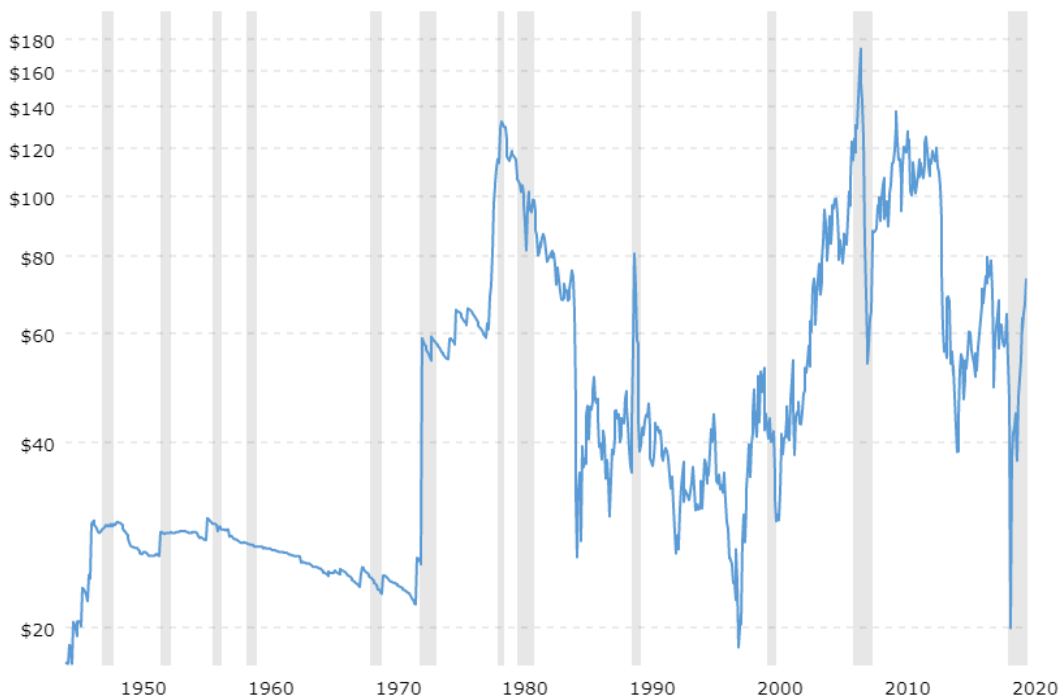


Figure 2.1 Historical Crude Oil Prices 1940-2020 (2020 dollars)

As shown in Figure 2.1, the price of crude oil was fairly stable before the 1970s, fluctuating around \$30 per barrel in 2020 dollars. At that time, recycling asphalt was still a novelty. According to NAPA, recycling was first used in Singapore in 1931 as a means of conserving petroleum when rehabilitating roads that showed premature distresses. After the roads in Singapore were rehabilitated, they lasted for 14 years before any type of major work was needed despite multiple problems brought on by World War II (NAPA, 1977). Taylor et. al., (1978) mentions that recycling was also used in Bombay (now Mumbai), India as early as 1948. Once these roads were rehabilitated with recycled mixture, they lasted almost 30 years before any repair was needed.

As seen in Figure 2.1, the first substantial rise in prices occurred in 1973 during the Arab Oil Embargo when the price per barrel doubled. The mid-70s are the beginning of the asphalt recycling era; the industry began developing processes for recycling and field experiments were initialized. In 1979, the second substantial rise in prices occurred due to the Iranian Revolution where the prices more than doubled. At this point, the interest in recycling and conserving the asphalt resources was maximized. Research supported guidance on technical issues, including the control of RAP, mix design procedures and plant operations. Roofing shingle manufacturers began supporting research into the use of waste shingles from manufacturing processes and a few contractors began using waste shingles as a way of extending their asphalt supplies (Newcomb et al., 2016).

Also, during this time, the use of rejuvenators was introduced to the asphalt mixture design. Rejuvenators are liquid additives, derived from petroleum which at the time were blended with virgin asphalt before the asphalt mix design. Even though the price of rejuvenators is higher than the price of virgin bitumen, rejuvenators are known to soften age-hardened bitumen. The earliest evidence on the use of rejuvenators was documented by (Little et al., 1979). In his research, Little

presented 12 projects in which asphalt recycling was used on an experimental basis. As shown in Table 2.1, these experimental projects employed a very high quantity of RAP and the use of soft asphalts and recycling agents. The reported issues of high RAP mixes and excessive pollution were related to the asphalt plants designs that were not optimized for the use of RAP. According to Newcombs et al., (1981) most of the asphalt plants were either parallel-flow drum or batch plants at that time. Later, double-drum, counter-flow drum, and heat-exchanger plants started being more common.

Table 2.1 Early Central Plant Recycling Projects (Little, 1979)

Road Project	Year	Layer	RAP %	Rejuvenator
I-8, Gila Bend, Ariz.	1978	Surface and Base	100	Cyclogen L (Recycling Oil)
US 666, Graham County, Ariz.	1977	Surface	80	AR-2000 and Extender Oil
Kossuth County, Iowa	1976	Surface	70	AC-10
I-94, Minnesota	1977	Surface and Base	50	AC (200/300 pen)
I-15, Henderson, Nev.	1974	Surface	100	AR-8000 and Paxole (Softening Agent)
Hillsboro to Silverton Hwy., Woodburn, Ore.	1977	Surface	70	AR-2000
I-20, Roscoe, Texas	1976	Base	85	AC-5
US 84, Snyder, Texas	1976	Base	30–100	E.A.11-M (Emulsified Asphalt) and AC-10
Loop 374, Mission, Texas	1975	Surface	85–100	AC-10 and Softening Agent
US 50, Holden, Utah	1975	Surface	77–100	AC-10 and Softening Agent
Blewitt Pass, Wash.	1977	Surface	93	AC-5
I-90, Rye Grass, Wash.	1977	Surface	72	Cyclopave (Recycling Oil)

Even though oil prices began to decrease during the 1980s, the use of RAP became a standard practice in the asphalt industry. At this time, contractors realized the great economical advantage RAP has. With the introduction of Superpave design system, agencies began applying

new approaches to both binder selection and mix design which had a negative effect on recycling. The novelty of the Superpave design method led many agencies to believe that RAP has a confounding effect on performance. Therefore, many agencies reduced the amount of RAP allowed in mixtures. For instance, Texas drastically reduced the amount of RAP from 50-100% to 20-30% during that time.

The necessity of accommodating RAP in the Superpave system was acknowledged in the late 1990s. In 2001, McDaniel and Anderson published the NCHRP Project 09-12, (NCHRP, 2000). This report provides comprehensive standard practices and recommendations for designing asphalt mixes containing RAP. The objectives of the NCHRP Project 09-12 were to develop guidelines for incorporating RAP in the Superpave system and to prepare a manual that can be used by laboratory and field technicians.

The first research project evaluating the performance of asphalt mixes containing Reclaimed Asphalt Shingles (RAS) began at the University of Nevada, Reno in 1986. This project consisted of an investigation of mixture properties and an economic analysis. Table 2.2 shows the main findings of this study of how RAS affects the asphalt mixture properties.

Table 2.2 Trends in RAS-Bearing Mixtures (Paulsen et al., 1986)

Property	Increased RAS Content	Increased RAS Size	Increased Asphalt Content	Use of Recycling Agent
Resilient Modulus	Increase	Decrease	Decrease	Decrease
Tensile Strength	Increase	Decrease	None	Decrease
Marshall Stability	None	None	Decrease	Decrease
Temperature Susceptibility	Decrease	Increase	None	Decrease

Overall, it was concluded that the incorporation of RAS in asphalt mixes increases the mix stiffness and the tensile strength. Paulsen suggests that up to 20% of RAS could be incorporated

in the asphalt mix if the increased mix stiffness is countered balanced through the use of recycling agent or an increased virgin asphalt content.

In 1993, the University of Minnesota investigated the use of recycled shingles and manufactured waste in asphalt mixtures (Newcomb et al., 1993). This research consisted in laboratory experiments with dense-graded and stone-matrix asphalt (SMA) mixtures and field mixtures. The research showed that the incorporation of RAS could improve the compatibility of mixtures and that the maximum amount of RAS that should be used in dense-graded mixes is 5% while up to 10% could be used in SMA mixtures. Following the results of this research, the Minnesota Department of Transportation implemented the use of 5% RAS in asphalt mixtures. Many state agencies and contractors were confident in using up to 12% RAP and 5% RAS in asphalt mixtures in the mid-2000s.

As depicted in Figure 2.2, the prices of oil began to rise dramatically in late 2007, following the burst of the housing bubble that year, and they continued to rise as the country entered the Great Recession in late 2008. Prices have declined and in 2012 they stabilized above pre-2008 levels before starting to fall again as oil prices dropped in 2015 (Newcomb et al., 2016).

In 2007, FHWA established the RAP Expert Task Group to coordinate, develop and improve national guidance and the recommendations for the use of RAP and RAS in asphalt mixtures. AASHTO and NAPA worked closely with FHWA to benchmark the acceptance and use of RAP and RAS by state the DOTs and asphalt pavement industry. Since then, many state DOT, Research Facilities and Universities began intensive research on the possibility of increasing the amount of RAP and RAS in asphalt mixes. NCHRP Project 09-46 concluded that asphalt overlays

with 30% RAP have shown performance equivalent to virgin mixtures and that mixtures with up to 50% RAP performed well in a wide variety of climatic and traffic conditions (West et al., 2013). Results from the National Center for Asphalt Technology (NCAT) Pavement Test Track have confirmed that using a softer grade of virgin binder reduced raveling and cracking. It was also observed that stiffer RAP mixes had a lower tensile strain under heavy truck loads. Florida DOT analyzed asphalt mixes containing 0, 30 and 50% RAP over a period of 11 years. They concluded that there is no significant difference in pavement life and performance between zero and 30% RAP content, (Copeland, 2011).

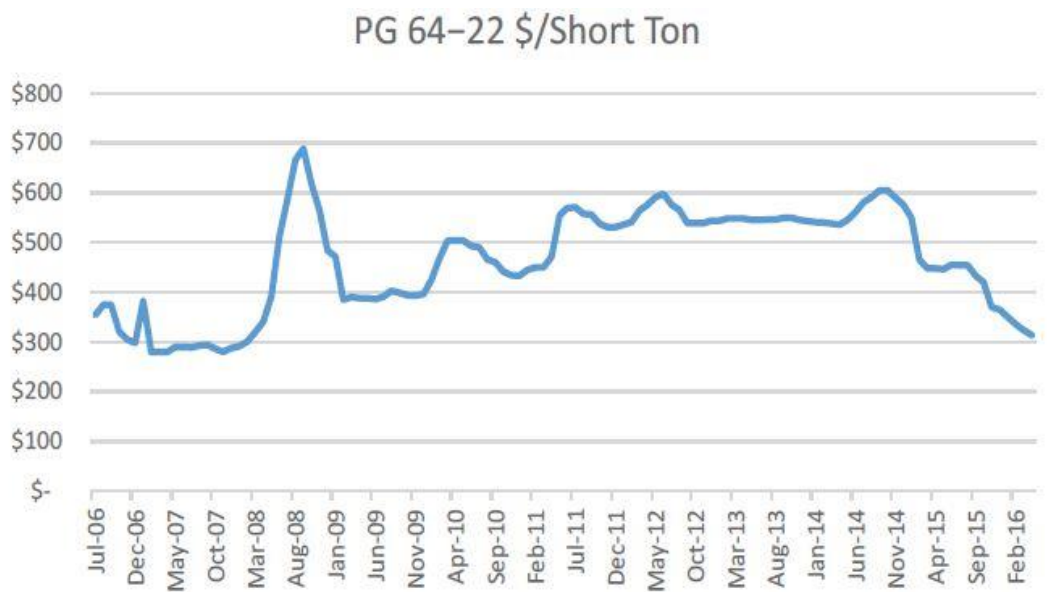


Figure 2.2 Kansas DOT Monthly Computed Asphalt Material Index, 2006-2016 (KDOT, 2016)

Referring to Figure 2.1, (MacroTrends,2021), it can be observed that the crude oil prices collapsed significantly in 2020. This drop is due to the global economic contraction driven by the COVID-19 pandemic and an oil market collapse. As seen in Figure 2.3, the current COVID-19 pandemic pushed the oil prices to a new low; the benchmark for US crude oil fell into negative territory for the first time ever in late April 2020. A year later, prices began recovering but it is

unlikely that there will be the same resilience in prices as witnessed following the 2008 global economic recession.



Figure 2.3 Oil price developments in USD dollars (BBC, 2015)

Considering the affordable price of renewable energy, the advancement in technological advances, and the growing commitment towards decarbonization, the fossil fuel industry is faced with the prospect of structural decline (Lahn et al., 2020). In the current context, continuing recycling asphalt pavement and shingles at higher rates has tremendous environmental and economic benefits. Nowadays, many agencies and DOTs all over the United States are actively researching options to introduce RAP/RAS in new asphalt mixtures at higher percentages.

2.2 Characterization of Recycled Materials

As mentioned previously, RAP consists of aggregates and aged binder. Adding RAP in a new asphalt mixture, can significantly increase its stiffness. The binder experiences two types of aging: short-term and long-term aging. The short-term aging is due to the combined effect of heat and oxygen during the mixing and hauling process. Depending on the RAP content, the inclusion

of aged binder changes the mixture performance. The long-term aging occurs during its service life and it is a result of multiple factors: oxidation, volatilization, polymerization, thixotropy, syneresis and separation (Vallerga et al., 1957). Some other influential factors in binder aging are the void content of mixtures, the layer position, the level of damage of the recycled pavement and stockpiling management (Al-Qadi et al., 2007).

The interaction between the virgin and aged binder is still a hot topic and different scenarios are considered. The first scenario assumes that there is no interaction between old and virgin materials, therefore RAP acts as a “black rock”. The second scenario assumes that all the aged binder in RAP blends effectively in the new mix. Previous research showed that depending on the RAP size and aggregate gradation, the available binder content in RAP varies. According to McDaniel et al. (2000), the inclusion of less than 15% RAP has no impact on the blended binder performance mix. Between 15% and 25% RAP, the virgin binder grade must be decreased by one grade (6°C) on both ends and for more than 25% RAP, the new binder needs to be graded using the performance-graded binder tests. Chen et al., (2007) concluded that RAP does not act like a black rock; but significant blending occurs between RAP and the virgin binder. Salianni et al., (2019) evaluated the blending aspect in RAP mixes. They concluded that the black rock assumption, which is commonly used, cannot be representative of the RAP contribution to the total binder content. They also concluded regarding the skeleton of the mix that the actual gradation lies somewhere in between these two extreme cases.

Despite the great economic and environmental benefits, the variability in RAP represents one of the main criteria for their limited use in asphalt mixtures, despite the great economic and environmental benefits. Currently, the Texas Department of Transportation (TxDOT) allows RAP

to replace up to 20 percent of virgin binder in surface course mixes, and up to 40 percent of virgin binder in the underlying layers, and up to 5 percent RAS, as shown in Table 2.3, (TxDOT, 2014).

Table 2.3. Allowable Amounts of RAP and RAS for Dense Graded Mixtures (TxDOT, 2014)

Mixture Description and Location	Maximum Ratio of Recycled Binder to Total Binder (%)	Maximum Allowable % (Percent by Weight of Total Mixture)		
		Unfractionated RAP	Fractionated RAP	RAS
Surface Mixes	20 (30 ^I)	10	20	5
Non-Surface Mixes < 8 in. From Final Riding Surface	20 (35 ^I)	10	30	5
Non-Surface Mixes > 8 in. From Final Riding Surface	20 (40 ^I)	10	40	5

The major concern of many DOTs is the variability in the RAP’s aggregate gradation, asphalt content, and the volumetric properties of the produced RAP mix. According to Zhou et al., (2010) the variability may be caused by the following:

- *Mixes of mixtures and treatments.* When RAP is removed from an old roadway, it includes pavement materials, plus patches, chip seals, and other maintenance treatments.
- *Mixes of layers.* Base, intermediate, and surface courses from the old roadway may all be mixed together in the RAP.
- *RAP stockpiles may also include “deleterious material,”* such as wood, concrete, trash.
- *RAP from several projects is sometimes mixed in a single stockpile.*

To reduce the RAP variability, the best practice is to collect the RAP from different projects in separate stockpiles. Another useful practice in reducing variability is RAP fractionation. As stated in Zhou et al. (2010), fractionating RAP is the act of processing it to screen, crush, size, and separate the various sizes into stockpiles that are more consistently uniform in size and composition. Regardless of whether the recycled materials are from the same project or different

projects, it was proved that RAP fractionation through separating coarse and fine RAP stockpiles will minimize segregation of RAP particles and allow greater flexibility in adjusting the RAP content for the final aggregate gradation. In Texas, most contractors crush and fractionate RAP into single maximum size of either 3/8 inch or 1/2 inch so it can be used mostly for asphalt overlay mixes (dense-graded Type C or D). The use of a paved, sloped storage area for RAP stockpiles greatly reduces the variability as well.

Another source used as recycled materials is the recycled asphalt shingles. The mineral aggregates and asphalt cement present in RAS makes it a candidate for product replacement in hot mix asphalt. RAS has two provenience sources: post-manufactured shingles and post-consumer shingles. Post-manufactured shingles are the waste products of the shingles manufacturing process, which include factory rejects and tab cut-outs, while post-costumer shingles are shingles that come directly from roofs of commercial and residential buildings after their service life including damage from severe weather (Williams et al., 2011). Shingles can be fabricated with organic backing (cellulose or wood fiber) or with fiberglass backing. The American Society for Testing and Materials (ASTM) has specifications for both types of shingles, ASTM D225 and ASTM D3462. Shingles are manufactured by saturating and coating the organic/fiberglass backing with liquid asphalt. Because of the “air-blown” technique used when adding the asphalt, the viscosity of asphalt increases due to the oxygen infused into the asphalt. The shingles are then covered with sand and crushed-stone granules to increase their durability and resistance to weathering. The percentage of the individual components is different in shingles manufactured with organic backing compared to shingles manufactured with fiberglass backing. Brook (2007) summarized the composition of each type of shingle in Table 2.4.

Table 2.4 Asphalt Shingle Composition, (Brock, 2007)

	Organic		Fiberglass		Post-consumer shingles	
	(lbs./100 sq.ft.)	%	(lbs./100 sq.ft.)	%	(lbs./100 sq.ft.)	%
Asphalt	68	30	38	19	72.5	31
Filler	58	26	83	40	58	25
Granules	75	33	79	38	75	32
Mat	0	0	4	2	0	0
Felt	22	10	0	0	27.5	12
Cut-out	2	1	2	1	2	0
TOTALS	221		202		235	

As observed in Table 2.4, the shingles manufactured with organic backbone contain more liquid asphalt than the fiberglass shingles due to the different absorption of the materials. Because of the loss of the surface granules caused by weathering, the post-consumer shingles have the higher content of asphalt. A higher asphalt content available implies a higher economic value but at the same time, a much brittle asphalt which directly affects the future mixture performance. Also, research suggests that the felt fibers may increase the tensile strength and toughness of the mixes. When RAS is added to asphalt mixes, a much larger percentage of virgin asphalt is reduced. Compared to adding RAP which contains 4-5% asphalt content, adding 10, 15 or 20% RAS in a mix will not make a significant reduction in virgin binder. Consequently, the percentage of RAS allowed by many agencies is low. Currently, Texas allows up to 5% RAS to be used separately or as a replacement for fractionated RAP.

Like RAP, fractionating the RAS could reduce the variability. The AASHTO provisional standard use of RAS as an additive in HMA requires that 100% of the RAS must pass sieve 12.5 mm. Some state agencies require an even smaller maximum particle size such as 9.5 mm or 4.75 mm. Currently, TxDOT specifies that the RAS used must 100% pass a 9.5 mm sieve. Research showed that gradation plays a major role in the HMA performance. Button et al., (1996) reported that a finer grind produced a more consistent and better performing mix. Also, a smaller RAS particle has a larger surface area with more exposed binder which has a higher probability to fully

blend with the virgin asphalt. Research conducted by the Iowa Department of Transportation, (Zhao et al., 2013) indicates that two-thirds of RAS binder behaves as liquid when heated and contributes to the final blending and the other third coated the RAS particles which behaves as aggregates coated with asphalt.

Williams et al., (2011) conducted an evaluation to determine the effects of post-consumer RAS on the laboratory performance of HMA and its compatibility with fractioned recycled asphalt pavement (FRAP). Eight mixes containing zero or five percent RAS and varying percentages of FRAP were placed on the pavement shoulder on the I-90 tollway in Illinois. Mixture characterization tests such as Dynamic Modulus, Flow Number, moisture sensitivity, beam fatigue and fracture energy test were employed to evaluate the stress strain response of the HMA samples. The results indicate that the mixes containing 5% RAS with less than 40% recycled materials exhibit an increased resistance to permanent deformation while maintaining satisfactory performance to fatigue stresses, low temperature cracking and freeze-thaw durability.

Zhou et al., (2013) investigated the impact of different percentages of RAS (0, 3% and 5%) on the optimum asphalt content (OAC). The research concluded that the OAC increases as the RAS content increases. This may be due to the higher stiffness of RAS. To achieve the desired viscosity, considering that the same mixing and compaction temperatures are intended, the amount of virgin binder should be increased but this increases the cost of the mix.

The inclusion of recycled materials in new asphalt mixes has a great economic and environmental benefit. However, because of the oxidative aging that recycled materials undergo over time, the mixes exhibit higher resistance to rutting but decreased resistance to low temperature and fatigue cracking.

2.3 Mix Design of RAP/RAS Asphalt Mixes

2.3.1 Current Mix Design of RAP/RAS Asphalt Mixes

Along time, many research studies proposed different approaches in designing asphalt mixes containing RAP and RAS. Most of these approaches were depended on volumetric considerations and, in some instances, problems have been reported with respect to the embrittlement of mixtures (Zhou et al., 2013). Kandhal and Mallick (1998) recommended a three-tier process for the evaluation of recycled asphalt in asphalt mixtures. McDaniel & Anderson et al. (2001) recommended similar tiers of RAP content to properly characterize the materials. Ultimately, these tiers were adopted by AASHTO and became the process for designing the RAP mixtures:

- For RAP content of less than 15 percent, there is no need to change the binder grade.
- For RAP content between 15 to 25 percent, the virgin binder should be one grade softer than desired final grade.
- For RAP content of more than 25 percent, blending charts should be used to determine the grade of virgin binder that must be added to the binder in the RAP.

AASHTO M 323 (AASHTO 2010) established the blending chart for RAP content of more than 25% as one of the following:

1. When the desired final binder grade, the percentage of RAP, and the properties of recovered RAP binder are known, the required properties of the virgin binder grade should be determined at every temperature (high, intermediate and low) separately:

$$T_{virgin} = \frac{T_{blend} - (\%RAP \times T_{RAP})}{(1 - \%RAP)}$$

Where:

T_{virgin} = Critical temperature of virgin asphalt binder (high, intermediate, low), C°

T_{blend} = Critical temperature of blended asphalt binder (final desired; high, intermediate, low), C°

$\%RAP$ = Percentage of RAP (in decimal)

T_{RAP} = Critical temperature of recovered RAP binder (high, intermediate, low), C°

According to Copeland et al., (2011), the critical high and intermediate temperatures are determined based on the Dynamic Shear Rheometer (DSR) tests performed on the recovered RAP binder before and after is aged through Rolling Thin Film Oven testing (RTFO). For example, the high temperature PG of the recovered RAP binder is the lowest of the original DSR and RTFO DSR critical temperatures. Following the same procedure but using Bending Beam Rheometer (BBR) testing instead of DSR testing, the low critical temperature is determined as the higher of the two lowest temperatures. Figure 2.4 shows an example of blending chart prepared using method A.

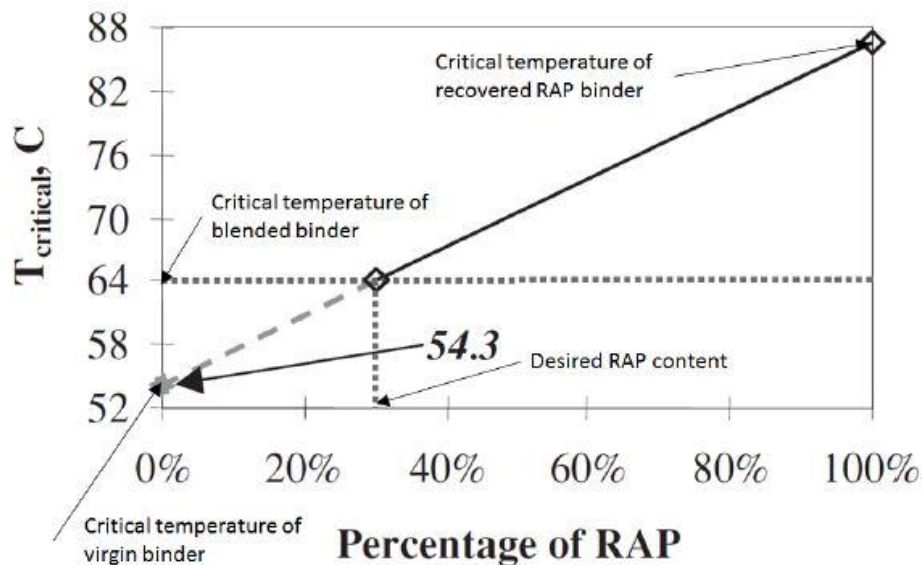


Figure 2.4 Blending chart for Method A (McDaniel et al., 2001)

2. When a specific virgin asphalt binder grade must be used and the desired binder grade and recovered RAP properties are known, the allowable percentage of RAP should be calculated for high, intermediate and low temperatures as follows:

$$\%RAP = \frac{T_{blend} - T_{virgin}}{T_{RAP} - T_{virgin}}$$

Figure 2.5 illustrates an example of blending chart prepared using method B.

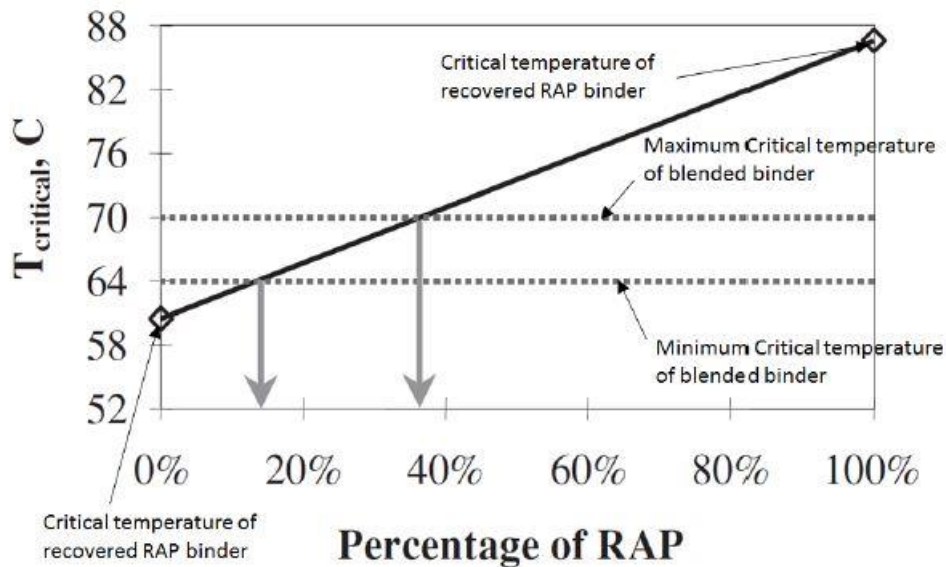


Figure 2.5 Blending chart for Method B (McDaniel et al., 2001)

A thorough characterization of the RAP and RAS must be performed to ensure they meet the governing specifications for aggregate gradation and quality, as well as binder quality when more than 25% binder replacement is used. Many State Departments of Transportation have adjusted the percentages in this guideline to reflect the local conditions.

Even though this procedure seems suitable for designing RAP mixes, more research on the topic concluded that it has several drawbacks. First, the blending charts assume a complete blending between the virgin and RAP aggregate and that the RAP is uniform in terms of binder grade and content. Second, the extraction of bitumen in the RAP to determine its viscosity or critical temperature is time consuming, creates disposal issues and involves hazardous solvents.

Bonaquist (2007) developed a methodology based on dynamic modulus and DSR measurements. The first step is measuring the mix dynamic modulus, E^* , using the Asphalt Mixture Performance Tester (AMPT). The second step consists in extracting the binder from the mix and measuring its shear modulus G^* using the DSR. It is assumed that the virgin and RAP binders become totally blended prior to the extraction process. Ultimately, the recovered binder's G^* value is used as an input into the Hirsch model or the Witczak model to estimate the mix E^* and then is compared to the measured E^* . Similar values suggest that there is a good blending of the virgin and RAP binders. Procedures based on the same principles but using different testing characterization, such as the Indirect Tension Test and the Bending Beam Rheometer are recommended by Stephens et al. (2001) and by Zofka et al. (2004).

Shirodkar et al. (2011), Bowers et al. (2014) and Bressi et al., (2015) studied the blending and diffusion between the RAP binder and virgin bitumen using staged extraction to isolate the recovered binder. Gel Permeation Chromatography and Fourier Transform Infrared Spectroscopy were utilized to analyze the properties of the recovered binder. However, none of these methods require performance tests for rutting or fatigue cracking, which leaves the estimation of the performance of the mixtures upon the local experience accumulated from previously constructed sections.

Even though RAS has been used as a component in asphalt mixtures for more than 20 years, it remains a relatively new application for many agencies. It was observed that the aggregates from RAS have an effect on the gradation properties of asphalt mixture. Therefore, the designer must determine the particle size and percentage of shingle aggregate and adjust the new aggregate composition accordingly. Also, adjustments must be done for the asphalt binder content requirements as part of the volumetric design procedure. RAS binders are much stiffer than virgin

asphalt binder, therefore agencies typically limit the use of RAS to a maximum of 5 percent by weight of aggregate. Although the amount of RAS in an asphalt mixture is relatively small, the non-asphalt components (aggregates and fibers) have an effect on the mixture. On one side, the presence of fibers and the angular properties of the RAS particles will generally increase the voids in the mineral aggregates (VMA). On the other side, the dust content of the RAS causes a reduction in VMA which is less than the increase from RAS particles and fibers, resulting in a net VMA increase. The dust to binder ratio and the fine aggregate angularity is also influenced by the use of shingles. To provide guidance with the incorporation of RAS in asphalt mixes, AASHTO published the Standard Practice for Design Considerations when using Reclaimed Asphalt Shingles in asphalt mixes in 2014, AASHTO PP78. Later on, this standard also proposed an approach to evaluate the embrittlement of the blended binder that affects the cracking properties of RAS mixtures. This approach is based on using the critical low temperature difference between the critical low temperature calculated for stiffness (S) and the one calculated for relaxation (m-value) derived from the Bending Beam Rheometer Test (BBR), as follows:

For stiffness (S):

$$T_c = \left[\frac{\log(300) - \log(S_1)}{\log(S_1) - \log(S_2)} \times (T_1 - T_2) \right] - 10$$

For relaxation (m-value):

$$T_c = T_1 + \left[\frac{0.300 - m_1}{m_1 - m_2} \times (T_1 - T_2) \right] - 10$$

From these two values, the critical low-temperature difference (ΔT_c) can be determined:

$$\Delta T_c = (S) \text{ critical temperature} - (m - \text{value}) \text{ critical temperature}$$

Where:

S_1 = Creep stiffness at T_1 , MPa

S_2 = Creep stiffness at T_2 , MPa

m_1 = Creep rate at T_1

m_2 = Creep rate at T_2

T_1 = Temperature at which S and m passes, °C

T_2 = Temperature at which S and m fails, °C

Figure 2.6 illustrates the graphical concept of the critical temperature values which may be interpolated between passing and failing temperatures, $T_{c,S}$ and $T_{c,m}$.

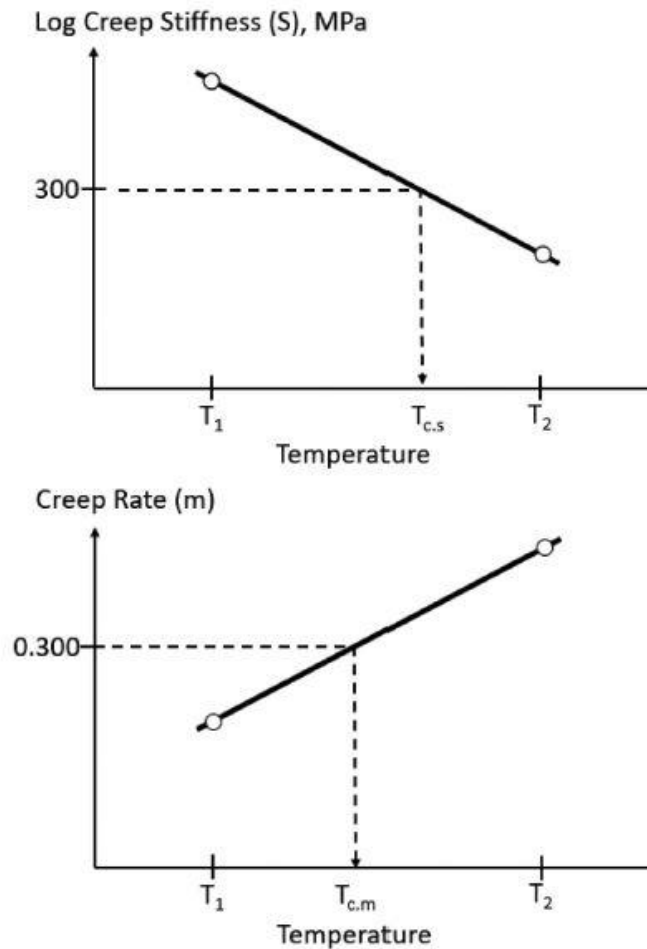


Figure 2.6 Graphical concept of $T_{c,S}$ and $T_{c,m}$ (Asphalt Institute, 2019)

The sign of ΔT_c , either positive or negative, indicates whether the performance grade is governed by its creep stiffness $S(+\Delta T_c)$ or creep rate $m(-\Delta T_c)$. S-controlled binders ($+\Delta T_c$) are

those that fail the 300 MPa limit at a warmer temperature than the m-value temperature. Alternately, m-controlled binders ($-\Delta T_c$) fail the 0.300 m-value at a warmer temperature than the S-value temperature (Asphalt Institute, 2019)

AASHTO recommends testing on blended binder to determine ΔT_c since is the most conservative condition. If blending is not complete, the impact of the aged binder on stiffening and relaxation is less that what the laboratory would predict. Also, the material must be PAV aged in accordance with AASHTO R28, with the exception that the aging time is increased to 40 hours. Research conducted by Anderson et al., (2011) indicated that when ΔT_c is less or equal to -5°C , a significant loss of cracking resistance occurs. This criterion can be adjusted on local experience or can be based on the specified low temperature of the binder grade from LTPPBind.

As mentioned earlier, the aged binder in RAP and RAS makes asphalt mixtures more brittle and creates long-term durability problems. It has been observed that using a softer and higher content of virgin binder may improve the resistance to cracking but it may become more susceptible to permanent deformation. Therefore, a balance of the combination of RAP and RAS content, virgin binder content and grade should be considered in the mix design.

2.3.2 Balanced Mix Design

With the introduction of Superpave, asphalt mixes are designed using a volumetric method; the design asphalt content is selected such that several volumetric parameters (Air Void ratio, Voids in the Mineral Aggregates and Voids Filled with Asphalt) are within specified ranges. However, there are no means to verify the mixture performance through mechanical tests before the field production and placement. To address these insufficiencies, Zhou et al., (2006) developed a new design method called Balanced Mixture Design (BMD) which promotes the use of rutting and fatigue cracking tests and criteria to achieve an optimum asphalt content.

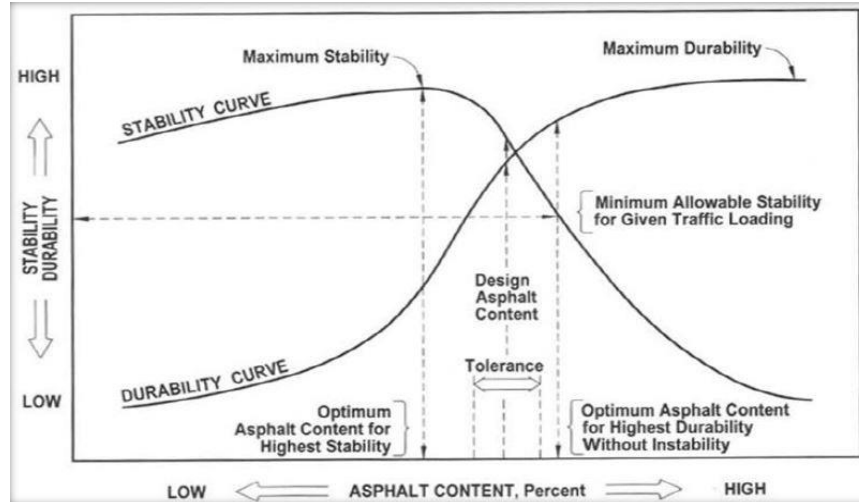


Figure 2.7 Proposed “Balanced” Mixture Design from Francis Hveem (Bennert, 2021)

The BMD concept is based on the same principle developed by Francis Hveem in the 1930s. As seen in Figure 2.7, the “balanced” area can be found where the optimum range of asphalt contents provides good rutting and durability in asphalt mixtures.

When first developed in 2006, Zhou’s BMD Texas method utilized the Hamburg Wheel Tracking Test (HWTT) and the Overlay Tester (OT) to determine the rutting and cracking resistance as performance tests (Figure 2.8 and Figure 2.9). However, in the past years, due to the lack of repeatability and high variability of the tests results of the OT test, researchers focused on developing and incorporating other tests. Recently, TxDOT partially adopted the IDEAL-CT test for the evaluation of cracking when designing BMD. Although the IDEAL-CT is simple, practical, and efficient and it shows a decent repeatability of the results, more research must be performed to ensure a good correlation to the field performance of the mixes.

Figure 2.10 summarizes the actions taken in the determination of the asphalt balanced content. According to Zhou et al., (2012), by examining the flow chart in Figure 2.10, there are four scenarios possible:



Figure 2.8 Hamburg Wheel Tracking Test



Figure 2.9 Overlay Tester

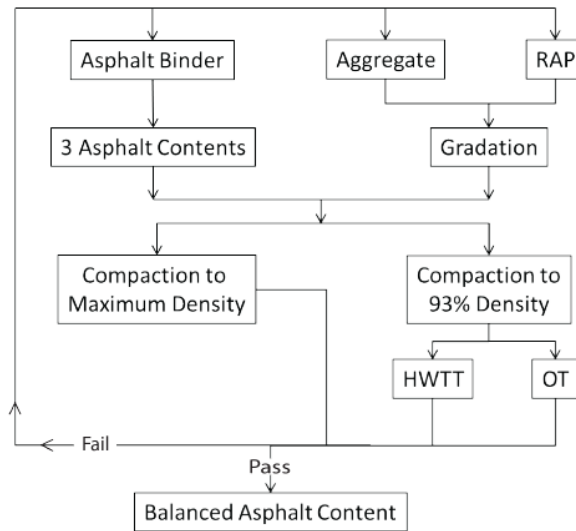


Figure 2.10 Balanced Mix Design Approach (Zhou et al., 2012)

- *Scenario 1.* The mixes fail both rutting and cracking requirements. In this case, the mix should be redesigned by using another PG binder, changing the aggregate gradation or use different types of aggregates.

- *Scenario 2.* The mixes fail rutting requirement but meet cracking requirement. The TxDOT mix design procedure used at that time tended to produce lean mixes, therefore reducing the asphalt content in order to increase the resistance to rutting is not considered a feasible option. The mix design must be redesigned by using aggregates with higher angularity and different gradation.
- *Scenario 3.* The mixes fail cracking requirement but meet rutting requirements. In this case, a viable solution would be to increase the asphalt content to improve its cracking resistance.
- *Scenario 4.* The mixes meet both rutting and cracking requirements. This is the ideal case where a balanced asphalt content can be further selected and then the mix design is complete.

Figure 2.11 illustrates a graphic example of the method. The BDM concept aims to find the range for the total binder content in which the lower bound is the minimum level to provide satisfactory cracking resistance, and the upper bound is the maximum asphalt content that does not cause excessive rutting. As seen in Figure 2.11, when the binder content increases, the mix is more prone to rutting but it has a better resistance to cracking. The mix must have less than 0.5-inch rutting after 20,000 cycles in the Hamburg Wheel Tracking test and it must last more than a predefined criterion (say 300 cycles) in the Overlay Tester. In this case, the asphalt binder content ranging from 5.3 to 5.8%, both criteria are met. (Romanoschi et al., 2014).

The performance criteria tests vary from state to state according to the regional climate and traffic conditions of the state. A survey performed by NCAT in 2017 shows the statistics of the most problematic distresses organized by states.

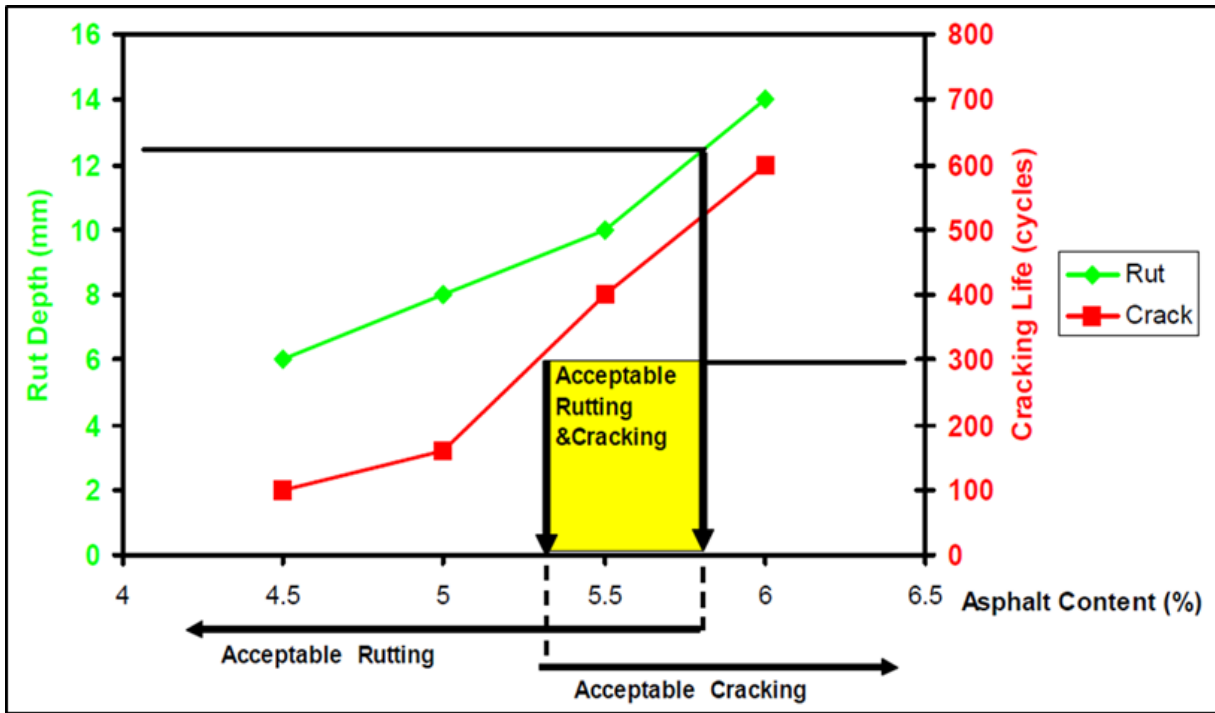


Figure 2.11 The Balanced Mixture Design Concept (Zhou et al. 2006)

Table 2.5 and Figure 2.12 shows the distress associated with the presence across the United States where the orange-colored states reported the presence of the given distress. As seen below, fatigue cracking is the most predominant distress reported by the DOTs, followed by rutting and thermal cracking.

Table 2.5 NCAT Survey results

<i>Answers (DOT)</i>	<i>Distress Percentage (%)</i>	<i>Response Percentage (%)</i>
Fatigue cracking	40	88
Rutting	33	70
Thermal cracking	30	64
Reflection cracking	29	62
Moisture damage	28	60
Raveling	23	49
Others (slippage, block cracking, etc.)	22	51





Figure 2.12 The most predominant asphalt distresses across United States (NCAT, 2017)

Based on the need of each state to better predict distresses and balance the mix design, different states select different performance measure tests. The variance is driven by two aspects: different pavement distresses (for example thermal cracking in Minnesota versus top-down cracking in Florida) and intended mix application or mix component of interest (for example high RAP/RAS mixes or specialty mixes).

Rutting resistance can be evaluated with Hamburg Wheel Tracking Test (HWTT), Asphalt Pavement Analyzer (APA), Asphalt Mixture Performance Tester (AMPT) and IDEAL-RT. HWTT and APA are the most used tests while the HWTT gained popularity due to the moisture susceptibility analysis. The IDEAL-RT was developed in 2020 by TTI as a much simple and more rapid alternative to test for rutting. At this time, according to TxDOT specifications, the IDEAL-

RT does not replace the HWTT, but it has a great potential to be added as a BMD performance test in the future. Regardless the type of test utilized, RAP/RAS mixtures are stiffer than virgin mixes, which gives them a better rutting resistance. Stroup-Gardiner et al., (1999), Willis et al., (2012), Tran et al., (2012), and Maupin Jr. et al., (2008) all demonstrated that RAP and RAP/RAS blend mixtures had significantly smaller rut depths in the APA than virgin mixtures. Only Apeageyi et al., (2011) reported that RAP mixes have a greater susceptibility for rutting than virgin mixes. However, they further explained that the RAP mixtures evaluated had lower effective asphalt contents which led to a mixture with lower stiffness characteristics.

The evaluation of durability/cracking resistance is significantly more complicated than that for stability/rutting, with aging being one of the main variables. The duration and temperature of the laboratory induced ageing is critical. Over-ageing the asphalt mixture in the laboratory increases the viscosity resulting in a stiffer mixture which is more prone to cracking. Not ageing the mixture enough, leads to a sub evaluation of the actual binder properties. Due to its complexities and high variability, ageing is a hot topic in the asphalt industry. More research must be conducted to correlate the laboratory ageing of mixtures with the naturally occurring ageing from the field.

There are numerous cracking tests available, each of which targets a specific cracking distress. For example, the fatigue cracking (bottom up or top down) can be determined through: IDEAL-CT Test, Bending Beam Fatigue Test, Texas Overlay Test, Semicircular Bending Test (SCB) and Direct Tension Cyclic Fatigue Test (S-VECD). According to McDaniel & Anderson (2001), the fatigue life decreases as the amount of RAP increases. They also stated that the beam fatigue tests showed that the number of cycles to 50% decrease in stiffness was greater for higher RAP, which implies a greater fatigue resistance. Hajj et al., (2007) also reported that RAP mixtures

had higher numbers of cycles to failure in the four-point beam fatigue test than virgin asphalt mixtures.

The low-temperature cracking resistance of the mixes can be evaluated through IDT Creep Compliance Test, SCB at Low Temperatures, Disk Shaped Compact Tension (DCT) and Thermal Stress Restrained Specimen Test (TSRST). Behnia et al., (2010) evaluated mixtures with different RAP percentages and different PG grade through DCT and concluded that RAP mixtures with softer binders had acceptable low-temperature fracture properties.

Reflection cracking resistance can be determined through IDEAL-CT Test, DCT, Overlay Test and SCB-IFIT Test. Mogawer et al., (2012) investigated a high number of plant-produced mixtures with up to 40% RAP content using the Overlay Tester, and his results showed that the RAP mixtures had lower fatigue resistance than that of virgin mixes. Tran et al., (2012) showed that the addition of 12% or more rejuvenating agent improves the fatigue behavior of RAP mixtures.

While some states have already established BMD approaches, other states DOTs are currently investigating performance testing (especially cracking tests) for integration into their mixture designs. As mentioned, Texas applied the BMD procedure to mixtures for high-volume surfacing since 2013. Currently, research is being conducted to investigate mixture design criteria based on climate, pavement layers, and traffic levels.

California uses the performance-modified volumetric design. As performance testing, Caltrans uses the Superpave Shear Tester (SST), Bending Beam Fatigue Test, HWTT and frequency sweep testing. Seven interstate highway projects were build using this approach. Caltrans is focusing on the mixture used on very-high volume pavements, (Wu et al., 2017).

Illinois uses the volumetric mixture design established by Superpave. IDOT is using HWTT as rutting performance evaluation and I-FIT SCB as a cracking test. The main objective is to address the use of high recycle content for RAP and RAS, (Newcomb, 2018).

Louisiana DOT is also using the volumetric design and a performance testing approach. The HWTT is used to evaluate rutting and the SCB-LSU method is used to evaluate the cracking resistance. This approach was implemented in 2016 and is used for both high and low volume roadways, (Newcomb, 2018).

New Jersey uses a procedure based on volumetric design with performance verification. For rutting, the APA is used and for cracking, both the OT and the bending beam fatigue test are used. This approach is used for approximately 10% of the high-volume surfaces. Also, Rutgers University developed and proposed a method based on performance properties, but it is still to be implemented, (Bennert et al., 2015).

The Wisconsin DOT is designing the mixtures with high recycled materials content based on the volumetric design. For rutting evaluation, the WisDOT uses the HWTT and to assess the cracking potential they use DCT test and low-temperature SCB, (West et al., 2021).

There are still many issues in using a volumetric method as the only approach to determining the composition of mixes. The amount of blending between RAP or RAS binders and virgin binders is a concern. Even though some states require using a softer grade of virgin asphalt, there is no guarantee that it is necessary or that a softer binder will have the desired results.

To date, the use of BMD approach seems to be the best option to design asphalt mixtures. The performance evaluation on durability and stability plays an essential role in the design of RAP/RAS.

2.4 Laboratory Evaluation of Recycled Asphalt Mixtures

Cracking and rutting are the most frequent distresses that drive the need for rehabilitation of asphalt pavements. Increasing the use of recycled materials, recycling agents and binder additives makes the asphalt mix design even more complex. To improve the design of mixes containing RAP and RAS, many research efforts focused on measuring the properties of these mixes using a multitude of laboratory tests. As briefly mentioned in the previous section, the laboratory rutting evaluation is well established and rutting does not seem to be a problem in RAP/RAS mixes. However, the laboratory cracking evaluation requires a lot of research effort. Many tests are readily available to evaluate the cracking performance. As shown in Figure 2.13, these tests are based on empirical and mechanistic principles.

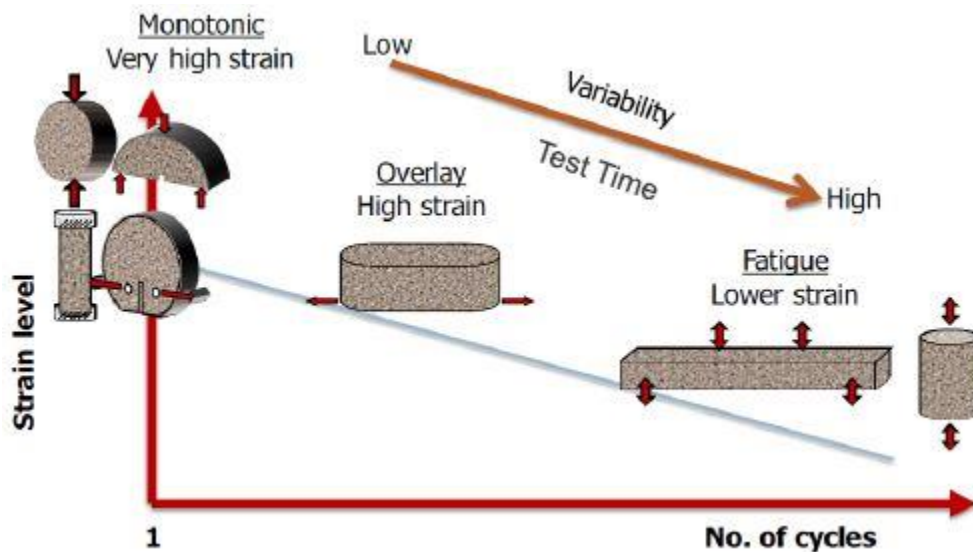


Figure 2.13

Typically, empirical tests have a monotonic loading and high strains, resulting in a much shorter completion time. Contrarily, mechanistic tests have a cyclic loading and low strains, which will require a longer test time. Mechanistic tests tend to have a better correlation to the field

performance than empirical tests, but the preparation of the specimens require more cutting, expert personnel and a longer testing time. Empirical tests are more practical in terms of cost and time and most showed repeatable and reproducible results. Empirical or mechanistic, the performance evaluation on durability and stability is essential in successfully designing RAP/RAS mixtures.

In 2002, Abdulshafi conducted an experiment to find a simple laboratory test that could determine the optimum RAP percentage based on mix durability. In this project, six sources of RAP and four RAP percentages varying between 0 and 30% were used. This study assumes that there is a complete blending between the RAP and virgin binder. To evaluate the durability of the mixes, Abdulshafi estimated the absorbed energy at failure for unconditioned and conditioned samples based on the indirect tensile strength test. The conditioning of the samples was performed by keeping the samples at constant saturation, followed by a freeze cycle and hot water soaking. The optimum RAP percentage was selected at the maximum percentage of absorbed energy. Based on this criterion, it was determined that a 30% RAP mixture containing a limestone aggregate withstands the maximum energy level. On the other side, a mixture produced with gravel aggregate showed the maximum absorbed energy at 10% RAP. The results did not show a specific trend, but it can be observed how many factors besides the blending affect the durability and how difficult is to predict it correctly.

McDaniel and Shah (2003) conducted a laboratory study to determine if the materials obtained from Indiana, Michigan and Missouri comply with the tiered approach developed by the FHWA and Superpave. The first part of the experiment consisted in comparing laboratory mixtures to plant produced mixes containing the same RAP content and source, virgin aggregate and binder. In the second part of the experiment, samples were prepared with a RAP content up to 50% to determine the effect of recycled materials on the mix performance. The mixes were then tested

using the Superpave Shear Tester. After examining the mixtures, it was determined that the plant produced mixes are similar in stiffness to the laboratory produced mixtures for the Michigan and Missouri samples. The plant-produced mixtures from Indiana were significantly stiffer than the laboratory mixes.

The analysis on the shear tester also showed the stiffening effect of RAP materials on the mixture properties compared to the virgin mixture. An increased stiffness may improve the rutting resistance but at the same time it may increase the potential to thermal and fatigue cracking. This confirmed the findings from NCHRP 9-12 study: recycled mixture with a RAP content greater than 20% have a lower fatigue life than virgin mixtures, (McDaniel et al., 2000). To improve the mixture fatigue performance, decreasing the virgin binder grade may be a good option. In this study, the authors also concluded that designing mixtures according to Superpave specifications may not be feasible at a RAP content greater than 40% due to the high fine content in RAP materials.

Huang et al., (2004) evaluated the fatigue performance using the indirect tensile strength test, the semicircular bending test and the four-point beam fatigue test. The mixtures tested were designed using the Marshall mix design with a RAP percentage varying between 0 to 30% and with the same aggregate structure and same asphalt content. This study concluded that the tensile strength increased with the increase in RAP content which suggests that RAP materials improved the fatigue life of HMA.

In 2008, the Virginia DOT analyzed how increasing the RAP content affects the performance of several high RAP and low RAP overlay projects. For this purpose, samples of mixture were collected from a single truck at the hot-mix plant for each paving project for laboratory testing. Afterwards, multiple mixes containing 21 to 30% RAP as well as a control

mixture with less than 20% RAP were designed using the Superpave method at 65 gyrations. For all the mixes, a PG 64-22 binder and a NMA of 9.5 mm to 19 mm was used. Table 2.6 shows the summary of high RAP mixes constructed in this study.

Table 2.6 Construction of High RAP mixes (Maupin et al., 2008)

<i>Route (s)</i>	<i>County or City</i>	<i>Mix Type</i>	<i>% RAP</i>
SR 40, CR 703	Dinwiddie	SM-12.5D	25
CR 611	Surry	SM-9.5D	25
I-664	Chesapeake	SM-12.5D	30
SR 6	Goochland	SM-12.5D	25
SR 6	Goochland	IM-19.0D	30
US 58	Carroll	SM-9.5D	30
US 221	Floyd	SM-9.5D	30
US 29	Nelson	SM-9.5D	25
SR 24, CR 691	Appomattox	SM-9.5D	25
US 29, SR 57, CR 729, CR 988	Pittsylvania	SM-9.5D	21

The samples were tested for: rut depth using the APA test, fatigue cracking using Beam fatigue test and moisture sensitivity using the Tensile Strength Ratio (TSR test and their results concluded that no significant statistical difference exists between the control mix and the higher RAP mixes.

Hajj et al. (2009) evaluated the impact of three RAP sources at three levels of RAP content 0, 15 and 30% in terms of mixture resistance to rutting, fatigue cracking, thermal cracking and moisture sensitivity. All the mixes except one indicated acceptable resistance to moisture damage. The resistance of HMA mixes to rutting was evaluated using the Asphalt Pavement Analyzer (APA) which subjects the mix to repeated wheel loads and measures the permanent deformation. Not only all mixes met the rut depth criterion for the State of Nevada but mixes containing RAP materials decreased rutting up to 33% when compared to the control mix with virgin materials. The resistance to fatigue cracking was evaluated using the flexural beam fatigue test with constant strain at three different levels. The results were not conclusive enough, although it was mentioned

that the introduction of RAP decreased the fatigue resistance of mixtures, especially at higher strain levels. However, some of these mixes could perform well in the field since stiffer mixtures produce lower tensile strains under vehicle loading. This indicates the need for testing the samples at similar strain levels in laboratory to those the mix will likely experience in field conditions.

Huang et al., (2011) conducted a laboratory study where he evaluated the performance of the most used mixture containing 0, 10, 20, and 30 % RAP in the state of Tennessee. Two types of aggregate (limestone and gravel) and three types of asphalt binders (PG 64-22, PG 70-22, and PG 76-22) were used in this study. Prior to testing, the plant produced HMA mixtures were short term and long term aged and tests were performed on both. The Superpave Indirect Tension, beam fatigue and semicircular bending tests were employed to determine the mixture cracking resistance. Figure 2.14 presents the IDT strength-test results of limestone and gravel mixtures. It can be observed that the mixtures that were long-term aged had higher ITS, lower strain at peak load, and lower toughness indices than the short-term aged mixtures. Also, it is noticeable that increasing the percentage of RAP increases the tensile strength and decreased the toughness indices for both short terms aged and long-term aged mixtures. Results from SCB tests also showed that the long-term aged limestone mixtures had a higher tensile strength, lower strains at peak load, and lower toughness indices. The addition of RAP in the gravel mixtures increased the tensile strength but significantly decreased the strain at peak load and toughness indices for both short-term and long-term aged mixtures. The results from the bending beam test showed than the inclusion of RAP generally decreased the crack resistance.

Zhou et al., (2011) conducted research on high RAP content mixes. Testing procedures such as aggregate gradation for the material variability, Hamburg Wheel Tracking Test (HWTT) for the rutting and moisture resistance and Overlay Test (OT) for the cracking resistance were performed.

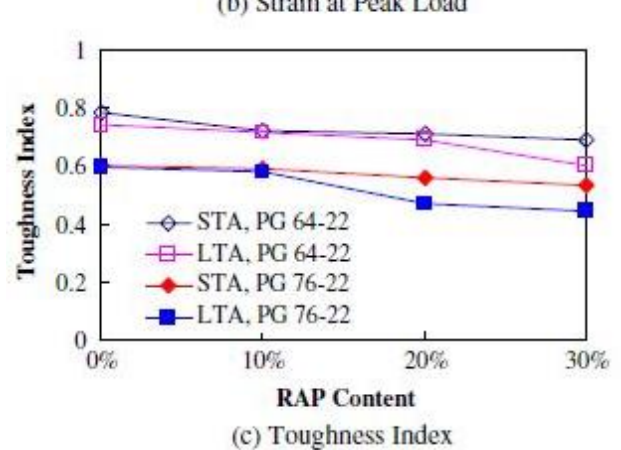
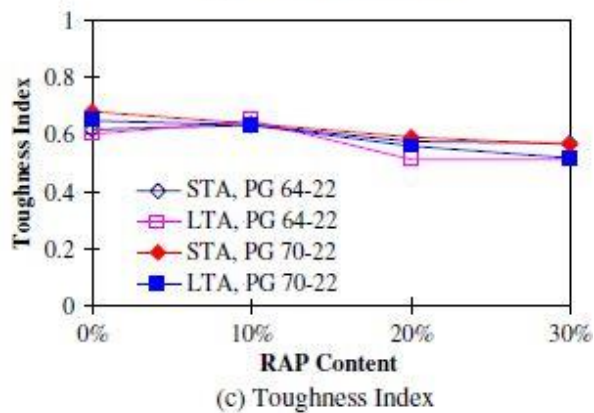
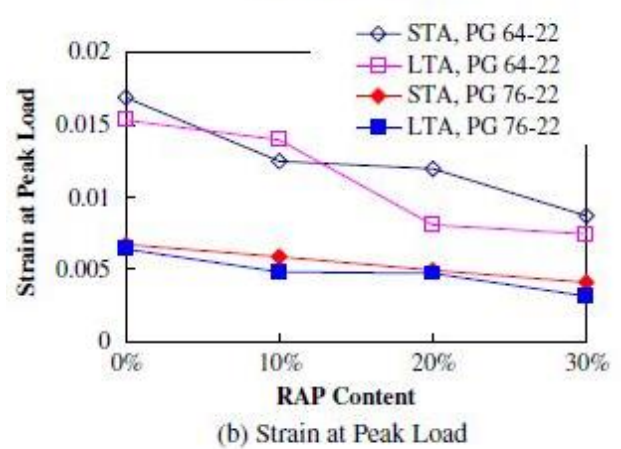
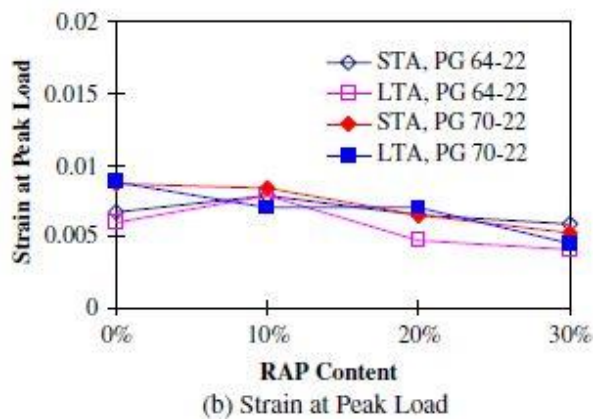
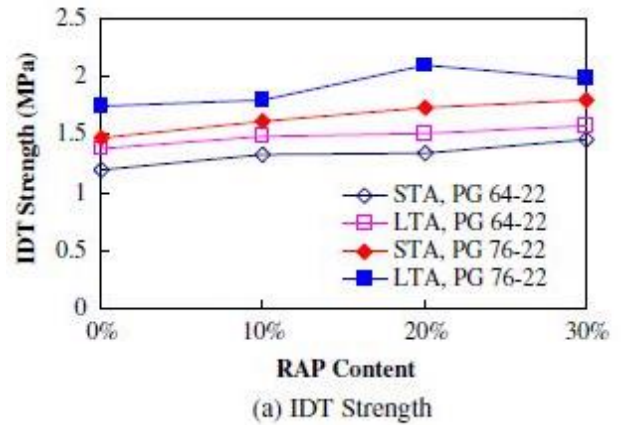
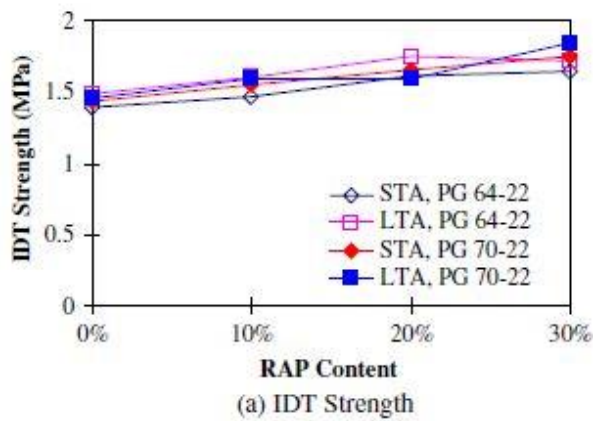


Figure 2.14 IDT strength test results for gravel mixtures-left and limestone mixtures-right, (Huang et al., 2011)

The research highlights that an increase in RAP content enhances the moisture resistance and causes a significant increase of optimum asphalt content (OAC) from a RAP content of 20%. However, a reverse reaction was observed with cracking resistance from 30% RAP content or a combination RAP and reclaimed asphalt shingles (RAS).

Apeageyi et al. (2013) evaluated the performance of high RAP asphalt mixtures by investigating the stiffness characteristics of 120 Virginia DOT dense-graded asphalt mixes containing 20% RAP or more. At the time, Virginia DOT considered high RAP mixes as the mixes with more than 20% for surface and intermediate, and 25% for base mixes. The Dynamic Shear Rheometer (DSR) and the Flow Number (FN) test were employed to determine the stiffness of the recovered asphalt binder and the rutting resistance of the mixes, respectively. Their analysis indicated that there is no statistically significant difference in FN for the majority (76%) of the mixtures even though they contained RAP amount ranging from 21 to 30%. Unexpectedly, the high-RAP mixtures were found to be softer than the mixtures with intermediate RAP content. A plausible explanation for that could be the practice of using softer asphalt binder for higher RAP contents led to a decrease in stiffness of the mixes.

Norouzi et al. (2017) examined the effects of RAP content and binder grade on the fatigue resistance of Georgia asphalt concrete mixtures. Asphalt mixtures with three asphalt binder PG 64-22, PG 67-22, and PG 76-22 were prepared and tested using dynamic modulus and controlled crosshead cyclic tension fatigue tests. Then, the test results were used as inputs in the S-VECD model and LVECD program to investigate the effects of RAP content and binder grade on the fatigue performance of pavements. The analysis showed that the addition of RAP up to 30% using corrected optimum asphalt content (COAC) method significantly improved the mixtures' fatigue resistance, especially for the mixtures with PG 64-22 and PG 67-22 binders. The COAC method reflects the original OAC plus the addition of virgin asphalt content in the amount of 25 percent of the RAP asphalt content. The non-RAP mixes with different binder grades showed a rapid decrease in material integrity with an increase in damage.

Xie et al., (2020) conducted an experiment to compare the effectiveness of different types of rejuvenators in mixtures with 30% RAP, 40% RAP, and 25%RAP & 5%RAS and to evaluate their cracking performance. Three bio-oils, one aromatic extract and one re-refined engine oil bottom were used as rejuvenators, as shown in Table 2.7. Four different methods of adding rejuvenators were used: terminal blend, belt spray, 48-h marination, and 14-day marination. Marination refers to the process of spraying the RAP and RAS with rejuvenator at room temperature and then kept in Ziploc bags.

Table 2.7 Rejuvenators used (Xie et al., 2020)

<i>Rejuvenator name</i>	<i>Description</i>	<i>Use information in this study</i>
RA1	Bio-based, made from crude tall oil	Used in all the three mixes
RA2	Bio-based, made from pine trees	Used in all the three mixes
RA3	Aromatic extract, refined crude oil	Used in all the three mixes
RA4	Re-refined engine oil bottom	Only used in 30% RAP mix
RA5	Bio-based, paper industry by-product	Used in 40% RAP mix and 25% RAP/5% RAS mix

Table 2.8 shows the tests were performed on the short-term aged and long-term aged mixtures.

Table 2.8 Proposed mix performance testing (Xie et al., 2020)

<i>Property evaluated</i>	<i>Test name</i>	<i>Test specification</i>
Raveling	Cantabro loss test	ASTM C131
Intermediate temperature cracking	Illinois Flexibility Index Test (I-FIT)	AASHTO TP 124
Reflective cracking	Overlay Tester (OT)	TxDOT Tex-248-F
Low-temperature cracking	Disc-Shaped Compact (DSC) tension test	ASTM D7313

It was concluded that the abrasion loss results in the raveling test for 40% RAP and 25% RAP/5%RAS was lower than those of the control mixes, regardless of the addition method utilized. This was expected because the rejuvenators soften aged asphalt binder and make the recycled mix less brittle.

In the I-FIT test, a higher fracture energy value represents a better resistance to cracking.

The I-FIT fracture energy indicated that all the rejuvenated mixes exhibited higher values than the control mix for short-term and long-term aged mixtures. This suggests that the rejuvenator improved the resistance to cracking of the recycled mixes.

Figures 2.15 and 2.16 show the number of cycles to failure obtained from the overlay tester and the fracture energy obtained from the DCT test, respectively. As seen in Figure 2.15, the rejuvenated mixes exhibited higher average values of cycles to failure compared to the corresponding control mix, indicating that the rejuvenator increased the cracking resistance of the recycled asphalt mixes.

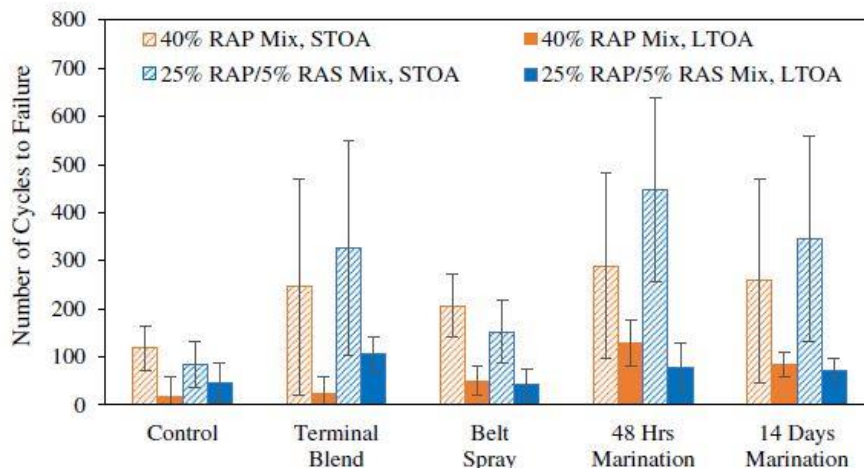


Figure 2.15 Overlay tester results (Xie et al., 2020)

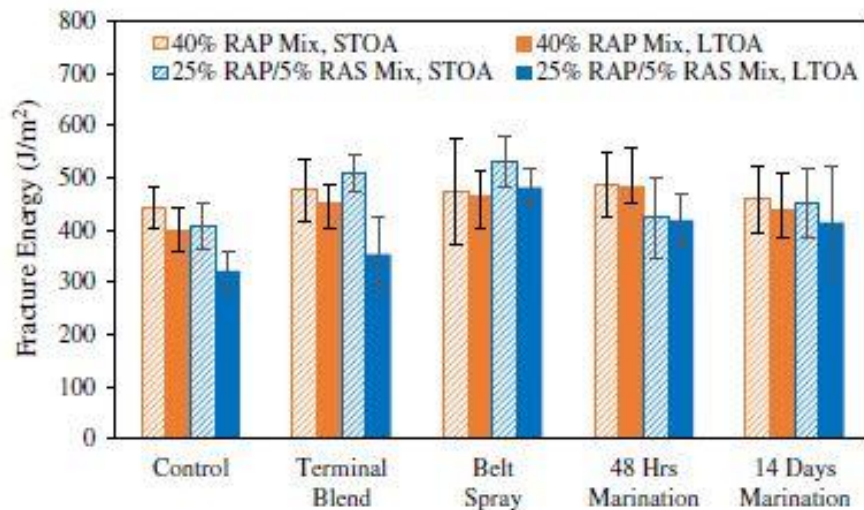


Figure 2.16 DCT fracture energy results (Xie et al., 2020)

In term of DCT fracture energy, the rejuvenators increased the fracture energy by 3-50%. Statistically, no significant difference was found between the rejuvenated and the control mixtures.

Many researchers have studied the mechanical properties and performance of RAP mixtures and some on the results were summarized above. The main takeaways are:

- The inclusion of RAP/RAS increases the resistance to rutting.
- Generally, the cracking resistance decreases with the increase of RAP and RAS content, although some cases showed the contrary.
- The use of rejuvenators and softer binders improve the cracking resistance especially for high RAP/RAS mixes.
- The use of RAP and RAS has none or minimal effect on the moisture sensitivity of mixtures.
- The performance of RAP/RAS mixtures is highly dependent on the aging phenomenon.
- Multiple performance evaluation tests are needed; a single approach may not be suitable for all the cases and locations.
- More research is needed to correlate the laboratory testing to the field performance.

2.5 Field Performance of RAP Mixtures

To validate the laboratory performance procedures employed in the characterization of recycled asphalt mixtures, evaluating the field performance, and establishing a correlation between laboratory and field performance is imperative. The optimization of the design of mixes containing RAP and RAS has used the recorded field performance of these mixes. Some studies have used specially built test sections in a controlled experimental design, others have collected performance data of existing in-service road sections.

2.5.1 Accelerated Pavement Testing

Accelerated Pavement Testing (APT) is an effective method to evaluate the performance of materials and pavement structures under controlled and accelerated loading and environmental conditions in a compressed time. The acceleration of damage is achieved by means of increased repetitions, modified loading conditions, imposed climatic condition, the use of thinner pavements with a decreased structural capacity and thus shorter design lives or a combination of all these factors (Metcalf, 1996). For many years, accelerated pavement testing was used to:

- Understand pavement behavior
- Identify and highlight deficiencies in current practices
- Evaluate new materials, designs, specifications, or constructions standards before full scale implementation
- Validate and calibrate new designs and performance models
- Compare different designs, materials, procedures, and products
- Link laboratory test results and field observations
- Assess impacts of new vehicles, tires, tire inflation pressures, load limits etc.

The data that can be generated by an APT facility is very vast and has the advantage of closely resembling the process that pavements are subjected to during their service lives. However, APT facilities are commonly associated with very high initial investments and operational costs. Even though the initial costs are higher, APT provides realistic results which might actually decrease the related costs in the long term. Brown et al., (2004) states that the benefit/cost ratio is 10 to 1 for his analysis; ratios of up to 50 have been reported elsewhere. Figure 2.17 illustrates a comparison of accelerated pavement testing and other evaluation methods in terms of reliability, time, and cost (Fosu-Saah et al., 2021).

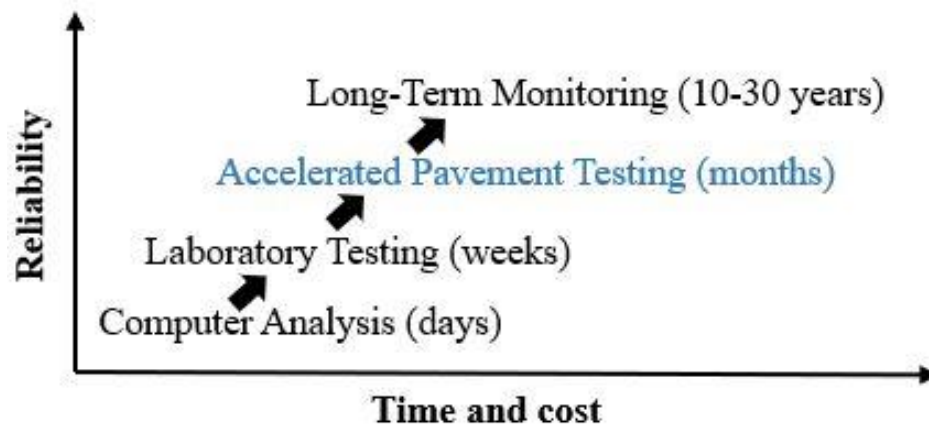


Figure 2.17 Pavement Testing Methods

There are two main types of APT facility: fixed and test track. The fixed APT can be linear (HVS, ALF, ATLAS) or circular (LCPC, CAPTIF). AASHO Road Test, Westtrack, NCAT and MnRoad are example of test tracks. Figure 2.18 shows the NCAT test track located in Alabama. Table 2.9 summarizes the main differences between fixed APT devices and Test Tracks. Regardless the type of APT selected and/or the way the load is applied, accelerated pavement testing is the best option to validate laboratory test and understand the pavement behavior.



Figure 2.18 NCAT Test Track – Alabama

Table 2.9 Differences between fixed APT and Test Tracks (Jones, 2011)

Fixed Devices	Test Tracks
Controlled temperature and moisture	Uncontrolled temperature and moisture
Slow speed trafficking	Highway speed trafficking
Ability to vary load and to overload	Limited ability to overload
Controlled wander	Uncontrolled wander
Little or no suspension interaction	Realistic suspension interaction
Ability to test short sections	Ability to test longer section
Difficult to measure roughness	Meaningful roughness measurements
Ability to be transported	Fixed location

2.5.2 Field Performance Studies of Recycled mixes in the United States

To compare the long-term performance of recycled and virgin asphalt overlays in an arid climate, the Arizona Department of Transportation constructed in 1981 eight overlay test sections on Interstate 8 in southwestern Arizona. The recycled overlay sections contained 50% RAP and a softer binder compared to the virgin mixtures. Roughness, skid number and cracking were collected over a period of 9 years. Hossain et al., (1993) reported that the recycled and asphalt sections performed similarly.

Paul (1996) evaluated the performance of five projects containing up to 50% RAP built between 1978 and 1981 in Louisiana. After evaluating the performance in terms of serviceability index, structural integrity and severity cracking, he concluded that no significant difference was found between the RAP and virgin mixes. However, the recycled asphalt mixture showed more longitudinal cracking.

Musselman (2009) investigated pavements constructed between 1991 and 1999 with 30 to 50% incorporated RAP. He focused on the age at which deficiencies due to cracking first appeared

in the sections. Then a comparison between the RAP and virgin mixes was performed. It was concluded that the performance decreases for the mixes containing more than 30% RAP.

In the recent years a variety of test sections with asphalt mixtures containing moderate and high RAP/ RAS were constructed and trafficked at the NCAT Pavement Test Track (Willis et al., 2009; West et al., 2012). Two test sections with mixtures containing 20% RAP and four sections with mixtures containing 45% RAP were built in 2006. All six mixtures were placed in two-inch thick surface layers. The same virgin aggregates and RAP were used for all six mixtures. The main difference among the RAP mixtures was the virgin binder type, as shown in Table 2.10.

Table 2.10 Summary of Test Sections and Binder Test Data (Willis et al., 2009)

Section	%RAP*	%RAP Binder**	Virgin Binder		Virgin Binder + RAP	
			PG Grade	True Grade	Predicted Grade	Recovered Grade
W3	20	18.2	PG 76-22	78.1 -23.8	80.1 -22.4	78.1 -30.3
W4	20	17.6	PG 67-22	68.4-31.2	72.0 -28.6	74.2 -29.7
W5	45	42.7	PG 52-28	54.7-32.8	69.4 -25.8	74.1 -30.2
E5	45	41.0	PG 67-22	68.4-31.2	76.9 -25.1	80.9 -26.2
E6	45	41.9	PG 76-22	78.1-23.8	82.7 -20.7	85.5 -25.7
E7	45	42.7	PG 76-22 +1.5% Sasobit	83.2 -20.6	85.7 -18.8	86.3 -24.3
N5	0	0	PG 67-22	68.4-31.2	68.4 -31.2	71.1 -32.4

After five years of traffic loading, which is the equivalent of more than 20 million ESALs, the test sections showed satisfactory performance in terms of rutting and cracking resistance. West et al. (2009; 2012) reported that all the sections had rut depths less than 5 mm and low-severity cracking was observed in all the sections except for the 20% RAP section with the PG 67–22 virgin binder. The dependency between the virgin binder grade and the percentage of cracking is easily noticeable: the softer the virgin binder, less cracking was observed. In an ascending order, the 45% RAP section with PG 52–28 had 3.5 feet of very-low-severity cracking, followed by the 45% RAP section with PG 67–22 binder containing 13.9 feet of cracking, then the 45% RAP

section with PG 76–22 containing 53.9 feet of cracking. The 45% RAP section with PG 76–22 with Sasobit had 145.5 feet of total crack length. Laboratory tests were also performed and then compared to the results obtained from the field experiment. The laboratory rutting results matched the field rut measurements and the master curves show that binder stiffness greatly influences mix stiffness. Softer binders decrease the mix stiffness which could decrease the durability of the pavement. The NCAT Test Track concludes that the use of softer binder grades in RAP mixes is not necessary. The RAP mixes showed very good rut resistance and high stiffness, but no fatigue cracking could be observed because of the very thick asphalt and strong pavement structure (24 inches) on top of a stiff base.

In 2009, further research was conducted, and additional high RAP test sections were constructed and evaluated. After 25 month of traffic loading, the equivalent of approximately 10 million ESALs, a 45% RAP test section showed 61 feet of low severity cracking and only 3 mm rutting. In the same project, two 50% RAP sections of the same thickness, one produced as HMA and the other as warm-mix asphalt (WMA), were compared to a control section of HMA and two WMA sections of the same thickness but without any RAP material. The two 50% RAP sections showed considerably less cracking and rutting than the two warm-mix sections. After 5 years of traffic, West et al. (2014) reported that the 50% RAP HMA showed no cracking and a rut depth of 4 mm and the 50% RAP WMA showed 3% cracking and 5 mm of rutting compared with the no-RAP WMA sections which showed 18% of cracking and a rut depth of 18 mm.

Several researchers evaluated the field performance of RAP mixtures based on the data collected over the past 25 years through the FHWA's Long-Term Pavement Performance (LTPP) program. West et al. (2011) evaluated the 20-year performance history of 18 projects constructed in United States and Canada. These projects are referred as the Specific Pavement Study 5 (SPS-

5) and each project consists of eight test sections with 30% or more RAP and one control virgin mixture section. West et al., (2011) compared seven exhibited distresses of the virgin sections with those of RAP sections including International Roughness Index (IRI), rutting, fatigue cracking, longitudinal cracking, transverse cracking, block cracking, and raveling. Table 2.11 shows the comparison of the performance sections. Statistical analyses indicated that the 30% RAP mixtures had proven equivalent performance to virgin mixtures in terms of raveling, block cracking, IRI and rutting. It has also been reported that approximately one third of the RAP sections showed more longitudinal and transverse cracking than the virgin mixture sections. However, further research attributed the increased cracking in the RAP sections to the high dust content present in those mixes, (West et al., 2014).

Table 2.11 Performance comparison: Virgin vs. 30% RAP Mixes (West et al., (2011))

Distress	Difference Between RAP and Virgin Mixes Not Significant (%)	Virgin Mixes Better Than RAP Mixes (%)	RAP Mixes Better Than Virgin Mixes (%)	RAP Mixes Equal to or Better Than Virgin Mixes (%)
IRI	19	42	39	58
Rutting	38	33	29	67
Fatigue Cracking	61	29	10	71
Longitudinal Cracking	75	15	10	85
Transverse Cracking	53	32	15	68
Block Cracking	96	3	1	97
Raveling	78	7	15	93

A national pooled fund study, TPF-5(213), was conducted at Iowa State University where a series of projects were built in Minnesota, Iowa, Missouri, Colorado, Illinois, Wisconsin, and Indiana with the main goal of investigating better ways to design asphalt mixtures with a higher content of RAS. Each demonstration project focused on evaluating different factors including RAS

grind size, RAS percentage, RAS source (post-consumers versus post-manufactured), RAS in combination with warm mix technology, RAS as a fiber replacement for stone matrix asphalt pavements, and RAS in combination with ground tire rubber (GTR). Some of these demonstration projects also included control sections to compare traditionally used mix designs containing either RAP only or no recycled product. The research interest corresponding to each state agency is showed in Table 2.12.

Table 2.12 Experimental plan for each demonstration project (Williams et al., 2012)

Agency	Research Interest	Mix designs developed		
CO	Replacement of RAP with RAS	0% RAS 20% RAP	3% RAS 15% RAP	
IL	5% RAS in SMA	PG 70-28 Lab Mix	PG 70-28 Plant Mix	PG 58-28 12% GTR
IN	RAS with foaming WMA	15% RAP	3% RAS	3% RAS WMA
IA	Percentage of RAS	0% RAS	4% RAS	5% RAS
MN	PM vs. PC RAS	0% RAS 30% RAP	5% MWAS RAS	5% PCAS RAS
MO	Coarse vs. Fine Grind RAS	0% RAS 15% RAP	5% Fine RAS 10% RAP	5% Coarse RAS 10% RAP
WY	RAS with RAP and 3G Compaction Aid	5% RAS No 3G	5% RAS 3G Evotherm	

The flow number test and the dynamic modulus test performed on each mix indicated good rutting resistance. The mixes also showed good fatigue cracking resistance in the four-point bending beam test with the SMA from Illinois having the most desirable fatigue characteristics. The SCB test was also performed, and the statistics showed no significant difference between the RAS mixes and the mixes without RAS from the Missouri, Minnesota, Indiana, Wisconsin, Illinois, and Colorado projects. Moreover, the fracture properties determined from the SCB test showed that the addition of RAS materials to HMA is beneficial, the fibers in RAS could be contributing to the mix performance.

Binder extraction was performed for each of the mixes and the average results showed that for every 1% increase in RAS, the low temperature grade of the base binder increased 1.9°C; and for every 1% increase in RAP, the low temperature grade of the base binder increased 0.3°C. Therefore, as a rule of thumb, 3 % RAS or 20 % RAP would be the maximum amount of recycled material allowed without requiring a low temperature grade bump (6°C) in the base binder (Williams et al., 2012). After 2 years, pavement condition surveys were performed on each section and there was no rutting, wheel path fatigue cracking or thermal cracking reported. However, transverse reflective cracking from the underlying jointed concrete pavement was reported in the Missouri, Colorado, Iowa, Indiana and Minnesota projects. The non-RAS pavement in Colorado showed lightly less cracking than the RAS pavement. The RAS pavements from Iowa, Indiana, Illinois and Wisconsin exhibited the same amount or less than the non-RAS sections. This pooled fund study shows a promising future for RAS application in HMA, and the results encouraged other State agencies in recycling more RAS.

2.5.3 Field Performance Studies of Recycled mixes in Texas

Over the past several years, the Texas DOT showed increased interest in understanding how RAP influences the asphalt concrete mixtures and how local climate and conditions affect the performance of mixes containing RAP in surface and underlying layers. To address this, several projects were constructed and evaluated, as given in Table 2.11. These field test sections covered different applications of RAP/RAS mixes, including: (1) asphalt overlays vs. new construction, (2) cold weather vs. hot weather, (3) heavy traffic vs. low traffic, (4) thicker vs. thin asphalt layer(s), and (5) virgin mix vs. RAP only (or RAP/RAS), (Zhou et al. 2014).

To demonstrate and validate the balanced mixed design approach on recycled mixtures, Zhou et al., (2011) overlaid four existing pavement sections with severe transverse cracking on

IH40 near Amarillo, Texas. The proposed mix design of the four overlays is summarized in Table 2.13. The 20% and 0% RAP mixes (Section 0 and 1, as shown in Figure 2.19) were designed by a contractor in accordance to the TxDOT standard mix procedure in which the OAC was selected based on a target 96.5% density and then it was checked to ensure the mix rutting and cracking requirement. The 35% RAP and 20% RAP placed on section 2 and 3 were designed by TTI following the BMD method. Based on previous experience, a maximum density of 98% was chosen in this study.



Figure 2.19 I-40 Experimental sections. Location and existing pavement condition after 4” milling, Zhou et al., (2011)

The sections were built in 2009 and surveys were conducted regularly. As summarized in Table 2.13 after three years of trafficking, the Section 0 and 1 showed 100% reflective cracking and Section 2 and 3 only 57% cracking. The Overlay Tester results showed that the mix from Section 2 had the best cracking resistance with 200 OT cycles performed. Zhou et al., (2011) concluded that the high RAP mixtures could perform well given that an appropriate mix design method such as BMD is used.

Table 2.13 Field RAP/RAS Test Sections and Observed Performance (Zhou, 2013)

Test Section				Weather	Traffic (mESA L/20 Years)	Overlay/ New Construction	Existing Condition if overlay	OT Cycles	Performance
Highway	RAP/RAS	Virgin Binder	HMA/WMA						
IH40	20%RAP	PG 64-28	HMA	Hot summer cold winter	30	4-inch overlay	Sever transverse cracking	10	100% reflect cracking after 3 years
	0%RAP	PG 64-28						90	
	20%RAP	PG 64-28						103	
	35%RAP	PG 58-28						200	57% reflect cracking after 3 years
FM1017	0%RAP	PG 76-22	HMA	Very hot summer, mild winter	0.8	New construction, 1.5-inch surface layer	N/A	28	Limited, fine cracking after 2.5 years
	20%RAP	PG 70-22						6	
	35%RAP	PG 70-22						7	
SH359	20% RAP	PG 70-22	HMA	Hot Summer Mild Winter	1	3-inch overlay	Sever transverse cracking	3	No cracking after 2.5 years
SH146	15%RAP / 5% TOAS	PG 64-22	HMA	Hot Summer Mild Winter	1.5	New construction, 2-inch surface layer	N/A	3	No cracking after 3 years
US87	5% TOAS	PG 64-28	HMA	Hot summer, very cold winter	3.5	3-inch overlay	Sever transverse cracking	48	50% reflective cracking after 2.5 years
		PG 64-28 with 0.4% more virgin binder						96	20% reflective cracking after 2.5 years
Loop820	15%RAP /5%MWAS	PG 54-22	WMA	Hot summer, mild winter	15	2-inch overlay	Fine transverse cracks in existing CRCP	8	Perfect condition after 1 year
		PG 64-22	WMA					12	
		PG 64-28	WMA					22	
		PG 64-22	WMA					24	

The sections were built in 2009 and surveys were conducted regularly. As summarized in Table 2.13, the Section 0 and 1 showed 100% reflective cracking and Section 2 and 3 only 57% cracking after three years of trafficking. The Overlay Tester results showed that the mix from Section 2 had the best cracking resistance with 200 OT cycles performed. Zhou et al., (2011)

concluded that the high RAP mixtures could perform well given that an appropriate mix design method such as BMD is used.

Another experimental project was constructed on FM1017, near Pharr, TX, on April 6th, 2010. This time, it was a new construction with a 1.5 in. surface asphalt layer. Three RAP mixes were used as shown in Table 2.13. Two of these mixtures, 0% RAP PG76-22 and 20% RAP PG64-22 were designed by contractors following Tex-204-F method and the third one was designed by TTI using 35% RAP and the BMD method. One year later, the sections were surveyed, and no distresses were observed. However, no conclusion could be drawn at the time since the period of performance was too short. Moreover, the traffic on this highway is very light, the climate is mild with no cold weather and there was almost no rainfall in that timeframe. No further research was documented regarding this case study.

In 2010, a new field test section constructed on SH 146 in the Houston area was evaluated by Zhou et al. (2013). A dense-graded TxDOT Type C mixture with 15% RAP/5% RAS and PG 64-22 was used in the top 2-inch surface layer. Laboratory testing of the mixture indicated good resistance to rutting but a poor cracking resistance. However, after three years of service, the test section was in an excellent condition: no rutting and cracking, as shown in Figure 2.20. It was concluded that on average, RAP sections tend to exhibit more cracking, but the differences are generally not significant.

In 2013, Texas Department of Transportation in collaboration with Texas A&M Transportation Institute investigated ways to mitigate cracking in RAS mixes. Based on previous experience and literature, there are four approaches that can be considered: reducing the RAS use, rejuvenating RAS binder in the mix design process, using softer virgin binders and increasing the design density.



Figure 2.20 Excellent condition of RAP/ RAS test sections on SH146, Houston (Zhou et al. (2013).

This study focused on validating two of these approaches: the use of softer binder and increasing design density. For this purpose, two 3-inch asphalt overlay sections were built on US87, Amarillo, Texas. The RAS mixes used are the same in terms of aggregates, gradation, virgin binder and RAS, except the OAC; the OAC for control section was 4.6% corresponding to 96.5% design density and the other one being 5% corresponding to 97.3% design density, Zhou et al. (2013). Three surveys were performed after 6, 14 and 18 months. The sections showed no rutting but reflecting cracking was observed on both test sections. As expected, increasing the design density improved the resistance to cracking, as shown in Figure 2.21 and Figure 2.22.



Figure 2.21 Reflective cracking of RAS test sections on US87, Amarillo (Zhou et al. (2013).

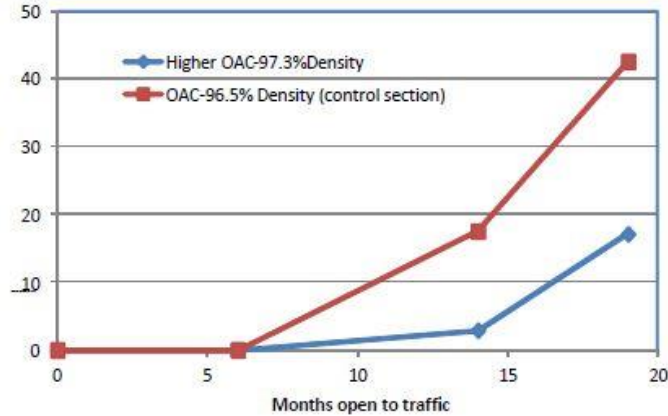


Figure 2.22 Reflective cracking of RAS test sections on US87, Amarillo (Zhou et al. (2013).

Romanoschi et al. (2014) conducted accelerated testing of mixes containing RAP and RAS and control mixes to validate the cracking and rutting potential. The entire experiment consisted of twelve sections built using typical Texas mixes, as shown in Table 2.14. To investigate the mix that performs best in North-East Texas, BMD mixes and RAP/RAS mixes were compared to the control mix. As seen in Table 2.14, this APT research project was divided in three parts: reflection cracking, rutting and fatigue cracking experiment.

Table 2.14. Experimental Pavement Structures (Romanoschi, 2014)

Reflection Cracking Experiment			
Test Section	Surface 2in.	Intermediate 2in.	Base 8in.
A	Type D	Type C	Cement (3.5%) Treated base
B	High RAP		
C	RAP&RAS		
D	BMD		
Rutting Experiment			
Test Section	Surface 2in.	Intermediate 6in.	Base 7in.
H	Type D	Type B	Cement (3.5%) Treated base
I	High RAP		
J	RAP&RAS		
K	BMD		
Fatigue Cracking Experiment			
Test Section	Surface 3in.	Base 8in.	Subbase 8in.
L	Type D	Bridgeport Rock	Cement (2%) Treated Subbase
E	High RAP		
F	RAP&RAS		
G	BMD		

Fatigue cracking and rutting sections were loaded bi-directionally while the reflection cracking sections were loaded uni-directionally for the reflection cracking sections using an 18,000 lbs. single axle load. The lateral wander was also considered; the lateral position of the Pavement Testing Machine was controlled during testing such that it followed a normal distribution with a standard deviation of 8 inches. The testing temperature for the fatigue cracking and reflection cracking sections was $\pm 68^{\circ}\text{F}$ and $\pm 104^{\circ}\text{F}$ for the rutting sections. Approximately 3 million passes of an 18,000 single axle load were applied to the experimental pavement sections. Also, the pavement response was recorded using the strain gauges installed at the bottom of the asphalt concrete layer. The data collected in field was used to verify two pavement design software (TxME and TxACOL). A program to predict the performance of asphalt mixes with RAP and RAS was developed by TTI, Tx-Recycol. Both pavement design software had reasonable prediction for the performance of the APT sections and Tx-Recycol gives the ability to evaluate the impact of RAP/RAS on pavement performance.

Also, the experiment showed that rutting does not represent a problem for Texas mixes, regardless of the RAP/RAS content. The virgin mixes showed a better resistance to cracking, but the mixes with recycled materials showed a fairly good resistance to cracking as well.

Zhou et al., (2017) investigated the most reliable cracking tests that can be used for routine mix designs to eliminate brittle mixes. The tests evaluated were the Overlay Tester, Disk-shaped Compact Tension test, Semi-Circular Bend test from the Louisiana Transportation Research Center (SCB-LTRC), and SCB test at room temperature from Illinois (SCB-IL). To validate these tests, the APT results provided by Romanoschi et al., (2014) and the measured performance from an older project located on US62 were utilized. It was concluded that the OT, DCT and SCB-IL matched the performance measured on US62 and the OT and SCB-LTRC were valid for six of the

APT section. A sensitivity analysis indicated that both the DCT and SCB-IL are not sensitive to asphalt binder content, and both showed an increase in cracking resistance with the inclusion of RAS.

Based on the information found in the literature the following can be concluded:

- RAP/RAS mixes have a good resistance to rutting
- Cracking performance is dependent upon many factors: traffic, climate, existing pavement conditions for overlays, pavement structure and thickness.
- Rejuvenating RAP/RAS binder, increasing the design density, using softer virgin binder and/or reducing RAP/RAS usage are approaches considered to improve cracking resistance.
- RAP/RAS mixes have the potential to perform equally or better than virgin mixes given that they are designed following a balanced mix design approach, as opposed to a purely volumetric approach.

2.6. Summary and Remarks

The beginning of the asphalt recycling era began during the Arab Oil Embargo of the 1970s, but because of the environmental and economic benefits, agencies encouraged its continued use. High RAP content mixes in the 1970s were attempted but due to the limited capacities of the asphalt plants, high RAP variability and limited knowledge about how to recycle asphalt material, the use of RAP was limited at lower percentages. The use of RAS as a component in HMA was introduced in the 1980s and continues to be researched to date. After the introduction of Superpave, specifications and standards were developed to aid and promote the use of recycled materials. However, due to factors such as traffic, climate, existing pavement conditions for overlays, pavement structure, thickness, types of rejuvenators and percentage of recycled material

used, the RAP/RAS mixes showed mixes results in terms of performance. To date, researchers across the world are continuously investigating ways to incorporate higher recycled material contents in new asphalt mixes without affecting its performance.

One of the primary issues of adding recycled materials to HMA is the rheological behavior change of the final binder blend. Because of the oxidative aging that recycled materials undergo over time, the mixes exhibit higher resistance to rutting but decreased resistance to low temperature and fatigue cracking.

Another problematic aspect in enhancing the performance of RAP/RAS mixes was that at the beginning, the design was solely based on the volumetric method to determining the composition of mixes. The amount of blending between RAP or RAS binders and virgin binders is still a concern. Some states require using a softer grade of virgin asphalt to account for the brittle binder from recycled materials but there is no guarantee that it is necessary or that a softer binder will have the desired results. To date, the use of BMD approach seems to be the best option to design asphalt mixtures. The performance evaluation on durability and stability plays an essential role in the design of RAP/RAS.

Along time, many researchers have studied the rheology of binder, the mechanical properties and the laboratory and field performance of recycled mixtures. The main takeaways are:

- The inclusion of RAP/RAS increases the resistance to rutting
- Generally, the cracking resistance decreases with the increase of RAP and RAS content, although some cases showed the contrary.
- Rejuvenating RAP/RAS binder, increasing the design density, using softer virgin binder and/or reducing RAP/RAS usage are approaches considered to improve cracking resistance.

- The use of RAP and RAS has none or minimal effect on the moisture sensitivity of mixtures.
- The performance of RAP/RAS mixtures is highly dependent on the aging phenomenon.
- RAP/RAS mixes have the potential to perform equally or better than virgin mixes given that they are designed following a balanced mix design approach, as opposed to a purely volumetric approach.
- Multiple performance evaluation tests are needed; a single approach may not be suitable for all the cases and locations.
- Accelerated testing is an efficient and realistic method to correlate laboratory performance to the field performance in a short period of time

More research is needed to correlate the laboratory testing to the field performance and to develop practices and standards based on the local conditions.

CHAPTER 3. PERFORMANCE OF FIELD SECTIONS AT APT FACILITY

3.1 Research tools

APT Facility and PTM

This research was conducted at the Accelerated Pavement Testing Facility (APTF) built by the University of Texas at Arlington in 2012, shown in Figure 3.1. The site is located near State Highway SH-820, approximately one mile north of Interstate Highway I-30, on the east side of Fort Worth, Texas. The testing site is conveniently located less than a mile away from an asphalt plant.



Figure 3.1 Layout of the APTF – University of Texas at Arlington

The loading device, named the Pavement Testing Machine (PTM), is a linear APT testing device. The PTM is 68 ft. x 10 ft. x 11ft. and it has a bogie with a dual wheel single axle that can move forwards and backwards. Figure 3.2 shows the PTM while is positioned on top of test sections.



Figure 3.2 Pavement Testing Machine

According to Romanoschi et al., (2020), the main components of the PTM (Figure 3.3) are:

- *A steel frame.* The frame is composed of two 45 ft. long beams bolted to four pillars. The beams are stabilized with transverse and diagonal bars at the top. A railroad rail is fixed underneath the bottom flange of each beam.
- *A moving bogie.* The bogie has the capability to move at a speed up to 5mph. Four rail wheels mounted at the top of the bogie push up into the rails mounted underneath the flanges of the main beams when load is applied to the test section. Four additional steel wheels travel on top of the inner part of the bottom flanges of the beams to support the bogie when the loading axle is lifted. A reinforced single axle of a truck with four bus tires is mounted at the bottom of the bogie.
- *A hydraulic pump.* The pump installed on the top of the bogie provides power to two hydraulic pistons that lift or push down the axle. When testing in bi-directional mode, the pistons push down continuously and when testing in uni-directional mode the pistons lift

the axle. The maximum axle load that can be applied is 36,000 lbf, which is twice the legal load limit for singles axles in most states across the USA. The load applied by each wheel is periodically calibrated using static scales.

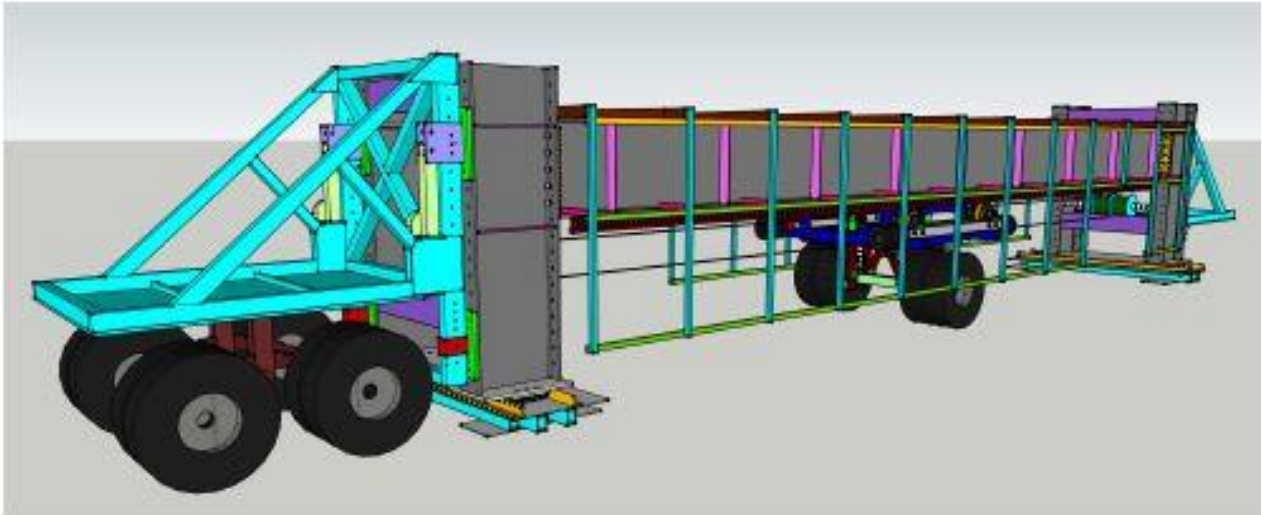


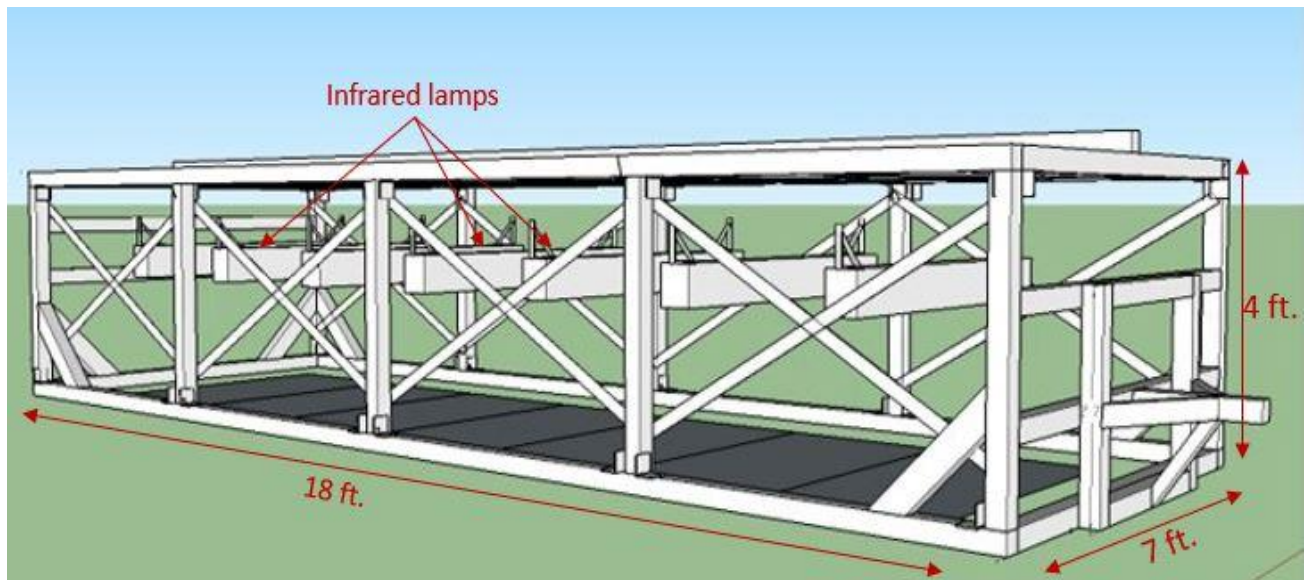
Figure 3.3 Schematic configuration of the PTM, Romanoschi et al., (2020)

- *An electrical motor.* It is mounted between the two front columns, and it pulls the bogie back and forth using a cable. A belt, sprockets, and drum system transmit the power from the motor to the cable.
- *Two transverse support footings.* They are mounted underneath the two front and the two rear columns. Each footing is fixed to the ground and attached with a screw jack system to the columns. The two screw jacks move in synchronized fashion the entire PTM sideways to provide the lateral wheel wander. The maximum lateral position the PTM can move on either side of the central position is 20 inches.
- *A fixed front platform.* A king pin mounted underneath aids in towing the PTM, if needed.
- *A rear platform.* It can move vertically relative to the frame, and it has a tandem truck axle mounted at its bottom.

- *A temperature control chamber.* It encases the main part of the PTM, and it is equipped with heating and cooling units and fans. A thermostat connected to temperature sensors glued to the surface of the pavement controls the inside air temperature between 32°F and 122°F.
- *Electrical and electronic equipment.* The equipment controls the main motor, the screw jack, and the pressure in the hydraulic system. The software controls all the components on the PTM, the position of the bogie, the lateral position of the machine and so on. The heating and cooling system are controlled separately. The electric power used is 460V.

Ageing Chambers

To account for the binder aging resulted from the environmental factors and age, artificial aging of all pavement sections was induced before applying accelerated loading. For this purpose, two artificial ageing chambers were built. Each chamber is 18 ft. long, 7ft. wide and 4 ft. tall. Figure 3.4 shows the schematic configuration of the chamber.



3.4 Schematic configuration of the oxidation chamber

Each chamber consists of:

- *An aluminum frame* made of four 18 ft. long 3x3 inches square tubing and four 6.5 ft. long 3x3 inches square tubing. The frame is stabilized with ten 4 ft. tall vertical aluminum square tubing and diagonal bars. The walls were insulated with 3 inches high-heat resistant insulation and then covered in aluminum sheets.



Figure 3.5 Construction of the oxidation chambers

- *Seven infrared lamps* were mounted on the interior ceiling at equally spaced intervals. The distance between two lamps is approximately 30 inches and it was calculated such that the areas of the pavement heated by any two adjacent lamps touch but do not overlap.
- *Electrical boxes* mounted on the outside are equipped with data loggers wired to temperature sensors glued on the surface of the pavement under each infrared lamp for recording the temperature, as shown in Figure 3.6.



3.6 Electrical box equipped with data logger

3.2 Construction of Pavement Sections and Instrumentation

In this research, eight test pavement sections were built and positioned, as shown in Figure 3.7. All pavement sections have the same foundation layers but different mixes in the surface layer; the mixes have different binder grades and rejuvenators. Each of the eight test sections consisted of:

- 3.0-inch asphalt concrete surface layer. Seven different mixes were paved on the eight sections.
- 10.0-inch Flex Base (Type A Grades 1 & 2). The same granular material was placed on all sections.
- 12.0-inch Subgrade soil. An imported soil was placed in lieu of the top 12 inches of existing subgrade soil for the sake of uniformity of the subgrade support.

Table 3.1 shows the mix designs of the pavement structures. Mix M was placed on section M and Q and serves as a reference mix. This mix is the most commonly used asphalt mixture on Farm-to- Market Roads (FM) in North Texas. It contains a PG64-22 bitumen and the recommended percentages of RAP and RAS according to TxDOT Specifications, 15% respectively 2%.

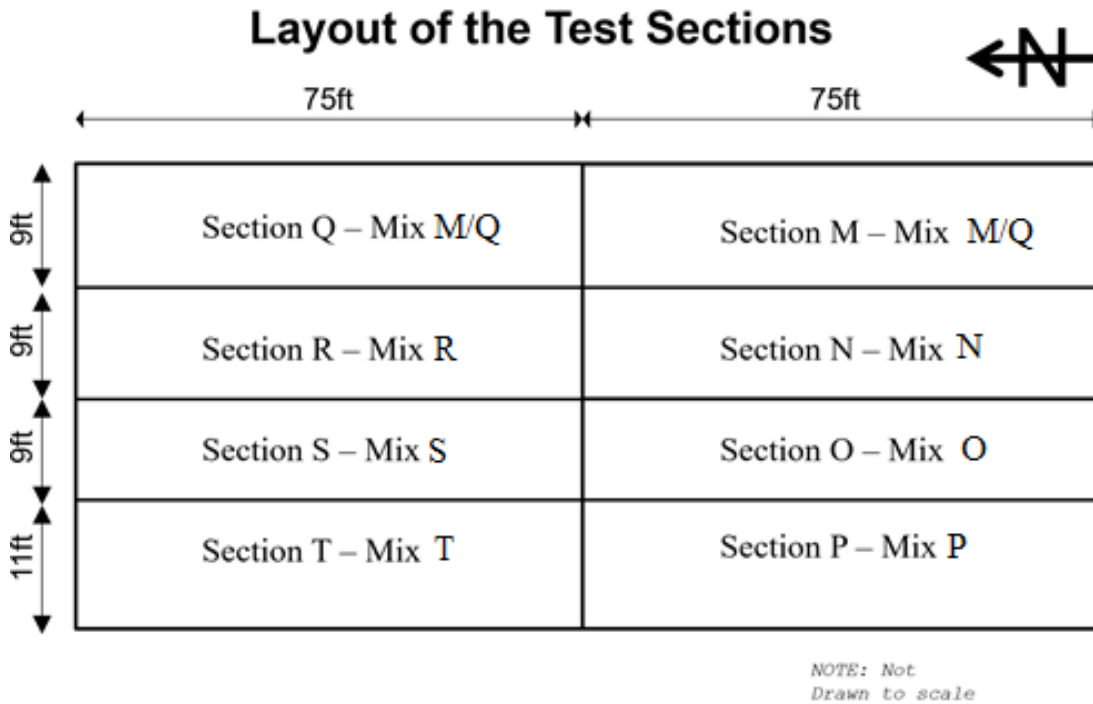


Figure 3.7 Layout of the experimental APT sections

Mixes S, T and R contain the same bitumen grade as Mix M/Q but different percentages of recycled materials and rejuvenators; these mixes were designed using the BMD concept. Mix P contains 15% RAP, follows the BMD approach, and has a PG 64-28 binder. Mixes O and N use a more brittle bitumen, PG 70-22, with only 15% RAP for Mix O and no RAP or RAS for Mix N. All mixes have the same source of aggregate, Mill Creek-Oklahoma, and contains 25% of Type C and 28.5-38% Type D coarse aggregates and 21.4-36% Manufactured Sand. The asphalt content varies between 4.8 and 5.3%. All seven mix designs were approved by TxDOT before being sent to the asphalt paving company for production. The detailed mix designs are attached in Appendix A-1.

Table 3.1 HMA Mix Designs of the Pavement Structures

Mix	% Rock (Mill Creek, OK)			Mineral filler	RAP %	RAS %	TD %	AC %	PG
	Type C	Type D	Man Sand						
M/Q	25.0	30.3	28.0	N/A	15.0	2.0	96.0	4.8	PG64-22 (Hunt)
O	25.0	30.0	30.0	N/A	15.0	0.0	96.0	4.8	PG70-22 (Ergon)
N	25.0	38.0	36.0	1	0.0	0.0	96.0	4.8	PG70-22 (Ergon)
P	25.0	30.0	30.0	N/A	15.0	0.0	96.0	4.8	PG64-28 (Jebro)
S	25.0	33.3	25.0	N/A	15.0	2.0	97.0	5.3	PG64-22 (Hunt)
T	25.0	30.3	28.0	N/A	15.0	2.0	96.5	5.0	PG64-22 (Hunt) 2% Cargill rejuvenator
R	25.0	28.5	21.4	N/A	25.0	0.0	97.6	5.3	PG64-22 (Hunt)

3.2.1 Construction of the top subgrade soil

To minimize the effect that the existing subgrade soil could have on the pavement sections, twelve inches of the existing soil was excavated and removed. New soil was brought and compacted in two 6-inch lifts. The new soil was a Type A material (Item 132) with low plasticity (LL=44, PL = 14, PI = 30). The moisture-density curve for the imported soil is given in Figure 3.8, while the complete test results are given in Appendix A-2. The Maximum Dry Density (MDD) was found to be 110 pcf for the Optimum Moisture Content (OMC) of 14.6%.

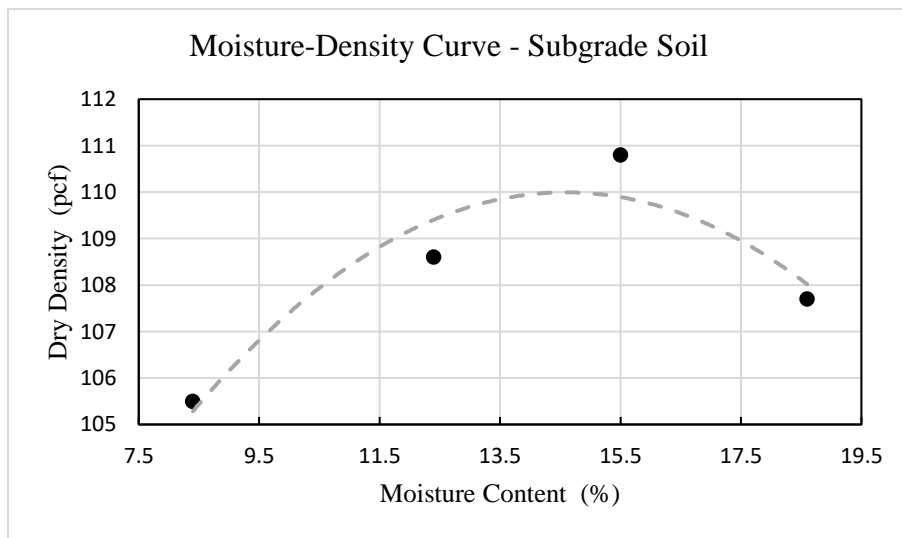


Figure 3.8 Moisture-density curve for the subgrade soil

Figure 3.9 shows the placement of the imported soil for the first 6-inch lift and Figure 3.10 shows the compaction of the imported soil. The top subgrade soil placement and compaction was finalized on November 19th, 2020.



Figure 3.9 Placement of new subgrade soil



Figure 3.10 Compaction of new subgrade soil

To verify that the compaction parameters were achieved, six nuclear density tests were conducted on each of the two 6-inch lifts of the compacted imported soil. The exact location of the nuclear density gauge is shown in Figure 3.11, while the measured density and moisture content results are showed in Table 3.2. As observed, more than 98 percent of Proctor density was recorded for all six locations.

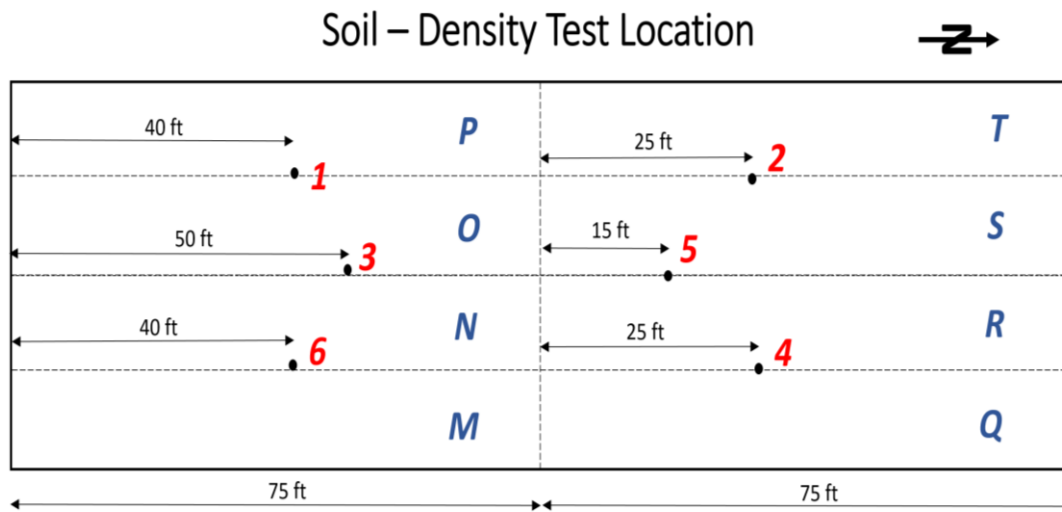


Figure 3.11 Location of the nuclear density measurements

Table 3.2 Moisture-density curve for the subgrade soil

Construction Lift	Point	Wet Density (pcf)	Moisture Content (%)	Dry Density (pcf)	Moisture Deviation (%)	Percent Proctor Density
Bottom	1	129.0	13.6	113.6	-1.0	103.3
	2	129.2	14.3	113.0	-0.3	102.7
	3	130.9	15.0	113.8	+0.4	103.5
	4	131.3	15.6	113.6	+1.0	103.3
	5	128.1	16.0	110.4	+1.4	100.4
	6	127.7	14.6	111.4	+0.0	101.3
Top	1	128.1	18.4	108.2	+3.8	98.4
	2	132.5	12.9	117.4	-1.7	106.7
	3	129.4	18.0	109.7	+3.4	99.7
	4	133.7	14.0	117.3	-0.6	106.6
	5	125.3	15.4	108.6	+0.8	98.7
	6	128.2	17.3	109.3	+2.7	99.4

3.2.2 Construction of the base layer

A 10-inch-thick Flex Base layer was placed and compacted on top of the imported soil embankment in two 5-inch lifts. The Flex Base consists of Type A Grades 1 & 2 Flex Base material (Item 247) brought from Martin Marietta – Chico Plant. The moisture-density curve for the flex base material is represented in Figure 3.12 while the details of the testing results can be found in Appendix A-3. The Maximum Dry Density (MDD) was found to be 141.8 pcf for the Optimum Moisture Content (OMC) of 6.3%.

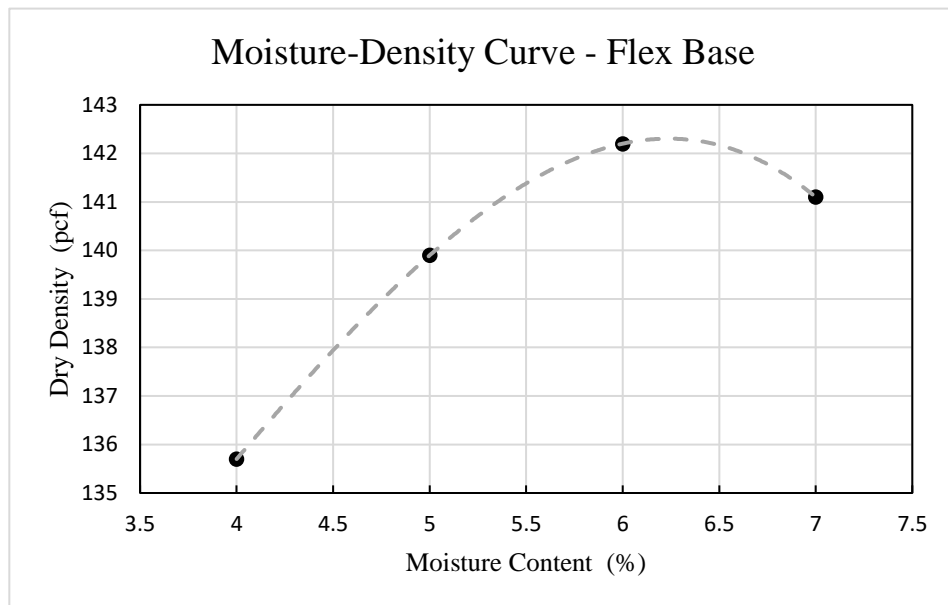


Figure 3.12 Moisture-density curve for the flex base material

Figure 3.13 and 3.14 shows photographs taken during the placement and the compaction of the flex base. The construction of the flex base layer was completed on November 20th, 2019.

To verify that the compaction parameters are achieved, nuclear density tests were conducted on each of the two 5-inch lifts of the compacted imported soil. The exact location of the nuclear density gauge is shown in Figure 3.15. The measured density and moisture content results are showed in Table 3.3. As observed, more than 100 percent of Proctor density was recorded for all six locations.



Figure 3.13 Placement of flex base



Figure 3.14 Compaction of flex base -top lift

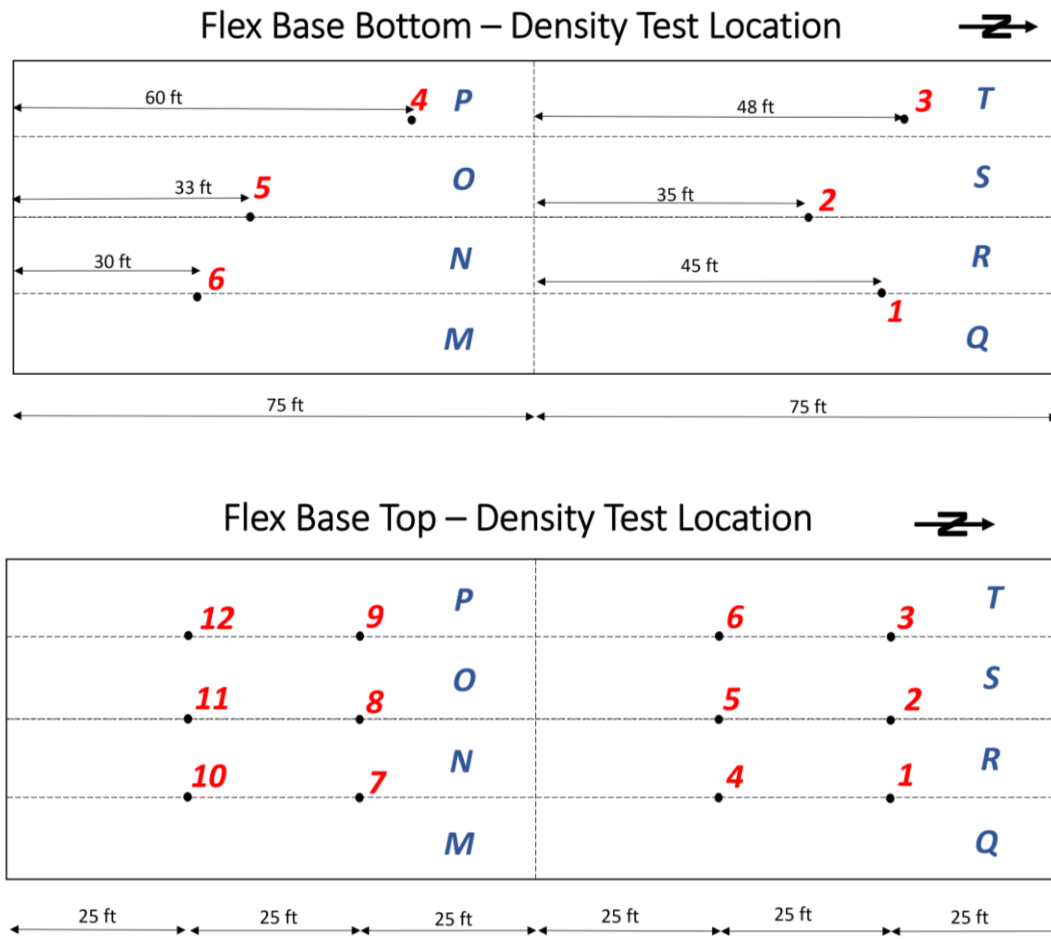


Figure 3.15 Location of the nuclear density measurements

Two days after the flex base construction was finalized, an AEP 50/50 asphalt emulsion prime coat was sprayed at a rate of 0.2 gal/sq.yd. The same emulsion and in the same quantity was sprayed again one day before the asphalt mixes were placed in September 2020. Asphalt emulsion priming consists of an application of low viscosity asphalt emulsion to an absorbent surface, in preparation for an asphalt surface course. This emulsion was used to bind the granular material together, to partially waterproof the base layer, to provide protection from environmental factors and to provide a bond in between the base and the next course. Figure 3.16 shows the Prime coat operations. Figure 3.17 shows the base layer with the applied Prime coat.

Table 3.3 In-situ and moisture-density data for the flex base

Construction Lift	Point	Wet Density (pcf)	Moisture Content (%)	Dry Density (pcf)	Moisture Deviation (%)	Percent Proctor Density
Bottom	1	152.0	6.6	142.6	+0.3	100.6
	2	154.5	5.8	146	-0.5	103.0
	3	152.7	7.3	142.3	+1.0	100.4
	4	152.4	7.3	142.0	+1.0	100.1
	5	158.2	6.4	148.7	+0.1	104.9
	6	155.9	7.2	145.4	+0.9	102.5
Top	1	148.5	4.7	141.8	-1.6	100.0
	2	151.5	5.8	143.2	-0.5	101.0
	3	152.0	5.1	144.6	-1.2	102.0
	4	149.5	5.0	142.4	-1.3	100.4
	5	150.9	5.8	142.6	-0.5	100.6
	6	153.4	5.6	145.3	-0.7	102.5
	7	148.7	4.6	142.2	-1.7	100.3
	8	150.9	5.3	143.3	-1.0	101.1
	9	150.2	5.1	142.9	-1.2	100.8
	10	148.1	4.2	142.1	-2.1	100.2
	11	152.4	4.8	145.4	-1.5	102.5
	12	152.7	5.3	145.0	-1.0	102.3



Figure 3.16 Spraying of Prime Coat on top of the flex base



Figure 3.17 Constructed base layer with Prime coat

3.2.3 Strain gauge instrumentation

To measure the dynamic strain responses at the bottom of the asphalt layer under moving traffic loads, four sections out of eight were instrumented with strain gauges. The instrumented sections were M, N, O and P. Figure 3.18 shows the strain gauge used in this project.



Figure 3.18 Strain gauge, model PMFLS-60-50-2LTSC, Tokyo Sokki

Model PMFLS-60-50-2LTSC were chosen because they are resistant to high temperatures, they are waterproof and able to withstand high loads, such as the compaction loads associated with pavement construction. Four strain gauges were incorporated in each pavement section during asphalt construction; two are aligned longitudinally and two in the transverse position. The gauge characteristics are given in Table 3.4.

Table 3.4 Tokyo Sokki PMFLS-60-50-2LTSC specifications

Parameter	Specification
Gauge length (mm)	60
Resistance (Ω)	120
Operational temperature ($^{\circ}\text{C}$)	-20 to +60
Maximum temperature ($^{\circ}\text{C}$)	+200
Leadwire	Φ 6mm 4-core sheathed chloroprene cable
Leadwire resistance per meter	0.11

As shown in Figure 3.18, two aluminum bars were glued at the ends of each gauge beforehand to improve the anchoring in the asphalt mix. For this purpose, JB Weld Extreme Heat metallic paste was used. Because the gauge measures the average strain between the anchors, the length of the sensor should be at least three times than the maximum aggregate size of the asphalt mix.

Two pairs of strain gauges, one in longitudinal and one in transverse direction were placed in the wheel path of each section. Figure 3.19 shows the configuration of the instrumentation used.

The installation consists of the following steps:

1. The strain gauges were checked for functionality prior to installation.
2. The location and gauge orientation were marked on the base with paint.
3. A patch of hot asphalt mix was placed in the desired location, Figure 3.20.
4. The gauges were pushed immediately in the correct location and the cables were secured with nails on each side, Figure 3.21.

- The strain gauges were covered with the respective HMA mixture right in front of the paver to safeguard the gauges from being damaged, Figure 3.22.
- After the paving operation was finalized, the electrical resistance of each gauge was measured to verify their functionality.

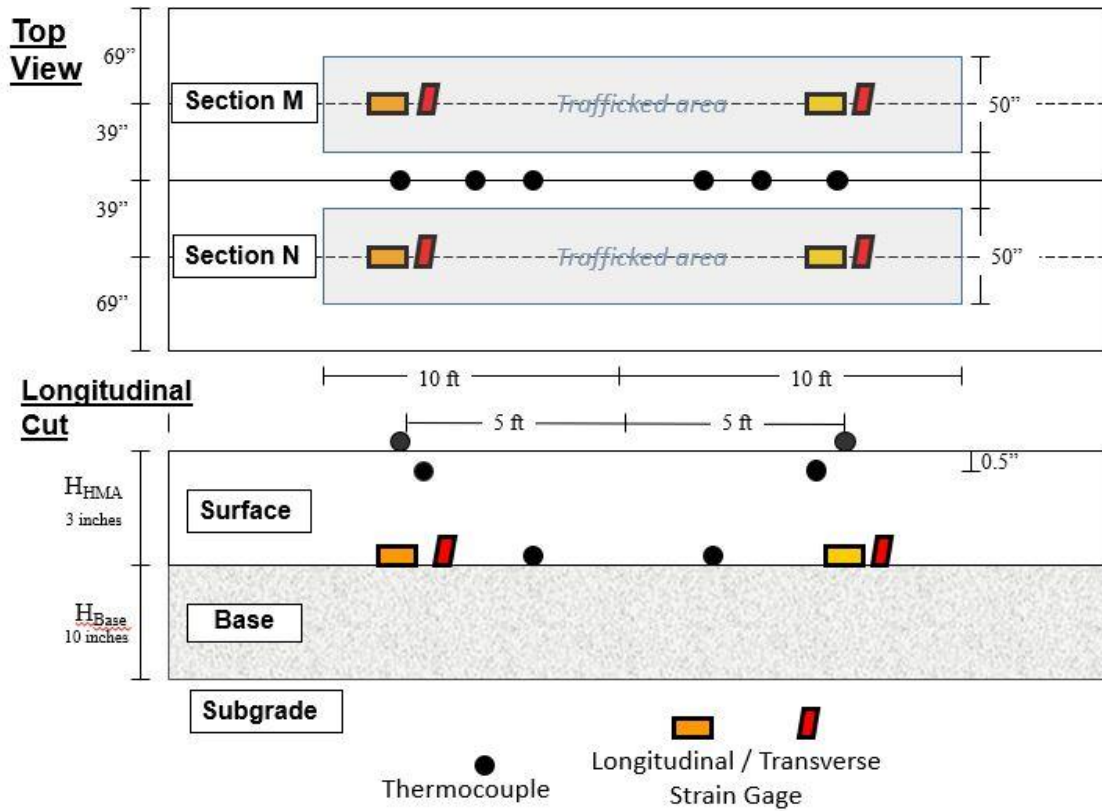


Figure 3.19 Schematic layout of the in-pavement instrumentation



Figure 3.20 Strain gauges on Sections M



Figure 3.21 Longitudinal and Transverse Strain Gauges on Sections O and P



Figure 3.22 Instrumented sections M and N-ready to be paved

Type K thermocouples (Figure 3.23) were placed in holes filled with oil and drilled at three depths: 0.0, 0.5 and 1.5 inches. This was done when the accelerated loading started in each respective section.

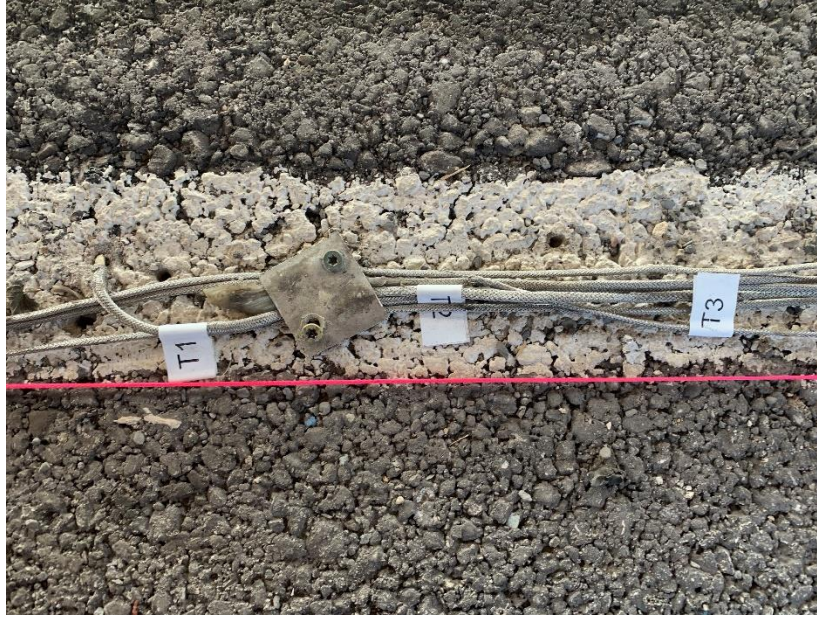


Figure 3.23 Thermocouples inside the PTM placed at surface pavement, 0.5 in and 3 in depth

3.2.4 Construction of the HMA layers

Sections P, T, M and Q were consecutively paved on September 3rd, 2020. Sections N, O, R and S were paved the following day, on September 4th, 2020. The lowest temperature recorded during the paving days was 71 °F and the highest temperature recorded was 85 °F. There was no rain, making those days the ideal time for paving the sections.

Two days before the paving started, a prime coat was sprayed, and the strain gauges were installed on top of the flex base. The sequence of paving included a dump truck full of HMA feeding the HMA into the Material Transfer Vehicle (MTV). Then the MTV continuously fed the paver which operated continuously without stopping (Figure 3.24). Immediately after paving, a steel roller compactor passed to compact the layers to the desired density (Figure 3.25). The rolling/compaction pattern included three vibration passes, followed by 1 pass of a low vibration (back drum only) and finalized with two static passes. The pictures showing the paving process of all sections are in Appendix A-4.



Figure 3.24 Sequence of Asphalt Mix Paving



Figure 3.25 Steel Roller Compacting the Pavement HMA Sections

During the paving, an Infra-red camera was used to capture the temperature of the HMA as it was being laid. Figure 3.26 shows the temperature as being recorded by the Infra-red camera, whereas Figure 3.27 shows a sample of the temperature map recorded in section P. The summary of the recorded temperatures is shown in Table 3.5.



Figure 3.26 The Infra-Red Camera Recording Pavement Construction Temperature

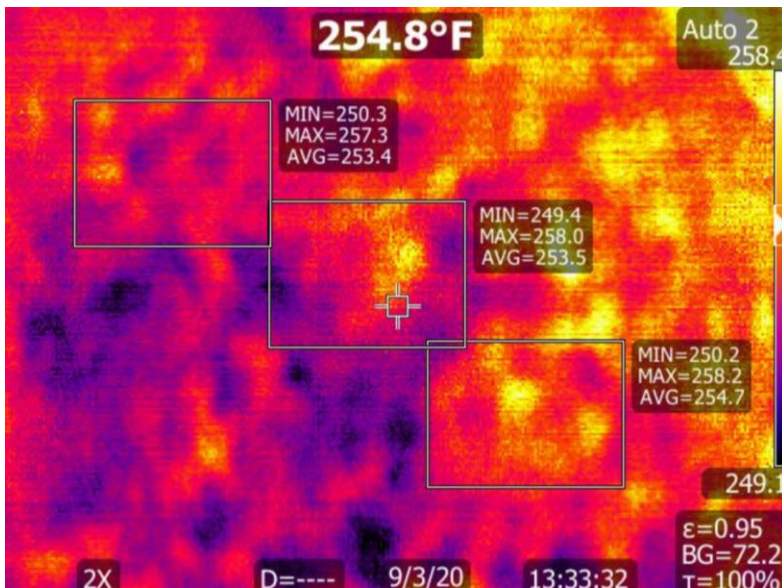


Figure 3.27 A Sample of Infra-Red Temperature Map captured during Section P Paving

Table 3.5 Paving temperatures recorded behind the paver

Section	P	T	M and Q	N	O	R	S						
Sequence of Paving	—————→												
Mixture	4	6	1	3	2	8	5						
IR Temp 1 (°F)	254.80	280.20	295.50	279.90	263.70	291.10	283.00						
IR Temp 2 (°F)	255.90	283.30	291.10	286.10	269.40	294.20	289.80						
IR Temp 3 (°F)	264.80	279.90	290.10	281.90	268.20	286.80	288.10						
IR Temp 4 (°F)	253.60	276.00	286.30	280.40	275.00	286.20	287.90						
IR Temp 5 (°F)	251.30	279.70	282.10	267.30	256.60	287.20	287.40						
IR Temp 6 (°F)		277.30	282.50	280.40									
IR Temp 7 (°F)		258.30	279.60	276.80									
IR Temp 8 (°F)		264.60	286.00	275.40									
IR Temp 9 (°F)		263.00	274.50	272.20									
IR Temp 10 (°F)		259.80	274.30										
IR Temp 11 (°F)			277.20										
IR Temp 12 (°F)			278.10										
IR Temp 13 (°F)			287.90										
IR Temp 14 (°F)			285.70										
IR Average Temp (°F)			256.08					272.21	283.64	277.82	266.58	289.10	287.24
IR-Temp (°F) Standard Dev			5.16					2.59	5.07	7.04	6.88	3.44	2.54
IR-Temp (°F) C. V			2.02	0.95				1.79	2.54	2.58	1.19	0.88	
Minimum compaction temp.		250	250	250				275	275	250	250		

The paving average temperatures varied from one section to another from 256 °F to 287 °F. The coefficient of variation was very small (C.V <3%). The maximum and minimum temperature maps for each section are in Appendix A-5.

To determine the percentage of density achieved on site, field densities were determined using a Nuclear Density Gauge (Figure 3.28). Besides that, three cores per section were extracted and subjected to laboratory density test. Table 3.6 shows the laboratory and field densities. The density data indicates that the coefficient of variation within each section was very small (CV<3.0), which implies that the compaction was relatively uniform. Also, the ANOVA analysis indicated no significant difference between lab and field density was observed at 95% confidence interval, with a p-value of 0.0321. The table also indicates that the densities of a few sections were close to the typical initial compaction field densities which are 93%±1%.



Figure 3.28 Measuring Field Density Using the Nuclear Density Gauge

Table 3.6 Compaction densities (pcf)

Section		M	N	O	P	Q	R	S	T
Maximum Theoretical (Rice) Density (pcf)		161.99	163.21	162.55	162.92	161.99	161.49	162.5	161.3
Gauge Reading (pcf)	1	148.4	154.7	163.8	151.4	152	152.7	153.6	153.2
	2	148.6	145.2	158.5	158.1	152.3	155.9	152	153
	3	149.4	154.4	154.6	158.2	146.9	156	156.4	151
	Average	148.8	151.4	159	155.9	150.4	154.9	154	152.4
	CV (%)	0.3	2.9	2.4	2.0	1.6	1.0	1.2	0.7
Gauge Density (% of Gmm)	1	91.6	94.6	100.8	92.9	93.8	94.6	94.5	95
	2	91.7	88.7	97.5	97	94	96.5	93.5	94.9
	3	92.2	94.4	95.1	97.1	90.7	96.6	96.3	93.6
	Average	91.9	92.6	96.3	95.7	92.8	95.9	94.8	94.5
	CV (%)	0.3	2.9	1.2	2.0	1.6	1.0	1.2	0.7
Core Lab Density (% of Gmm)	1	91.7	92.7	95.4	94.2		96.2	94.3	94.4
	2	93.4	92.5	94.3	93.5		97.3	95.2	94.8
	3	91.9	91.8	93.2	93.3		96.1	93.1	95.3
	Average	92.3	92.3	94.3	93.7		96.5	94.2	94.8
	CV (%)	0.8	0.5	1.0	0.4		0.6	0.9	0.4

In addition to the temperature and field densities recorded in the field, laboratory quality control tests on extracted field cores were performed by the Texas Transportation Institute (TTI). The TTI team extracted the cores from the pavement test sections (Figure 3.29).



Figure 3.29 TTI extracting cores from Section S

TTI evaluated the performance data in terms of cracking and rutting potential. The IDEAL-CT and IDEAL-RT were performed, and the results are showed in Table 3.7. The current criteria for interpreting these tests are for all mixes the CT Index should be greater than 90, and the RT Index greater than 60, 65 and 75 for the PG 64, PG 70, and PG 76 binders respectively. For cracking, the best cracking resistance was recorded on mixes N and T, where N is the mix with no RAP or RAS and uses the stiffer PG 70 binder, whereas T has 15% RAP and 2% RAS with 2%

Cargill rejuvenator with a PG 64 binder. The worse cracking resistance was observed for mix S which is identical to the mixture placed on Section T but without the rejuvenator.

Table 3.7 QC test results performed on field cores

Section	Construction QC Data				
	Rice Specific Gravity	QC Density (%)	Total AC (%)	CT Index	RT Index
M and Q	2.596	96.1	5.2	80.2	66.3
O	2.605	96.6	4.8	112.8	88.9
N	2.622	95.7	5.6	143.5	124.3
P	2.611	96.6	5.4	127.2	107.6
R	2.588	97.5	5.0	99.9	80.6
S	2.604	96.9	5.0	45.4	36.6
T	2.585	97.1	5.2	138.9	114.8

To check uniformity and thickness, TTI collected two types of Ground Penetrating Radar (GPR) on September 11th, 2020, Figure 3.30. A typical data display from the Pavecheck system is shown in Figure 3.31. During GPR testing one trace was captured for every 1 foot of travel. The color display in the top of Figure 3.31 has the surface as the top line in the display. The red line at a depth of approximately 3.0 inches being the reflection from the top of the base layer. The photograph shown was taken at the location of the vertical solid red line in the color display. The plot at the bottom right of Figure 3.31 is the GPR reflection from the location of the photo. The computation shows that the surface dielectric at this location is 6.5 and the computed layer thickness is 3.3 inches.

The surface dielectric is an indicator of mat density. The blue line at the bottom of the color plot shows the surface dielectric from the entire run. The dips at either end of the plot are where the data was collected off the test pad. In the test pads the surface dielectric is reasonable uniform with a mean value of 6.4 and a standard deviation of 0.23. One output from processing the GPR data is shown in Figure 3.32. All the data collected is included in Appendix A-5.



Figure 3.30 GPR with 1.0 GHz Horn Antenna and GPR with 3 Channel Rolling Density Meter

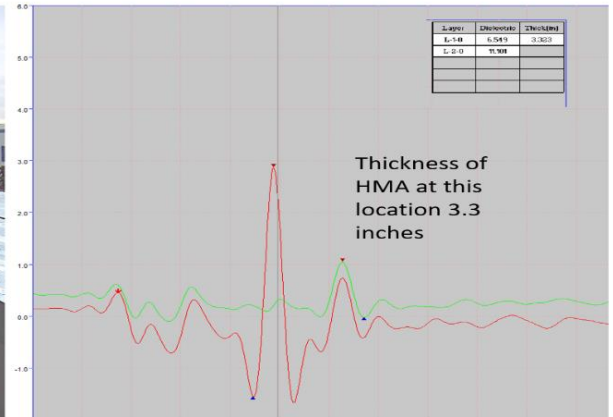
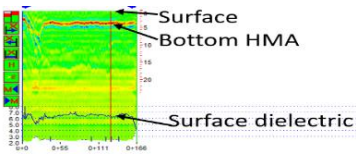


Figure 3.31 GPR data display from the run over sections M and Q

The measured thickness for the asphalt layer in the area where accelerated testing load is applied is shown in Figure 3.33 and 3.34, the 0.0 ft coordinate being the longitudinal center of each test section, and the positive values being to the North of the longitudinal center. The figures indicate that the seven sections had an average thickness of the asphalt concrete layer of about 3.25 inches in the APT loading area. For Section O, the asphalt concrete layer was 2.9 inches in average.

TTI PavCheck Backcalculation Analysis Result (Version 1.0)											247	247	4.89	4.50	6.32	3.40	0.00	0.00	6.46	12.01	0.00

Basic Information:																					
Project folder name:	E:\easystore Aug 2019\APT at UTA 2019\APT Site RADAR										250	250	4.93	4.54	6.40	3.51	0.00	0.00	6.38	11.57	0.00
Project name :	Q-M C.PRJ										251	251	4.95	4.54	6.38	3.43	0.00	0.00	6.33	12.31	0.00
FWD test file name :											252	252	4.95	4.54	6.36	3.37	0.00	0.00	6.39	11.91	0.00
GPR test file name :	q-m c.DAT										253	253	4.93	4.54	6.36	3.44	0.00	0.00	6.30	12.49	0.00
Metal plate file :	mtp.dat										254	254	4.93	4.52	6.36	3.42	0.00	0.00	6.36	12.23	0.00
Image list file :	q-m c.IMG (67 total images)										255	255	4.93	4.52	6.36	3.42	0.00	0.00	6.39	11.54	0.00
GPS file name :	(45 total GPS reading)										256	256	4.95	4.54	6.34	3.32	0.00	0.00	6.41	11.80	0.00
Core image file :											257	257	4.95	4.54	6.28	3.22	0.00	0.00	6.23	12.26	0.00

GPR Test File Information:																					
Metal Plate Peak :	7.24 (volts)										258	258	4.93	4.52	6.26	3.19	0.00	0.00	6.35	12.50	0.00
Total traces :	339										259	259	4.89	4.50	6.22	3.19	0.00	0.00	6.35	12.41	0.00
Velocity factor :	11.8										260	260	4.89	4.49	6.26	3.26	0.00	0.00	6.46	13.45	0.00

GPR CALCULATION SUMMARY REPORT (in ASCII Format):																					

Trace	Feet	Time1	Time2	Time3	Thick1	Thick2	Thick3	E1	E2	E3											
181	181	5.15	4.74	6.63	3.69	0.00	0.00	5.93	9.94	0.00	268	268	4.84	4.45	6.28	3.37	0.00	0.00	6.76	12.04	0.00
182	182	5.13	4.72	6.59	3.70	0.00	0.00	5.75	8.80	0.00	269	269	4.84	4.45	6.30	3.36	0.00	0.00	6.97	12.15	0.00
183	183	5.09	4.70	6.49	3.51	0.00	0.00	5.87	10.66	0.00	270	270	4.86	4.45	6.34	3.47	0.00	0.00	6.72	11.43	0.00
184	184	5.05	4.66	6.47	3.51	0.00	0.00	6.04	11.69	0.00	271	271	4.86	4.45	6.32	3.45	0.00	0.00	6.60	10.61	0.00
185	185	5.05	4.64	6.49	3.57	0.00	0.00	6.03	11.14	0.00	272	272	4.86	4.45	6.32	3.46	0.00	0.00	6.56	10.17	0.00
186	186	5.01	4.60	6.45	3.55	0.00	0.00	6.10	11.56	0.00	273	273	4.86	4.47	6.32	3.47	0.00	0.00	6.53	11.62	0.00
187	187	4.99	4.60	6.43	3.52	0.00	0.00	6.20	12.28	0.00	274	274	4.86	4.45	6.32	3.45	0.00	0.00	6.60	11.52	0.00
188	188	4.95	4.54	6.40	3.47	0.00	0.00	6.35	11.70	0.00	275	275	4.88	4.49	6.34	3.45	0.00	0.00	6.60	10.81	0.00
189	189	4.93	4.52	6.38	3.46	0.00	0.00	6.41	11.57	0.00	276	276	4.88	4.49	6.34	3.49	0.00	0.00	6.47	10.64	0.00
190	190	4.91	4.52	6.38	3.49	0.00	0.00	6.46	14.42	0.00	277	277	4.86	4.47	6.32	3.48	0.00	0.00	6.50	9.59	0.00
191	191	4.95	4.54	6.36	3.44	0.00	0.00	6.13	16.49	0.00	278	278	4.86	4.47	6.30	3.42	0.00	0.00	6.55	9.67	0.00
192	192	4.97	4.56	6.38	3.38	0.00	0.00	6.33	6.33	0.00	279	279	4.86	4.45	6.30	3.40	0.00	0.00	6.64	10.13	0.00
193	193	4.97	4.56	6.40	3.43	0.00	0.00	6.35	11.01	0.00	280	280	4.86	4.47	6.30	3.40	0.00	0.00	6.61	9.77	0.00
194	194	4.93	4.52	6.30	3.27	0.00	0.00	6.41	11.71	0.00	281	281	4.88	4.47	6.36	3.54	0.00	0.00	6.46	10.08	0.00
195	195	4.91	4.50	6.28	3.28	0.00	0.00	6.38	11.85	0.00	282	282	4.89	4.50	6.40	3.56	0.00	0.00	6.53	11.46	0.00
196	196	4.95	4.54	6.32	3.30	0.00	0.00	6.29	12.33	0.00	283	283	4.89	4.49	6.34	3.47	0.00	0.00	6.38	10.34	0.00
197	197	4.97	4.56	6.32	3.27	0.00	0.00	6.21	11.73	0.00	284	284	4.91	4.50	6.34	3.31	0.00	0.00	6.82	12.21	0.00
198	198	5.03	4.62	6.40	3.35	0.00	0.00	6.13	11.54	0.00	285	285	4.91	4.50	6.32	3.35	0.00	0.00	6.46	11.78	0.00
199	199	5.05	4.64	6.42	3.35	0.00	0.00	6.10	11.71	0.00	286	286	4.89	4.49	6.28	3.32	0.00	0.00	6.39	12.85	0.00
200	200	5.05	4.64	6.42	3.38	0.00	0.00	6.01	6.01	0.00	287	287	4.88	4.47	6.28	3.35	0.00	0.00	6.47	12.13	0.00
201	201	5.03	4.64	6.42	3.49	0.00	0.00	5.78	15.82	0.00	288	288	4.88	4.49	6.26	3.28	0.00	0.00	6.55	12.27	0.00
202	202	5.03	4.62	6.42	3.38	0.00	0.00	6.18	13.58	0.00	289	289	4.89	4.49	6.24	3.20	0.00	0.00	6.50	11.37	0.00
203	203	5.01	4.60	6.36	3.27	0.00	0.00	6.21	10.62	0.00	290	290	4.89	4.49	6.28	3.29	0.00	0.00	6.52	11.54	0.00
204	204	5.01	4.60	6.32	3.21	0.00	0.00	6.10	12.68	0.00	291	291	4.89	4.49	6.26	3.26	0.00	0.00	6.47	12.05	0.00
205	205	4.99	4.60	6.24	3.07	0.00	0.00	6.10	10.25	0.00	292	292	4.89	4.50	6.26	3.28	0.00	0.00	6.38	10.94	0.00
206	206	5.01	4.62	6.24	3.03	0.00	0.00	6.07	9.79	0.00	293	293	4.91	4.50	6.20	3.08	0.00	0.00	6.44	11.05	0.00
207	207	5.03	4.64	6.30	3.14	0.00	0.00	6.01	11.89	0.00	294	294	4.89	4.49	6.22	3.23	0.00	0.00	6.18	6.18	0.00
208	208	5.01	4.62	6.28	3.15	0.00	0.00	5.97	10.66	0.00	295	295	4.91	4.50	6.20	3.08	0.00	0.00	6.44	11.05	0.00
209	209	5.01	4.62	6.28	3.11	0.00	0.00	6.11	11.13	0.00	296	296	4.93	4.54	6.24	3.21	0.00	0.00	6.11	10.28	0.00
210	210	5.01	4.60	6.32	3.19	0.00	0.00	6.16	12.12	0.00	297	297	4.93	4.54	6.26	3.22	0.00	0.00	6.26	10.73	0.00
211	211	4.95	4.56	6.34	3.38	0.00	0.00	6.18	12.93	0.00	298	298	4.95	4.54	6.28	3.21	0.00	0.00	6.27	10.81	0.00
212	212	4.91	4.50	6.32	3.36	0.00	0.00	6.44	13.48	0.00	299	299	4.95	4.54	6.30	3.28	0.00	0.00	6.18	10.93	0.00
213	213	4.88	4.47	6.28	3.31	0.00	0.00	6.63	14.40	0.00	300	300	4.95	4.54	6.28	3.20	0.00	0.00	6.33	9.78	0.00
214	214	4.86	4.45	6.24	3.24	0.00	0.00	6.74	15.40	0.00	301	301	4.93	4.54	6.32	3.36	0.00	0.00	6.26	10.86	0.00
215	215	4.84	4.43	6.24	3.30	0.00	0.00	6.68	16.59	0.00	302	302	4.93	4.52	6.34	3.45	0.00	0.00	6.08	10.73	0.00
216	216	4.84	4.45	6.24	3.25	0.00	0.00	6.86	15.02	0.00	303	303	4.95	4.54	6.34	3.40	0.00	0.00	6.11	10.33	0.00
217	217	4.86	4.45	6.26	3.30	0.00	0.00	6.66	15.30	0.00	304	304	4.97	4.56	6.40	3.39	0.00	0.00	6.49	11.62	0.00
218	218	4.86	4.45	6.24	3.20	0.00	0.00	6.87	14.76	0.00	305	305	4.99	4.58	6.42	3.36	0.00	0.00	6.60	11.11	0.00
219	219	4.86	4.47	6.24	3.27	0.00	0.00	6.61	13.36	0.00	306	306	4.99	4.58	6.43	3.39	0.00	0.00	6.68	11.85	0.00

220	220	4.86	4.47	6.20	3.18	0.00	0.00	6.58	13.35	0.00											
221	221	4.86	4.45	6.18	3.12	0.00	0.00	6.63	12.72	0.00											
222	222	4.86	4.45	6.18	3.11	0.00	0.00	6.68	13.38	0.00											
223	223	4.86	4.47	6.20	3.17	0.00	0.00	6.61	13.59	0.00											

											Trace	Feet	Time1	Time2	Time3	Thick1	Thick2	Thick3	E1	E2	E3
											Average :		4.92	4.52	6.32	3.34	0.00	0.00	6.42	11.83	0.00
											Stdev :		0.066	0.066	0.075	0.123	0.000	0.000	0.236	1.662	0.000

Figure 3.32 Detailed dielectric and thickness data computed for the sections Q and M

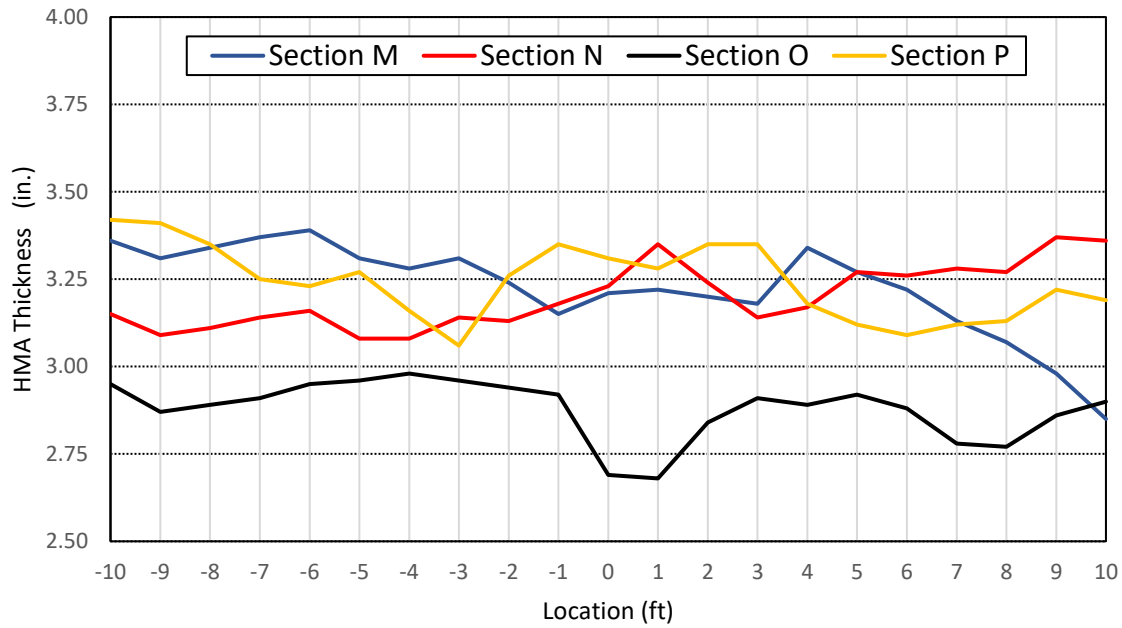


Figure 3.33 HMA thickness for Lane M, N, O and P

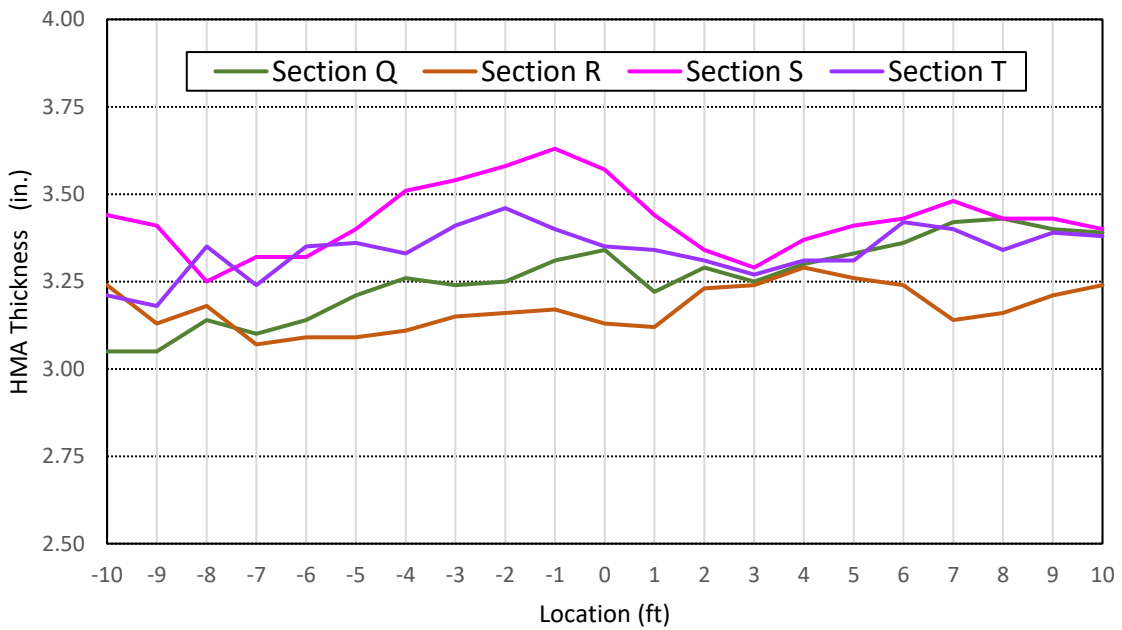


Figure 3.34 HMA thickness for Lane Q, R, S and T

Five days after placement, the TTI team collected Falling Weight Deflectometer data, with the equipment shown in Figure 3.35. The measurements were taken in nine locations on each section. The exact locations were marked with white paint. As an example, Sections S and T are shown in Figure 3.36 for a better visualization. The five circles marked with numbers are within the area where the APT loading is applied while the white filled circles are outside the PTM trafficked area.



Figure 3.35 FWD testing on Section M

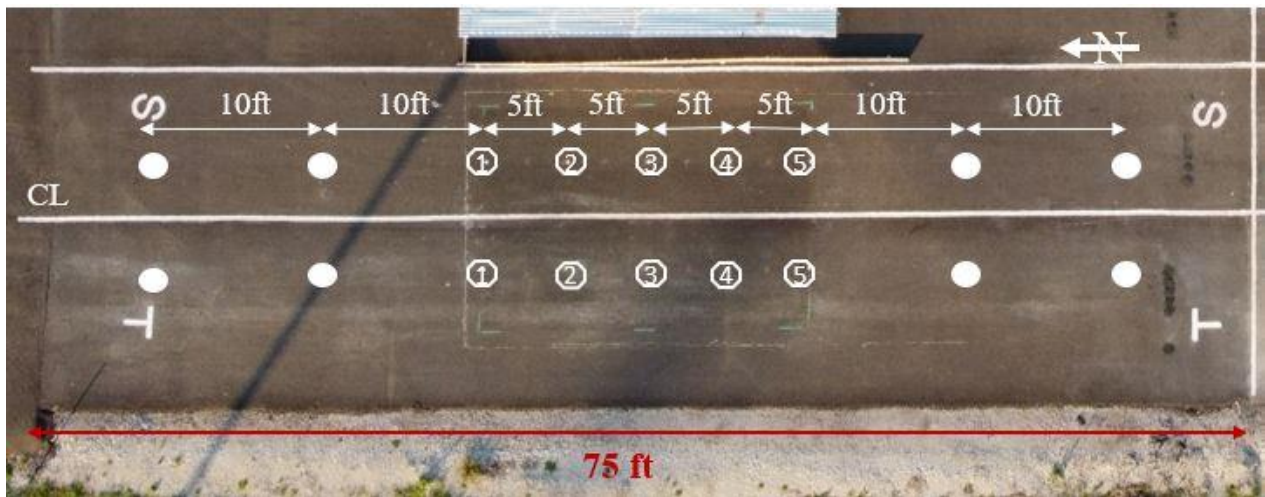


Figure 3.36 Location of the FWD testing, Section S and T

The FWD data was used to back-calculate the Base and Subgrade Modulus using the MODULUS 7 backcalculation program. The detailed results are attached in Appendix A-6 while Table 3.8 gives the average backcalculated moduli of the PTM trafficked area for the eight pavement test sections.

Table 3.8 Summary of deflection data from all sections after construction

Section	Average Central Deflection (mils)	Base Modulus (ksi)	Subgrade Modulus (ksi)
M	14.9	40	26
N	9.0	105	34
O	9.3	83	40
P	9.9	82	36
Q	15.6	49	17
R	12.5	63	24
S	15.3	52	19
T	14.1	60	21

As observed, the highest average deflection recorded was on section Q, 15.6 mils. The variation between sections is substantial; the average maximum deflections range from 9.0 mils to 15.6 mils. This appears primarily related to the support from the subgrade layer. Sections P, O and N have average subgrade modulus values of greater than 30 ksi, whereas Sections S and Q have values less than 20 ksi.

On June 17th, 2021, a new series of FWD deflection were collected only for the North sections, Q, R, S and T, in the PTM trafficked area using the TxDOT equipment. The data was back calculated using the same software and the summary of the results are shown in Table 3.9.

Table 3.9 Deflection data from the north section after artificial aging and 10 months after construction

Section	Average Central Deflection (mils)	Base Modulus (ksi)	Subgrade Modulus (ksi)
Q	36.5	20.7	7.2
R	33.1	22.6	7.6
S	26.2	32.7	11.2
T	31.1	29.6	9.1

The results showed an increase in the average deflection of 134% for lane Q, 165% for lane R, 71% for lane S and 120% for lane T. Implicitly, the subgrade modulus decreased significantly: 58% for lane Q, 68% for lane R, 41% for lane S and 57% for lane T. A possible factor contributing to this change may be attributed to the different FWD equipment used for collecting the data. Contrary to the expectations, the deflection values recorded were higher. Ageing increases stiffness which should decrease the deflections.

3.3 Artificial Ageing of Pavement Sections

Two ageing boxes were specially built to age artificially the new flexible pavement structure before applying the APT loading. To determine for how long and what is the temperature needed to obtain a desired aging, a much smaller box containing only one infra-red lamp and binder from a previous APT project were used. The dimensions of the small box were 6ft x 4ft x4 ft., Figure 3.37 and 3.38.



Figure 3.37 Small artificial aging box

Since mix N is the only virgin mix included in this APT experiment, it was decided that this mix containing bitumen PG 70-22 with no RAP or RAS should be analyzed and correlated to an older similar mix in terms of stiffness. Many efforts were made to find a pavement in the Dallas and Fort Worth District that has PG 70-22 in the top layer, contains no RAP or RAS and is at least ten years old. Since Texas DOT has allowed RAP and RAS during this period, such a surface mix was not available anywhere in the Dallas and Fort Worth District. Therefore, it was decided to use data from an older APT research project even though the performance grade of that particular section was PG 64-22. One of the advantages of using the older APT section was the availability of the extracted binder characteristics from when the pavement was constructed in February 2013.

To determine a stiffness equivalency factor between the two asphalt mixtures the following were performed:

- Six cores were extracted; three from the 2013 APT section and three from the 2020 APT experiment, Lane N. The cores were sent to TTI for binder extraction and stiffness evaluation.
- The small ageing box was positioned on Section N as seen in Figure 3.37, and the oxidation process was run continuously for three weeks.
- Three samples were cored, and binder extraction was performed, Figure 3.39.
- The same process was followed, and cores were extracted after 4 and 5 weeks.

Table 3.10 shows the binder extraction results. According to the stiffness data obtained, five weeks of artificial ageing correspond to about seven-and-a-half years of naturally occurring ageing.



Figure 3.38 Coring after 4 weeks of artificial aging



Figure 3.39 Extracted cores after 3 weeks of artificial aging

Table 3.10 Binder extraction data

APT Section	2013		2020			
	No aging	After 7.5 years	No aging	3 weeks	4 weeks	5 weeks
G* (kPa)	2.376	22.363	1.711	4.933	7.08	23.52
δ (degree)	84.45	71.61	78.38	74.73	73.18	65.67
G*/sin δ	2.387	23.57	1.747	5.114	7.396	25.813
Aging ratio	9.9		N/A	2.9	4.2	14.8

Soon after establishing the ageing period, the sections were aged in pairs using the larger oxidation chambers. The sequencing of artificially ageing was pair M and N, followed by O and P, S and T and lastly, Q and R. After being placed on the section, the ageing chambers were waterproofed with rubber strips and sealant, as shown in Figure 3.40.



Figure 3.40 Ageing chambers places on Lane Q and R

Temperature data was extracted weekly from the data loggers to ensure functionality and uniformity. The temperature data was recorded every 60 minutes. Figures 3.41 to 3.48 shows the temperature recorded for all lanes.

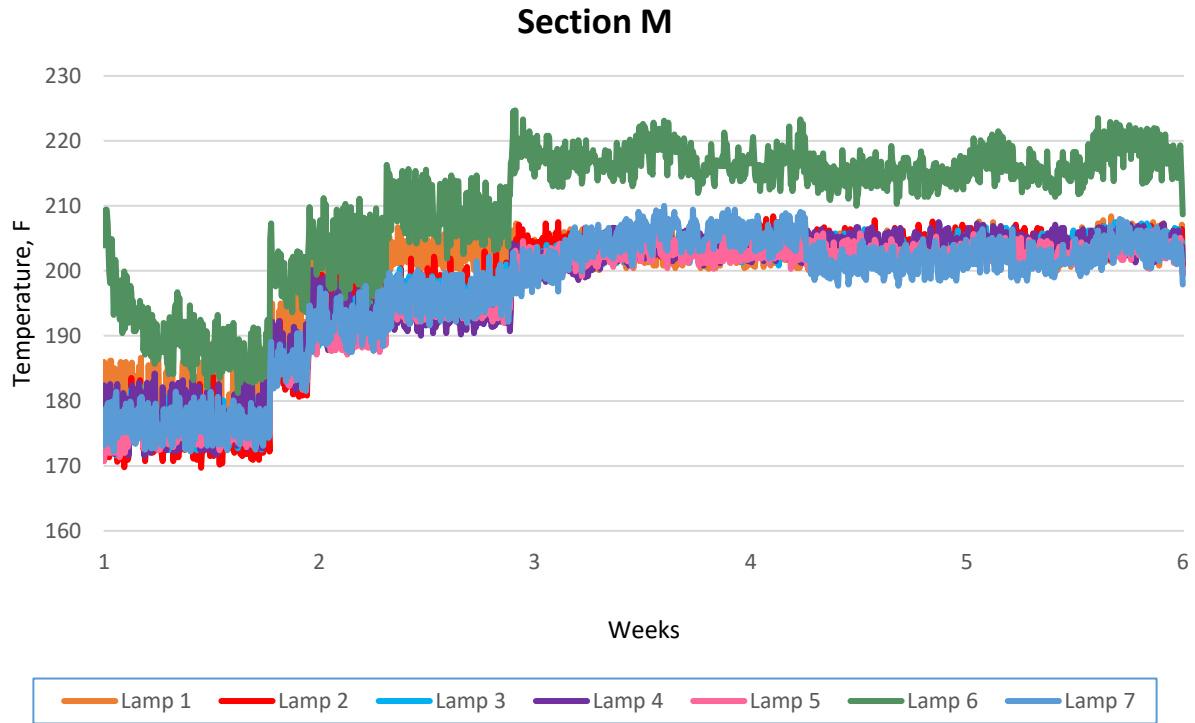


Figure 3.41 Thermal data recorded on Lane M

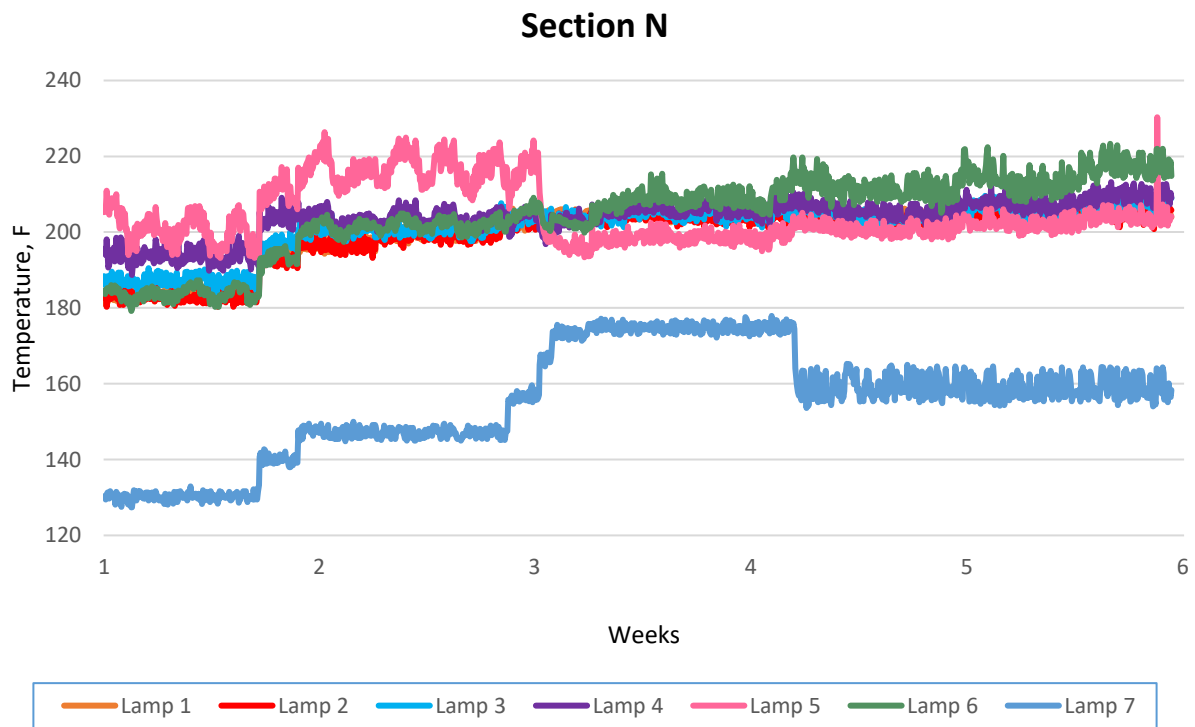


Figure 3.42 Thermal data recorded on Section N

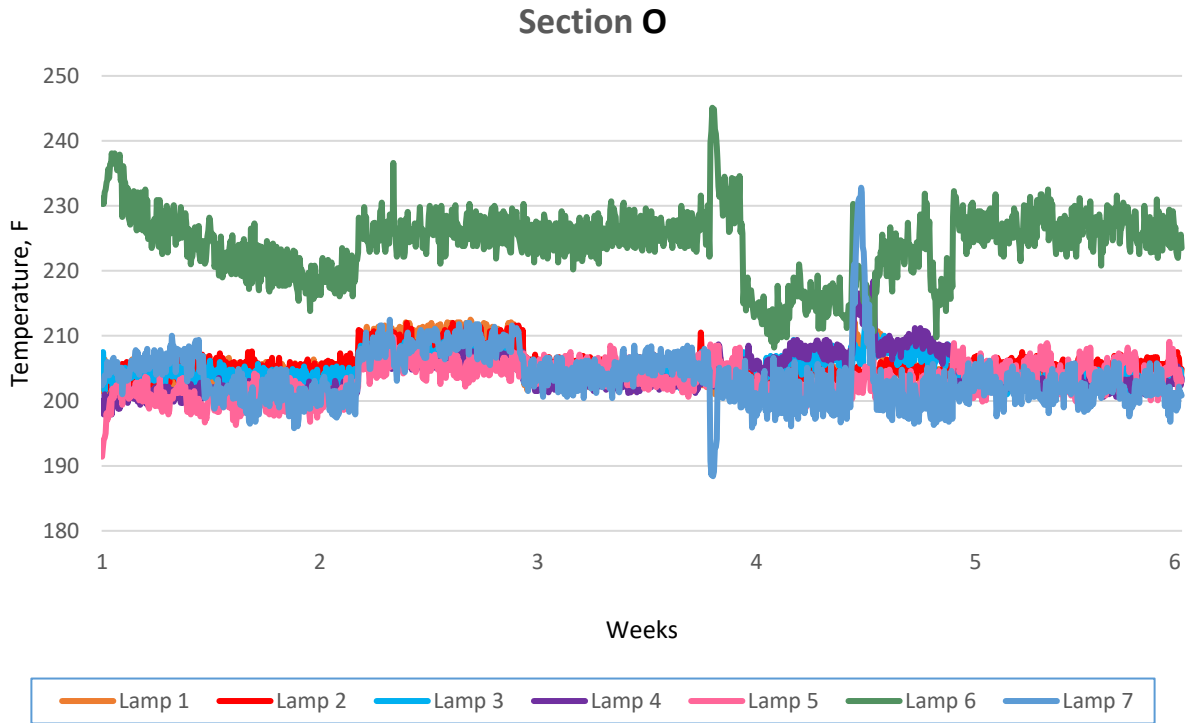


Figure 3.43 Thermal data recorded on Section O

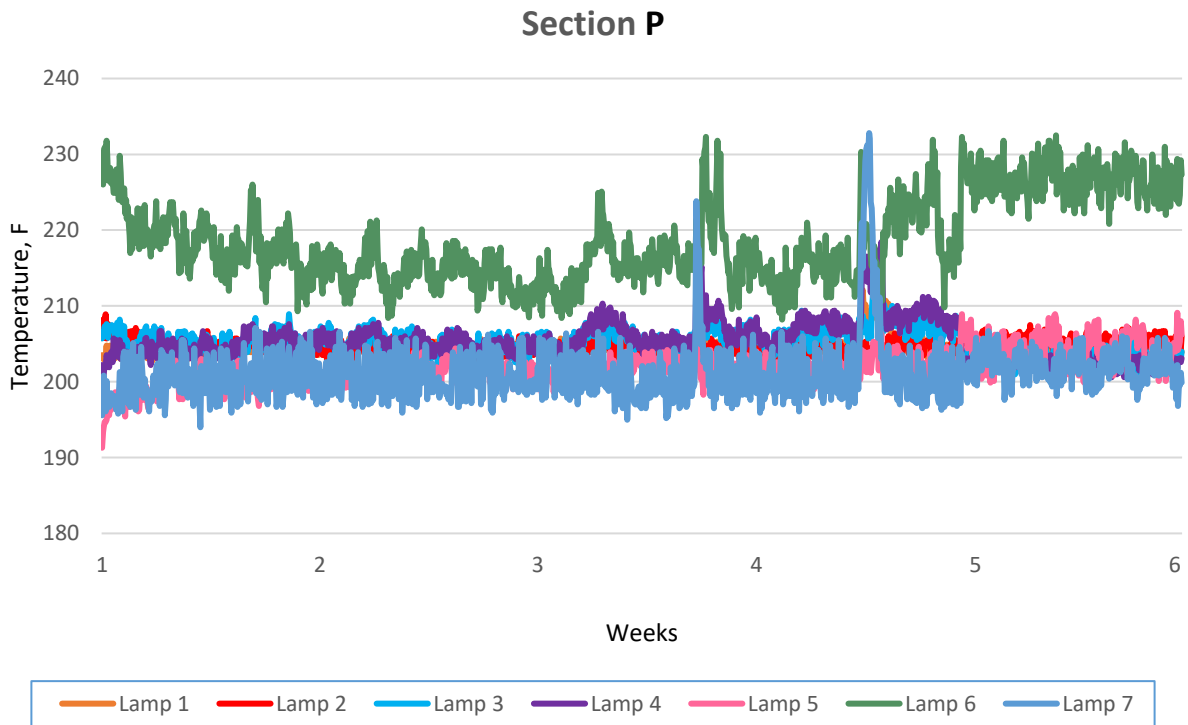


Figure 3.44 Thermal data recorded on Section P

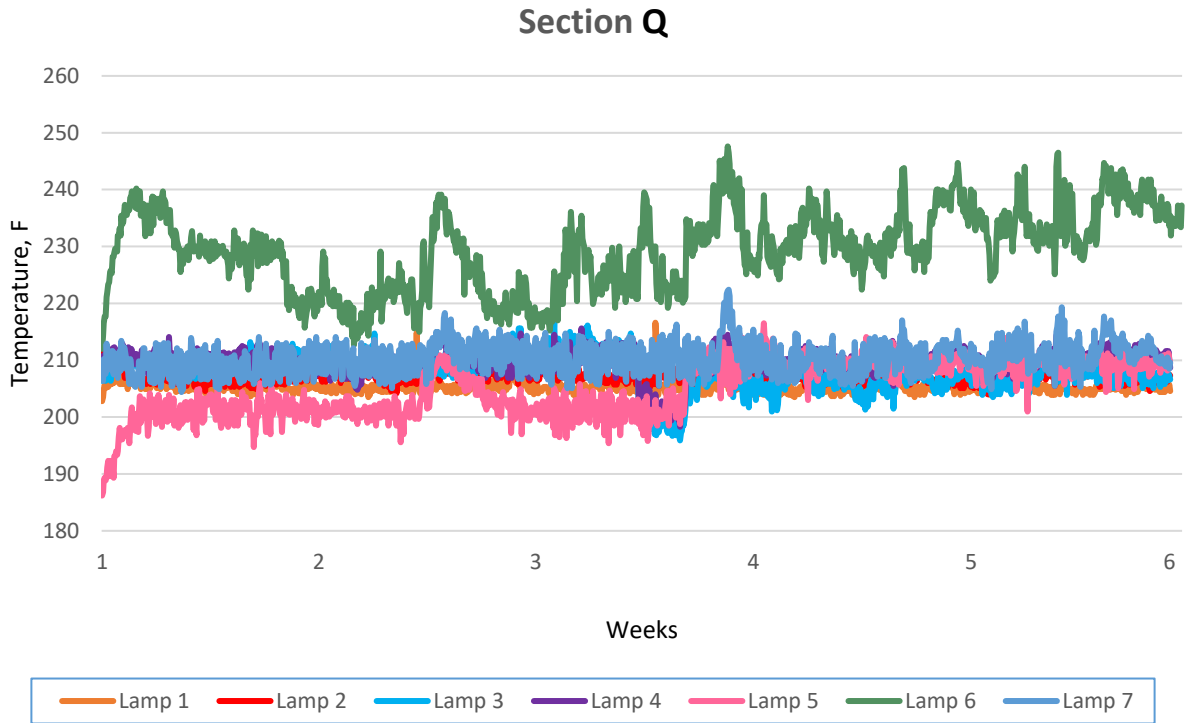


Figure 3.45 Thermal data recorded on Section Q

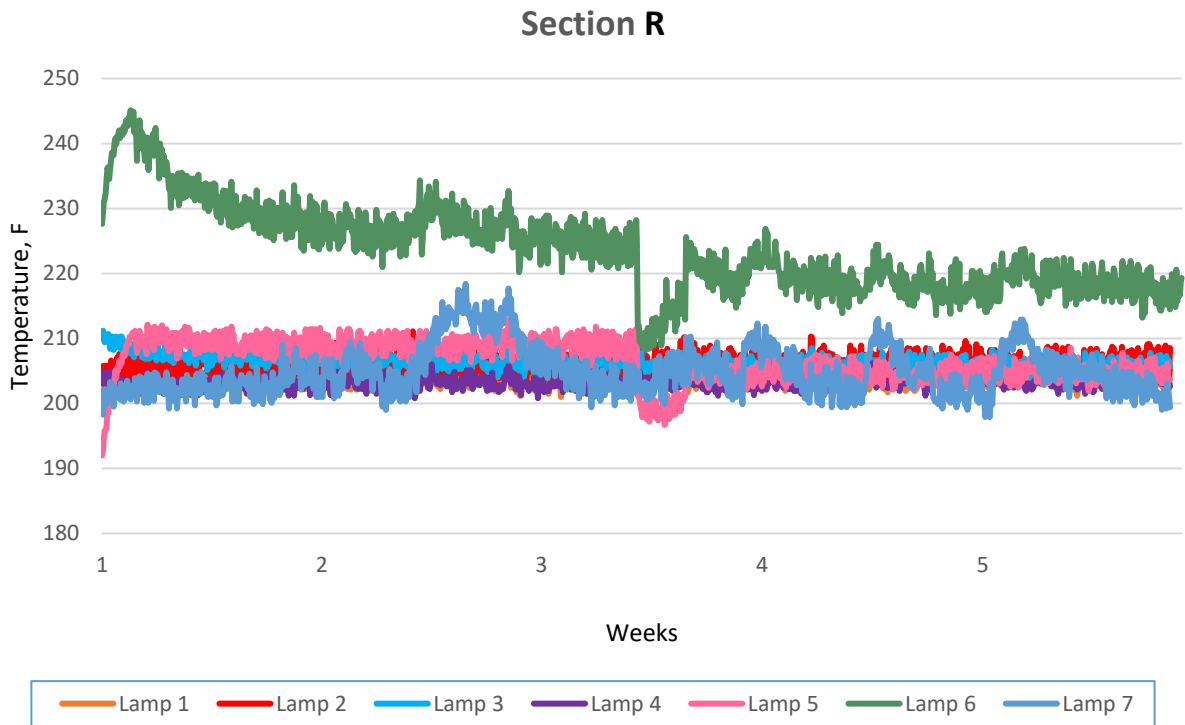


Figure 3.46 Thermal data recorded on Section R

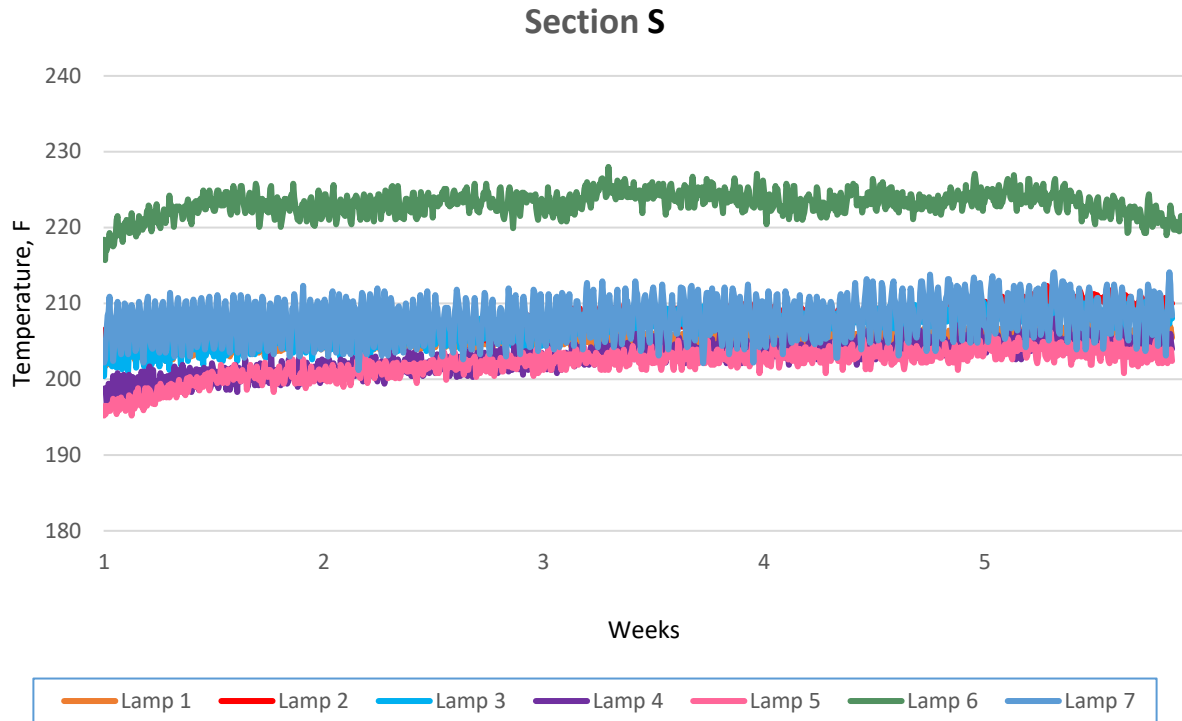


Figure 3.47 Thermal data recorded on Section S

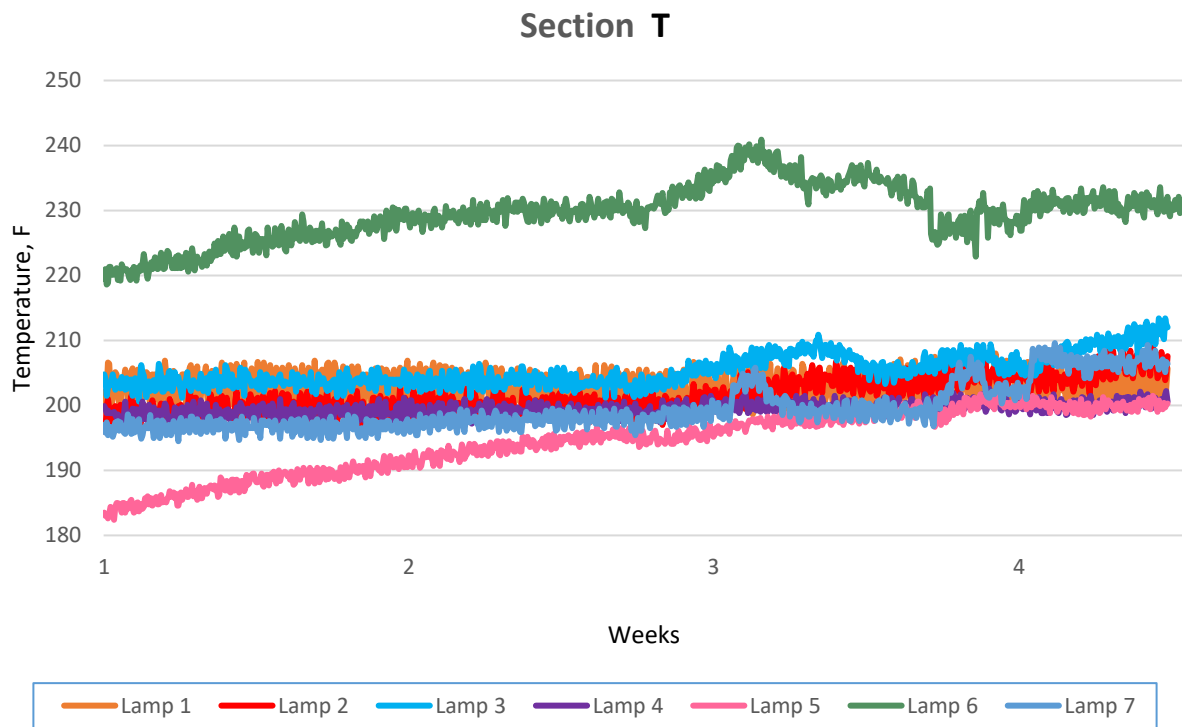


Figure 3.48 Thermal data recorded on Section T

The data recorded indicates that the temperature was overall uniform and in the 195 to 210°F range. The thermocouple installed under Lamp 6 indicated higher temperatures. In some instances, the temperatures recorded for this lamp were as high as 240°F. This can be due to the overlapping with lamp 7 since the distance between these two lamps is slightly smaller than 30 inches or it could be due to the malfunction of the Omega data logger used. On the other hand, for section N, lamp 7 recorded temperatures with about 50°F lower than expected. However, analyzing the pattern of the other lanes it seems like lamp 7 functioned normally on the other sections.

3.4 APT Testing of Pavement Sections

3.4.1 Loading conditions

The test sections are tested in pairs. The pairs tested together are sections M with N, sections O with P, sections S with T and sections Q with R. Bidirectional loading was applied for all the sections. Figure 3.49 shows the inside of the PTM machine while testing sections Q and R.



Figure 3.49 PTM positioned on sections Q and R

An 18,000 lbs. (81.6 kN) single axle, dual tire, load and a tire inflation pressure of 100 psi (690 kPa) was used throughout this experiment. The axle load and tire inflation pressure were checked periodically. The APT wheel loads were calibrated twice using a pair of highway patrol scales placed under the wheels. The axle load was maintained constant by always selecting the same setting for the hydraulic valve that controls the oil pressure in the hydraulic system. The correct setting was obtained in the calibration. The tire inflation pressure was measured using a tire pressure gauge.

Lateral wheel wander was also applied. The PTM is moving laterally following the pattern of a normal distribution with a standard deviation of 8.0 inches truncated at the maximum lateral position of 15 inches, Figure 3.50. This covers 93.9 percentile of the entire area of the normal distribution. This wander pattern was repeated every 1,028 passes starting from the center position (Position 0.0).

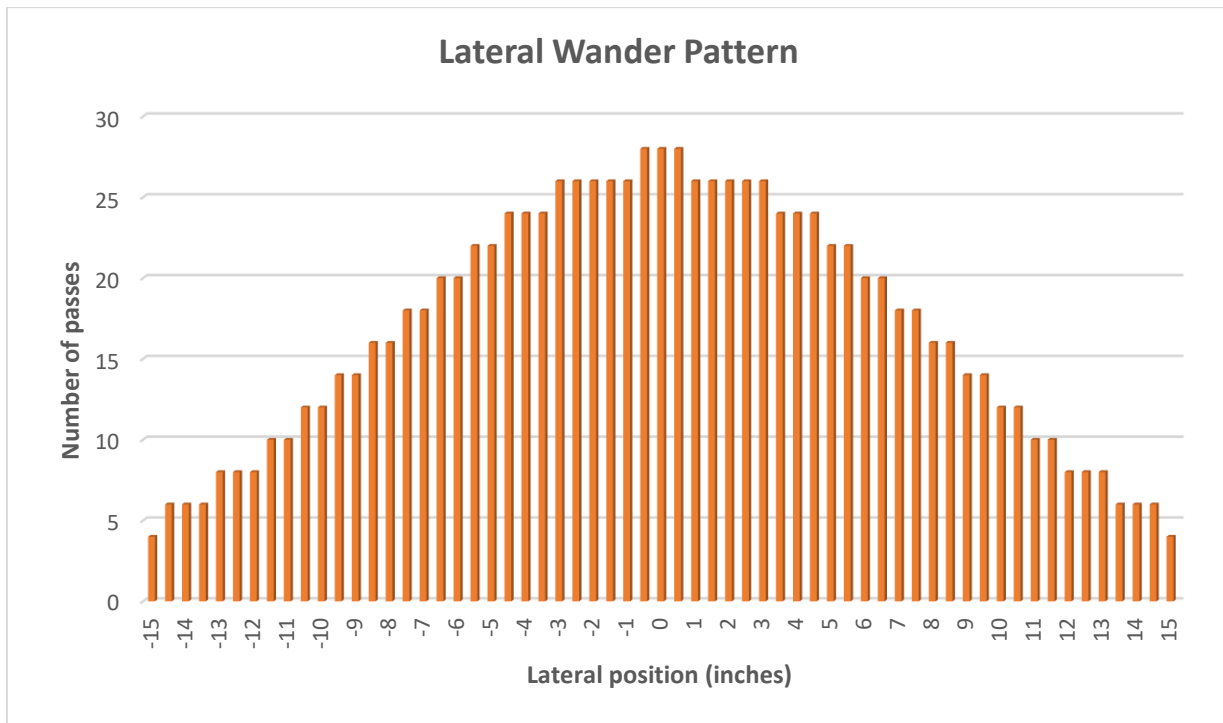


Figure 3.50 Lateral wander pattern followed by the PTM

Rutting measurements, deflection testing, and crack mapping were done when APT loading was started (0 passes), at 5,000, 10,000, 25,000, 100,000 passes, and every 100,000 passes after that. The pavement sections are considered failed when 50% of the trafficked area was cracked or a rut depth of 0.75 in. (19 mm) was measured at the pavement surface.

3.4.2 Temperature during APT testing

The temperature between two tested sections was measured at the surface, 0.5 inches below the surface and at the bottom of the asphalt layer. Thermocouples were placed in drilled holes filled with oil when the accelerated loading started on each respective section. Two sets of three thermocouples were installed 30 feet apart on the longitudinal orientation of the PTM, one was installed towards North and the other towards South. The temperature at each depth was recorded and the average temperature is reported, as seen in Figure 3.51. The goal was to maintain a surface temperature of 68-70°F.

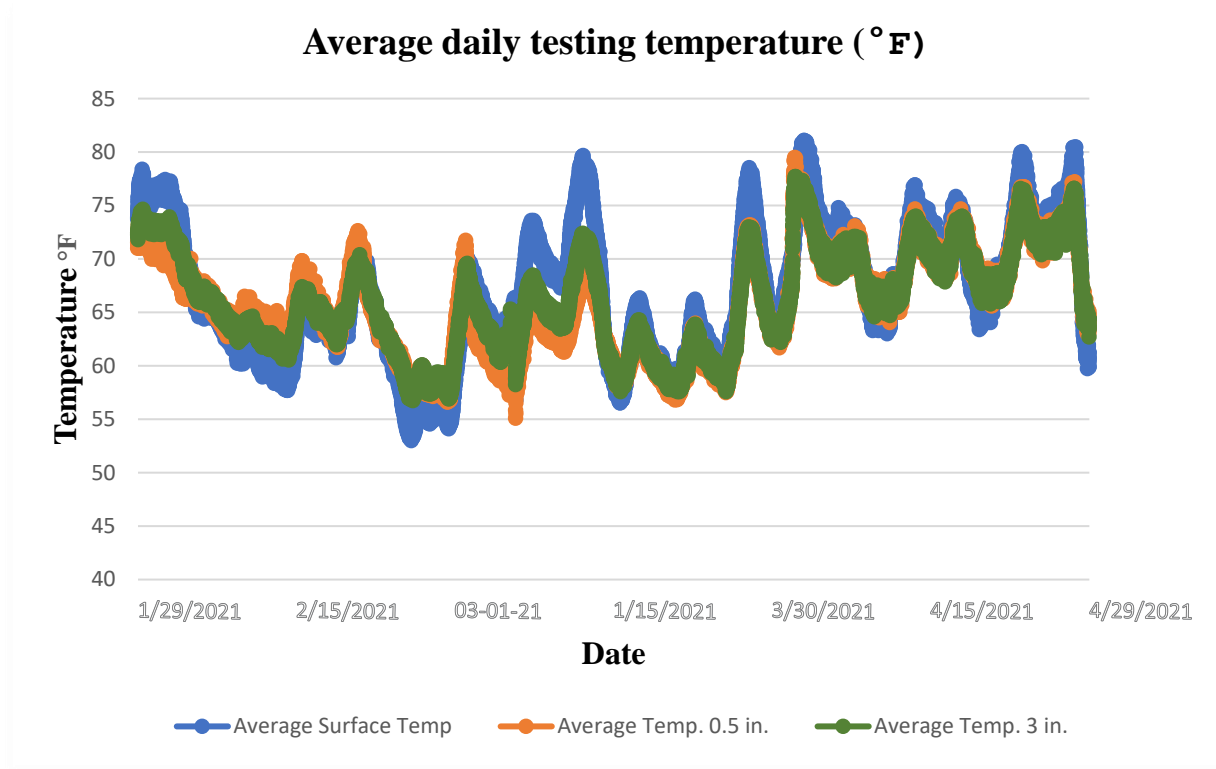


Figure 3.51 Temperature recorded during APT testing on Section O and P

3.5 Rutting measurements

Rutting measurements were performed in five locations for each section as shown in Figure 3.36. The locations are 5 ft. apart and numbered from 1 to 5, section 1 being toward North. Transverse profile measurements were performed when APT loading was started (0 passes), at 5,000, 10,000, 25,000, 100,000 passes, and every 100,000 passes after that. To do so, an in-house built profiler was used. Figure 3.52 shows the main components of the profiler:

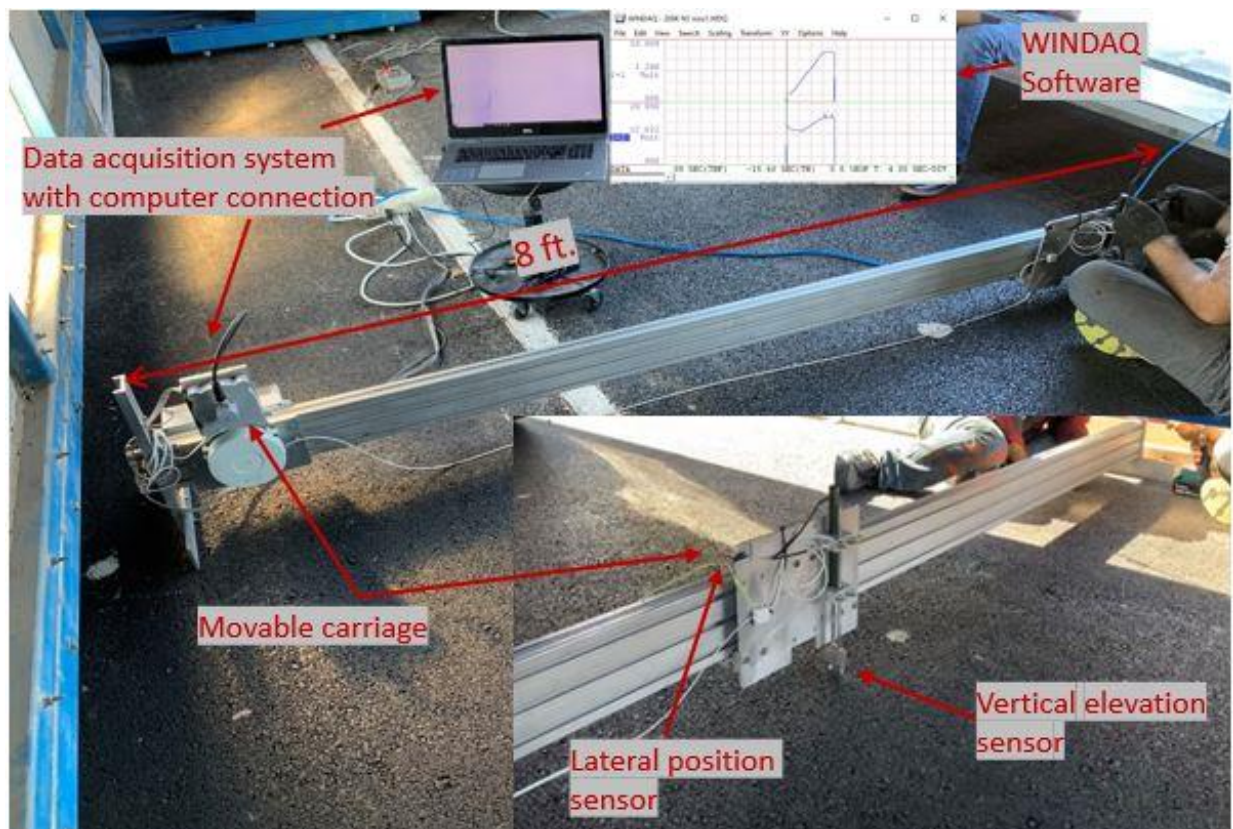


Figure 3.52 Main components of the transverse profiler

The following steps are employed when performing the profile measurements:

- The data acquisition system mounted on the profiler was connected to a laptop computer and the WINDAQ software application was opened.

- The beam was positioned transversally on the testing section in a predetermined, fixed position. The testing location was marked with driven nails; one nail was fixed on the center line that separates one section from the other and the second nail was fixed 7 ft. away.
- The data recording was started, and the carriage was moved along the aluminum beam at a constant speed until it reached the second reference nail. The recording was then stopped. The vertical and lateral position sensors recorded voltage signals which were converted afterwards to distances using conversions factors derived in a prior calibration.
- Microsoft Excel was used to process the data and obtain a transverse profile with elevation data every 1.0inch interval starting from the first nail, which was considered as the lateral position 0.0. Figure 3.53 shows an example of a transverse profile recorded in one of the five longitudinal locations. The complete transverse data is provided in Appendix B-1.

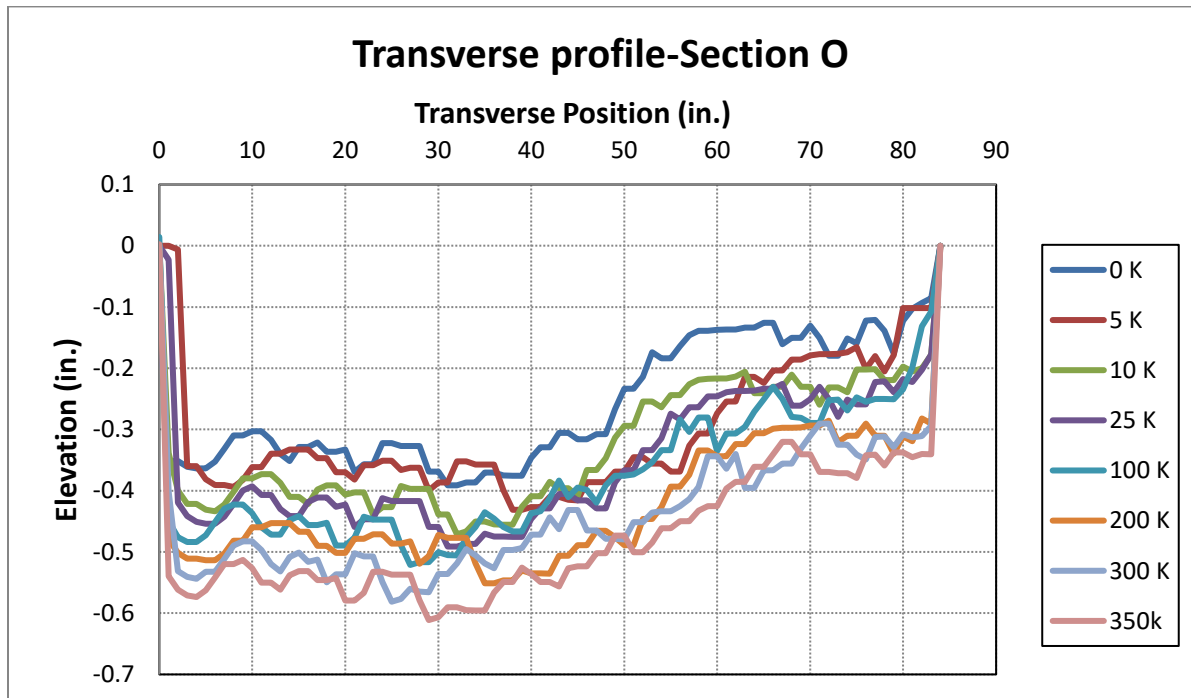


Figure 3.53 Example of transverse profile, Lane O-Profile 3

- Using the elevation data recorded in each transverse profile, the Permanent Deformation (PD) was calculated in each point by subtracting the measured elevation after a given number of APT passes from the initial elevation data. When the elevation of a point is lower than the initial elevation, the permanent deformation in that point was considered positive.
- For each transverse profile the permanent deformation was computed as the maximum value obtained from the 84 points. Finally, the average of the permanent deformation for the five transverse profiles was computed.

Over 400 transverse profiles were measured and analyzed. To ease the workload, two Excel VBA codes were developed (Appendix B-2). Figure 3.54 to 3.56 show the progression of the computed average permanent deformation.

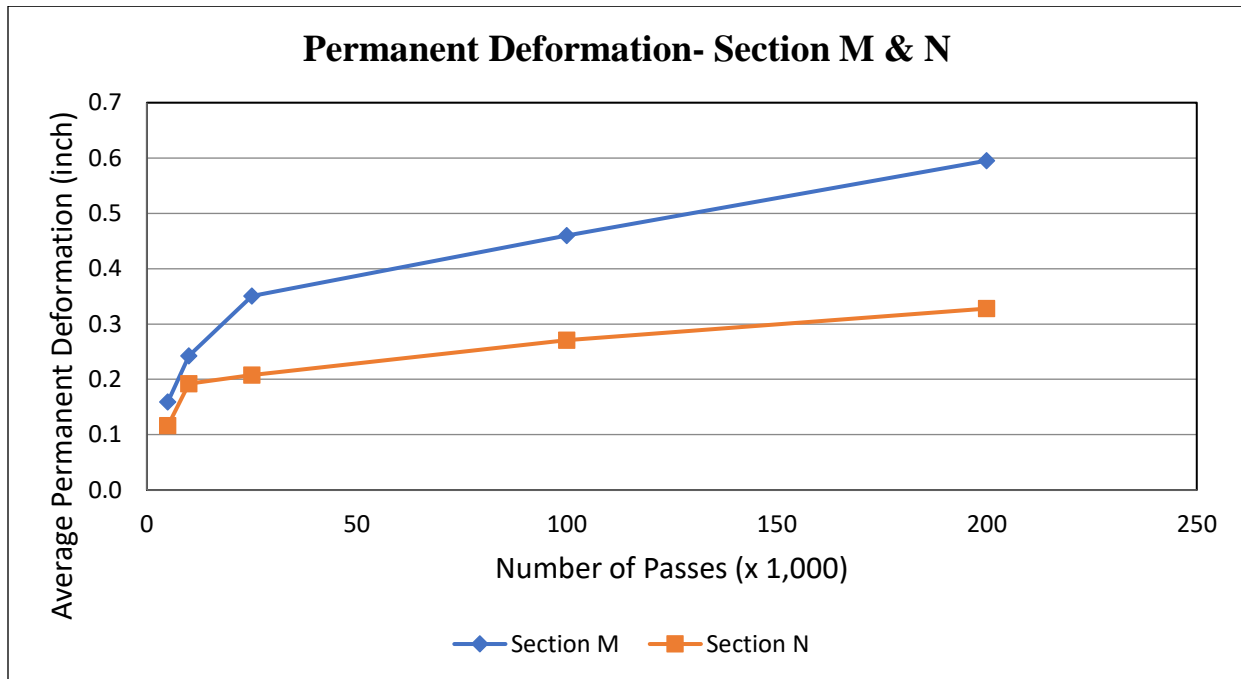


Figure 3.54 Progression of permanent deformation in Section M and N

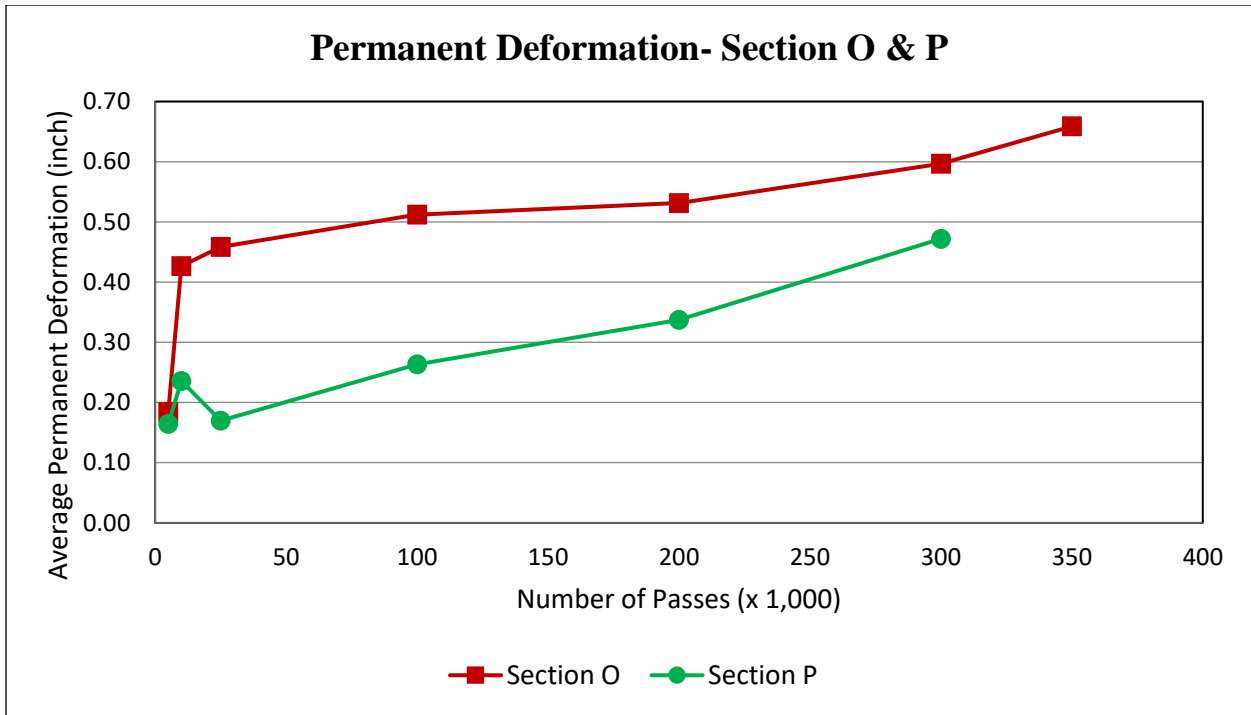


Figure 3.55 Progression of permanent deformation in Section O and P

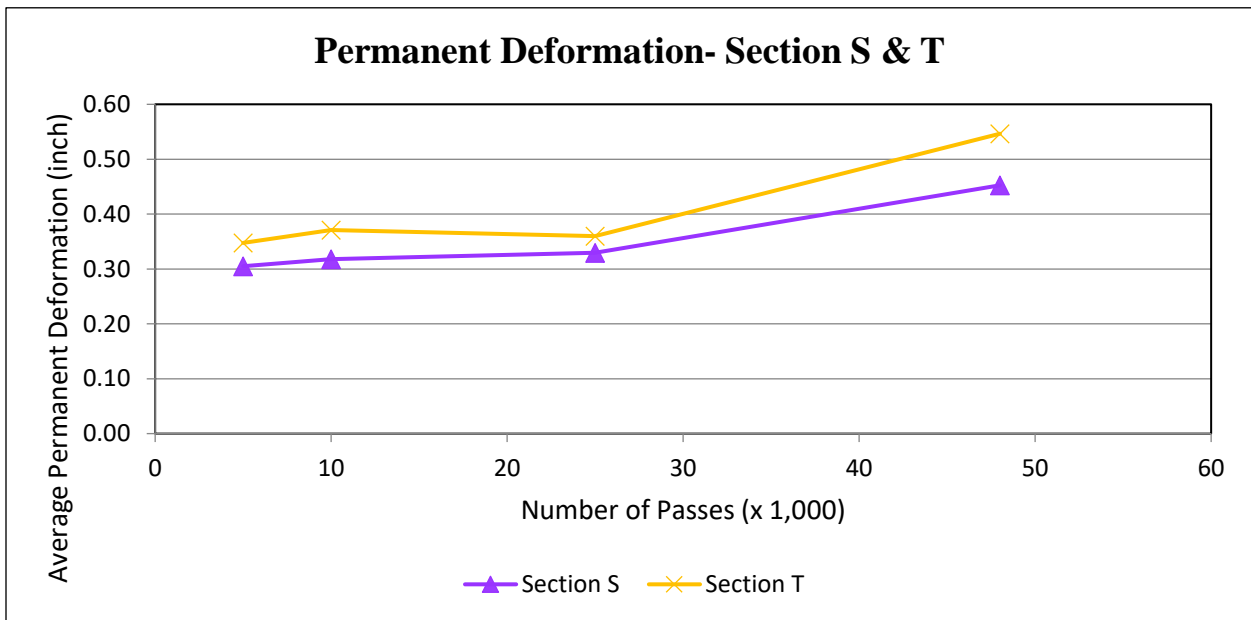


Figure 3.56 Progression of permanent deformation in Section S and T

Section N did not fail. However, the loading of Section N was stopped because of the high extent of cracking present on the adjacent section, Section M. Testing of Section N will resume after the failed section M is excavated and a concrete pad will be poured. This is a necessary for the proper positioning of the PTM in the testing location.

As noticeable from the graphs, none of the sections exhibited rutting failure; cracking has been the main cause of failure. Out of the mixes tested, the mix exhibiting the lower rut depth is ranked 1st while the one exhibiting the highest rut depth exhibits the lowest rut resistance and it is ranked 6th, Figure 3.57.

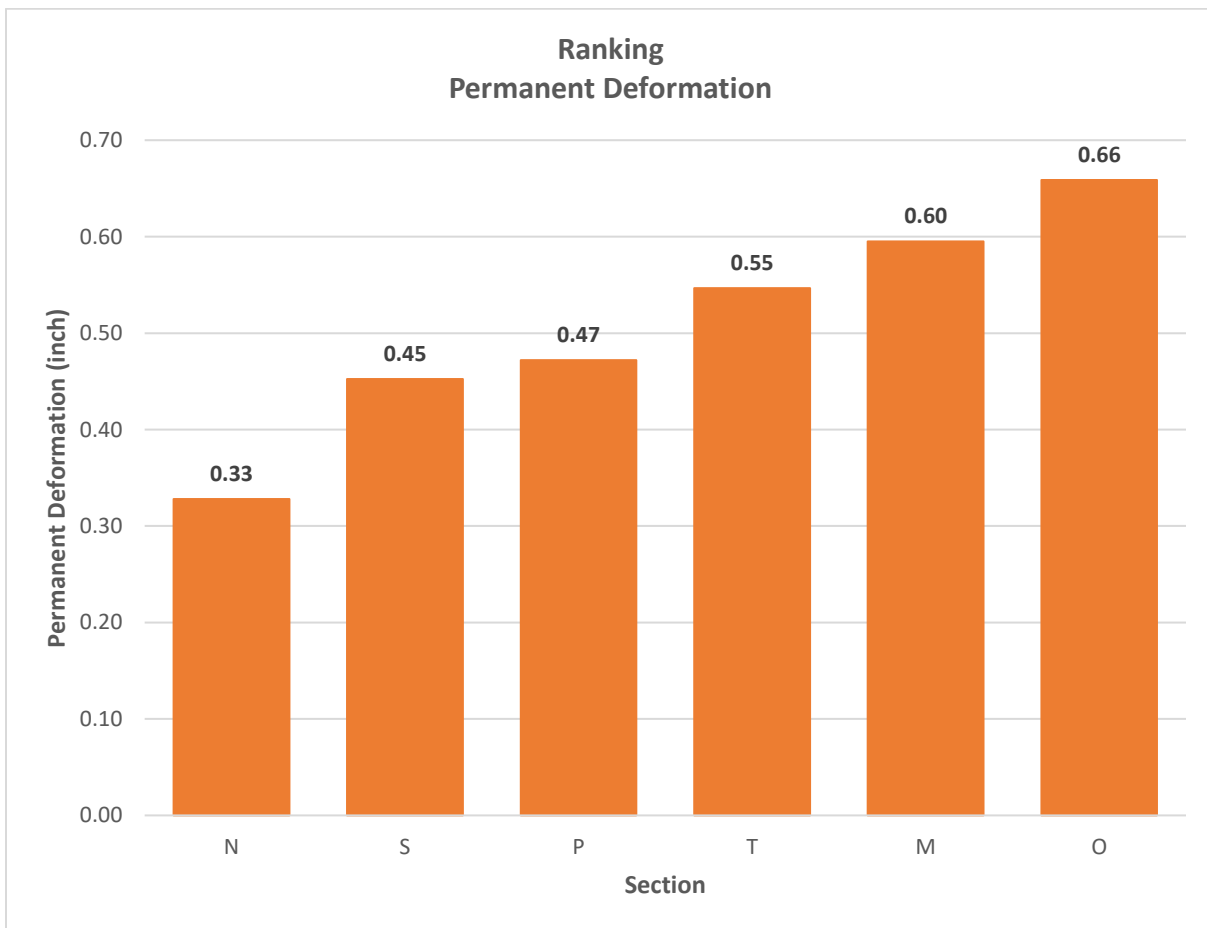


Figure 3.57 Ranking of computed permanent deformation

3.6 Deflection Measurements

A Light Falling Weight Deflectometer (LWD) was used to measure the structural capacity and the change in the layer moduli (Figure 3.58). A L-FWD test is performed by dropping a weight from a known height on a loading plate placed on top of the pavement. The impact load is measured with a load cell mounted at the bottom of the device while the vertical deflection of the pavement is measured in three locations, including the center of the loading plate, is measured using three geophones.

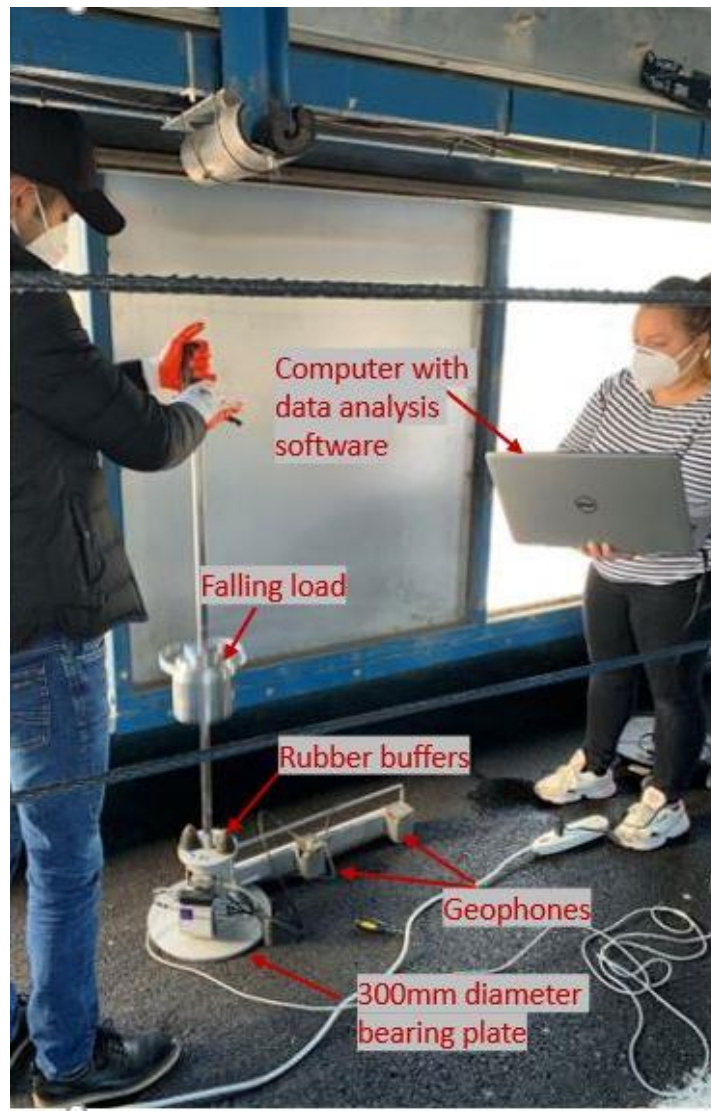


Figure 3.58 Light Falling Weight Deflectometer measurements

The L-FWD has the advantage of being small enough to fit inside the PTM. The deflection measurements were performed at five different locations which were permanently marked on the sections. For each point, five drops were performed to ensure a good positioning of the device on the testing pad. Using the deflections recorded, the overall pavement stiffness was then calculated as the ratio between the applied impact pressure and the central deflection.

$$S = \frac{P}{d_0 \times \pi R^2}$$

Where:

S – Overall pavement stiffness (Kip/inch)

P – Applied load (lbs.)

d_0 – Central deflection (in.)

R – Radius of the loading plate, 5.94 inches.

Table 3.11 shows the central deflection and the calculated overall pavement stiffness for the fifth drop of the L-FWD test. Figures 3.59 and 3.60 show the average overall pavement stiffness and the central deflection for the sections tested while the detailed graphs for each point are attached in Appendix C.

The results show that all the sections are very stiff. There is significant variance within the six tested sections, S and T recorded the highest deflections. This could suggest that the use of rejuvenators does not work as well as expected under aging conditions. The deflection recorded for sections M, N, O and P seem to follow a similar trend, the central deflections increase after the first 5,000 of APT loading, followed by a slightly decrease and overall uniform values thereafter.

Table 3.11 Central deflection and the calculated overall pavement stiffness

Passes ×1,000	Central deflection; d0 (mils)					Overall Pavement Stiffness, S (Kip/in)				
	Location					Location				
	1	2	3	4	5	1	2	3	4	5
Section M										
0	6.3	4.6	4.4	4.2	5.4	4473.1	6093.6	6423.3	6832.9	5532.2
5	7.0	5.0	5.7	2.8	5.9	4106.7	5772.0	5101.7	9736.9	4929.7
10	5.4	1.7	2.4	3.0	5.4	5433.4	18054.5	12222.1	9966.3	5438.8
25	7.5	6.1	7.2	5.2	5.9	4032.1	4994.2	4242.8	5818.8	5209.4
100	12.6	8.2	8.3	7.3	6.7	2302.8	3665.1	3705.6	4215.8	4648.3
200	4.0	4.9	3.2	4.2	4.5	6319.4	5209.1	8573.0	6614.2	5928.6
Section N										
0	4.9	2.4	2.9	2.9	3.1	5965.7	11578.0	9822.5	9850.3	9174.7
5	6.8	2.7	3.5	3.3	3.7	4290.9	11037.7	8288.6	8151.4	7924.4
10	5.1	4.6	5.4	4.7	6.1	5472.4	6004.1	5234.7	6060.5	4672.8
25	6.0	3.4	4.1	4.6	3.7	5066.7	8793.3	7251.2	6365.1	7992.8
100	2.8	3.8	4.2	4.8	3.9	5265.1	8177.9	7386.9	6413.9	8070.6
200	4.8	4.5	4.9	4.7	5.3	5807.1	6244.4	5708.1	5713.8	5178.3
300	7.2	4.0	5.0	4.6	4.0	3651.0	6957.0	5467.8	5565.3	6797.8
Section O										
0	4.0	4.9	3.2	4.2	4.5	6319.4	5209.1	8573.0	6614.2	5928.6
5										
10										
25				5.7	5.0				4959.6	5650.3
100	4.8	8.0	3.9	7.2	5.6	5922.0	3489.8	7154.2	3957.9	5072.2
200	7.1	7.0	5.5	6.9	5.4	3916.2	4004.7	5258.9	3980.6	5305.6
300	5.9	6.1	4.6	6.9	7.8	4773.6	4332.5	6173.0	3956.3	3540.6
350	6.5	20.0	7.5	14.2	6.6	4242.9	1356.8	3776.8	1911.7	4286.7
Section P										
0	4.8	4.5	4.9	4.7	5.3	5807.1	6244.4	5708.1	5713.8	5178.3
5										
10										
25	6.9	6.5	6.9	9.3	6.5	4147.8	4184.0	3965.1	3027.3	4313.5
100	6.1	7.4	5.7	7.7	5.8	4656.3	3772.3	4922.1	3561.3	4920.1
200	6.6	8.3	8.0	11.3	6.1	4364.8	3354.5	3585.6	2439.8	4656.1
300	4.3	6.6	5.2	9.4	6.5	6361.3	4136.6	5089.4	2816.1	4027.5
350	6.0	7.1	6.6	8.3	5.6	4670.2	3916.2	4145.7	3195.3	4852.4
Section S										
0	4.5	4.6	4.5	5.1	6.6	6509.1	6265.5	6284.7	5577.2	4486.0
5	5.6	5.7	5.7	6.2	7.7	1895.5	1737.2	1754.1	1548.5	1946.1
10	3.8	4.0	3.9	4.5	5.9	7344.7	7030.1	7067.9	6164.9	4814.2
25	4.2	4.2	3.5	3.5	3.9	6619.1	6793.1	7624.1	8207.9	7294.4
48	32.7	17.1	15.7	18.1	12.0	773.6	1611.9	1764.4	1477.0	2411.3

Table 3.11 Central deflection and the calculated overall pavement stiffness - continued

Lane T										
0	7.3	6.8	6.6	5.9	7.9	4029.2	4307.1	4410.0	5092.8	3707.1
5	8.4	7.9	7.7	7.0	9.0	3432.7	3629.2	3703.2	4205.1	3189.8
10	6.7	6.1	6.0	5.3	7.3	4277.9	4606.5	4728.1	5534.9	3907.9
25	4.0	3.7	4.4	3.9	5.4	7272.6	8048.4	6523.6	7448.5	5192.5
48	8.2	10.9	22.3	26.7	23.0	3177.1	2457.1	1153.8	1002.2	1199.4

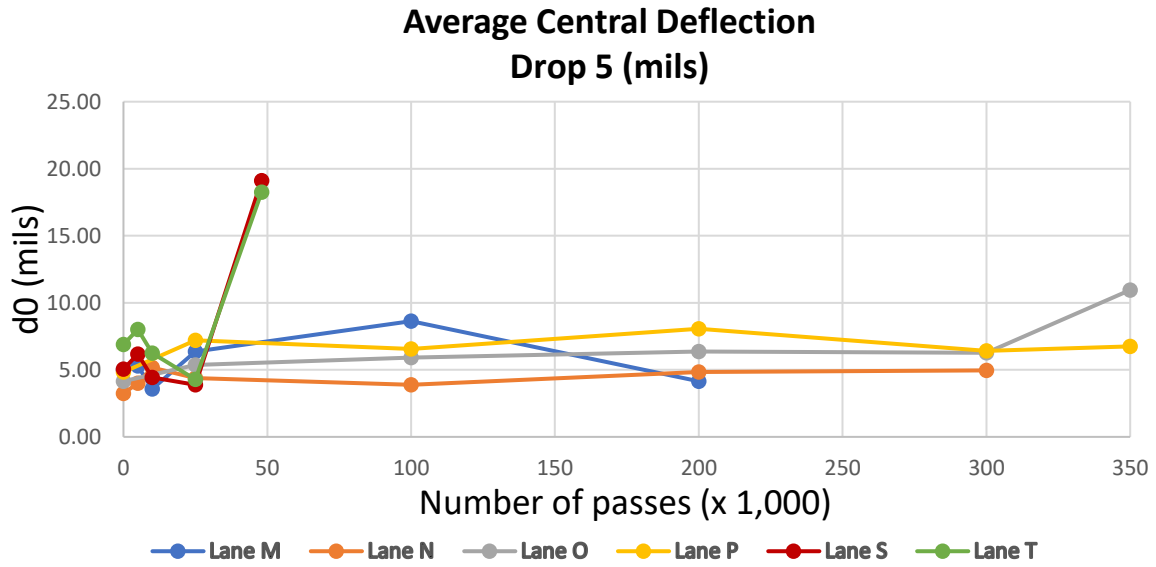


Figure 3.59 Average central deflection for all sections

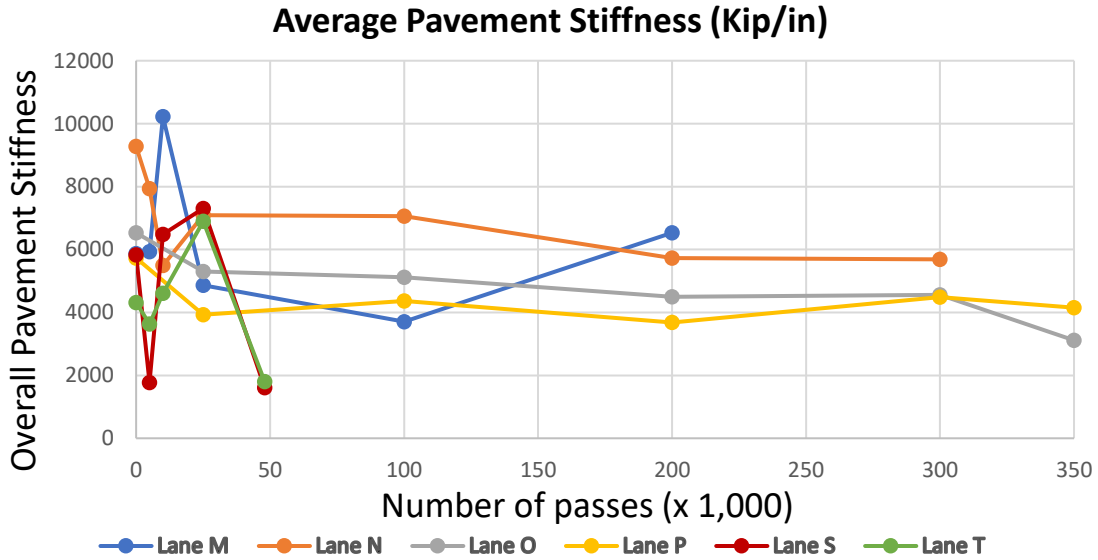


Figure 3.60 Average pavement stiffness for all sections

Because the thickness of the asphalt layer has an impact on the stiffness and the layer moduli, the asphalt thickness corresponding to each testing location was extracted from the GPR data.

Table 3.12. Asphalt layer thickness in the testing location

Lane	Asphalt layer thickness in the testing location (in)					
	Point 1	Point 2	Point 3	Point 4	Point 5	Average
M	3.28	3.03	3.13	3.2	3.31	3.19
N	3.44	3.37	3.17	3.18	3.16	3.26
O	3.02	2.86	2.89	2.92	2.95	2.93
P	3.05	3.22	3.18	3.35	3.23	3.21
Q	3.39	3.33	3.34	3.21	3.05	3.26
R	3.24	3.26	3.13	3.09	3.24	3.19
S	3.4	3.41	3.57	3.4	3.15	3.39
T	3.38	3.31	3.35	3.36	3.21	3.32

Figure 3.61 illustrates the ranking based on the central deflection. Section M recorded the smallest deflection and is ranked at 1st and section S had the highest deflection and is ranked as 6th. It is believed that the deflection recorded after failure on section M is not fully reliable because the section presented extensive cracking at that time. Thus, section N should be ranked as 1st. Because section S has the thickest asphalt layer, in average 3.39 inches, it was expected have the highest stiffness. However, the evolution of the overall pavement stiffness does not show a trend pattern; too little data points were collected since this section completely failed at only 48,000 passes of APT loading.

It is important to note here that, when all L-FWD tests were done, the temperatures in the asphalt layer were very similar. The temperature control chamber on the PTM machine had been started for at least three days before each L-FWD test was performed; the same temperature control settings have been used during the entire project.

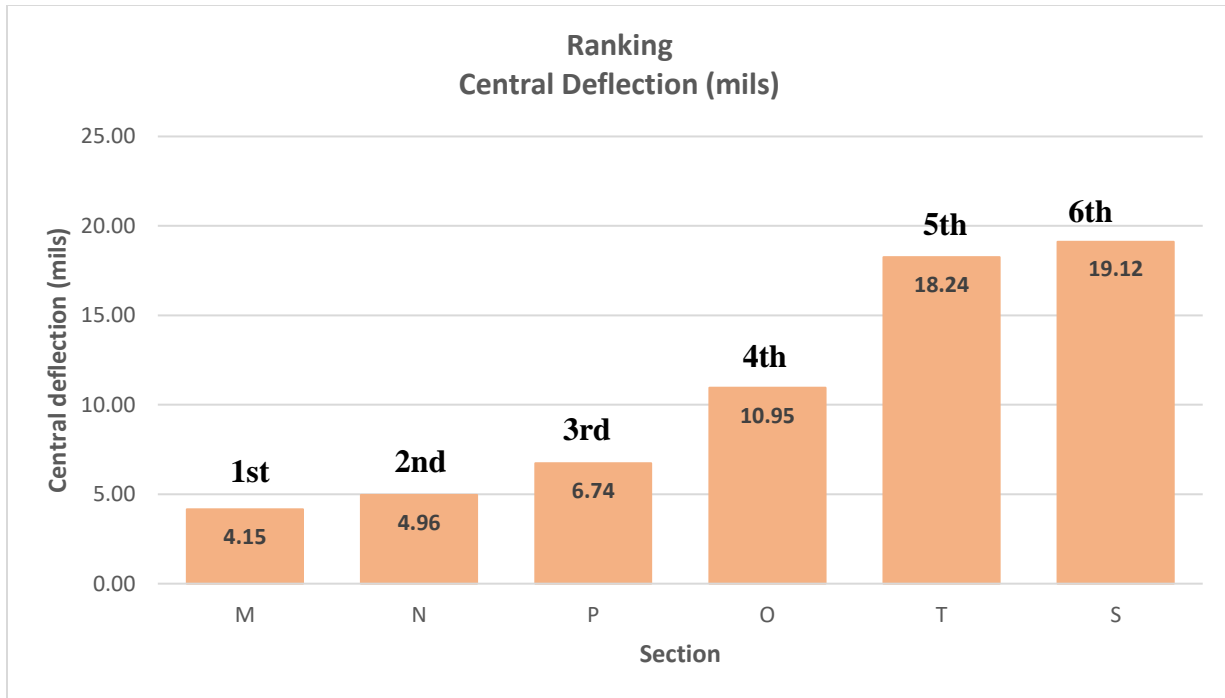


Figure 3.61 Ranking of the central deflection measured by L-FWD

3.7 Cracking Measurements

The extent of surface cracks was measured using a grid panel with 6-inch square openings. Two 4 ft. x 10 ft. long panels were built and positioned on the trafficked area, one to the North and one to the South from the middle point of the center line. After placing the grid on the pavement surface, the observed crack pattern was drawn on a paper template using the string grid as the reference. The percentage of the cracked area was calculated based on the numbers of squares with cracks. Figure 3.62 shows the grid panel used in the crack mapping while Figures 3.63 to 3.77 show the evolution of cracks for sections M, N, O, P, S and T. The first cracks observed on sections M and O were after 200,000 passes, on section P after 100,000 passes, and on section S and T at 46,000 passes. No cracks were observed at the end of loading on Section N.



Figure 3.62. Crack extent evaluation using a grid panel of squares

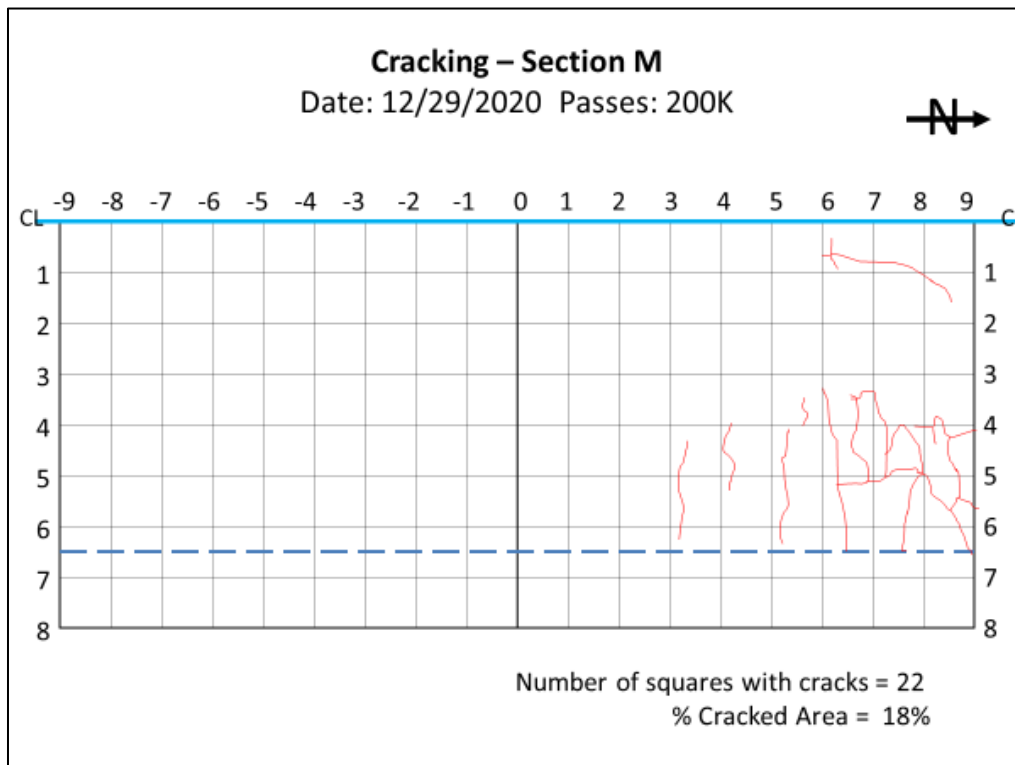


Figure 3.63 Cracking in section M after 200,000 passes

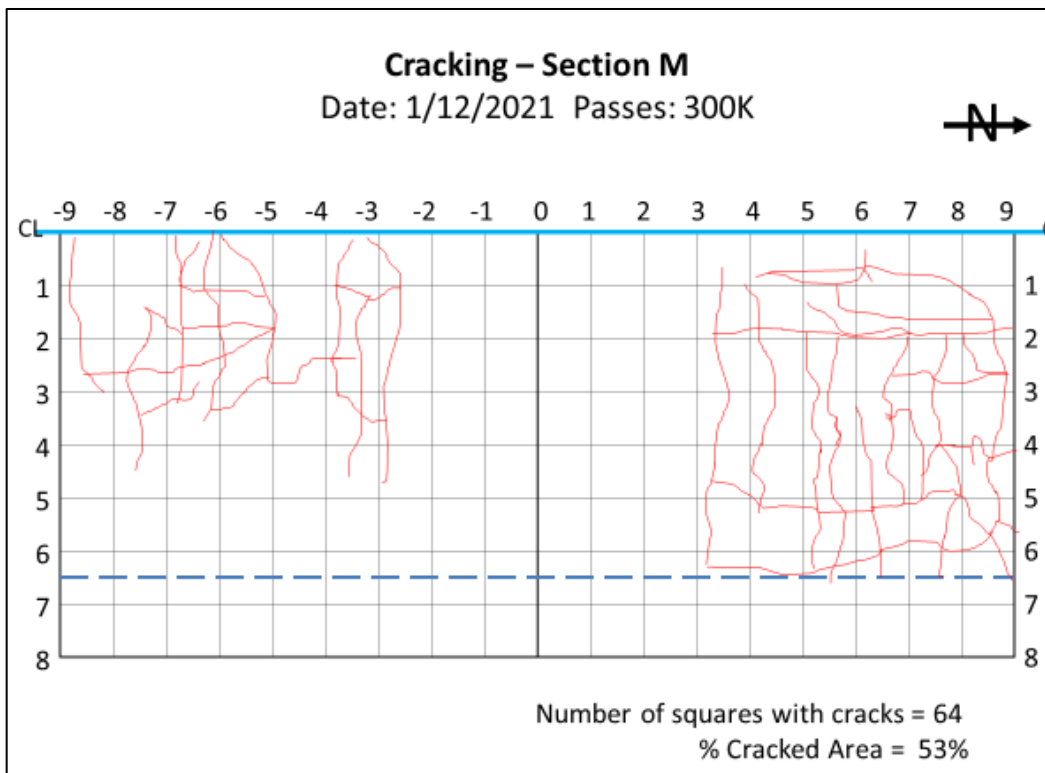


Figure 3.64 Cracking in section M after 300,000 passes

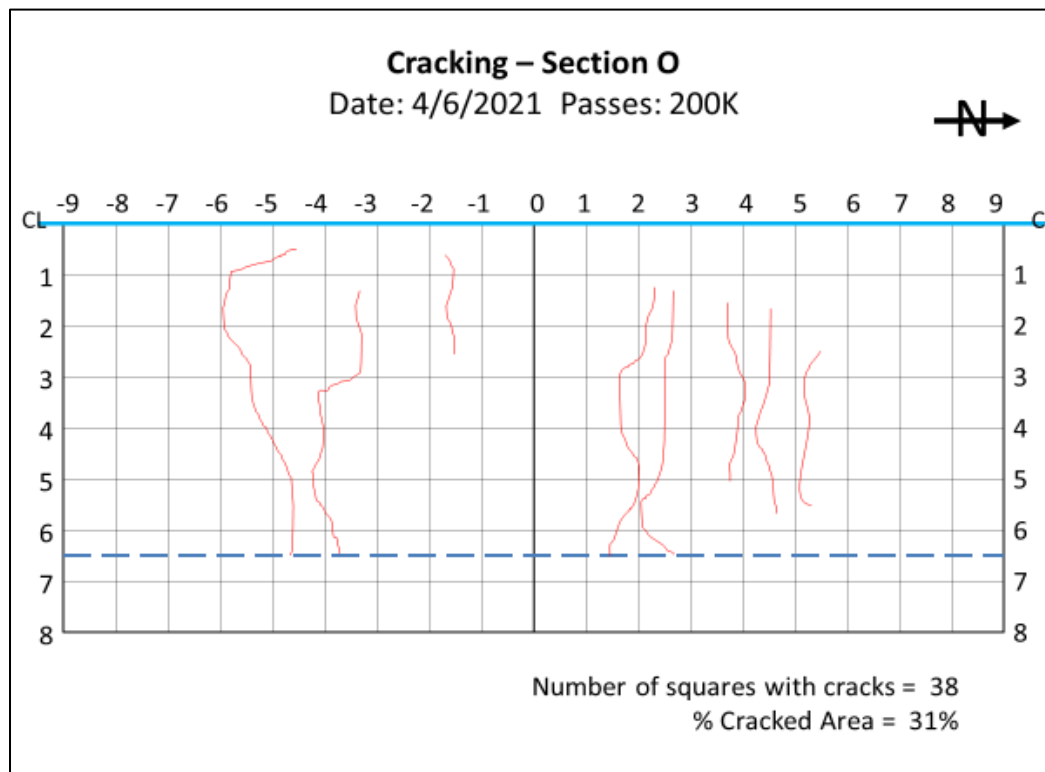


Figure 3.65 Cracking in section O after 200,000 passes

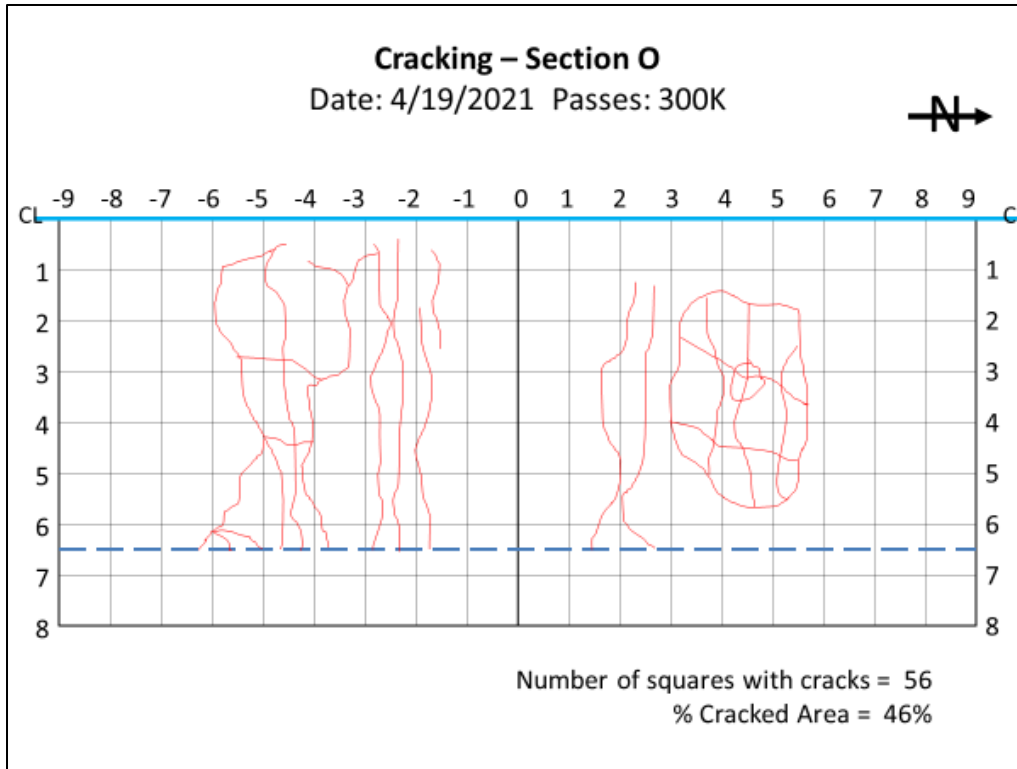


Figure 3.66 Cracking in section O after 300,000 passes

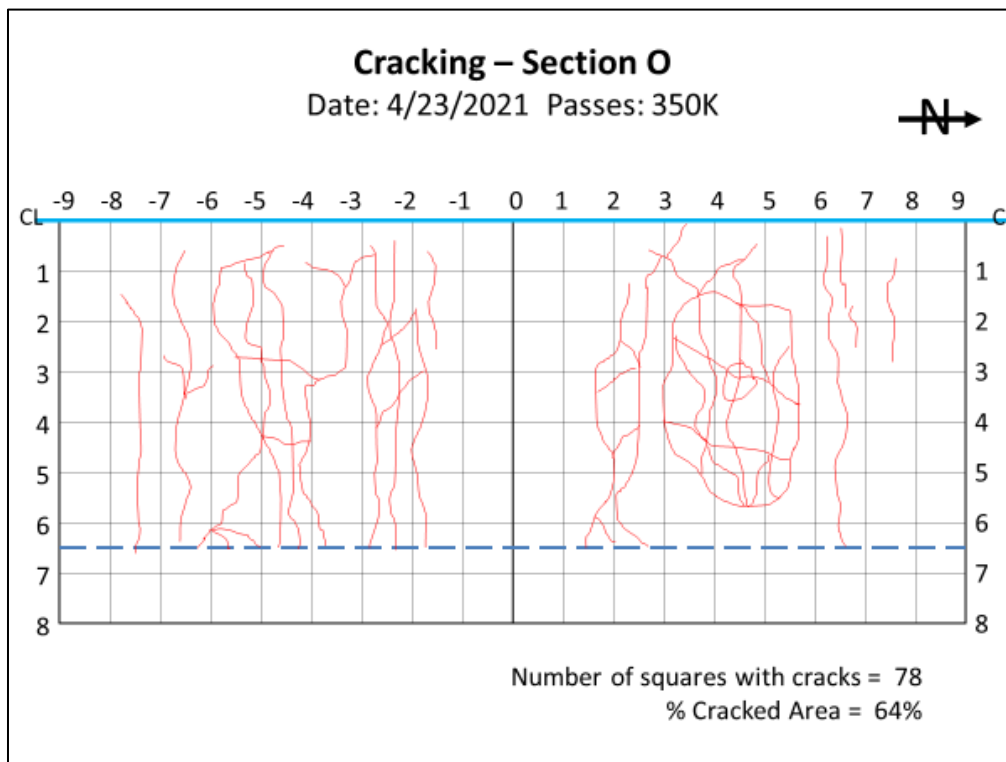


Figure 3.67 Cracking in section O after 350,000 passes

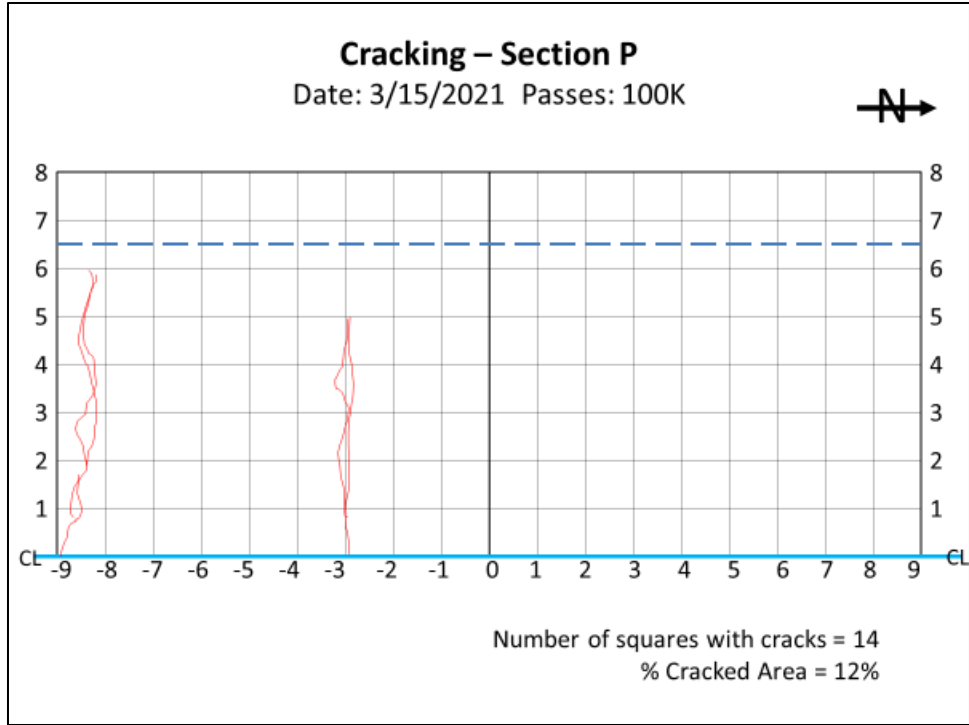


Figure 3.68 Cracking in section P after 100,000 passes

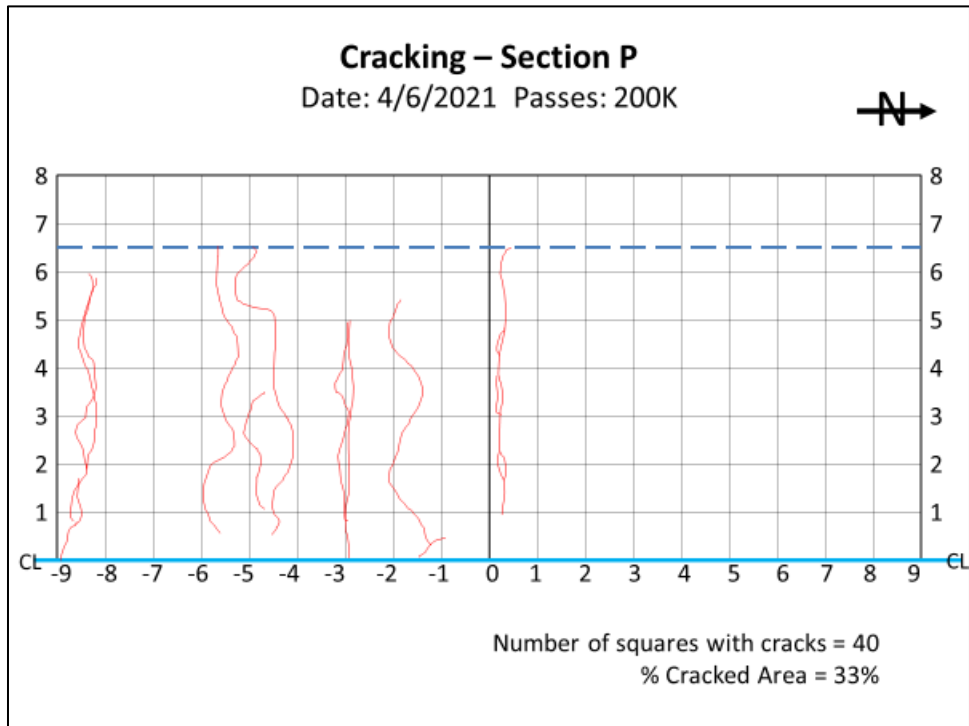


Figure 3.69 Cracking in section P after 200,000 passes

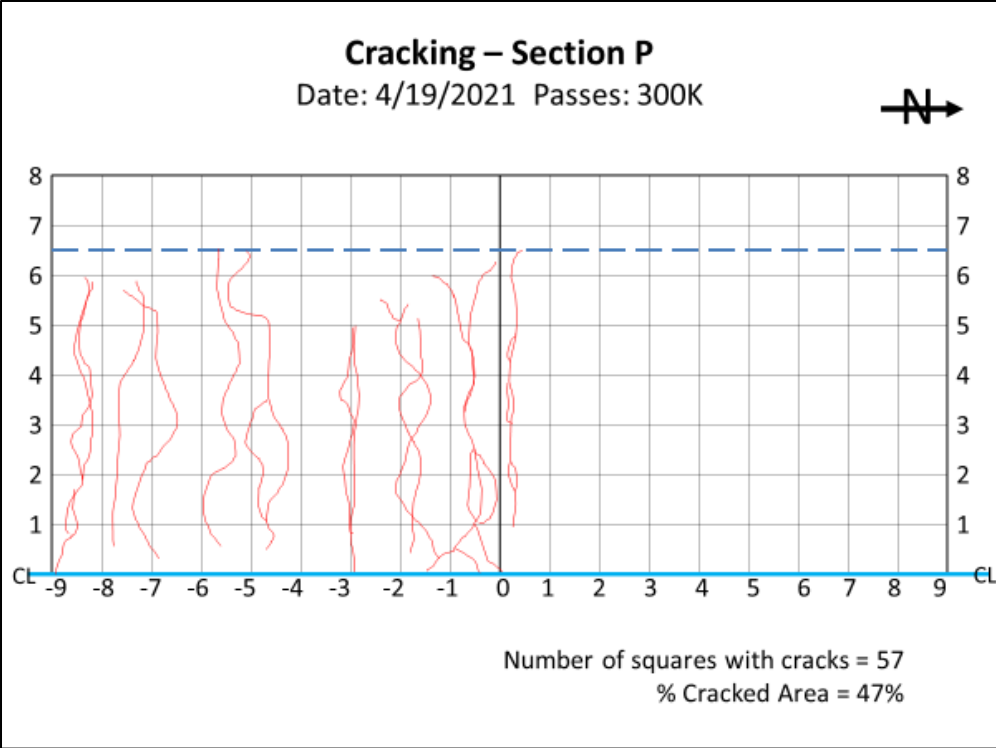


Figure 3.70 Cracking in section P after 300,000 passes

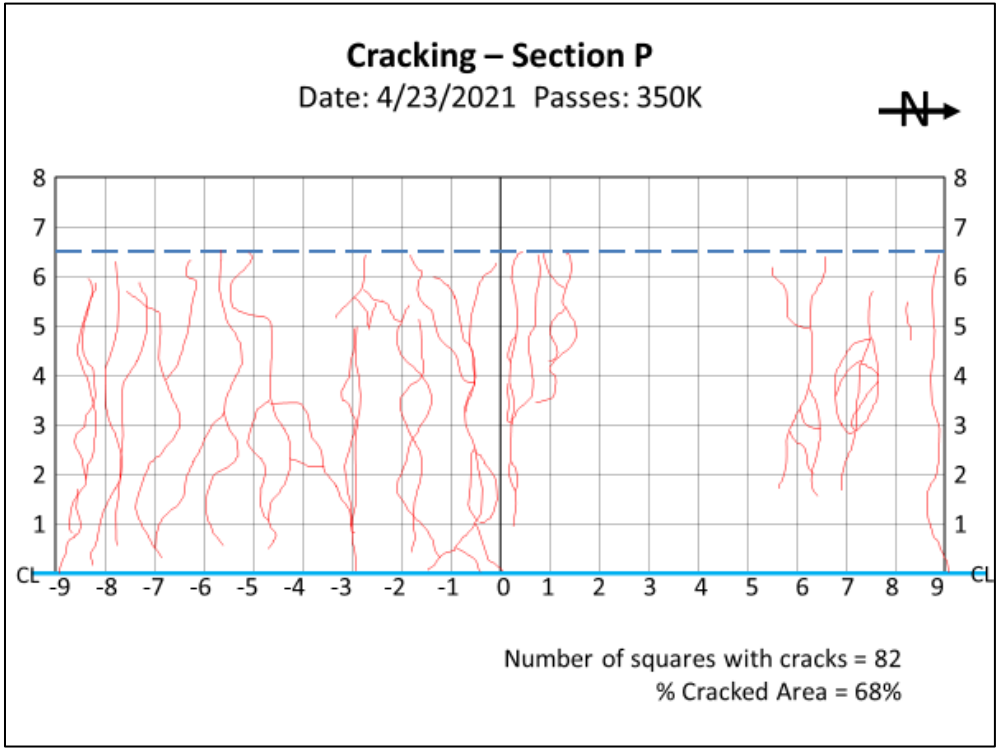


Figure 3.71 Cracking in section P after 350,000 passes

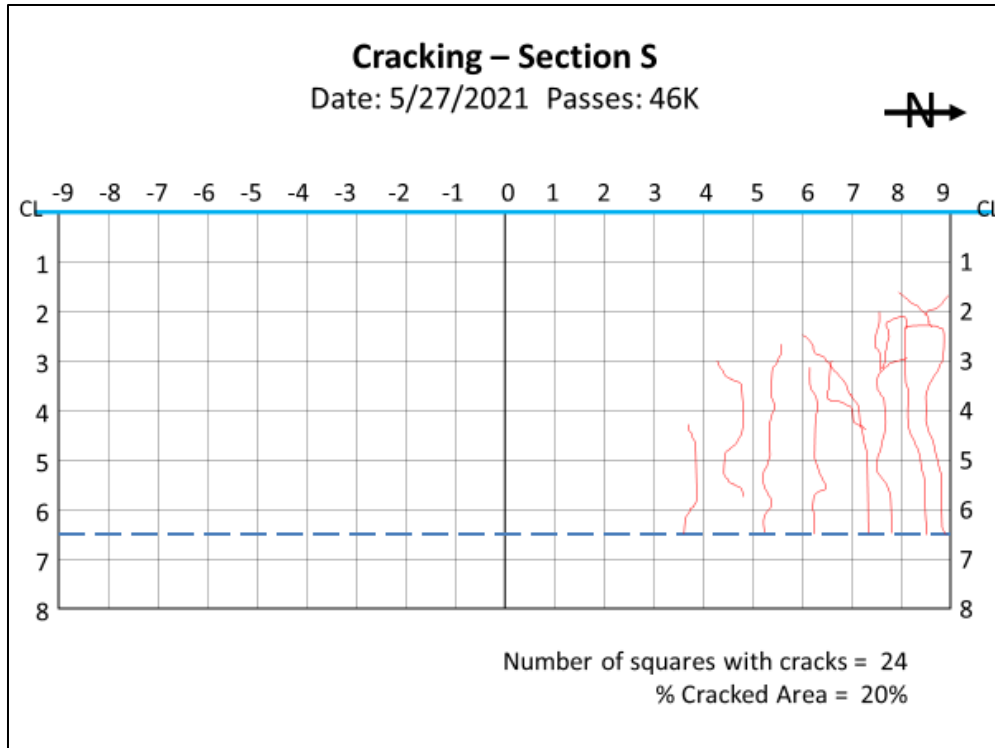


Figure 3.72 Cracking in section S after 46,000 passes

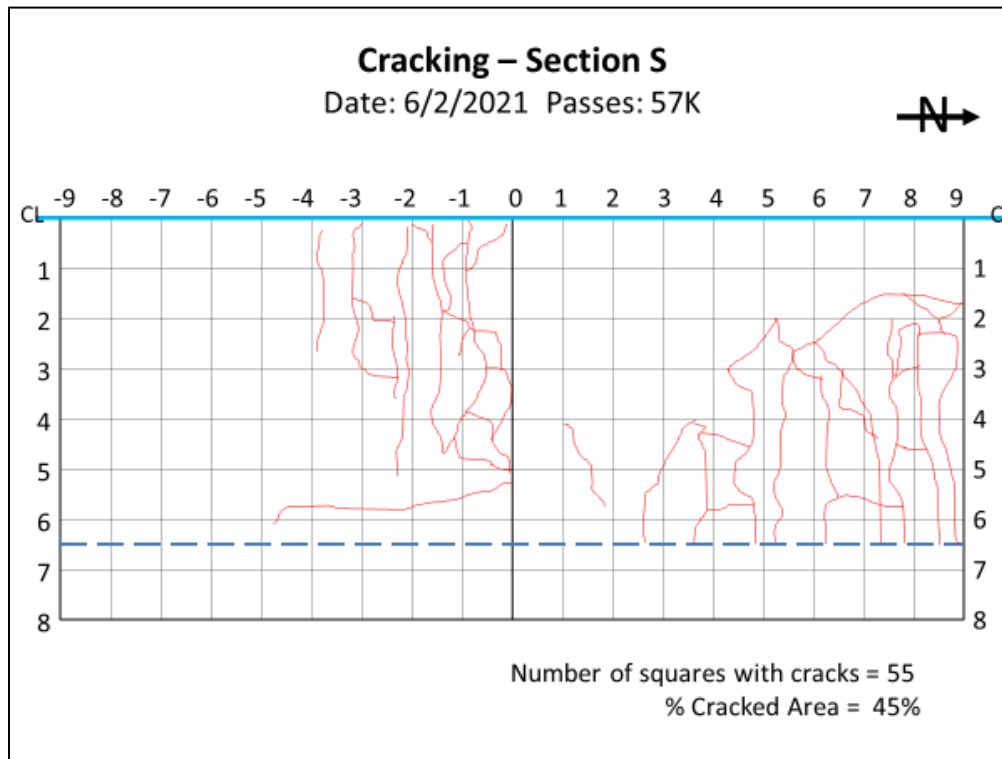


Figure 3.73 Cracking in section S after 57,000 passes

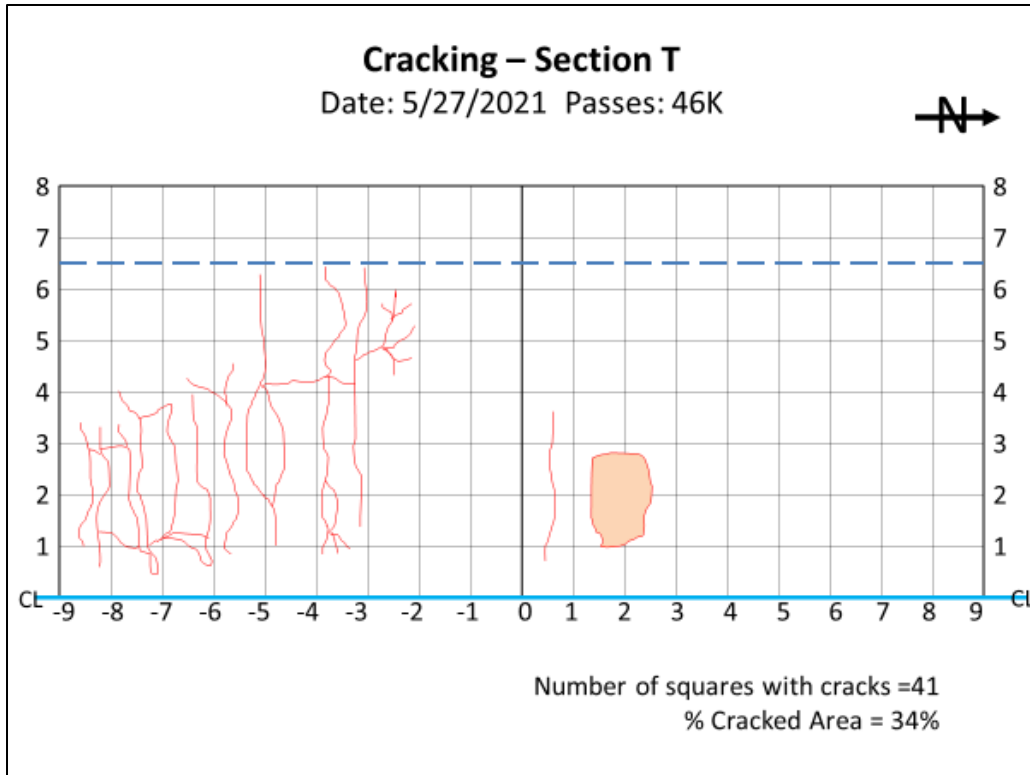


Figure 3.74 Cracking in section T after 46,000 passes

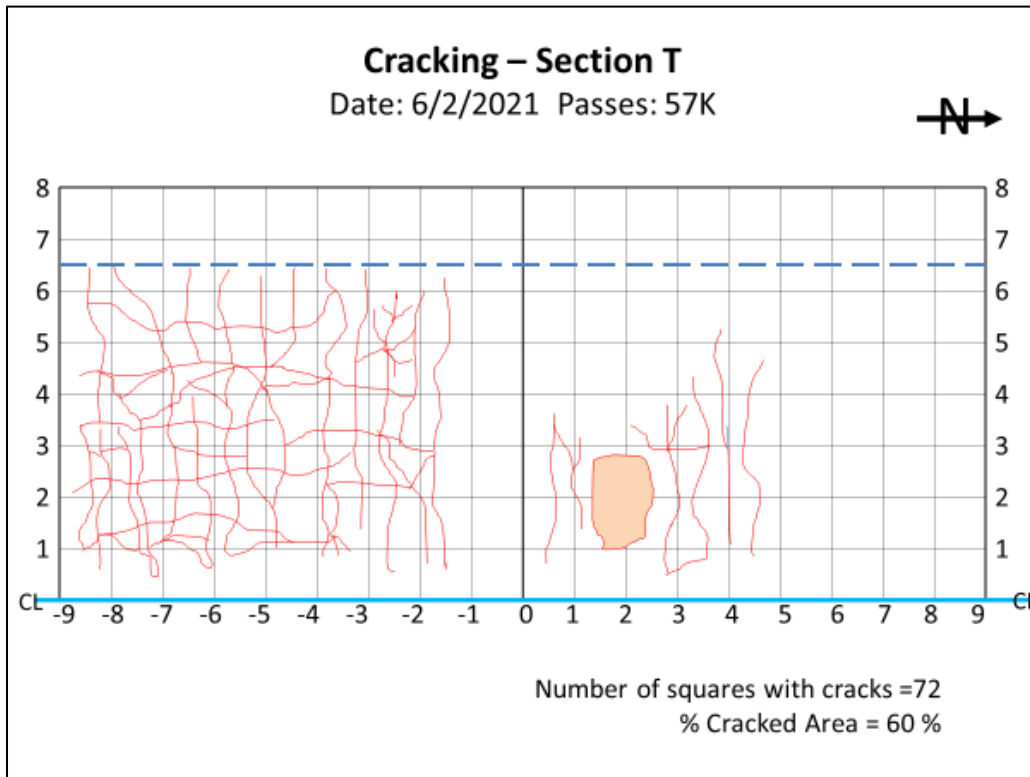


Figure 3.75 Cracking in section T after 57,000 passes

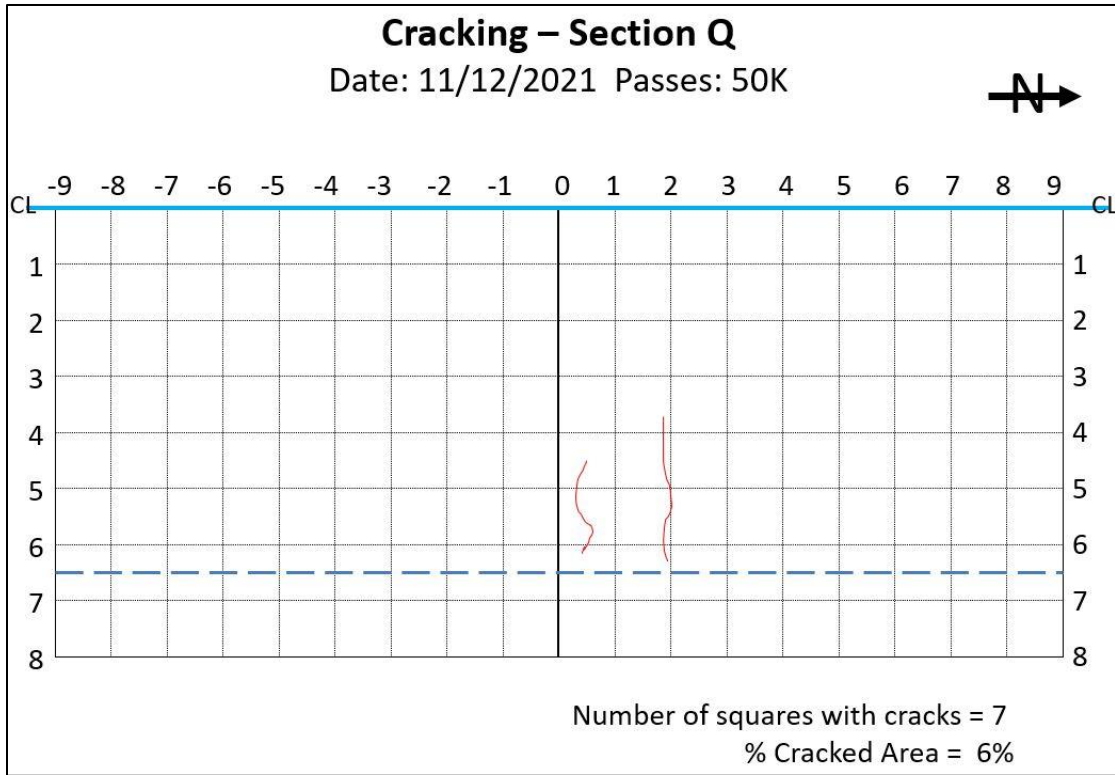


Figure 3.76 Cracking in section Q after 50,000 passes

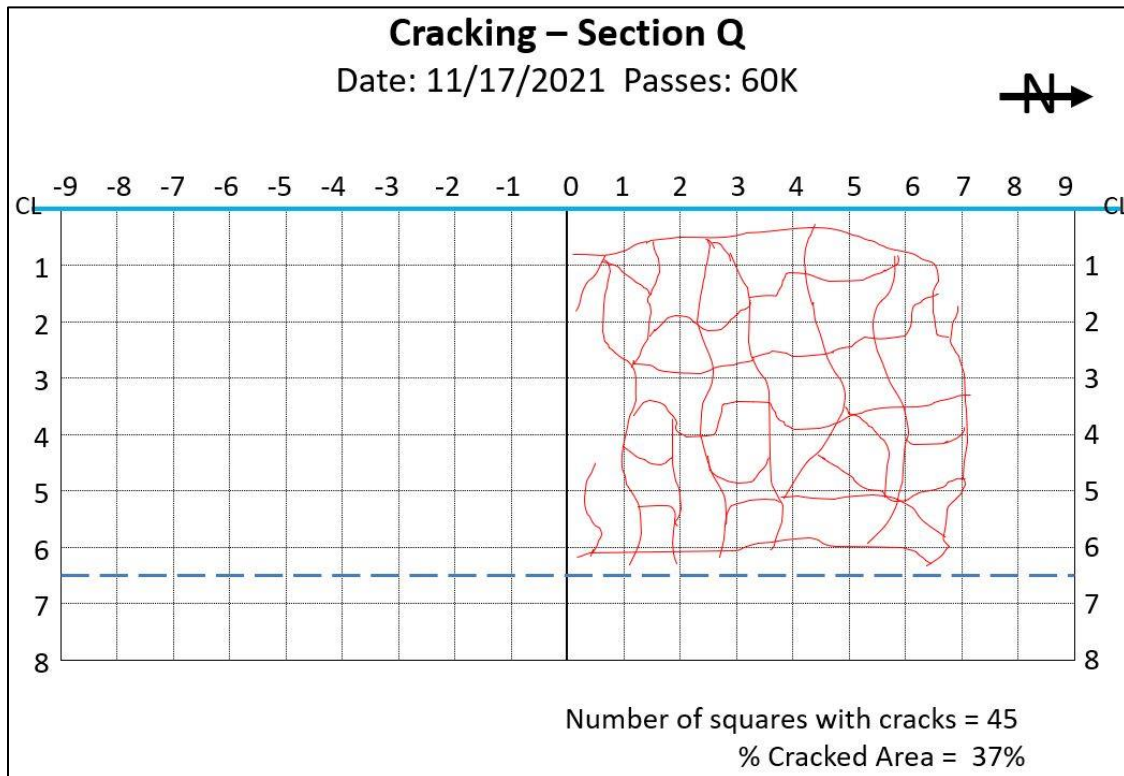


Figure 3.77 Cracking in section Q after 60,000 passes

Figure 3.78 summarizes the evolution of cracking extent with the number of load repetitions for each APT tested section while Figure 3.79 to 3.82 show photographs of the tested sections taken after failure. The surface cracking patterns were similar for all the sections: alligator cracking appeared in section M, O, P and T; moderate longitudinal cracking appeared in section M, low severity potholes occurred in section O and S and a combination of alligator cracking and transverse cracking was observed in section S. The alligator cracking was the most predominant distress in all sections. It may be associated with the fatigue resistance of the asphalt concrete layer and with the condition of the aggregate base and subgrade layers. Typically, a more brittle and thinner asphalt concrete layer or a weaker foundation produces more alligator cracking. Section T (Figure 3.82) had severe alligator cracking. Water bleeding and pumping occurred in section S and T. Water pumping is a clear indication of water moving freely within the pavement which leads to weakening of base and subgrade materials. As supported by the backcalculated moduli values (Table 3.8), all north sections seem to have a weaker foundation, which likely caused their premature cracking failure.

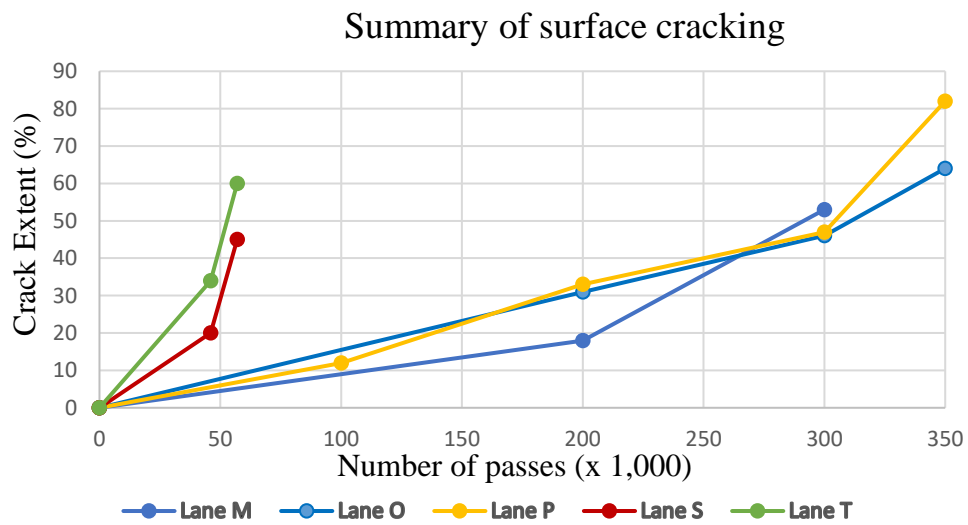


Figure 3.78 Cracking extent during APT loading



Figure 3.79 Surface cracking on section M after 300,000 passes



Figure 3.80 Surface cracking on section O after 350,000 passes



Figure 3.81 Surface cracking on section P after 350,000 passes



Figure 3.82 Surface cracking on section T (left) and S (right) after 57,000 passes

3.8 Strain Measurements

As discussed in *Subchapter 3.2.3 Strain gauge instrumentation*, the south sections, M, N, O and P were instrumented with two longitudinal and two transversal strain gauges each. Referring to Figure 3.19, each strain gauge was labeled as follows:

- The first letter indicates the section where the gauge was installed.
- The second letter indicates the orientation of the gauge; L for longitudinal and T for transverse.
- The number at the end indicates the replicate gauge. Number “1” was used for the gauges installed in the South end of the section and Number “2” was used for the gauges installed at the North end of the section.

Strain measurements under the passing axle were performed at 0, 5,000, 10,000, 25,000 and 100,000 and then every 100,000 passes of the PTM axle until failure. To collect the data, a National Instruments acquisition system was used. The data was collected at a frequency of 1,000 Hz. The strain measurements were recorded for two lateral positions, as depicted in Figure 3.82:

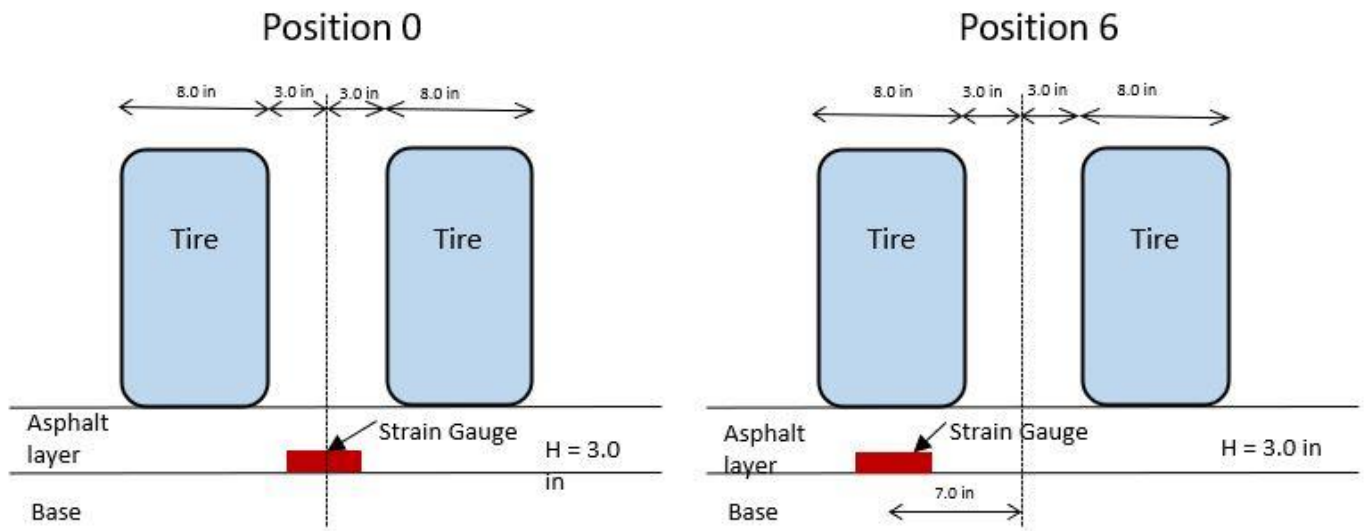


Figure 3.82 Wheel position during strain measurements

- Position 0 – The symmetry axis of the wheel was placed above the strain gauges. The two tires of the wheel straddled the sensors.
- Position 6 – The symmetry axis of the wheel was 6 inches away transversally from the gauges (one tire is passing above the strain gauges).

After the PTM was positioned in the desired position (Position 0 or 6), the machine was turned on and the loading was applied to the pavement. Data recording was started when the axle was at the north end of travel and started traveling south. The strain values were recorded for at least four cycles (eight passes). All the strain data was converted to Excel spreadsheet files for further analysis.

Using the change in output voltage recorded, the excitation voltage and the gauge factor, all the strain values were computed as follows:

$$\varepsilon = \frac{4 \times \Delta V_0}{V_i \times G_F}$$

Where:

ε - strain (microstrains)

ΔV_0 – change in output voltage

V_i – excitation voltage

G_F – gauge factor, 2.

Figure 3.83 shows the two typical shapes of the strain signal that were observed for one pass (half a cycle). Type 1 was observed for the longitudinal strain and Type 2 was observed for the transverse strain.

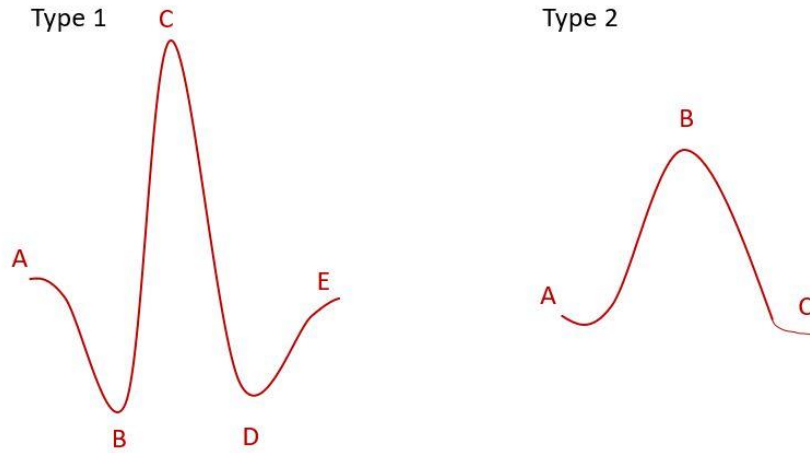


Figure 3.83 Typical strain signal observed

All strain signals were graphed, and the peak strain values were extracted. The average peak values are given in Table 3.13. No strains were recorded for Position 6 for sections M and N. Also, two out of the eight strain gauges installed on sections M and N malfunctioned: NL2 and MT1. For sections O and P, the strains were recorded in both position 0 and 6” and the results are showed in Table 3.14 and 3.15. Gauge OL1 was destroyed during the construction of the sections and gauge OT1 did not record realistic values. The detailed data is available in Appendix D-1. Peak 1 is the highest strain recorded when the buggy travels from North to South and Peak 2 is the maximum strain signal value recorded when the buggy travels from South to North.

Table 3.13 Longitudinal and transverse strain signals recorded for sections M and N

Passes	Position 0						
	Gauge	ML1	ML2	NL1	MT1	NT1	NT2
10k	Peak 1	150.3	244.4	391.8	55.0		210.9
	Peak 2	159.6	242.1	385.4	89.3		192.2
25k	Peak 1	279.6	365.8	345.3	167.7	186.8	75.7
	Peak 2	319.3	327.0	348.6	196.0	198.2	95.3
100k	Peak 1	193.1	407.5	223.8		75.2	191.1
	Peak 2	196.5	395.9	224.9		73.3	161.5
200k	Peak 1	147.93	433.8	300.3			298.4
	Peak 2	162.5	426.4	236.5			289.5
300k	Peak 1						
	Peak 2						

Table 3.14 Longitudinal strain signals recorded for sections O and P

Passes		Position 0			Position 6		
	Gauge	OL2	PL1	PL2	OL2	PL1	PL2
0	Peak 1	241.07	297.37	235.88	248.29	314.71	239.40
	Peak 2	223.44	257.82	241.68	225.90	271.52	246.09
5k	Peak 1	300.16	371.29	282.89	306.10	373.83	284.20
	Peak 2	266.51	318.16	290.25	275.37	330.57	291.45
10k	Peak 1	340.42	476.48	324.28			
	Peak 2	301.86	424.98	332.83			
25k	Peak 1	399.56	447.79	367.96	429.19	527.68	419.84
	Peak 2	367.79	441.65	373.49	401.17	469.13	423.92
100k	Peak 1	389.30		304.79	388.49	144.46	326.53
	Peak 2	380.75		334.26	386.32	166.04	358.62
200k	Peak 1	581.24	371.53	380.34	595.45	362.32	433.23
	Peak 2	515.77	390.28	379.88	544.22	424.61	432.12
300k	Peak 1	481.90		381.38	324.05	254.65	315.28
	Peak 2	502.84		416.90	318.87	257.49	367.50

Table 3.15 Transverse strain signals recorded for sections O and P

Passes		Position 0			Position 6		
	Gauge	OT2	PT1	PT2	OT2	PT1	PT2
0	Peak 1	69.56	89.90	154.02		93.84	184.61
	Peak 2	68.52	77.52	151.81		78.35	179.08
5k	Peak 1	40.17	112.62		-0.15	116.30	
	Peak 2	40.43	100.40		43.27	101.99	
10k	Peak 1		138.70	63.65			
	Peak 2		111.62	59.06			
25k	Peak 1	19.86	126.16	64.89	6.84	357.65	234.07
	Peak 2	39.17	106.29	66.16	208.65	318.94	245.85
100k	Peak 1		118.56		10.15	564.79	198.34
	Peak 2		99.43		188.97	523.57	208.21
200k	Peak 1				7.27	661.69	262.45
	Peak 2				294.17	692.10	250.70
300k	Peak 1						
	Peak 2						

Figure 3.84 illustrates an example of the longitudinal and transverse strain plotted for gauge OL2 and OT2 for one complete cycle. All the strain signals recorded are plotted and attached in Appendix D.

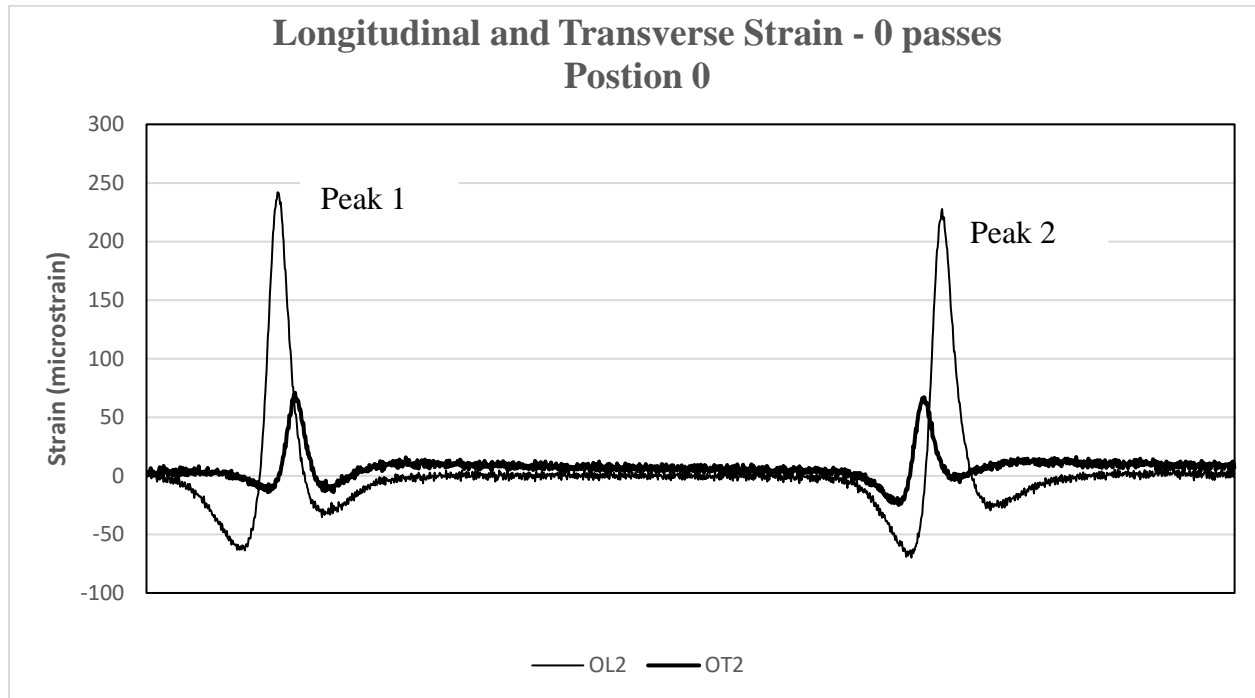


Figure 3.82 Example of longitudinal and transverse strain signal

The overall conclusions that can be drawn regarding the measured strain are:

- The longitudinal strains are always larger than the corresponding transverse strains.
- The recorded strains in Position 6" are slightly larger than the strains recorded in Position 0; larger strains are observed when the tire is right above the strain gauge.
- The measured horizontal strains at the bottom of the asphalt layer are higher for the thinner sections, section O has an average thickness of 2.93" and measured slightly higher strains than section M which has an average thickness of 3.19".
- The measured strains are sometimes different when the wheel moves toward South versus North, the difference being less than 20%.

CHAPTER 4. LABORATORY PERFORMANCE OF RAP MIXES

Cracking and rutting are the most frequent distresses that require the rehabilitation of asphalt pavements. The increasing use of recycled materials, recycling agents and binder additives makes the asphalt mix design even more complex. To improve the design of mixes containing RAP and RAS, many research efforts focused on measuring the properties of these mixes using a multitude of laboratory tests with the intent of predicting their field performance. Finding the laboratory test that best correlates to the field performance is crucial and much needed. Most of the laboratory tests currently used as performance measures in designing virgin asphalt mixes show satisfactory correlations with the field performance. The problematic issue arises when recycled materials are incorporated into asphalt concrete mixtures.

To find the laboratory tests that best predict the field performance resulted from this APT experiment, a series of laboratory tests were conducted and analyzed in terms of rutting and cracking resistance. To reduce the variability given by the gyratory compaction of the specimens in the laboratory, the tests were conducted on cores extracted from the in situ APT pavement test sections. Moreover, to better replicate the field conditions and to gather more information about the artificial ageing process applied to the sections, the cores were extracted from the artificially aged area. Initially, it was envisioned that the cores can be extracted right next from the APT trafficked area, but it was not feasible because of the limited space available. Therefore, the ageing chambers were placed right in the middle of all sections, in the transverse direction. The sections were aged for 5 weeks, and the temperature was measured continuously by thermocouples glued to the surface of the pavement under the infra-red lamps, the temperature data is shown in Figure 4.1.

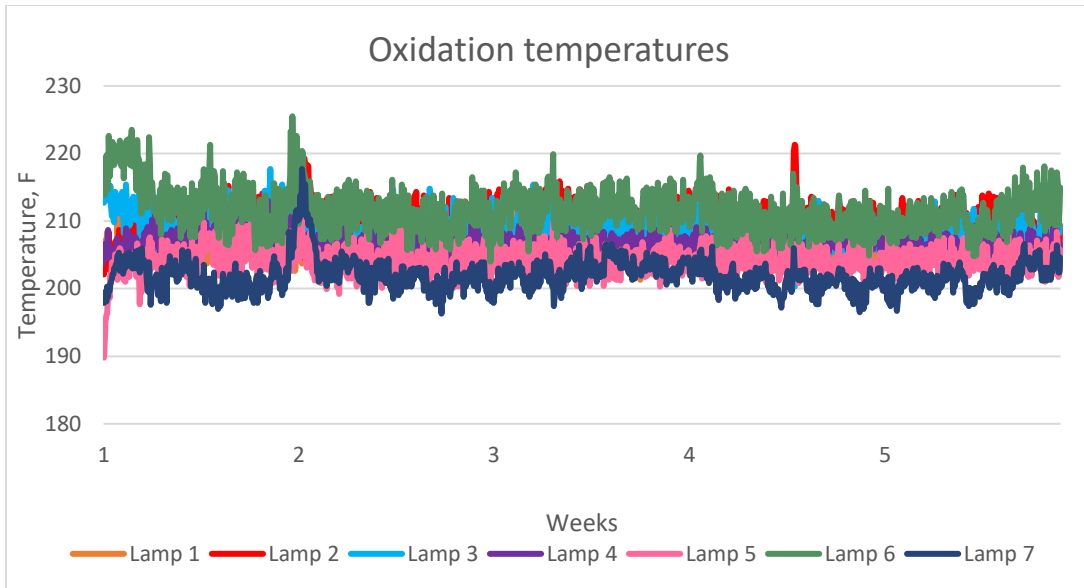


Figure 4.1 Temperature data recorded during the artificial oxidation

After the aging was done, the boxes were removed, and the sections were let to cool off one week before coring. A total of 224 cores were extracted and prepared for testing. After extraction, the holes were sealed with bitumen emulsion and covered with cold patch asphalt mix to prevent intrusion of water underlayers. This was necessary since the North sections were under APT testing.



Figure 4.2 Sequence of covering the core holes

4.1 Evaluation of Rutting Resistance

4.1.1 Hamburg Wheel Track Test (HWTT)

The Hamburg wheel-tracking test is commonly used to evaluate the rutting resistance and moisture susceptibility of asphalt mixtures. Many State Departments of Transportation currently require HWTT in their mix design specifications. Some DOTs use this test only as a rutting test and some of them use it as a combined rutting and moisture damage test. Texas DOT uses this test as a performance test when designing balanced asphalt mixtures.

In this test, two sets of cylindrical specimens or field cores are placed in mounting trays (Figure 4.3) and submerged in a hot water bath. A steel wheel with a load of 158 lbs. applies repetitive passes over the specimens. The rate of load application is 52 passes per minute. To measure the rut depth along the center of the wheel path, two linear variable differential transducers are mounted on each side of the device.

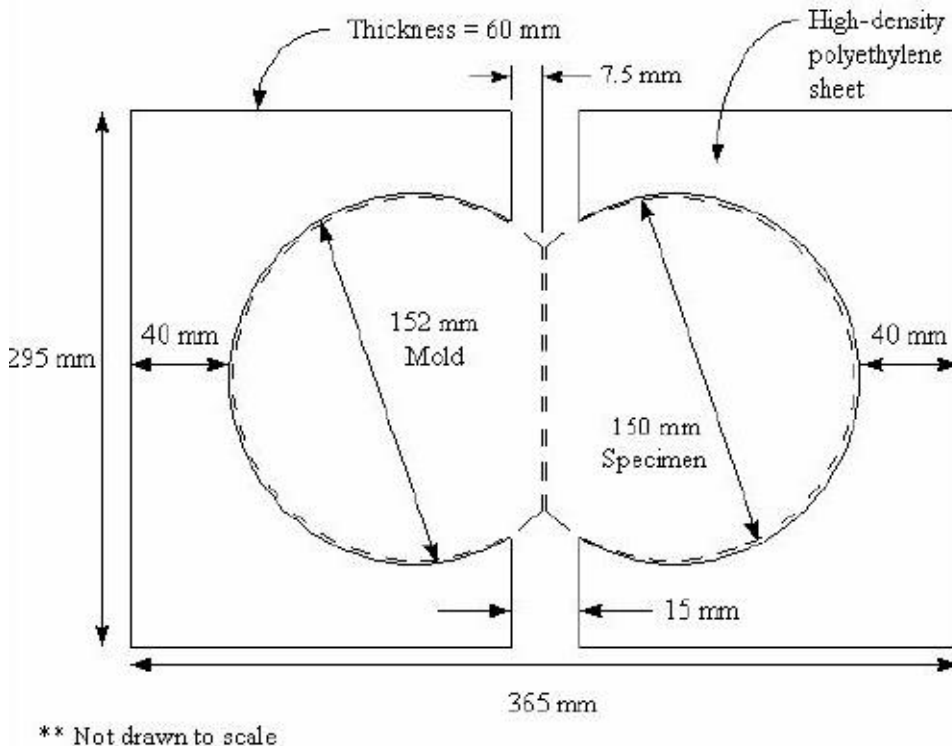


Figure 4.3 Top view of test specimen configuration for the HWT device (Tex-242-F)

The AASHTO specification, T324, does not mention the number and locations of rut depth reading; therefore, different practices are used among different States. Table 4.1 shows the HWT requirements used in Texas. Figure 4.4 shows the schematic rut depth measurement points according to Tex-242-F.

Table 4.1 Hamburg Wheel Test Requirements

High-Temperature Binder Grade	Minimum # of <u>Passes at 12.5 mm</u> Rut depth, tested at 50°C
PG 64 or lower	10,000
PG 70	15,000
PG 76 or higher	20,000

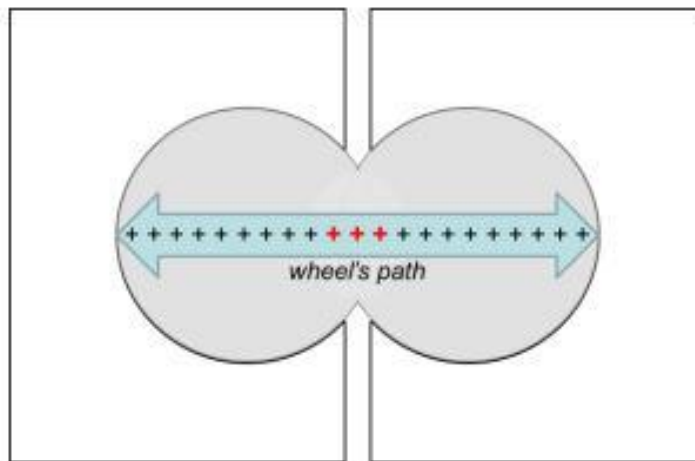


Figure 4.4 Schematic rut depth measurement points

Because the cores were extracted using a 6-inch diameter core drill bit, they did not fit in the 150mm diameter mold, therefore a new set of four molds were fabricated to accommodate the 6-inch specimens. Two pairs (four specimens) were tested for each mix. The samples were cut to a thickness of 62 mm using a saw cutter equipped with a diamond blade (Figure 4.5). After trimming the samples to the specified thickness, the bulk specific gravity test was performed according to the AASHTO T166 test protocol. The bulk specific gravity and the theoretical maximum specific gravity were used to calculate the air voids percentage of the mix, they are given in Table 4.2. The samples were paired for testing based on the air void percentage and loaded into the HWT. The

failure criterion is selected based on the PG grade, according to the TxDOT specifications. All samples were tested at 50°C in accordance with TxDOT specifications. The samples are considered to pass the Hamburg test if the rut depth at 10,000 passes (for Sections M, P, S, T and R where a PG64 was used) or 15,000 passes (for Sections N and O where a PG70 was used) is less than 12.5mm. Figure 4.6 shows for all mixes the average rut depth obtained from the HWTT.



Figure 4.5 Cutting of the specimens and testing assembling in the HWT device

Because Sections M and Q have the same mix in the top layer and there is no significant difference in the air content percentage, the test was conducted only on the samples extracted from section M. Appendix E contains the rut depth graphs for each lane individually. The results obtained by the pairs of samples for a given section show overall a good repeatability of the results, except section O. As seen in Figure E3, there is a 2 mm rut depth difference between Pair 1 and 2. This difference can be attributed to the high air void content in Sample O4 (6.75%) compared to the air void percentage from Sample O1, O2 and O3 (4.46%, 4.25% respectively 4.45%). The

highest rut depth recorded was for section T (9.93 mm), and the smallest rut recorded was for section S, (3.43 mm).

Table 4.2 Sample dimensions and characteristics

Sample	Dry (g)	Water (g)	SSD (G)	Gmb	Gmm	AV (%)	Height (mm)	Diameter (mm)
M1	2,860.0	1,717.7	2,863.9	2.50	2.59	3.81	64.1	151.8
M2	2,849.8	1,710.7	2,852.7	2.50	2.59	3.80	64.0	151.9
M3	2,878.3	1,728.5	2,883.9	2.49	2.59	3.96	64.7	151.4
M4	2,894.2	1,741.4	2,898.7	2.50	2.59	3.59	64.9	151.4
N1	2,870.4	1,739.8	2,874.2	2.53	2.62	3.50	64.1	151.6
N2	2,789.1	1,654.1	2,802.4	2.43	2.62	7.36	65.2	151.1
N3	2,872.7	1,732.7	2,879.1	2.51	2.62	4.43	64.4	151.7
N4	2,717.2	1,640.7	2,720.9	2.52	2.62	4.06	60.4	151.2
O1	2,773.9	1,663.2	2,777.7	2.49	2.61	4.46	62.5	151.6
O2	2,854.6	1,715.1	2,859.6	2.49	2.61	4.25	63.9	154.6
O3	2,861.3	1,720.6	2,870.1	2.49	2.61	4.45	62.5	151.7
O4	2,803.5	1,744.3	2,898.4	2.43	2.61	6.75	62.6	151.5
P1	2,755.7	1,667.6	2,757.6	2.53	2.61	3.14	63.2	148.8
P2	2,802.4	1,701.2	2,804.4	2.54	2.61	2.67	62.6	148.8
P3	2,778.9	1,684.8	2,783.1	2.53	2.61	3.06	62.9	148.6
P4	2,612.5	1,574.7	2,614.5	2.51	2.61	3.74	62.0	148.3
Q1	2,782.5	1,675.2	2,786.4	2.50	2.59	3.47	62.4	152.2
Q2	2,899.0	1,748.9	2,904.1	2.51	2.59	3.26	64.5	151.5
Q3	2,811.3	1,677.8	2,817.6	2.47	2.59	4.92	64.0	152.1
Q4	2,774.2	1,668.4	2,778.8	2.50	2.59	3.69	61.5	152.1
R1	2,735.9	1,636.9	2,741.8	2.48	2.59	4.32	62.2	151.7
R2	2,821.8	1,683.7	2,825.3	2.47	2.59	4.49	64.6	151.5
R3	2,761.1	1,657.1	2,765.7	2.49	2.59	3.76	62.2	151.4
R4	2,740.2	1,637.8	2,743.7	2.48	2.59	4.26	61.8	151.1
S1	2,772.7	1,665.8	2,783.8	2.48	2.60	4.76	63.0	151.2
S2	2,717.5	1,613.1	2,732.5	2.43	2.60	6.77	63.0	151.0
S3	2,793.8	1,671.1	2,803.8	2.47	2.60	5.28	64.0	151.3
S4	2,860.5	1,716.5	2,869.8	2.48	2.60	4.75	64.8	151.3
T1	2,746.5	1,658.6	2,749.8	2.52	2.59	2.63	64.2	149.6
T2	2,695.0	1,620.2	2,699.5	2.50	2.59	3.40	61.6	148.8
T3	2,705.6	1,625.7	2,708.6	2.50	2.59	3.34	63.0	148.5
T4	2,263.6	1,597.9	2,667.2	2.12	2.59	3.68	62.6	148.3

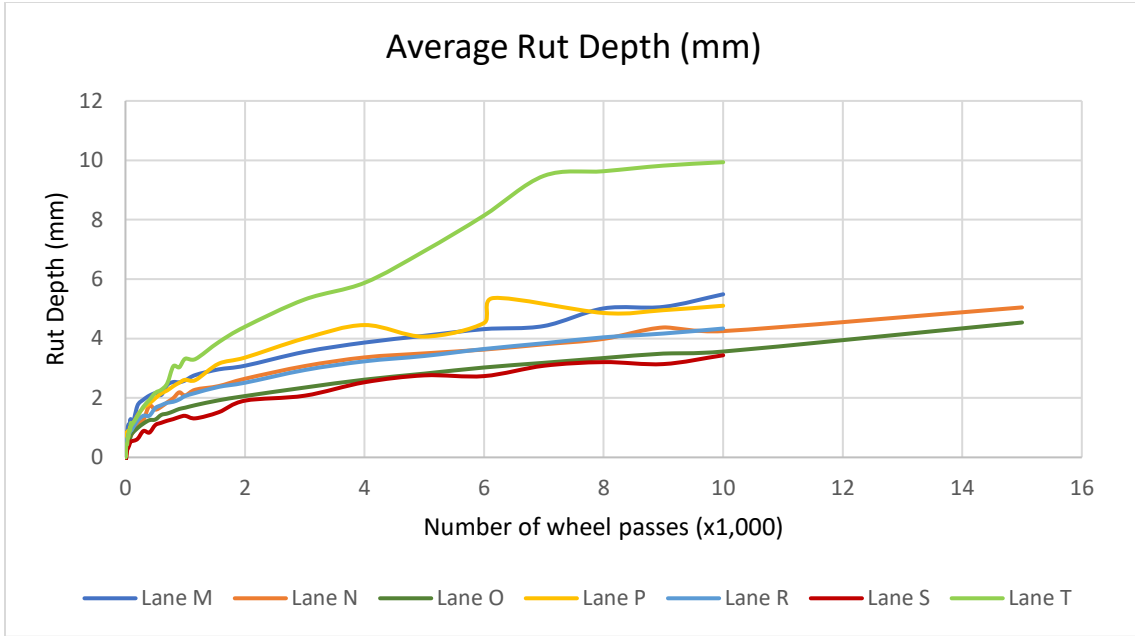


Figure 4.6 Average central rut depth for all mixes

The HWTT was performed on unaged samples, cored after the construction of the sections to examine the effect of artificial aging on the asphalt mixes. Figure 4.7 compares the rut depths obtained from the unaged compacted samples and aged field cores.

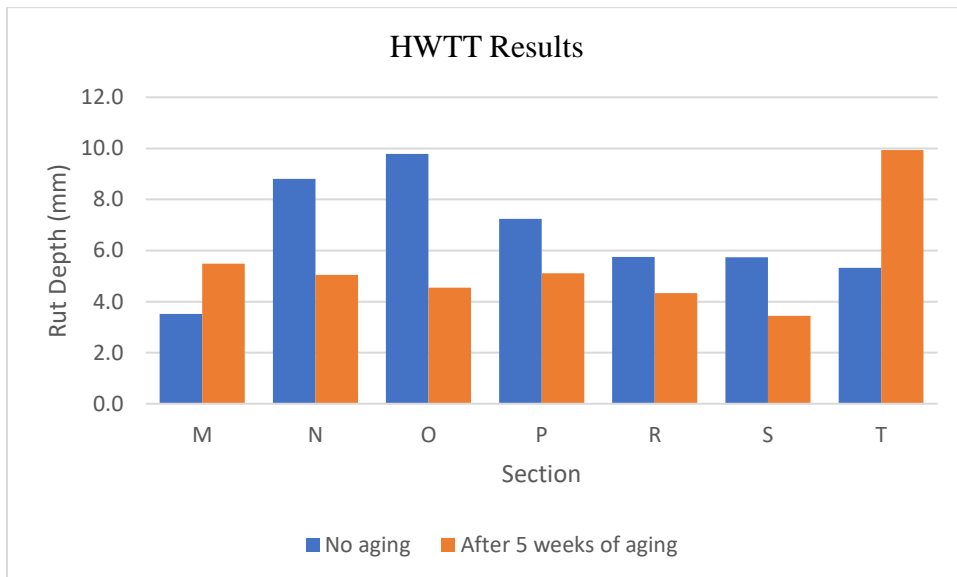


Figure 4.7 HWTT Rut Depths recorded for aged and unaged samples

As expected, artificial aging increased the resistance to rutting for most sections. The virgin mix placed on section N recorded an increase in resistance to rutting of 43%. Also, the mixes containing recycled materials and placed on O, P, R, and S showed an increase of 54%, 29%, 25% and 40%, respectively. The reference mix, 15%RAP 2%RAS showed a decrease in rutting resistance of 36%. This was not anticipated since aging makes the asphalt stiffer, therefore more resistant to permanent deformation. In the same manner, the mix placed on section T showed a decrease in resistance to rutting of 46%.

4.1.2 Dynamic Modulus Test

Another test performed was the Dynamic Modulus Test. According to AASHTO, based on the Maximum Aggregate Size used in the asphalt mixes, the sample height for this test must be 6.0 inches. Since the thickness of the constructed asphalt layers is only 3.0 inches, samples were compacted in the laboratory using the Superpave Gyratory compactor on plant asphalt mixes collected during the paving process. Three trials of compaction were required to achieve similar air voids as the voids in the constructed field sections. As recommended by AASHTO T-320, the asphalt mix was first compacted to 1.0 % air void percentage higher than the target percentage of the test specimens. It turns out that 1.0 % percent offset was not enough to achieve an appropriate percentage of air voids in the test specimen. This is because the air void content of the test specimen reduces after the cutting of the top and bottom ends of the compacted specimen. The air void percentage was increased in 1.0 % increments and similar air void content as the one present in the field sections was achieved for a 3.0% offset.

The samples were first compacted using a 150 mm diameter mold and then a 100 mm diameter specimen was extracted. The testing specimen has a diameter of 100 mm and a height of

150 mm. For each section, three samples were prepared and tested at different temperatures, 15°C, 20°C and 25°C. Figure 4.8 shows the preparation of the testing specimens starting from compaction to assembling in the UTM 25 test equipment. Table 4.3 summarizes the characteristics of the test specimens.

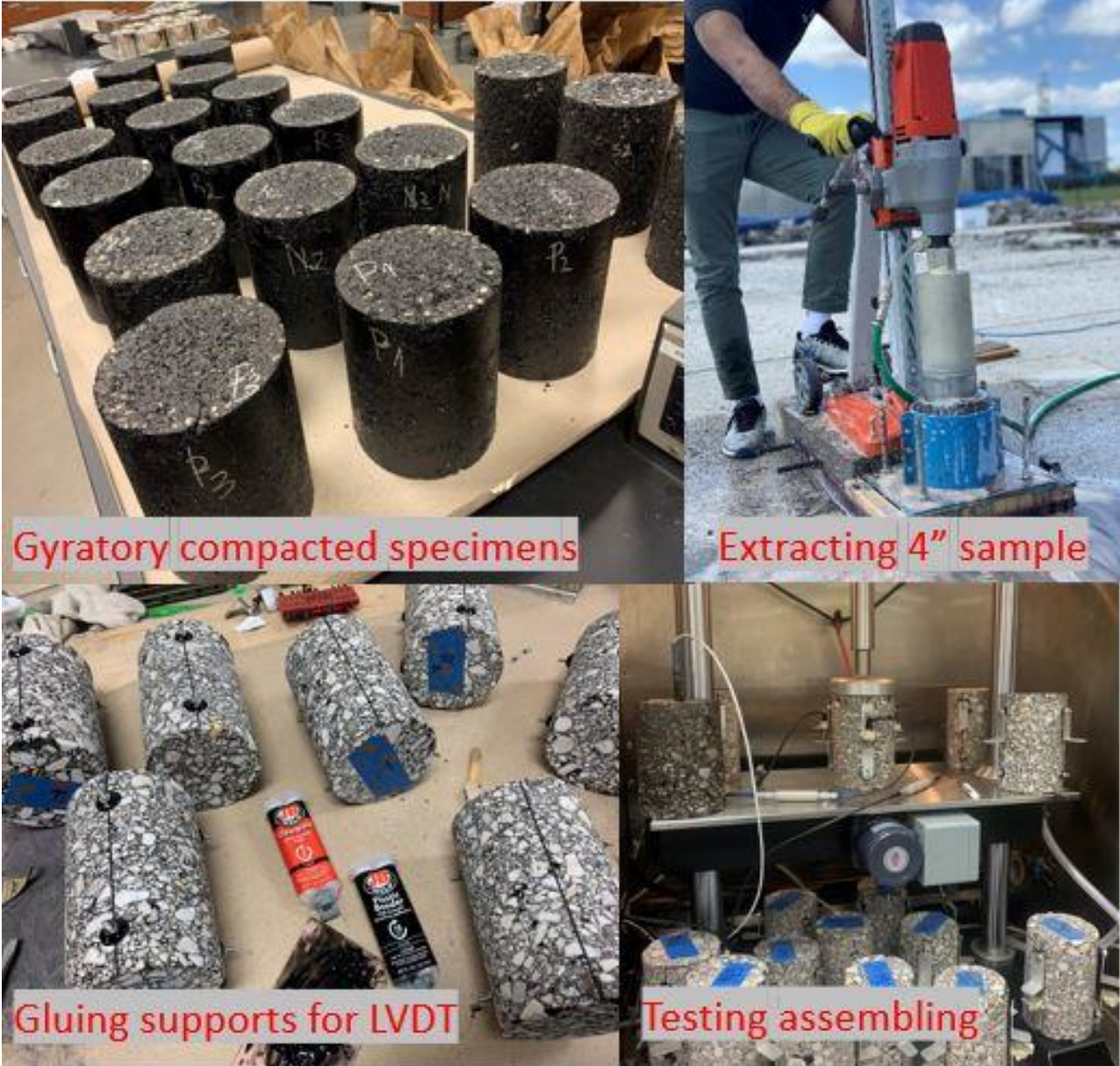


Figure 4.8 Sample preparation for the Dynamic Modulus Test

Table 4.3 Air Voids of the Dynamic Modulus specimens

Sample	Dry (g)	Water (g)	SSD (G)	Gmb	Gmm	AV (%)
M1	2,999.4	1,808.4	3,002.5	2.51	2.59	3.17
M2	2,984.6	1,798.9	2,987.9	2.51	2.59	3.23
M3	2,957.8	1,784.0	2,961.0	2.51	2.59	3.12
N1	3,019.7	1,837.3	3,022.3	2.55	2.62	2.81
N2	3,055.0	1,855.8	3,058.0	2.54	2.62	3.08
N3	3,038.9	1,847.0	3,041.7	2.54	2.62	2.99
O1	2,955.6	1,761.0	2,961.4	2.46	2.60	5.48
O2	2,979.8	1,788.2	2,983.4	2.49	2.60	4.29
O3	2,992.9	1,791.5	2,997.4	2.48	2.60	4.73
P1	2,977.5	1,792.7	2,980.7	2.51	2.61	3.97
P2	2,991.2	1,805.4	2,994.5	2.52	2.61	3.62
P3	2,972.2	1,789.8	2,975.8	2.51	2.61	3.98
Q1	2,999.4	1,808.4	3,002.5	2.51	2.59	3.17
Q2	2,984.6	1,798.9	2,987.9	2.51	2.59	3.23
Q3	2,957.8	1,784.0	2,961.0	2.51	2.59	3.12
R1	2,974.3	1,793.7	2,975.9	2.52	2.58	2.79
R2	2,971.5	1,795.2	2,972.9	2.52	2.58	2.51
R3	2,966.4	1,788.1	2,968.3	2.51	2.58	2.88
S1	2,982.6	1,800.0	2,984.1	2.52	2.60	3.27
S2	2,972.4	1,791.1	2,974.0	2.51	2.60	3.51
S3	2,995.8	1,807.9	2,997.5	2.52	2.60	3.29
T1	2,903.5	1,731.3	2,906.6	2.47	2.58	4.43
T2	2,939.4	1,753.8	2,942.1	2.47	2.58	4.31
T3	2,921.2	1,742.0	2,923.2	2.47	2.58	4.33

In the Dynamic Modulus Test, a sinusoidal axial compressive load is applied to the cylindrical specimen at a sweep of loading frequencies. During testing, the UTM system measures the vertical stress and the resulting vertical compression strain. The dynamic resilient modulus is then calculated by dividing the peak-to-peak vertical compressive stress to the peak-to-peak vertical strain. The dynamic load and stress, microstrain, dynamic modulus, maximum and minimum load displacement, temperature, duration of test and phase angle are recorded periodically during testing. Figure 4.9 to 4.11 summarizes the averaged results obtained from the Dynamic Modulus test for 15°C, 20°C and 25°C.

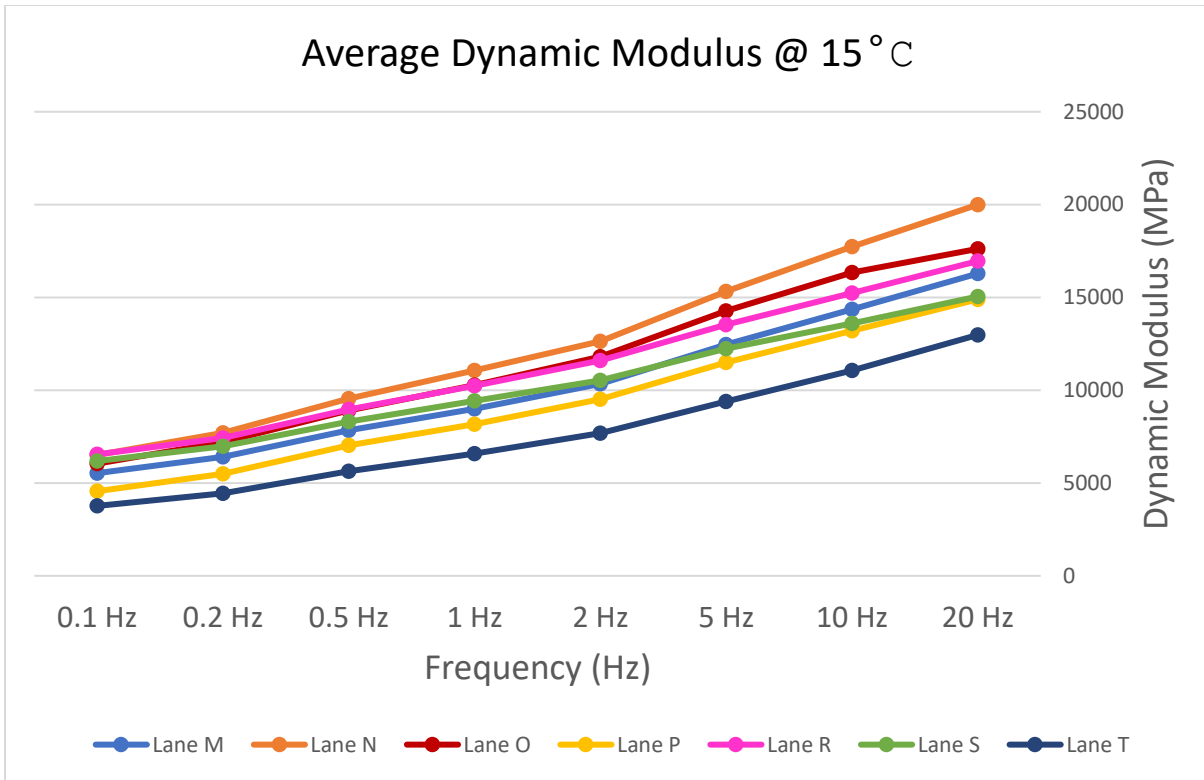


Figure 4.9 Dynamic Modulus Results @15°C

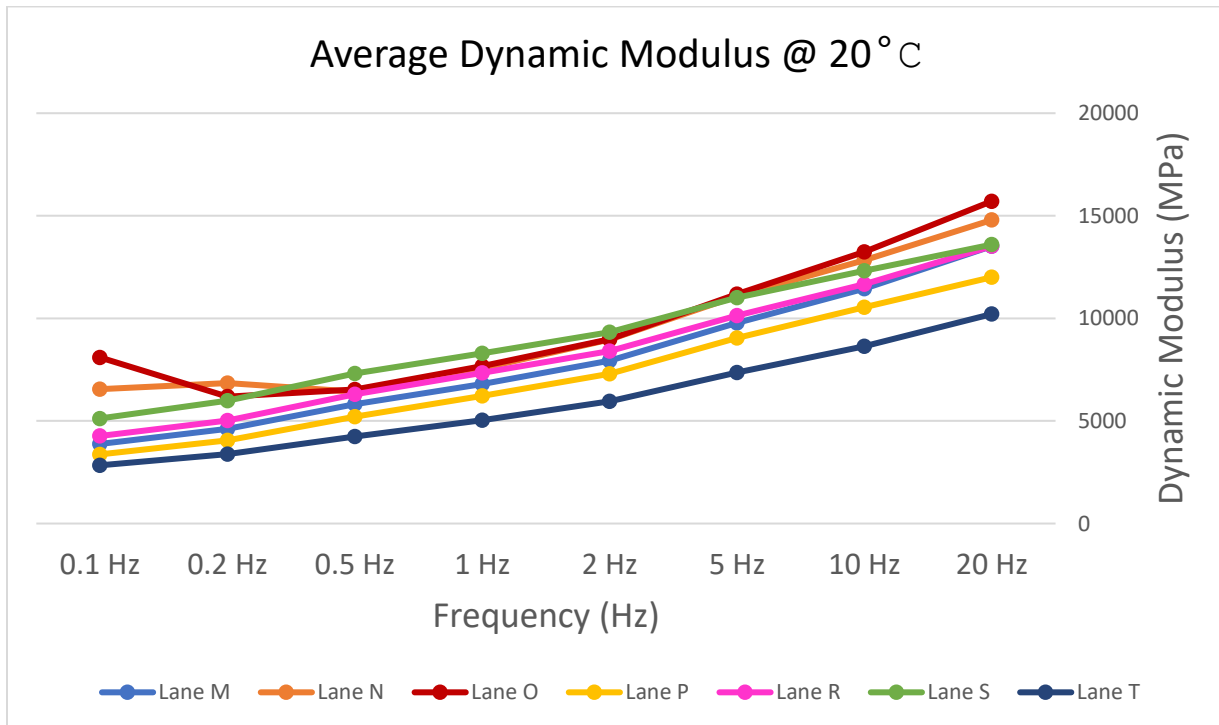


Figure 4.10 Dynamic Modulus Results @20°C

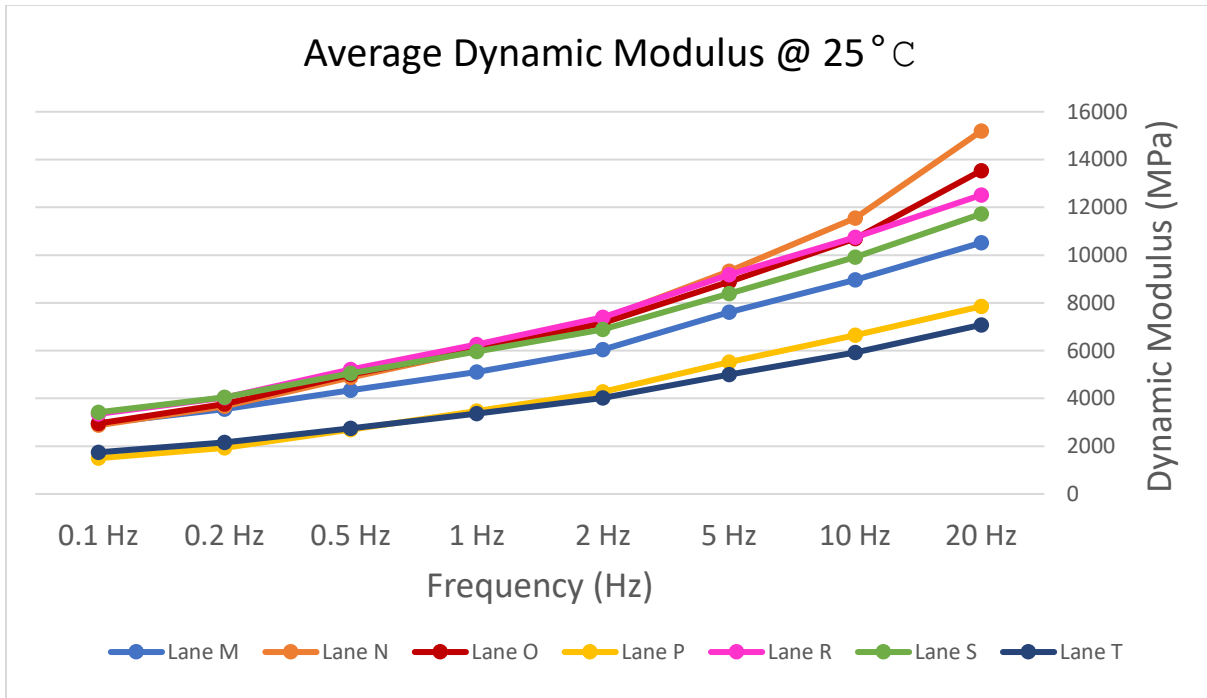


Figure 4.11 Dynamic Modulus Results @25°C

As expected, the dynamic modulus decreased with an increase in temperature and increased with loading frequency. For an increase in temperature of 5°C, the dynamic modulus decreased the least for section S by approximately 12% and increased the most for section R by 28%. For an increase in temperature of 10°C, the dynamic modulus decreased the least for section S by circa 35% and increased the most for section P by 57%. An increase in the loading frequency, from 0.1 Hz to 20 Hz for a test performed at 15°C, 20°C and 25°C increases the dynamic modulus value by 66%, 64% and respectively 76%. Figures 4.12 to 4.14 summarize the averaged phase angle values obtained from the Dynamic Modulus test for 15°C, 20°C and 25°C.

The phase angle increased with an increase in temperature and decreased with loading frequency. For an increase in temperature of 5°C, the phase angle increased the least for section N by approximately 5% and increased the most for section S by 30%.

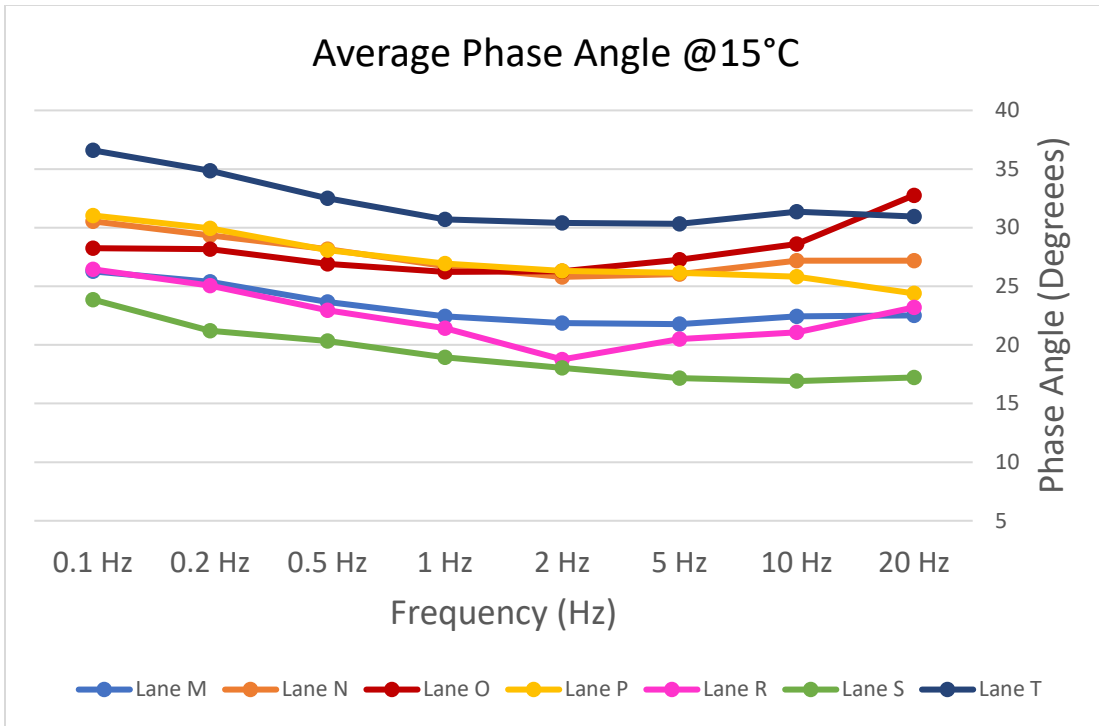


Figure 4.12 Phase Angle values obtained from the Dynamic Modulus test @15°C

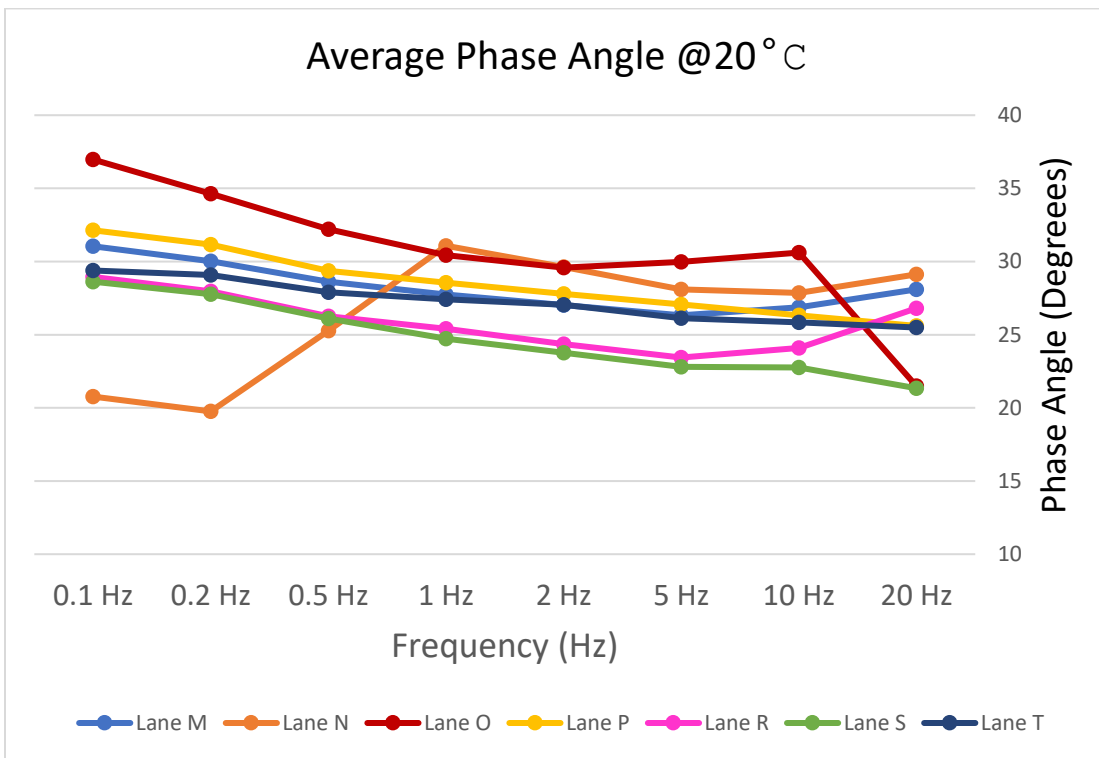


Figure 4.13 Phase Angle values obtained from the Dynamic Modulus test @20°C

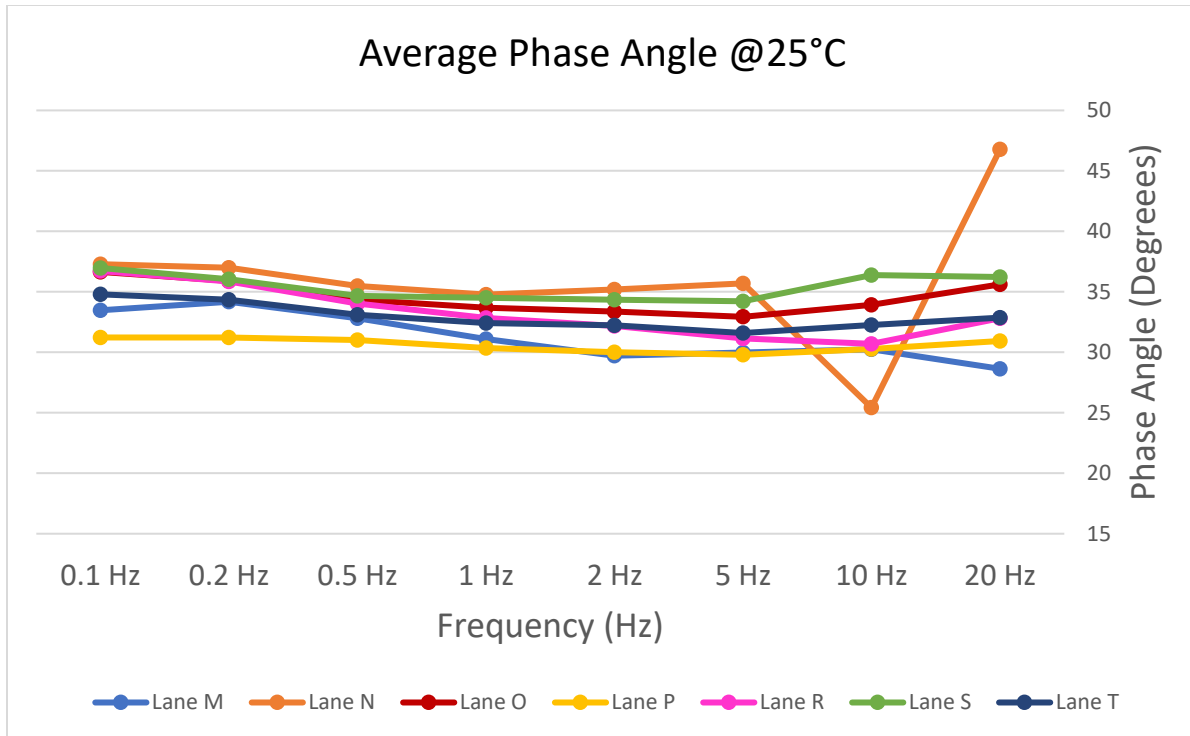


Figure 4.14 Phase Angle values obtained from the Dynamic Modulus test @25°C

The phase angle increased with an increase in temperature and decreased with loading frequency. For an increase in temperature of 5°C, the phase angle increased the least for section N by approximately 5% and increased the most for section S by 30%. For an increase in temperature of 10°C, the phase angle increased the least for section T by circa 8% and increased the most for section S by roughly 55%. An increase in the loading frequency, from 0.1 Hz to 20 Hz for a test performed at 15°C, 20°C and 25°C decreased the phase angle values by 16%, 20% and respectively 3%. As observed in Figure 4.13 and 4.14, the phase angles values for section N show inconsistency with the change in loading frequency. Most likely, the LVDTs slipped away from the supports when the loading frequency increased. Generally, a higher dynamic modulus value signifies a higher resistance to permanent deformation and a lower phase angle translates in a more elastic asphalt mixture.

Because most of the APT loading was performed at 20°C, further discussion is based on the dynamic modulus test performed at the same temperature. As seen in Figure 4.10, all mixes containing RAP and RAS except the mix O exhibited lower stiffness than the virgin mix N, which contains no recycled materials. However, this can be justified by the higher performance grade of the bitumen used in that mixture. Mixes T and P seem to be the softest mixtures out of all seven. This reinforces the benefits of using a Balanced Mix Design approach while designing asphalt mixtures. This also implies that a softer mix likely has a better cracking resistance. However, the field data for section T proves the contrary; Section T was failed completely after only 57,000 of load repetitions. A detailed summary of the results and the Dynamic Modulus graphs are plotted individually for each test sample and included in Appendix F.

4.1.3 Ideal Rutting Test

To simplify rutting testing during mixture design and QA/QA phases, the Texas Transportation Institute developed the indirect tensile asphalt rutting test in early 2020. This test is designed as a shear test since rutting is caused mainly by shear movement of the mix. The development of IDEAL-RT test aimed for simplicity (no cutting, gluing or nothing required), efficiency (test completion within 3 minutes), practicality (minimum training for routine operation), sensitivity (sensitive to asphalt components), and cost.

The concept of the IDEAL RT test is based on the three-point bending and Semi-Circular Bending test. In this test, a 62mm high specimen is used and the test is performed at 50°C to match the Hamburg Wheel Tracking Test criteria in Texas. The test can be performed in any Marshall stability frame using a specially designed jig. Figure 4.15 shows the schematic design of the IDEAL-RT test. As seen, the specimen is placed and constrained in a rigid fixture. The vertical

load is applied at a rate of 50 mm/min. Two shear planes are developed upon the load being applied to the specimen.

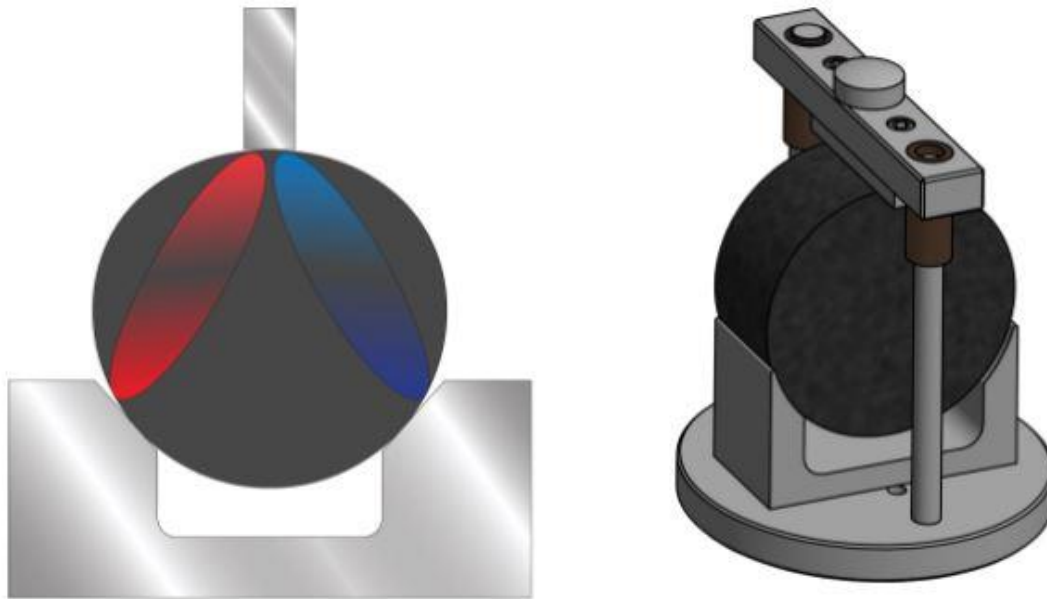


Figure 4.15. IDEAL RT test jig and sample showing shear planes caused by compression

Because this test is relatively new, there is insufficient research that supports its feasibility. However, few research projects determined that it correlates well with the field performance observation of mixes and showed good repeatability. This test relies on shear deformation to predict rutting. In addition, the samples are loaded from the top using a small contact area which does not reflect field conditions, where the rutting distress is caused by large tires from heavy trucks (Nsengiyumva et al., 2020).

For the laboratory evaluation of this test, three asphalt specimens were tested for each section. The testing specimens were extracted from the APT sections, trimmed to 62 mm thickness and the AASHTO T166 protocol was followed to determine the air voids. Table 4.4 shows the summary of the testing samples dimensions and the calculated air voids.

Table 4.4 Air Voids of the Ideal-RT specimens

Sample	Dry (g)	Water (g)	SSD (G)	Gmb	Gmm	AV (%)	Thickness (mm)
M1	2,626.8	1,566.9	2,636.7	2.46	2.59	5.34	64.92
M2	2,621.4	1,559.7	2,636.1	2.44	2.59	6.12	64.05
M3	2,798.6	1,673.4	2,801.0	2.48	2.59	4.32	62.71
N1	2,663.6	1,592.0	2,674.2	2.46	2.62	6.13	62.81
N2	2,657.8	1,582.1	2,669.3	2.44	2.62	6.76	64.80
N3	2,651.0	1,584.0	2,661.3	2.46	2.62	6.15	62.98
O1	2,762.9	1,653.9	2,769.6	2.48	2.61	4.94	64.40
O2	2,693.6	1,612.1	2,701.8	2.47	2.61	5.11	63.54
O3	2,651.0	1,598.2	2,656.2	2.51	2.61	3.81	63.04
P1	2,716.3	1,642.8	2,721.0	2.52	2.61	3.48	63.11
P2	2,730.0	1,648.9	2,735.2	2.51	2.61	3.71	63.81
P3	2,712.9	1,634.1	2,718.1	2.50	2.61	4.11	62.65
R1	2,701.6	1,616.7	2,708.3	2.47	2.59	4.37	63.91
R2	2,670.1	1,595.2	2,676.4	2.47	2.59	4.58	65.69
R3	2,674.2	1,597.8	2,679.0	2.47	2.59	4.43	64.76
S1	2,495.8	1,494.4	2,526.3	2.42	2.60	7.12	61.07
S2	2,662.8	1,590.8	2,672.6	2.46	2.60	5.47	64.38
S3	2,683.7	1,606.4	2,697.8	2.46	2.60	5.57	64.40
T1	2,698.2	1,611.7	2,700.6	2.48	2.59	4.14	62.66
T2	2,705.2	1,620.2	2,715.1	2.47	2.59	4.42	62.91
T3	2,656.2	1,590.6	2,662.0	2.48	2.59	4.09	63.75

Before being tested, all the samples were conditioned for 2 hours at 50°C. The test was performed using a Humboldt Marshall frame and an IDEAL-RT jig made by Instrotek. Figure 4.16 shows a specimen positioned in the IDEAL-RT jig, ready to be tested. As shown, the deformation is recorded using a LVDT mounted on the top of the frame. A tablet equipped with a software collects the data and calculates the output parameters. Because this test is performed in the same manner as the IDEAL-CT test, the software uses the same template file to export the results. Two failed specimens are shown in Figure 4.16 where the two shear planes are visible. The rutting parameter computed from this test is called RT_{INDEX} or shear strength. The output displays the applied load versus the vertical displacement. Three area of the curve development are considered:



Figure 4.16 IDEAL-RT Test setup and failed specimens

- The non-damage stage – ranges between 0 and 20-30% of the peak load
- The deformation damage stage- develops between 20-30% of the peak load and the peak load
- The cracking damage stage – ranges between the peak load and failure.

To calculate the RT_{INDEX} , only the first two stages are considered. The third one is used to estimate the cracking index.

To gain better insight about the IDEAL-RT results, the load corresponding to a 5 mm deformation was identified for all the tested samples and the findings are summarized in Table 4.5.

Table 4.5 Load at 5mm deformation

Section	Load (kN) @ 5mm deformation			
	Sample 1	Sample 2	Sample 3	Average
M	6.26	-	5.10	5.68
N	6.75	7.06	6.44	6.75
O	7.13	7.00	6.88	7.00
P	2.02	1.80	2.42	2.08
R	5.55	4.54	5.28	5.12
S	3.23	7.10	4.91	5.08
T	3.23	4.08	3.79	3.70

The mixes can be categorized based on the load corresponding to a fixed deformation of 5 mm; a higher load translates into a higher resistance to permanent deformation. Accordingly, mix O has the highest resistance to rutting and mix P has the lowest resistance to rutting.

The mixes were also ranked based on the RT_{INDEX} values calculated by the software included with the Smart jig. However, when comparing the load corresponding to a fixed deformation and the RT_{INDEX} values, a disagreement between the ranking is observed, as shown in Figure 4.17. According to the RT_{INDEX} , mix S has the highest resistance to rutting and mix T has the lowest resistance to rutting.

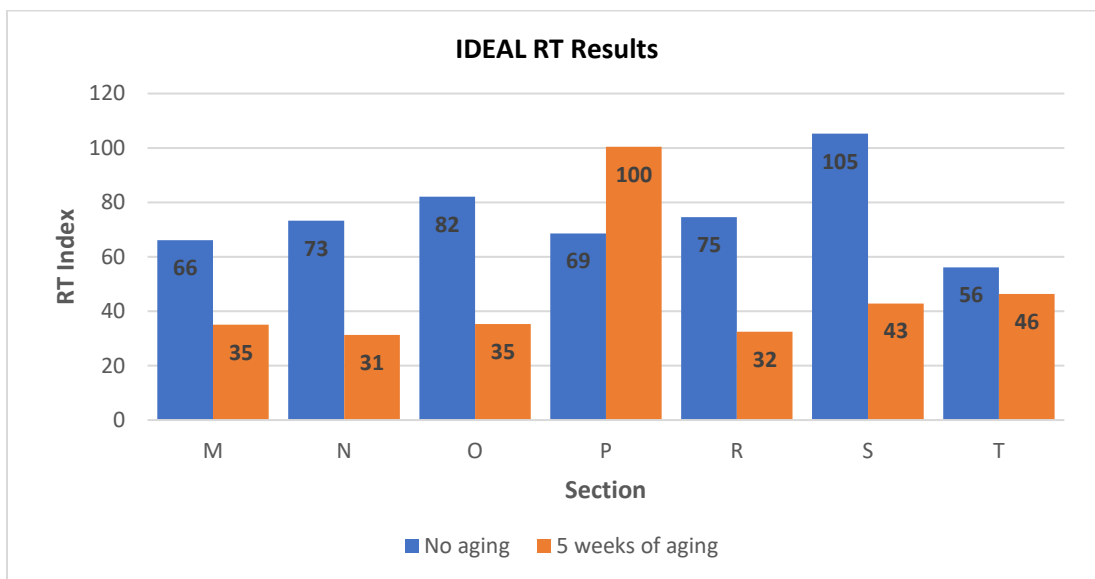


Figure 4.17 RT_{INDEX} values obtained on aged field cores and unaged compacted specimens

The unaged IDEAL-RT test was performed on compacted specimens to an AV of 7 percent, according to the TxDOT specification. However, the density of the field cores is approximately 5 percent for most sections. It is not reasonable to compare both, further testing should be performed on unaged field cores. However, the ranking is illustrated for a better visualization.

A correlation between the laboratory rutting tests was performed and is displayed in Figure 4.18 to 4.20. The best correlation is observed between the Dynamic Modulus test and the IDEAL RT load-deformation parameter. Also, the Dynamic Modulus correlates well with the HWT test; it seems that the rut depth decreases exponentially with an increase in stiffness. The worse correlation is between the IDEAL RT and HWT test with an R^2 of 0.116. Zhou et al., (2020) reported a good correlation between these two tests; however, it is likely that the RT_{INDEX} deformation needs to be improved.

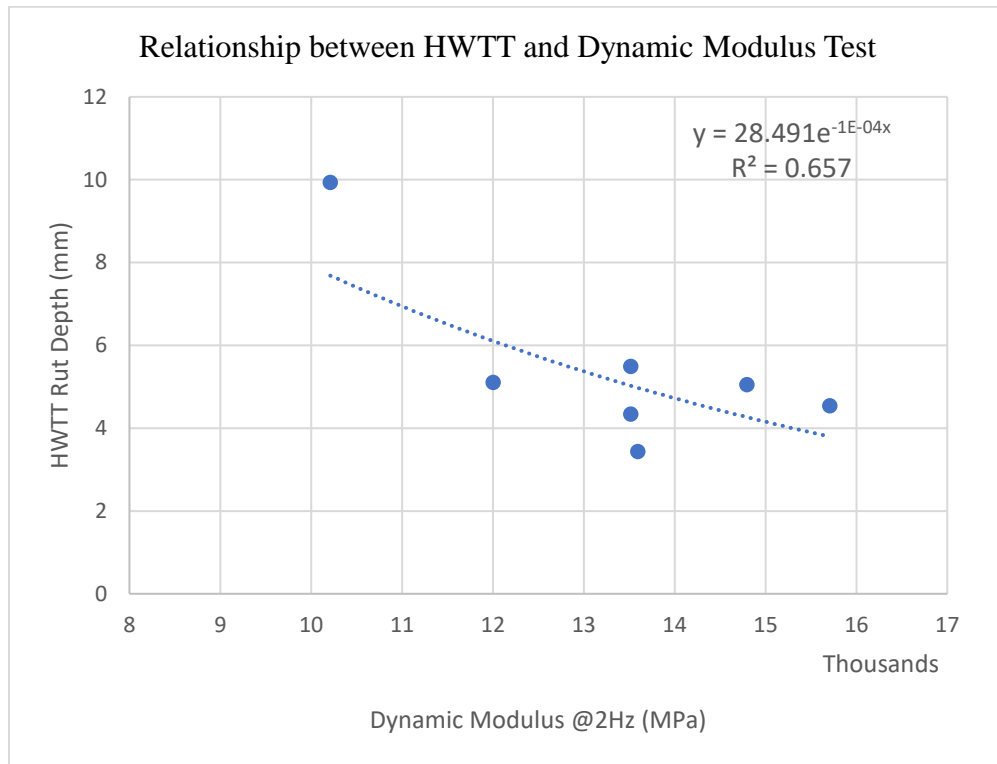


Figure 4.18 Correlation between HWT and Dynamic Modulus Test

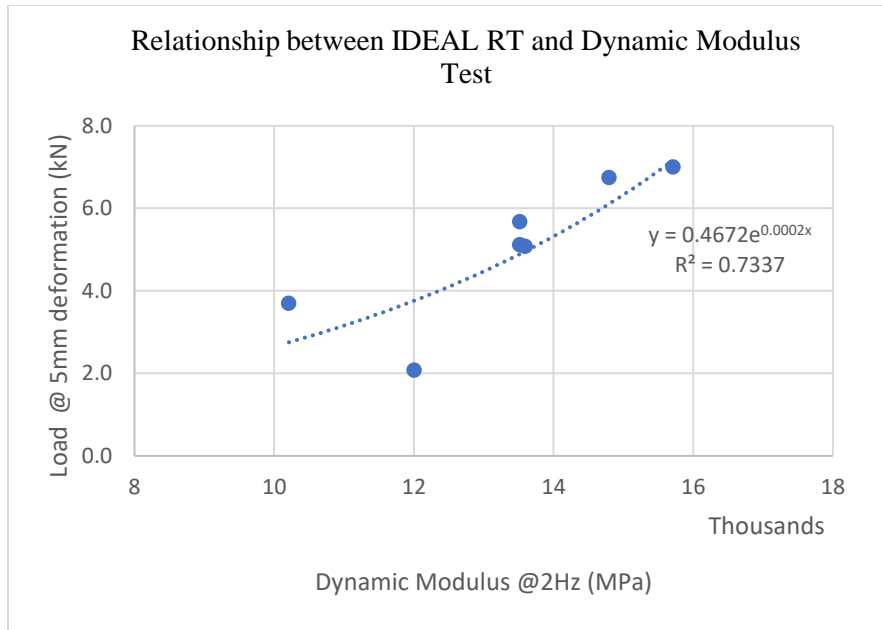


Figure 4.19 Correlation between IDEAL RT and Dynamic Modulus Test

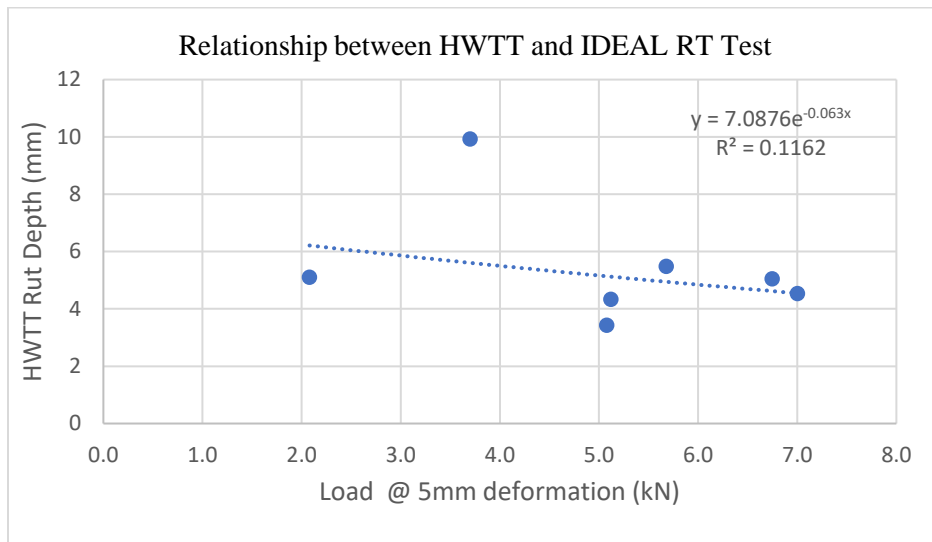


Figure 4.20 Correlation between IDEAL RT and HWT Test

4.1.4 Ranking of Rutting Tests and correlation with the Field Performance

Out of the seven mixes tested, the mix exhibiting the lower rut depth is ranked as 1st while the one exhibiting the highest rut depth exhibits the lowest rut resistance and it is ranked as the 7th.

Figure 4.21 shows the ranking of the results obtained from the Hamburg Wheel Test.

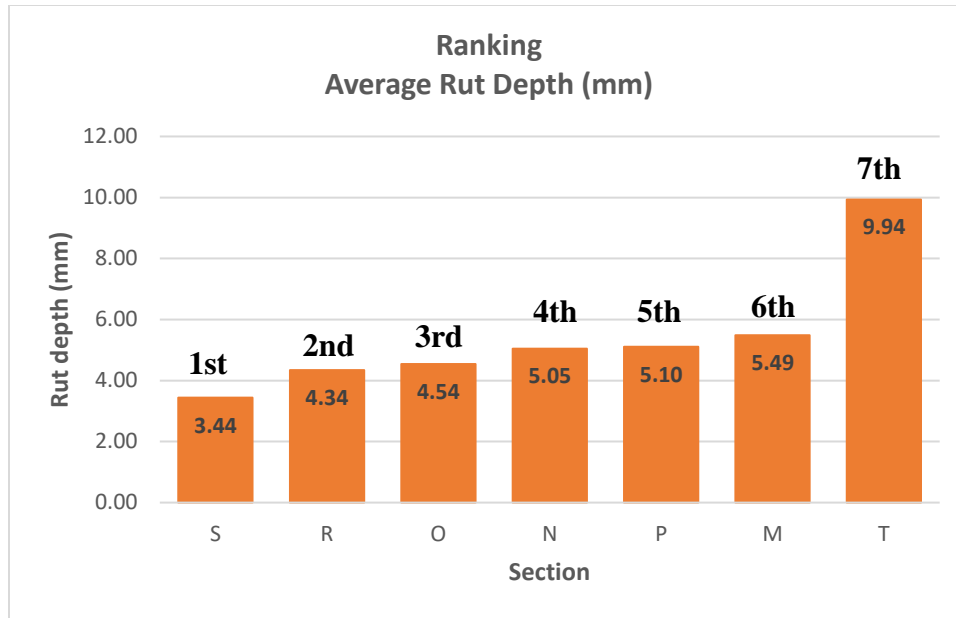


Figure 4.21 Ranking of HWTT results

According to these results, Section S has the best rutting resistance and mix T has the worse resistance to permanent deformation. From a mix design standpoint, both mixtures, S and T were designed using the BMD approach and contain the same bitumen, PG 64-22. The only difference is that mix T contains rejuvenators. The addition of rejuvenators in Mix T led to an increase of rut depth of 65%. Mixes O, N and P measured almost the same rut depth. To be noted, the mix P was subjected to 10,000-wheel passes while mixes O and P were subjected to 15,000. Mix R recorded a 4.34 mm central rut depth after 10,000 passes and it was ranked as 2nd.

Based on the performance data collected from the APT testing, Section M failed at 200,000 passes, section O and P failed at 350,000 passes and section S and T failed at 57,000 passes. Sections N and R did not fail, but because of the high extent of cracking present on the adjacent lanes, M and Q, accelerated loading was temporarily stopped until the adjacent lanes are reconstructed. The cracked section M was excavated, and a concrete pad was poured, therefore, testing on section N will resume in December 2021. On November 16th, Section Q failed abruptly

after only 60,000 passes of the wheels. After 25,000 passes, rutting measurements were performed on section Q and the permanent deformation recorded was below 2 mm. After another 25,000 passes of the wheel, the PTM was stopped, and the section was inspected for distresses. In terms of rutting, no rut depth was observed. However, two cracks, 12” and 16” long and were identified toward the middle of section Q. Also, minor pumping was visible. This is a clear indication for a weak base layer and water moving within the pavement structure. Accelerated loaded testing resumed after two days and after 10,000-wheel passes, Section Q failed completely. Figure 4.22 shows a photograph of the failed section. Because of the 3.75-inch rut depth, the transverse profiler could not be positioned on the pavement to measure the elevation.



Figure 4.22 Rut depth measured on lane Q

Figure 4.23 depicts the average permanent deformation measured on all sections. Mix M has the lowest resistance to rutting; after 200,000 passes the maximum rut depth recorded was 15.11 mm. The average rut obtained from the HWTT was 5.49 mm and it was ranked as 6th. It can be observed that there is a good correlation between the results of the Hamburg Wheel Test and the rutting performance recorded under APT loading. Mix O had a similar performance in the APT test as mix T. However, Ground Penetrating Radar test recorded a thinner surface layer for section O (2.93 inches) than for all other sections.

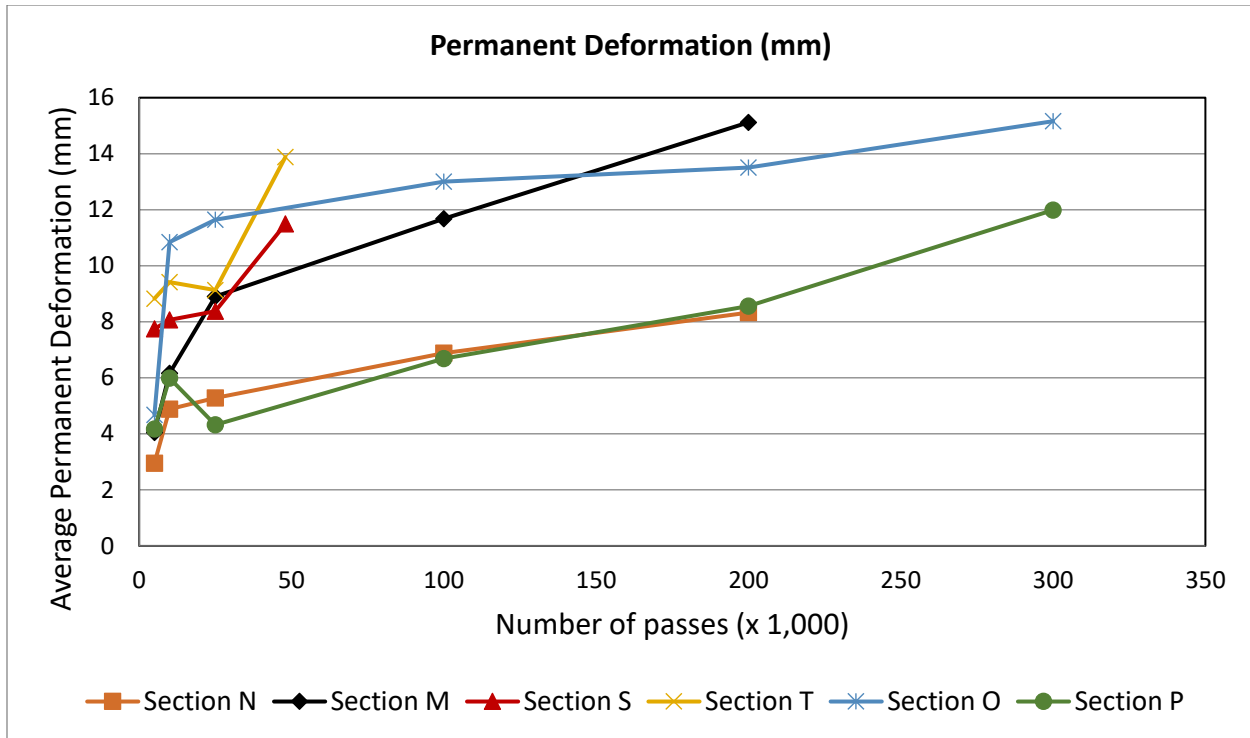


Figure 4.23 Average permanent deformation (mm)

Mixes N and P exhibited the best resistance to permanent deformation, 8.32 mm respectively 11.98 mm. According to the Hamburg measurements, these mixtures are ranked as 4th and 5th. Not many conclusions can be drawn based on mixes N and R since they were not tested to failure yet.

Figure 4.24 depicts the ranking performance based on the Dynamic Modulus Test. A higher dynamic modulus value signifies a higher resistance to permanent deformation. The mixes containing RAP are expected to have a higher dynamic modulus, implicitly a higher resistance to rutting. Once again, based on the Dynamic Modulus results and the prior comments, mix O proves to have the best resistance to rutting. All the other results show a good correlation between the Dynamic Modulus results and the performance recorded by the APT experiment. Mix T was ranked as 7th for both tests. This proves a good correlation between the Dynamic Modulus test and the HWT test in terms of evaluation of the laboratory performance.

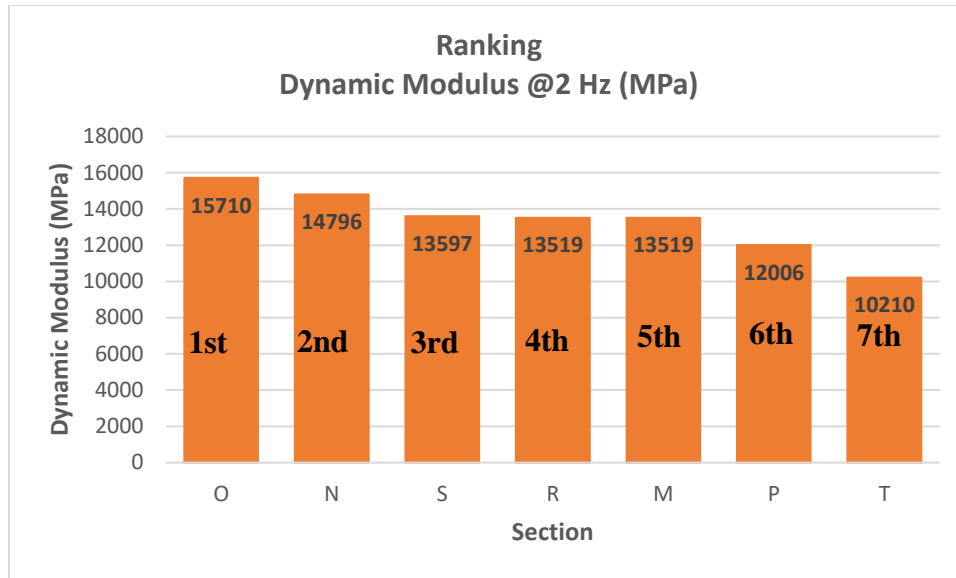


Figure 4.24 Ranking performance based on the Dynamic Modulus Test

Figure 4.25 shows the ranking performance of the parameters obtained from the load-deformation curve from the IDEAL-RT test. According to the results, mix O is ranked as the mix with the best resistance to rutting while mix P ranks as the 7th. On the other side, the measured permanent deformation ranks section O as 3rd and section P as 5th. The only mix that is ranked the same is mix N. It can be concluded that the IDEAL RT test is highly sensitive to recycled materials and the parameter estimated is not a good indicator of rutting performance.

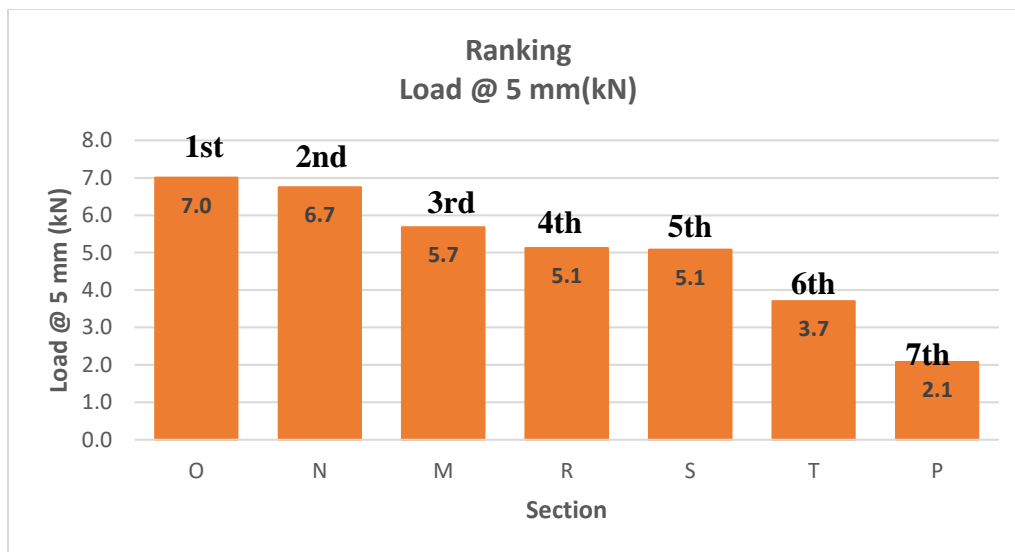


Figure 4.25 Ranking performance based on the data from IDEAL-RT test

To visualize the ranking from the laboratory tests and the measured permanent deformation from the APT experiment, all the rankings are illustrated in Figure 4.26. However, it is not feasible to compare the North and South sections together because of the weak foundation observed in the North sections.

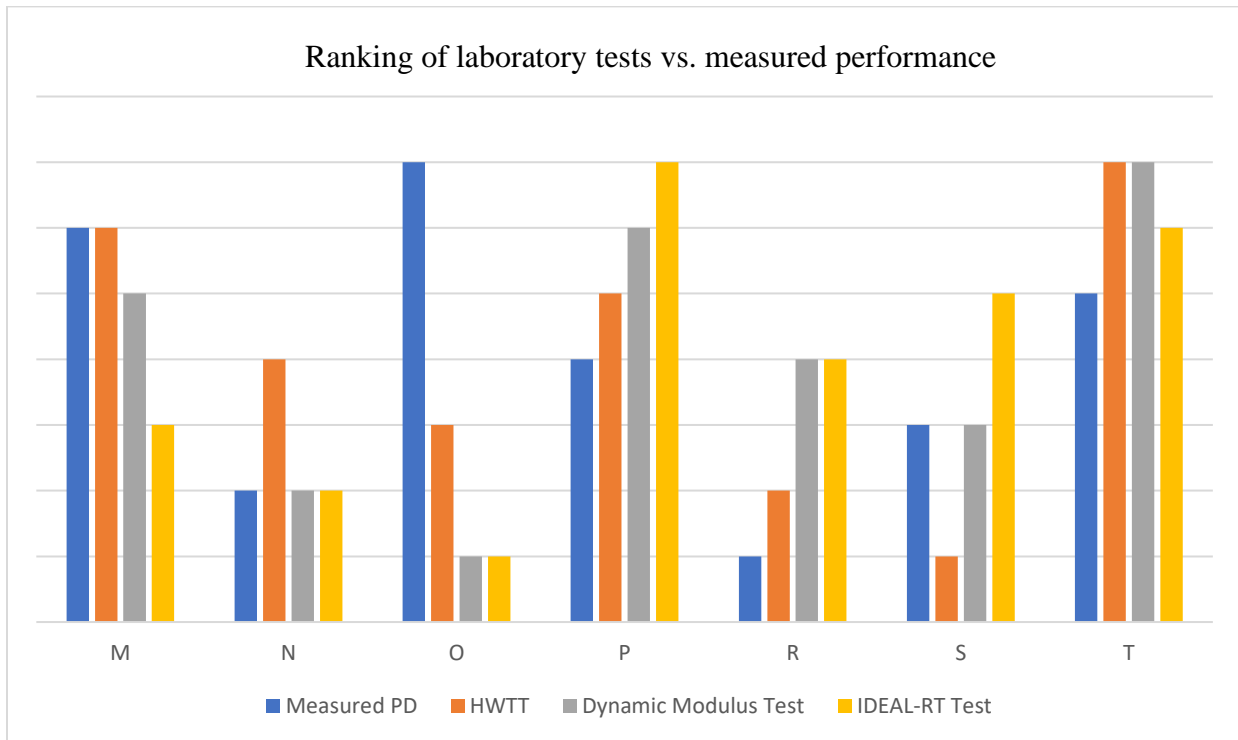


Figure 4.26 Ranking of laboratory tests vs. measured performance

The resistance to rutting of mixes M and Q was predicted as being the best by the HWTT and the Dynamic Modulus test. The IDEAL-RT test underestimated the potential rutting. The virgin mix N was equally predicted by the Dynamic Modulus test and the IDEAL-RT test as having good performance. However, since this section was not tested to failure yet, it can be concluded that the HWTT prediction is accurate. For the asphalt mix O, all the tests performed underestimated its resistance to permanent deformation. Because it has the thinnest asphalt layer out of all sections, this mix proved to have a good field performance. Mix P ranked 4th in terms of field performance and its resistance to rutting was overestimated by the Dynamic Modulus test and the IDEAL RT

parameter. The HWTT had the best prediction in terms of rutting. It is difficult to rank Sections Q, S and T; they experienced large rates of rutting (95.25 mm, 11.49 and 13.88, respectively) after a relatively low number of passes, likely because of plastic deformation and water infiltration in the aggregate base. This was proved through high FWD deflections measured on those sections. Moreover, sections Q and M had the same asphalt mix in the top layer. However, section M recorded a permanent deformation of 15.11 mm after 200,000 passes while section Q had a permanent deformation of 92.55 mm after only 60,000 passes. A final determination of rutting distribution between layers can be determined from trenching after the completion of the APT experiment.

Based on the results of the IDEAL-RT test, artificial ageing of the sections increased the resistance to rutting of all the BMD mixes containing recycled materials by approximately 50 percent.

4.2 Evaluation of Cracking Resistance

4.2.1 Overlay Tester (OT), Tex-248-F

The Overlay Tester was developed in the early 2000s by the Texas A&M Transportation Institute as a method to determine the susceptibility of asphalt mixes to fatigue or reflective cracking. This test has been continuously researched, improved, and updated. Currently, Texas DOT uses the Overlay Test as a performance evaluation cracking test in designing balanced mix asphalt. The Overlay Tester machine is an electro-hydraulic system that applies repeated direct tension loads to specimens. As seen in Figure 4.27, the OT machine features two plates: the left one is fixed and the right one slides horizontally. The right plate applies tension in a cyclic triangular waveform to a constant displacement of 0.025 inches. The displacement is measured by two linear variable differential transducers (LVDTs). A load cell measures the force needed to

impose the displacement. The duration of a complete cycle is 10 seconds. One cycle is defined as the movement of the sliding plate from the initial position until it reaches the maximum displacement and then it returns to its initial position. This test is performed in a controlled temperature chamber at a temperature of 25°C.

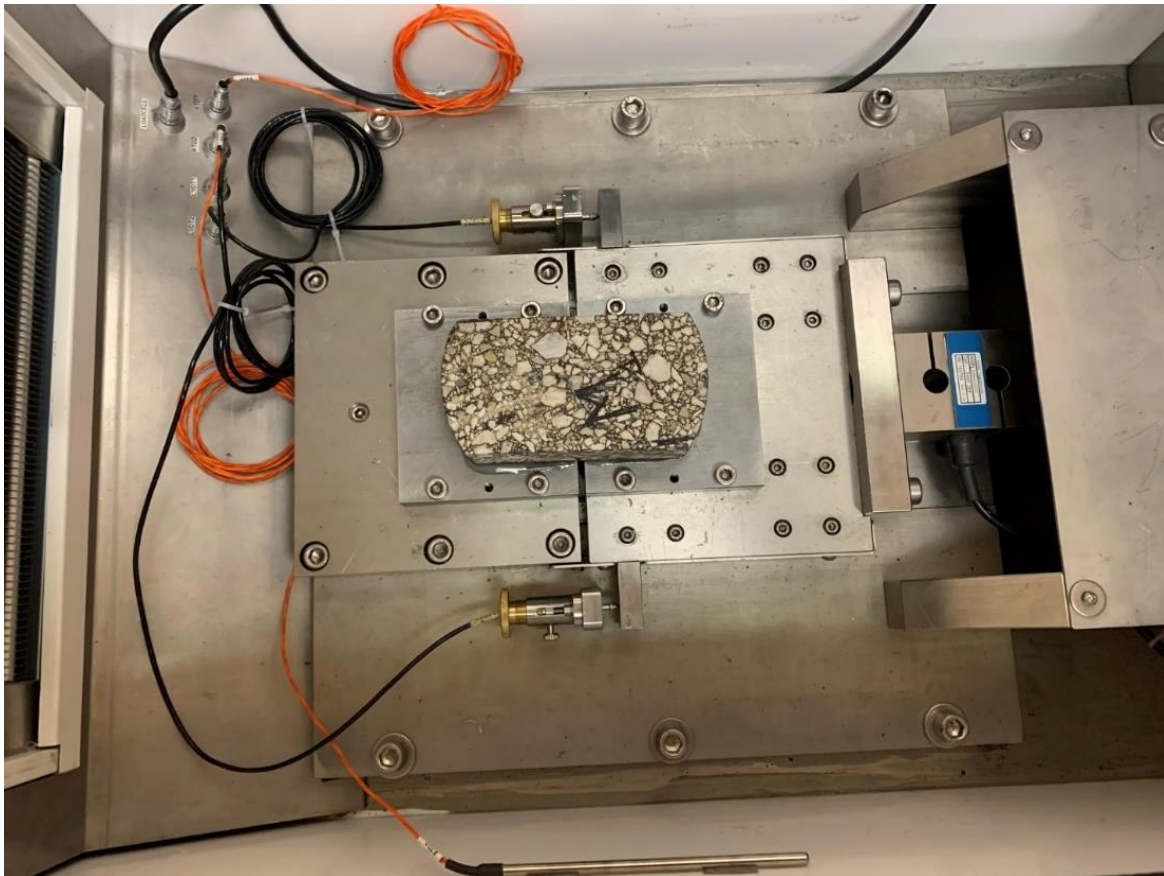


Figure 4.27 Overlay Tester equipment

The preparation of the testing specimens is a long and tedious process. First, the 6.0 inches diameter cores were trimmed from a thickness of 3.0 inches to 1.5 inches. The trimmed top and bottom slice were discarded. The next step was to trim the sides of the circular core to obtain a 3.0 inches wide rectangular shaped size specimen. After the specimen was prepared, the air void percentage was determined according to AASHTO T166 and summarized in Table 4.5 together with the sample dimensions.

Table 4.5 OT Sample Dimensions and AV%

Sample	Dry (g)	Water (g)	SSD (g)	Gmb	Gmm	AV (%)	Height (mm)	Length (mm)	Width (mm)
M1	1,120.2	674.3	1,121.6	2.5	2.6	3.5	41.1	80.4	154.2
M2	1,087.4	649.7	1,090.2	2.5	2.6	4.8	39.5	80.5	152.9
M3	1,133.3	681.3	1,134.5	2.5	2.6	3.6	40.8	80.6	152.1
N1	1,025.6	620.5	1,027.7	2.5	2.6	3.9	37.4	79.4	152.4
N2	1,072.3	648.8	1,074.1	2.5	2.6	3.8	39.8	80.1	152.2
N3	1,035.6	617.3	1,039.8	2.5	2.6	6.5	39.7	80.6	152.3
O1	1,118.9	672.9	1,120.9	2.5	2.6	4.1	41.4	79.9	152.4
O2	1,109.0	666.6	1,110.5	2.5	2.6	4.1	40.9	79.8	152.9
O3	1,119.1	676.6	1,120.5	2.5	2.6	3.2	40.8	80.2	152.3
P1	1,014.1	608.8	1,015.8	2.5	2.6	4.5	39.9	77.9	150.2
P2	1,070.3	643.1	1,071.3	2.5	2.6	4.2	41.6	78.0	150.0
P3	1,029.4	624.5	1,030.7	2.5	2.6	2.9	39.6	80.1	149.7
Q1	1,079.6	650.5	1,081.0	2.5	2.6	3.3	39.8	80.7	152.5
Q2	1,105.3	668.6	1,107.0	2.5	2.6	2.8	39.0	80.9	152.1
Q3	995.1	592.7	1,000.8	2.4	2.6	6.0	38.5	80.0	152.0
R1	1,074.0	645.9	1,076.4	2.5	2.6	3.6	39.6	80.2	152.3
R2	1,046.6	626.3	1,048.7	2.5	2.6	4.3	38.9	79.4	152.5
R3	1,066.8	639.1	1,068.8	2.5	2.6	4.1	38.5	80.3	152.5
S1	1,007.3	598.4	1,014.8	2.4	2.6	7.1	39.2	77.9	152.3
S2	1,015.3	606.3	1,022.4	2.4	2.6	6.3	39.5	79.5	152.2
S3	1,034.7	618.6	1,038.8	2.5	2.6	5.4	39.8	79.2	152.1
T1	1,044.8	627	1,046.2	2.5	2.6	3.6	38.8	80.4	149.4
T2	1,042.9	623.5	1,044.1	2.5	2.6	4.1	38.5	80.8	151.4
T3	1,097.9	654.9	1,099.2	2.5	2.6	4.4	40.6	80.9	150.1

The preparation of the testing samples was continued by gluing the specimens to the testing plates. To do so, a mounting jig and a 4.2 mm spacer bar was used. Figure 4.28 shows the steps employed in the gluing process. The sequence of gluing was as follows: the middle of the sample was marked, and a small amount of petroleum jelly was applied along the line and then a 4 mm wide tape was placed along the line to ease the removal of the specimen from the base plates (Figure 4.28 A and B). A two-part epoxy was mixed, and 16 grams were used for each specimen. The epoxy was carefully poured on each half of the specimen without touching the middle tape, as shown in Figure 4.28 C. The specimen was then mounted on the base after making sure that is

centered and aligned with the edges, as shown in Figure 4.28 D. Finally, a 5-lb. weight was placed on top of the specimens to ensure full contact with the base plate.

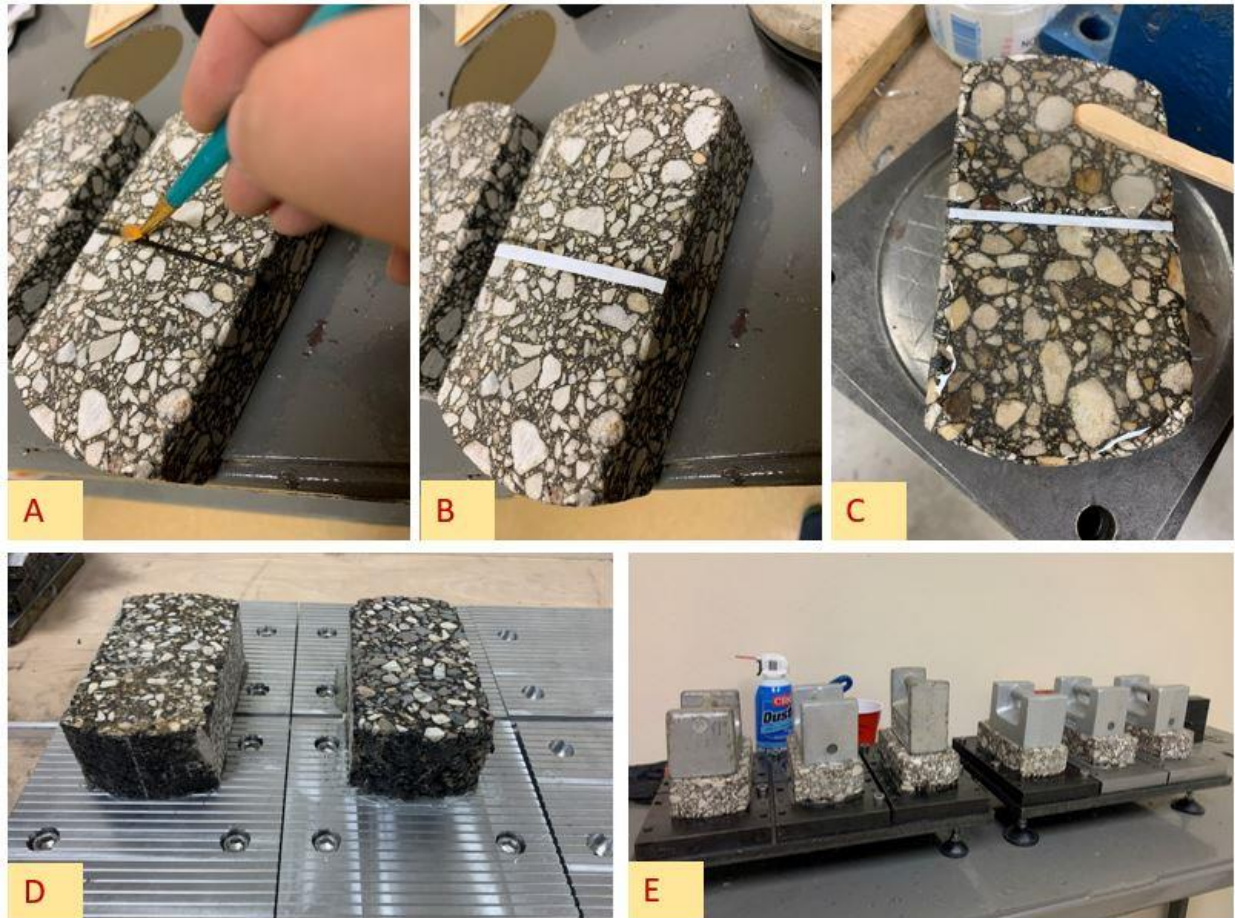


Figure 4.28 OT Sample preparation

Before being tested, the samples were conditioned for two hours at 25°C. The sample was then loaded into the Overlay Tester machine and testing was started, Figure 4.27. The test was run until a 93% reduction in maximum load occurred or when 1,000 cycles were reached. The number of cycles to failure, the critical fracture energy (CFE) at the maximum peak load and the crack progression rate (CPR) were reported. As represented in Figure 4.29, the CFE is calculated at the maximum peak load and the cracked cross-sectional area is considered as the specimen total cross-sectional area for practical purposes.

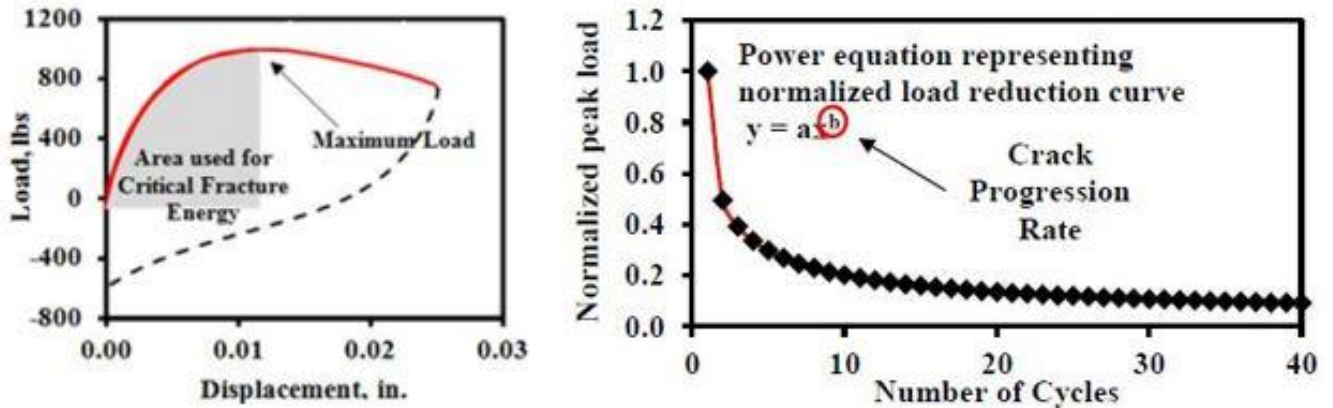


Figure 4.29 CFE and CPR representation and calculation

To reduce the OT variability, instead of the number of cycles to failure, the CPR parameter was introduced. The smaller the CPR, the better the cracking resistance of a mix. This parameter is calculated by fitting a power equation to the normalized peak load versus number of cycles as illustrated in Figure 4.29. This assumes that the reduction in the maximum tensile load per cycle is attributed to fatigue damage in terms of cracking. However, the viscoelastic relaxation of the asphalt mixture also contributed to the load reduction and is not accounted for.

Table 4.6 summarizes the results obtained from the Overlay Tester for all mixes.

Table 4.6 Overlay Tester Results

Section	M/Q		N		O		P		R		S		T	
Cycles	221	54	327	519	137	21	1000	648	35	82	6	6	1000	30
Load (kN)	4.3	4.7	3.9	3.4	6.1	5.7	3.9	3.5	5.6	4.6	3.8	3.7	3.2	2.8
CFE (J)	395	356	369	582	620	649	465	541	618	633	503	324	529	233
CPR	-0.5	-0.6	-0.5	-0.4	-1	-1	-0.3	-0.3	-1	-0	-1.6	-1.6	-0.3	-0.7
CRI	68	56	70	77	60	23	91	79	22	69	75	73	96	34
Load drop	96	93	93	93	93	93	88	93	93	93	93	93	93	93

Because of the high variability recorded within the samples of the same mix, an average of the calculated CFE cannot be reported, instead a summary of the results is showed in Figure 4.30 while the CPR is depicted in Figure 4.31. The variation between the number of cycles to failure indicates high variability and questions the veracity of the results. The percentage change in

between the two samples made from the same mix is as high as 85% for mix O. The only mix that showed consistent results was mix S. The other mixes showed the following percentage change in the number of cycles to failure: 76% for mix M, 37% for mix N, 35% for mix P and 57% for mix R.

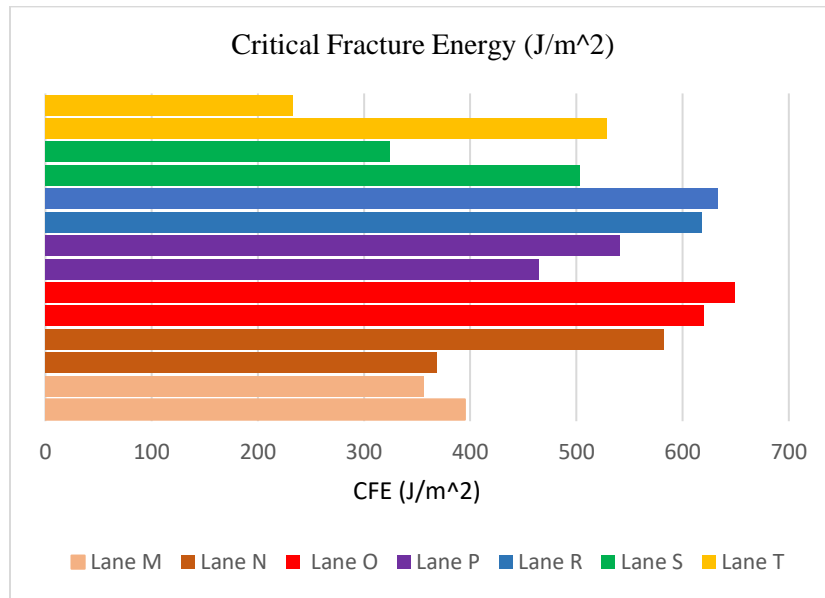


Figure 4.30 Critical Fracture Energy for all mixes

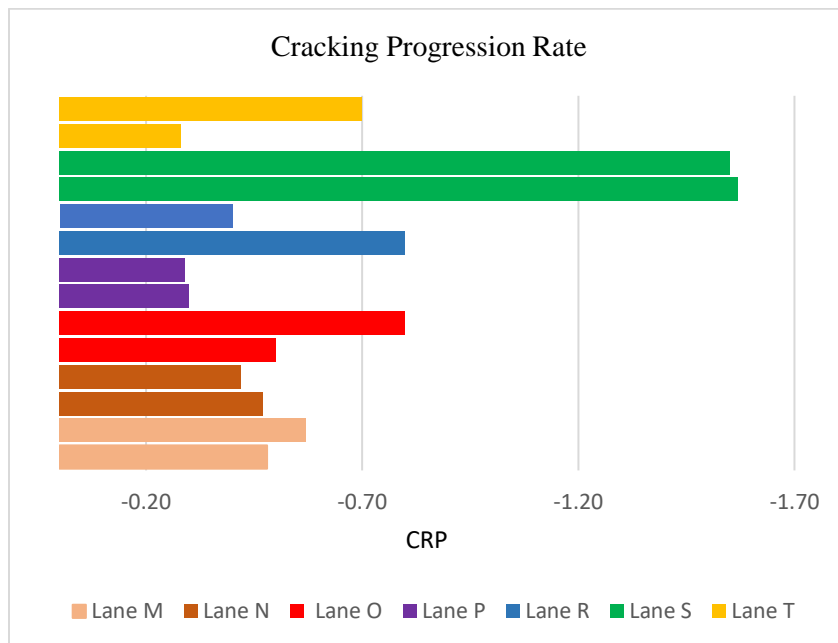


Figure 4.31 Cracking Progression Rate for all mixes

Mixes P, S, T and R are BMD mixes. This implies that their resistance in the Overlay Tester should be approximately 300 cycles. However, that is not true for mixes S and R. On one side, this could indicate that the artificial ageing induced to the pavement sections greatly affects the cracking performance. On the other side, the results of the OT are not included in the mix design file of the mixtures, so no comparison can be done. It is recommended that some sort of cracking performance test should always be performed before starting the HMA fabrication and adjustments shall be made according to the results obtained. However, the OT may not be the ideal candidate as a cracking QC/QA test since the process is so lengthy and laborious.

Zhou et al., (2020) evaluated and collected cracking resistance data of asphalt mixes for more than a decade. Based on this data, mixes were classified as into five groups:

- *Very poor cracking resistance:* OT cycles < 20,
- *Poor cracking resistance:* 20 < OT cycles < 50.
- *Intermediate cracking resistance:* 50 < OT cycles < 200.
- *Good cracking resistance:* 200 < OT cycles < 750,
- *Very good cracking resistance:* OT cycles > 750.

According to this classification, mix S pertains to the very poor cracking resistance category with only 6 OT cycles. Mix P classifies as a mix with a very good cracking resistance. However, this categorization is empirical and supported by high variable data. Moreover, this classification does not consider the type of asphalt mix, the use of recycled materials, type of binder and so on.

To evaluate the effect of induced aging, a comparison between the overlay data obtained from the unaged compacted specimens and an average of the results obtained on the aged field cores is illustrated in Figure 4.32. As theoretically expected, the resistance to cracking decreased

with the aging period for most mixes. Mixes N, O, P, R and S experienced a drop in cracking resistance of 26%, 38%, 8%, 25% and 70%, respectively. Contrary to the expectations, mix M exhibited a 17% better cracking resistance after artificial ageing. Although, this might be attributed to the different air void content since the compacted specimens do not replicate well the field density. The mix containing rejuvenators exhibited a better resistance to cracking than the unaged asphalt mix.

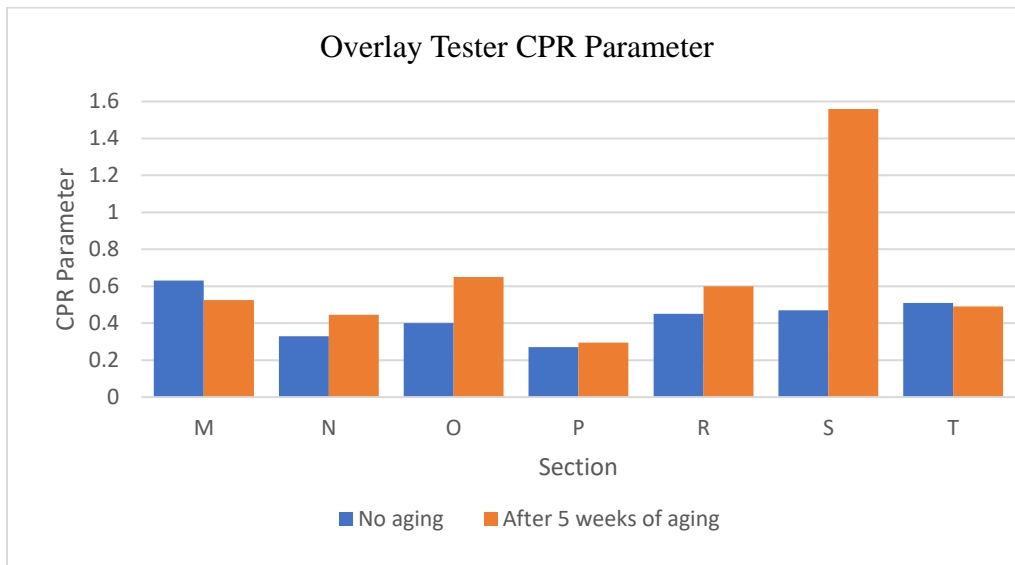


Figure 4.32 CPR values obtained on aged and unaged field cores

4.2.2 IDEAL-CT Test, Tex-250-F

The IDEAL-CT test is similar to the indirect tensile strength test in terms of crosshead displacement, testing temperature (25°C) and rate of loading (50 mm/min). The test can be conducted in any device that has the capability to measure displacement data and apply compressive load at a controlled deformation rate until the specimen completely fractures.

For each asphalt mix, four specimens were tested, and their dimensions and characteristics are summarized in Table 4.6. Figure 4.33 shows the testing setup for the IDEAL-CT test.

Table 4.6 IDEAL-CT Sample Dimensions and AV%

Sample	Dry (g)	Water (g)	SSD (G)	Gmb	Gmm	AV (%)	H(mm)	Ø(mm)
M1	2,755.0	1,643.7	2,760.4	2.47	2.59	4.89	64.7	151.6
M2	2,612.1	1,548.8	2,618.7	2.44	2.59	5.88	61.0	151.4
M3	2,759.7	1,639.7	2,771.2	2.44	2.59	5.98	65.6	150.7
M4	2,806.4	1,681.2	2,810.6	2.48	2.59	4.21	64.7	151.5
N1	2,753.0	1,648.1	2,768.2	2.46	2.62	6.26	64.5	152.2
N2	2,772.4	1,662.9	2,786.0	2.47	2.62	5.85	64.8	152.0
N3	2,865.6	1,723.7	2,870.0	2.50	2.62	4.66	65.5	152.1
N4	2,761.2	1,647.8	2,769.6	2.46	2.62	6.13	64.0	151.9
O1	2,762.7	1,659.1	2,766.6	2.49	2.61	4.24	63.4	152.5
O2	2,825.4	1,702.4	2,831.0	2.50	2.61	3.90	65.2	152.0
O3	2,838.0	1,702.6	2,843.0	2.49	2.61	4.47	65.8	152.2
O4	2,904.1	1,750.0	2,906.9	2.51	2.61	3.64	66.0	152.1
P1	2,847.6	1,721.1	2,852.5	2.52	2.61	3.57	67.5	149.6
P2	2,811.3	1,698.9	2,815.1	2.52	2.61	3.50	66.2	149.6
P3	2,733.3	1,651.3	2,737.4	2.52	2.61	3.58	65.0	149.8
P4	2,707.5	1,647.9	2,711.1	2.55	2.61	2.43	64.0	149.9
Q1	2,762.0	1,645.8	2,766.9	2.46	2.59	5.02	64.4	152.4
Q2	2,696.8	1,601.3	2,704.9	2.44	2.59	5.80	63.8	152.7
Q3	2,879.5	1,735.5	2,884.2	2.51	2.59	3.36	65.5	152.9
Q4	2,861.2	1,707.6	2,866.1	2.47	2.59	4.79	66.5	152.6
R1	2,828.3	1,696.0	2,833.6	2.49	2.59	3.93	65.0	153.5
R2	2,761.8	1,647.2	2,765.8	2.47	2.59	4.60	64.5	153.0
R3	2,787.8	1,679.3	2,790.8	2.51	2.59	3.09	63.2	152.8
R4	2,818.7	1,683.1	2,823.0	2.47	2.59	4.45	65.0	152.7
S1	2,815.0	1,692.8	2,825.4	2.49	2.60	4.55	65.1	151.7
S2	2,739.5	1,637.6	2,748.8	2.47	2.60	5.32	64.5	151.9
S3	2,768.3	1,662.5	2,776.8	2.48	2.60	4.60	63.5	152.0
S4	2,850.5	1,710.0	2,856.3	2.49	2.60	4.50	65.5	152.3
T1	2,754.4	1,661.7	2,766.3	2.49	2.59	3.54	65.7	149.4
T2	2,735.0	1,634.5	2,742.8	2.47	2.59	4.54	65.8	150.0
T3	2,703.8	1,627.8	2,709.0	2.50	2.59	3.26	64.7	150.3
T4	2,702.2	1,618.4	2,708.9	2.48	2.59	4.14	64.3	149.8

The IDEAL-CT test is based on deriving the performance-related cracking parameter from the measured load versus displacement curve (Figure 4.34). The parameter developed for this test is called the CT_{INDEX} and is inspired by the Paris's law and the research done by Bazant and Prat for crack propagation.

$$CT_{INDEX} = \frac{t}{2.4} \times \frac{l_{75}}{D} \times \frac{G_f}{|m_{75}|}$$

Where:

CT_{INDEX} – cracking tolerance index normalized to a 62 mm thick specimen

G_f – Failure energy, lbs./in.

$|m_{75}|$ – absolute value of the post-peak slope, in.

l_{75} – Displacement at 75% of the peak load after the peak, in.

D – diameter of specimen, in.



Figure 4.33 Testing setup for the IDEAL-CT Test

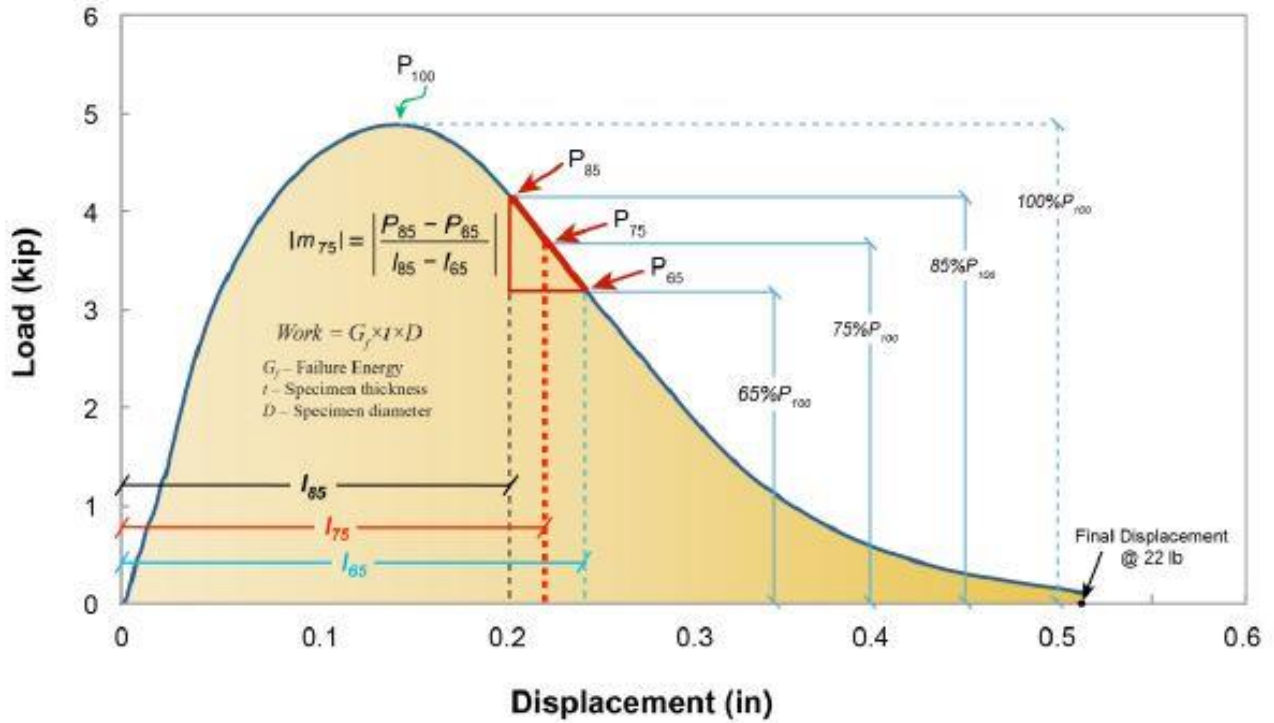


Figure 4.34 Load versus displacement curve for IDEAL-CT

All the samples were tested, and the load and displacement data obtained were stored in Excel spreadsheet. The data analysis was performed in the Rutgers Analysis Tool Pack developed by Rutgers Center for Advanced Infrastructure and Transportation. The results for each sample are attached in Appendix G while a summary is showed in Table 4.7. Generally, a higher CT_{INDEX} value translates in a better cracking resistance. The CT_{INDEX} varies with mix types and recycled materials.

According to the results, mixes T and P have the highest resistance to cracking and the mixes S and M have the lowest resistance to cracking. Based on these findings, it can be concluded that a mix containing 15% RAP and 2% RAS can have a better cracking resistance than a virgin mix. Figure 4.35 compares the CT_{INDEX} values obtained right after paving (no aging) versus the CT_{INDEX} values obtained after 5 weeks of artificial aging.

Table 4.7 IDEAL-CT Results

Specimen	Peak Load (kN)	Displacement (mm)	Tensile Strength (kPa)	Fracture Energy (J/m ²)	Slope (S)	Gf/S	CT Index
M1	17	5	1,096	7,706	7	1,165	40
M2	16	6	1,106	9,163	7	1,306	52
M3	17	7	1,067	9,189	8	1,136	52
M4	18	6	1,149	8,849	9	934	38
N1	20	5	1,286	9,261	4	2,250	70
N2	22	5	1,428	8,022	12	693	23
N3	22	6	1,414	10,721	8	1,390	52
N4	22	5	1,450	10,032	5	1,866	61
O1	21	7	1,376	13,489	5	2,589	116
O2	18	8	1,183	11,876	5	2,329	120
O3	17	5	1,074	7,548	7	1,141	39
O4	21	7	1,325	12,990	5	2,493	112
P1	15	7	932	9,505	3	3,419	165
P2	13	8	849	10,947	2	5,865	294
P3	16	7	1,028	8,806	5	1,865	84
P4	14	7	944	9,056	3	2,785	130
Q1	16	7	1,059	9,729	8	1,224	55
Q2	17	5	1,118	7,126	7	1,060	33
Q3	18	5	1,121	8,693	4	1,959	65
Q4	16	6	988	9,323	4	2,286	87
R1	16	7	992	9,822	3	3,825	171
R2	15	7	979	9,685	3	3,257	152
R3	16	8	1,050	11,103	5	2,192	111
R4	20	6	1,311	10,446	6	1,893	72
S1	20	6	1,307	9,006	7	1,360	51
S2	17	5	1,078	8,165	6	1,385	47
S3	17	4	1,098	7,440	7	1,117	33
S4	19	6	1,235	8,267	7	1,227	45
T1	12	6	800	7,622	3	2,476	104
T2	13	9	861	10,812	2	4,902	302
T3	13	6	870	8,099	3	2,546	106
T4	12	7	804	8,274	2	3,941	176

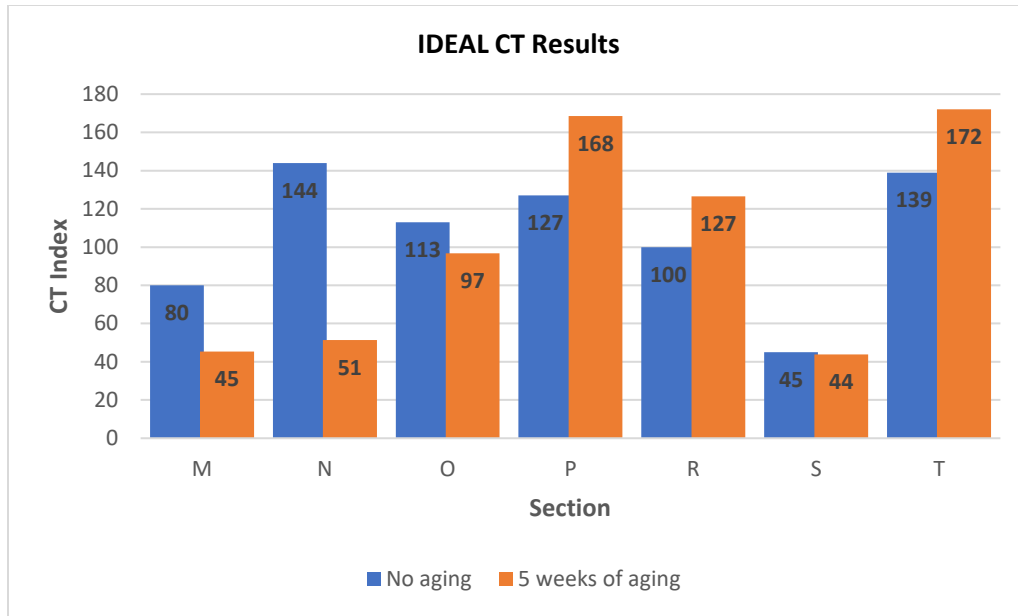


Figure 4.35 CT_{INDEX} before and after artificial aging

Normally, ageing, or induced ageing is expected to increase the asphalt stiffness, making them more resistant to rutting and more prone to cracking. That was the case for mixes M, N and O. The decrease in cracking resistance was 43% for mix M, 64% for mix N and 14% for mix O. Unusually, mixes P, R and T showed the opposite. The increase in cracking resistance was 33% for mix P, 27% for mix R and 24% for mix T. The common factor between these three mixes is that they were designed using the Balanced Mix Design approach. The results obtained for mix T advocates the benefit of using rejuvenators, since section T showed the best resistance to cracking out of all mixes.

To address the sensitivity of the IDEAL-CT test to aging, additional testing was performed on the mixes placed on lane S and T. Figure 4.36 shows the calculated CT_{INDEX} performed on cores in three different stages: no aging (laboratory compacted), 5 weeks of artificial ageing (equivalent of 7.5 years) and 26 weeks plus 5 weeks of artificial ageing (equivalent to 8 years of aging).

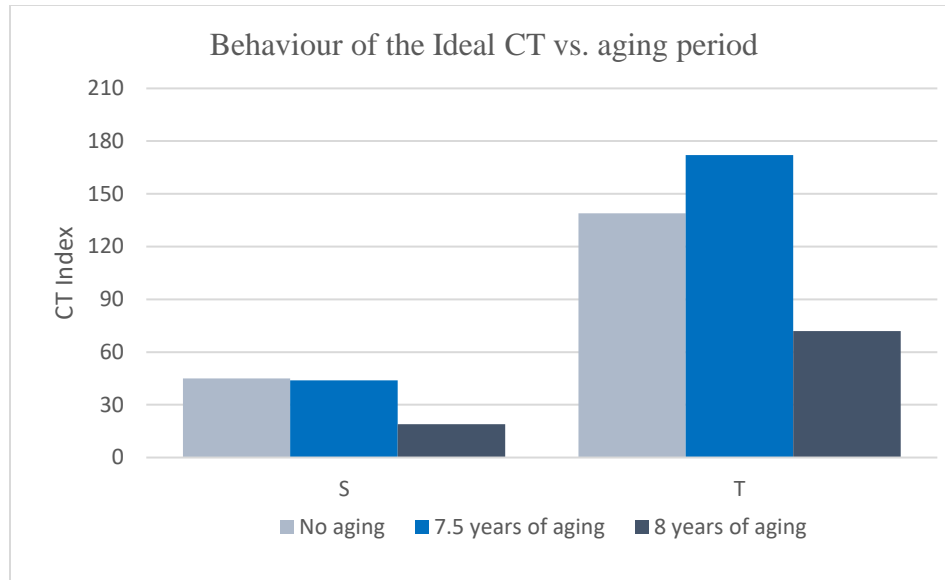


Figure 4.36 Variation of the CT_{INDEX} over aging period

As expected, mix S showed decreased cracking resistance over longer aging period. The cracking resistance dropped by 58% after 22 weeks of ageing. Mix T exhibited an increase in cracking resistance after 5 weeks of artificial ageing (23%), followed by a decrease of 48%. This is primarily due to the fact that the test performed on unaged mixture was on gyratory compacted specimens. Also, the variability of test results within the same mix was high.

4.2.3 Semi-circular Bending Test (SCB), ASTM D8044-16

The SCB test is based on fracture mechanics which is known to be an effective tool to characterize crack initiation and propagation in materials. Compared to other fracture tests used in the asphalt community, such as disk-shaped compact tension (DCT) test and single edge notched beam (SEB) test, the SCB test uses a half-moon shaped specimen which can be easily prepared. Also, this test can accommodate easily field cores, and it showed good repeatability of the results in the past. In this test, a semi-circular specimen is loaded monotonically until fracture occurs under a constant rate of deformation in a three-point bending load configuration. Being based on fracture mechanics, a notch is cut in each specimen. The length of the notch is variable and is based

on the mixture properties, aggregates size, binder type and so on. One research study showed that notch depths greater than 25mm show no sensitivity to NMAS. Under this test, the load and deformation are continuously recorded and used to compute the fracture energy. Marasteanu et al., (2004) defined the fracture energy as:

$$G_f = \frac{W_0 + mg\delta_0}{A_{lig}}$$

Where:

G_f – fracture energy (J/m^2)

W_0 – the fracture work, the area below the load-displacement curve

m – mass

g – gravitational acceleration

δ_0 - deformation

A_{lig} = thickness x (radius-notch length).

In 2015, Al-Qadi et al., (2015) developed a new fracture indicator, Flexibility Index (F.I.) which better differentiate mixtures.

$$F.I.=0.01 \times \frac{\text{Fracture energy}}{\text{post peak slope}}$$

A good correlation of F.I. was established after evaluating and correlating the parameter with the field performance as follows:

- *Poor cracking resistance:* F.I. < 2,
- *Intermediate cracking resistance:* 2 < F.I. < 6.
- *Good cracking resistance:* F.I. > 6.

Table 4.8 summarizes the dimensions and characteristics of the specimen fabricated for the SCB test while Figure 4.37 show the SCB test setup.

Table 4.8 SCB Test Sample Dimensions and AV%

Sample	Dry (g)	Water (g)	SSD (G)	Gmb	Gmm	AV (%)	Notch (mm)	Thick. (mm)	Height (mm)
M1-1	2,587.3	1,541.2	2,594.5	2.5	2.6	5.3	24.1	60.2	75.0
M1-2	2,617.8	1,560.8	2,623.0	2.5	2.6	5.0	23.8	61.2	75.7
M2-1	2,587.3	1,541.2	2,594.5	2.5	2.6	5.3	25.1	61.1	75.2
M2-2	2,617.8	1,560.8	2,623.0	2.5	2.6	5.1	23.8	61.6	75.0
N1-1	2,627.2	1,589.9	2,632.6	2.5	2.6	3.9	22.1	59.9	75.6
N1-2	2,549.1	1,508.5	2,564.2	2.4	2.6	7.9	24.0	59.6	75.1
N2-1	2,627.2	1,589.9	2,632.6	2.5	2.6	3.9	24.1	60.8	78.9
N2-2	2,549.1	1,508.5	2,564.2	2.4	2.6	7.9	26.2	60.8	74.2
O1-1	2,595.3	1,554.4	2,599.2	2.5	2.6	4.6	23.8	58.1	73.6
O1-2	2,610.0	1,570.0	2,613.7	2.5	2.6	4.0	25.0	60.1	73.8
O2-1	2,595.3	1,554.4	2,599.2	2.5	2.6	4.6	23.8	58.9	73.4
O2-2	2,610.0	1,570.0	2,613.7	2.5	2.6	4.1	23.5	58.9	74.3
P1-1	2,506.9	1,515.3	2,510.0	2.5	2.6	3.4	25.2	58.4	71.4
P1-2	2,477.8	1,497.5	2,481.9	2.5	2.6	3.6	26.1	58.9	73.0
P2-1	2,506.9	1,515.3	2,510.0	2.5	2.6	3.4	27.5	57.5	72.7
P2-2	2,477.8	1,497.5	2,481.9	2.5	2.6	3.6	25.1	59.6	74.3
R1-1	2,654.9	1,598.5	2,661.1	2.5	2.6	3.5	23.8	59.6	74.1
R1-2	2,601.0	1,568.0	2,605.4	2.5	2.6	3.1	24.6	59.9	73.9
R2-1	2,654.9	1,598.5	2,661.1	2.5	2.6	3.5	25.0	57.9	73.9
R2-2	2,601.0	1,568.0	2,605.4	2.5	2.6	3.1	25.1	58.2	74.1
S1-1	2,556.8	1,527.3	2,567.3	2.5	2.6	5.6	23.9	59.6	73.2
S1-2	2,587.1	1,553.0	2,597.2	2.5	2.6	4.9	24.8	59.9	74.0
S2-1	2,556.8	1,527.3	2,567.3	2.5	2.6	5.6	24.0	58.7	73.3
S2-2	2,587.1	1,553.0	2,597.2	2.5	2.6	4.9	24.8	58.7	73.7
T1-1	2,510.4	1,501.5	2,515.6	2.5	2.6	4.2	26.1	59.5	71.7
T1-2	2,552.0	1,533.0	2,555.7	2.5	2.6	3.5	24.8	59.4	72.7
T2-1	2,510.4	1,501.5	2,515.6	2.5	2.6	4.2	22.9	59.8	73.4
T2-2	2,552.0	1,533.0	2,555.7	2.5	2.6	3.5	23.8	59.8	71.1

Four replicates were tested for each mix and the average results are summarized in Table 4.9. The detailed results are given in Appendix H.

Based on the data obtained, mixes M and S classify as mixes with intermediate resistance to cracking, and the rest of the mixes fall under the category of mixes with good cracking resistance.



Figure 4.37 SCB Test setup and failed specimens

Table 4.9 Summary of results -SCB Test

Sample	Max Load (KN)	Fracture Energy (J/m ²)	Slope (KN/mm)	F.I.
M	1.12	393.78	-0.85	8.4
N	1.09	753.27	-1.08	8.77
O	1.32	946.00	-1.04	9.98
P	0.60	655.09	-0.27	25.81
R	1.08	779.34	-0.87	9.30
S	1.13	576.22	-1.50	3.91
T	0.65	584.80	-0.45	13.34

As shown in the Appendix H, the coefficient of variance is relatively high, therefore the results are might not be a true representation of the actual cracking performance. It is envisioned

to perform additional SCB testing in the future using three different notch depths, 15 mm, 20 mm and 25 mm and three different rates of loading.

Figure 4.38 displays the correlation between the CT_{INDEX} determined from the IDEAL CT test and the FI from the SCB test. It can be observed that these two tests correlate relatively well. The CT_{INDEX} seem to be linearly proportional to the FI value; the larger FI, the bigger CT_{INDEX} value. This indicates that there is a decent level of confidence in using these two tests interchangeably. For example, a FI value of 10 corresponds to a CT_{INDEX} value of 100.

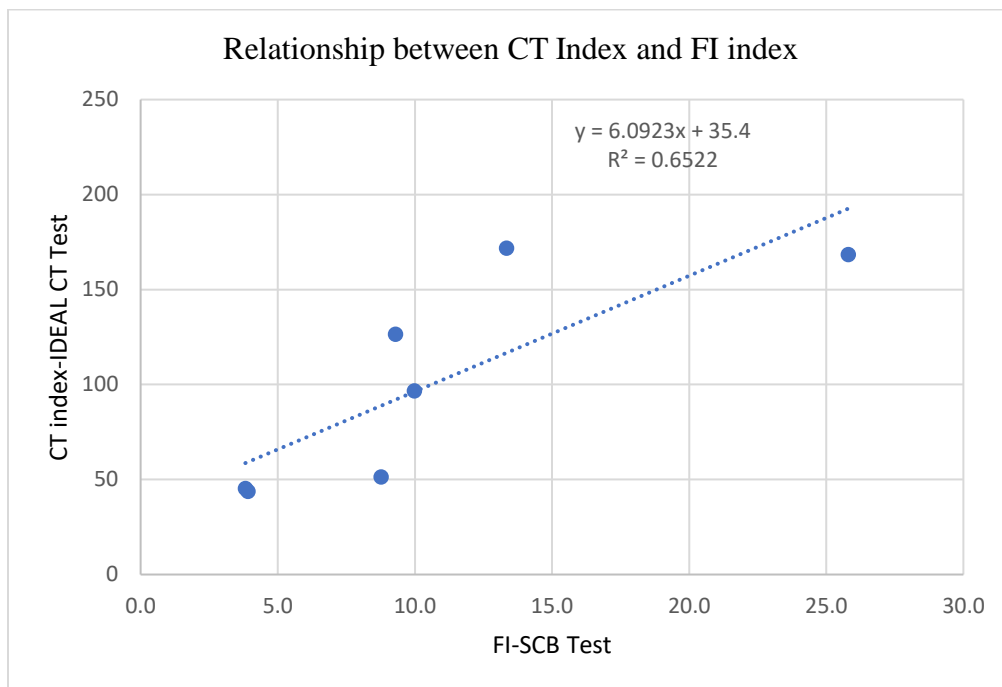


Figure 4.38 Relationship between the CT_{INDEX} and FI-SCB

Figures 4.39 and 4.40 show the corresponding relationship between the Overlay tester and SCB Test and IDEAL-CT test, respectively. As observed, these tests do not seem to correlate very well. The high variability in the results obtained for the Overlay Test might be at fault for the poor correlation. To draw conclusions on the possible correlation, additional testing is needed.

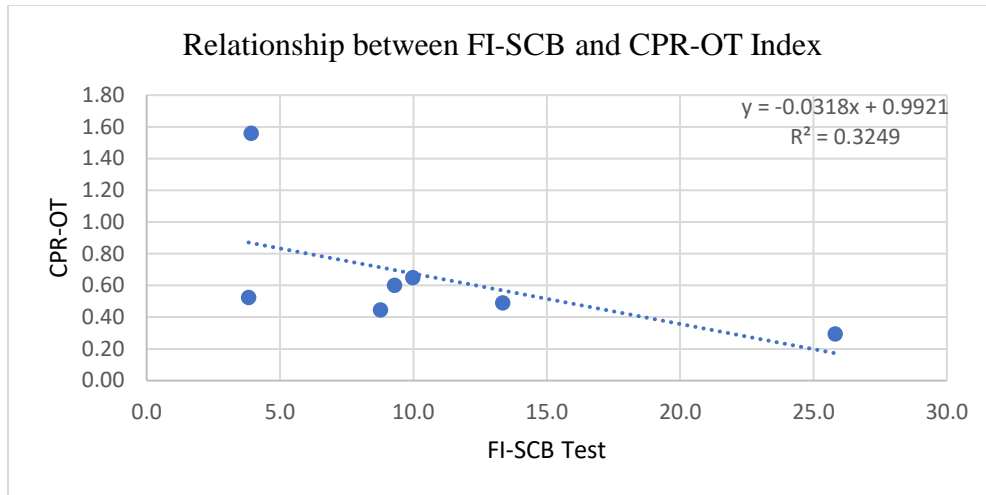


Figure 4.39 Relationship between the FI-SCB and Overlay Tester

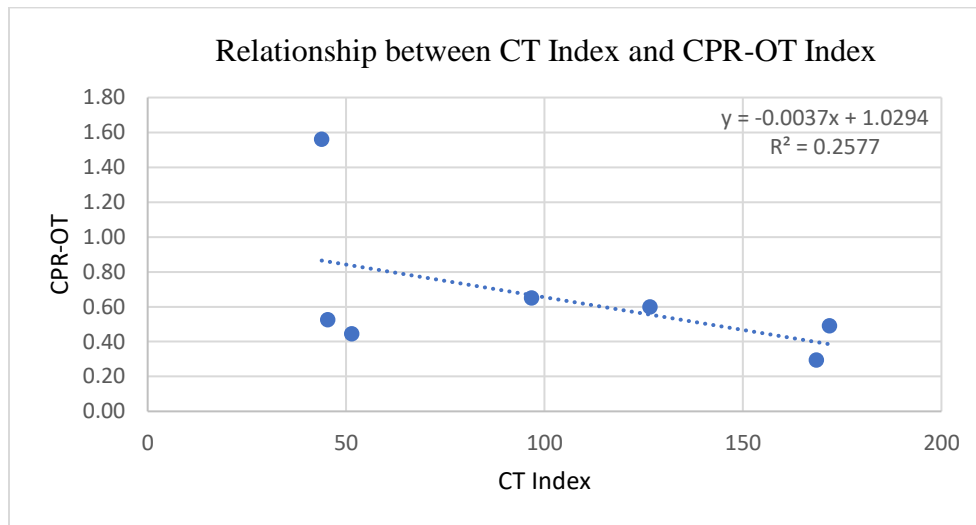


Figure 4.40 Relationship between the CT_{INDEX} and Overlay Tester

4.2.4 Ranking of cracking tests and correlation with the field performance

For a better visualization of the results obtained from the laboratory cracking tests, all the results were ranked and illustrated in the Figures 4.41 to 4.43 in a similar manner as the results obtained from the rutting tests.

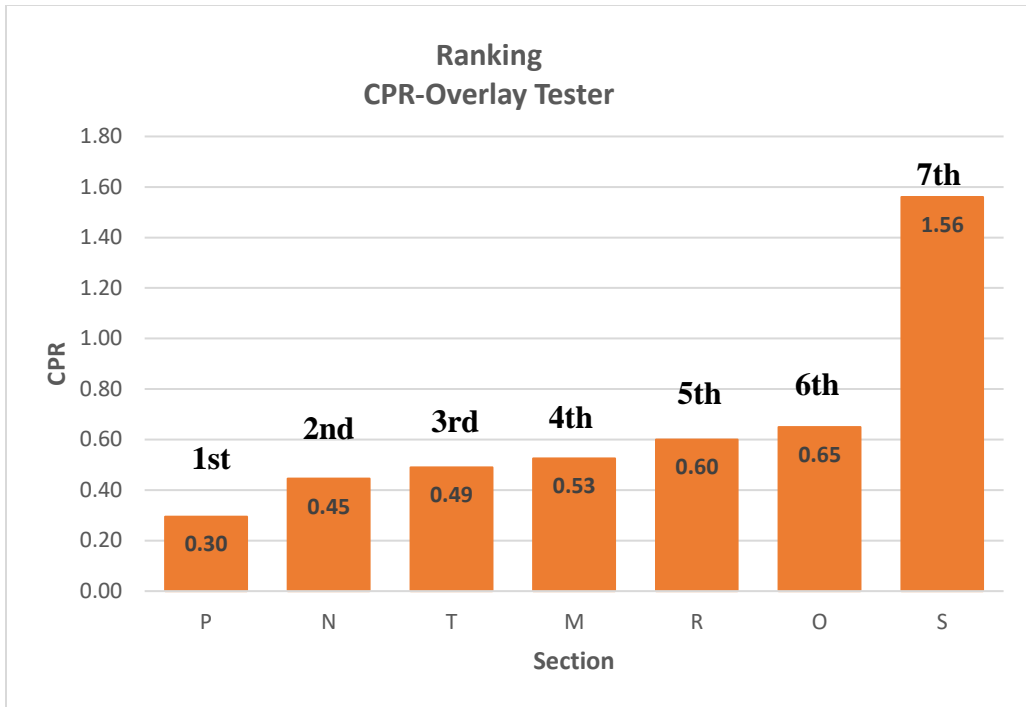


Figure 4.41 Ranking of the CPR values -Overlay Test

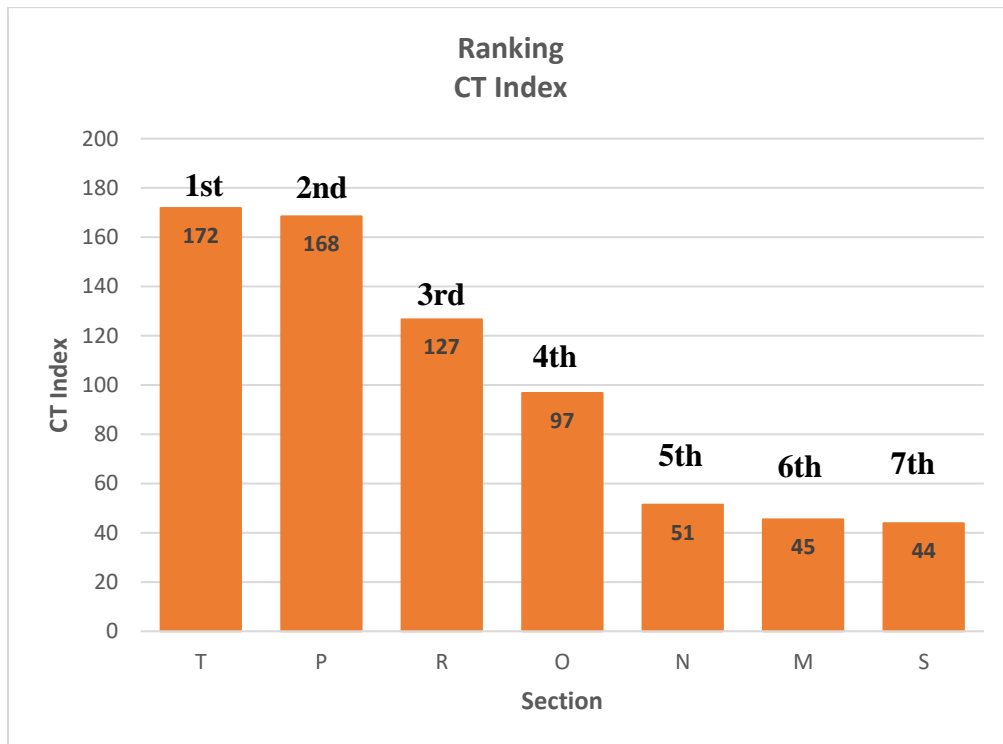


Figure 4.42 Ranking of the CT_{INDEX} values -IDEAL-CT Test

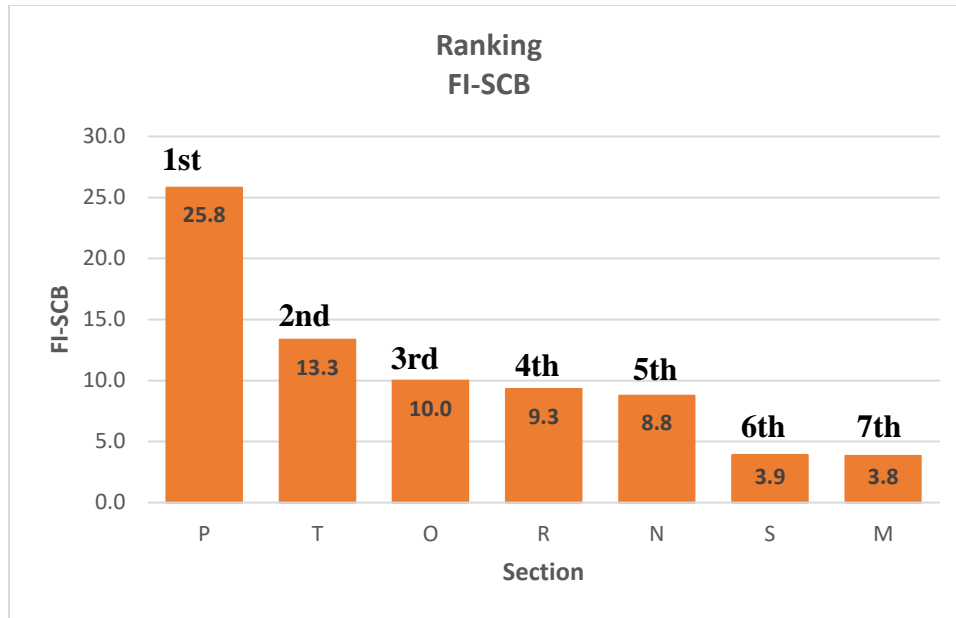


Figure 4.43 Ranking of the *FI* values -SCB Test

To compare the laboratory cracking tests with the field performance, the fatigue life was represented by the number of load passes to failure, considered as the number of passes of the PTM when 50 percent of the loaded area has cracked. Even though, all experimental pavement sections were designed to have the same structure with the only difference being the asphalt mixture, the constructed lanes varied in terms of asphalt layer thickness and properties of the base and subgrade. To properly compare the laboratory mixtures results with the field performance, adjustment needs to be done to the measured APT fatigue cracking data.

To do so, the horizontal tensile strain at the bottom of the asphalt layer was computed using the Flexible Pavement Design System, FPS21. This software was developed by TTI for the Texas Department of Transportation and is a mechanistic-empirically based design software widely used by the TxDOT for structural design, overlay design, stress-strain response analysis and pavement life prediction. The FPS21 is based on a linear-elastic analysis system and the material inputs are

the backcalculated modulus values of the pavement layers. For the purpose needed, the Mechanistic design check was used.

Figure 4.44 shows the interface of the FPS software and the inputs required for the mechanistic design check. As shown, the loading type is done with a dual tire, with the same pressure, load, and wheel dimensions as the PTM.

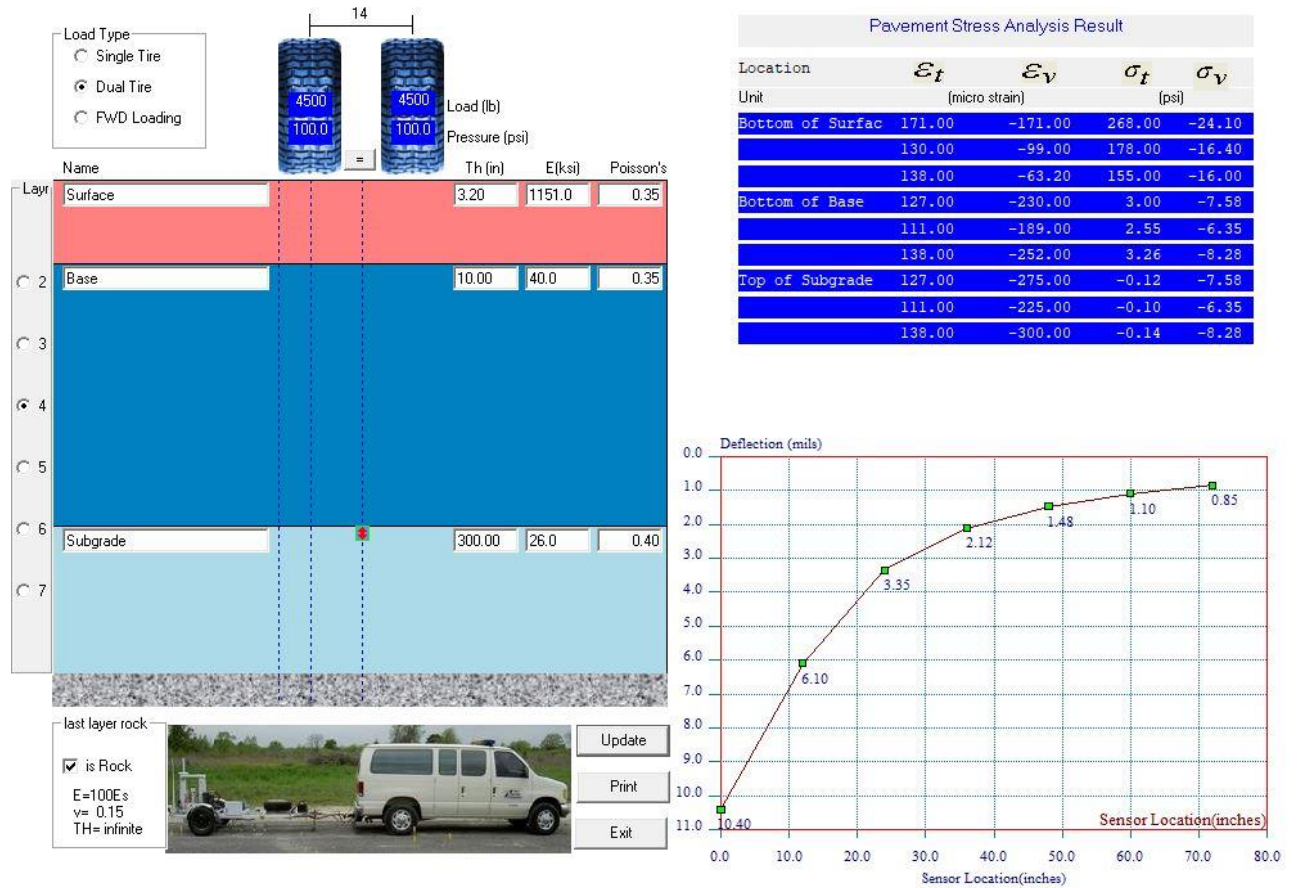


Figure 4.44 FPS21-Mechanistic Design Check

A mechanistic design check was performed for each section and the horizontal tensile strains recorded at the bottom of the asphalt layer are showed in Table 4.10 while the FPS21 screenshots for all sections are shown in Appendix I. Table 4.10 summarizes the data used in the mechanistic check.

Is important to note that even though sections N and R were not tested to failure to date, for the purpose of this analysis, an estimative APT fatigue data was assumed; 500,000 APT passes for section N and 150,000 for section R.

Table 4.10 FPS21- Input parameters

Section	M	N	O	P	Q	R	S	T
As-constructed structure								
HMA Thickness (in.)	3.19	3.26	2.93	3.21	3.26	3.19	3.39	3.32
Base Thickness (in.)	10	10	10	10	10	10	10	10
HMA E (ksi)	1,151	1,301	1,302	1,059	1,151	1,220	1,353	863
Base E (ksi)	40	105	83	82	49	63	52	60
Subgrade E (ksi)	26	34	40	36	17	24	19	21
Benchmark structure								
HMA Thickness (in.)	3	3	3	3	3	3	3	3
Base Thickness (in.)	10	10	10	10	10	10	10	10
HMA E (ksi)	1,150	1,300	1,302	1,059	1,150	1,220	1,353	863
Base E (ksi)	50	50	50	50	50	50	50	50
Subgrade E (ksi)	25	25	25	25	25	25	25	25

The k_2 parameter was recalculated using the classic fatigue equation developed by the Asphalt Institute, the k_2 parameter was calculated using the other known parameters.

$$N_f = k_1 \left(\frac{1}{\varepsilon_t} \right)^{k_2} \left(\frac{1}{E^*} \right)^{k_3}$$

Where:

N_f - the number of repetitions of load to cause fatigue cracking,

ε_t – the tensile strain at the critical location, at the bottom of the asphalt layer,

E^* - dynamic modulus of the material,

k_1, k_2, k_3 – constants from laboratory and field calibration, $k_1 = 0.0796$ and $k_3 = -0.854$

After the k_2 parameter was calculated for each mix, the number of load repetition was recalculated again, this time using the horizontal tensile strains computed at the bottom of the

asphalt layer for the design thickness, which was 3.0 inches and the design moduli, 50.0 ksi for the flex base and 25.0 ksi for the subgrade soil. A correlation factor was established between the measured and adjusted fatigue life. The adjusted APT fatigue life is showed in Table 4.11.

Table 4.11 Adjustment of the APT fatigue performance based on k_2 calibration

Section	Measured Cracking Life	ϵ (microstrain) As constructed	k_2	ϵ (microstrain) Ref. structure	CF	Adjusted fatigue life
M	291,429	138	-3.227	127	1.31	381,014
N	500,000	73	-3.080	121	0.21	107,209
O	311,111	86	-3.083	121	0.35	109,368
P	307,143	92	-3.082	130	0.34	104,048
Q	60,000	128	-3.023	127	1.02	61,440
R	150,000	107	-3.070	124	0.64	95,391
S	60,000	114	-3.000	119	0.88	52,750
T	50,632	123	-2.964	139	0.70	35,238

A comparison between the results obtained from each laboratory cracking test performed and the adjusted APT fatigue performance estimated after calibrating the k_2 parameter is illustrated in Figures 4.45 to 4.48.

As shown in the figures, there is minimal or no correlation between the cracking tests and the APT performance. The higher R^2 value determined was showed for the IDEAL-CT test. However, with a R^2 value of 0.12 the correlation is insignificant. This lack of correlation can be explained by the weaker subgrade layer of the North sections (Q, R, S and T) than that of the South sections (M, N, P and Q) . Regardless of that issue, it is indisputable that aging has a major influence on the cracking resistance. The IDEAL CT tests performed at different aging period highlighted the decline in cracking resistance.

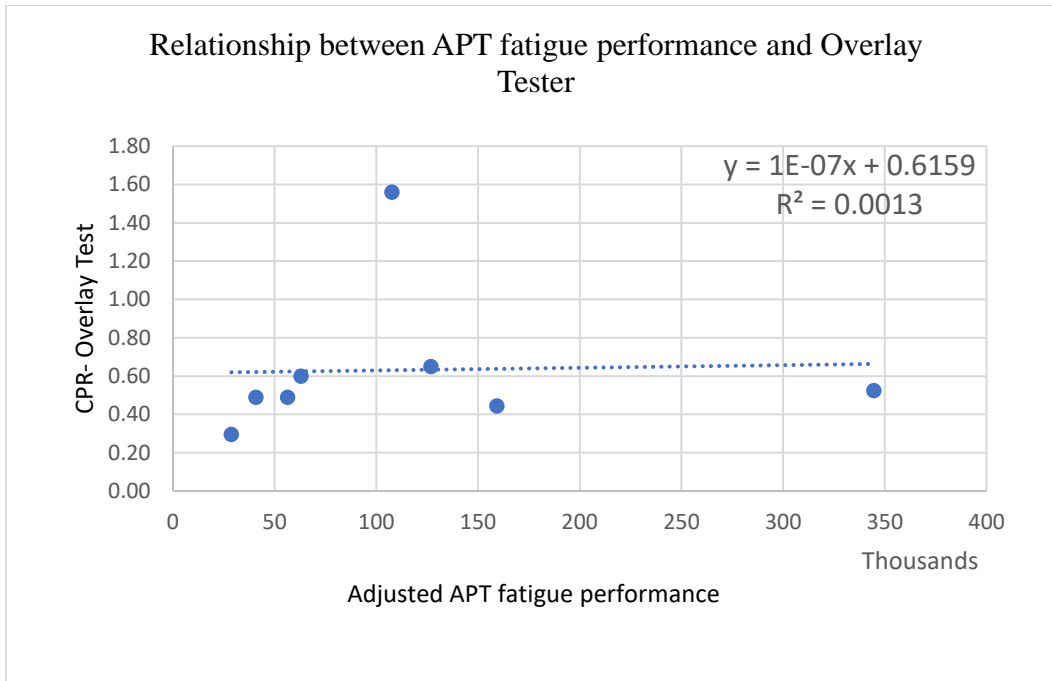


Figure 4.45 Correlation between CPR and APT performance

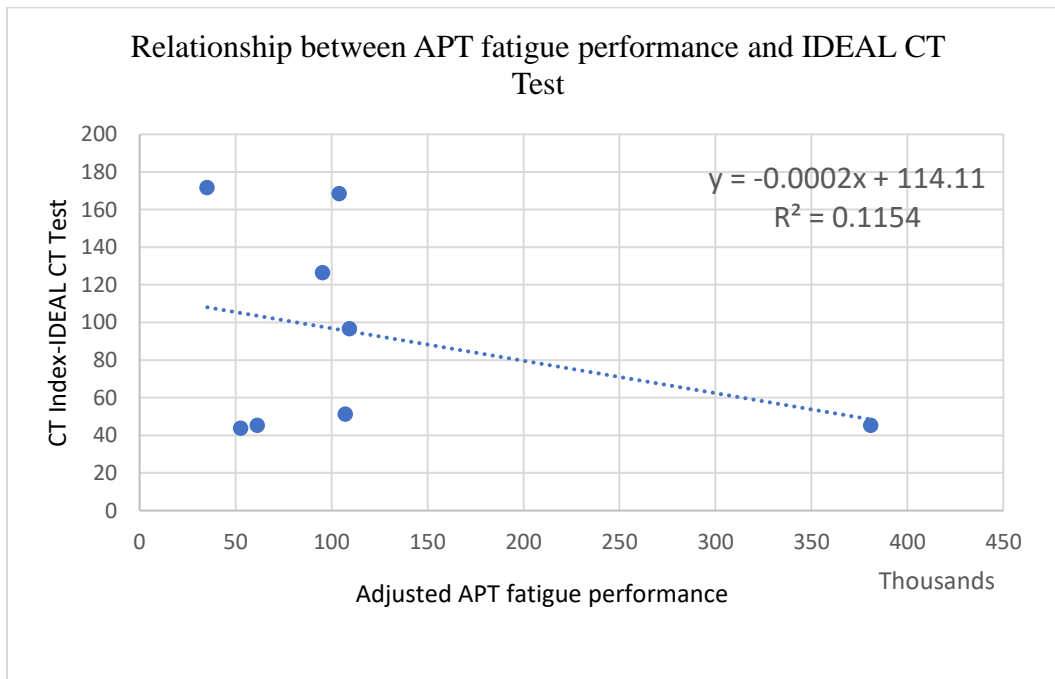


Figure 4.46 Correlation between CT Index and APT performance

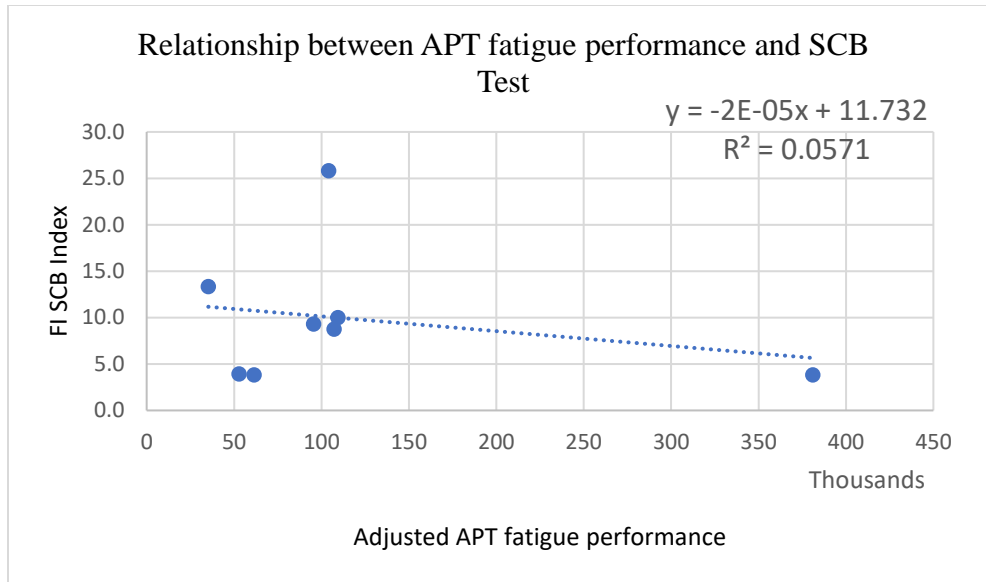


Figure 4.47 Correlation between FI-SCB and APT performance

One other limitation is that in the estimation of the adjustment fatigue performance approach, the results of the Dynamic modulus tests done on laboratory compacted field produced mix were used as the values of the elastic moduli of the mixes in the FPS21 program. At the time of the writing of this research dissertation no other stiffness values were available. It is therefore recommended that further laboratory tests, such as Dynamic Modulus or beam fatigue, be conducted on specimens extracted from the experimental sections and not on laboratory compacted specimens. In this way, the effect of artificial ageing as well as of different densities of the field compacted mixes will be reflected in the obtained stiffness values.

These results draw attention on the laboratory cracking tests employed in characterizing the recycled mixtures. Evidently, the addition of recycled materials completely changes the way the mixture behaves which implies that the testing criteria used by the Superpave virgin mixes cannot coincide with the testing criteria used for examining recycled asphalt mixtures. Because of the weak correlation between the measured APT performance and the laboratory tests, no ranking can be established.

CHAPTER 5. SUMMARY AND RECOMMENDATIONS

While virgin material for pavement applications is depleting the resources, the volume of pavement material reclaimed from in-service pavements is increasing. Consequently, there is an increased interest in the use of reclaimed asphalt materials in the production of new asphalt mixes to reduce costs and preserve nonrenewable resources. Reclaimed asphalt pavement (RAP) and Reclaimed Asphalt Shingles (RAS) has proved to be an effective alternative to virgin materials in HMA production. Despite that recycling asphalt creates a cycle that optimizes the use of natural resources and sustains the pavement industry, State transportation departments have limited the maximum amount of RAP used in surface layers because of the variability concerns and lack of guidance provided. Even though at the moment, the United States recycles more RAP than Europe does in terms of percentage of the total RAP extracted from old pavements, it still lags Japan and other countries.

A special concern is the use of RAP and RAS in asphalt surface mixes and overlays, which are subjected while in service to higher stresses from the action of vehicle traffic and environment than the mixes in the lower layers. More effort and evaluation of field performance are necessary to develop guidance on best practices when using RAP for surface layers. Currently, Texas Department of Transportation (TxDOT) allows RAP to replace up to 20 percent of virgin binder in surface course mixes, and up to 40 percent of virgin binder in the underlying layers. Despite many efforts, past asphalt recycling projects showed mixed results in terms of performance, even for mixes that fulfilled the requirements for maximum content of RAP/RAS and maximum percentage of recycled binder.

In response to this need, an accelerated pavement test project was sponsored by the Texas Department of Transportation. For this project, eight pavement test sections were built and tested

under accelerated loading conditions with the Pavement Testing Machine (PTM). All test sections have the same foundation layers but different mixes in the surface layer as shown below:

Test Section	Superpave-C HMA, SAC B 3.0 in. thick	Base Material 10.0 in. thick
M, Q	PG 64-22 (15%RAP +2%RAS) = Reference Mix	Type A Gr 1&2 Flex Base
O	PG 70-22 (15%RAP)	
N	PG 70-22 (no RAP or RAS)	
P	PG 64-28 (15% RAP + BMD)	
S	PG 64-22 (15% RAP+2%RAS + BMD)	
T	PG 64-22 (15% RAP+2%RAS + BMD + Rejuvenator)	
R	PG 64-22 (25% RAP + BMD)	

The primary objective was to assess the correlations between the laboratory evaluation results and the APT field performance and to evaluate the effect of artificial induced aging of asphalt mixtures. The test data was analyzed using the latest test standards and relevant literature. The conclusions drawn based on the rutting resistance are:

- Rutting is not a problem for Texas mixes, regardless the percent of recycled materials incorporated.
- The performance of RAP/RAS mixtures is highly dependent on the aging phenomenon and as expected, aging increased the stiffness of the asphalt mixtures by 50 % which implicitly translates in a better resistance to rutting.
- The Superpave mixes were most of the times outperformed in the laboratory by the BMD mixes.
- All the mixes performed as expected in terms of rutting; the mix placed on section O, PG 70-22 with 15% RAP, performed relatively better in terms of rutting resistance and correlated with laboratory test predictions. The mixes designed with the Balanced Mix Design concept showed a better correlation between laboratory tests and field performance.

- Section Q experienced large rates of deformations from plastic deformation in the aggregate base.
- The HWT test correlated the best with the field performance. At the same time, the Dynamic Modulus showed a good correlation to the HWT results. Furthermore, it is envisioned that the dynamic modulus might have had a better correlation to the field performance if the test would have been performed on field cores rather than laboratory compacted specimens.
- The RT_{INDEX} derived from the IDEAL RT test showed contradictory results to the field performance and to the HWT and Dynamic Modulus test. However, when evaluating the force for a given deformation, the results were relevant.

The conclusions drawn based on the cracking resistance are:

- As expected, the addition of recycled materials increased the stiffness of the asphalt mix making it more prone to cracking.
- Aging greatly lowers the fatigue cracking resistance. Aging affected less mix S which performed better than mix T which was expected to perform significantly better because of the rejuvenator component.
- The IDEAL CT test predicted a better resistance to cracking for the mix containing the rejuvenators, but the APT field data showed the opposite.
- From a material evaluation standpoint, IDEAL CT testing on field cores from section T before aging, after the equivalent of 7 years of aging and 7.5 years of aging reinforced the use of rejuvenators to combat a poor cracking resistance.
- The Overlay Tester showed high variability of the results while no correlation to the field performance.

- The SCB test has the potential to better estimate the cracking resistance. However, the variation of the results obtained were relatively high. Therefore, the results cannot be considered a representation of the actual cracking performance. Testing at different rates of loading and different notch depths may increase the correlation to the field performance.
- The CT index derived from the IDEAL CT test was linearly proportional to the FI index derived from the SCB test.
- There was minimal or no correlations between the cracking tests and the performance recorded by the APT.
- More research is needed to correlate the laboratory testing to the field performance and to develop practices and standards based on the local conditions.

Having a better understanding of the correlation between the observed field performance and laboratory test results for asphalt surface mixes containing RAP is crucial and much needed. This research promotes the use of recycled materials in the construction of roads to the maximum economical and practical extent possible and with equal or improved performance.

Recommendations:

The following recommendations result from this research:

- Further laboratory testing must be performed on aged and unaged mixes to evaluate the increase in stiffness for different type of mixtures containing different percentages of recycled materials and rejuvenators.
- The use of rejuvenators, the increase of design density, the use of softer virgin binder and/or the reduction of RAP/RAS usage approaches must be considered in order to improve the cracking resistance.
- The correlation between a direct tension cyclic fatigue test and the APT fatigue cracking performance needs to be evaluated.
- Further SCB testing considering different notch lengths and different loading rate should be performed to study the potential correlation to field performance.

References

1. Aguiar-Moya J., Vargas-Nordbeck A., Leiva-Villacorta F., Loría-Salazar L. (eds) *The Roles of Accelerated Pavement Testing in Pavement Sustainability*. Springer, Cham. https://doi.org/10.1007/978-3-319-42797-3_56
2. Alavi, M.Z.; He, Y.; Harvey, J.; Jones, D. (2015) Evaluation of the Combined Effects of Reclaimed Asphalt Pavement (RAP), Reclaimed Asphalt Shingles (RAS), and Different Virgin Binder Sources on the Performance of Blended Binders for Mixes with Higher Percentages of RAP and RAS, *Technical Memorandum UCPRC-RR-2015-06*
3. Apeagyei, A.K., & S.D. Diefenderfer (2011). *Asphalt Material Design Inputs for Use with the Mechanistic-Empirical Pavement Design Guide in Virginia*. Report FHWA/ VCTIR 12-R6. Virginia Center for Transportation Innovation and Research, Charlottesville, Virginia
4. Brock, B. (2007, November). Economics of RAS in HMA. In *Presentation at the 3rd Asphalt Shingle Recycling Forum, Chicago, Illinois*.
5. Brown, S. F. (2004). Accelerated pavement testing in highway engineering. *Proceedings of the Institution of Civil Engineers - Transport*, 157(3), 173–180. <https://doi.org/10.1680/tran.2004.157.3.173>
6. Button, J. W., Williams, D., & Scherocman, J. A. (1996). *Roofing shingles and toner in asphalt pavements* (No. FHWA/TX-97/1344-2F).
7. Cao, W., Mohammad, L. N., Barghabany, P., & Cooper, S. B. (2019). Relationship between laboratory and full-scale fatigue performance of asphalt mixtures containing recycled materials. *Materials and Structures*, 52(1), 1-15.
8. Chen, J.S.; Huang, C.C.; Chu, P.Y.; Lin, K.Y. Engineering characterization of recycled asphalt concrete and aged bitumen mixed recycling agent. *Journal of Material Science*. 2007, 42, 9867–9876.
9. Cooper III, S. B., Mohammad, L. N., Kabir, S., & King Jr, W. (2014). Balanced asphalt mixture design through specification modification: Louisiana's experience. *Transportation Research Record*, 2447(1), 92-100.
10. Copeland, A. (2009). *Reclaimed Asphalt Pavement in Asphalt Mixes: State-of-the-Practice* Washington, DC: Federal Highway Administration.
11. Cosentino, P. J., Kalajian, E. H., Shieh, C. S., Mathurin, W. J. K., Gomez, F. A., Cleary, E. D., & Treeratrakoon, A. (2003). *Developing specifications for using recycled asphalt pavement as base, subbase or general fill materials, phase II* (No. FL/DOT/RMC/06650-7754,).

12. Dong, Q., & B. Huang (2014). Evaluation of Influence Factors to Crack Initiation of LTPP Resurfaced Asphalt Pavements Using Parametric Survival Analysis. *Journal of Performance of Constructed Facilities*, Vol. 28, No. 2, pp. 412–421. doi:10.1061/(ASCE)CF.1943-5509.0000409.
13. El-Hmrawey, S. , Abu El-Maaty, A. and Elmohr, A. (2015) Durability of Hot Asphalt Mixtures Containing Reclaimed Asphalt Pavements. *Open Access Library Journal*, **2**, 1-18. doi: [10.4236/oalib.1101508](https://doi.org/10.4236/oalib.1101508).
14. Fujie Zhou, Soohyok Im, Sheng Hu, David Newcomb & Tom Scullion (2017) Selection and preliminary evaluation of laboratory cracking tests for routine asphalt mix designs, *Road Materials and Pavement Design*, 18:sup1, 62-86, DOI: 10.1080/14680629.2016.1266741
15. Hajj, E.Y., P.E. Sebaaly, R.C. West, N. Morian, & L. Loria (2012b). Recommendations for the Characterization of RAP Aggregate Properties Using Traditional Testing and Mixture Volumetrics. *Road Materials and Pavement Design*, Vol. 13, Sup. 1, pp. 209–233. doi:10.1080/14680629.2012.657072.
16. Harvey, J. T. (2009). Use of Accelerated Pavement Testing to Evaluate Maintenance and Pavement Preservation Treatments: Introduction. *Transportation Research Circular*, (E-C139).
17. Hong, F., D.-H. Chen, & M.M. Mikhail (2010). Long-Term Performance Evaluation of Recycled Asphalt Pavement Results from Texas: Pavement Studies Category 5 Sections from the Long-Term Pavement Performance Program. In *Transportation Research Record: Journal of Transportation Research Board*, No. 2180. Transportation Research Board of the National Academies, Washington, D.C. pp. 58–66. doi:10.3141/2180-07.
18. Hossain, M., Metcalf, D. G., & Scofield, L. A. (1993). Performance of recycled asphalt concrete overlays in Southwestern Arizona. *Transportation Research Record*, 30-37.
19. IDOT (2013). *Use of Reclaimed Asphalt Shingles in Illinois: 2nd Edition*. Report No. IL-PRR-163. Illinois Department of Transportation, Springfield, Illinois.
20. Jones, D. (2011). An Overview of Accelerated Pavement Accelerated Pavement Testing. Arizona. Retrieved October 10, 2021, from <https://pavement.engineering.asu.edu/wp-content/uploads/2013/02/Jones.pdf>.
21. Li, X., M. Marasteanu, R.C. Williams, & T.R. Clyne (2008). Effect of Reclaimed Asphalt Pavement (Proportion and Type) and Binder Grade on Asphalt Mixtures. *Transportation Research Record: Journal of the Transportation Research Board*, No. 2051. Transportation Research Board of the National Academies, Washington, D.C.

22. McDaniel, R. S., & Anderson, R. M. (2001). *Recommended use of reclaimed asphalt pavement in the Superpave mix design method: technician's manual* (No. Project D9-12 FY'97). National Research Council (US). Transportation Research Board.
23. McDaniel, R.S., & R.M. Anderson (2001). *NCHRP Report 452: Recommended Use of Reclaimed Asphalt Pavement in the Superpave Mix Design Method: Technician's Manual*. TRB, National Research Council, Washington, D.C.
24. McDaniel, R.S., K.J. Kowalski, & A. Shah (2012a). *Evaluation of Reclaimed Asphalt Pavement for Surface Mixtures*. Report FHWA/IN/JTRP-2012/03. Indiana Department of Transportation and Purdue University, West Lafayette, Indiana. doi:10.5703/1288284314665
25. Metcalf, J. B. (1996). *Synthesis of Highway Practice 235-Application of full scale accelerated Pavement Testing*. National Cooperative Highway Research Program.
26. Musselman, J. (2009). High RAP Performance in Florida. *HMA Recycling Expert Task Group, Department of Transportation, Washington, DC*. Obtained from: http://www.morerap.us/12-09/Musselman_High_RAP_Performance_Florida.pdf. Site last accessed October 24, 2021.
27. Paul, H. R. (1996). *Evaluation of Recycled Projects for performance* (Vol. 65, Ser. pp. 231-254). Journal of the Association of Asphalt Paving Technologists.
28. Pouranian, M. R.; Shishehbor, Mehdi. (2019). Sustainability Assessment of Green Asphalt Mixtures: A Review. *Environments* 6, no. 6: 73.
29. Roberts, F.L.; Kandhal, P.S.; Brown, E.R.; Lee, D.Y. and Kennedy, T.W. (1996). *Hot Mix Asphalt Materials, Mixture Design, and Construction*. National Asphalt Pavement Association Education Foundation. Lanham, MD.
30. Romanoschi S.A., Scullion T., Zhou F., Saeedzadeh R. (2016) *Evaluation of the Optimum Percentage of RAP and RAS in Asphalt Mixes in Texas Using Accelerate Pavement Testing*.
31. Romanoschi, S.A., T. Scullion. *Validation of the Maximum Allowable Amounts of Recycled Binder, RAP, & RAS Using Accelerated Pavement Testing*. Interim Report. Report No. FHWA/TX-14/0-6682-1, The University of Texas at Arlington, May 2014.
32. Stroup-Gardiner, M. *Use of Reclaimed Asphalt Pavement and Recycled Asphalt Shingles in Asphalt Mixtures*; Transportation Research Board: Washington, DC, USA, 2016; No. Project 20-05, Topic 46-05.
33. Vallerger, B.A.; Monismith, C.L. and Granthem, K. (1957). A Study of Some Factors Influencing the Weathering of Paving Asphalts. *Asphalt Paving Technology: Proceedings*, vol. 26. Association of Asphalt Paving Technologists.

34. West, R.C., & J.R. Willis (2014). *Case Studies on Successful Utilization of Reclaimed Asphalt Pavement and Recycled Asphalt Shingles in Asphalt Pavements*. NCAT Report 14-06. National Center for Asphalt Technology, Auburn University, Auburn, Alabama.
35. West, R.C., J. Michael, R. Turochy, & S. Maghsoodloo (2011). Use of Data from Specific Pavement Studies Experiment 5 in the Long-Term Pavement Performance Program to Compare Virgin and Recycled Asphalt Pavements. In *Transportation Research Record: Journal of the Transportation Research Board*, No. 2208. Transportation Research Board of the National Academies, Washington, D.C. pp. 82–89. doi:10.3141/2208-11.
36. Williams, R. C. (2013). *Performance of Recycled Asphalt Shingles in Hot Mix Asphalt: TPF-5 (213)*, Iowa DOT's Project Involvement.
37. Williams, R. C., Cascione, A., Haugen, D. S., Buttlar, W. G., Bentsen, R. A., & Behnke, J. (2011). Characterization of hot mix asphalt containing post-consumer recycled asphalt shingles and fractionated reclaimed asphalt pavement. *Report to the Illinois State Toll Highway Authority*.
38. Willis R., Timm D., West R., Powell B., Robbins M., Taylor A., Smit A., Tran N., Heitzman M. and A. Bianchini (2009). *Accelerated Performance Testing on the 2006 NCAT Test Track*. NCAT Report, National Center for Asphalt Technology, December 2009.
39. Zhou, F., Im, S., Hu, S., Newcomb, D., & Scullion, T. (2017). Selection and preliminary evaluation of laboratory cracking tests for routine asphalt mix designs. *Road Materials and Pavement Design*, 18(sup1), 62-86.
40. Zhou, F., Im, S., Sun, L., & Scullion, T. (2017). Development of an IDEAL cracking test for asphalt mix design and QC/QA. *Road Materials and Pavement Design*, 18(sup4), 405-427.
41. Zhou, F., Li, H., Hu, S., Button, J. W., & Epps, J. A. (2012). *Characterization and best use of recycled asphalt shingles in hot-mix asphalt* (No. FHWA/TX-13/0-6614-2). Texas. Dept. of Transportation. Research and Technology Implementation Office.
42. Zhou, F., S. Hu, & T. Scullion (2013a). *Balanced RAP/RAS Mix Design and Performance Evaluation System for Project Specific Service Conditions*. Report FHWA/ TX-13/0-6092-3. Texas A&M Transportation Institute, Texas A&M University, College Station, Texas.
43. Zofka, A., M.O. Marasteanu, T.R. Clyne, X. Li, & O. Hoffman (2004). *Development of Simple Asphalt Test for Determination of RAP Blending Charts*. Report MN/ RC-2004-44. Minnesota Department of Transportation, St. Paul, Minnesota.
44. Cooper, S. B., King, W., & Kabir, S. (2016). *Testing and analysis of LWT and SCB properties of asphalt concrete mixtures*, LTRC Project No. 11-3B

45. Flintsch, G. W., Loulizi, A., Diefenderfer, S. D., Diefenderfer, B. K., & Galal, K. A. (2008). Asphalt material characterization in support of mechanistic–empirical pavement design guide implementation in Virginia. *Transportation Research Record*, 2057(1), 114-125.
46. Romanoschi, S., & Scullion, T. (2014). *Validation of the maximum allowable amounts of recycled binder, RAP, and RAS using accelerated pavement testing-interim report* (No. FHWA/TX-14/0-6682-1). Texas. Dept. of Transportation. Research and Technology Implementation Office.
47. Lee, H., Mokhtari, A., & Williams, C. (2018). *TR 693: Development of Quality Standards for Inclusion of High Recycled Asphalt Pavement Content in Asphalt Mixtures, Phase III* (No. TR-693). University of Iowa. Center for Computer-Aided Design.
48. Newcomb, D. E., Epps, J. A., & Zhou, F. (2016). *Use of RAP & RAS in High Binder Replacement Asphalt Mixtures: A Synthesis. National Asphalt Pavement Association, Special Report, 213.*
49. Arshadi, A., Steger, R., Ghabchi, R., Zaman, M., Hobson, K., & Commuri, S. (2017). Performance evaluation of plant-produced warm mix asphalts containing RAP and RAS. *Road Materials and Pavement Design*, 18(sup4), 293-310.
50. Pouranian, M. R., & Shishehbor, M. (2019). Sustainability assessment of green asphalt mixtures: A review. *Environments*, 6(6), 73.
51. Bell, C. A. (1990). Relationship between laboratory aging tests and field performance of asphalt-concrete mixtures. In *Serviceability and Durability of Construction Materials* (pp. 745-754). ASCE.
52. Alavi, Z., He, Y., Harvey, J., & Jones, D. W. (2015). *Evaluation of the combined effects of reclaimed asphalt pavement (RAP), reclaimed asphalt shingles (RAS), and different virgin binder sources on the performance of blended binders for mixes with higher percentages of RAP and RAS: a research report from t* (No. UCPRC-RR-2015-06). University of California (System). Pavement Research Center.
53. Pasetto, M., Partl, M. N., & Tebaldi, G. (Eds.). (2019). *Proceedings of the 5th International Symposium on Asphalt Pavements & Environment (APE)* (Vol. 48). Springer Nature.
54. Golalipour, A., Veginati, V., & Mensching, D. J. (2021). Evaluation of Asphalt Mixture Performance Using Cracking and Durability Tests at a Full-Scale Pavement Facility. *Transportation Research Record*, 03611981211021856.
55. Zhou, F., Hu, S., & Newcomb, D. (2020). Development of a performance-related framework for production quality control with ideal cracking and rutting tests. *Construction and Building Materials*, 261, 120549.

APPENDIX A

Item 1

Mix Design of the Asphalt mixtures

TEXAS DEPARTMENT OF TRANSPORTATION
HMCP MIXTURE DESIGN : MATERIAL PROPERTIES

SAMPLE ID:	HSC18AUSTA1711	SAMPLE DATE:	3/2/2017
LOT NUMBER:	DA6C111960	LETTING DATE:	10/05/2016
SAMPLE STATUS:	COMPLETE	CONTROLLING CSJ:	0196-03-272
COUNTY:	DALLAS	SPEC YEAR:	2014
SAMPLED BY:	MITCHELL PAGE	SPEC ITEM:	03446032
SAMPLE LOCATION:	GOODNIGHT LANE PLANT	SPECIAL PROVISION:	
MATERIAL CODE:	0344CM0000	MIX TYPE:	344-SP-C
MATERIAL NAME:	ITEM 344 COMPLETE MIX QCQA ALL MIX TYPES		
PRODUCER:	D18AUSTIN-ASPH:AUSTIN ASPHALT GOODNIGHT LANE PLANT		
AREA ENGINEER:	JASON MASHELL	PROJECT MANAGER:	FREDRICK POLK

COURSE/LIFT:	Surface	STATION:		DIST. FROM CL:		CONTRACTOR DESIGN # :	DA6C111960
--------------	---------	----------	--	----------------	--	-----------------------	------------

	Bin No.1	Bin No.2	Bin No.3	Bin No.4	Bin No.5	Bin No.6	Bin No.7
Individual Bin (%):	Bin No.1 = 25 %	Bin No.2 = 30.3 %	Bin No.3 = 28 %				
Aggregate Source:	Limestone_Dolomite	Limestone_Dolomite	Limestone_Dolomite				
Aggregate Number:	50445	50445	50445				
Sample ID:	TY C	TY D	Man Sand				

Test Name	Site Manager Test Template	Test Method	Spec. Min or Max	Spec. Limit	Modified Spec. Limit	Result	Sample ID	Result	Sample ID	Result	Sample ID	Result	Sample ID	Result	Sample ID	Result	Sample ID	Result	Sample ID
Stockpile						Bin No.1		Bin No.2		Bin No.3		Bin No.4		Bin No.5		Bin No.6		Bin No.7	
Decantation	Tx217	Tex-217-F	Max.	1.5		0.60	TY B	0.40	TY D										
Deleterious Mat'l	Tx217	Tex-217-F	Max.	1.0		0.00	TY B	0.00	TY D	0.00	Man Sand								
Surface Aggregate Classification	Tx4AgClas	Tex-438-A, Tex-612-J	Min.		B	B	RS-SAC	B	RS-SAC	B	RS-SAC								
Magnesium Sulfate Soundness	Tx411M	Tex-411-A	Max.	25		6.00	RSSM	6.00	RSSM	6.00	RSSM								
LA Abrasion	Tx410	Tex-410-A	Max.	35		30.00	RSLA	30.00	RSLA	30.00	RSLA								
Crushed Faces Count	Tx460	Tex-460-A	Min.	95	NA														
Flat & Elongated	Tx280	Tex-280-F	Max.	10		0.00	TY B	0.00	TY D										
Micro-Deval Abrasion	Tx461	Tex-461-A	Use results to estimate the Mg Sulfate Soundness Loss			11.00	RSMD	11.00	RSMD										
Fine Aggregate						Bin No.1		Bin No.2		Bin No.3		Bin No.4		Bin No.5		Bin No.6		Bin No.7	
Bar Linear Shrinkage	Tx107	Tex-107-E	Max.	3						1.00	Man Sand								
Methylene Blue	-	AASHTO T330	Max.																
Combined Aggregate						Bin No.1		Bin No.2		Bin No.3		Bin No.4		Bin No.5		Bin No.6		Bin No.7	
Sand Equivalent	Tx203	Tex-203-F	Min.	45		80.00	Combined agg												
User Defined Testing						Bin No.1		Bin No.2		Bin No.3		Bin No.4		Bin No.5		Bin No.6		Bin No.7	
Use this area to enter any test methods, specifications & test result that apply to this material(s) but are not listed above.	1																		
	2																		
	3																		
	4																		
	5																		

Recycled Materials						Bin No.8		Bin No.9		Bin No.10	
Deleterious Mat'l	Tx217	Tex-217-F, Part III	Max.	0.5		0.2	Frac Rap				
Decantation	Tx406	Tex-406-A, Part I	Max.	5		2.0	Frac Rap				
Plasticity Index	Tx104-6	Tex-106-E	Max.	8							
User Defined Testing											

Remarks:
Reference: BRSQC dated 04/01/17.



TEXAS DEPARTMENT OF TRANSPORTATION
AUSTIN ASPHALT

2014 HMAP MIXTURE DESIGN : COMBINED GRADATION

Refresh Workbook

TX2MIXDE14 - File Version: 01/19/17 15:32:54

SAMPLE ID:	HSC18AUSTA1711	SAMPLE DATE:	3/2/2017
LOT NUMBER:	DA6C111960	LETTING DATE:	10/05/2016
SAMPLE STATUS:	COMPLETE	CONTROLLING CSJ:	0196-03-272
COUNTY:	DALLAS	SPEC YEAR:	2014
SAMPLED BY:	MITCHELL PAGE	SPEC ITEM:	03446032
SAMPLE LOCATION:	GOODNIGHT LANE PLANT	SPECIAL PROVISION:	
MATERIAL CODE:	0344CM0000	MIX TYPE:	344-SP-C
MATERIAL NAME:	ITEM 344 COMPLETE MIX QCQA ALL MIX TYPES		WMA Additive in Design? Yes
PRODUCER:	D18AUSTIN-ASPH:AUSTIN ASPHALT GOODNIGHT LANE PLANT		Target Discharge Temp., °F: 275
AREA ENGINEER:	JASON MASHELL	PROJECT MANAGER:	FREDRICK POLK
		WMA RATE:	0.5 UNITS: % by weight of asphalt
COURSE/LIFT:	Surface	STATION:	
		DIST. FROM CL:	
		CONTRACTOR DESIGN #:	DA6C111960

Maximum Allowable, %	
Frac RAP:	20.0
Unfrac RAP:	10.0
RAS:	5.0
RB Ratio:	20.0

Recycled Binder, %	
Bin No.8 :	0.8
Bin No.9 :	0.0
Bin No.10 :	0.0
Total	0.8

Use this value in the QC/QA template>>

Ratio of Recycled to Total Binder, %	
(based on binder percent (%) entered below in this worksheet)	
15.6	

Aggregate	AGGREGATE BIN FRACTIONS							"RECYCLED MATERIALS"						Material Type						
	Bin No.1	Bin No.2	Bin No.3	Bin No.4	Bin No.5	Bin No.6	Bin No.7	Bin No.8	Bin No.9	Bin No.10										
Source:	limestone_Dolomit	limestone_Dolomit	limestone_Dolomit					Fractionated RAP	RAS			Material Source								
Pit:	Mill Creek, OK	Mill Creek, OK	Mill Creek, OK					Austin Asphalt Dallas Plant	Sustainable Pavement			RAS Type								
Number:	50445	50445	50445						Tear-off			RAP/RAS Producer								
Producer:	Martin Marietta	Martin Marietta	Martin Marietta					Austin Asphalt Dallas Plant	Sustainable Pavement Technologies			Sample ID								
Sample ID:	TY C	TY D	Man Sand					Fine 1/2"	RAS											
Recycled Asphalt Binder (%)																				
												5.0	19.0			Combined Gradation				
Hydrated Lime?:								15.0	% of Tot. Mix	0.0	% of Tot. Mix	% of Tot. Mix	Total Bin	Lower & Upper Specification Limits						
Individual Bin (%):	25.0	Percent	30.0	Percent	30.0	Percent	Percent	Percent	Percent	Percent	Percent	15.0	% of Aggreg		% of Aggreg	% of Aggreg	100.0%			
Sieve Size:	Cum.% Passing	Wtd Cum. %	Cum.% Passing	Wtd Cum. %	Cum.% Passing	Wtd Cum. %	Cum.% Passing	Wtd Cum. %	Cum.% Passing	Wtd Cum. %	Cum.% Passing	Wtd Cum. %	Cum.% Passing	Wtd Cum. %	Cum.% Passing	Wtd Cum. %	Cum. % Passing	Lower	Upper	Within Spec's
1"	100.0	25.0	100.0	30.0	100.0	30.0											100.0	100.0	100.0	Yes
3/4"	100.0	25.0	100.0	30.0	100.0	30.0											100.0	98.0	100.0	Yes
1/2"	74.7	18.7	100.0	30.0	100.0	30.0											93.7	90.0	100.0	Yes
3/8"	41.6	10.4	96.0	28.8	100.0	30.0											84.2	58.0	90.0	Yes
No. 4	5.0	1.3	45.0	13.5	99.3	29.8											54.5	28.0	90.0	Yes
No. 8	1.9	0.5	6.6	2.0	87.7	26.3											35.3	28.0	58.0	Yes
No. 16	1.1	0.3	4.4	1.3	59.7	17.9											24.8	2.0	58.0	Yes
No. 30	1.1	0.3	2.3	0.7	44.5	13.4											18.5	2.0	58.0	Yes
No. 50	1.1	0.3	1.3	0.4	23.6	7.1											11.2	2.0	58.0	Yes
No. 200	1.1	0.3	1.1	0.3	4.2	1.3											2.9	2.0	10.0	Yes

(Bold Italic) Not within specifications (Bold Italic) Not within specifications- Restricted Zone (Italic) Not cumulative

Lift Thickness, in:	2.00	Binder Substitution?	No	Binder Originally Specified:	PG 70-22	Substitute Binder:	
Asphalt Source:	Ergon PG70-22	Binder Percent, (%):	4.8	Asphalt Spec. Grav.:	1.028		
Antistripping Agent:	Evotherm	Percent, (%):	0.5				

Dry Rodded Unit Weight of Coarse Agg. (pcf)	92.000
---	--------

Remarks:
Designed by Danny Meek (Level 2 Cert. # 595).

Combined Gradation

Notes:

Page 3 of 10

TEXAS DEPARTMENT OF TRANSPORTATION
HMCP MIXTURE DESIGN : MATERIAL PROPERTIES

SAMPLE ID:	HSC18AUSTA1711	SAMPLE DATE:	3/2/2017
LOT NUMBER:	DA6C111960	LETTING DATE:	10/05/2016
SAMPLE STATUS:	COMPLETE	CONTROLLING CSJ:	0196-03-272
COUNTY:	DALLAS	SPEC YEAR:	2014
SAMPLED BY:	MITCHELL PAGE	SPEC ITEM:	03446032
SAMPLE LOCATION:	GOODNIGHT LANE PLANT	SPECIAL PROVISION:	
MATERIAL CODE:	0344CM0000	MIX TYPE:	344-SP-C
MATERIAL NAME:	ITEM 344 COMPLETE MIX QCQA ALL MIX TYPES		
PRODUCER:	D18AUSTIN-ASPH:AUSTIN ASPHALT GOODNIGHT LANE PLANT		
AREA ENGINEER:	JASON MASHELL	PROJECT MANAGER:	FREDRICK POLK

COURSE/LIFT:	Surface	STATION:		DIST. FROM CL:		CONTRACTOR DESIGN # :	DA6C111960
--------------	---------	----------	--	----------------	--	-----------------------	------------

	Bin No.1	Bin No.2	Bin No.3	Bin No.4	Bin No.5	Bin No.6	Bin No.7
Individual Bin (%):	Bin No.1 = 25 %	Bin No.2 = 30 %	Bin No.3 = 30 %				
Aggregate Source:	Limestone_Dolomite	Limestone_Dolomite	Limestone_Dolomite				
Aggregate Number:	50445	50445	50445				
Sample ID:	TY C	TY D	Man Sand				

Test Name	Site Manager Test Template	Test Method	Spec. Min or Max	Spec. Limit	Modified Spec. Limit	Result	Sample ID	Result	Sample ID	Result	Sample ID	Result	Sample ID	Result	Sample ID	Result	Sample ID	Result	Sample ID
Stockpile							Bin No.1		Bin No.2		Bin No.3		Bin No.4		Bin No.5		Bin No.6		Bin No.7
Decantation	Tx217	Tex-217-F	Max.	1.5		0.60	TY B	0.40	TY D										
Deleterious Mat'l	Tx217	Tex-217-F	Max.	1.0		0.00	TY B	0.00	TY D	0.00	Man Sand								
Surface Aggregate Classification	Tx4AgClas	Tex-438-A, Tex-612-J	Min.		B	B	RS-SAC	B	RS-SAC	B	RS-SAC								
Magnesium Sulfate Soundness	Tx411M	Tex-411-A	Max.	25		6.00	RSSM	6.00	RSSM	6.00	RSSM								
LA Abrasion	Tx410	Tex-410-A	Max.	35		30.00	RSLA	30.00	RSLA	30.00	RSLA								
Crushed Faces Count	Tx460	Tex-460-A	Min.	95	NA														
Flat & Elongated	Tx280	Tex-280-F	Max.	10		0.00	TY B	0.00	TY D										
Micro-Deval Abrasion	Tx461	Tex-461-A	Use results to estimate the Mg Sulfate Soundness Loss			11.00	RSMD	11.00	RSMD										
Fine Aggregate							Bin No.1		Bin No.2		Bin No.3		Bin No.4		Bin No.5		Bin No.6		Bin No.7
Bar Linear Shrinkage	Tx107	Tex-107-E	Max.	3						1.00	Man Sand								
Methylene Blue	-	AASHTO T330	Max.																
Combined Aggregate							Bin No.1		Bin No.2		Bin No.3		Bin No.4		Bin No.5		Bin No.6		Bin No.7
Sand Equivalent	Tx203	Tex-203-F	Min.	45		80.00	Combined agg												
User Defined Testing							Bin No.1		Bin No.2		Bin No.3		Bin No.4		Bin No.5		Bin No.6		Bin No.7
Use this area to enter any test methods, specifications & test result that apply to this material(s) but are not listed above.	1																		
	2																		
	3																		
	4																		
	5																		

Recycled Materials						Bin No.8	Bin No.9	Bin No.10
Deleterious Mat'l	Tx217	Tex-217-F, Part III	Max.	0.5		0.2	Frac Rap	
Decantation	Tx406	Tex-406-A, Part I	Max.	5		2.0	Frac Rap	
Plasticity Index	Tx104-6	Tex-106-E	Max.	8				
User Defined Testing								

Remarks:
Reference: BRSQC dated 04/01/17.

TEXAS DEPARTMENT OF TRANSPORTATION
HMCP MIXTURE DESIGN : MATERIAL PROPERTIES

SAMPLE ID:	HSC18AUSTA1711	SAMPLE DATE:	3/2/2017
LOT NUMBER:	DA6C111960	LETTING DATE:	10/05/2016
SAMPLE STATUS:	COMPLETE	CONTROLLING CSJ:	0196-03-272
COUNTY:	DALLAS	SPEC YEAR:	2014
SAMPLED BY:	MITCHELL PAGE	SPEC ITEM:	03446032
SAMPLE LOCATION:	GOODNIGHT LANE PLANT	SPECIAL PROVISION:	
MATERIAL CODE:	0344CM0000	MIX TYPE:	344-SP-C
MATERIAL NAME:	ITEM 344 COMPLETE MIX QCQA ALL MIX TYPES		
PRODUCER:	D18AUSTIN-ASPH:AUSTIN ASPHALT GOODNIGHT LANE PLANT		
AREA ENGINEER:	JASON MASHELL	PROJECT MANAGER:	FREDRICK POLK

COURSE/LIFT:	Surface	STATION:		DIST. FROM CL:		CONTRACTOR DESIGN # :	DA6C111960
--------------	---------	----------	--	----------------	--	-----------------------	------------

	Bin No.1	Bin No.2	Bin No.3	Bin No.4	Bin No.5	Bin No.6	Bin No.7
Individual Bin (%):	Bin No.1 = 25 %	Bin No.2 = 38 %	Bin No.3 = 36 %	Bin No.4 = 1 %			
Aggregate Source:	Limestone_Dolomite	Limestone_Dolomite	Limestone_Dolomite				
Aggregate Number:	50445	50445	50445				
Sample ID:	TY C	TY D	Man Sand	filler			

Test Name	Site Manager Test Template	Test Method	Spec. Min or Max	Spec. Limit	Modified Spec. Limit	Result	Sample ID	Result	Sample ID	Result	Sample ID	Result	Sample ID	Result	Sample ID	Result	Sample ID	Result	Sample ID
Stockpile							Bin No.1		Bin No.2		Bin No.3		Bin No.4		Bin No.5		Bin No.6		Bin No.7
Decantation	Tx217	Tex-217-F	Max.	1.5		0.60	TY B	0.40	TY D										
Deleterious Mat'l	Tx217	Tex-217-F	Max.	1.0		0.00	TY B	0.00	TY D	0.00	Man Sand								
Surface Aggregate Classification	Tx4AgClas	Tex-438-A, Tex-612-J	Min.		B	B	RS-SAC	B	RS-SAC	B	RS-SAC								
Magnesium Sulfate Soundness	Tx411M	Tex-411-A	Max.	25		6.00	RSSM	6.00	RSSM	6.00	RSSM								
LA Abrasion	Tx410	Tex-410-A	Max.	35		30.00	RSLA	30.00	RSLA	30.00	RSLA								
Crushed Faces Count	Tx460	Tex-460-A	Min.	95	NA														
Flat & Elongated	Tx280	Tex-280-F	Max.	10		0.00	TY B	0.00	TY D										
Micro-Deval Abrasion	Tx461	Tex-461-A	Use results to estimate the Mg Sulfate Soundness Loss			11.00	RSMD	11.00	RSMD										
Fine Aggregate							Bin No.1		Bin No.2		Bin No.3		Bin No.4		Bin No.5		Bin No.6		Bin No.7
Bar Linear Shrinkage	Tx107	Tex-107-E	Max.	3						1.00	Man Sand								
Methylene Blue	-	AASHTO T330	Max.																
Combined Aggregate							Bin No.1		Bin No.2		Bin No.3		Bin No.4		Bin No.5		Bin No.6		Bin No.7
Sand Equivalent	Tx203	Tex-203-F	Min.	45		80.00	Combined agg												
User Defined Testing							Bin No.1		Bin No.2		Bin No.3		Bin No.4		Bin No.5		Bin No.6		Bin No.7
Use this area to enter any test methods, specifications & test result that apply to this material(s) but are not listed above.	1																		
	2																		
	3																		
	4																		
	5																		

Recycled Materials						Bin No.8	Bin No.9	Bin No.10
Deleterious Mat'l	Tx217	Tex-217-F, Part III	Max.	0.5		0.2	Frac Rap	
Decantation	Tx406	Tex-406-A, Part I	Max.	5		2.0	Frac Rap	
Plasticity Index	Tx104-6	Tex-106-E	Max.	8				
User Defined Testing								

Remarks:
Reference: BRSQC dated 04/01/17.



TEXAS DEPARTMENT OF TRANSPORTATION
AUSTIN ASPHALT

2014 HMAP MIXTURE DESIGN : COMBINED GRADATION

Refresh Workbook

TX2MIXDE14 - File Version: 01/19/17 15:32:54

SAMPLE ID:	HSC18AUSTA1711	SAMPLE DATE:	3/2/2017
LOT NUMBER:	DA6C111960	LETTING DATE:	10/05/2016
SAMPLE STATUS:	COMPLETE	CONTROLLING CSJ:	0196-03-272
COUNTY:	DALLAS	SPEC YEAR:	2014
SAMPLED BY:	MITCHELL PAGE	SPEC ITEM:	03446032
SAMPLE LOCATION:	GOODNIGHT LANE PLANT	SPECIAL PROVISION:	
MATERIAL CODE:	0344CM0000	MIX TYPE:	344-SP-C
MATERIAL NAME:	ITEM 344 COMPLETE MIX QCQA ALL MIX TYPES		WMA Additive in Design? Yes
PRODUCER:	D18AUSTIN-ASPH:AUSTIN ASPHALT GOODNIGHT LANE PLANT		Target Discharge Temp., °F: 275
AREA ENGINEER:	JASON MASHHELL	PROJECT MANAGER:	FREDRICK POLK
		WMA RATE:	0.5 UNITS: % by weight of asphalt
COURSE/LIFT:	Surface	STATION:	
		DIST. FROM CL:	
		CONTRACTOR DESIGN #:	DA6C111960

Maximum Allowable, %	
Frac RAP:	20.0
Unfrac RAP:	10.0
RAS:	5.0
RB Ratio:	30.0

Recycled Binder, %	
Bin No.8 :	0.8
Bin No.9 :	0.0
Bin No.10 :	0.0
Total	0.8

Use this value in the QC/QA template>>

Ratio of Recycled to Total Binder, %	
(based on binder percent (%) entered below in this worksheet)	
15.6	

Aggregate	AGGREGATE BIN FRACTIONS							"RECYCLED MATERIALS"						Material Type				
	Bin No.1	Bin No.2	Bin No.3	Bin No.4	Bin No.5	Bin No.6	Bin No.7	Bin No.8	Bin No.9	Bin No.10								
Source:	limestone_Dolomit	limestone_Dolomit	limestone_Dolomit					Fractionated RAP	RAS				Material Source					
Pit:	Mill Creek, OK	Mill Creek, OK	Mill Creek, OK					Austin Asphalt Dallas Plant	Sustainable Pavement				RAS Type					
Number:	50445	50445	50445						Tear-off				RAP/RAS Producer					
Producer:	Martin Marietta	Martin Marietta	Martin Marietta					Austin Asphalt Dallas Plant	Sustainable Pavement Technologies				Sample ID					
Sample ID:	TY C	TY D	Man Sand					Fine 1/2"	RAS									
Recycled Asphalt Binder (%)												Combined Gradation						
												5.0	19.0					
Hydrated Lime?:								15.0	% of Tot. Mix	0.0	% of Tot. Mix	% of Tot. Mix	Total Bin	Lower & Upper Specification Limits				
Individual Bin (%):	25.0	Percent	30.0	Percent	30.0	Percent	Percent	Percent	Percent	Percent	Percent	100.0%						
Sieve Size:	Cum.% Passing	Wtd Cum. %	Cum.% Passing	Wtd Cum. %	Cum.% Passing	Wtd Cum. %	Cum.% Passing	Wtd Cum. %	Cum.% Passing	Wtd Cum. %	Cum.% Passing	Wtd Cum. %	Cum.% Passing	Wtd Cum. %	Cum. % Passing	Lower	Upper	Within Spec's
1"	100.0	25.0	100.0	30.0	100.0	30.0									100.0	100.0	100.0	Yes
3/4"	100.0	25.0	100.0	30.0	100.0	30.0									100.0	98.0	100.0	Yes
1/2"	74.7	18.7	100.0	30.0	100.0	30.0									93.7	90.0	100.0	Yes
3/8"	41.6	10.4	96.0	28.8	100.0	30.0									84.2	58.0	90.0	Yes
No. 4	5.0	1.3	45.0	13.5	99.3	29.8									54.5	28.0	90.0	Yes
No. 8	1.9	0.5	6.6	2.0	87.7	26.3									35.3	28.0	58.0	Yes
No. 16	1.1	0.3	4.4	1.3	59.7	17.9									24.8	2.0	58.0	Yes
No. 30	1.1	0.3	2.3	0.7	44.5	13.4									18.5	2.0	58.0	Yes
No. 50	1.1	0.3	1.3	0.4	23.6	7.1									11.2	2.0	58.0	Yes
No. 200	1.1	0.3	1.1	0.3	4.2	1.3									2.9	2.0	10.0	Yes

(Bold Italic) Not within specifications **(Bold Italic)** Not within specifications- Restricted Zone **(Italic)** Not cumulative

Lift Thickness, in:	2.00	Binder Substitution?	No	Binder Originally Specified:	PG 64-28	Substitute Binder:	
Asphalt Source:	Jebro PG64-28	Binder Percent, (%):	4.8	Asphalt Spec. Grav.:	1.028		
Antistripping Agent:	Evotherm	Percent, (%):	0.5				

Dry Rodded Unit Weight of Coarse Agg. (pcf) 92.000

Remarks:
Designed by Danny Meek (Level 2 Cert. # 595).

Combined Gradation

Notes:

Page 3 of 10

TEXAS DEPARTMENT OF TRANSPORTATION
HMCP MIXTURE DESIGN : MATERIAL PROPERTIES

SAMPLE ID:	HSC18AUSTA1711	SAMPLE DATE:	3/2/2017
LOT NUMBER:	DA6C111960	LETTING DATE:	10/05/2016
SAMPLE STATUS:	COMPLETE	CONTROLLING CSJ:	0196-03-272
COUNTY:	DALLAS	SPEC YEAR:	2014
SAMPLED BY:	MITCHELL PAGE	SPEC ITEM:	03446032
SAMPLE LOCATION:	GOODNIGHT LANE PLANT	SPECIAL PROVISION:	
MATERIAL CODE:	0344CM0000	MIX TYPE:	344-SP-C
MATERIAL NAME:	ITEM 344 COMPLETE MIX QCQA ALL MIX TYPES		
PRODUCER:	D18AUSTIN-ASPH:AUSTIN ASPHALT GOODNIGHT LANE PLANT		
AREA ENGINEER:	JASON MASHELL	PROJECT MANAGER:	FREDRICK POLK

COURSE/LIFT:	Surface	STATION:		DIST. FROM CL:		CONTRACTOR DESIGN # :	DA6C111960
--------------	---------	----------	--	----------------	--	-----------------------	------------

	Bin No.1	Bin No.2	Bin No.3	Bin No.4	Bin No.5	Bin No.6	Bin No.7
Individual Bin (%):	Bin No.1 = 25 %	Bin No.2 = 30 %	Bin No.3 = 30 %				
Aggregate Source:	Limestone_Dolomite	Limestone_Dolomite	Limestone_Dolomite				
Aggregate Number:	50445	50445	50445				
Sample ID:	TY C	TY D	Man Sand				

Test Name	Site Manager Test Template	Test Method	Spec. Min or Max	Spec. Limit	Modified Spec. Limit	Result	Sample ID	Result	Sample ID	Result	Sample ID	Result	Sample ID	Result	Sample ID	Result	Sample ID	Result	Sample ID
Stockpile						Bin No.1		Bin No.2		Bin No.3		Bin No.4		Bin No.5		Bin No.6		Bin No.7	
Decantation	Tx217	Tex-217-F	Max.	1.5		0.60	TY B	0.40	TY D										
Deleterious Mat'l	Tx217	Tex-217-F	Max.	1.0		0.00	TY B	0.00	TY D	0.00	Man Sand								
Surface Aggregate Classification	Tx4AgClas	Tex-438-A, Tex-612-J	Min.		B	B	RS-SAC	B	RS-SAC	B	RS-SAC								
Magnesium Sulfate Soundness	Tx411M	Tex-411-A	Max.	25		6.00	RSSM	6.00	RSSM	6.00	RSSM								
LA Abrasion	Tx410	Tex-410-A	Max.	35		30.00	RSLA	30.00	RSLA	30.00	RSLA								
Crushed Faces Count	Tx460	Tex-460-A	Min.	95	NA														
Flat & Elongated	Tx280	Tex-280-F	Max.	10		0.00	TY B	0.00	TY D										
Micro-Deval Abrasion	Tx461	Tex-461-A	Use results to estimate the Mg Sulfate Soundness Loss			11.00	RSMD	11.00	RSMD										
Fine Aggregate						Bin No.1		Bin No.2		Bin No.3		Bin No.4		Bin No.5		Bin No.6		Bin No.7	
Bar Linear Shrinkage	Tx107	Tex-107-E	Max.	3						1.00	Man Sand								
Methylene Blue	-	AASHTO T330	Max.																
Combined Aggregate						Bin No.1		Bin No.2		Bin No.3		Bin No.4		Bin No.5		Bin No.6		Bin No.7	
Sand Equivalent	Tx203	Tex-203-F	Min.	45		80.00	Combined agg												
User Defined Testing						Bin No.1		Bin No.2		Bin No.3		Bin No.4		Bin No.5		Bin No.6		Bin No.7	
Use this area to enter any test methods, specifications & test result that apply to this material(s) but are not listed above.	1																		
	2																		
	3																		
	4																		
	5																		

Recycled Materials						Bin No.8		Bin No.9		Bin No.10	
Deleterious Mat'l	Tx217	Tex-217-F, Part III	Max.	0.5		0.2	Frac Rap				
Decantation	Tx406	Tex-406-A, Part I	Max.	5		2.0	Frac Rap				
Plasticity Index	Tx104-6	Tex-106-E	Max.	8							
User Defined Testing											

Remarks:
Reference: BRSQC dated 04/01/17.

TEXAS DEPARTMENT OF TRANSPORTATION
HMCP MIXTURE DESIGN : MATERIAL PROPERTIES

SAMPLE ID:	HSC18AUSTA1711	SAMPLE DATE:	3/2/2017
LOT NUMBER:	DA6C111960	LETTING DATE:	10/05/2016
SAMPLE STATUS:	COMPLETE	CONTROLLING CSJ:	0196-03-272
COUNTY:	DALLAS	SPEC YEAR:	2014
SAMPLED BY:	MITCHELL PAGE	SPEC ITEM:	03446032
SAMPLE LOCATION:	GOODNIGHT LANE PLANT	SPECIAL PROVISION:	
MATERIAL CODE:	0344CM0000	MIX TYPE:	344-SP-C
MATERIAL NAME:	ITEM 344 COMPLETE MIX QCQA ALL MIX TYPES		
PRODUCER:	D18AUSTIN-ASPH:AUSTIN ASPHALT GOODNIGHT LANE PLANT		
AREA ENGINEER:	JASON MASHELL	PROJECT MANAGER:	FREDRICK POLK

COURSE/LIFT:	Surface	STATION:		DIST. FROM CL:		CONTRACTOR DESIGN # :	DA6C111960
--------------	---------	----------	--	----------------	--	-----------------------	------------

	Bin No.1	Bin No.2	Bin No.3	Bin No.4	Bin No.5	Bin No.6	Bin No.7
Individual Bin (%):	Bin No.1 = 25 %	Bin No.2 = 33.3 %	Bin No.3 = 25 %				
Aggregate Source:	Limestone_Dolomite	Limestone_Dolomite	Limestone_Dolomite				
Aggregate Number:	50445	50445	50445				
Sample ID:	TY C	TY D	Man Sand				

Test Name	Site Manager Test Template	Test Method	Spec. Min or Max	Spec. Limit	Modified Spec. Limit	Result	Sample ID	Result	Sample ID	Result	Sample ID	Result	Sample ID	Result	Sample ID	Result	Sample ID	Result	Sample ID
Stockpile							Bin No.1		Bin No.2		Bin No.3		Bin No.4		Bin No.5		Bin No.6		Bin No.7
Decantation	Tx217	Tex-217-F	Max.	1.5		0.60	TY B	0.40	TY D										
Deleterious Mat'l	Tx217	Tex-217-F	Max.	1.0		0.00	TY B	0.00	TY D	0.00	Man Sand								
Surface Aggregate Classification	Tx4AgClas	Tex-438-A, Tex-612-J	Min.		B	B	RS-SAC	B	RS-SAC	B	RS-SAC								
Magnesium Sulfate Soundness	Tx411M	Tex-411-A	Max.	25		6.00	RSSM	6.00	RSSM	6.00	RSSM								
LA Abrasion	Tx410	Tex-410-A	Max.	35		30.00	RSLA	30.00	RSLA	30.00	RSLA								
Crushed Faces Count	Tx460	Tex-460-A	Min.	95	NA														
Flat & Elongated	Tx280	Tex-280-F	Max.	10		0.00	TY B	0.00	TY D										
Micro-Deval Abrasion	Tx461	Tex-461-A	Use results to estimate the Mg Sulfate Soundness Loss			11.00	RSMD	11.00	RSMD										
Fine Aggregate							Bin No.1		Bin No.2		Bin No.3		Bin No.4		Bin No.5		Bin No.6		Bin No.7
Bar Linear Shrinkage	Tx107	Tex-107-E	Max.	3						1.00	Man Sand								
Methylene Blue	-	AASHTO T330	Max.																
Combined Aggregate							Bin No.1		Bin No.2		Bin No.3		Bin No.4		Bin No.5		Bin No.6		Bin No.7
Sand Equivalent	Tx203	Tex-203-F	Min.	45		80.00	Combined agg												
User Defined Testing							Bin No.1		Bin No.2		Bin No.3		Bin No.4		Bin No.5		Bin No.6		Bin No.7
Use this area to enter any test methods, specifications & test result that apply to this material(s) but are not listed above.	1																		
	2																		
	3																		
	4																		
	5																		

Recycled Materials						Bin No.8	Bin No.9	Bin No.10
Deleterious Mat'l	Tx217	Tex-217-F, Part III	Max.	0.5		0.2	Frac Rap	
Decantation	Tx406	Tex-406-A, Part I	Max.	5		2.0	Frac Rap	
Plasticity Index	Tx104-6	Tex-106-E	Max.	8				
User Defined Testing								

Remarks:
Reference: BRSQC dated 04/01/17.



TEXAS DEPARTMENT OF TRANSPORTATION
AUSTIN ASPHALT

2014 HMAP MIXTURE DESIGN : COMBINED GRADATION

Refresh Workbook

TX2MIXDE14 - File Version: 01/19/17 15:32:54

SAMPLE ID:	HSC18AUSTA1711	SAMPLE DATE:	3/2/2017
LOT NUMBER:	DA6C111960	LETTING DATE:	10/05/2016
SAMPLE STATUS:	COMPLETE	CONTROLLING CSJ:	0196-03-272
COUNTY:	DALLAS	SPEC YEAR:	2014
SAMPLED BY:	MITCHELL PAGE	SPEC ITEM:	03446032
SAMPLE LOCATION:	GOODNIGHT LANE PLANT	SPECIAL PROVISION:	
MATERIAL CODE:	0344CM0000	MIX TYPE:	344-SP-C
MATERIAL NAME:	ITEM 344 COMPLETE MIX QCQA ALL MIX TYPES		WMA Additive in Design? Yes
PRODUCER:	D18AUSTIN-ASPH:AUSTIN ASPHALT GOODNIGHT LANE PLANT		Target Discharge Temp., °F: 275
AREA ENGINEER:	JASON MASHELL	PROJECT MANAGER:	FREDRICK POLK
		WMA RATE:	0.5 UNITS: % by weight of asphalt
COURSE/LIFT:	Surface	STATION:	
		DIST. FROM CL:	
		CONTRACTOR DESIGN #:	DA6C111960

Maximum Allowable, %	
Frac RAP:	20.0
Unfrac RAP:	10.0
RAS:	5.0
RB Ratio:	30.0

Recycled Binder, %	
Bin No.8 :	0.8
Bin No.9 :	0.4
Bin No.10 :	0.0
Total	1.1

Use this value in the QC/QA template>>

Ratio of Recycled to Total Binder, %	
(based on binder percent (%) entered below in this worksheet)	
22.6	

Aggregate	AGGREGATE BIN FRACTIONS							"RECYCLED MATERIALS"			Material Type									
	Bin No.1	Bin No.2	Bin No.3	Bin No.4	Bin No.5	Bin No.6	Bin No.7	Bin No.8	Bin No.9	Bin No.10										
Source:	limestone_Dolomit	limestone_Dolomit	limestone_Dolomit					Fractionated RAP	RAS		Material Source									
Pit:	Mill Creek, OK	Mill Creek, OK	Mill Creek, OK					Austin Asphalt Dallas Plant	Sustainable Pavement		RAS Type									
Number:	50445	50445	50445						Tear-off		RAP/RAS Producer									
Producer:	Martin Marietta	Martin Marietta	Martin Marietta					Austin Asphalt Dallas Plant	Sustainable Pavement Technologies		Sample ID									
Sample ID:	TY C	TY D	Man Sand					Fine 1/2"	RAS											
								Recycled Asphalt Binder (%)												
								5.0	19.0		Combined Gradation									
Hydrated Lime?:								15.0	% of Tot. Mix	2.0	% of Tot. Mix	% of Tot. Mix	Total Bin	Lower & Upper Specification Limits						
Individual Bin (%):	25.0	Percent	30.3	Percent	28.0	Percent		Percent		Percent		Percent	100.0%							
Sieve Size:	Cum.% Passing	Wtd Cum. %	Cum.% Passing	Wtd Cum. %	Cum.% Passing	Wtd Cum. %	Cum.% Passing	Wtd Cum. %	Cum.% Passing	Wtd Cum. %	Cum.% Passing	Wtd Cum. %	Cum.% Passing	Wtd Cum. %	Cum.% Passing	Wtd Cum. %	Cum. % Passing	Lower	Upper	Within Spec's
1"	100.0	25.0	100.0	30.3	100.0	28.0											100.0	100.0	100.0	Yes
3/4"	100.0	25.0	100.0	30.3	100.0	28.0											100.0	98.0	100.0	Yes
1/2"	74.7	18.7	100.0	30.3	100.0	28.0											93.7	90.0	100.0	Yes
3/8"	41.6	10.4	96.0	29.1	100.0	28.0											84.2	58.0	90.0	Yes
No. 4	5.0	1.3	45.0	13.6	99.3	27.8											54.3	28.0	90.0	Yes
No. 8	1.9	0.5	6.6	2.0	87.7	24.6											35.2	28.0	58.0	Yes
No. 16	1.1	0.3	4.4	1.3	59.7	16.7											24.9	2.0	58.0	Yes
No. 30	1.1	0.3	2.3	0.7	44.5	12.5											18.6	2.0	58.0	Yes
No. 50	1.1	0.3	1.3	0.4	23.6	6.6											11.6	2.0	58.0	Yes
No. 200	1.1	0.3	1.1	0.3	4.2	1.2											3.2	2.0	10.0	Yes

(Bold Italic) Not within specifications (Bold Italic) Not within specifications- Restricted Zone (Italic) Not cumulative

Lift Thickness, in:	2.00	Binder Substitution?	No	Binder Originally Specified:	PG 64-22	Substitute Binder:	
Asphalt Source:	Hunt 64-22		Binder Percent, (%):	5.0	Asphalt Spec. Grav.:	1.028	
Antistripping Agent:	Evotherm		Percent, (%):	0.5			

Dry Rodded Unit Weight of Coarse Agg. (pcf)	92.000
---	--------

Remarks:
Designed by Danny Meek (Level 2 Cert. # 595).

Combined Gradation

Notes:

Page 3 of 10

TEXAS DEPARTMENT OF TRANSPORTATION
HMCP MIXTURE DESIGN : MATERIAL PROPERTIES

SAMPLE ID:	HSC18AUSTA1711	SAMPLE DATE:	3/2/2017
LOT NUMBER:	DA6C111960	LETTING DATE:	10/05/2016
SAMPLE STATUS:	COMPLETE	CONTROLLING CSJ:	0196-03-272
COUNTY:	DALLAS	SPEC YEAR:	2014
SAMPLED BY:	MITCHELL PAGE	SPEC ITEM:	03446032
SAMPLE LOCATION:	GOODNIGHT LANE PLANT	SPECIAL PROVISION:	
MATERIAL CODE:	0344CM0000	MIX TYPE:	344-SP-C
MATERIAL NAME:	ITEM 344 COMPLETE MIX QCQA ALL MIX TYPES		
PRODUCER:	D18AUSTIN-ASPH:AUSTIN ASPHALT GOODNIGHT LANE PLANT		
AREA ENGINEER:	JASON MASHELL	PROJECT MANAGER:	FREDRICK POLK

COURSE/LIFT:	Surface	STATION:		DIST. FROM CL:		CONTRACTOR DESIGN # :	DA6C111960
--------------	---------	----------	--	----------------	--	-----------------------	------------

	Bin No.1	Bin No.2	Bin No.3	Bin No.4	Bin No.5	Bin No.6	Bin No.7
Individual Bin (%):	Bin No.1 = 25 %	Bin No.2 = 30.3 %	Bin No.3 = 28 %				
Aggregate Source:	Limestone_Dolomite	Limestone_Dolomite	Limestone_Dolomite				
Aggregate Number:	50445	50445	50445				
Sample ID:	TY C	TY D	Man Sand				

Test Name	Site Manager Test Template	Test Method	Spec. Min or Max	Spec. Limit	Modified Spec. Limit	Result	Sample ID	Result	Sample ID	Result	Sample ID	Result	Sample ID	Result	Sample ID	Result	Sample ID	Result	Sample ID
Stockpile						Bin No.1		Bin No.2		Bin No.3		Bin No.4		Bin No.5		Bin No.6		Bin No.7	
Decantation	Tx217	Tex-217-F	Max.	1.5		0.60	TY B	0.40	TY D										
Deleterious Mat'l	Tx217	Tex-217-F	Max.	1.0		0.00	TY B	0.00	TY D	0.00	Man Sand								
Surface Aggregate Classification	Tx4AgClas	Tex-438-A, Tex-612-J	Min.		B	B	RS-SAC	B	RS-SAC	B	RS-SAC								
Magnesium Sulfate Soundness	Tx411M	Tex-411-A	Max.	25		6.00	RSSM	6.00	RSSM	6.00	RSSM								
LA Abrasion	Tx410	Tex-410-A	Max.	35		30.00	RSLA	30.00	RSLA	30.00	RSLA								
Crushed Faces Count	Tx460	Tex-460-A	Min.	95	NA														
Flat & Elongated	Tx280	Tex-280-F	Max.	10		0.00	TY B	0.00	TY D										
Micro-Deval Abrasion	Tx461	Tex-461-A	Use results to estimate the Mg Sulfate Soundness Loss			11.00	RSMD	11.00	RSMD										
Fine Aggregate						Bin No.1		Bin No.2		Bin No.3		Bin No.4		Bin No.5		Bin No.6		Bin No.7	
Bar Linear Shrinkage	Tx107	Tex-107-E	Max.	3						1.00	Man Sand								
Methylene Blue	-	AASHTO T330	Max.																
Combined Aggregate						Bin No.1		Bin No.2		Bin No.3		Bin No.4		Bin No.5		Bin No.6		Bin No.7	
Sand Equivalent	Tx203	Tex-203-F	Min.	45		80.00	Combined agg												
User Defined Testing						Bin No.1		Bin No.2		Bin No.3		Bin No.4		Bin No.5		Bin No.6		Bin No.7	
Use this area to enter any test methods, specifications & test result that apply to this material(s) but are not listed above.	1																		
	2																		
	3																		
	4																		
	5																		

Recycled Materials						Bin No.8		Bin No.9		Bin No.10	
Deleterious Mat'l	Tx217	Tex-217-F, Part III	Max.	0.5		0.2	Frac Rap				
Decantation	Tx406	Tex-406-A, Part I	Max.	5		2.0	Frac Rap				
Plasticity Index	Tx104-6	Tex-106-E	Max.	8							
User Defined Testing											

Remarks:
Reference: BRSQC dated 04/01/17.

TEXAS DEPARTMENT OF TRANSPORTATION
HMCP MIXTURE DESIGN : MATERIAL PROPERTIES

SAMPLE ID:	HSC18AUSTA1711	SAMPLE DATE:	3/2/2017
LOT NUMBER:	DA6C111960	LETTING DATE:	10/05/2016
SAMPLE STATUS:	COMPLETE	CONTROLLING CSJ:	0196-03-272
COUNTY:	DALLAS	SPEC YEAR:	2014
SAMPLED BY:	MITCHELL PAGE	SPEC ITEM:	03446032
SAMPLE LOCATION:	GOODNIGHT LANE PLANT	SPECIAL PROVISION:	
MATERIAL CODE:	0344CM0000	MIX TYPE:	344-SP-C
MATERIAL NAME:	ITEM 344 COMPLETE MIX QCQA ALL MIX TYPES		
PRODUCER:	D18AUSTIN-ASPH:AUSTIN ASPHALT GOODNIGHT LANE PLANT		
AREA ENGINEER:	JASON MASHELL	PROJECT MANAGER:	FREDRICK POLK

COURSE/LIFT:	Surface	STATION:		DIST. FROM CL:		CONTRACTOR DESIGN # :	DA6C111960
--------------	---------	----------	--	----------------	--	-----------------------	------------

	Bin No.1	Bin No.2	Bin No.3	Bin No.4	Bin No.5	Bin No.6	Bin No.7
Individual Bin (%):	Bin No.1 = 25 %	Bin No.2 = 28.5 %	Bin No.3 = 21.4 %				
Aggregate Source:	Limestone_Dolomite	Limestone_Dolomite	Limestone_Dolomite				
Aggregate Number:	50445	50445	50445				
Sample ID:	TY C	TY D	Man Sand				

Test Name	Site Manager Test Template	Test Method	Spec. Min or Max	Spec. Limit	Modified Spec. Limit	Result	Sample ID	Result	Sample ID	Result	Sample ID	Result	Sample ID	Result	Sample ID	Result	Sample ID	Result	Sample ID
Stockpile						Bin No.1	Bin No.2	Bin No.3	Bin No.4	Bin No.5	Bin No.6	Bin No.7							
Decantation	Tx217	Tex-217-F	Max.	1.5		0.60	TY B	0.40	TY D										
Deleterious Mat'l	Tx217	Tex-217-F	Max.	1.0		0.00	TY B	0.00	TY D	0.00	Man Sand								
Surface Aggregate Classification	Tx4AgClas	Tex-438-A, Tex-612-J	Min.		B	B	RS-SAC	B	RS-SAC	B	RS-SAC								
Magnesium Sulfate Soundness	Tx411M	Tex-411-A	Max.	25		6.00	RSSM	6.00	RSSM	6.00	RSSM								
LA Abrasion	Tx410	Tex-410-A	Max.	35		30.00	RSLA	30.00	RSLA	30.00	RSLA								
Crushed Faces Count	Tx460	Tex-460-A	Min.	95	NA														
Flat & Elongated	Tx280	Tex-280-F	Max.	10		0.00	TY B	0.00	TY D										
Micro-Deval Abrasion	Tx461	Tex-461-A	Use results to estimate the Mg Sulfate Soundness Loss			11.00	RSMD	11.00	RSMD										
Fine Aggregate						Bin No.1	Bin No.2	Bin No.3	Bin No.4	Bin No.5	Bin No.6	Bin No.7							
Bar Linear Shrinkage	Tx107	Tex-107-E	Max.	3						1.00	Man Sand								
Methylene Blue	-	AASHTO T330	Max.																
Combined Aggregate						Bin No.1	Bin No.2	Bin No.3	Bin No.4	Bin No.5	Bin No.6	Bin No.7							
Sand Equivalent	Tx203	Tex-203-F	Min.	45		80.00	Combined agg												
User Defined Testing						Bin No.1	Bin No.2	Bin No.3	Bin No.4	Bin No.5	Bin No.6	Bin No.7							
Use this area to enter any test methods, specifications & test result that apply to this material(s) but are not listed above.	1																		
	2																		
	3																		
	4																		
	5																		

Recycled Materials						Bin No.8	Bin No.9	Bin No.10
Deleterious Mat'l	Tx217	Tex-217-F, Part III	Max.	0.5		0.2	Frac Rap	
Decantation	Tx406	Tex-406-A, Part I	Max.	5		2.0	Frac Rap	
Plasticity Index	Tx104-6	Tex-106-E	Max.	8				
User Defined Testing								

Remarks:
Reference: BRSQC dated 04/01/17.

APPENDIX A

Item 2

Laboratory results for the imported soil



TEXAS DEPARTMENT OF TRANSPORTATION

Moisture-Density Relationship of Subgrade and Embankment Soils
Tex-114-E

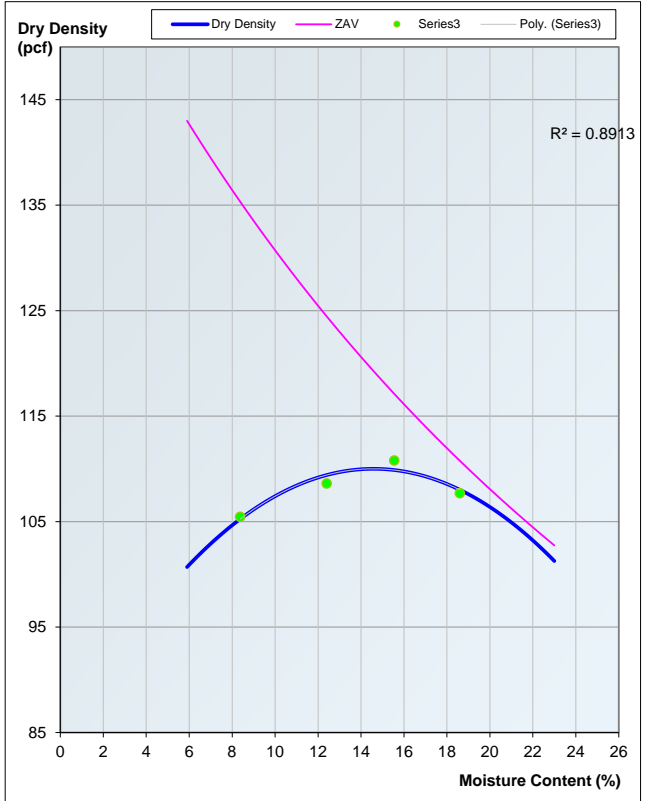
Refresh Workbook

File Version: 03/09/15 10:25:36

Table with sample details including SAMPLE ID: BOON & UTA- UTP, SAMPLED DATE, TEST NUMBER, LETTING DATE, SAMPLE STATUS, CONTROLLING CSJ, COUNTY, SPEC YEAR, SAMPLED BY, SPEC ITEM, SAMPLE LOCATION, SPECIAL PROVISION, MATERIAL CODE, GRADE, MATERIAL NAME, PRODUCER, AREA ENGINEER, PROJECT MANAGER, COURSE/LIFT, STATION, DIST. FROM CL.

Moisture-Density Work Sheet

Moisture-Density Work Sheet table containing data for Oven Dry Weight, Weight of Pycnometer & Water, Weight of Aggr., Pycn. & Water, Specific Gravity, Hygroscopic Moisture, Percent Water Content, Mass Material, Mass Water Added, Wet Mass Specimen & Mold, Tare Mass Mold, Wet Mass Specimen, Height of Specimen, Volume per Linear mm., Volume of Specimen, Wet Density of Specimen, Wet Mass of Pan & Specimen, Dry Mass Pan & Specimen, Tare Mass Pan, Dry Mass Material, Mass Water, Percent Water on Total, Dry Density, Estimated Dry Density, Max Density, and Optimum Moisture.



For technical support call Mike Arellano at (512) 465-7305: Version 7 (4/23/99)

Remarks:

Blank remarks box

Form with fields for Test Method (TX114), Tested By (CHRIS NGUYEN), Tested Date (10/30/19), Test Stamp Code, Omit Test, Completed Date, Reviewed By, Locked By, TxDOT, District, Area, Authorized By, and Authorized Date.



TEXAS DEPARTMENT OF TRANSPORTATION

Moisture-Density Relationship of Subgrade and Embankment Soils
Tex-114-E

Refresh Workbook

File Version: 03/09/15 10:25:35

SAMPLE ID:	BOON & UTA APT	SAMPLED DATE:	
TEST NUMBER:		LETTING DATE:	
SAMPLE STATUS:		CONTROLLING CSJ:	
COUNTY:		SPEC YEAR:	
SAMPLED BY:		SPEC ITEM:	
SAMPLE LOCATION:		SPECIAL PROVISION:	
MATERIAL CODE:		GRADE:	
MATERIAL NAME:			
PRODUCER:			
AREA ENGINEER:	PROJECT MANAGER:		
COURSE/LIFT:	STATION:	DIST. FROM CL:	

Moisture-Density Work Sheet

Oven Dry Weight, (g):					
Weight of Pycnometer & Water, (g):					
Weight of Aggr., Pycn. & Water, (g):					
Specific Gravity (Apparent):					
Hygroscopic Moisture, (%):					
	1	2	3	4	5
Percent Water Content, (%):			6 %	9 %	12 %
Mass Material, (lb):			6	6	6
Mass Water Added, (lb):			.36	.54	.72
Wet Mass Specimen & Mold, (lb):			10.462	10.801	11.059
Tare Mass Mold, (lb):			5.49		
Wet Mass Specimen, (lb):			4.972	5.311	5.569
Height of Specimen, (in.):			6		
Volume per Linear mm., (in.):			.00725		
Volume of Specimen, (ft ³):			.0435		
Wet Density of Specimen, (g):			114.299	122.092	128.023
Wet Mass of Pan & Specimen, (g):			8.121	8.532	8.769
Dry Mass Pan & Specimen, (lb):			7.740	7.951	8.019
Tare Mass Pan, (lb):			3.196	3.225	3.197
Dry Mass Material, (lb):					
Mass Water, (lb):					
Percent Water on Total, (%):					
Dry Density, (pcf):					
Estimated Dry Density, (pcf):			107.829	112.011	114.306
Max Density, (pcf):					
Max Density, (kg/m ³):					
Optimum Moisture, (%):					

For technical support call Mike Arellano at (512) 465-7305; Version 7 (4/23/99)

Remarks:

Test Method:	Tested By:	Tested Date:
X114	CHRIS ARELLANO	10-30
Test Stamp Code:	Omit Test:	Completed Date: Reviewed By:
Checked By:	TxDOT:	District: Area:
Authorized By:	Authorized Date:	

APPENDIX A

Item 3

Laboratory results for the flex base material



TEXAS DEPARTMENT OF TRANSPORTATION

Moisture-Density Relations of Base Material & Sand or Subgrade & Embankment Soils
Tex-113-E or Tex-114-E

File Version: 07/06/15 14:42:05

Refresh Workbook

SAMPLE ID: BOON & UTA	SAMPLED DATE:
TEST NUMBER:	LETTING DATE:
SAMPLE STATUS:	CONTROLLING CSJ:
COUNTY:	SPEC YEAR:
SAMPLED BY:	SPEC ITEM:
SAMPLE LOCATION:	SPECIAL PROVISION:
MATERIAL CODE:	GRADE:
MATERIAL NAME:	
PRODUCER:	
AREA ENGINEER:	PROJECT MANAGER:
COURSE/LIFT:	STATION:
	DIST. FROM CL:

Moisture-Density Work Sheet

Oven Dry Weight, (g):	1000
Weight of Pycnometer & Water, (g):	2020
Weight of Aggr., Pycn. & Water, (g):	2650
Specific Gravity (Apparent)(Override):	
Specific Gravity (Apparent)(Calc):	2.70
Hygroscopic Moisture, (%):	
Sample Number :	
Percent Water Content, (%)	
Mass Material, (lb):	19
Mass Water Added, (lb):	0.76
Wet Mass Specimen & Mold, (lb):	29.334
Mass of Mold, (lb):	11.208
Wet Mass Specimen, (lb):	18.126
Height of Specimen, (in.):	7.83
Volume per Linear mm., (in.):	0.0164
Volume of Specimen, (ft³):	0.128412
Wet Density of Specimen, (lb/ft³):	141.16
Wet Mass of Pan & Specimen, (lb):	21.902
Dry Mass Pan & Specimen, (lb):	21.18
Tare Mass Pan, (lb):	3.761
Dry Mass Material, (lb):	17.419
Mass Water, (lb):	0.722
Percent Water on Total, (%):	4.14
Dry Density, (pcf):	135.55
Estimated Dry Density, (pcf):	135.73

Import Data								
SCA Energy Data								
	Total Energy (lb-ft)	Avg Energy/ Blow (lb-ft)	Total Energy (lb-ft)	Avg Energy/ Blow (lb-ft)	Total Energy (lb-ft)	Avg Energy/ Blow (lb-ft)	Total Energy (lb-ft)	Avg Energy/ Blow (lb-ft)
Lift 1:	755.7	13.5	757.5	13.5	752.7	13.4	751.6	13.4
Lift 2:	761.7	13.4	761.7	13.4	759.8	13.3	758.8	13.3
Lift 3:	750.4	13.2	759.1	13.1	761.0	13.1	760.7	13.1
Lift 4:	750.7	12.9	759.1	12.9	755.6	12.8	761.8	12.9

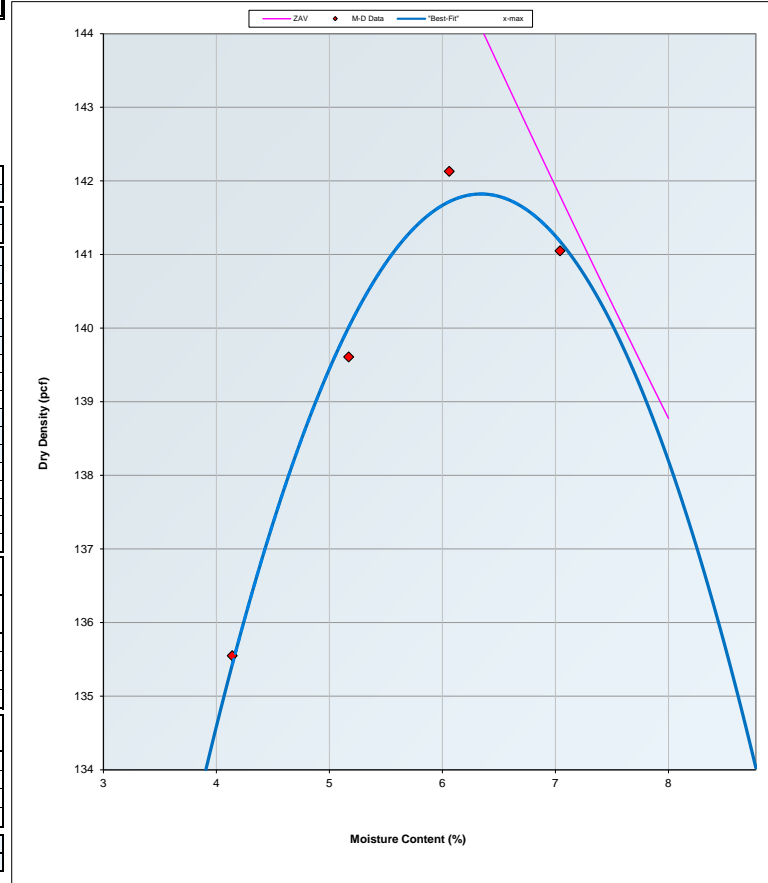
SCA Drop Data								
	Avg. Drop Ht. (in)	Blows	Avg. Drop Ht. (in)	Blows	Avg. Drop Ht. (in)	Blows	Avg. Drop Ht. (in)	Blows
Lift 1:	18.37	56	18.37	56	18.37	56	18.36	56
Lift 2:	18.35	57	18.36	57	18.36	57	18.36	57
Lift 3:	18.34	57	18.35	58	18.35	58	18.35	58
Lift 4:	18.33	58	18.33	59	18.34	59	18.33	59

Unconfined Strength Data (psi):							
Percent Strain (%):							

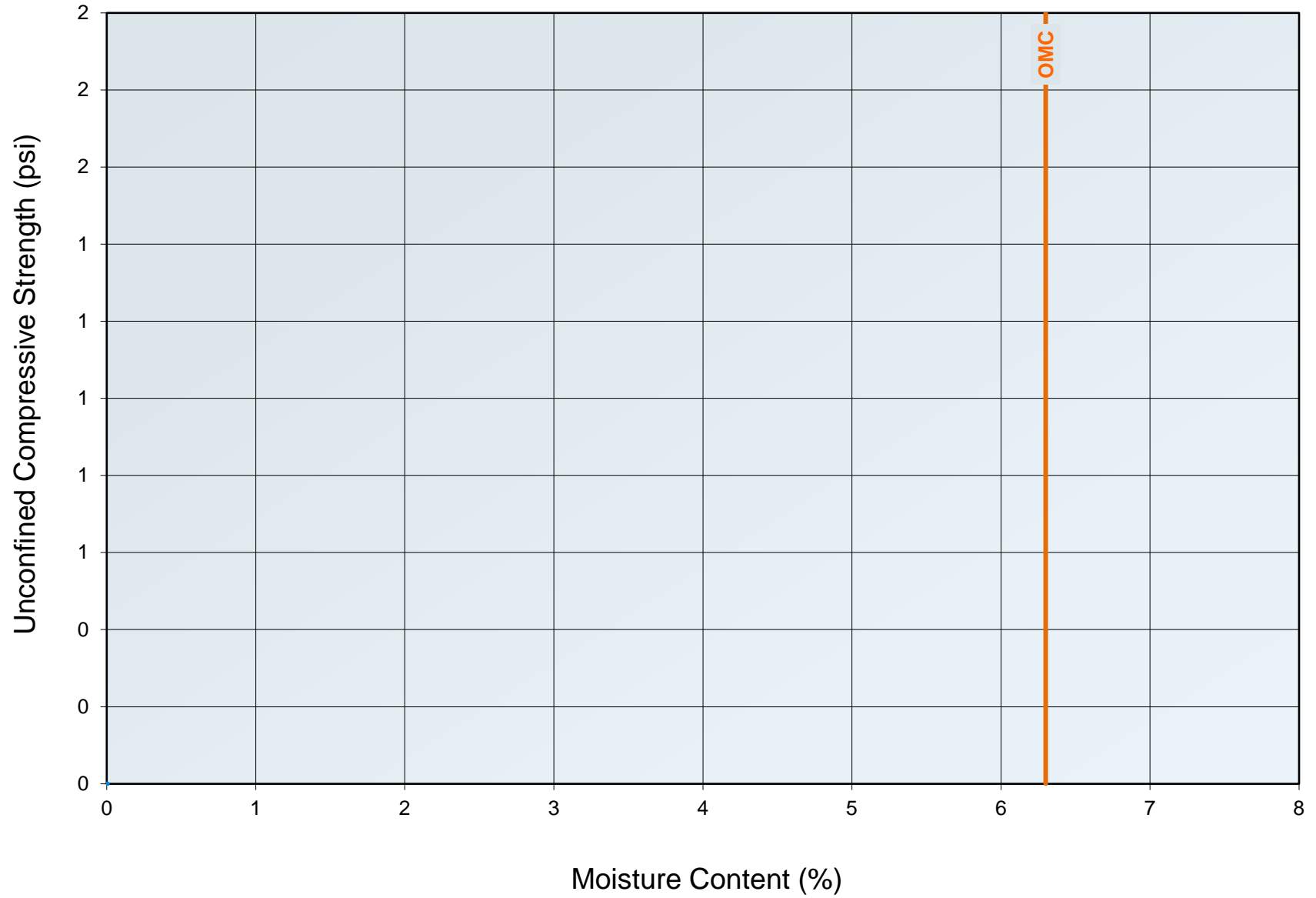
Max Dry Density, (pcf):	141.8
Optimum Moisture Content, (%):	6.3
M-D Graph R ² Value:	0.99

Remarks:

Test Method:	Tested By:	Tech Cert No:	Tested Date:
TX113	Chris Nguyen		11/08/19
TX114			
Test Stamp Code:	Omit Test:	Completed Date:	Reviewed By:
Locked By:	TxDOT:	District:	Area:
Authorized By:	Authorized Date:		



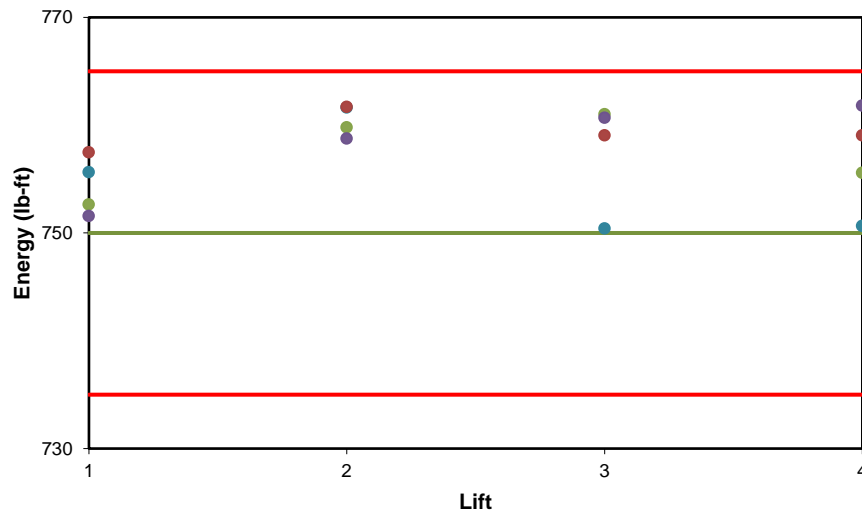
UCS vs Moisture Content



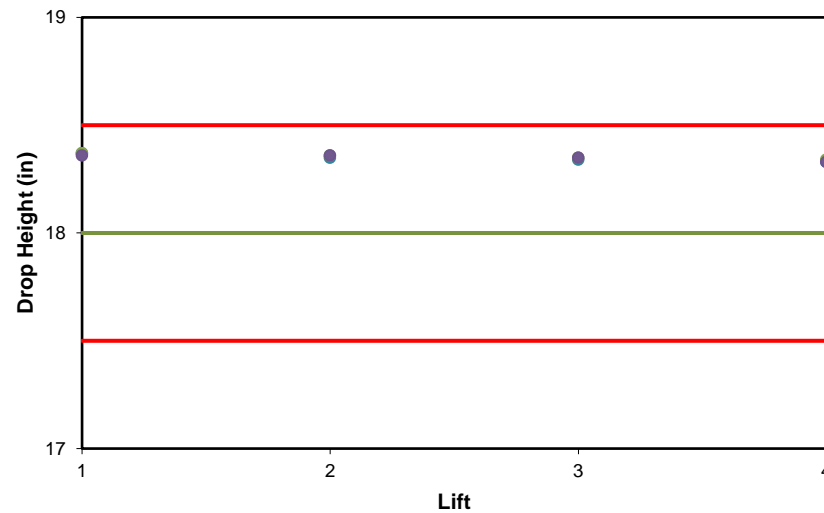
Energy Data

Drop Data

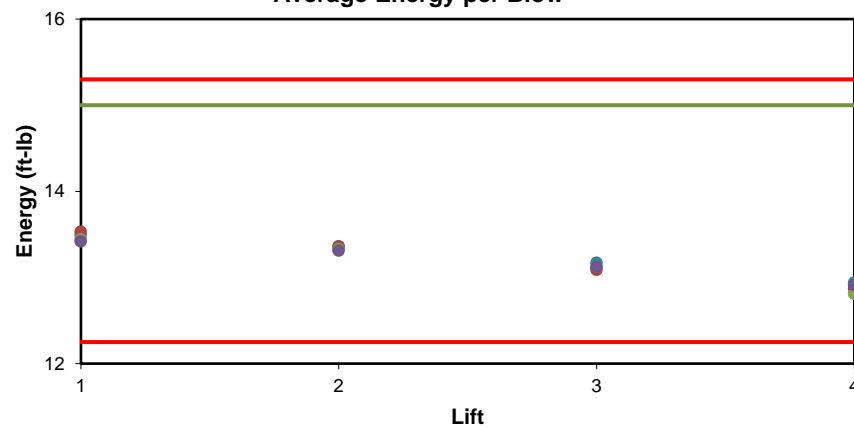
Total Energy per Lift



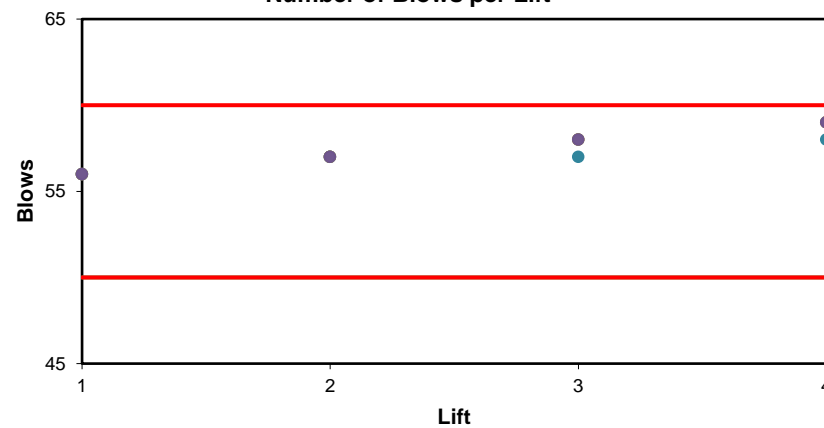
Average Drop Height per Blow



Average Energy per Blow



Number of Blows per Lift



● Specimen 1 ● Specimen 2 ● Specimen 3 ● Specimen 4



TEXAS DEPARTMENT OF TRANSPORTATION

Moisture-Density Relationship of Subgrade and Embankment Soils
Tex-114-E

Refresh Workbook

File Version: 03/09/15 10:25:36

SAMPLE ID:	Bonn & UTA		SAMPLED DATE:	
TEST NUMBER:			LETTING DATE:	
SAMPLE STATUS:			CONTROLLING CSJ:	
COUNTY:			SPEC YEAR:	
SAMPLED BY:			SPEC ITEM:	
SAMPLE LOCATION:			SPECIAL PROVISION:	
MATERIAL CODE:			GRADE:	
MATERIAL NAME:				
PRODUCER:				
AREA ENGINEER:			PROJECT MANAGER:	
COURSE/LIFT:		STATION:		DIST. FROM CL:

Moisture-Density Work Sheet

Oven Dry Weight, (g):					
Weight of Pycnometer & Water, (g):					
Weight of Aggr., Pycn. & Water, (g):					
Specific Gravity (Apparent):					
Hygroscopic Moisture, (%):					
	1	2	3	4	5
Percent Water Content, (%):			4	5%	6%
Mass Material, (lb):			19	19	19
Mass Water Added, (lb):			.75	.95	1.14
Wet Mass Specimen & Mold, (lb):			29.334	30.203	30.767
Tare Mass Mold, (lb):			-1-	11.208	11.208
Wet Mass Specimen, (lb):			18.126	18.995	19.559
Height of Specimen, (in.):			7.830	7.888	7.912
Volume per Linear mm., (in.):			-1-	.0164	-1-
Volume of Specimen, (ft ³):			.12841	.12936	.12976
Wet Density of Specimen, (g):			141.157	146.838	150.732
Wet Mass of Pan & Specimen, (g):			21.902	22.722	23.267
Dry Mass Pan & Specimen, (lb):			21.180	21.788	22.149
Tare Mass Pan, (lb):			3.761	3.708	3.702
Dry Mass Material, (lb):					
Mass Water, (lb):					
Percent Water on Total, (%):					
Dry Density, (pcf):					
Estimated Dry Density, (pcf):			135.728	139.846	142.2
Max Density, (pcf):					
Max Density, (kg/m ³):					
Optimum Moisture, (%):					

For technical support call Mike Arellano at (512) 465-7305: Version 7 (4/23/99)

Remarks:

Test Method:	Tested By:	Tested Date:
114		
Test Stamp Code:	Omit Test:	Completed Date: Reviewed By:
Checked By:	TxDOT:	District: Area:
Authorized By:	Authorized Date:	

APPENDIX A

Item 4

Photographs taken during paving



Figure A4-1 Paving of Section P



Figure A4-2 Paving of sections M and Q (same mixtures for two sections)



Figure A4-3 Paving Section N



Figure A4-4 Paving Section O



Figure A4-5 Paving Section R



Figure A4-6 Paving Section S

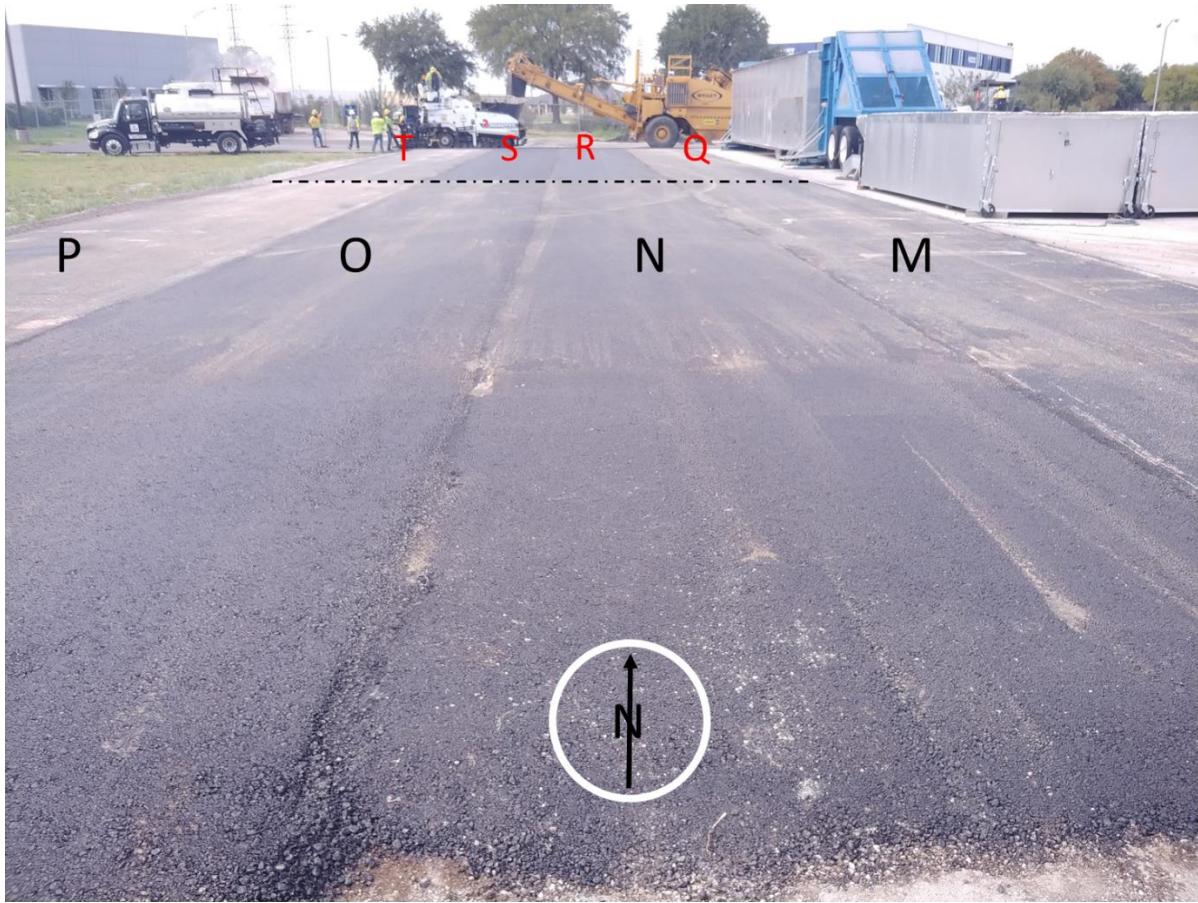


Figure A4-7 View of all sections after Paving

APPENDIX A

Item 5

Infrared camera temperatures

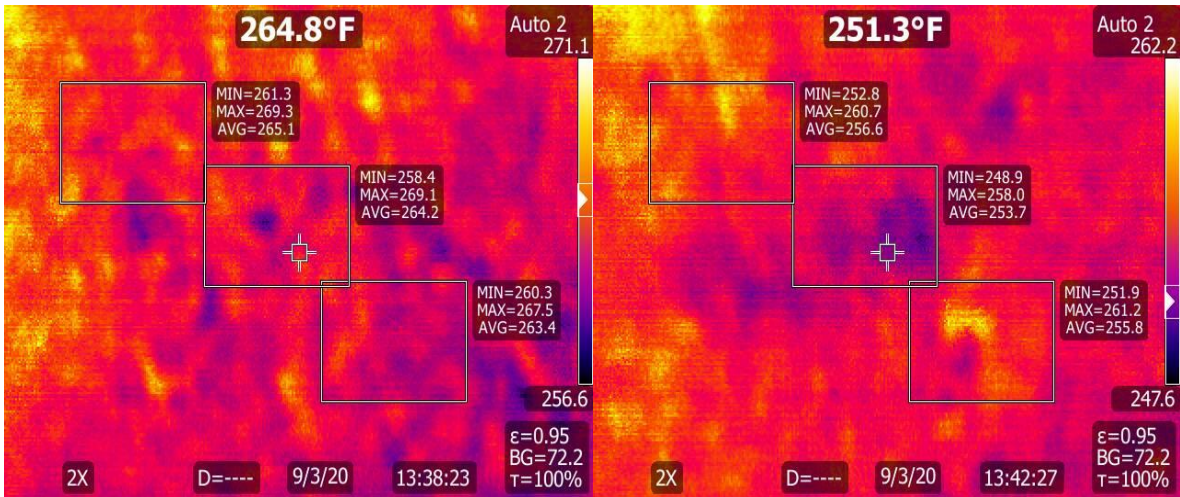


Figure A5-1 Maximum and Minimum Temperature Maps for Section P

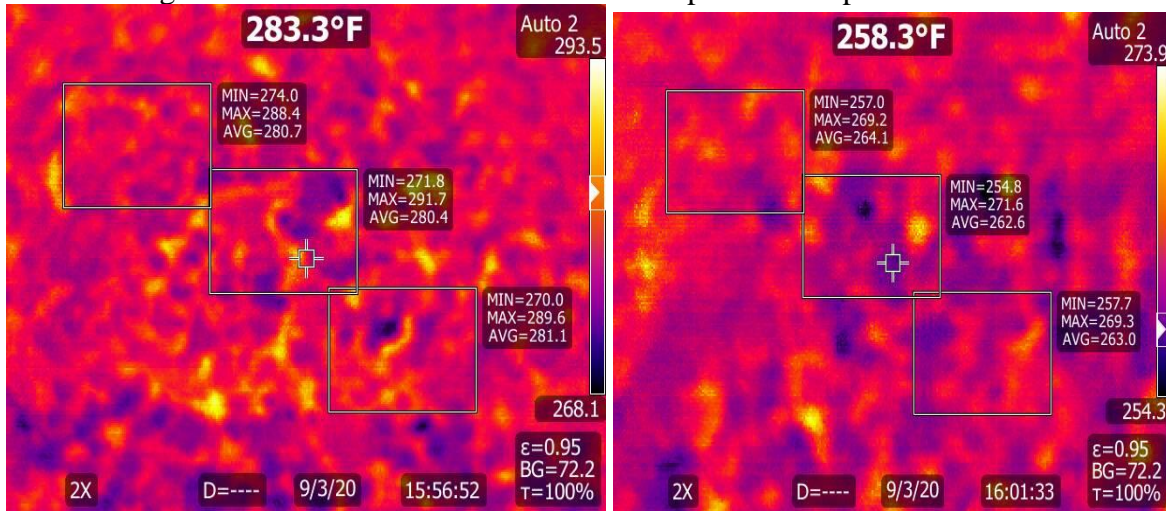


Figure A5-2 Maximum and Minimum Temperature Maps for Section T

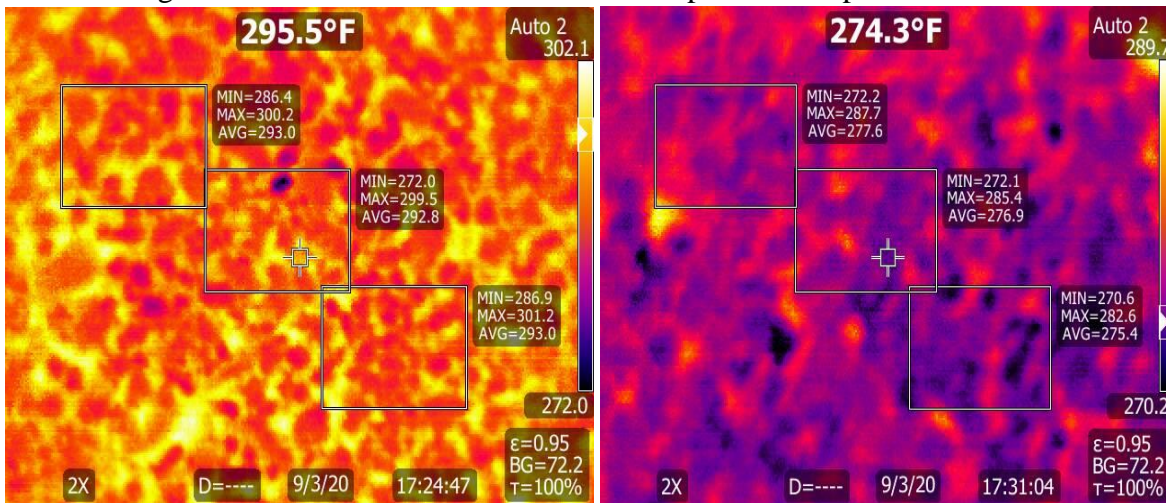


Figure A5-3 Maximum and Minimum Temperature Maps for Section M and Q

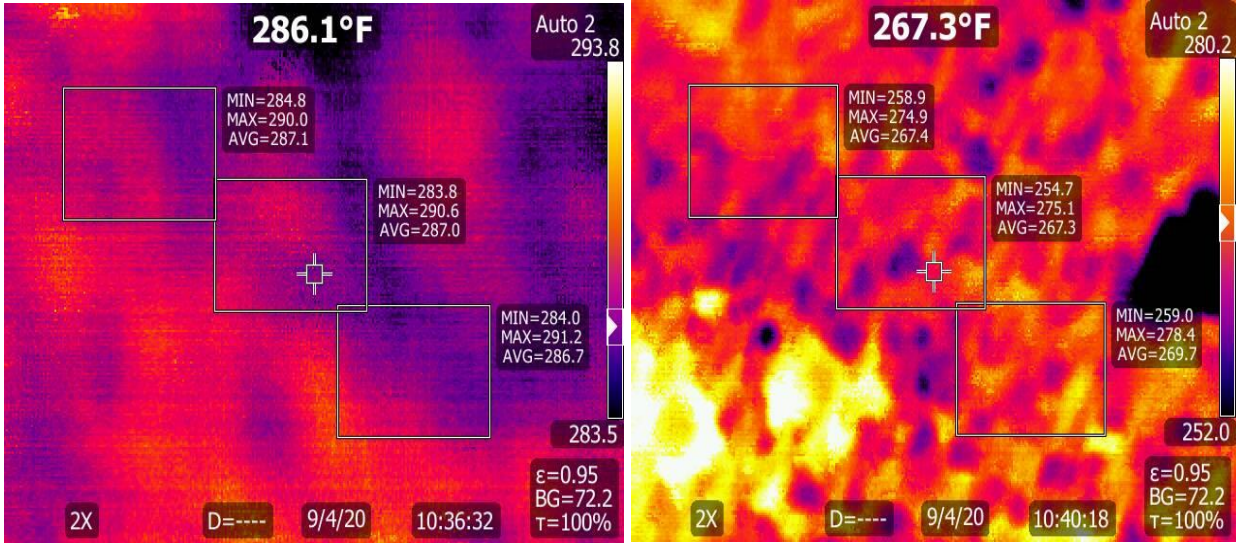


Figure A5-4 Maximum and Minimum Temperature Maps for Section N

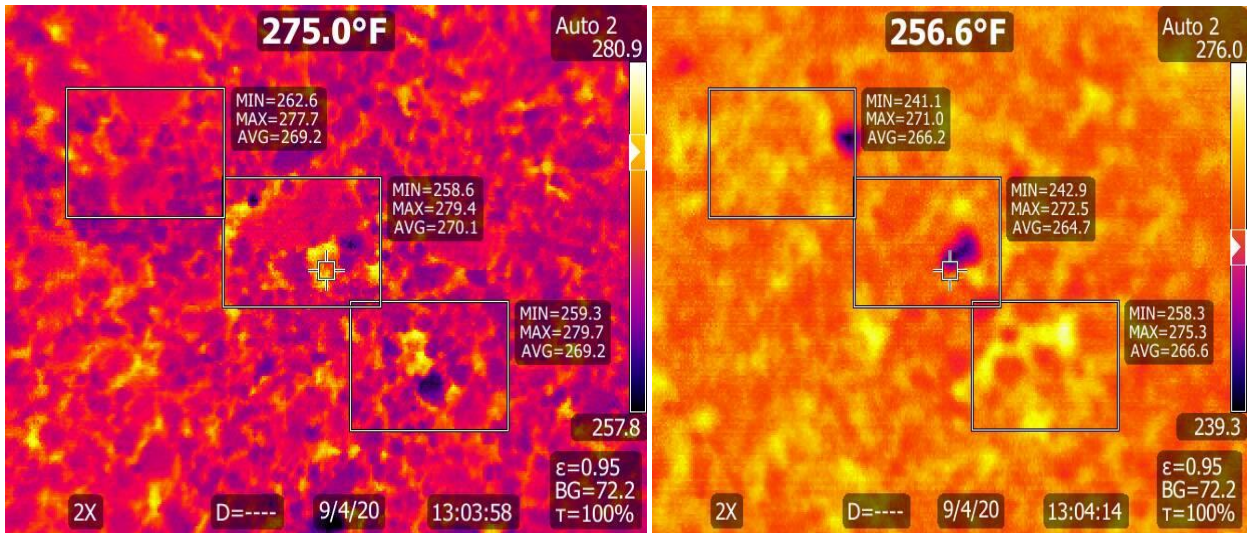


Figure A5-5 Maximum and Minimum Temperature Maps for Section O

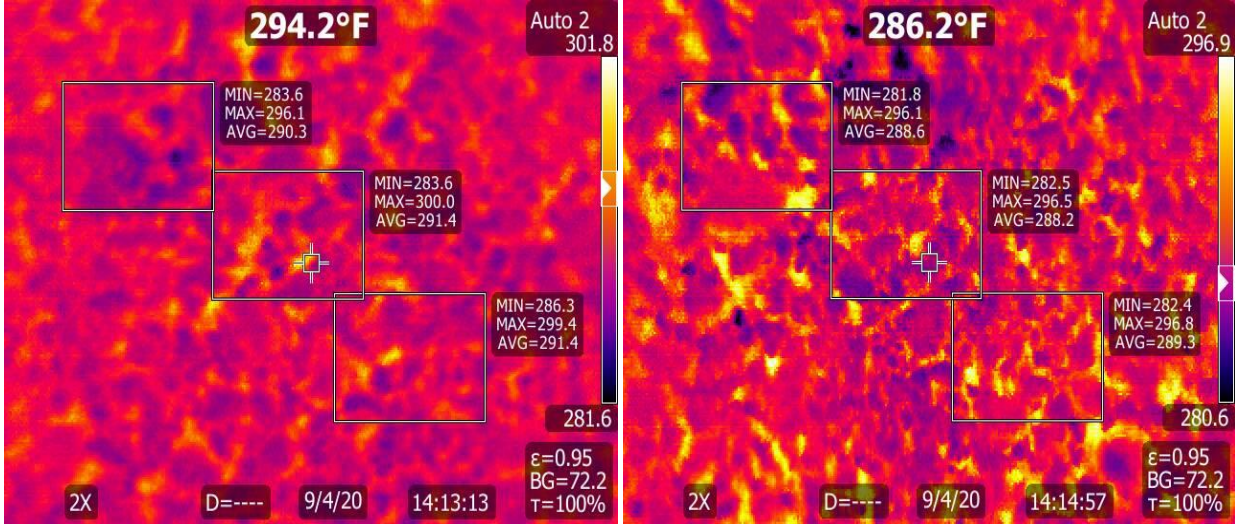


Figure A5-6 Maximum and Minimum Temperature Maps for Section R

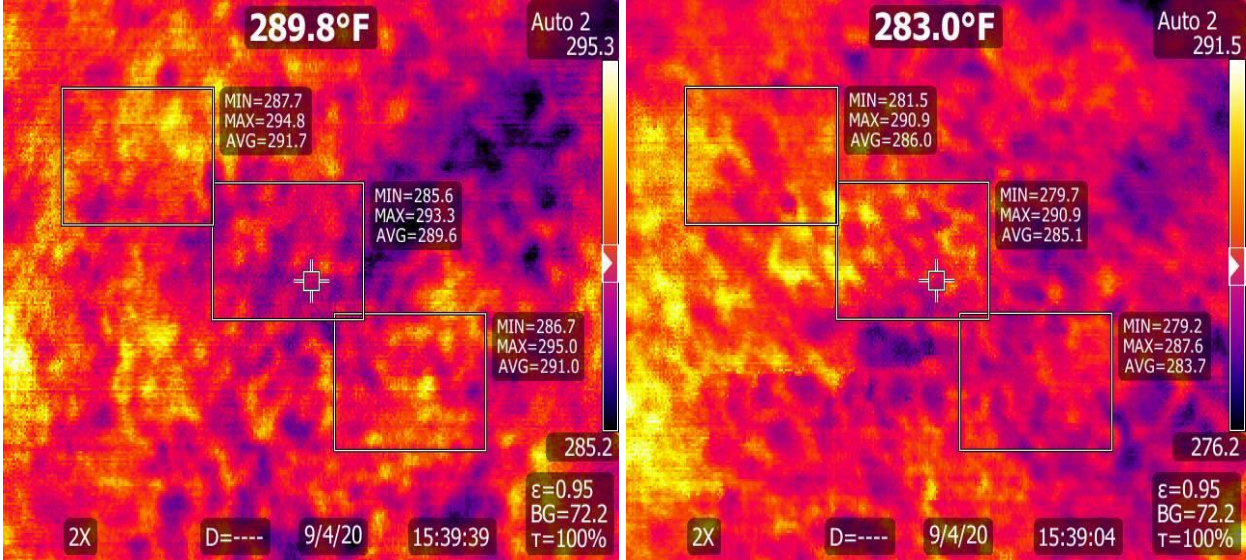


Figure A5-7 Maximum and Minimum Temperature Maps for Section R

APPENDIX A

Item 6

FWD Data - Collected on September 10th, 2020

TABLE A6-1 Section M

M - Notepad

File Edit Format View Help

TTI MODULUS ANALYSIS SYSTEM (SUMMARY REPORT)														(Version 7.0)	
District:									MODULI RANGE(psi)						
County :									Minimum	Maximum	Poisson Ratio Values				
Highway/Road:		Pavement:	Thickness(in)				460,000	1,240,000	H1: v = 0.35						
		Base:	10.00				10,000	200,000	H2: v = 0.35						
		Subbase:	0.00						H3: v = 0.00						
		Subgrade:	70.00(User Input)				10,000		H4: v = 0.40						
Station	Load (lbs)	Measured Deflection (mils):							Calculated Moduli values (ksi):				Absolute Dpth to		
		W1	W2	W3	W4	W5	W6	W7	SURF(E1)	BASE(E2)	SUBB(E3)	SUBG(E4)	ERR/Sens	Bedrock	
0.000	10,034	11.26	5.31	2.04	1.11	0.70	0.44	0.26	772.2	64.3	0.0	33.9	8.59	76.2	
10.000	9,947	12.04	6.92	2.34	1.04	0.64	0.47	0.35	1240.0	40.3	0.0	31.7	10.93	56.6 *	
20.000	9,738	16.15	8.54	2.83	1.41	0.88	0.59	0.35	1123.4	25.3	0.0	25.0	10.67	54.8	
25.000	9,881	13.38	6.93	2.58	1.35	0.89	0.61	0.41	936.3	46.5	0.0	26.6	11.27	69.1	
30.000	9,804	13.46	6.87	2.55	1.54	1.02	0.68	0.17	700.5	55.5	0.0	24.9	12.11	68.5	
35.000	9,388	13.14	6.31	2.68	1.71	1.07	0.69	0.43	460.0	69.5	0.0	22.8	10.53	122.8 *	
40.000	9,651	17.41	9.71	3.35	1.65	0.94	0.61	0.20	1219.3	21.7	0.0	21.7	8.05	58.2	
50.000	9,673	19.12	10.34	3.31	1.48	0.89	0.61	0.41	1046.4	18.4	0.0	22.4	10.04	52.4	
60.000	9,585	18.41	10.16	3.00	1.31	0.87	0.63	0.26	1085.6	17.8	0.0	24.0	14.18	48.9	
Mean:		14.93	7.90	2.74	1.40	0.88	0.59	0.32	953.7	39.9	0.0	25.9	10.71	59.3	
Std. Dev:		2.89	1.84	0.43	0.23	0.14	0.08	0.10	261.8	20.2	0.0	4.2	1.82	13.2	
Var Coeff(%):		19.37	23.23	15.73	16.15	15.58	14.35	30.48	27.5	50.5	0.0	16.4	16.98	22.3	

TABLE A6-2 Section N

N - Notepad

File Edit Format View Help

TTI MODULUS ANALYSIS SYSTEM (SUMMARY REPORT)														(Version 7.0)	
District:									MODULI RANGE(psi)						
County :									Minimum	Maximum	Poisson Ratio Values				
Highway/Road:		Pavement:	Thickness(in)				460,000	1,240,000	H1: v = 0.35						
		Base:	10.00				10,000	200,000	H2: v = 0.35						
		Subbase:	0.00						H3: v = 0.00						
		Subgrade:	80.00(User Input)				10,000		H4: v = 0.40						
Station	Load (lbs)	Measured Deflection (mils):							Calculated Moduli values (ksi):				Absolute Dpth to		
		W1	W2	W3	W4	W5	W6	W7	SURF(E1)	BASE(E2)	SUBB(E3)	SUBG(E4)	ERR/Sens	Bedrock	
0.000	10,155	9.30	5.01	1.79	0.99	0.60	0.41	0.09	1240.0	68.5	0.0	41.1	8.22	62.7 *	
10.000	10,089	7.57	4.15	1.78	0.98	0.59	0.42	0.11	1240.0	110.3	0.0	42.1	6.48	125.7 *	
20.000	10,220	7.57	4.10	1.97	1.28	0.87	0.60	0.35	1024.0	157.3	0.0	35.3	9.15	300.0	
25.000	10,089	8.83	4.17	1.98	1.31	0.87	0.59	0.39	560.0	132.6	0.0	35.0	11.26	300.0	
30.000	10,100	7.79	4.82	2.23	1.35	0.90	0.62	0.33	1240.0	137.8	0.0	31.7	8.73	126.2 *	
35.000	9,892	10.04	4.92	2.19	1.37	0.89	0.62	0.42	636.9	97.9	0.0	31.6	8.96	181.2	
40.000	9,979	8.80	5.06	2.32	1.39	0.89	0.61	0.42	1240.0	106.3	0.0	30.8	7.35	174.5 *	
50.000	9,947	12.00	6.26	2.63	1.55	0.96	0.63	0.12	886.8	64.3	0.0	27.5	6.73	114.6	
60.000	10,012	9.89	5.83	2.55	1.34	0.80	0.56	0.41	1240.0	76.8	0.0	30.2	6.58	103.4 *	
Mean:		9.09	4.92	2.16	1.28	0.82	0.56	0.29	1034.2	105.7	0.0	33.9	8.16	153.3	
Std. Dev:		1.44	0.75	0.31	0.19	0.13	0.09	0.14	277.6	32.5	0.0	5.0	1.56	73.9	
Var Coeff(%):		15.81	15.21	14.21	14.47	16.30	15.29	48.90	26.8	30.7	0.0	14.7	19.16	48.2	

TABLE A6-3 Section O

TTI MODULUS ANALYSIS SYSTEM (SUMMARY REPORT)														(Version 7.0)	
District:									MODULI RANGE(psi)						
County :			Thickness(in)						Minimum	Maximum	Poisson Ratio Values				
Highway/Road:			Pavement:	3.00					460,000	1,240,000	H1: v = 0.35				
			Base:	10.00					10,000	200,000	H2: v = 0.35				
			Subbase:	0.00							H3: v = 0.00				
			Subgrade:	99.08(by DB)					10,000		H4: v = 0.40				
Station	Load (lbs)	Measured Deflection (mils):							Calculated Moduli values (ksi):				Absolute Dpth to		
		W1	W2	W3	W4	W5	W6	W7	SURF(E1)	BASE(E2)	SUBB(E3)	SUBG(E4)	ERR/Sens	Bedrock	
0.000	10,122	10.31	5.86	2.31	1.24	0.81	0.57	0.38	1240.0	63.0	0.0	35.7	6.92	83.6 *	
10.000	10,089	8.77	4.88	2.09	1.22	0.78	0.52	0.10	1240.0	88.7	0.0	38.5	5.32	130.6 *	
20.000	10,089	10.60	5.56	2.19	1.26	0.81	0.54	0.17	1240.0	57.8	0.0	37.0	5.88	83.4 *	
25.000	9,979	11.65	5.39	1.83	1.06	0.70	0.47	0.02	1050.0	42.6	0.0	42.6	7.14	57.0	
30.000	10,056	7.20	3.76	1.63	1.01	0.64	0.46	0.28	1240.0	116.3	0.0	48.0	6.32	143.6 *	
35.000	10,089	9.98	3.77	1.75	1.11	0.74	0.51	0.34	460.0	88.3	0.0	46.6	11.07	300.0 *	
40.000	10,078	7.80	3.98	1.86	1.17	0.78	0.55	0.37	911.7	128.0	0.0	41.7	6.74	300.0	
50.000	10,078	8.98	4.88	2.09	1.24	0.78	0.52	0.36	1240.0	84.6	0.0	38.4	4.89	130.6 *	
61.000	9,990	8.58	5.31	2.33	1.20	0.70	0.52	0.32	1240.0	81.6	0.0	37.9	7.48	96.8 *	
Mean:		9.32	4.82	2.01	1.17	0.75	0.52	0.26	1095.8	83.4	0.0	40.7	6.86	112.1	
Std. Dev:		1.43	0.80	0.25	0.09	0.06	0.04	0.13	265.7	27.1	0.0	4.3	1.79	60.3	
Var Coeff(%):		15.30	16.61	12.50	7.57	7.77	6.81	50.55	24.3	32.5	0.0	10.6	26.13	47.6	

TABLE A6-4 Section P

TTI MODULUS ANALYSIS SYSTEM (SUMMARY REPORT)														(Version 7.0)	
District:									MODULI RANGE(psi)						
County :			Thickness(in)						Minimum	Maximum	Poisson Ratio Values				
Highway/Road:			Pavement:	3.00					460,000	1,240,000	H1: v = 0.35				
			Base:	10.00					10,000	200,000	H2: v = 0.35				
			Subbase:	0.00							H3: v = 0.00				
			Subgrade:	87.05(by DB)					10,000		H4: v = 0.40				
Station	Load (lbs)	Measured Deflection (mils):							Calculated Moduli values (ksi):				Absolute Dpth to		
		W1	W2	W3	W4	W5	W6	W7	SURF(E1)	BASE(E2)	SUBB(E3)	SUBG(E4)	ERR/Sens	Bedrock	
0.000	10,122	8.86	4.80	2.32	1.44	0.95	0.64	0.40	979.7	119.0	0.0	32.1	6.58	154.6	
10.000	10,122	7.98	4.22	1.94	1.26	0.85	0.57	0.37	994.0	131.4	0.0	37.1	8.24	265.6	
20.000	10,144	9.21	4.81	2.02	1.24	0.77	0.49	0.30	1205.8	84.0	0.0	37.4	6.25	114.6	
25.000	10,100	9.26	4.55	2.04	1.19	0.72	0.47	0.31	888.4	91.7	0.0	38.2	4.11	135.4	
30.000	10,034	10.58	5.35	1.92	1.07	0.66	0.43	0.31	1240.0	50.4	0.0	40.4	6.72	63.3 *	
35.000	9,990	9.76	4.21	1.92	1.15	0.70	0.47	0.33	460.0	97.5	0.0	40.0	6.71	138.5 *	
40.000	10,045	9.30	5.04	2.01	1.17	0.74	0.48	0.35	1240.0	75.7	0.0	37.5	6.88	87.8 *	
50.000	9,914	13.30	6.70	2.19	1.18	0.76	0.54	0.40	1149.6	33.5	0.0	34.5	8.73	53.9	
60.000	9,979	11.31	5.78	2.34	1.29	0.80	0.59	0.46	1117.0	56.2	0.0	33.1	6.93	93.8	
Mean:		9.95	5.05	2.08	1.22	0.77	0.52	0.36	1030.5	82.1	0.0	36.7	6.79	100.1	
Std. Dev:		1.58	0.80	0.17	0.10	0.09	0.07	0.05	247.4	32.0	0.0	2.9	1.29	44.3	
Var Coeff(%):		15.90	15.82	7.95	8.57	11.23	13.22	14.90	24.0	39.0	0.0	7.9	19.04	44.3	

TABLE A6-5 Section Q

TTI MODULUS ANALYSIS SYSTEM (SUMMARY REPORT)													(Version 7.0)	
District:														
County :														
Highway/Road:														
			Thickness(in)		MODULI RANGE(psi)					Poisson Ratio Values				
			Pavement:	3.00	Minimum	460,000	Maximum	1,240,000	H1: v = 0.35					
			Base:	10.00		10,000		200,000	H2: v = 0.35					
			Subbase:	0.00							H3: v = 0.00			
			Subgrade:	42.05(by DB)				10,000			H4: v = 0.40			
Station	Load (lbs)	Measured Deflection (mils):							Calculated Moduli values (ksi):				Absolute Dpth to	
		W1	W2	W3	W4	W5	W6	W7	SURF(E1)	BASE(E2)	SUBB(E3)	SUBG(E4)	ERR/Sens	Bedrock
0.000	9,760	14.81	7.82	2.69	1.46	0.90	0.63	0.44	704.7	52.7	0.0	17.6	19.13	58.1
10.000	9,662	16.68	8.67	2.61	1.33	0.85	0.60	0.44	605.6	40.4	0.0	17.7	22.06	49.6
20.000	9,684	15.32	7.79	2.48	1.26	0.80	0.58	0.38	594.5	47.5	0.0	18.9	21.14	52.2
25.000	9,738	13.84	7.18	2.39	1.23	0.76	0.56	0.40	679.1	55.9	0.0	19.8	20.00	55.2
30.000	9,684	14.12	7.90	2.66	1.27	0.80	0.57	0.41	902.8	49.6	0.0	18.1	19.91	56.1
35.000	9,749	14.64	7.69	2.72	1.45	0.93	0.68	0.44	682.9	55.2	0.0	17.5	19.79	61.2
40.000	9,706	14.89	8.25	2.87	1.48	0.99	0.73	0.47	866.4	49.6	0.0	16.5	20.70	59.2
50.000	9,541	19.20	10.42	3.24	1.67	1.07	0.79	0.50	568.8	36.1	0.0	14.0	21.95	50.9
60.000	9,662	17.74	9.00	3.49	1.93	1.23	0.87	0.65	460.0	53.0	0.0	13.7	18.56	78.3 *
Mean:		15.69	8.30	2.79	1.45	0.93	0.67	0.46	673.9	48.9	0.0	17.1	20.36	55.1
Std. Dev:		1.80	0.96	0.36	0.23	0.15	0.11	0.08	140.7	6.7	0.0	2.1	1.20	6.5
Var Coeff(%):		11.50	11.59	12.77	15.60	16.34	16.30	17.48	20.9	13.7	0.0	12.1	5.89	11.8

TABLE A6-6 Section R

TTI MODULUS ANALYSIS SYSTEM (SUMMARY REPORT)													(Version 7.0)	
District:														
County :														
Highway/Road:														
			Thickness(in)		MODULI RANGE(psi)					Poisson Ratio Values				
			Pavement:	3.00	Minimum	460,000	Maximum	1,240,000	H1: v = 0.35					
			Base:	10.00		10,000		200,000	H2: v = 0.35					
			Subbase:	0.00							H3: v = 0.00			
			Subgrade:	51.57(by DB)				10,000			H4: v = 0.40			
Station	Load (lbs)	Measured Deflection (mils):							Calculated Moduli values (ksi):				Absolute Dpth to	
		W1	W2	W3	W4	W5	W6	W7	SURF(E1)	BASE(E2)	SUBB(E3)	SUBG(E4)	ERR/Sens	Bedrock
0.000	9,574	15.86	8.50	2.62	1.30	0.80	0.56	0.39	887.4	32.3	0.0	21.2	17.47	50.6
10.000	9,881	13.94	6.77	2.35	1.20	0.76	0.55	0.39	588.5	53.4	0.0	24.0	16.18	59.1
20.000	9,804	12.06	6.08	2.14	1.07	0.67	0.49	0.33	785.0	59.2	0.0	26.5	15.94	60.7
25.000	9,892	11.85	6.09	1.95	0.99	0.63	0.48	0.35	938.6	53.3	0.0	28.7	18.07	52.7
30.000	9,925	10.91	5.63	1.91	1.04	0.71	0.51	0.38	835.0	70.4	0.0	28.4	18.64	56.9
35.000	9,793	12.37	6.41	2.33	1.20	0.78	0.56	0.42	747.2	62.5	0.0	24.0	16.40	65.0
40.000	9,826	11.54	6.05	2.46	1.38	0.90	0.63	0.20	668.3	84.6	0.0	22.2	15.10	95.8
51.000	9,815	12.18	6.40	2.43	1.39	0.92	0.66	0.48	667.6	74.7	0.0	22.0	16.67	73.2
61.000	9,859	11.82	6.63	2.71	1.52	1.07	0.81	0.55	842.9	83.3	0.0	19.9	17.31	98.2
Mean:		12.50	6.51	2.32	1.23	0.80	0.58	0.39	773.4	63.7	0.0	24.1	16.86	64.6
Std. Dev:		1.50	0.82	0.28	0.18	0.14	0.10	0.10	115.2	16.6	0.0	3.2	1.11	13.5
Var Coeff(%):		12.00	12.64	11.91	14.58	17.19	17.82	25.13	14.9	26.1	0.0	13.1	6.58	21.0

TABLE A6-7 Section S

TTI MODULUS ANALYSIS SYSTEM (SUMMARY REPORT)														(Version 7.0)	
District:											MODULI RANGE(psi)				
County :											Minimum	Maximum	Poisson	Ratio Values	
Highway/Road:	Pavement:	Thickness(in)							460,000	1,240,000	H1:	v = 0.35			
	Base:	10.00							10,000	200,000	H2:	v = 0.35			
	Subbase:	0.00									H3:	v = 0.00			
	Subgrade:	51.05(by DB)							10,000		H4:	v = 0.40			
Station	Load (lbs)	Measured Deflection (mils):							Calculated Moduli values (ksi):				Absolute Dpth to		
		W1	W2	W3	W4	W5	W6	W7	SURF(E1)	BASE(E2)	SUBB(E3)	SUBG(E4)	ERR/Sens	Bedrock	
0.000	9,541	18.07	8.75	2.72	1.31	0.82	0.61	0.43	573.3	31.3	0.0	20.1	17.32	51.0	
10.000	9,673	19.03	9.68	2.90	1.28	0.83	0.61	0.44	672.9	26.1	0.0	19.6	18.49	49.4	
20.000	9,771	13.80	7.09	2.61	1.37	0.85	0.60	0.44	632.0	57.7	0.0	21.2	15.28	67.1	
25.000	9,826	14.11	7.06	2.54	1.37	0.85	0.60	0.39	564.1	57.3	0.0	21.6	15.64	63.5	
30.000	9,837	13.16	7.15	2.73	1.48	0.92	0.65	0.32	839.4	60.9	0.0	20.3	15.11	74.5	
35.000	9,695	15.30	8.45	3.35	1.72	1.02	0.71	0.50	784.0	50.6	0.0	16.9	13.12	85.2	
40.000	9,651	17.66	9.50	3.30	1.69	1.08	0.77	0.56	593.4	40.5	0.0	16.4	17.05	59.0	
50.000	9,881	12.15	7.14	3.14	1.81	1.20	0.86	0.31	1018.3	87.7	0.0	17.1	14.67	160.7	
60.000	9,749	14.96	8.11	3.18	1.83	1.27	0.94	0.64	677.0	60.5	0.0	16.6	18.09	81.6	
Mean:		15.36	8.10	2.94	1.54	0.98	0.71	0.45	706.0	52.5	0.0	18.9	16.08	64.1	
Std. Dev:		2.38	1.06	0.31	0.22	0.17	0.13	0.11	149.7	18.4	0.0	2.1	1.76	17.9	
Var Coeff(%):		15.51	13.04	10.47	14.41	17.25	17.83	23.86	21.2	35.1	0.0	11.2	10.95	27.9	

TABLE A6-8 Section T

TTI MODULUS ANALYSIS SYSTEM (SUMMARY REPORT)														(Version 7.0)	
District:											MODULI RANGE(psi)				
County :											Minimum	Maximum	Poisson	Ratio Values	
Highway/Road:	Pavement:	Thickness(in)							460,000	1,240,000	H1:	v = 0.35			
	Base:	10.00							10,000	200,000	H2:	v = 0.35			
	Subbase:	0.00									H3:	v = 0.00			
	Subgrade:	63.38(by DB)							10,000		H4:	v = 0.40			
Station	Load (lbs)	Measured Deflection (mils):							Calculated Moduli values (ksi):				Absolute Dpth to		
		W1	W2	W3	W4	W5	W6	W7	SURF(E1)	BASE(E2)	SUBB(E3)	SUBG(E4)	ERR/Sens	Bedrock	
0.000	9,782	13.67	7.27	2.77	1.39	0.81	0.57	0.42	1030.0	43.7	0.0	24.2	9.61	74.0	
10.000	9,749	16.41	8.32	2.56	1.34	0.85	0.63	0.44	865.5	28.9	0.0	24.6	14.56	50.5	
20.000	9,673	17.74	8.55	2.88	1.54	0.96	0.66	0.46	585.8	33.3	0.0	21.6	12.28	56.1	
25.000	9,870	15.31	7.37	2.39	1.44	0.98	0.68	0.46	584.0	44.1	0.0	24.7	16.41	53.4	
30.000	9,881	12.65	6.48	2.67	1.56	1.06	0.78	0.57	602.9	74.3	0.0	22.9	13.69	102.4	
35.000	10,089	9.83	6.05	3.03	1.84	1.18	0.83	0.51	1240.0	123.7	0.0	20.7	8.70	175.9 *	
40.000	9,826	13.24	7.03	3.05	1.79	1.22	0.89	0.65	598.7	75.9	0.0	20.0	13.08	143.3	
50.000	9,892	12.70	7.43	2.85	1.71	1.21	0.91	0.70	970.4	66.3	0.0	20.8	16.09	75.6	
60.000	9,771	16.11	8.40	3.29	1.96	1.39	1.07	0.81	507.4	55.5	0.0	17.9	15.86	81.2	
Mean:		14.18	7.43	2.83	1.62	1.07	0.78	0.56	776.1	60.6	0.0	21.9	13.36	76.4	
Std. Dev:		2.43	0.86	0.27	0.22	0.19	0.16	0.14	257.9	29.1	0.0	2.3	2.77	27.7	
Var Coeff(%):		17.13	11.63	9.66	13.37	17.82	20.60	24.28	33.2	48.0	0.0	10.6	20.76	36.3	

APPENDIX B

Item 1

Measured transverse profiles -All sections

Figure 1. Transverse Profiles – Section M, Profile 1

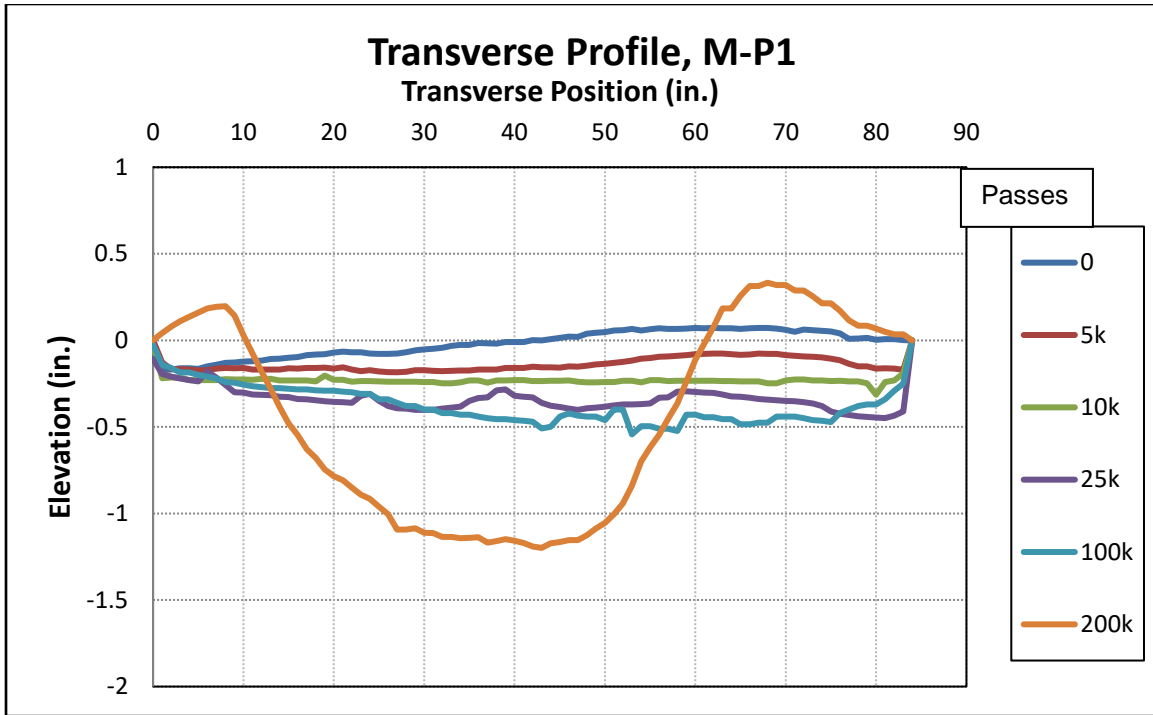


Figure 2. Transverse Profiles – Section M, Profile 2

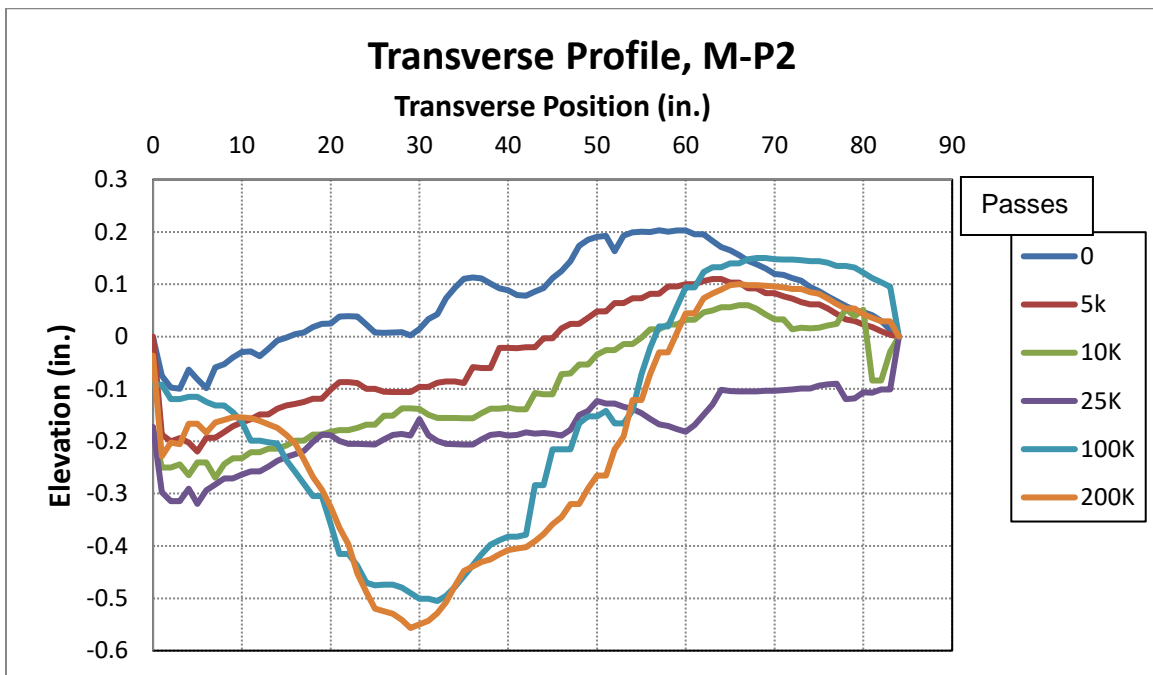


Figure 3. Transverse Profiles – Section M, Profile 3

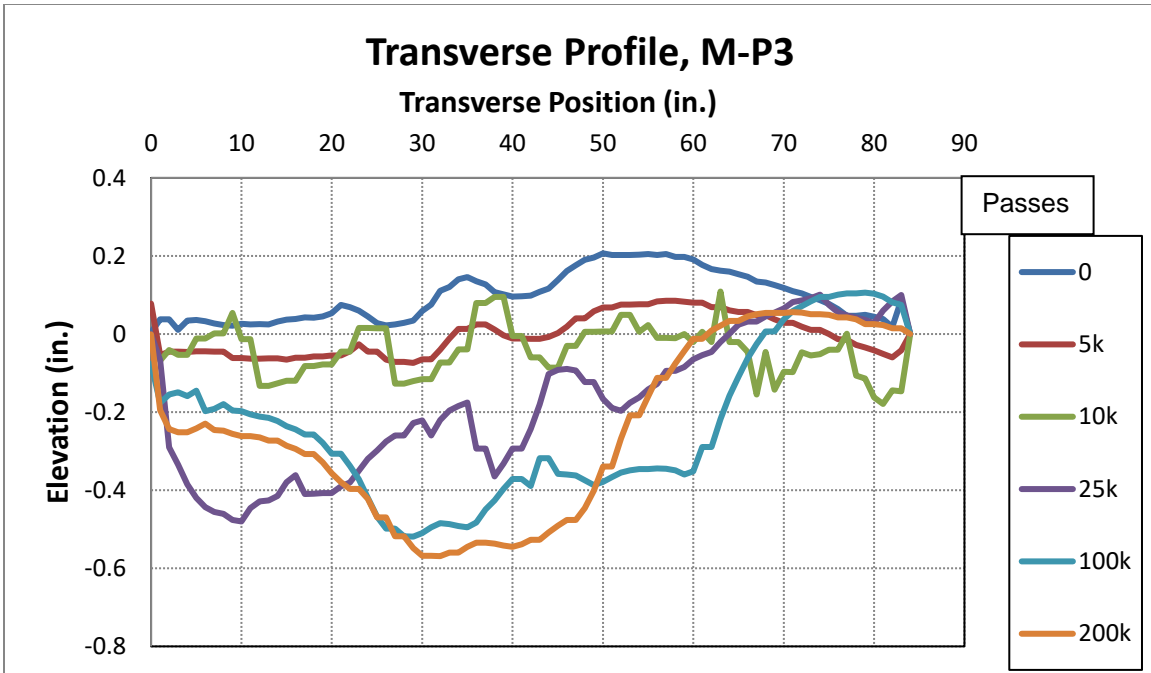


Figure 4. Transverse Profiles – Section M, Profile 4

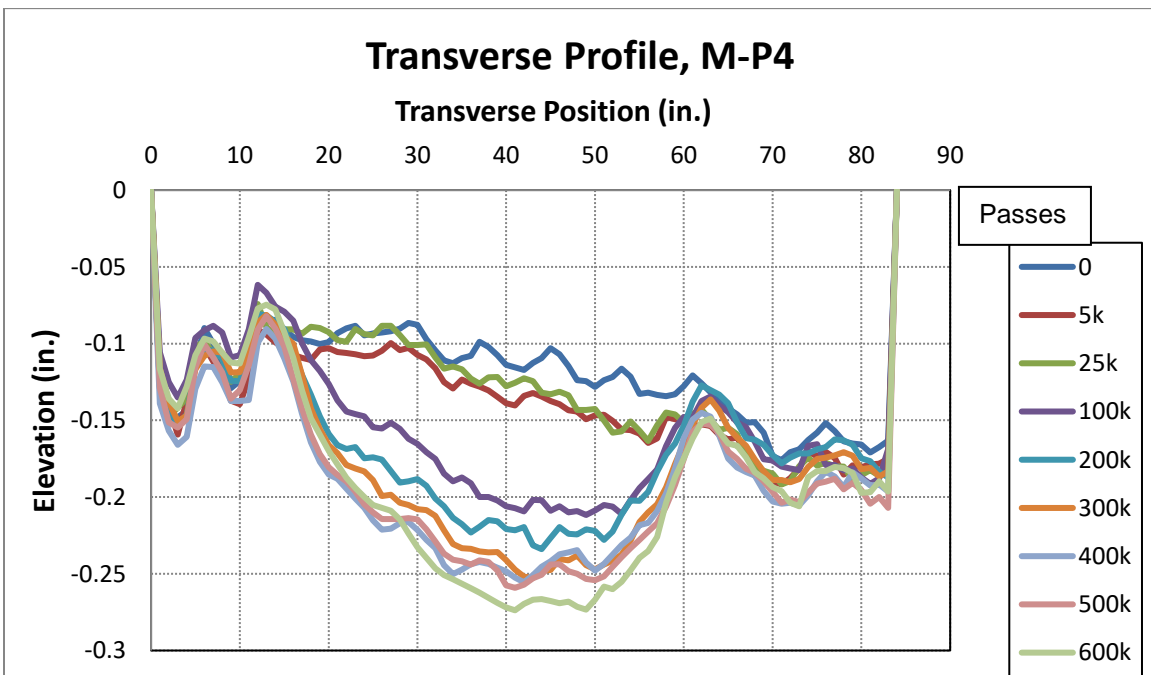


Figure 5. Transverse Profiles – Section M, Profile 5

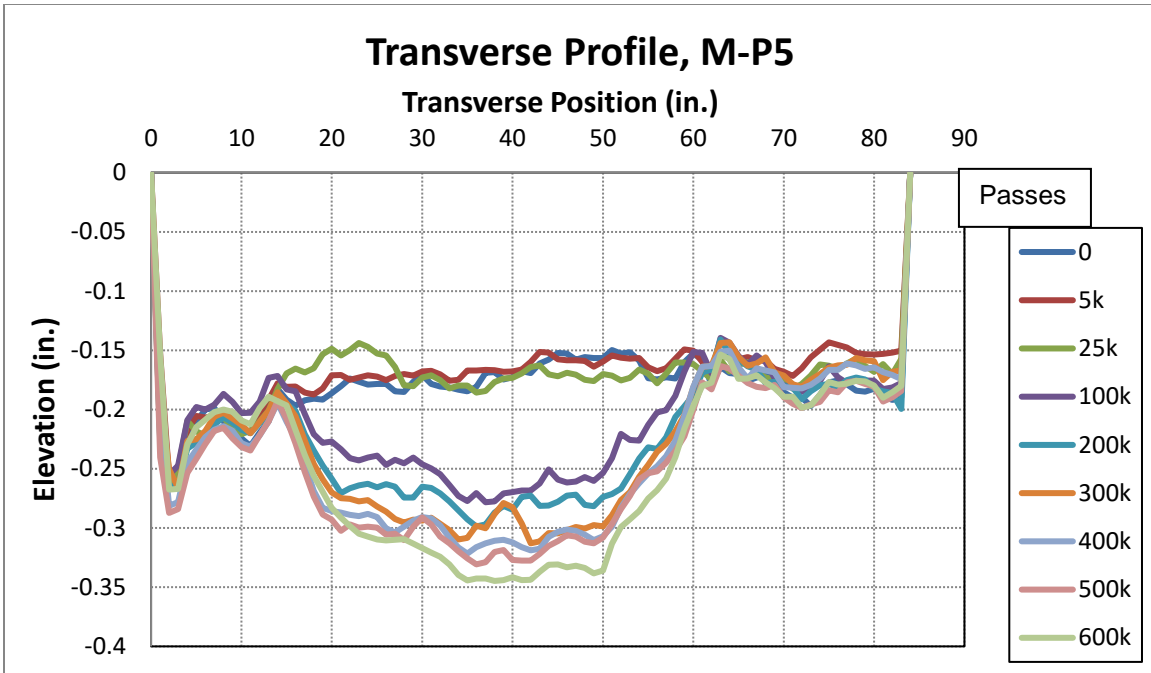


Figure 6. Transverse Profiles – Section N, Profile 1

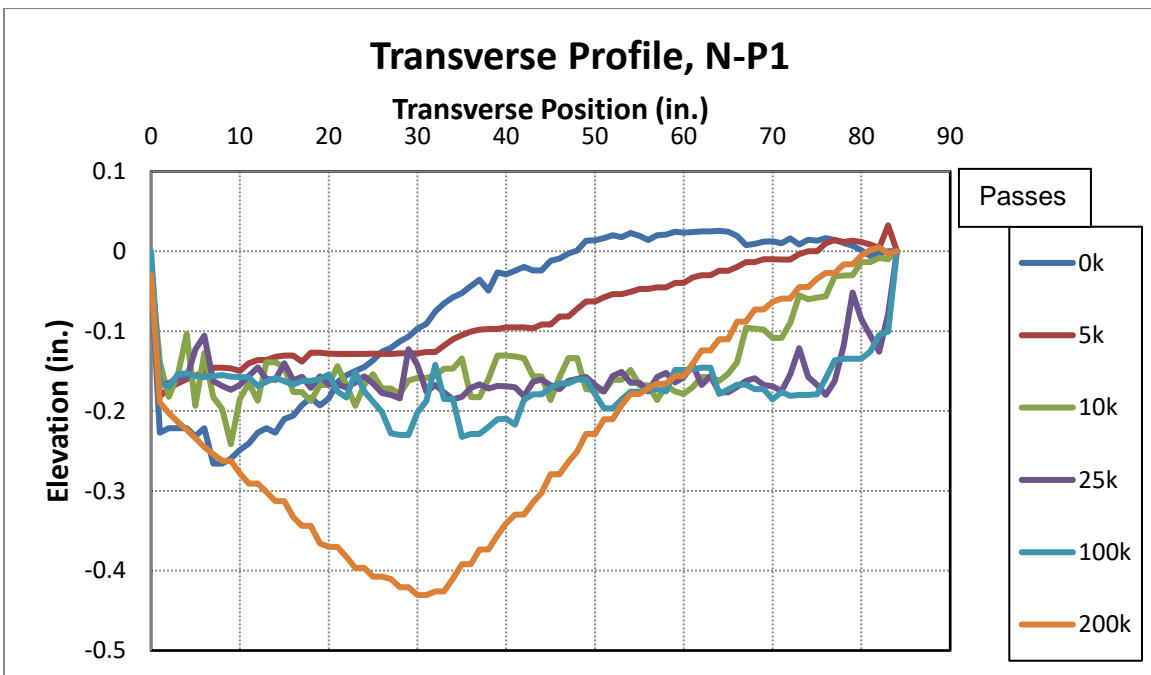


Figure 7. Transverse Profiles – Section N, Profile 2

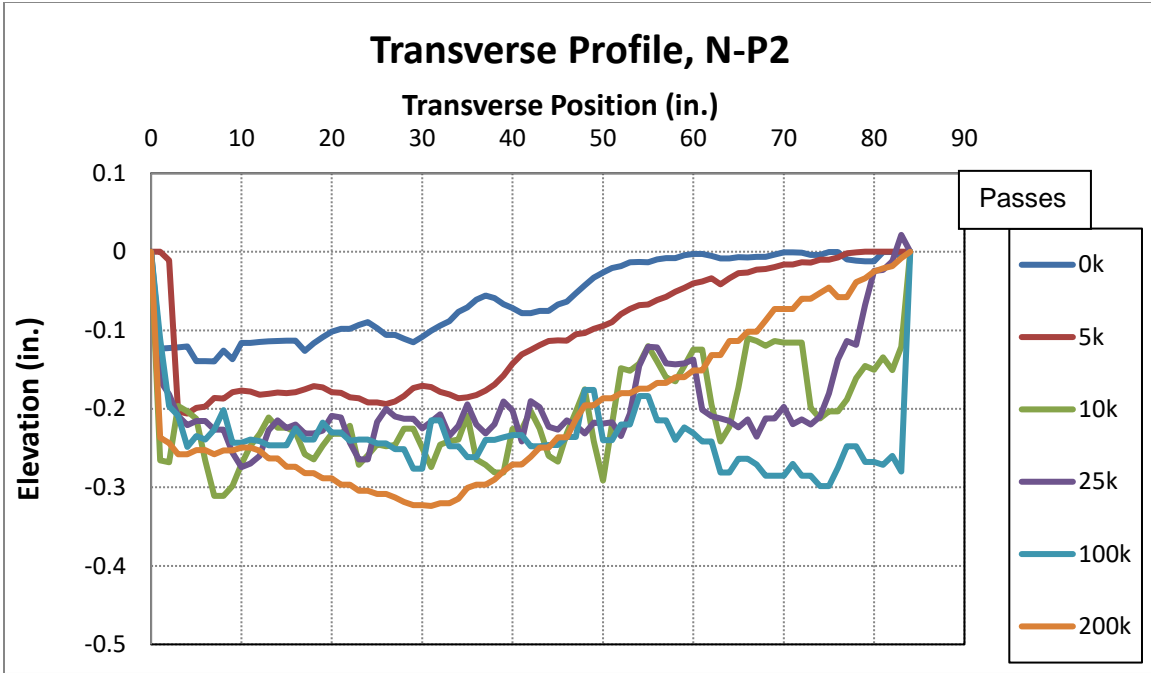


Figure 8. Transverse Profiles – Section N Profile 3

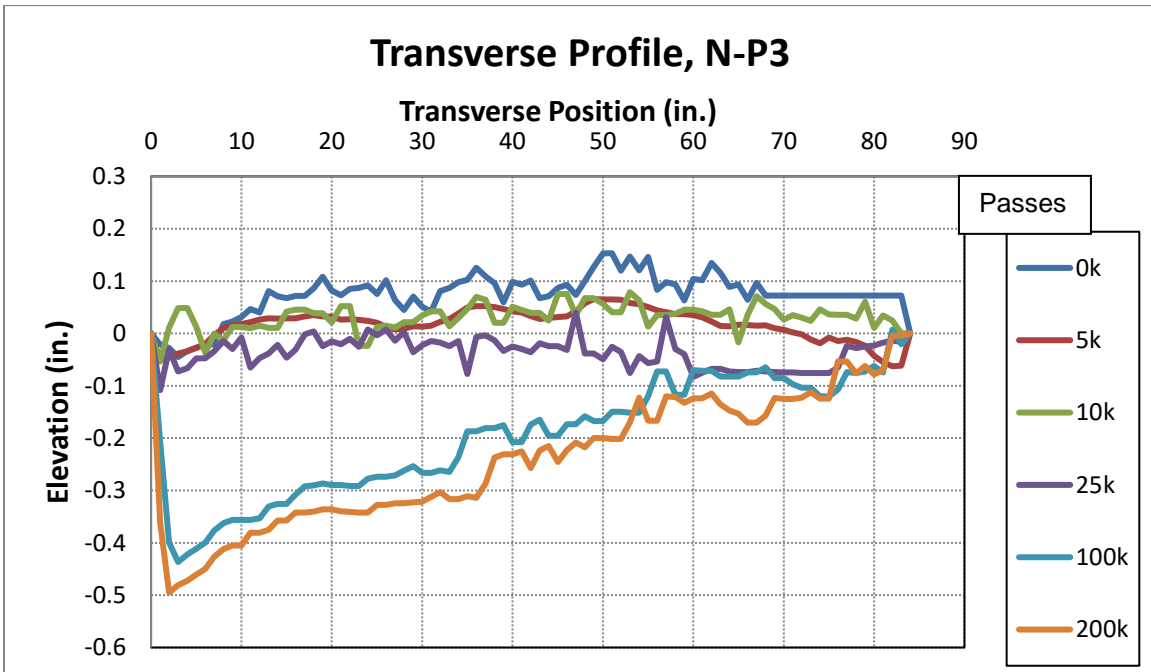


Figure 9. Transverse Profiles – Section N, Profile 4

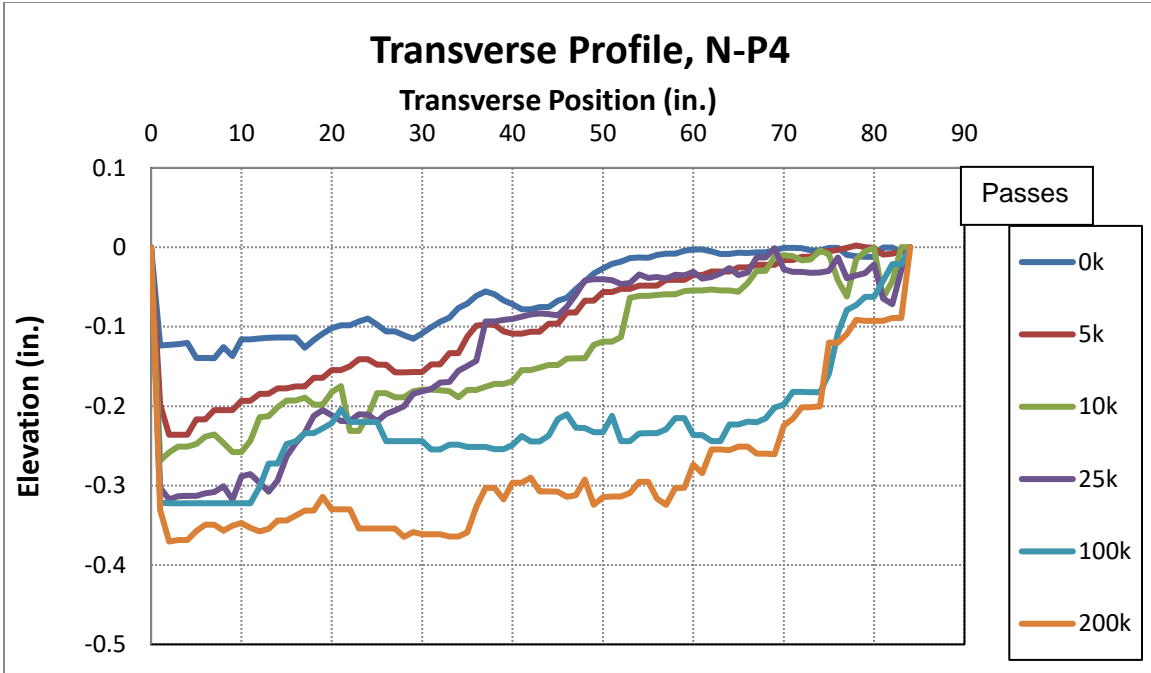


Figure 10. Transverse Profiles – Section N, Profile 5

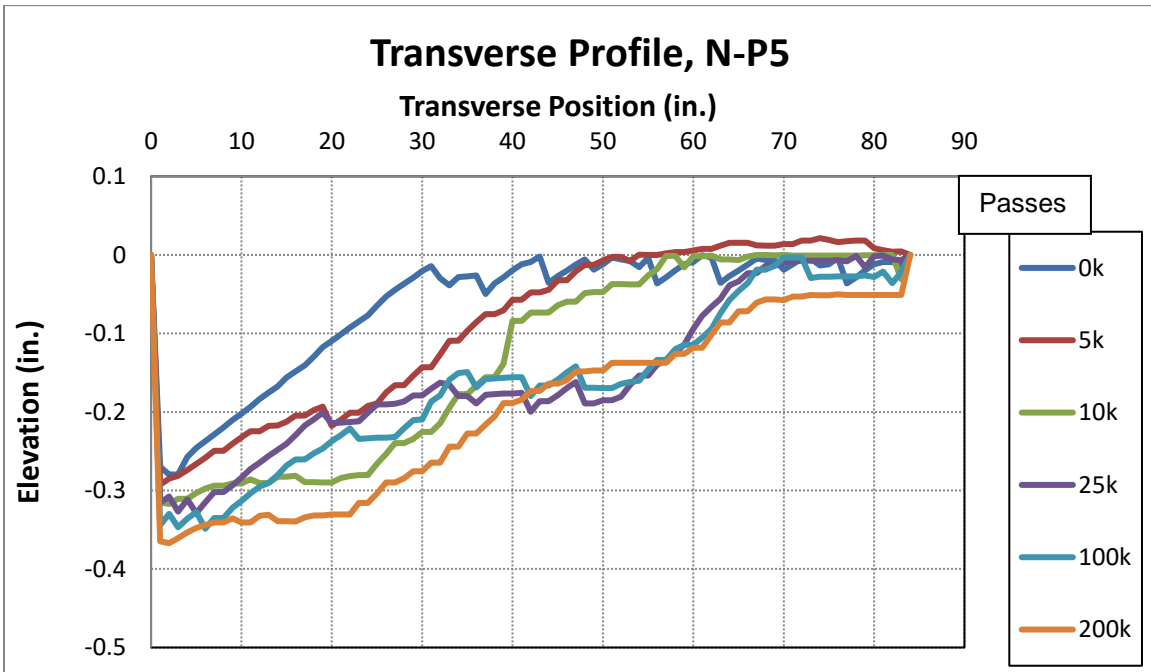


Figure 11. Transverse Profiles – Section O, Profile 1

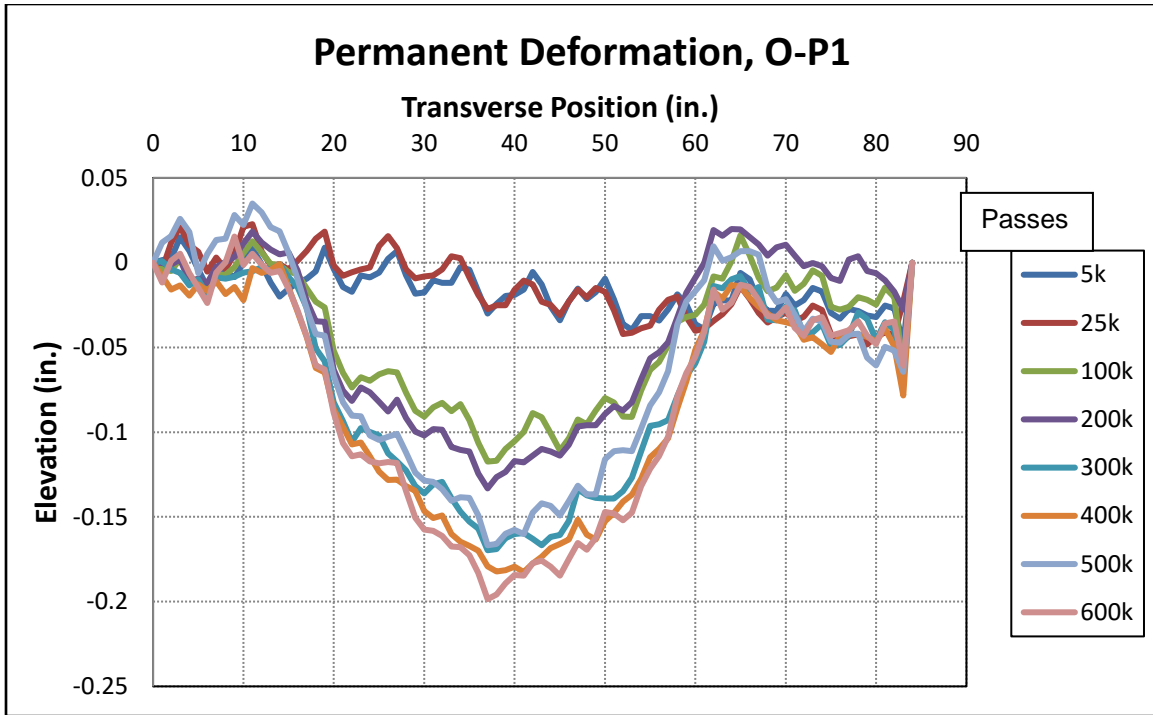


Figure 12. Transverse Profiles – Section O, Profile 2

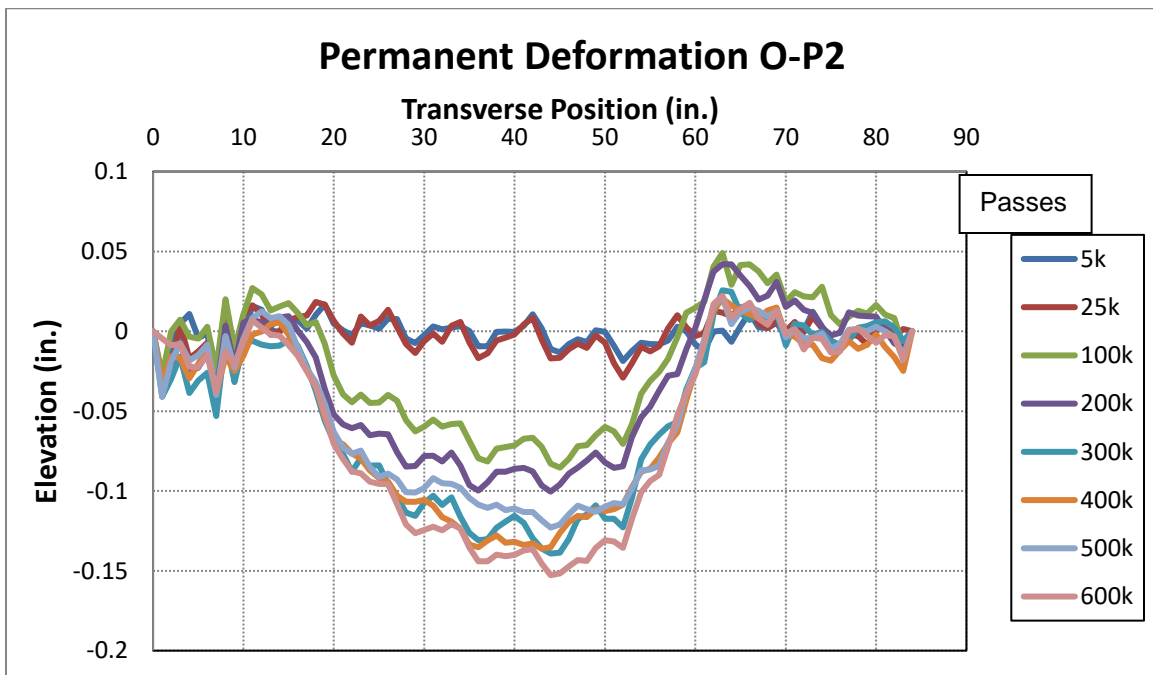


Figure 13. Transverse Profiles – Section O, Profile 3

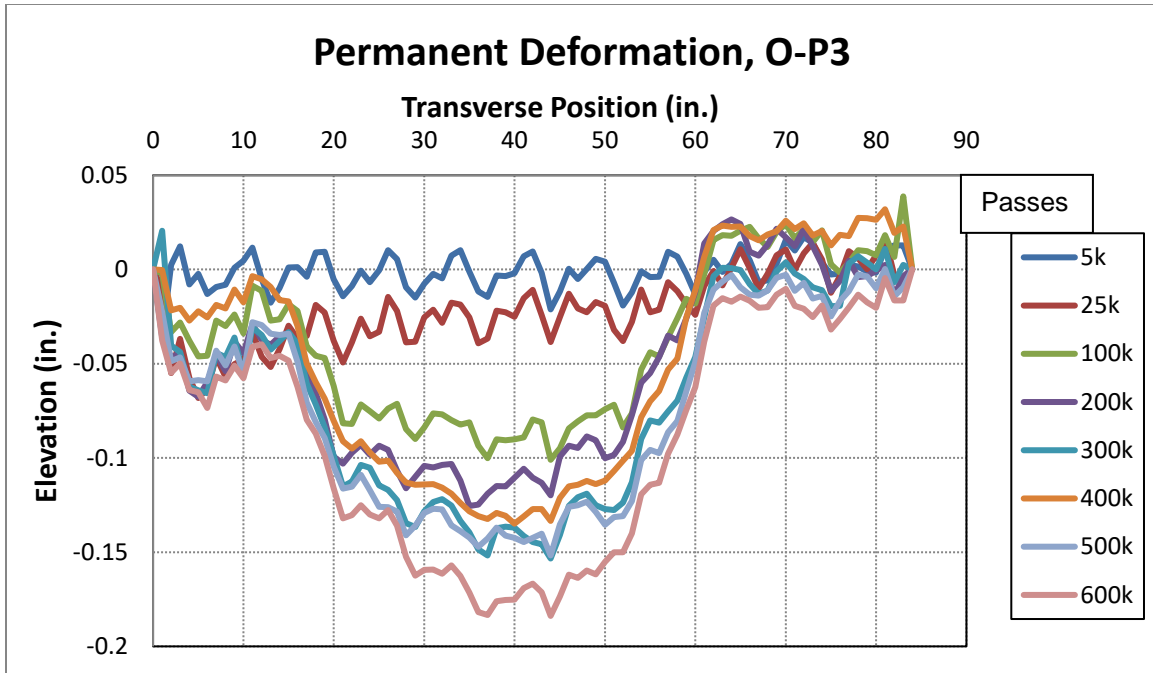


Figure 14. Transverse Profiles – Section O, Profile 4

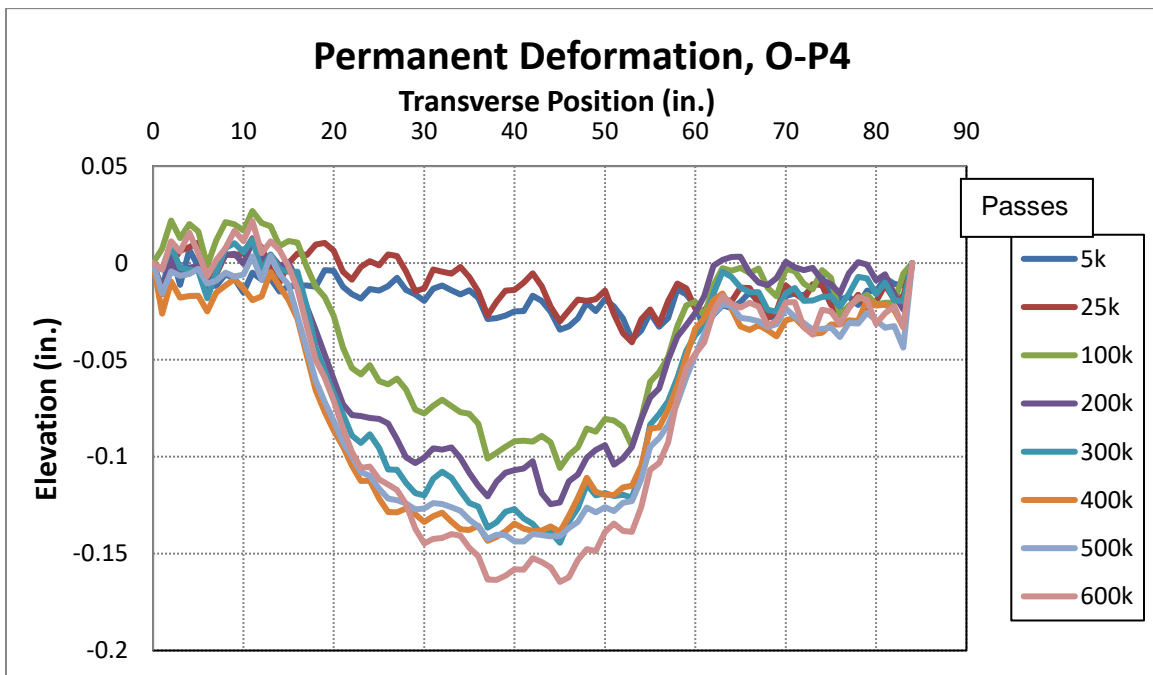


Figure 15. Transverse Profiles – Section O, Profile 5

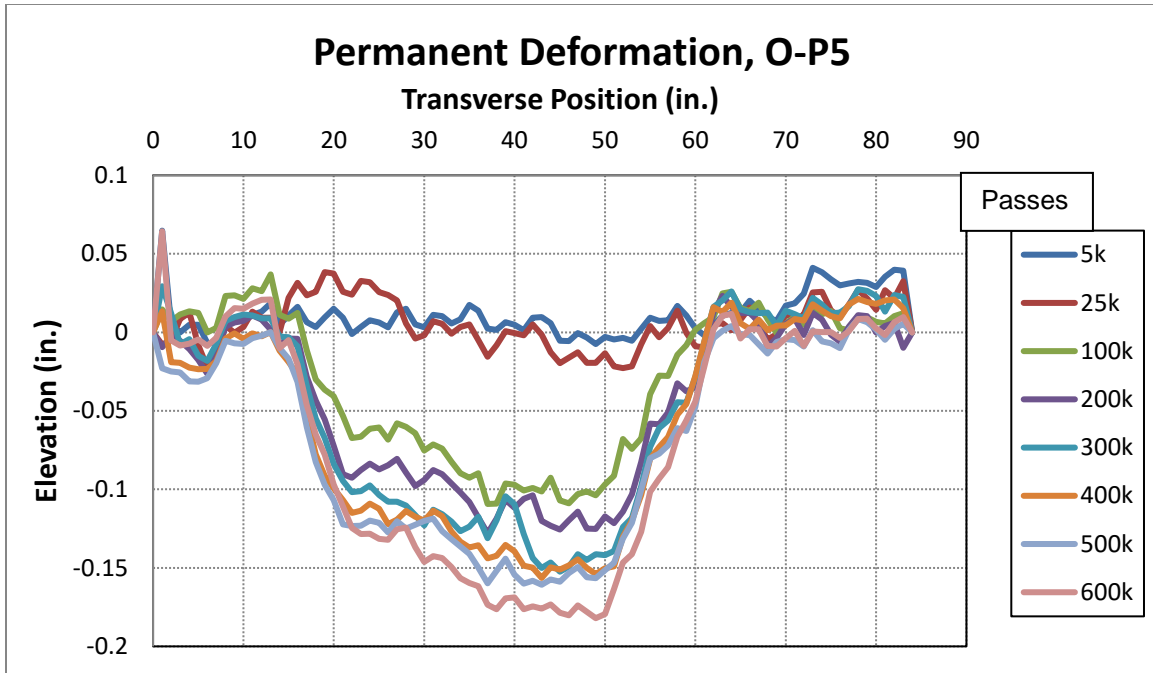


Figure 16. Transverse Profiles – Section P, Profile 1

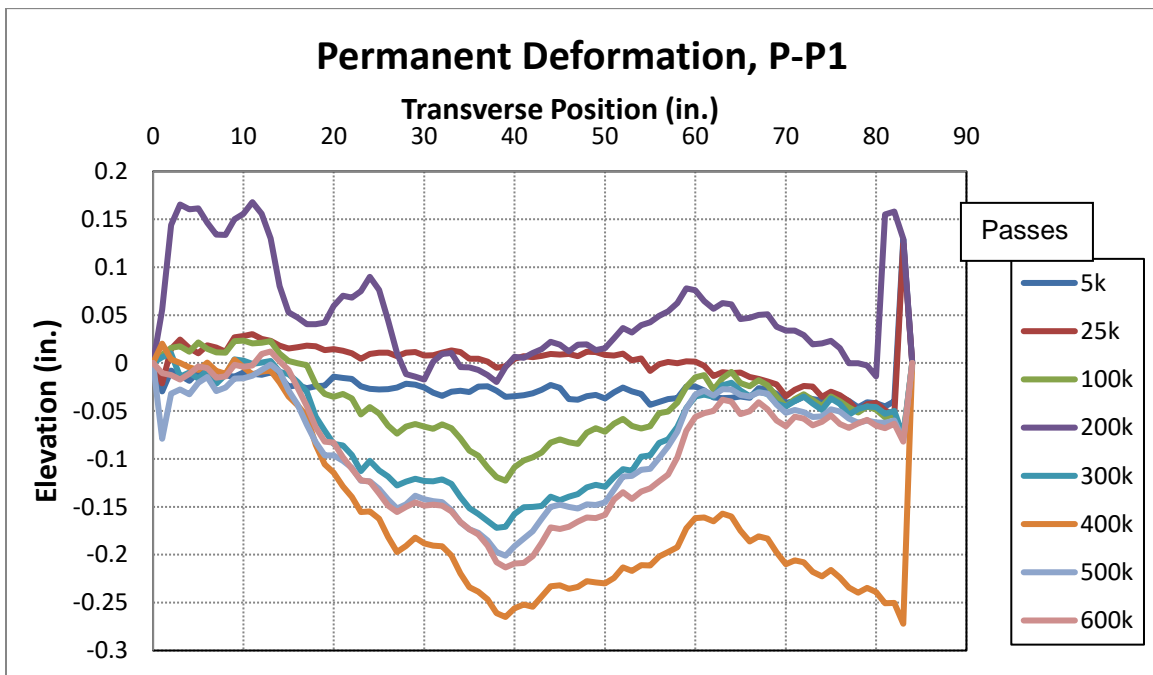


Figure 17. Transverse Profiles – Section P, Profile 2

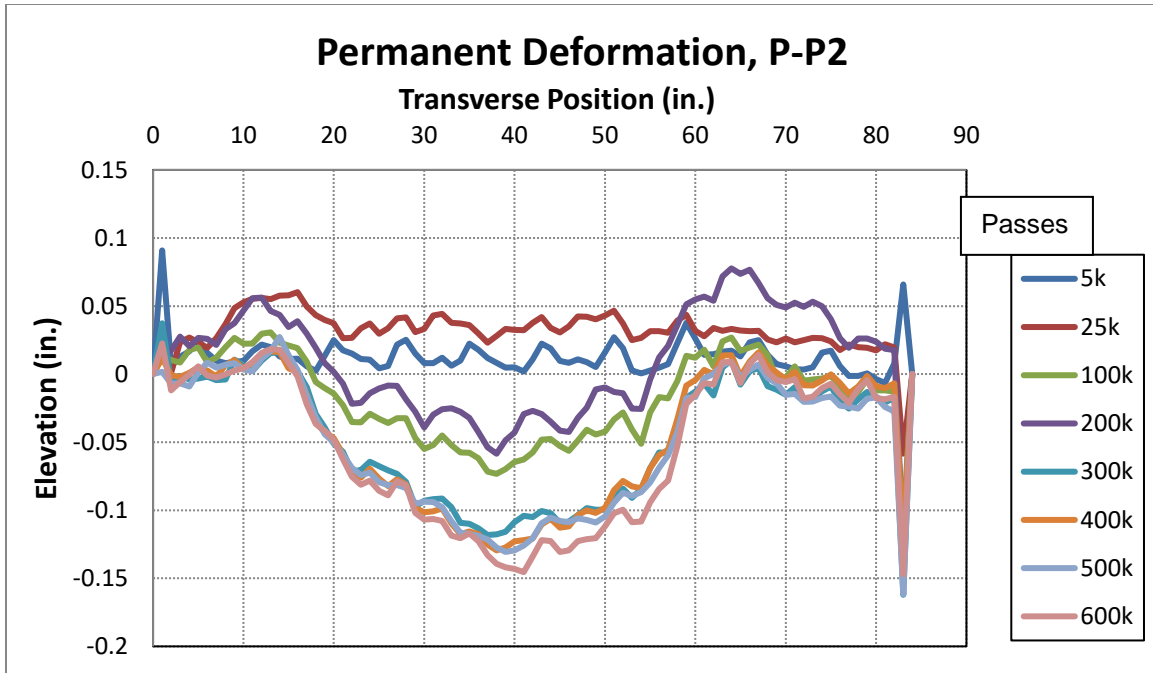


Figure 18. Transverse Profiles – Section P, Profile 3

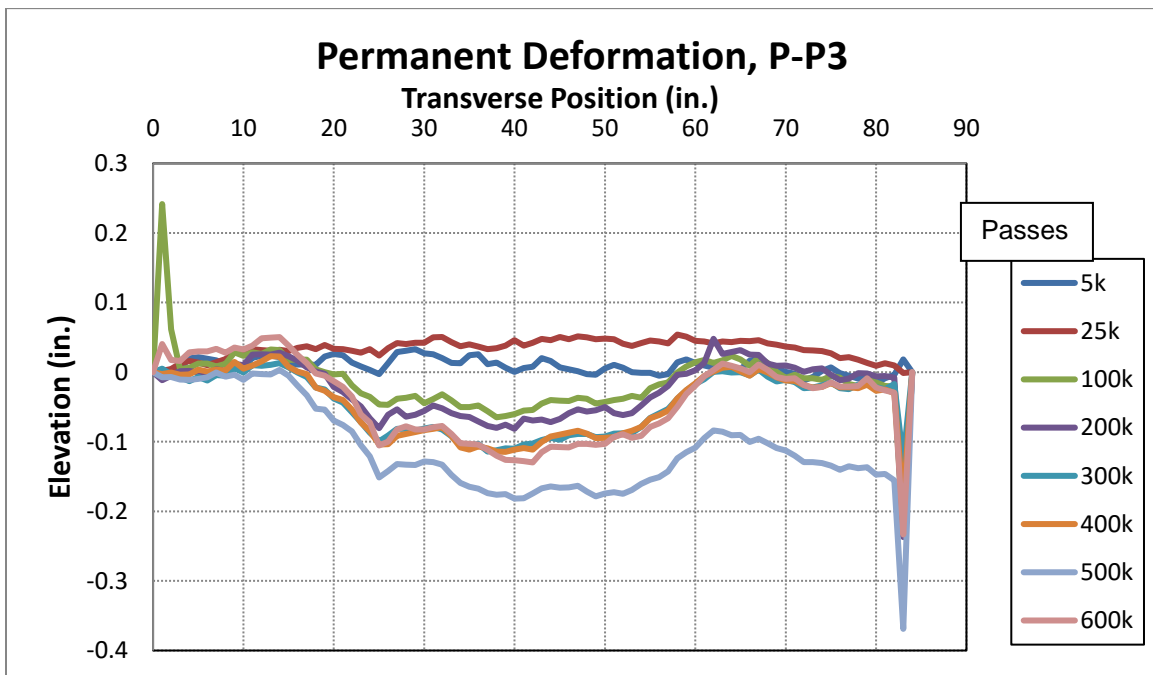


Figure 19. Transverse Profiles – Section P, Profile 4

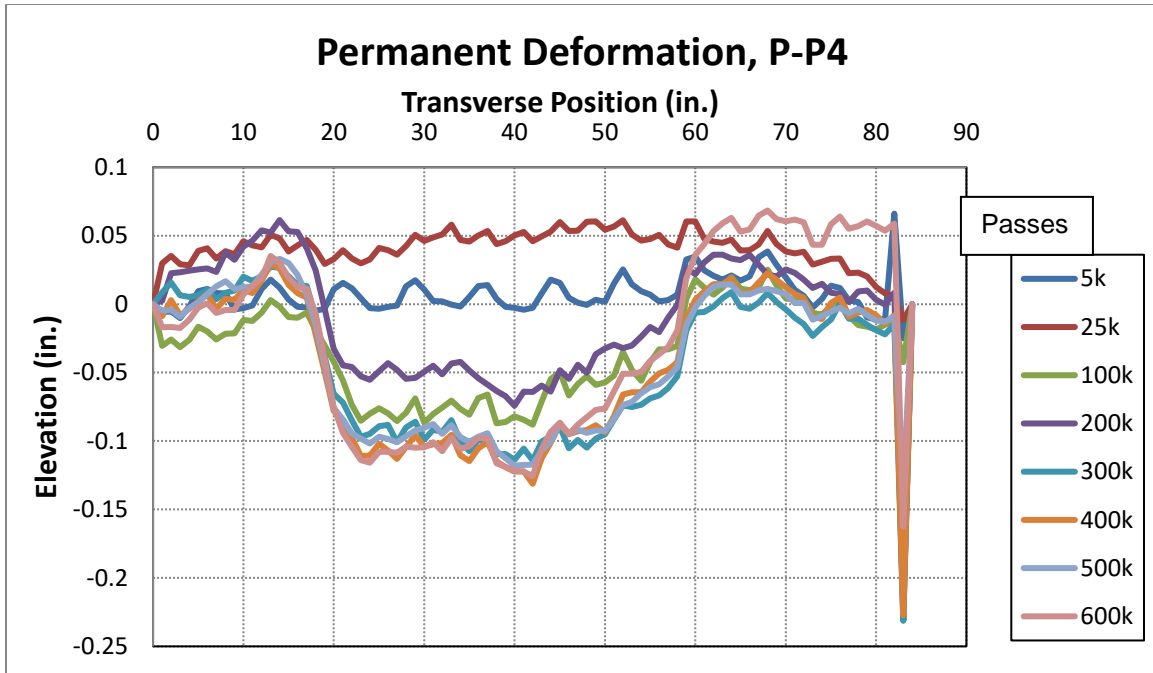


Figure 20. Transverse Profiles – Section P, Profile 5

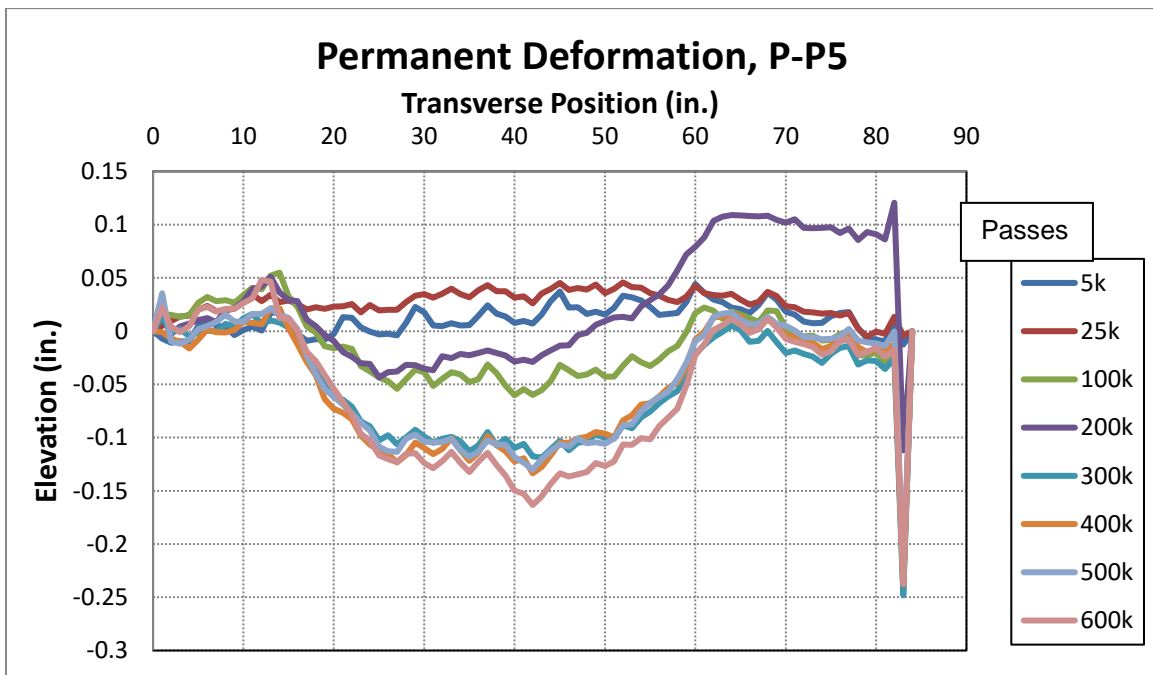


Figure 21. Transverse Profiles – Section S, Profile 1

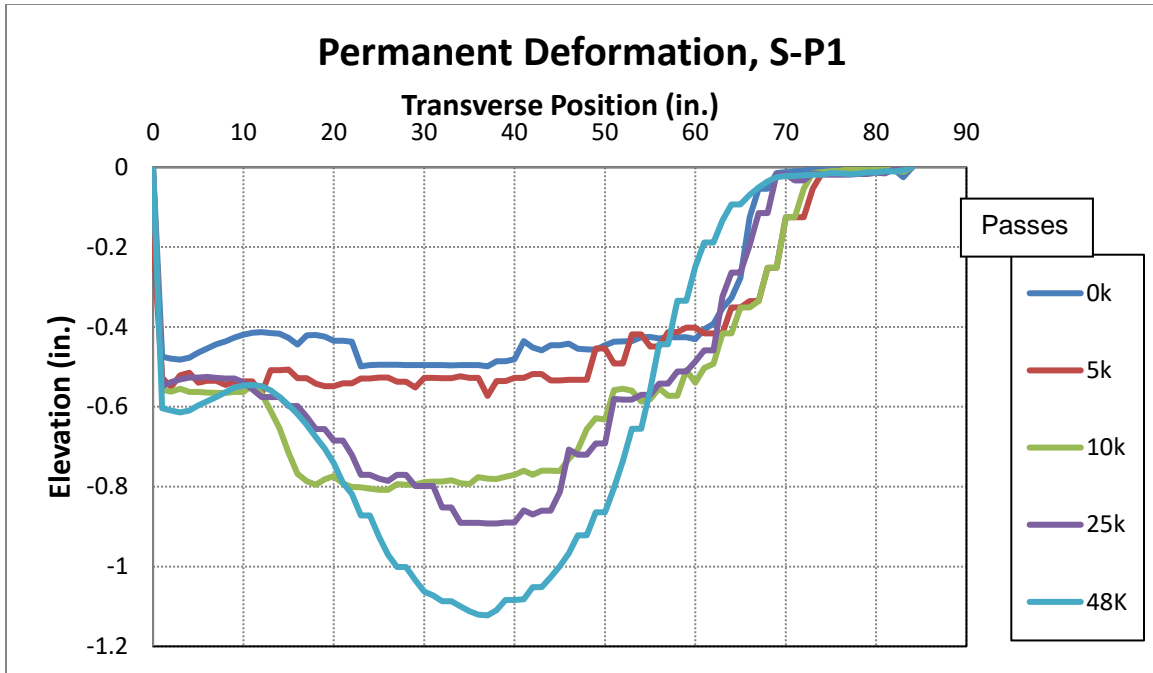


Figure 22. Transverse Profiles – Section S, Profile 2

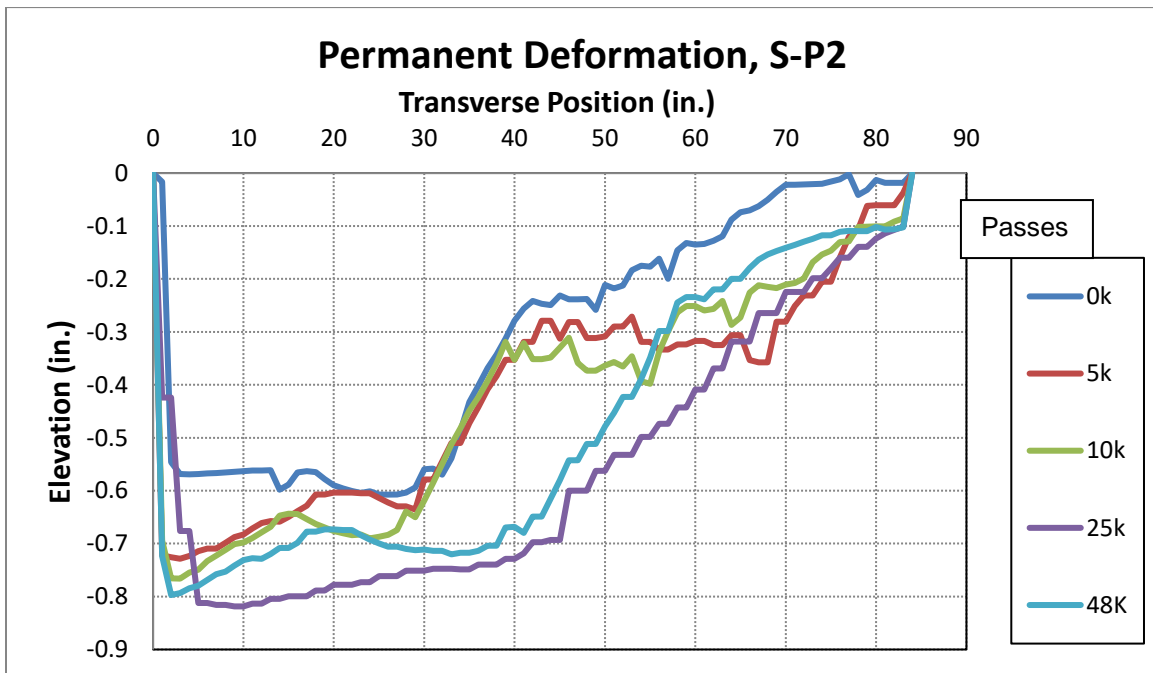


Figure 23. Transverse Profiles – Section S, Profile 3

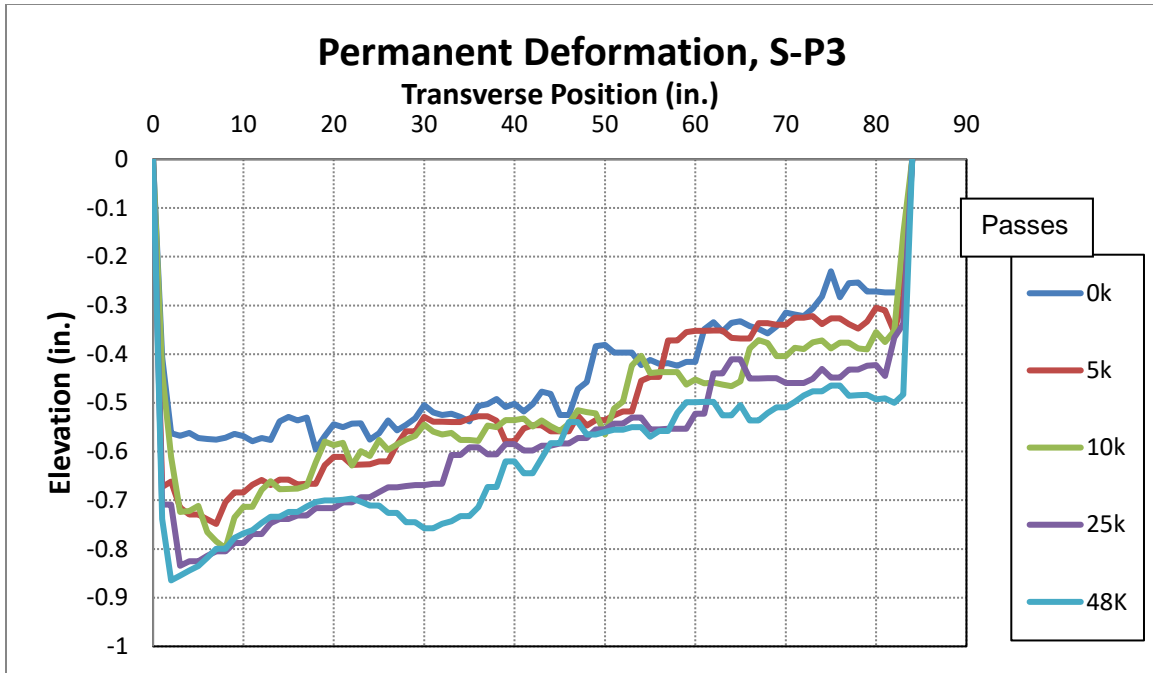


Figure 24. Transverse Profiles – Section S, Profile 4

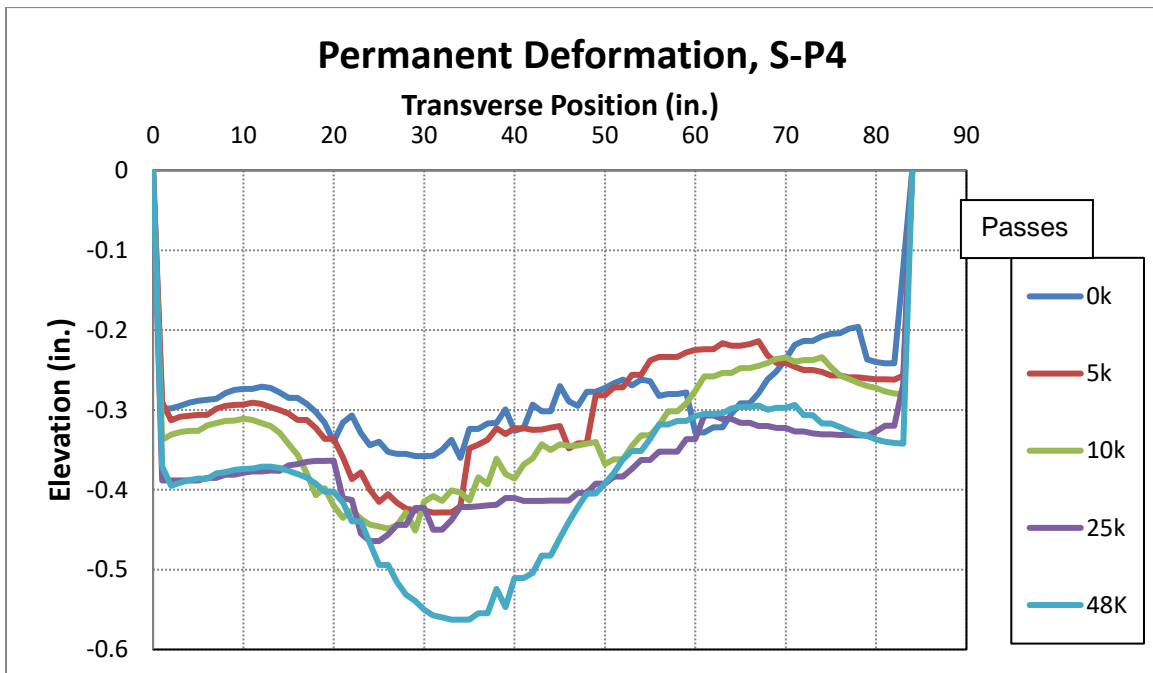


Figure 25. Transverse Profiles – Section S, Profile 5

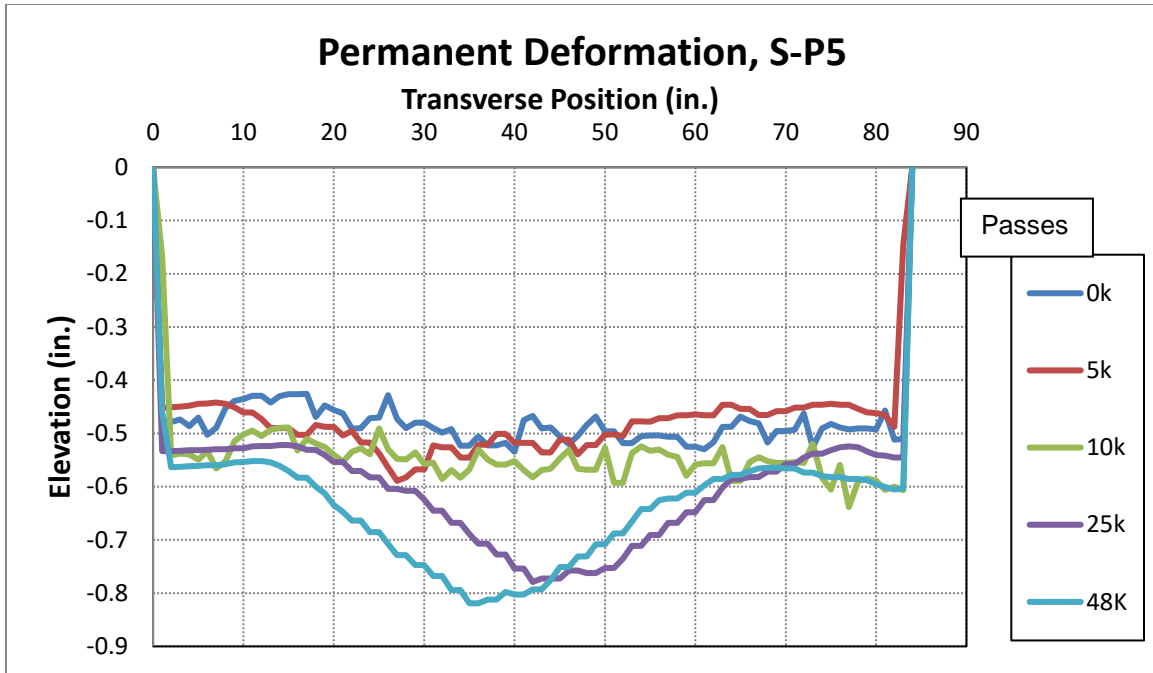


Figure 26. Transverse Profiles – Section T, Profile 1

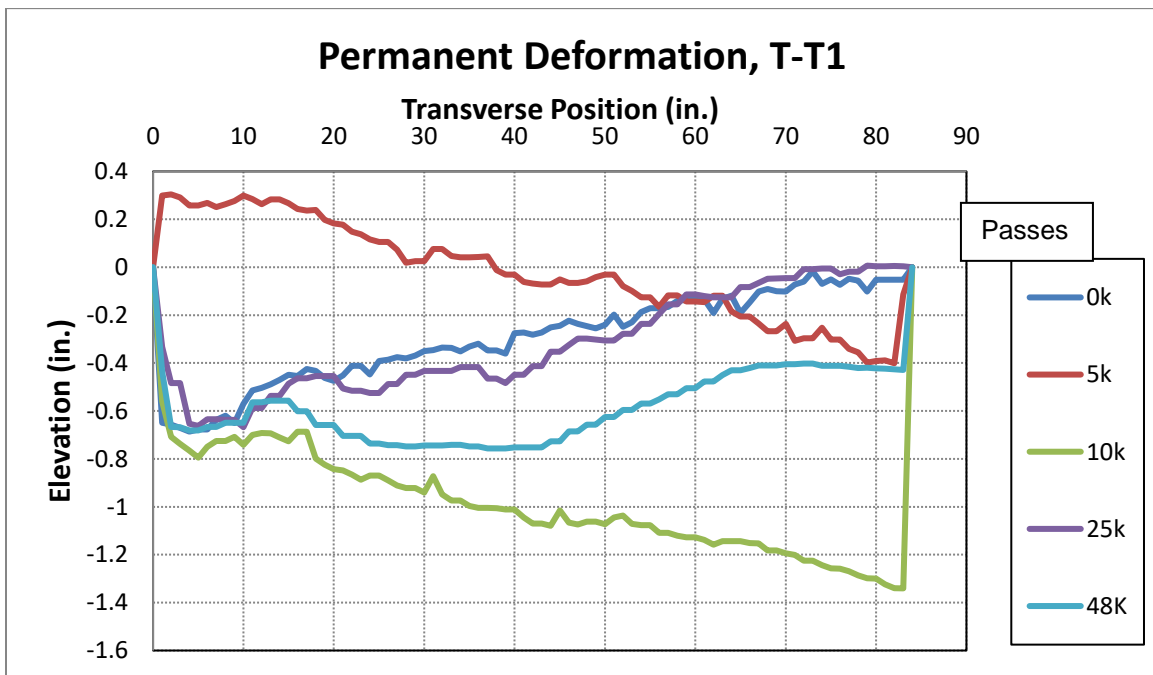


Figure 27. Transverse Profiles – Section T, Profile 2

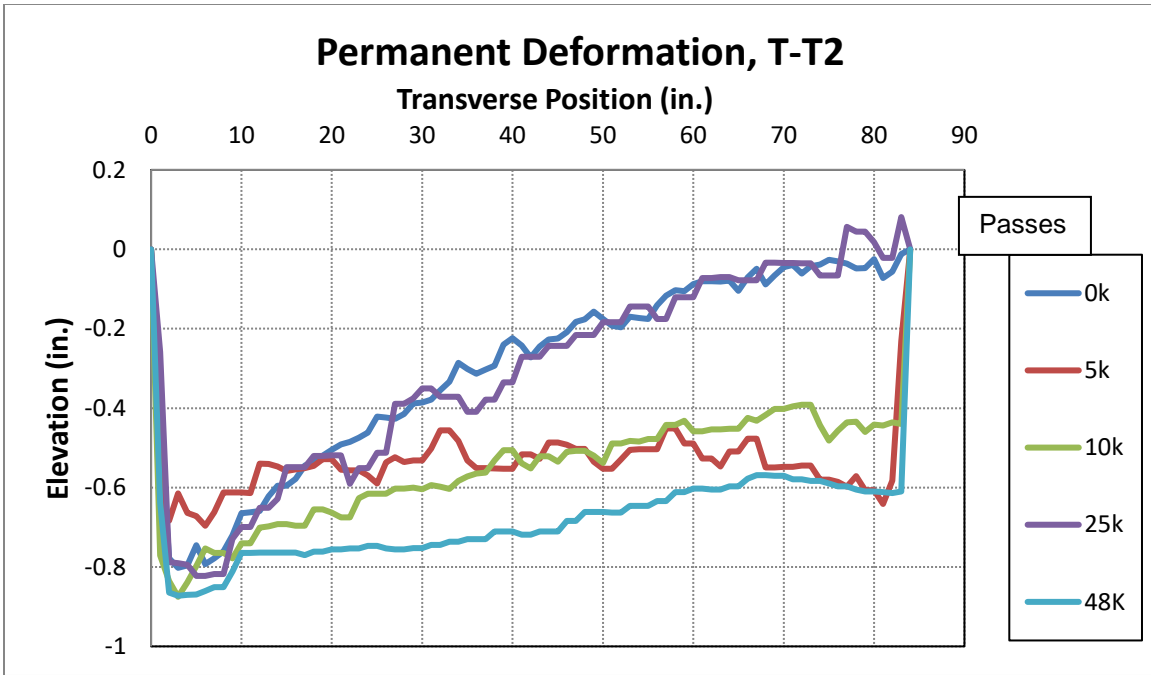


Figure 28. Transverse Profiles – Section T, Profile 3

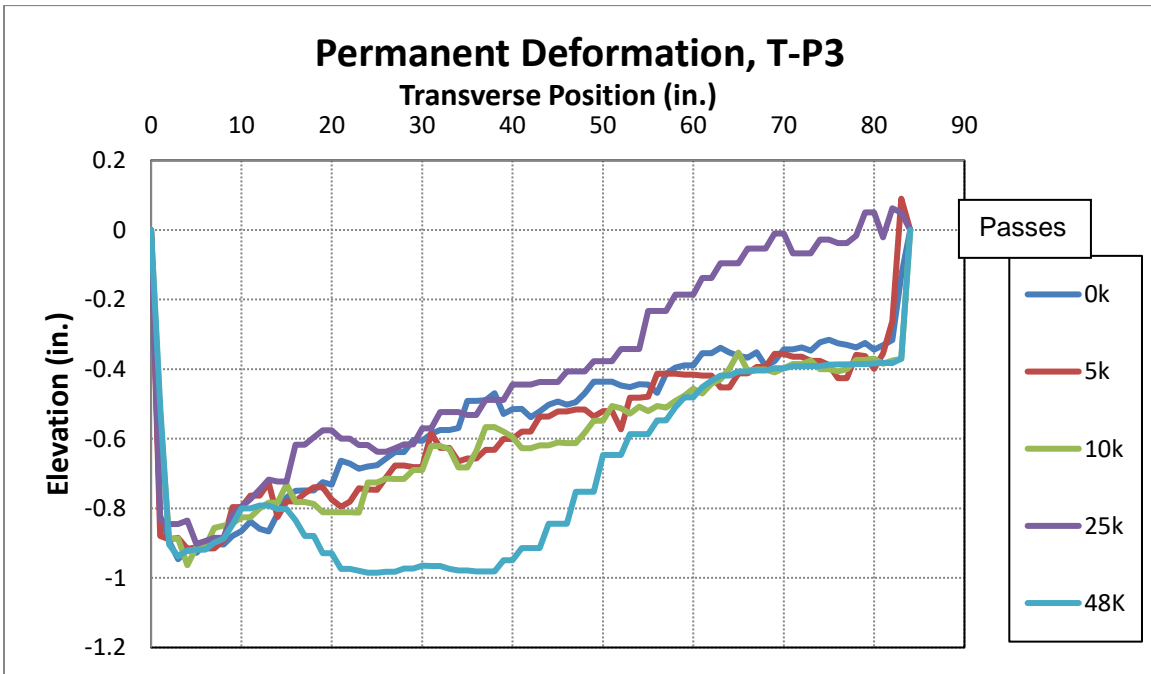


Figure 29. Transverse Profiles – Section T, Profile 4

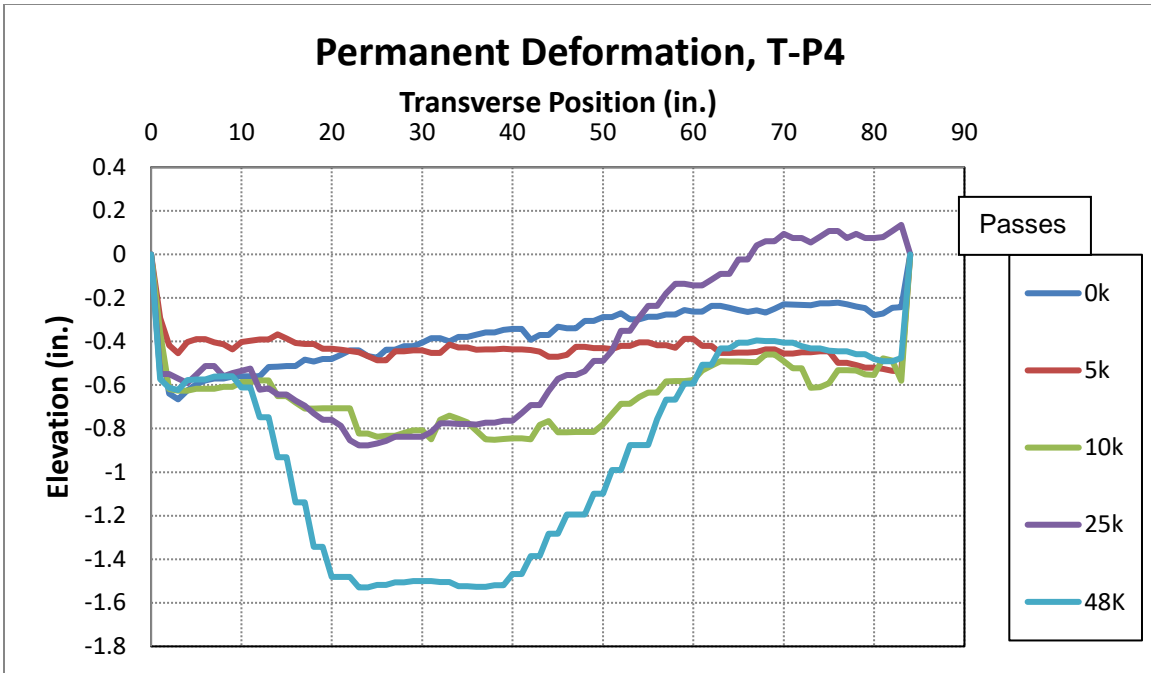
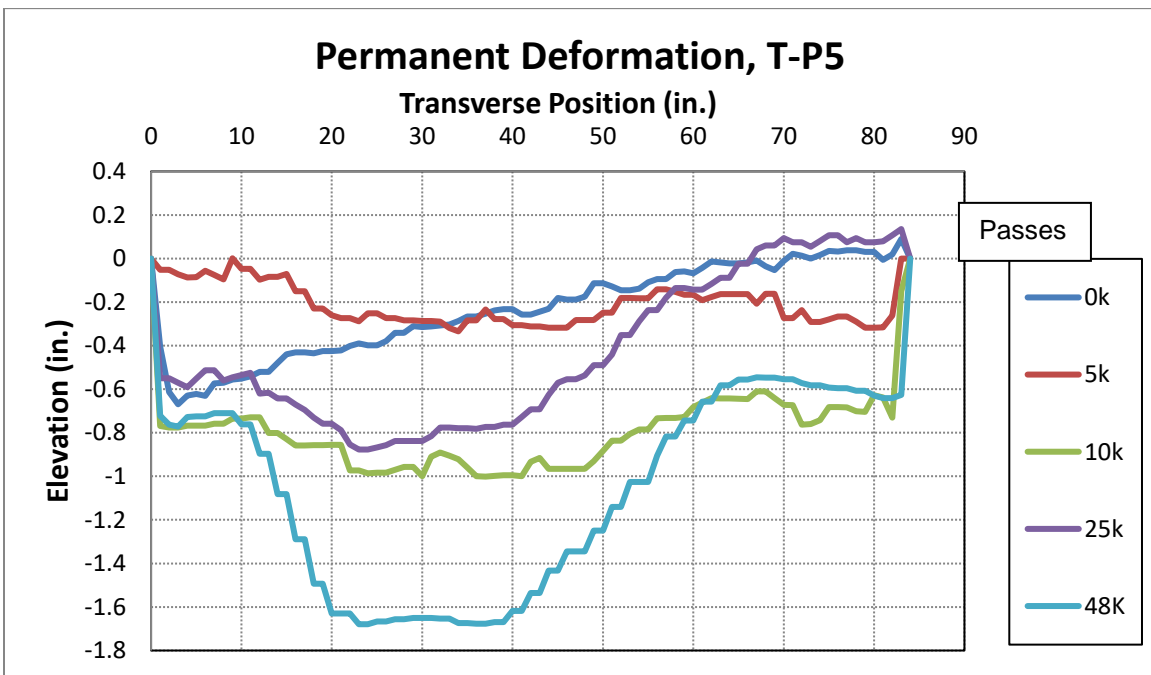


Figure 30. Transverse Profiles – Section T, Profile 5



APPENDIX B

Item 2

VBA Code

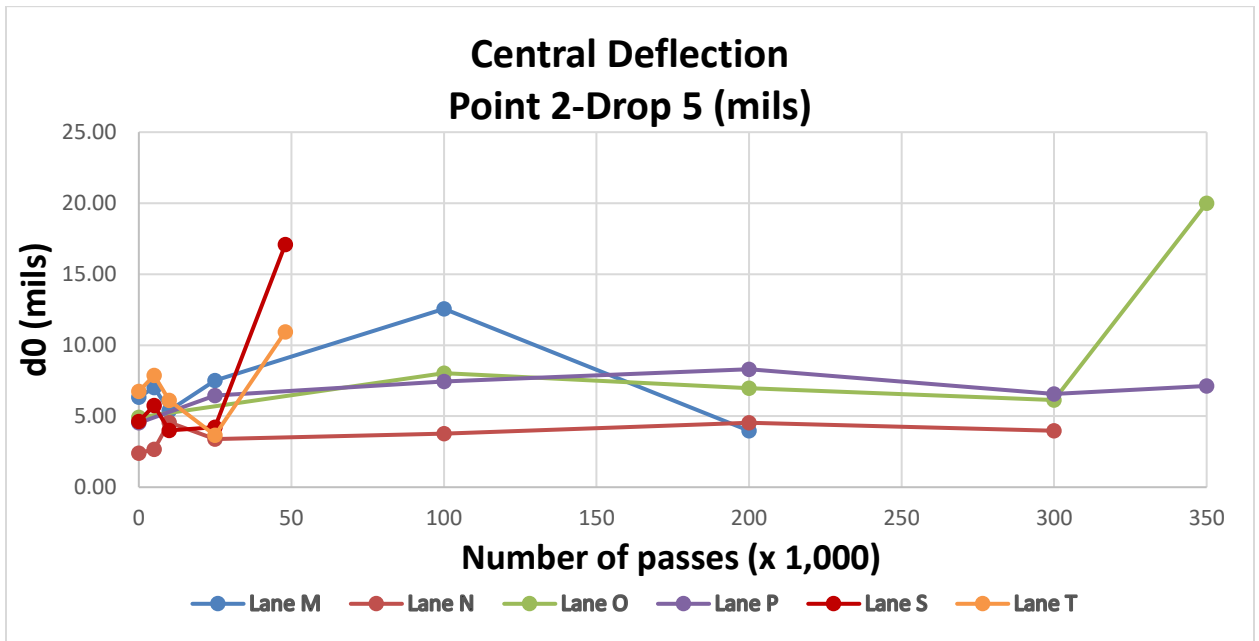
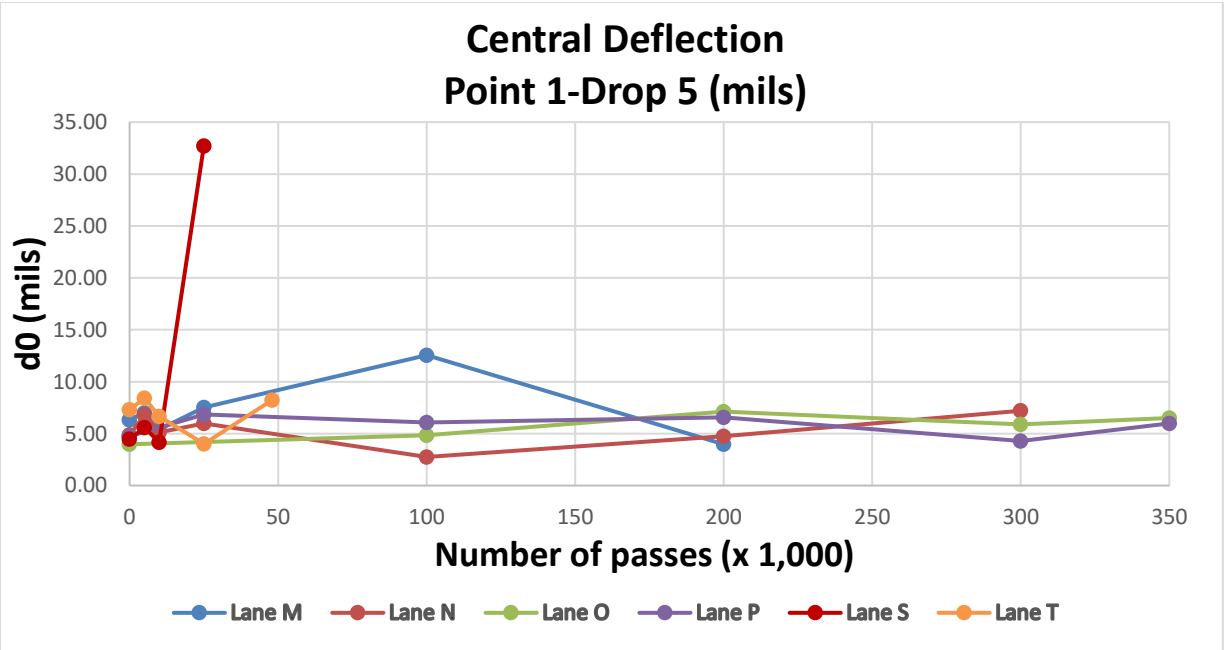
```

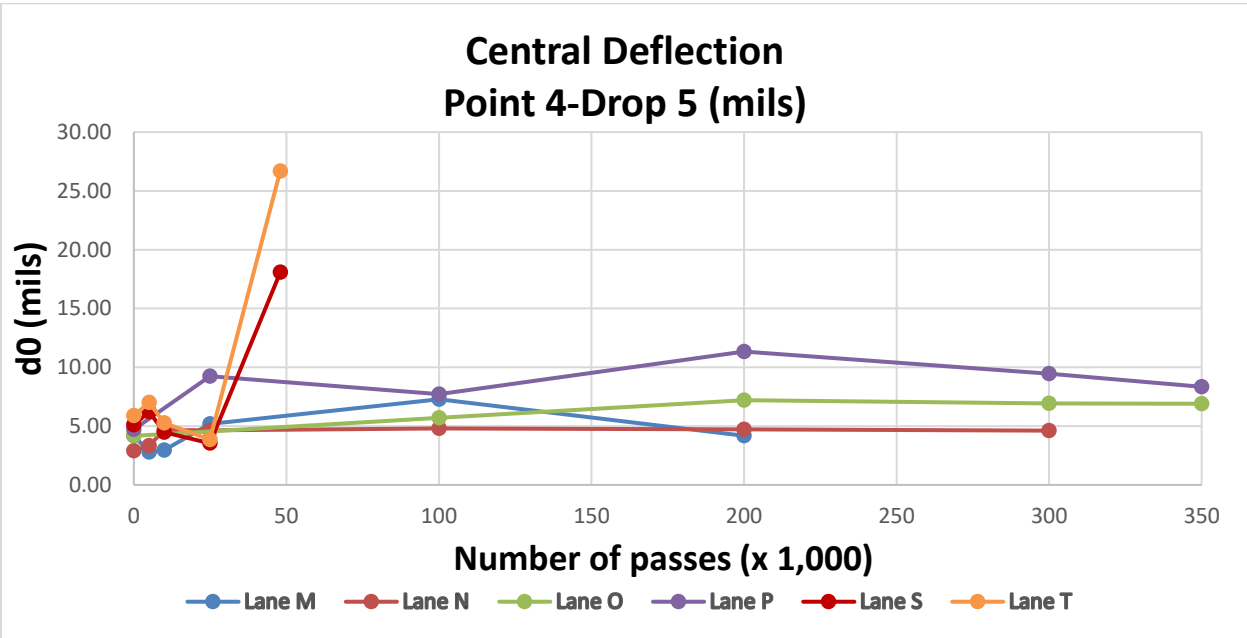
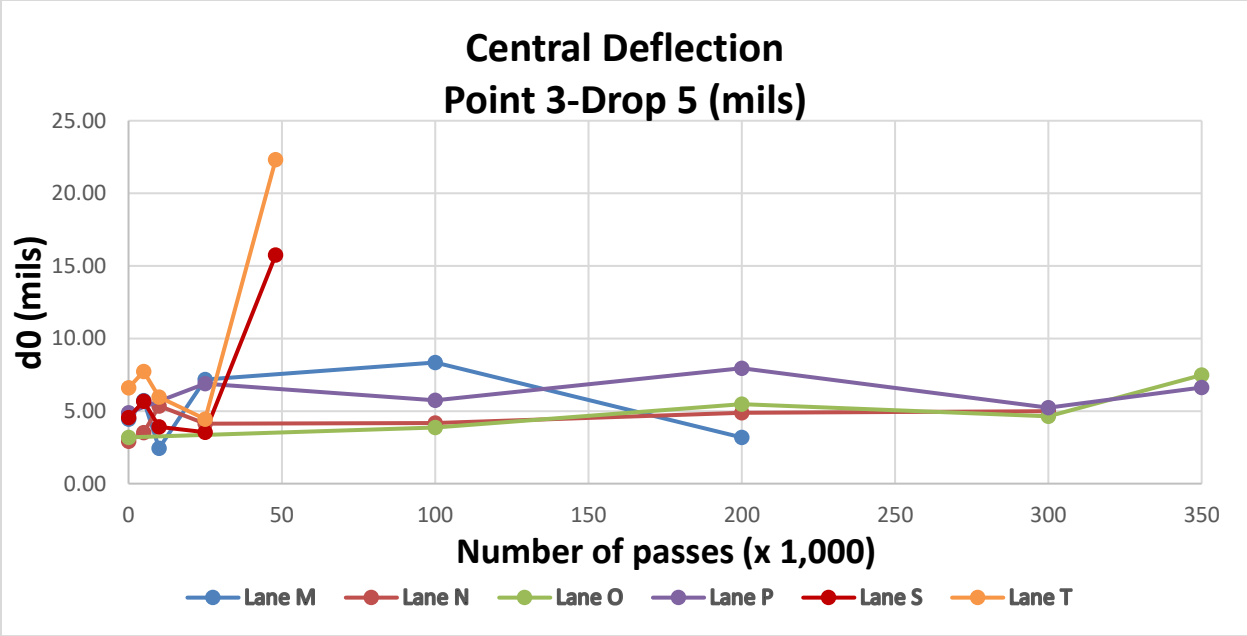
Sub secondpart()
'
' secondpart Macro
'
' Keyboard Shortcut: Ctrl+Shift+A
'
Range("A1:B1").Select
Range(Selection, Selection.End(xlDown)).Select
ActiveWorkbook.PivotCaches.Create(SourceType:=xlDatabase, SourceData:= _
    "Sheet2!R1C1:R106C2", Version:=6).CreatePivotTable TableDestination:= _
    "Sheet2!R1C4", TableName:="PivotTable12", DefaultVersion:=6
Sheets("Sheet2").Select
Cells(1, 4).Select
With ActiveSheet.PivotTables("PivotTable12").PivotFields("x axis")
    .Orientation = xlRowField
    .Position = 1
End With
ActiveSheet.PivotTables("PivotTable12").AddDataField ActiveSheet.PivotTables( _
    "PivotTable12").PivotFields("Corrected"), "Sum of Corrected", xlSum
With ActiveSheet.PivotTables("PivotTable12").PivotFields("Sum of Corrected")
    .Caption = "Average of Corrected"
    .Function = xlAverage
End With
Range("H2").Select
ActiveCell.FormulaR1C1 = "=VLOOKUP(RC[-1],R2C4:R82C5,2)"
Range("H3").Select
ActiveWindow.SmallScroll Down:=-6
Range("H2").Select
Selection.AutoFill Destination:=Range("H2:H86")
Range("H2:H86").Select
Range("L19").Select
ActiveWindow.SmallScroll Down:=69
Range("H86").Select
ActiveCell.FormulaR1C1 = "=VLOOKUP(RC[-1],R2C4:R82C5,2)"
Range("K76").Select
ActiveWindow.SmallScroll Down:=-75
End Sub
Sub thirdpart()
'
' thirdpart Macro
'
' Keyboard Shortcut: Ctrl+b
'
Range("H3").Select
Range(Selection, Selection.End(xlDown)).Select
Selection.ClearContents
Range("D1:E1").Select
Range(Selection, Selection.End(xlDown)).Select
Selection.ClearContents
Range("A2:B2").Select
Range(Selection, Selection.End(xlDown)).Select
Selection.ClearContents
End Sub

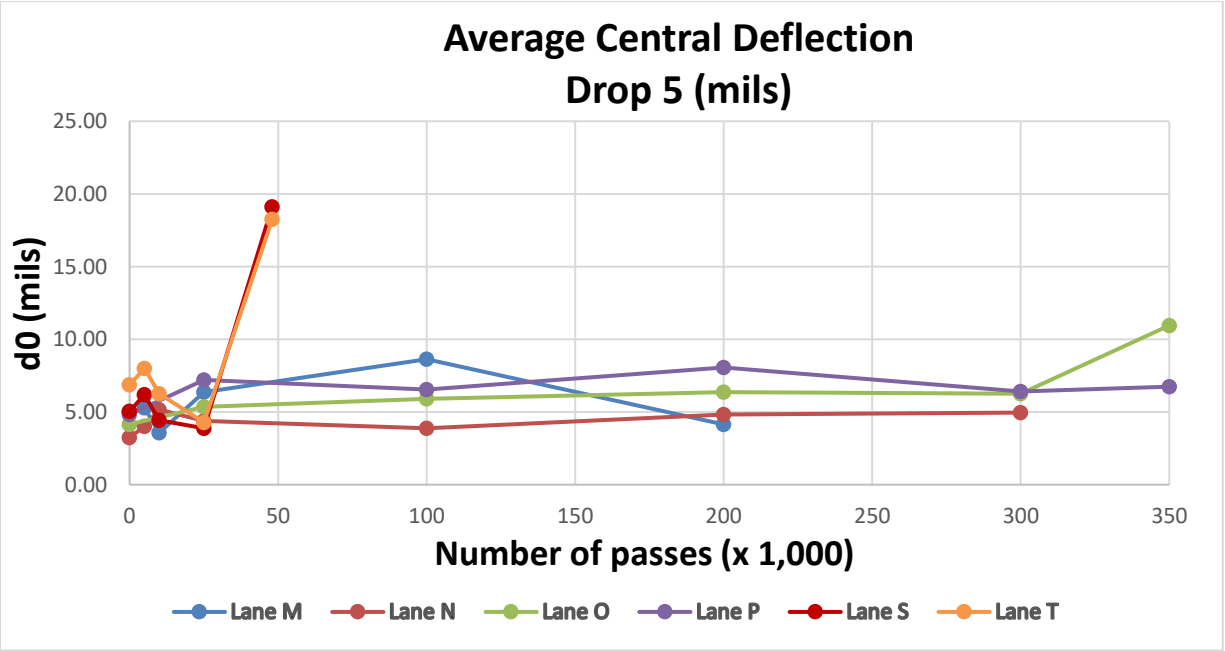
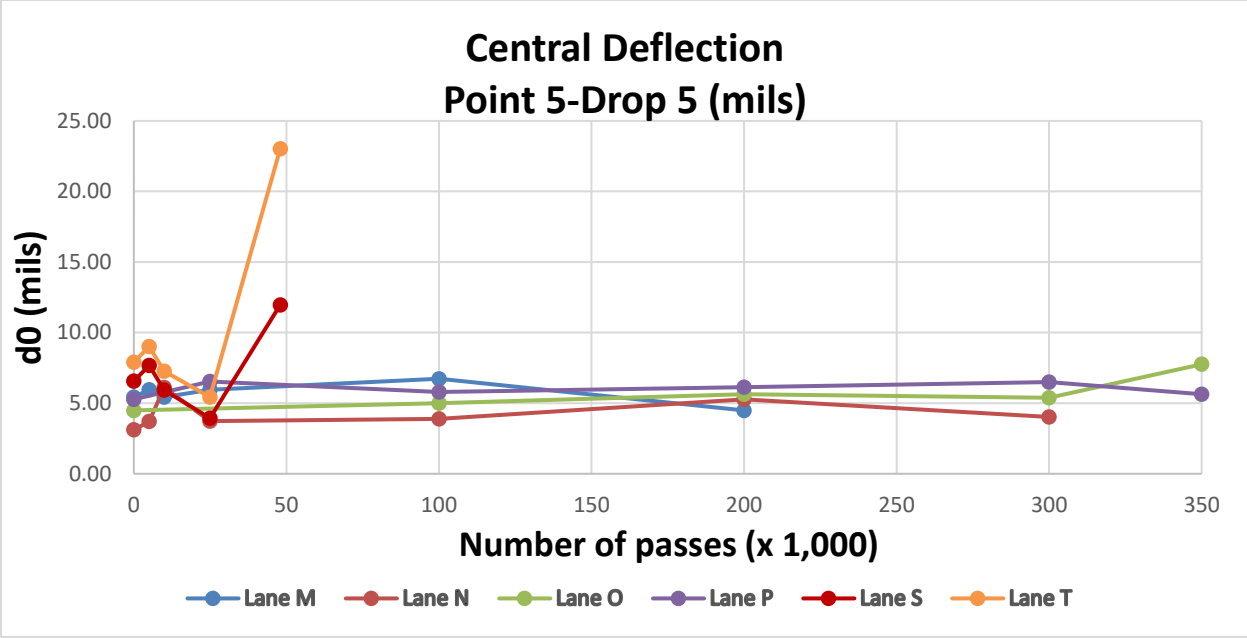
```

APPENDIX C

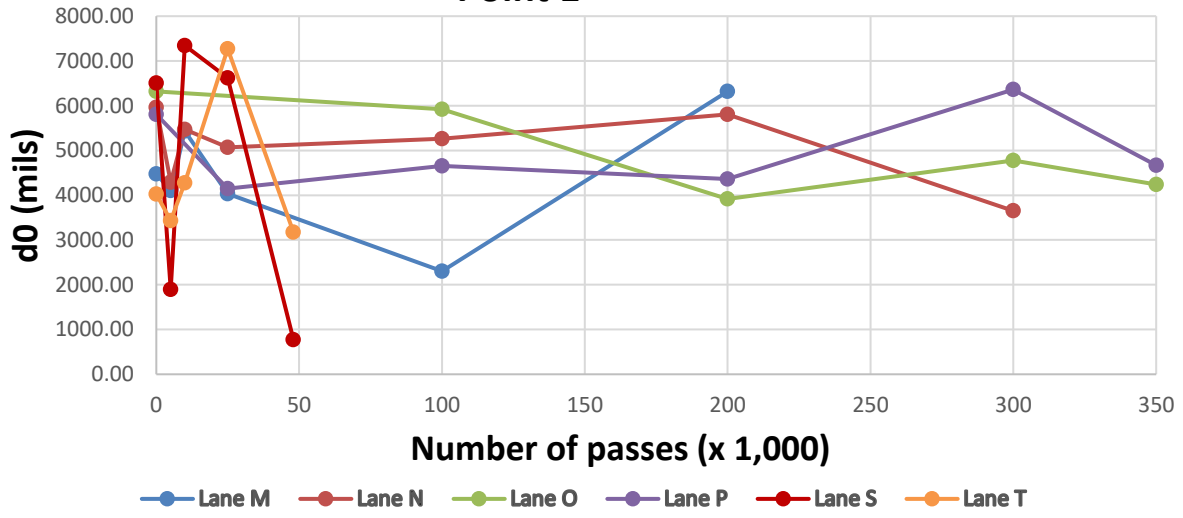
Overall pavement stiffness and Central Deflection recorded by the L-FWD



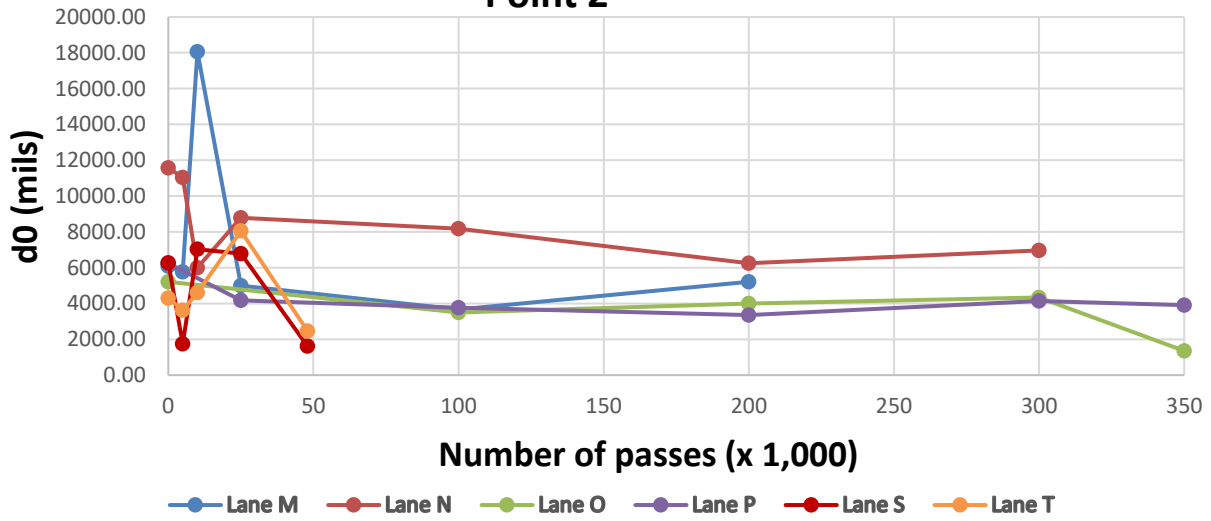




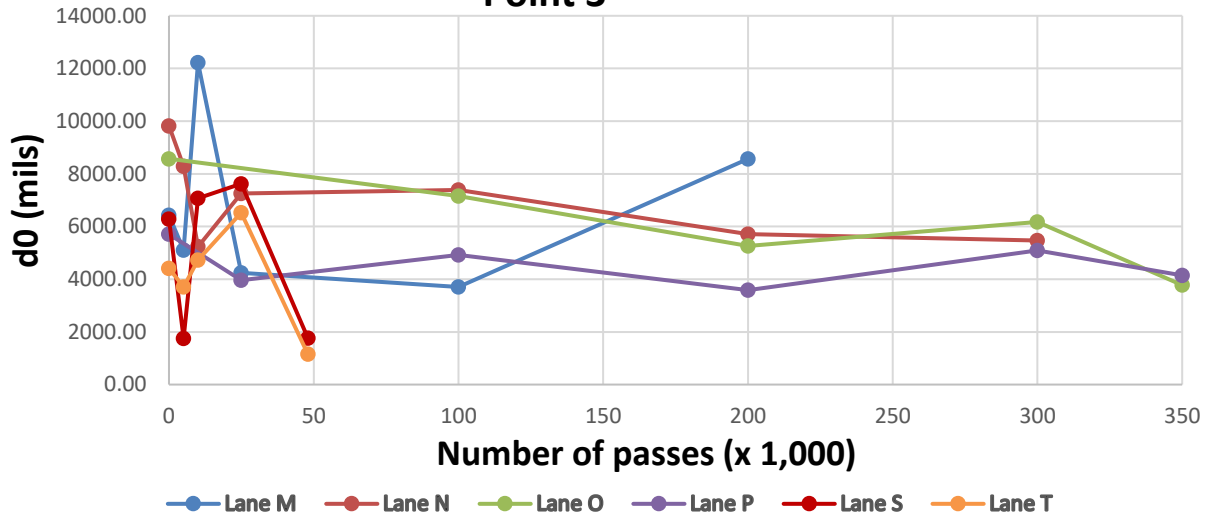
Overall Pavement Stiffness (pci) Point 1



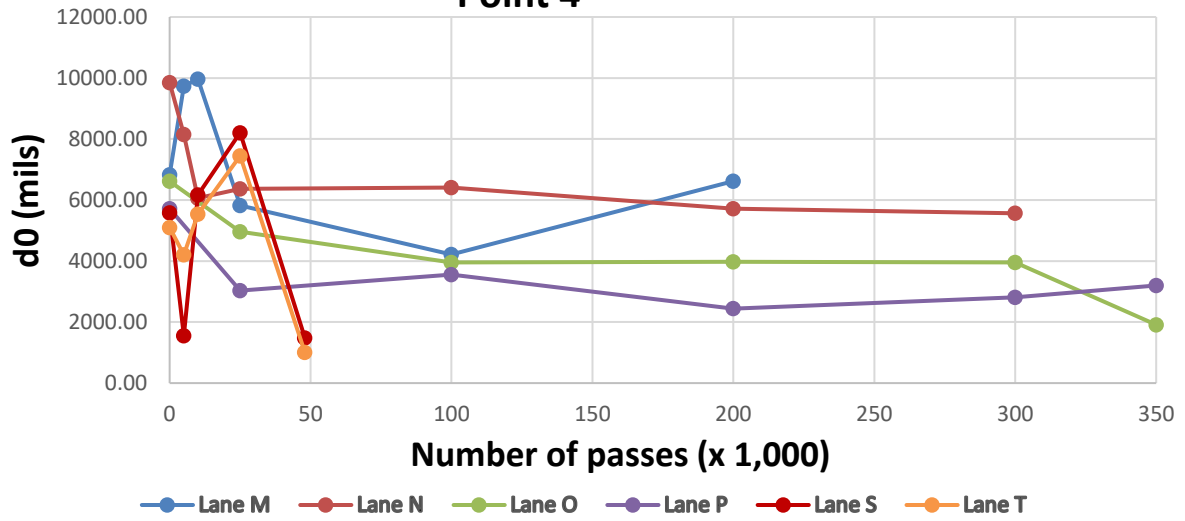
Overall Pavement Stiffness (pci) Point 2



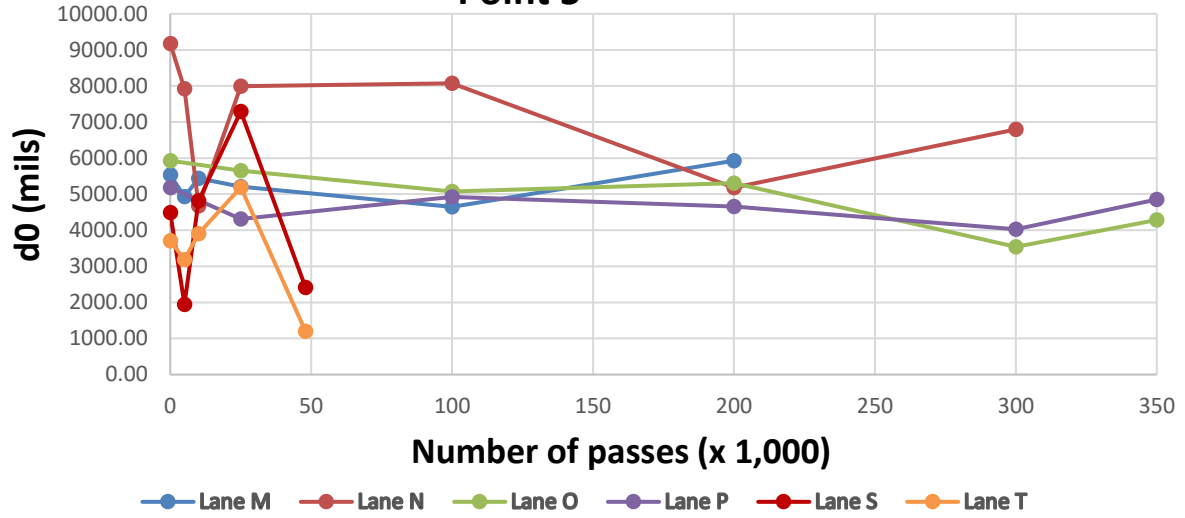
Overall Pavement Stiffness (pci) Point 3



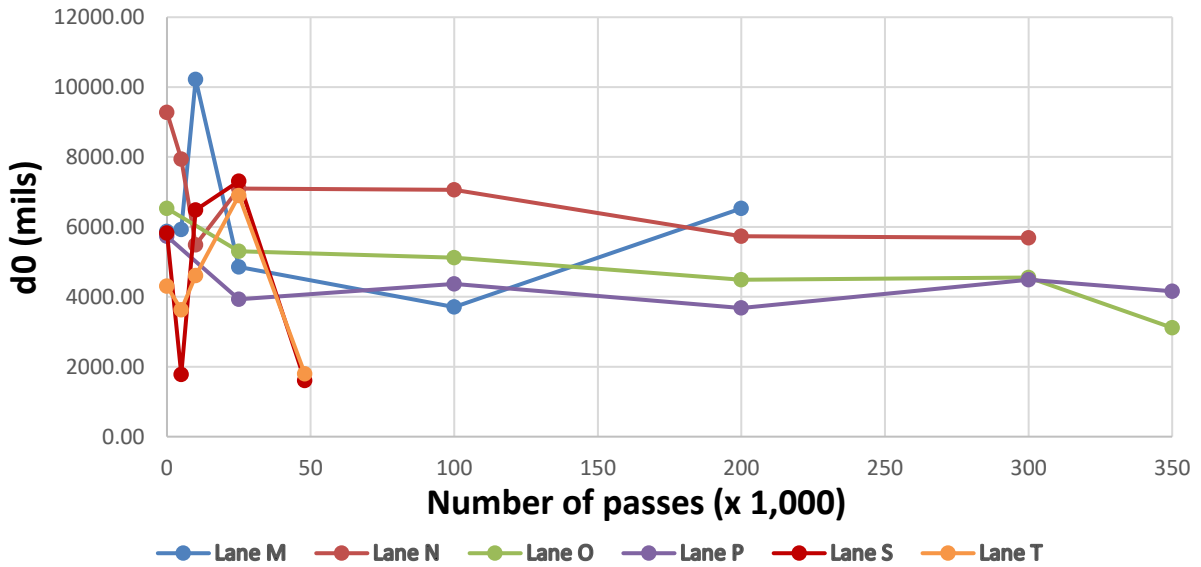
Overall Pavement Stiffness (pci) Point 4



Overall Pavement Stiffness (pci) Point 5



Average Pavement Stiffness (pci)



APPENDIX D

Item 1. Summary of the Longitudinal and Transverse Strain Signals

Item 2. Longitudinal and Transverse Strain Signals - Graph Representation

Table D1-1 Longitudinal Strain Signal Values-Lane M&N -10k passes

Run	Gauge	Position 0				
		A	B	C	D	E
1	ML1	-0.09	-27.44	153.08	-38.95	5.39
	ML2	6.59	-79.01	244.81	-17.45	5.42
	NL1	-9.85	-101.64	388.59	-69.67	3.43
	NL2					
2	ML1	2.12	-57.42	161.09	-11.34	0.66
	ML2	8.52	-34.43	240.66	-56.88	5.15
	NL1	-6.34	-114.03	388.8	-48.01	-4.77
	NL2					
3	ML1	4.8	-26.93	147.68	-39.18	4.7
	ML2	3.39	-81.37	243.47	-18.46	8.57
	NL1	-11.33	-98.38	388.17	-68.44	-1.25
	NL2					
4	ML1	1.2	-58.28	156.97	-11.21	0.53
	ML2	5.1	-36.61	244.56	-58.23	0.75
	NL1	-13.34	-116.94	381.37	-53.13	-1.32
	NL2					
5	ML1	6.45	-28.27	148.97	-38.58	4.33
	ML2	-30.7	-78.94	245.31	-20.24	7.9
	NL1	-4.94	-98.81	398.69	-70.25	-2.12
	NL2					
6	ML1	1.89	-58.24	159.36	-11.32	7.28
	ML2	9.05	-36.91	242.89	-59.53	1.81
	NL1	-6.5	-111.95	389.53	-46.51	0.91
	NL2					
7	ML1	6.61	-26.6	151.27	-38.11	3.15
	ML2	2.97	-81.72	243.85	-19.12	8.16
	NL1	1.14	-104.26	391.57	-68.31	-1.72
	NL2					
8	ML1	1.11	-56.02	160.82	-11.98	6.53
	ML2	3.15	-43.17	240.4	-59.39	-0.76
	NL1	-3.16	-114.31	381.88	-49.26	-1.92
	NL2					

Table D1-2 Longitudinal Strain Signal Values-Lane M&N -25k passes

Run	Gauge	Position 0				
		A	B	C	D	E
1	ML1	-3.88	-50.44	279.44	-53.43	0.57
	ML2	-2.28	-118.42	368.57	-47.14	3.64
	NL1	-1.27	-139.88	343.67	-76.48	-5.39
	NL2					
2	ML1	-1.97	-94.31	321.26	-19.66	12.18
	ML2	-1.74	-82.92	328.53	-86.3	-2.78
	NL1	-4.5	-114.05	349.89	-77.09	3.41
	NL2					
3	ML1	1.83	-55.3	279.96	-55.82	5.63
	ML2	-1.42	-117.58	362.16	-47.05	5.85
	NL1	-0.27	-138.82	347.25	-84.62	0.14
	NL2					
4	ML1	-0.83	-92.32	319.65	-14.22	3.78
	ML2	9.68	-76.49	326.54	-84.32	1.38
	NL1	-7.06	-109.26	346.25	-77.25	3.02
	NL2					
5	ML1	5	-55.12	280.87	-55.12	4.25
	ML2	-3.15	-118.1	366.84	-49.69	-8.44
	NL1	6.83	-135.55	344.25	-83.45	-2.76
	NL2					
6	ML1	-2.38	-90.94	315.93	-16.1	12.97
	ML2	1	-77.27	327.16	-83.97	0.32
	NL1	-5.07	-112.08	351	-75.76	5.36
	NL2					
7	ML1	1.68	-48.28	278	-53.16	4.49
	ML2	-3.46	-115.5	365.78	-47.42	5.64
	NL1	-2.53	-137.25	346.04	-73.81	-2.18
	NL2					
8	ML1	3.91	-89.51	320.23	-24.67	12.88
	ML2	0.33	-75.49	325.92	-85.33	-6.33
	NL1	-6.5	-109.17	347.15	-76.51	0.73
	NL2					

Table D1-3 Longitudinal Strain Signal Values-Lane M&N -100k passes

Run	Gauge	Position 0				
		A	B	C	D	E
1	ML1	7.87	-61.93	190.46	-97.78	5.65
	ML2			391.58		
	NL1	4.32	-183.32	224.62	-70.53	3.27
	NL2					
2	ML1	-1.1	-120.67	190.49	-48.53	0.22
	ML2			392.45		
	NL1	-1.76	-120.42	226.45	-114.87	2.57
	NL2					
3	ML1	7.94	-66.12	186.85	-94.01	2.15
	ML2			382.58		
	NL1	4.68	-181.85	223.44	-65.07	3.44
	NL2					
4	ML1	-2.11	-119.83	205.31	-46.91	1.31
	ML2			358.69		
	NL1	-6.7	-123.72	219.07	-106.19	4.2
	NL2					
5	ML1	0.17	-63.27	185.27	-92.99	3
	ML2			428.33		
	NL1	0.71	-182.08	223.61	-68.48	1.98
	NL2					
6	ML1	5.08	-118.81	193.17	-48.51	10
	ML2			408.71		
	NL1	4.41	-121.78	225.1	-113.02	-0.22
	NL2					
7	ML1	-0.24	-65.8	209.93	-90.74	10.22
	ML2			427.66		
	NL1	1.47	-192.68	223.42	-73.17	4.84
	NL2					
8	ML1	-0.9	-118.89	197.08	-49.69	0.3
	ML2			423.74		
	NL1	-1.28	-120.96	228.79	-116.61	1.86
	NL2					

Table D1-4 Longitudinal Strain Signal Values-Lane O&P -200k passes

Run	Gauge	Position 0				
		A	B	C	D	E
1	ML1	0.07	218.77	-78.3	5.29	5.29
	ML2	-7.96	-142.12	421.89	-70.44	2.78
	NL1	-5.41	-133.4	299.32	-122.87	-27.86
	NL2					
2	ML1	1.11	-101.61	234.54	-21.01	8.07
	ML2	10.93	-101.82	420.33	-113.11	3.47
	NL1	-61.23	-296.49	236.75	-59.25	-5.18
	NL2					
3	ML1	11.29	-39.87	226.68	-74.99	4.55
	ML2	-5.54	-143.39	450.79	-69.68	1.18
	NL1	-1.87	-136.01	300.65	-123.54	-33.36
	NL2					
4	ML1	0.92	218.63	-20.26	-20.26	-7.47
	ML2	8.3	-104.76	434.48	-104.45	-12.57
	NL1	-52.45	-294.92	236.32	-62.47	-2.53
	NL2					
5	ML1	5.64	-38.2	221.16	-78.63	2.45
	ML2	-3.33	-140.7	434.03	-69.88	-5.74
	NL1	-4.7	-132.68	300.6	-121.8	-27.33
	NL2					
6	ML1	2.04	-105.65	214.52	-21.96	5.89
	ML2	-3.05	-103.62	436.46	-103.02	5.78
	NL1	-57.43	-297.58	237.1	-57.27	-2.69
	NL2					
7	ML1	6.36	-38.99	222.18	-81.44	-3.17
	ML2	-6.35	-140.63	428.33	-69.81	-2.38
	NL1	-0.98	-133.52	300.8	-122.85	-24.66
	NL2					
8	ML1	-2.69	-108.33	221.01	-25.87	4.87
	ML2	-8.4	-99.43	414.34	-102.29	5.78
	NL1	-56.35	-297.37	235.86	-62.77	-2.84
	NL2					

Table D1-5 Transversal Strain Signal Values-Lane O&P -0 passes

Run	Gauge	Position 0			Position 6		
		A	B	C	A	B	C
1	OT1						
	OT2	0.22	70.88	-0.13			
	PT1	3.97	90.18	4.5	2.53	95.32	4.11
	PT2	-3.76	155.95	-0.47	3.88	185.43	6.05
2	OT1	Not Working					
	OT2	0.44	66.44	4.39			
	PT1	5.25	76.8	1.41	2.67	78.81	1.2
	PT2	-4.15	153.18	3.99	3.58	184.36	0.94
3	OT1	Not Working					
	OT2	1.14	66.55	-1.16			
	PT1	1.71	90.59	6.44	5.2	94.04	1.29
	PT2	6.36	157.07	3.26	5.15	185.76	2.7
4	OT1						
	OT2	-3.07	68.97	-3.03			
	PT1	4.16	77.16	4.68	3.32	79.25	1.71
	PT2	-4.13	148.55	1.59	1.89	187.56	6.69
5	OT1						
	OT2	-4.22	69.33	-5.34			
	PT1	5.14	88.94	5.48	1.94	92.39	2.07
	PT2	4.51	160.48	10.63	4.33	187.37	11.65
6	OT1						
	OT2	-7.32	67.88	9.18			
	PT1	6.85	77.14	2.31	3.63	77.73	1.01
	PT2	8.9	158.5	-2.02	3.89	171.87	-4.61
7	OT1						
	OT2	-0.68	71.46	4.51			
	PT1	5.08	89.9	2.85	1.53	93.61	0.59
	PT2	-2.13	142.58	2.27	5.76	179.86	9.55
8	OT1						
	OT2	-8.62	70.79	6.42			
	PT1	3.08	78.99	2.5	1.55	77.61	-2.13
	PT2	6.62	147	3.78	7.57	172.54	2.85

Table D1-6 Transversal Strain Signal Values-Lane O&P -5k passes

Run	Gauge	Position 0			Position 6		
		A	B	C	A	B	C
1	OT1	Not Working			Not Working		
	OT2	1.93	43.2	0.45	6.42	42.89	1.76
	PT1	11.65	122.89	4.43	3.71	125.49	2.2
	PT2						
2	OT1	Not Working			Not Working		
	OT2	2.87	44.42	-0.39	4.03	46.66	-0.94
	PT1	4.77	106.48	1.48	5.48	108.55	3.41
	PT2						
3	OT1	Not Working			Not Working		
	OT2	1.48	41.22	0.22	4.52	41.72	0.57
	PT1	4	112.44	1.65	4.41	116.34	3.5
	PT2						
4	OT1	Not Working			Not Working		
	OT2	0.54	42.18	-2.76	1.13	44.15	-0.44
	PT1	4.49	102.24	-4.49	4.15	106.43	-0.86
	PT2						
5	OT1	Not Working			Not Working		
	OT2	2.41	38.78	-2.04	2.3	41.08	-0.68
	PT1	2.78	106.73	-3.36	5.41	112.59	0.62
	PT2						
6	OT1	Not Working			Not Working		
	OT2	0.73	38.06	-5.41	1.48	41.82	-0.63
	PT1	0.18	96.84	-1.48	2.62	96.06	-0.03
	PT2						
7	OT1	Not Working			Not Working		
	OT2	1.02	37.46	-3.88	1.86	37.89	-0.35
	PT1	-0.21	108.43	-4.78	3.71	110.79	-1.34
	PT2						
8	OT1	Not Working			Not Working		
	OT2	-0.82	37.07	-6.84	1.3	40.43	1.08
	PT1	-3.78	96.02	-6.79	1.78	96.93	0.23
	PT2						

Table D1-7 Transversal Strain Signal Values-Lane O&P -10k passes

Run	Gauge	Position 0		
		A	B	C
1	OT1			
	OT2			
	PT1	0	145.03	2.31
	PT2	6.94	65.69	-0.71
2	OT1			
	OT2			
	PT1	-0.45	115.29	-3.1
	PT2	5.85	60.91	-0.22
3	OT1			
	OT2			
	PT1	-0.71	132.36	-4.78
	PT2	7.02	61.6	-0.5
4	OT1			
	OT2			
	PT1	-2.71	107.94	-11.37
	PT2	1.7	57.21	-1.24

D1-8 Transversal Strain Signal Values-Lane O&P -25k passes

Run	Gauge	Position 0			Position 6		
		A	B	C	A	B	C
1	OT1						
	OT2	-5.41	25.48	-7.34	-0.76	183.75	5.62
	PT1	6.11	131.02	-0.06	2.36	361.89	1.19
	PT2	0.89	67.11	0.77	11.34	233.36	11.38
2	OT1						
	OT2	2.11	39.28	-8.48	7.26	205.75	4.19
	PT1	5.25	109.11	-0.13	2.91	316.84	5.89
	PT2	6.45	68.79	-0.33	0.41	248.72	13.8
3	OT1						
	OT2	2.51	18	-10.32	-0.75	189.27	5.85
	PT1	4.58	121.29	-2.11	-3.92	356.25	11.43
	PT2	-0.37	65.41	-2.6	7.78	233.14	9.72
4	OT1						
	OT2	-2.39	39.05	-9.9	3.89	211.54	8.96
	PT1	-1.48	103.46	-11.29	9.49	325.41	8.98
	PT2	5.46	63.53	-7.09	7.19	242.98	5.68
5	OT1						
	OT2	-4.65	16.09	-9.76	4.36	189.67	7.82
	PT1				-2.2	354.8	10.48
	PT2	7.06	62.15	-3.91	13.21	235.71	11.78
6	OT1						
	OT2						
	PT1				8.87	314.56	10.71
	PT2						

Table D1-9 Transversal Strain Signal Values-Lane O&P -100K passes

Run	Gauge	Position 0			Position 6		
		A	B	C	A	B	C
1	OT1	Not Working			Not Working		
	OT2				6.96	171.55	5.57
	PT1	1.66	119.3	-13.42	11.33	552.94	12.33
	PT2				-2	197.53	3.78
2	OT1						
	OT2				5.55	186.8	6.98
	PT1	1.64	99.33	-7.13	2.31	521.76	17.14
	PT2				1.24	207.94	2.8
3	OT1						
	OT2				7	168.15	9.04
	PT1	7.12	122.89	-5.73	7.27	569.3	7.58
	PT2				1.91	198.78	3.52
4	OT1						
	OT2				8.57	188.2	12.68
	PT1	1.01	100.67	-7.89	5.08	526.05	3.45
	PT2				0.66	208.7	1.49
5	OT1						
	OT2				11.45	174.69	11.25
	PT1	5.17	116.4	-3.59	-2.1	572.13	14.26
	PT2				-4.24	198.72	3.92
6	OT1						
	OT2				7.91	191.92	7.89
	PT1	0.96	98.28	-11.15	3.78	522.89	14.55
	PT2				2.78	207.99	-2.21
7	OT1						
	OT2						
	PT1	5.42	115.63	-14.82			
	PT2						

Table D1-10 Transversal Strain Signal Values-Lane O&P -200K passes

Run	Gauge	Position 6		
		A	B	C
1	OT1			
	OT2	10.21	200.1	-3.38
	PT1	9.5	668.39	-8.65
	PT2	-7.69	263.68	3.48
2	OT1			
	OT2	-2.41	297.94	4.16
	PT1	5.21	694.33	-4.65
	PT2	4.15	252.61	-1.28
3	OT1			
	OT2	11.22	210.71	5.41
	PT1	12.12	664.4	12.38
	PT2	2.75	262.56	2.83
4	OT1			
	OT2	11.78	280.45	5.67
	PT1	1.04	689.66	10.95
	PT2	3.98	250.04	-1.5
5	OT1			
	OT2	12.3	226.34	9.12
	PT1	1.25	655.81	15.1
	PT2	2.44	261.12	11.78
6	OT1			
	OT2	1.36	304.11	11.33
	PT1	7.19	692.3	12.67
	PT2	2.09	249.44	-1.14
7	OT1			
	OT2			
	PT1	5.96	658.17	12.73
	PT2			

Table D1-11 Longitudinal Strain Signal Values-Lane O&P -0 passes

Run	Gauge	Position 0					Position 6				
		A	B	C	D	E	A	B	C	D	E
1	OL1	Not Working					Not Working				
	OL2	-4.25	-63.8	237.65	-35.2	2	-4	-69.34	249.14	-40.19	-1.99
	PL1	0.1	-85.29	299.28	-42.37	2.19	6.22	-94.5	314.74	-56.73	2.71
	PL2	0.25	-73.55	236.24	-63.3	0.55	0.16	-75.44	242.11	-73.75	-4.87
2	OL1	Not Working					Not Working				
	OL2	-3.44	-69.83	225.48	-29.48	2.21	-1.78	-75.61	224.41	-34.03	0.8
	PL1	-3	-73.28	255.8	-47.17	2.41	-2.74	-86.38	270.14	-63.67	3.95
	PL2	-3.46	-90.97	241.31	-49.75	-3.27	-1.61	-92.16	246.63	-64.24	-1.46
3	OL1	Not Working					Not Working				
	OL2	2.25	-64.26	239.14	-33.23	0.85	-3.61	-68.86	246.35	-41.65	-1.02
	PL1	-2.34	-87.26	291.26	-48.96	1.68	-0.8	-97.56	313.33	-57.89	2.29
	PL2	-4.16	-74.51	233.27	-61.57	-3.18	-3.64	-79.21	240.89	-67	-3.55
4	OL1	Not Working					Not Working				
	OL2	1.68	-69.84	220.84	-26.93	1.97	-2.41	-74.51	225.13	-33.86	0.98
	PL1	0.47	-72.51	259.17	-43.34	2.51	2.6	-84.01	274.23	-59.8	-0.22
	PL2	-0.96	-92.25	244.17	-53.7	0.23	-4.6	-95.15	244.85	-56.58	-2.87
5	OL1	Not Working					Not Working				
	OL2	-1.36	-64.28	242.39	-34	2.02	-3.96	-69.86	249.21	-48.12	-0.85
	PL1	0.44	-81.69	297.86	-42.79	0.59	-1.78	-98.92	314.1	-59.81	4.06
	PL2	-2.88	-78.48	239.34	-61.29	-2.63	-4.26	-78.66	236.83	-67.95	0.3
6	OL1	Not Working					Not Working				
	OL2	-3.06	-66.88	223.53	-29.85	1.4	-4.23	-74.86	226.94	-35.74	1.3
	PL1	0.48	-73.07	257.13	44.29	2.52	1.61	-86.3	269.18	-61.75	1.84
	PL2	-2.24	-92.42	238.63	-47.65	-0.26	-0.01	-94.93	244.26	-55.68	-0.18
7	OL1	Not Working					Not Working				
	OL2	-2.87	-63.69	245.11	-34.16	1.13	-2.66	-69	248.47	-39.56	-1.32
	PL1	-3.39	-83.24	301.08	44.58	1.78	0.65	-95.46	316.66	-59.58	4
	PL2	-3.12	-72.53	234.68	-60.63	2.37	-2.45	-76.49	237.76	-68.03	2.67
8	OL1	Not Working					Not Working				
	OL2	-2.65	-70.68	223.9	-26.59	0.47	0.5	-73.74	227.1	-33.75	-0.54
	PL1	8.63	-70.95	259.16	-39.53	0.45	-1.49	-85.93	272.54	-60.4	1.9
	PL2	-0.57	-89.02	242.6	-51.35	-0.31	-0.33	-93.73	248.6	-55.97	0.84

Table D1-12 Longitudinal Strain Signal Values-Lane O&P -5k passes

Run	Gauge	Position 0					Position 6				
		A	B	C	D	E	A	B	C	D	E
1	OL1	Not Working					Not Working				
	OL2	-0.52	-78.63	299.28	-46.78	-7.43	1.21	-74.27	304.58	-39.45	4.34
	PL1	0.61	-125.75	369.5	-83.6	0.23	-1.67	-133.99	378.04	-94.03	-1.02
	PL2	3.3	-86.64	277.86	-71.79	-3.45	-2.19	-85.96	281.81	-74.67	0.41
2	OL1	Not Working					Not Working				
	OL2	1.52	-86.31	267.59	-38.9	-6.45	-0.13	-83.63	273.76	-33.47	7.41
	PL1	-2.1	-120.26	311.65	-79.49	-1.2	-3.7	-125.68	327.55	-89.69	-7.17
	PL2	0.46	-103.59	292.62	-63.88	-1.3	0.18	-109.78	287.45	-62.62	6.08
3	OL1	Not Working					Not Working				
	OL2	-1.77	-78.49	302.67	-45.96	-9.1	4.58	-71.9	309.43	-43.95	2.55
	PL1	-8.35	-123.67	369.74	-87.36	0.34	-2.78	-134.63	369.89	-93.85	-5.21
	PL2	-2.41	-84.22	289.53	-73.05	-2.14	-4.39	-85.49	278.36	-73.88	4.16
4	OL1	Not Working					Not Working				
	OL2	0.66	-86.17	270.65	-46.25	-7.8	-2.08	-83.61	280.08	-33.61	6.18
	PL1	-1.74	-119.37	319.51	-80.69	-2.12	-1.49	-127.11	327.87	-85.89	-8.38
	PL2	-3.98	-105.25	286.25	-60.6	-1.18	-1.56	-107.93	293.57	-62.84	0.52
5	OL1	Not Working					Not Working				
	OL2	1.79	-75.77	300.9	-46.32	-8.66	3.15	-71.13	304.23	-44.48	2.58
	PL1	-5.32	-128.02	373.44	-85.27	-0.64	0.61	-134.69	374.94	-93.43	-7.54
	PL2	1.13	-83.62	280.94	-71.32	2.74	-1.63	-84.13	290.87	-75.12	2.94
6	OL1	Not Working					Not Working				
	OL2	1.19	-84.1	263.4	-34.81	-8.35	3.44	-84.69	271.32	-33.86	3.59
	PL1	-6.19	-121.08	318.51	-83.23	0.55	-0.57	-128.64	333.89	-89.96	-5.68
	PL2	-3.13	-106.85	290.95	-61.46	4.6	0.16	-110.15	295.25	-59.9	3.45
7	OL1	Not Working					Not Working				
	OL2	1.15	-74.4	297.79	-44.78	-6.62	6.45	-71.71	306.15	-42.56	5.66
	PL1	-1.48	-128.03	372.47	-89.06	0.46	-1.87	-134.06	372.46	-97.06	-6.49
	PL2	-3.86	-84.09	283.21	-71.84	-1.3	-0.82	-87.64	285.74	-74.47	-8.6
8	OL1	Not Working					Not Working				
	OL2	0.74	-87.53	264.4	-46.15	-4.6	-3.63	-83.56	276.32	-34.41	4.33
	PL1	-7.28	-118.8	322.97	-80.43	0.26	-3.09	-131.26	332.96	-89.22	-9.21
	PL2	0.64	-104.68	291.17	-61.76	-1.8	-4.89	-109.91	289.52	-62.44	0.55

Table D1-13 Longitudinal Strain Signal Values-Lane O&P -10k passes

Run	Gauge	Position 0				
		A	B	C	D	E
1	OL1	Not Working				
	OL2	-4.41	-81.91	340.55	-48.74	-4.02
	PL1	0.53	-117.84	480.53	-71.34	-7.2
	PL2	-1.8	-81.41	324.72	-72.74	2.9
2	OL1	Not Working				
	OL2	-6.2	-90.24	296.47	-37.59	-0.52
	PL1	-6.78	-98.99	420.23	-80.34	-7.1
	PL2	-196	-105.39	330.64	-58.14	-0.18
3	OL1	Not Working				
	OL2	-3.72	-82.29	340.29	-47.25	3.29
	PL1	-3.04	-126.35	472.42	-74.36	-2.3
	PL2	-2.09	-85.04	323.83	-71	2.9
4	OL1	Not Working				
	OL2	-4.6	-92.84	307.24	-37.39	-2.52
	PL1	-5.1	-118.29	429.73	-75.79	-2.35
	PL2	-5.59	-105.98	335.02	-59.44	-1.77

Table D1-14 Longitudinal Strain Signal Values-Lane O&P -25k passes

Run	Gauge	Position 0					Position 6				
		A	B	C	D	E	A	B	C	D	E
1	OL1	Not Working					Not Working				
	OL2	-5.25	-106.43	398.53	-67.29	-1.43	3.23	-105.74	432.14	-62.41	1.05
	PL1	-9.27	-179.18	405.78	-149.45	-11.25	-3.95	-140.33	526.38	-156.6	1.01
	PL2	-7.13	-110.64	369.99	-99.43	-3.64	-4.2	-103.48	422.85	-72.78	4.58
2	OL1	Not Working					Not Working				
	OL2	-6.82	-116.29	366.47	-61.82	-2.75	-0.3	-119.99	401.87	-55.39	4.75
	PL1	-3.71	-196.47	435	-119.89	-12.5	-2.07	-279.06	467.52	-93.29	-1.88
	PL2	-11.99	-132.61	380.74	-87.29	-2.31	0.19	-103.68	421.65	-79.27	7.17
3	OL1	Not Working					Not Working				
	OL2	-2.89	-108.35	397.35	-66.4	-7.96	-0.77	-102.86	428.06	-61.73	1.93
	PL1	-7.11	-183.26	437	-153.05	-15.24	-2.95	-139.66	527.65	-156.55	4.26
	PL2	-6.9	-115.25	369.45	-102.39	-8.97	-2.33	-104.81	418.55	-79.41	3.25
4	OL1	Not Working					Not Working				
	OL2	-7.11	-117.51	369.11	-60.31	0.67	-1.85	-118.6	400.1	-68.26	-5.91
	PL1	-5.42	-251	441.36	-122.12	-24.7	-3.3	-279.67	468.42	-89.75	6.3
	PL2	-12.1	-134.36	375.3	-88.44	-2.36	1.58	-109.04	421.01	-83.34	5.05
5	OL1	Not Working					Not Working				
	OL2	-5.42	-109.73	402.8	-71.23	-6.99	-2.91	-110.29	431.23	-60.48	-0.37
	PL1	-6.29	-176.3	500.58	-153.48	-20.38	0.27	-136.94	529.02	-156.75	-5.36
	PL2	-7.84	-115.11	364.43	-103.66	-10.53	5.8	-107.58	417.99	-80.61	0.26
6	OL1	Not Working					Not Working				
	OL2						-2.02	-118.56	401.54	-53.62	2.14
	PL1	-7.08	-257.78	448.58	-125.21	-25.5	-8.47	-277.48	471.46	-91.57	-1.85
	PL2						-2.85	-108.14	429.09	-83.3	6.43
7	OL1	Not Working					Not Working				
	OL2							-102.87	425.32	-55.78	3.54
	PL1										
	PL2							-107.89	419.95	-79.79	3.35

Table D1-15. Longitudinal Strain Signal Values-Lane O&P -100K passes

Run	Gauge	Position 0					Position 6				
		A	B	C	D	E	A	B	C	D	E
1	OL1	Not Working					Not Working				
	OL2	-2.39	-164.72	382.38	-46.28	-1.22	-0.75	-178.12	388.14	-52.24	3.47
	PL1	Not Working					-5.33	-159.6	143.32	-53.28	-0.55
	PL2	-0.62	-147.36	298.51	-55.07	-0.2	-2.3				
2	OL1	Not Working					Not Working				
	OL2	-0.83	-103.26	380.91	-84.04	0.75	-0.3	-101.41	389.58	-77.21	-5.36
	PL1	Not Working					-6.07	-142.88	165.94	-48.54	-0.62
	PL2	-5.57	-94.61	335.15	-77.58	-0.02	-0.13	-89.05	359.11	-117.48	5.33
3	OL1	Not Working					Not Working				
	OL2	-4.51	-163.71	393.27	-48.39	-4.44	-0.77	-177.89	387.33	-49.71	2.43
	PL1	Not Working					-0.96	-160.38	144.32	-52.88	0.71
	PL2	-2.83	-146.77	308.47	-62.7	2.81	-0.96	-207.66	325.12	-50.14	4.05
4	OL1	Not Working					Not Working				
	OL2	-2.54	-98.96	379.31	-79.32	3.19	-1.85	-99.15	384.3	-77.89	7.61
	PL1	Not Working					-2.11	-140.39	169.13	-45.96	0.93
	PL2	-4.68	-93.55	331.36	-77.91	3.81	-2.07	-80.37	363.91	-118.11	-0.17
5	OL1	Not Working					Not Working				
	OL2	-4.77	-164.19	392.25	-51.72	-1.93	0.36	-177.7	389.94	-63.87	5.38
	PL1	Not Working					-3.55	-157.96	145.73	-52.31	1.53
	PL2	-5.23	-148.01	307.39	-55.9	2.35	-1.91	-206.86	328.34	-51.31	4.07
6	OL1	Not Working					Not Working				
	OL2	-9.23	-96.67	382.03	-81.12	3.61	0.55	-96.76	388.53	-79.26	9.1
	PL1	Not Working					-1.62	-139.62	163.06	-47.12	-1.14
	PL2	-2.5	-94.75	336.26	-78.61	1.33	-4.09	-79.26	359.33	-115.62	4.96
7	OL1	Not Working					Not Working				
	OL2							-176.29	388.54	-48.65	5.94
	PL1										
	PL2							-207.64	326.13	-51.78	2.54
8	OL1	Not Working					Not Working				
	OL2							-100.97	382.85	-80.366	6.42
	PL1										
	PL2							-89.74	352.13	-120.92	1.56

Table D1-16 Longitudinal Strain Signal Values-Lane O&P -200K passes

Run	Gauge	Position 0					Position 6				
		A	B	C	D	E	A	B	C	D	E
1	OL1	Not Working					Not Working				
	OL2	0.09	-207.55	585.65	-101.32	6.74	1.61	-259.8	598.58	-71.99	-1.38
	PL1	-1.55	-147	361.6	-65.1	9.8	0.01	-136.19	361.36	-80.06	1.25
	PL2	-3.01	-162.58	382.78	-55.89	4.36	-5.45	-264.21	432.35	-42.45	14.54
2	OL1	Not Working					Not Working				
	OL2	-0.75	-197.2	483.39	-146.52	-1.95	3.84	-180.36	541.69	-79.63	9.62
	PL1	3.59	-110.6	387.75	-43.89	-10.24	-0.59	-173.51	424.55	-40.48	-3.17
	PL2	-3.74	-136.45	339.68	-110.34	3.64	6.55	-67.7	433	-142.57	2.78
3	OL1	Not Working					Not Working				
	OL2	1.73	-206.73	570.86	-98.3	5.83	0.98	-246.22	595.82	-78.78	3.78
	PL1	-0.36	-116.1	373.97	-36.81	15.45	-3.16	-135.41	363.22	-99.74	1.14
	PL2	-0.99	-151.8	377.19	-59.87	6.75	0.45	-264.31	436.57	-44.97	4.12
4	OL1	Not Working					Not Working				
	OL2	-6.02	-152.25	524.33	-102.17	0.25	-3.12	-182.2	544.57	-82.34	6.14
	PL1	5.85	-109.52	389.75	-38.04	-4.75	-0.11	-169.79	425.72	-23.44	-2.48
	PL2	3.27	-80.68	389.05	-75.94	-10.13	0.75	-80.9	428.65	-144.03	4.89
5	OL1	Not Working					Not Working				
	OL2	0.68	-197.45	584.98	-91.28	12.46	-3.85	-243.41	591.95	-69.71	5.93
	PL1	-2.9	-115.66	376.53	-36.92	25.71	-1.13	-132.33	362.38	-78.55	6.14
	PL2	-5.45	-150.82	380.82	-53.62	8.76	-4.81	-262.21	430.78	-43.59	3.78
6	OL1	Not Working					Not Working				
	OL2	2.4	-151.16	519.46	-95.66	-5.45	-4.83	-176.71	546.39	-97.1	2.18
	PL1	0.78	-103.56	393.35	-35.44	-4.75	-3.4	-169.45	423.57	-36.3	-2.85
	PL2	-2.9	-79.19	393.89	-62.38	15.86	3.89	-65.21	434.7	-142.33	3.78
7	OL1	Not Working									
	OL2	-0.99	-204.95	583.46	-87.59	-0.28					
	PL1	-1.62	-117.85	374	-36.84	8.43					
	PL2	-2.71	-152.99	383.02	-53.33	9.14					
8	OL1	Not Working									
	OL2	-1.26	-147.89	535.9	-96.54	7.85					
	PL1	0									
	PL2	-2.78	-76.79	396.88	-57.56	13.12					

Table D1-17 Longitudinal Strain Signal Values-Lane O&P -300K passes

Run	Gauge	Position 0					Position 6				
		A	B	C	D	E	A	B	C	D	E
1	OL1	Not Working					Not Working				
	OL2	-3.71	-64.55	464.94	-42.75	9.26	-6.98	-97.81	320.68	-52.02	6.87
	PL2	-3.75	-247.68	368.23	-29	-3.47	-0.88	-318.87	315.88	-5.36	-2.42
2	OL2	-2.16	-33.46	523.61	-38.88	11.25	-4.94	-41.64	319.78	-34.51	8.14
	PL1						2.36	-147.04	258.48	-12.35	1.77
	PL2	-1.53	-72.8	437.28	-72.8	15.42	-1.37	-45.35	363.98	-124.98	17.63
3	OL2	-0.55	-115.97	464.99	-37.63	9.1	-2.17	-93.44	325.33	-42.5	-4.36
	PL1						3.32	-29.52	253.56	-20.57	20.88
	PL2	1.25	-228.08	381.13	-26.26	0.11	-1.37	-318.65	317.12	-21.09	1.25
4	OL2	1.57	-40.48	495.07	-39.15	12.13	-2.07	-40.57	317.12	-30.99	-2.52
	PL1						3.85	-146.02	258.52	-12.77	-3.23
	PL2	-3.75	-61.17	404.54	-69.51	19.64	-1.38	-43.43	370.04	-122.77	18.25
5	OL2	-1.33	-88.1	515.78	-36.54	-8.48	-2.16	-98.1	326.15	74.3	-2.78
	PL1						-1.21	-28.7	256.13	-20.58	21.79
	PL2	-0.52	-220.42	395.69	-29.02	-5.88	-0.55	-314.25	309.34	-23.49	3.48
6	OL2	-2.09	-38.41	489.83	-12.26	9.68	-4.56	-41.23	319.7	-39.76	5.37
	PL1						3.74	-147.32	255.47	-10.98	1.53
	PL2	0.07	-58.61	408.89	-68.58	16.9	2.1	-44.32	369.74	-122.69	8.53

Table D1-18 Transversal Strain Signal Values-Lane M&N -10k passes

Run	Gauge	Position 0		
		A	B	C
1	MT1	3.39	51	6.12
	NT2	2.02	204.74	-0.4
2	MT1	3.88	88.75	7.78
	NT2	2.49	193.09	7.79
3	NT2	1.17	210.18	8.11
4	MT1	3.01	90.55	6.78
	NT2	6.78	191.61	7.62
5	MT1	3.97	54.26	4.37
	NT2	10.72	218.06	4.98
6	MT1	2.07	90.13	10.01
	NT2	5.26	190.81	10.29
7	MT1	4.57	56.41	5.86
	NT2	8.29	210.81	8.45
8	MT1	2.78	87.71	8.3
	NT2	9.85	193.34	12.38

Table D1-19 Transversal Strain Signal Values-Lane M&N -25k passes

Run	Gauge	Position 0		
		A	B	C
1	MT1	2.83	152.05	3.74
	NT1	1.66	188.39	6.85
	NT2	1.35	71.91	0.82
2	MT1	-1.22	184.81	10.44
	NT1	6.45	204.56	12.44
	NT2	3.14	81.94	3.76
3	MT1	-1.89	159.92	6.82
	NT1	10.89	174.83	11.78
	NT2	9.76	74.99	1.29
4	MT1	8.81	197.39	14.23
	NT1	7.48	203.86	14.58
	NT2	6.04	94.76	7.12
5	MT1	6.78	179.56	14.56
	NT1	7.92	172.25	6.78
	NT2	8.71	79.15	2.36
6	MT1	7.88	202.69	12.38
	NT1	11.91	207.48	17.05
	NT2	7.01	102.83	8.12
7	MT1	1.44	179.15	8.99
	NT1	8.41	211.56	15.25
	NT2	10.78	76.82	3.86
8	MT1	10.69	199	5.64
	NT1	12.58	176.85	5.53
	NT2	4.96	101.5	4.78

Table D1-20 Transversal Strain Signal Values-Lane M&N -100k passes

Run	Gauge	Position 0		
		A	B	C
1	NT1	6.2	77.73	8.53
	NT2	-4.03	188.36	-3.48
2	NT1	3.49	73.18	11.99
	NT2	-6.93	162.86	2.17
3	NT1	8.32	74.45	9.16
	NT2	-3.66	193.11	-2.78
4	NT1	7.57	75.14	9.72
	NT2	-5.01	160.4	4.27
5	NT1	2.87	74.15	10.29
	NT2	-4.28	192.3	-2.47
6	NT1	3.21	71.76	5.79
	NT2	1.4	160.27	2.52
7	NT1	4.15	74.51	9.26
	NT2	-4.04	190.54	-5.79
8	NT1	3.66	73.11	3.38
	NT2	-5.95	162.6	3.1

Table D1-21 Transversal Strain Signal Values-Lane O&P -200k passes

Run	Gauge	Position 0		
		A	B	C
1	NT2	-2.91	296.17	-15.3
3	NT2	1.75	297.13	-14.95
4	NT2	-24.99	288.41	5.51
5	NT2	3.39	302.44	-14.65
6	NT2	-23.19	288.9	3.45
7	NT2	-6.24	297.87	-14.01
8	NT2	-25.21	291.93	4.03

**Longitudinal and Transverse Strain - 0 passes
Position 0**

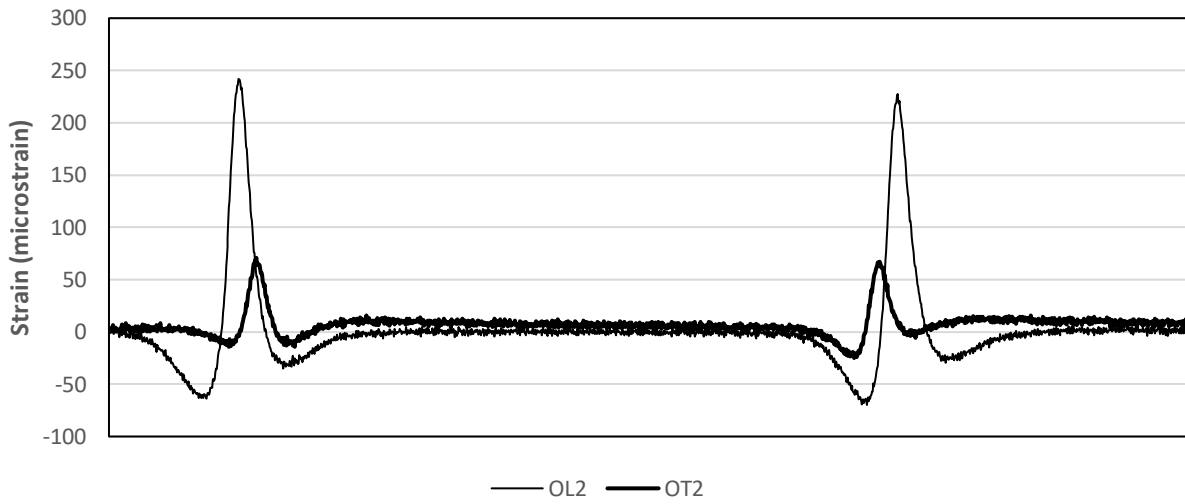


Figure D2-1 Strain Signals Recorded by OL2 and OT2 - 0 Passes

**Longitudinal and Transverse Strain - 0 passes
Position 0**

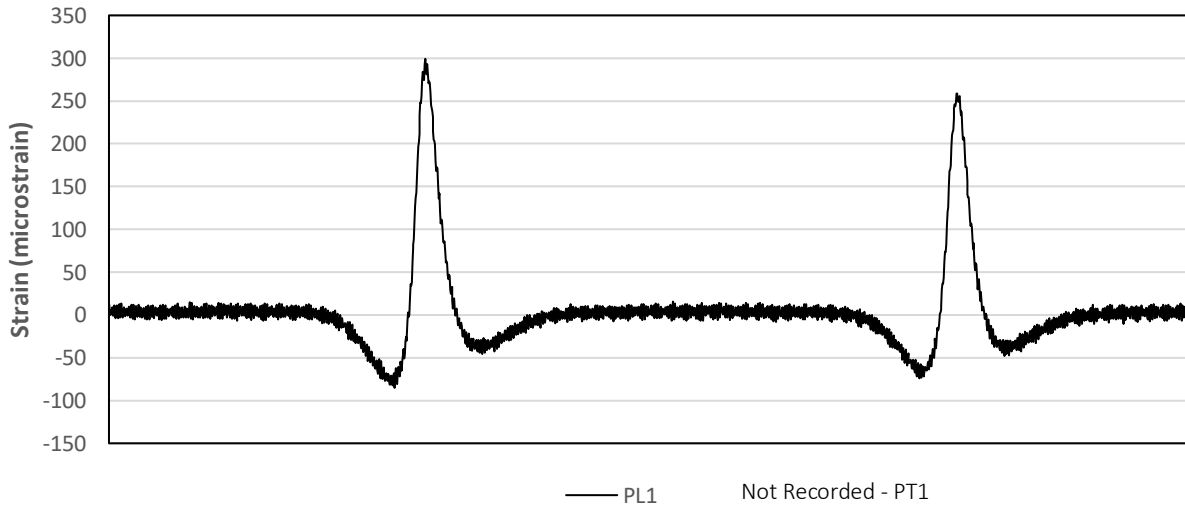


Figure D2-2 Strain Signals Recorded by PL1 - 0 Passes

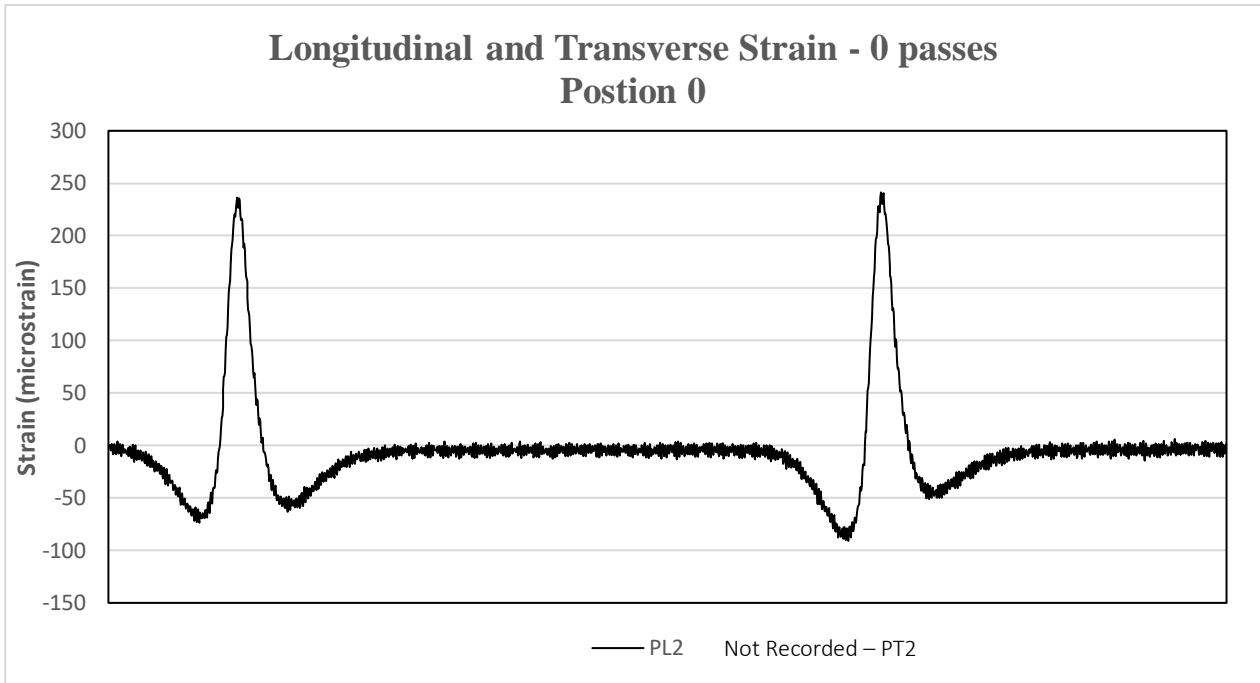


Figure D2-3 Strain Signals Recorded by PL2 – 0 Passes

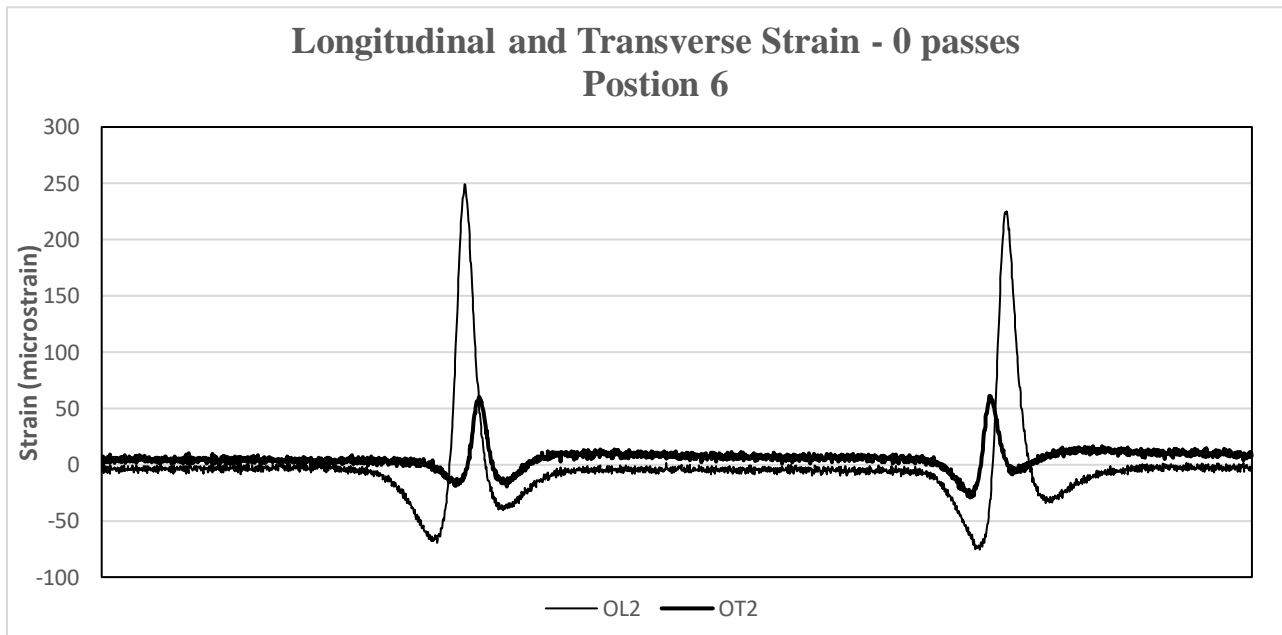


Figure D2-4 Strain Signals Recorded by OL2 and OT2 – 0 Passes

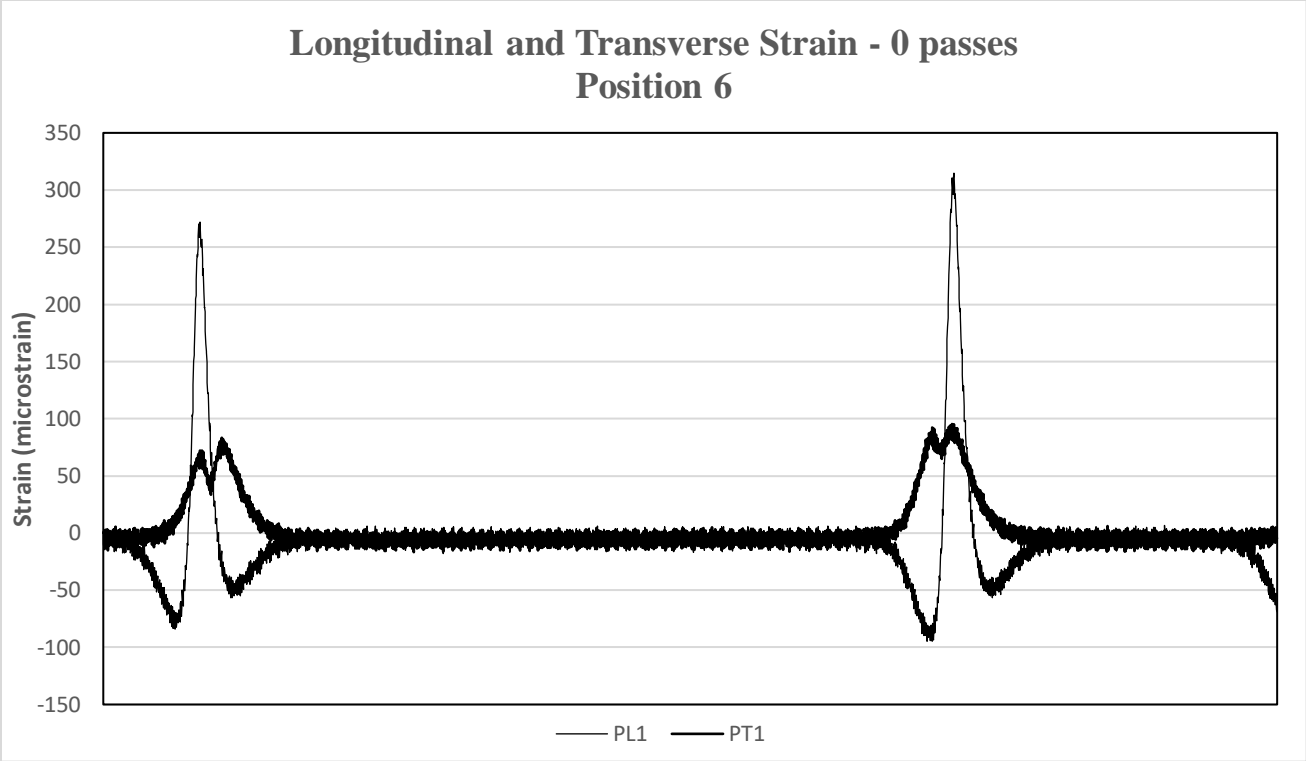


Figure D2-5 Strain Signals Recorded by PL1 and PT1 – 0 Passes

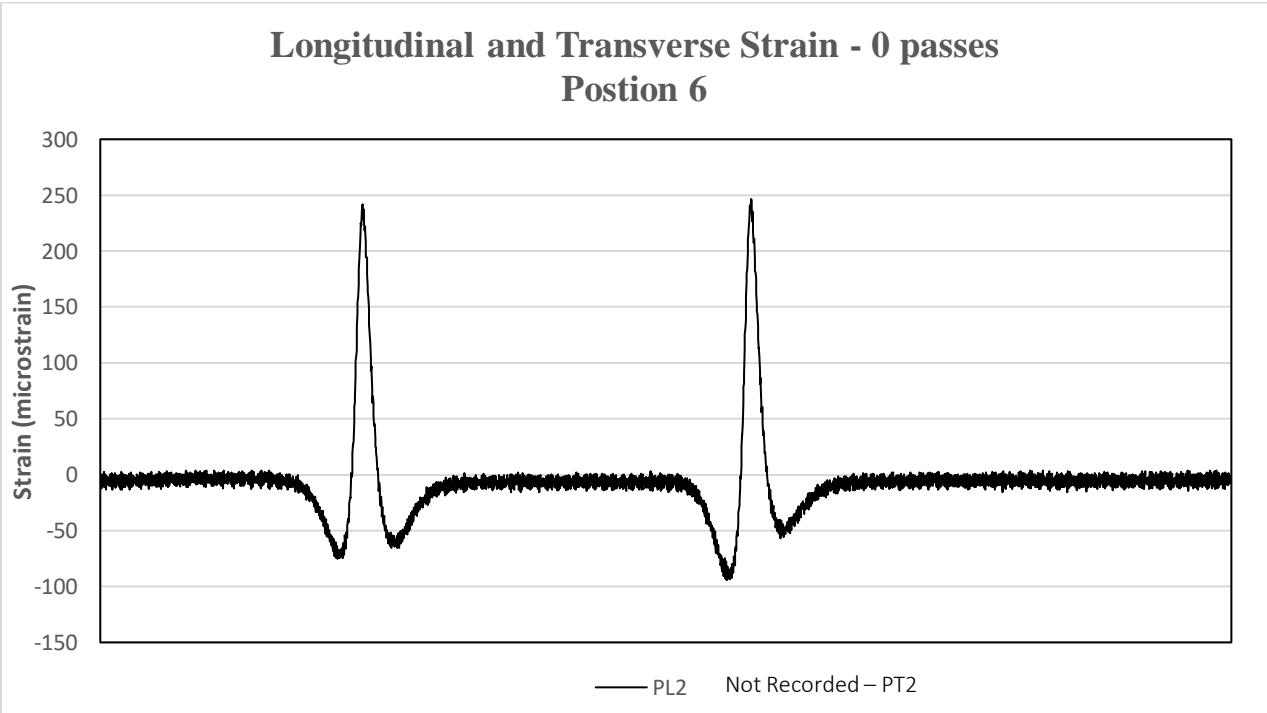


Figure D2-6 Strain Signals Recorded by PL2 – 0 Passes

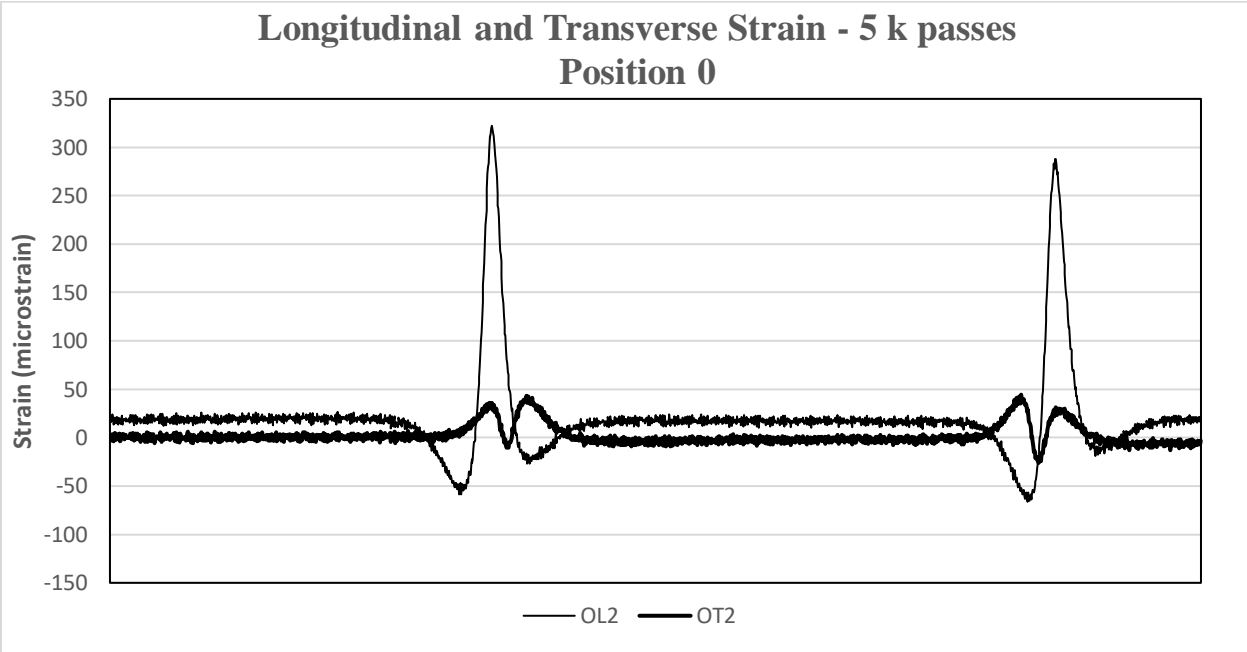


Figure D2-7 Strain Signals Recorded by OL2 OT2 - 5,000 Passes

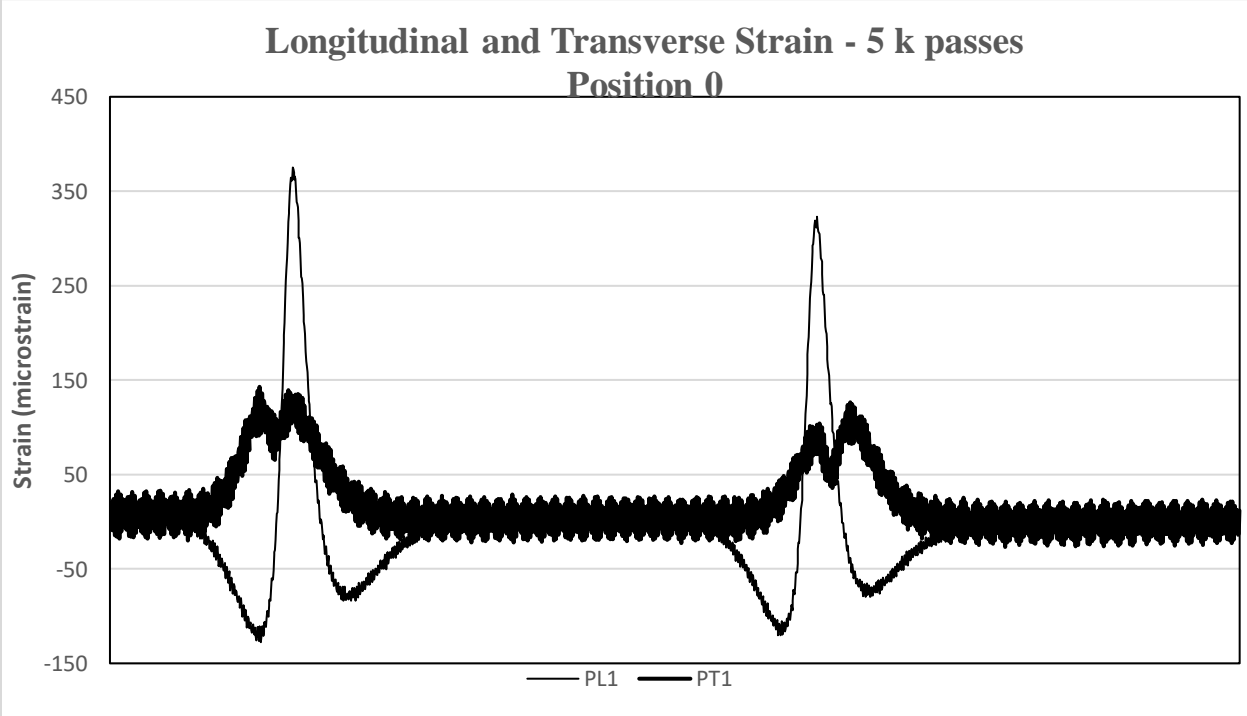


Figure D2-8 Strain Signals Recorded by PL1 and PT1 – 5,000 Passes

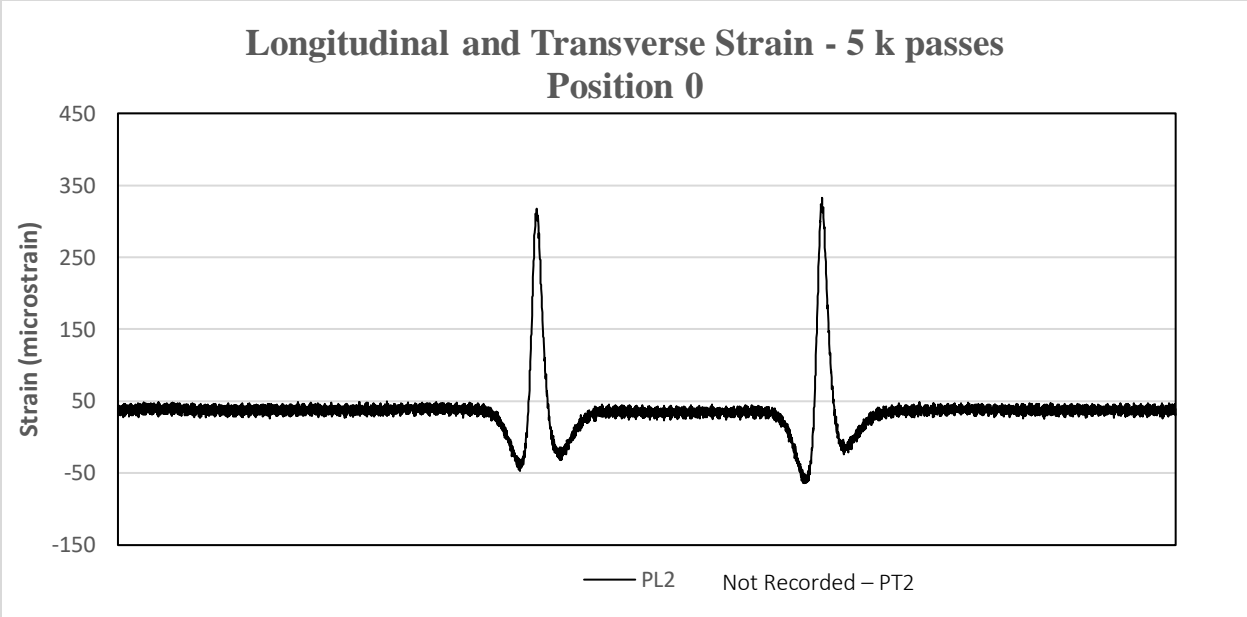


Figure D2-9 Strain Signals Recorded by PL2 – 5,000 Passes

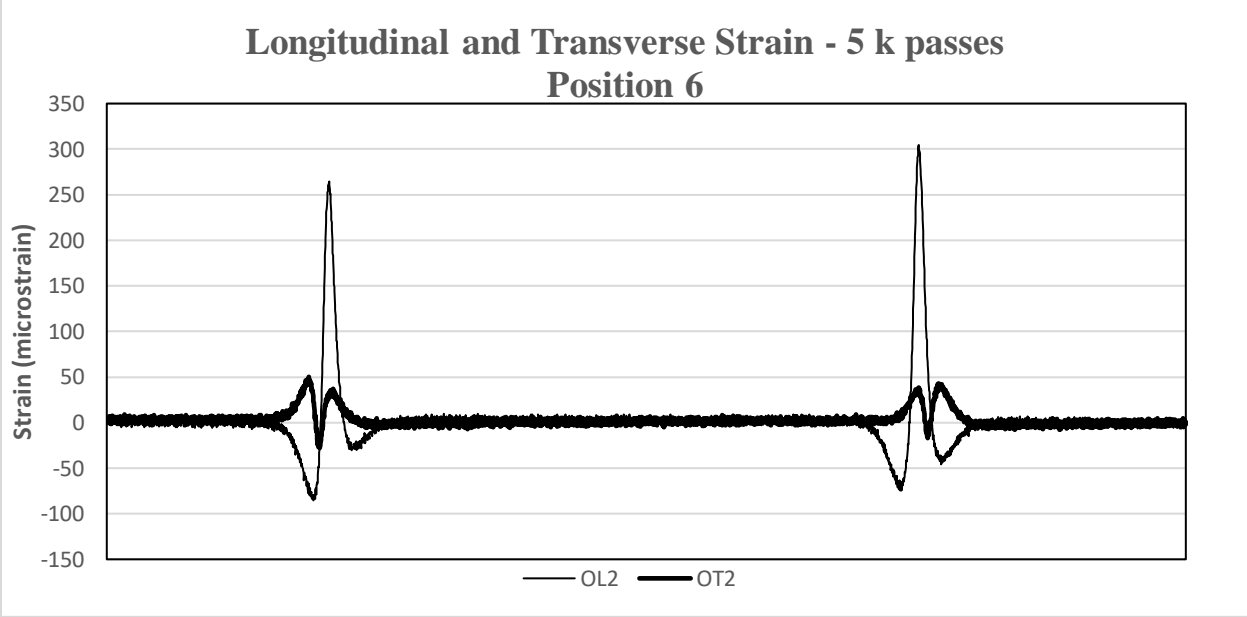


Figure D2-10 Strain Signals Recorded by OL2 and OT2 – 5,000 Passes

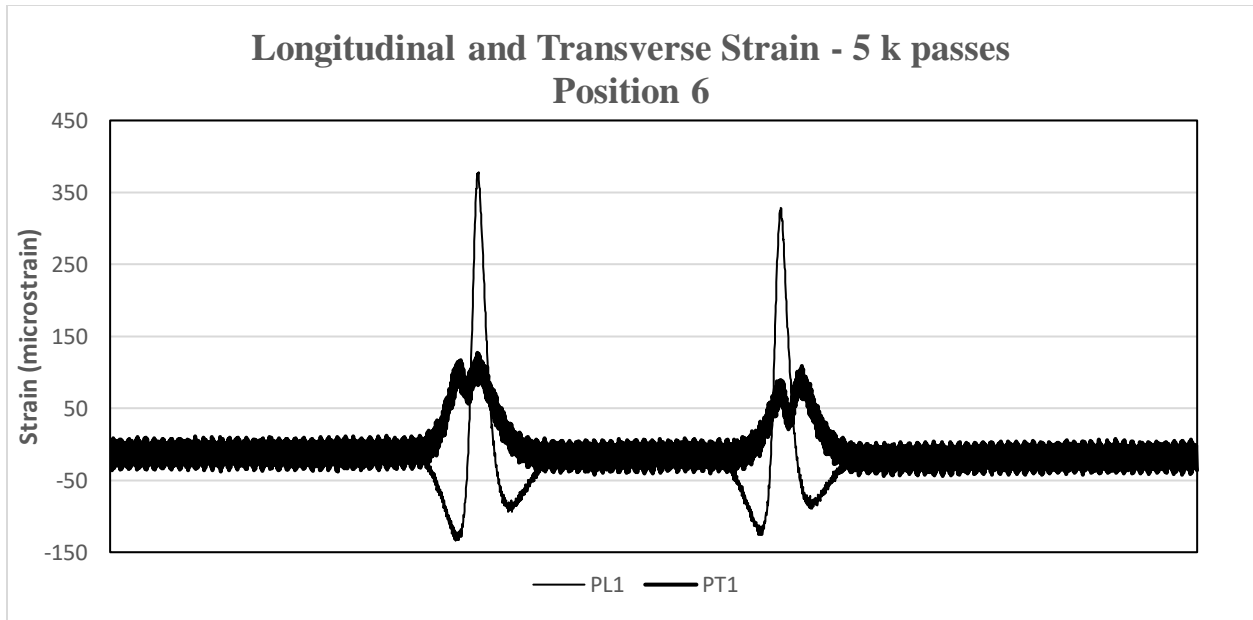


Figure D2-11 Strain Signals Recorded by PL1 and PT2 – 5,000 Passes

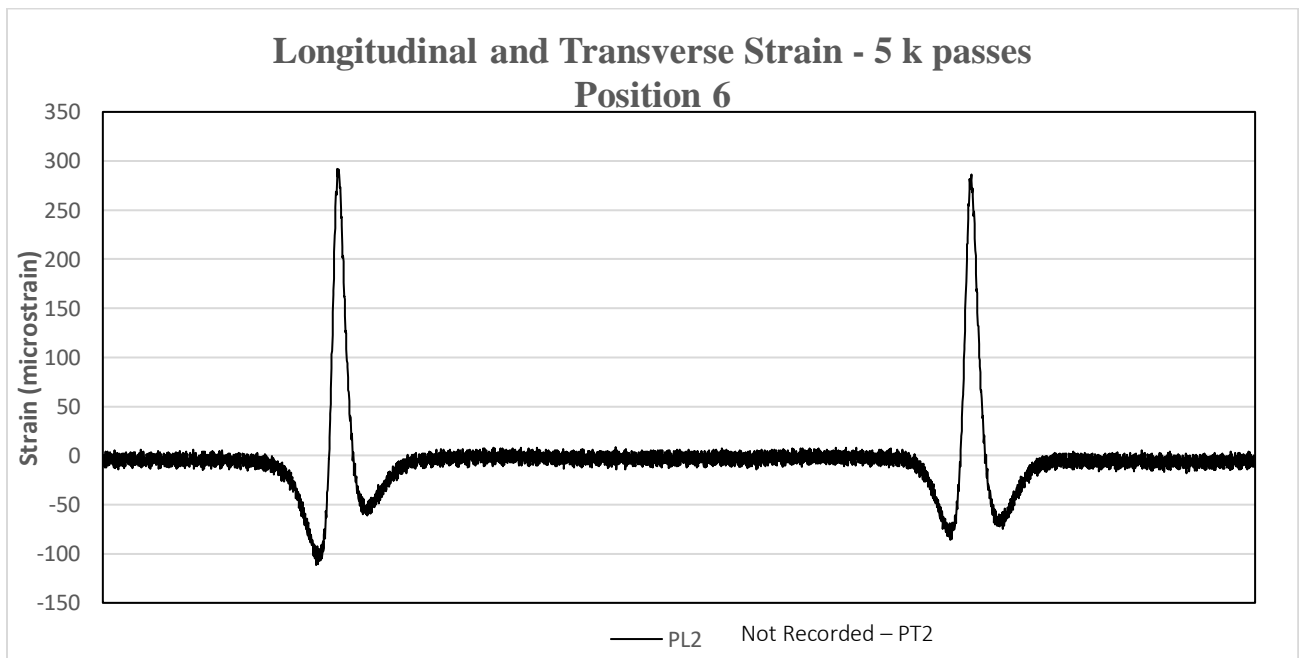


Figure D2-12 Strain Signals Recorded by PL2 – 5,000 Passes

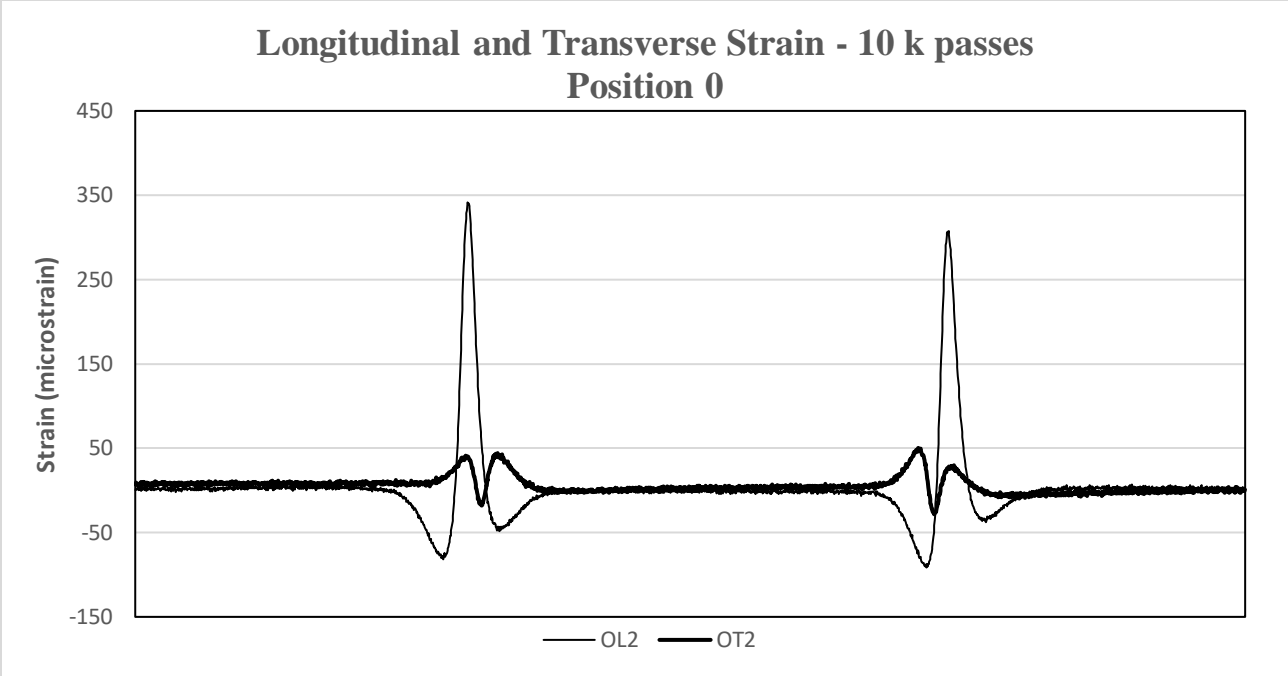


Figure D2-12 Strain Signals Recorded by OL2 and OT2 – 10,000 Passes

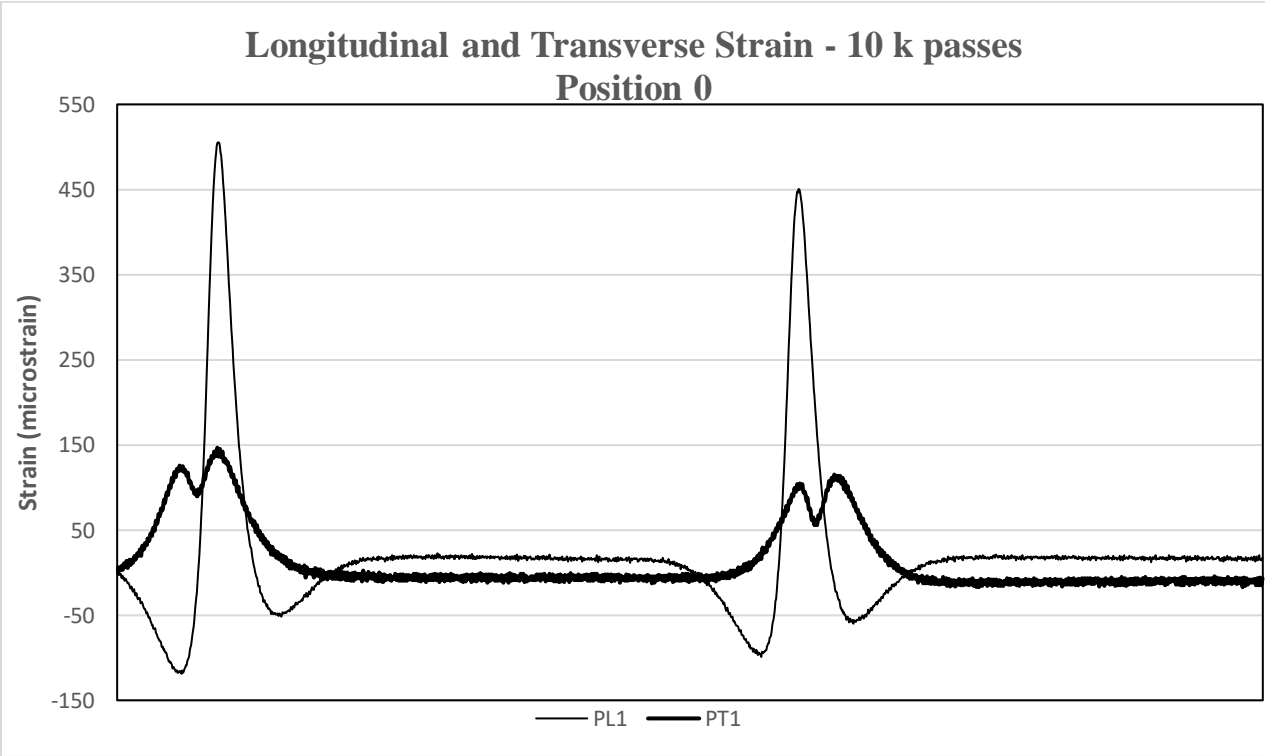


Figure D2-13 Strain Signals Recorded by PL1 and PT1 – 10,000 Passes

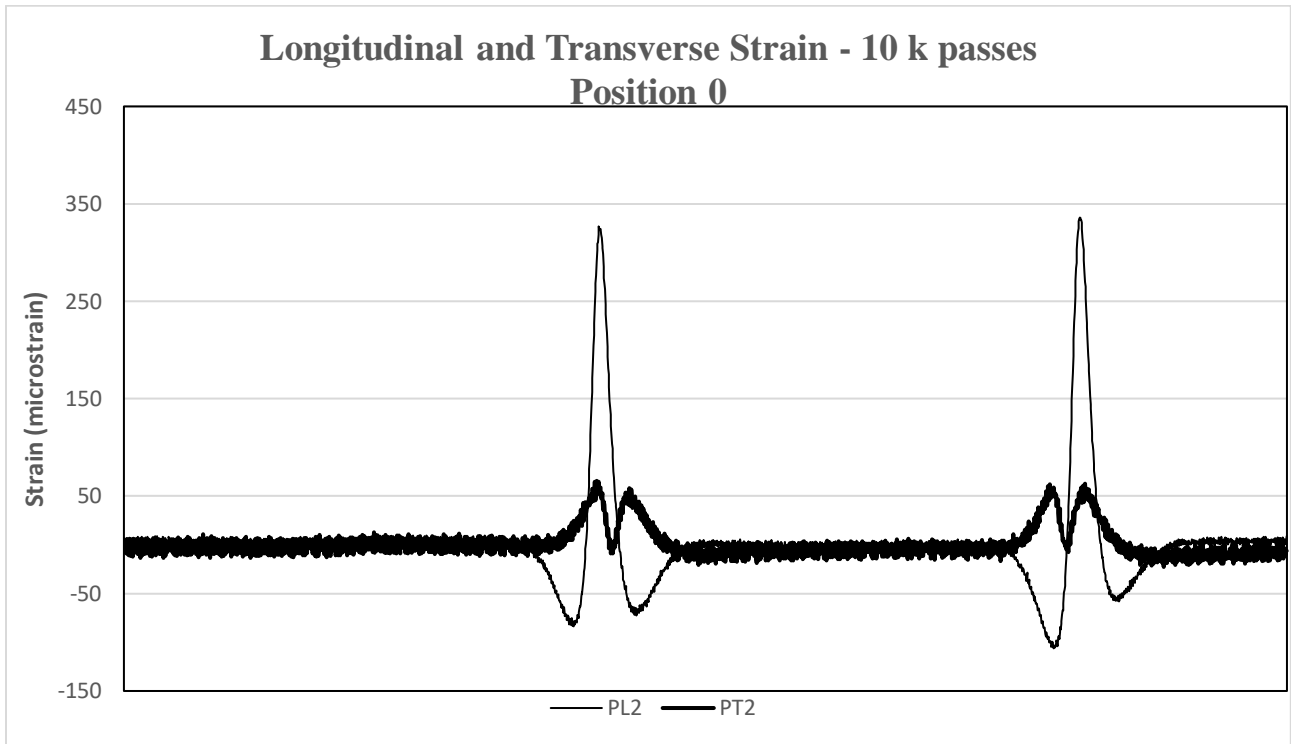


Figure D2-14 Strain Signals Recorded by PL2 and PT2 – 10,000 Passes

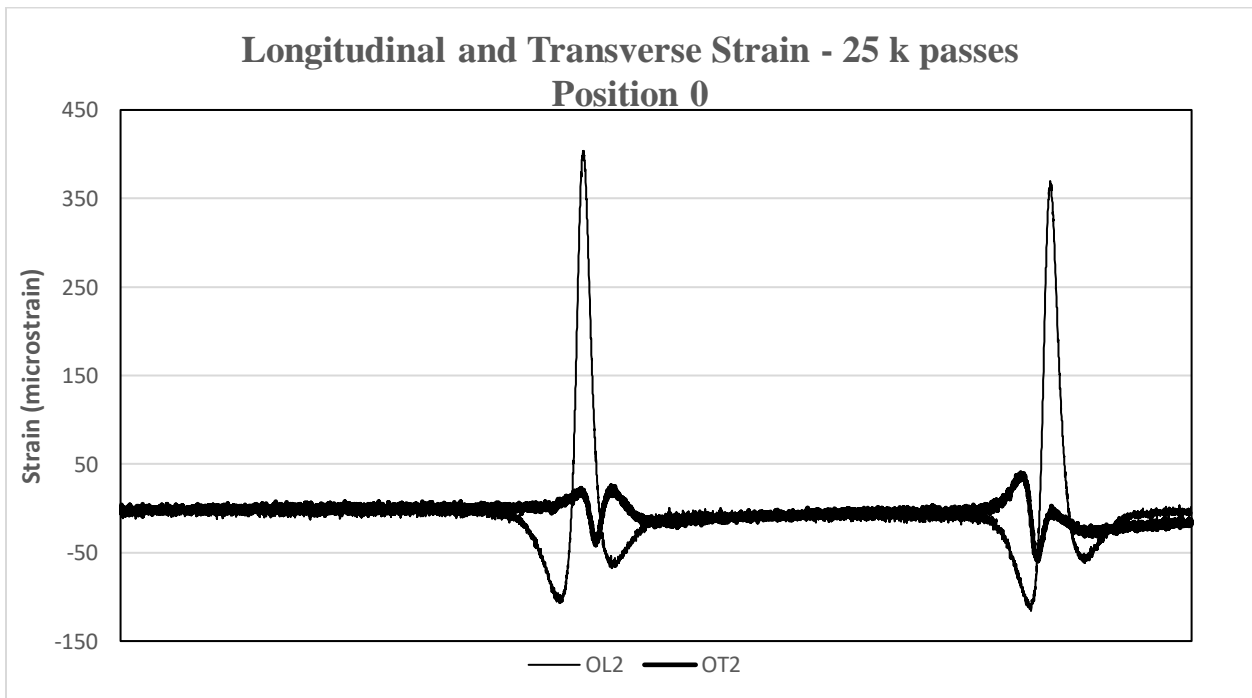


Figure D2-15 Strain Signals Recorded by OL2 OT2 – 25,000 Passes

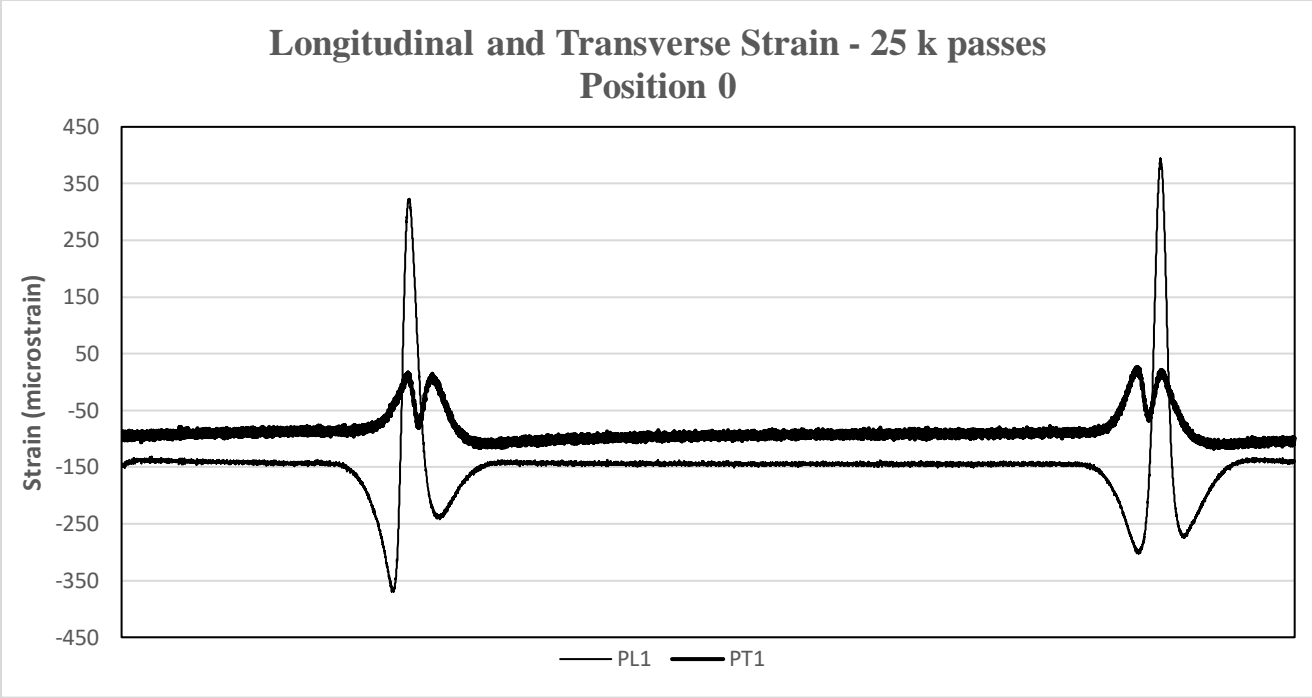


Figure D2-16 Strain Signals Recorded by PL1 and PT1 – 25,000 Passes

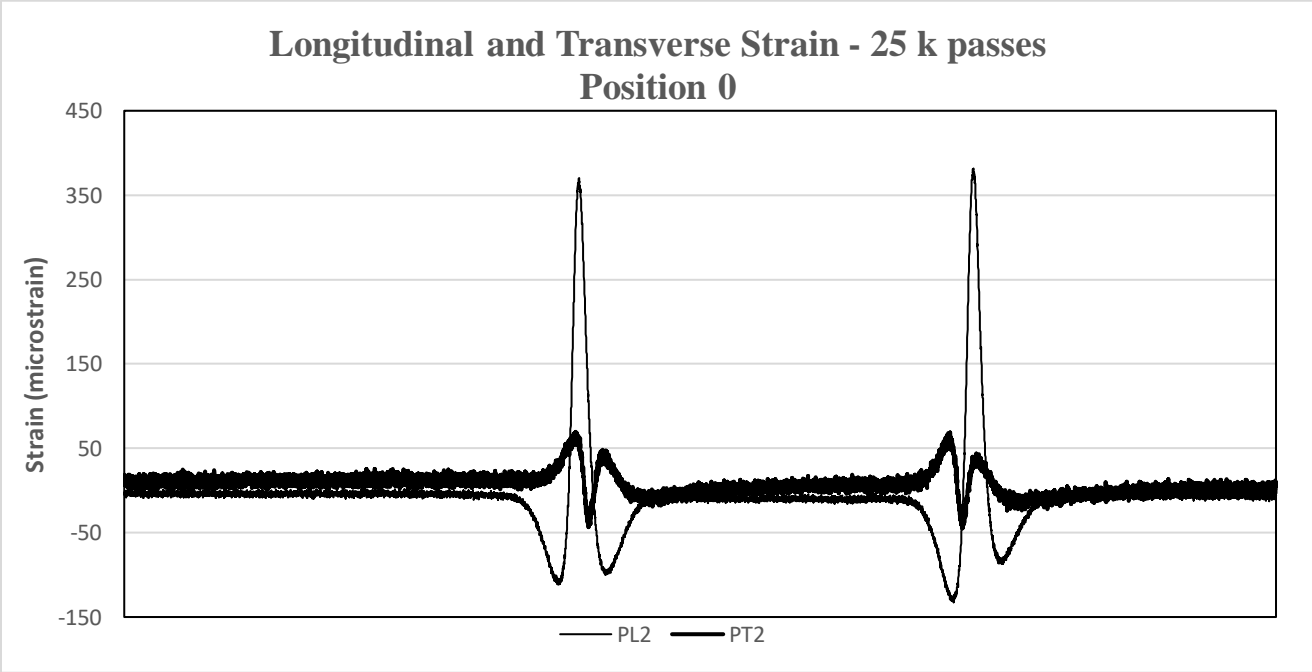


Figure D2-17 Strain Signals Recorded by PL2 and PT2 – 25,000 Passes

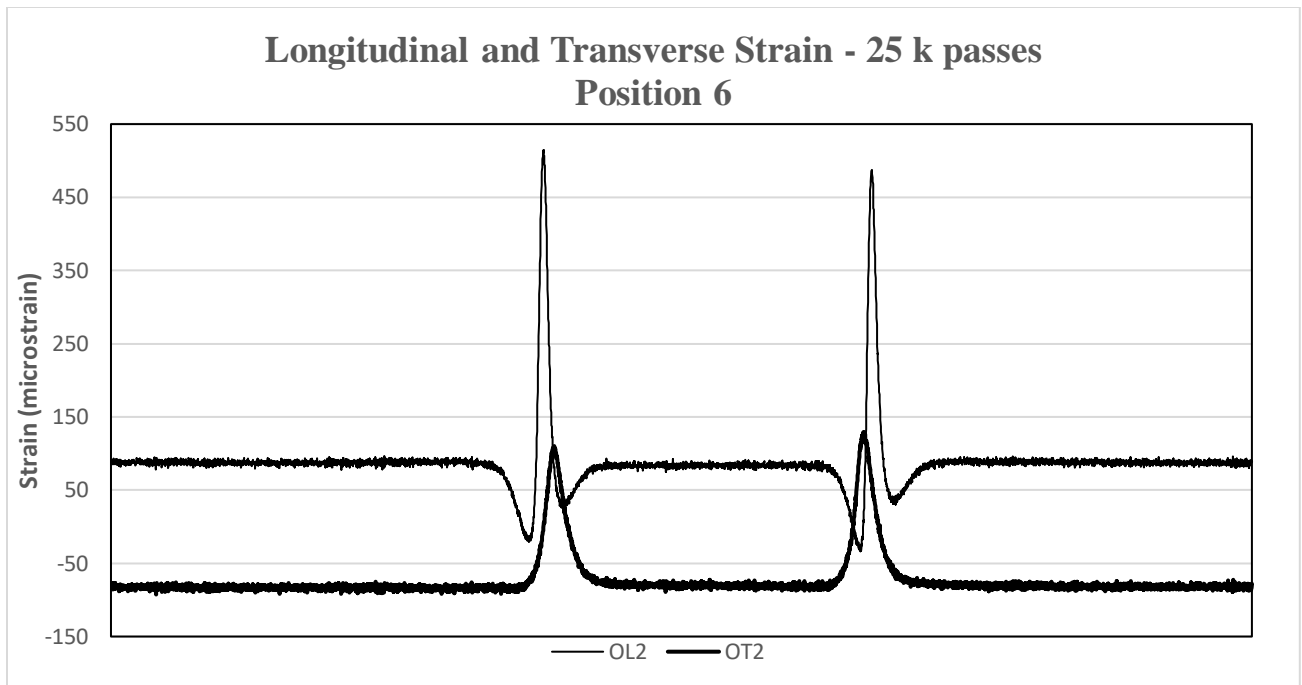


Figure D2-18 Strain Signals Recorded by OL2 and OT2 – 25,000 Passes

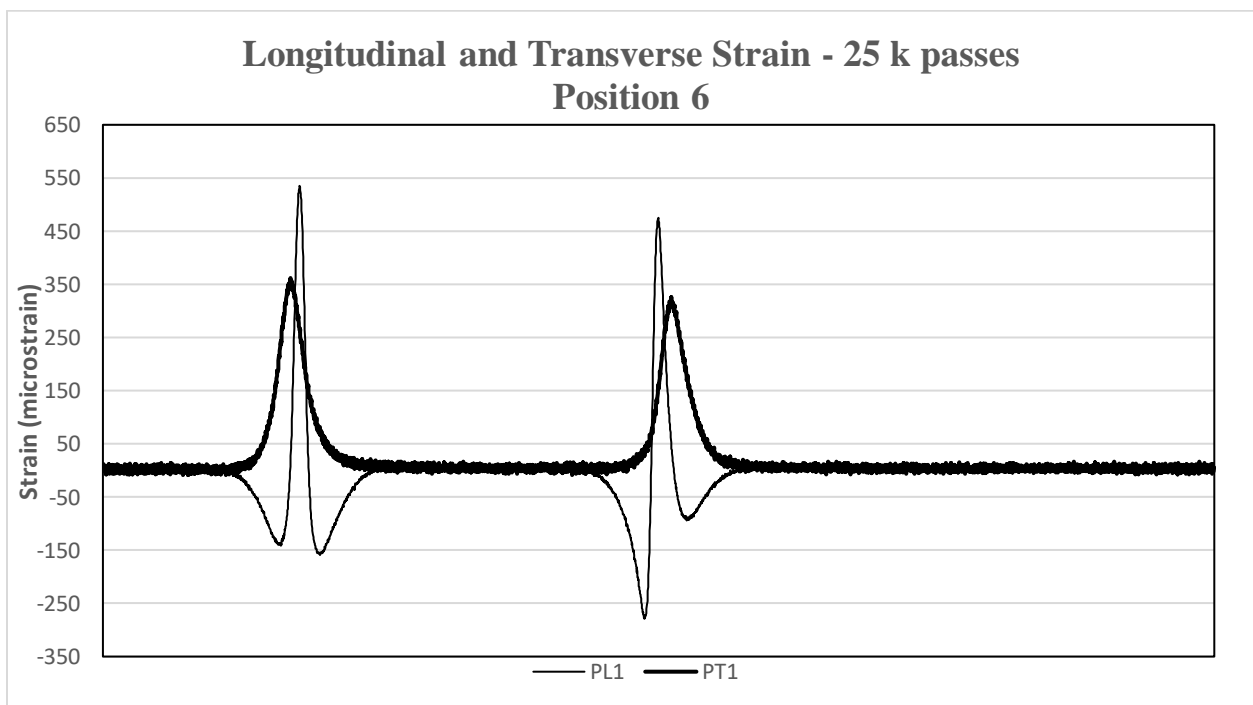


Figure D2-19 Strain Signals Recorded by PL1 and PT1 – 25,000 Passes

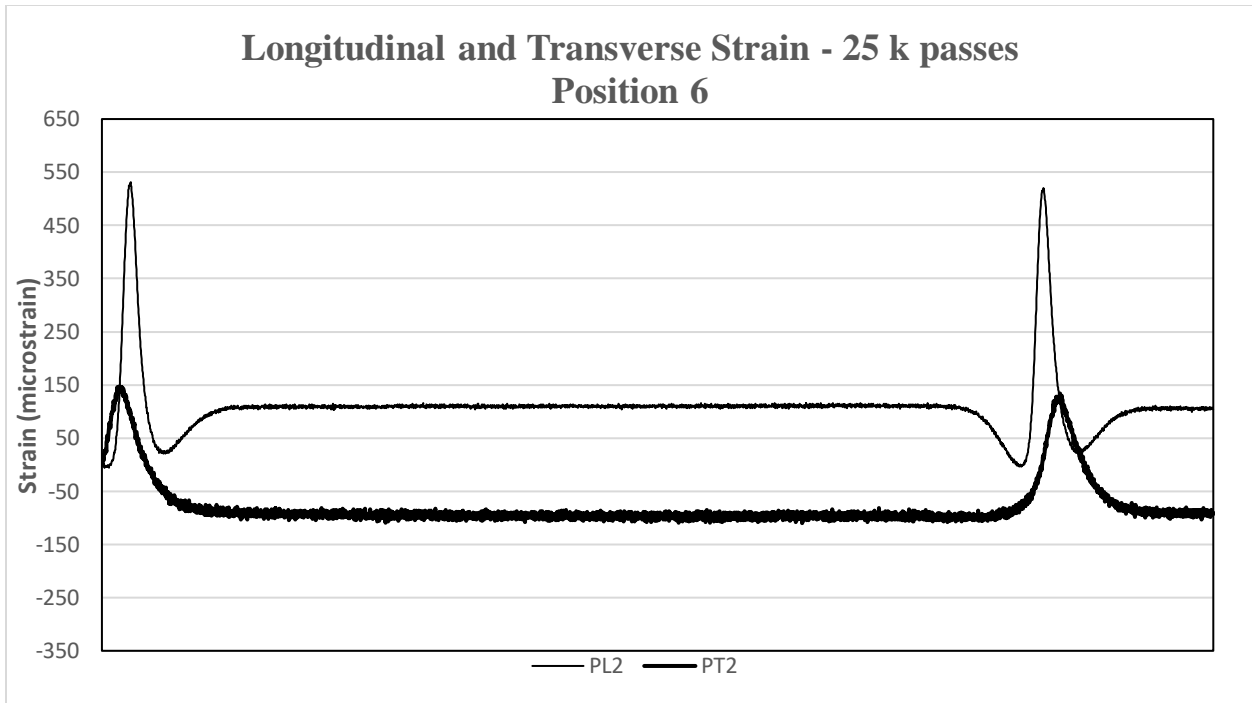


Figure D2-20 Strain Signals Recorded by PL2 and PT2 – 25,000 Passes

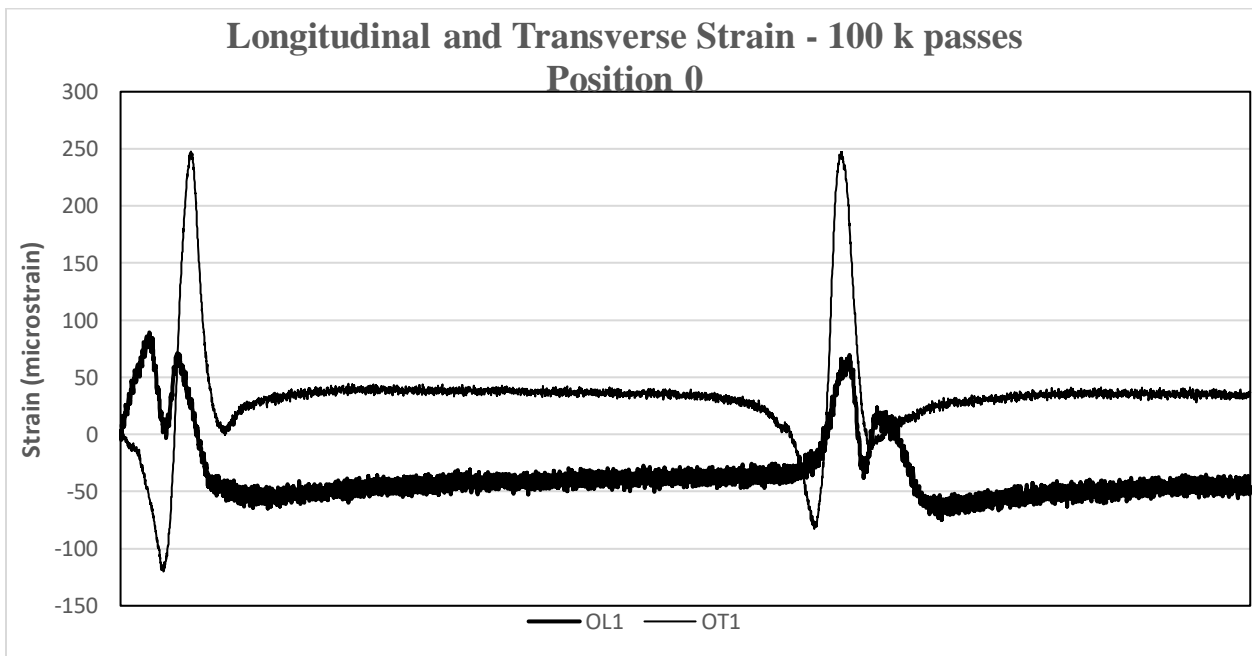


Figure D2-21 Strain Signals Recorded by OL1 and OT1 – 100,000 Passes

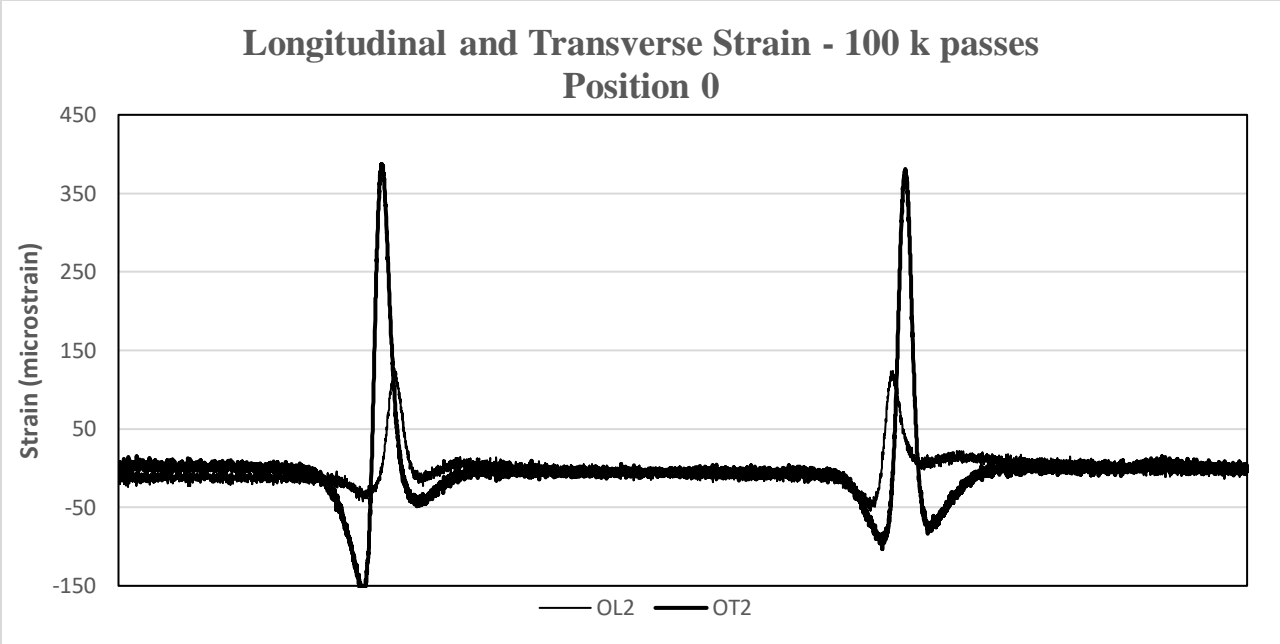


Figure D2-22 Strain Signals Recorded by OL2 and OT2 – 100,000 Passes

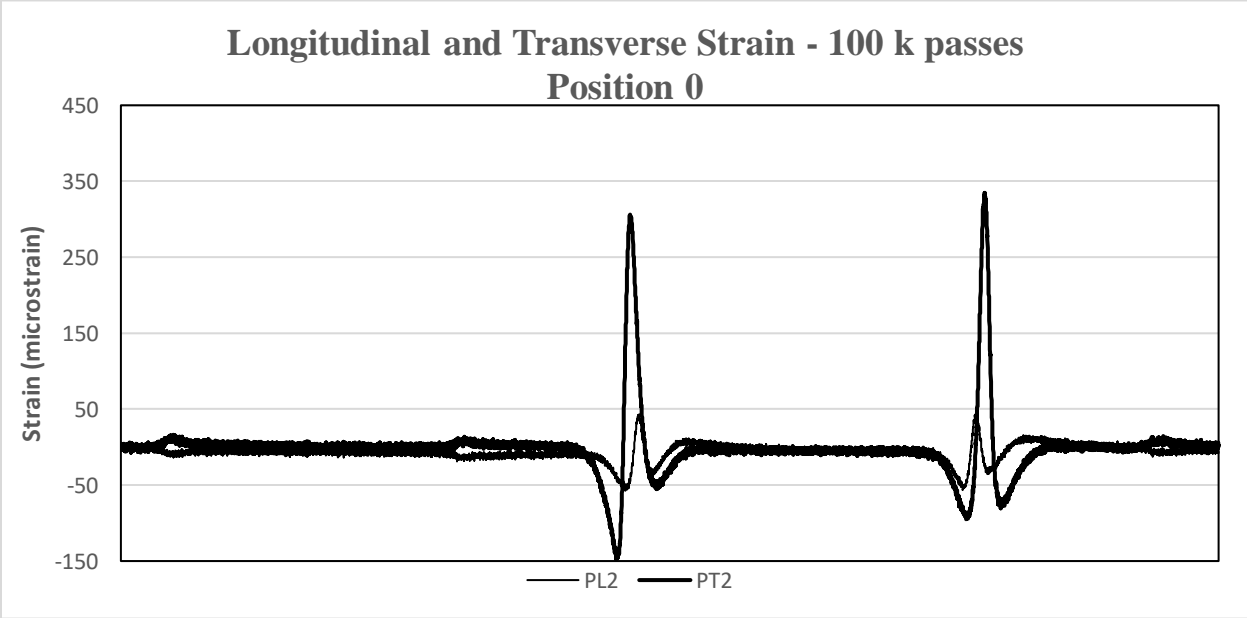


Figure D2-23 Strain Signals Recorded by PL2 and PT2 – 100,000 Passes

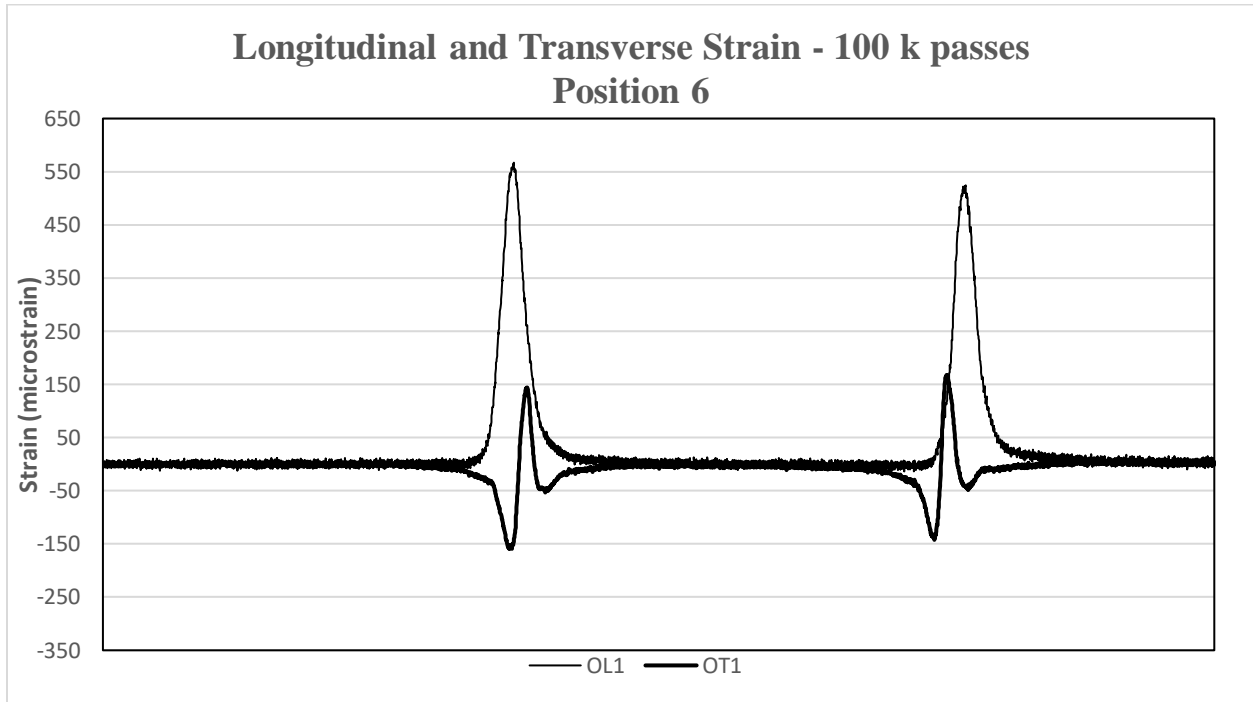


Figure D2-24 Strain Signals Recorded by OL1 and OT1 – 100,000 Passes

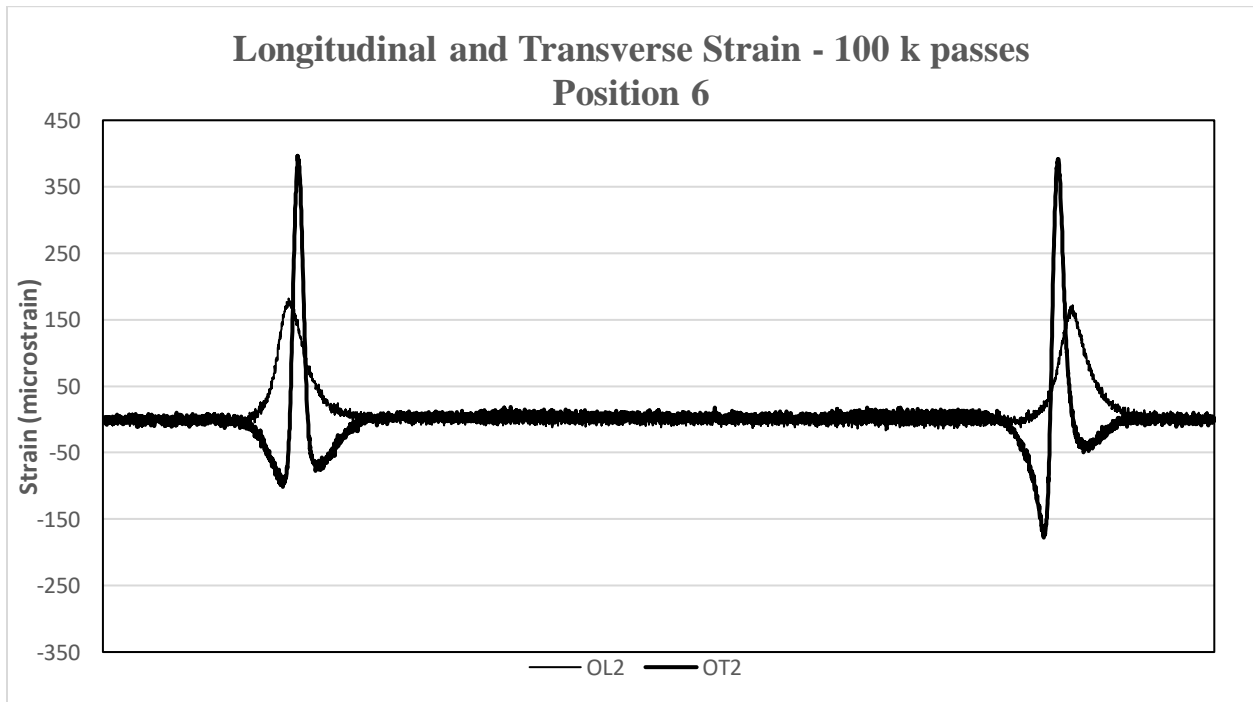


Figure D2-25 Strain Signals Recorded by OL2 and OT2 – 100,000 Passes

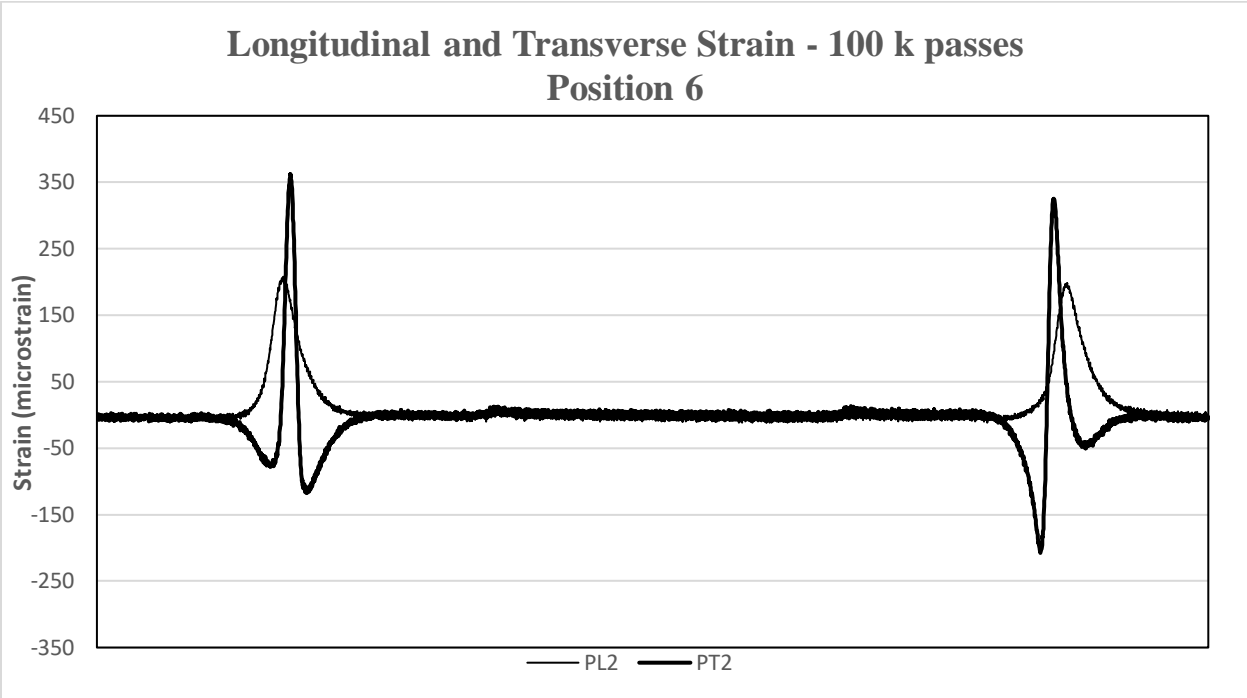


Figure D2-26 Strain Signals Recorded by PL2 and PT2 – 100,000 Passes

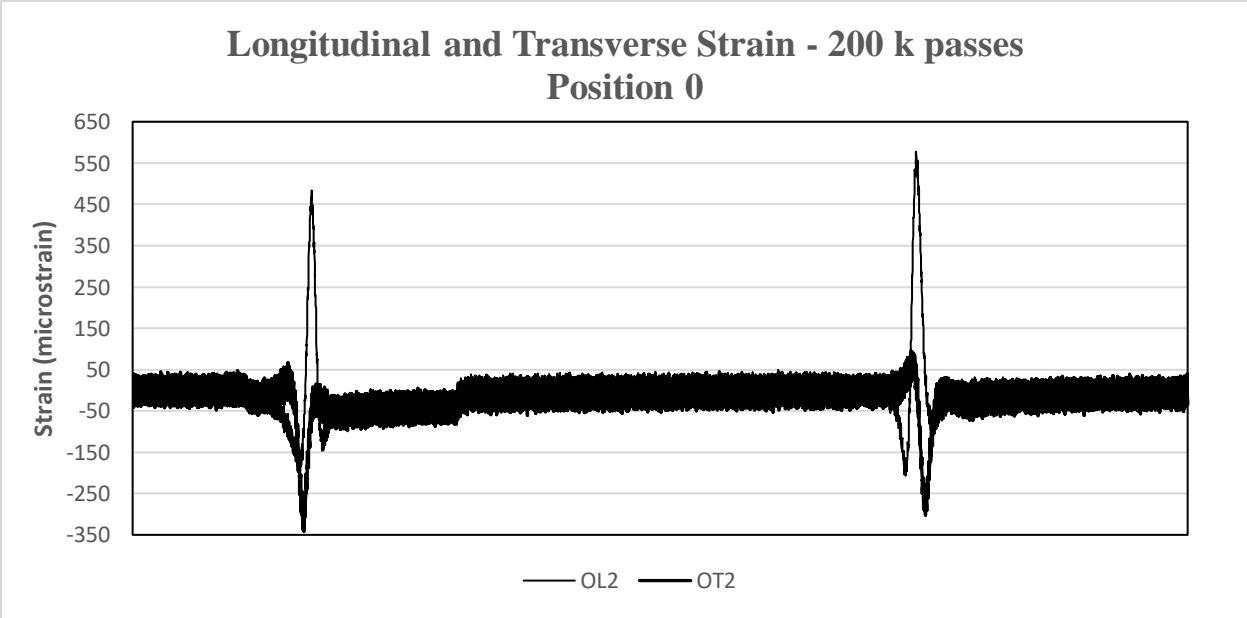


Figure D2-27 Strain Signals Recorded by OL2 and OT2 – 200,000 Passes

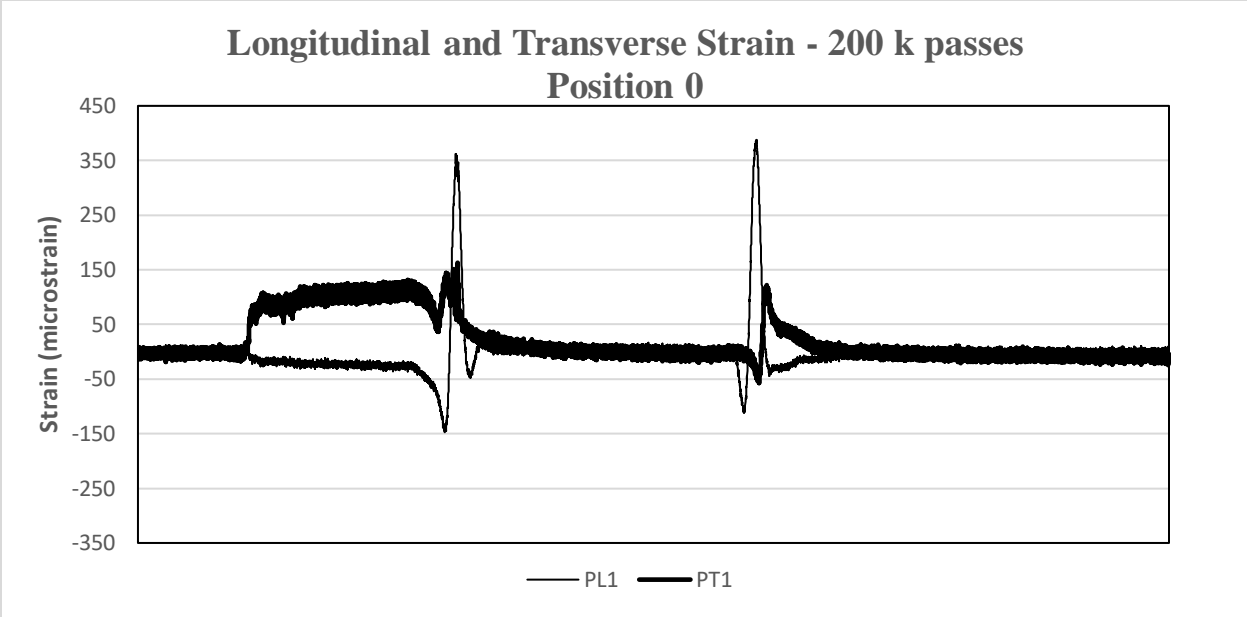


Figure D2-28 Strain Signals Recorded by PL1 and PT1 – 200,000 Passes

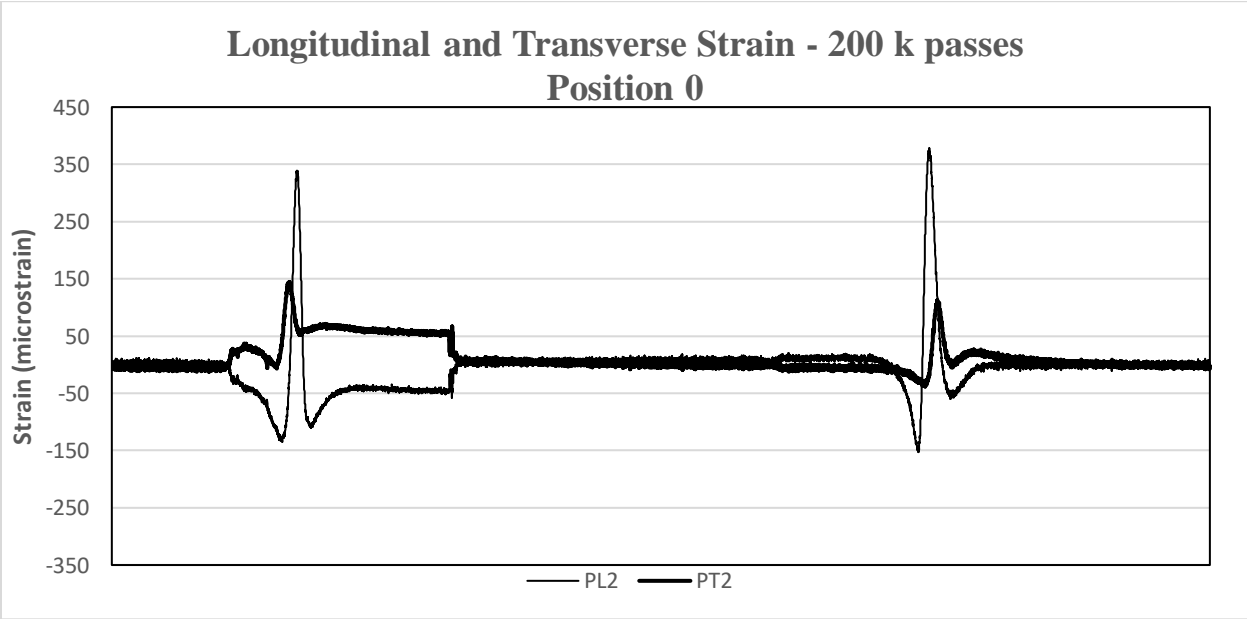


Figure D2-29 Strain Signals Recorded by PL2 and PT2 200,000 Passes

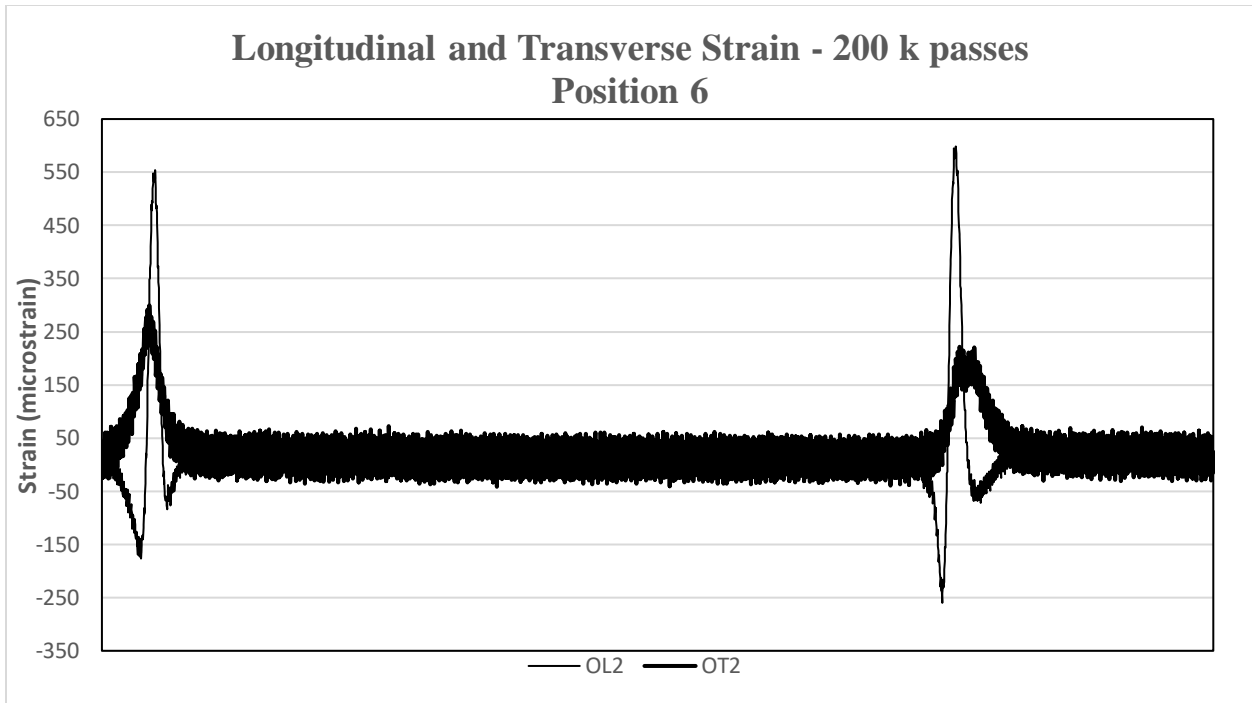


Figure D2-30 Strain Signals Recorded by OL2 and OT2 – 200,000 Passes

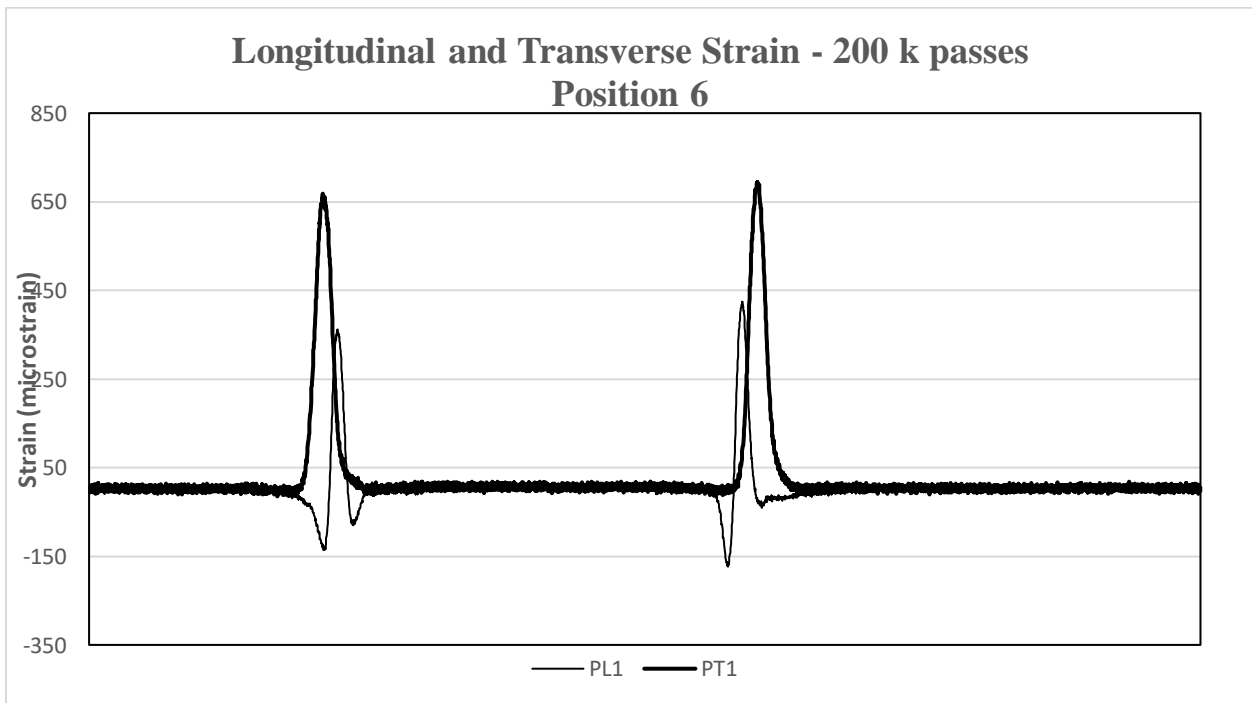


Figure D2-31 Strain Signals Recorded by PL1 and PT1 – 200,000 Passes

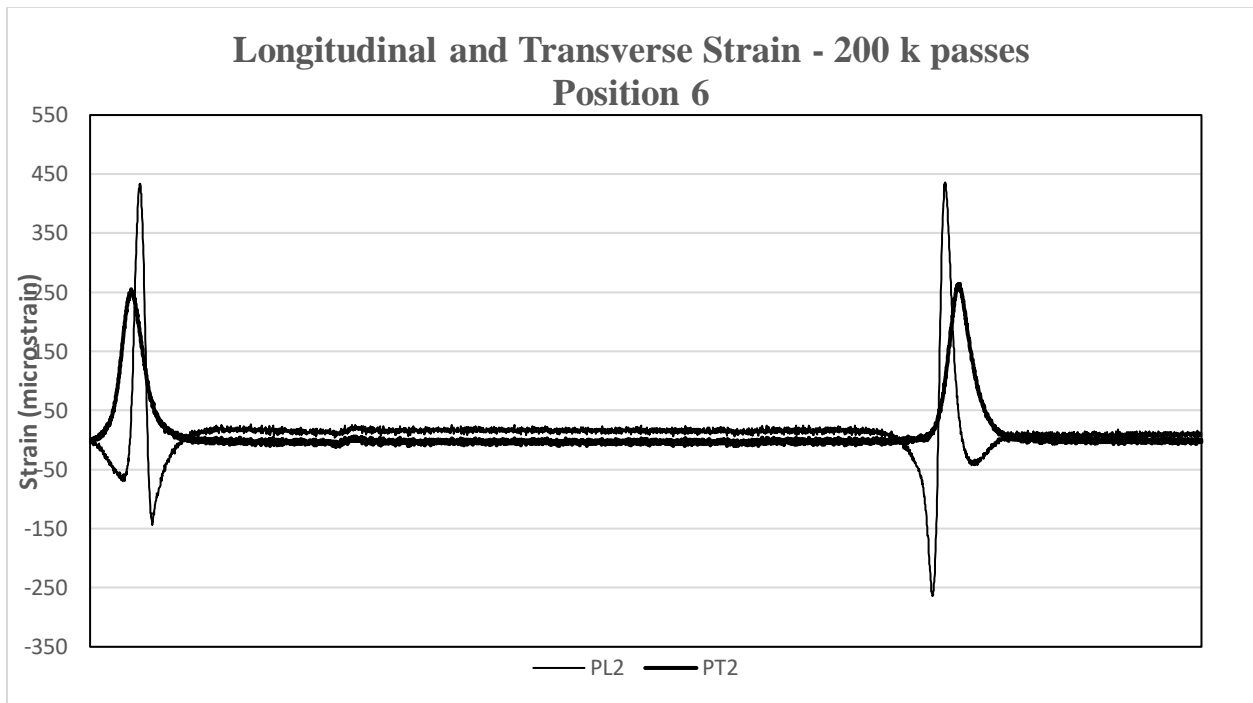


Figure D2-32 Strain Signals Recorded by PL2 and PT2 – 200,000 Passes

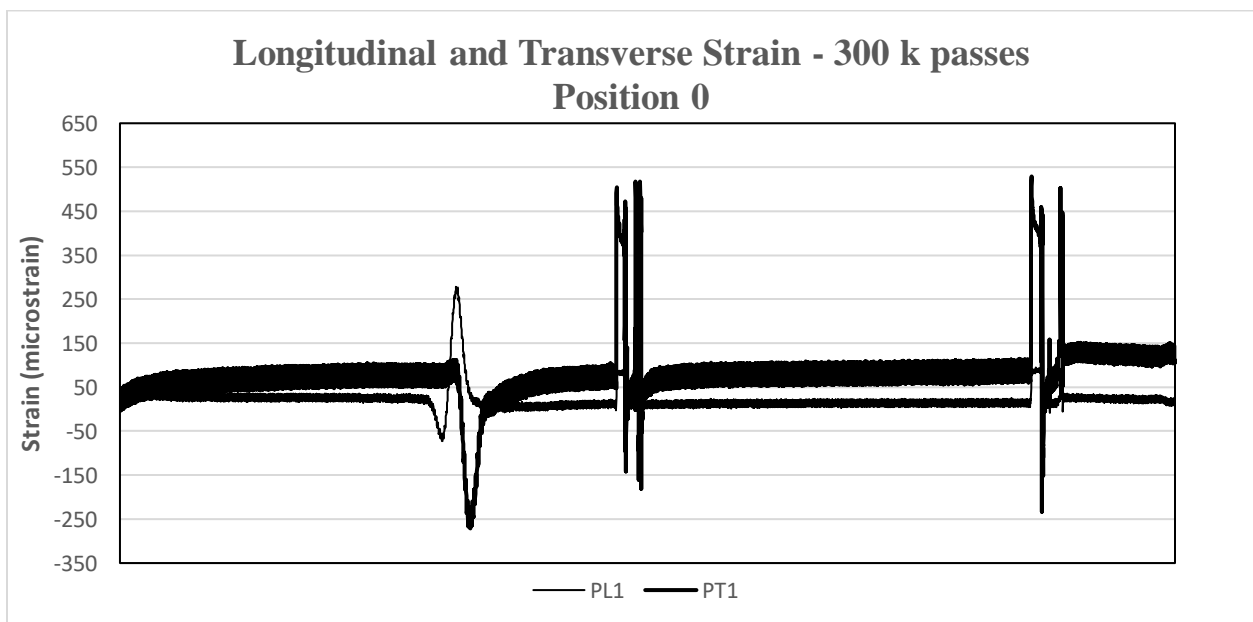


Figure D2-33 Strain Signals Recorded by PL1 and PT1 – 300,000 Passes

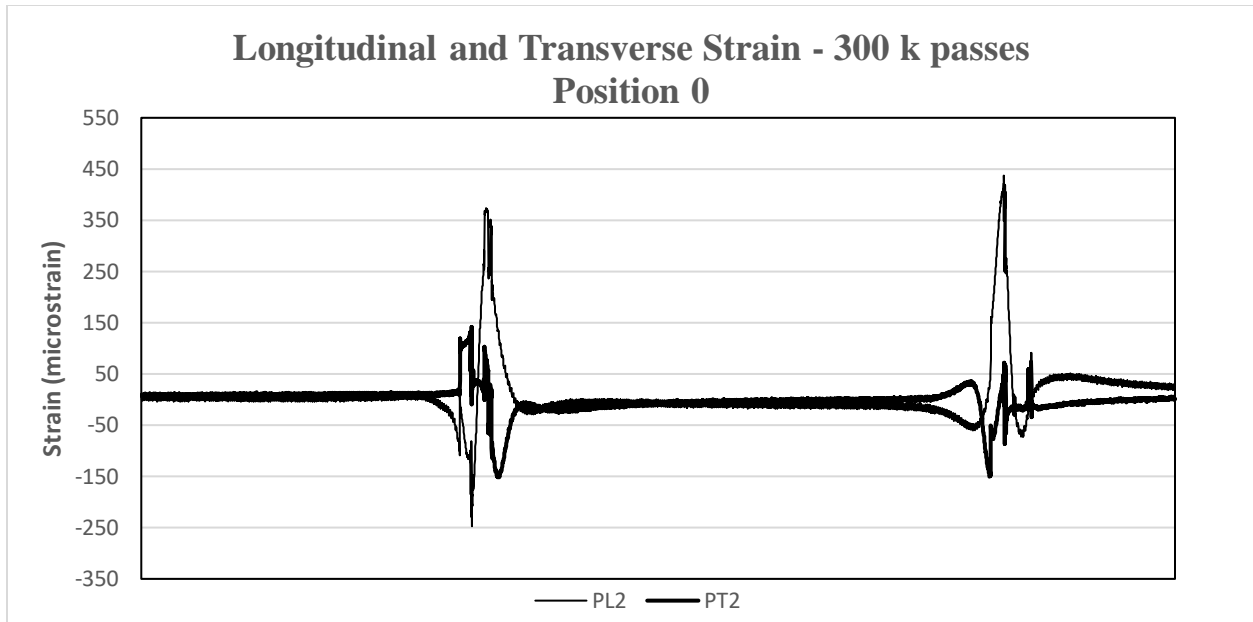


Figure D2-34 Strain Signals Recorded by PL2 and PT2 – 300,000 Passes

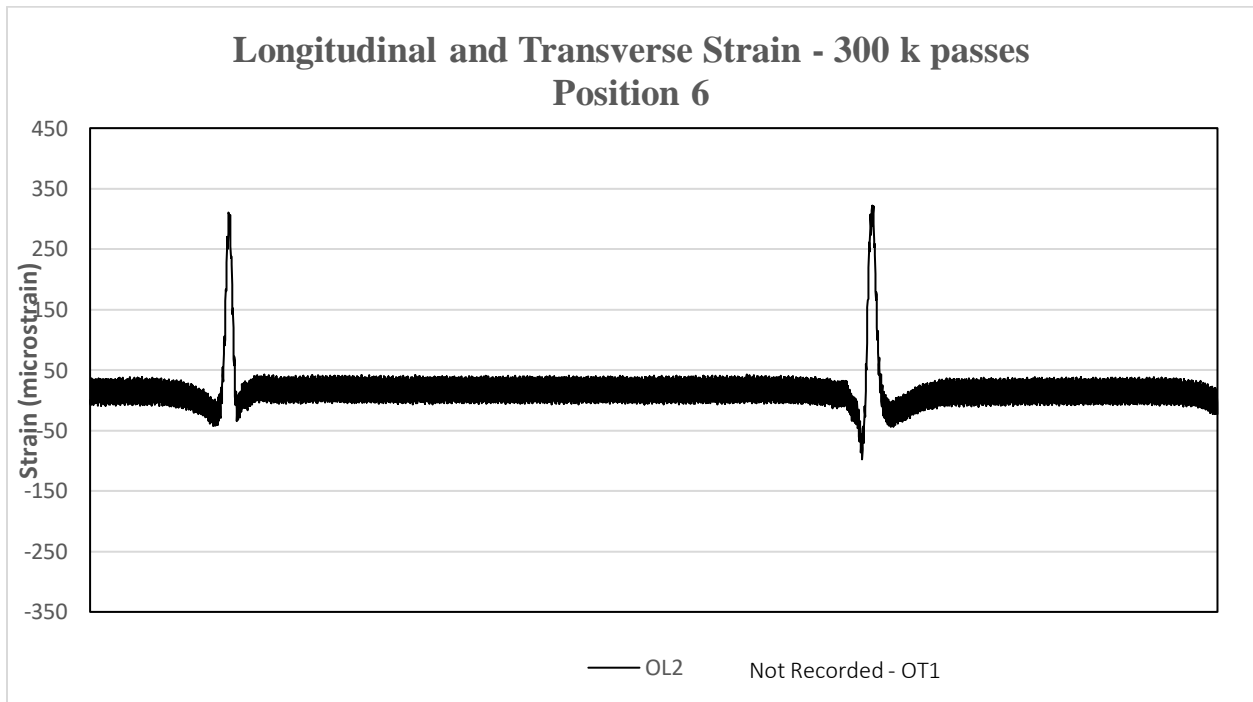


Figure D2-35 Strain Signals Recorded by OL2 – 300,000 Passes

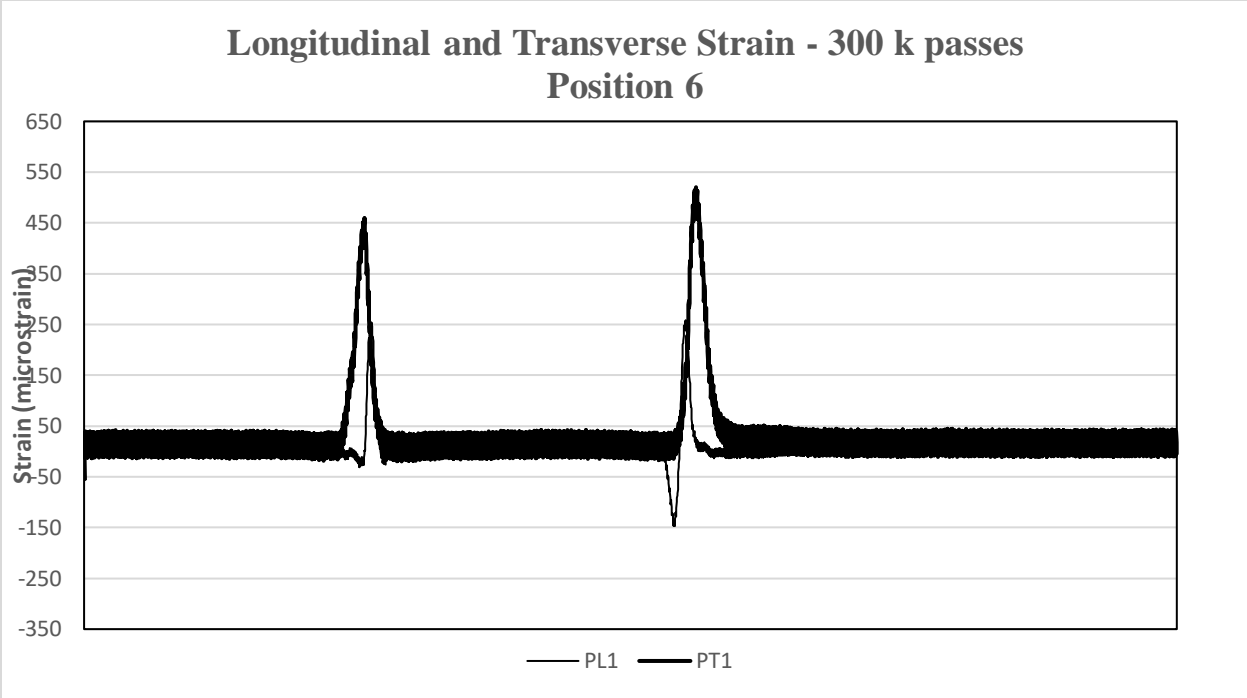


Figure D2-36 Strain Signals Recorded by PL1 and PT1 – 300,000 passes

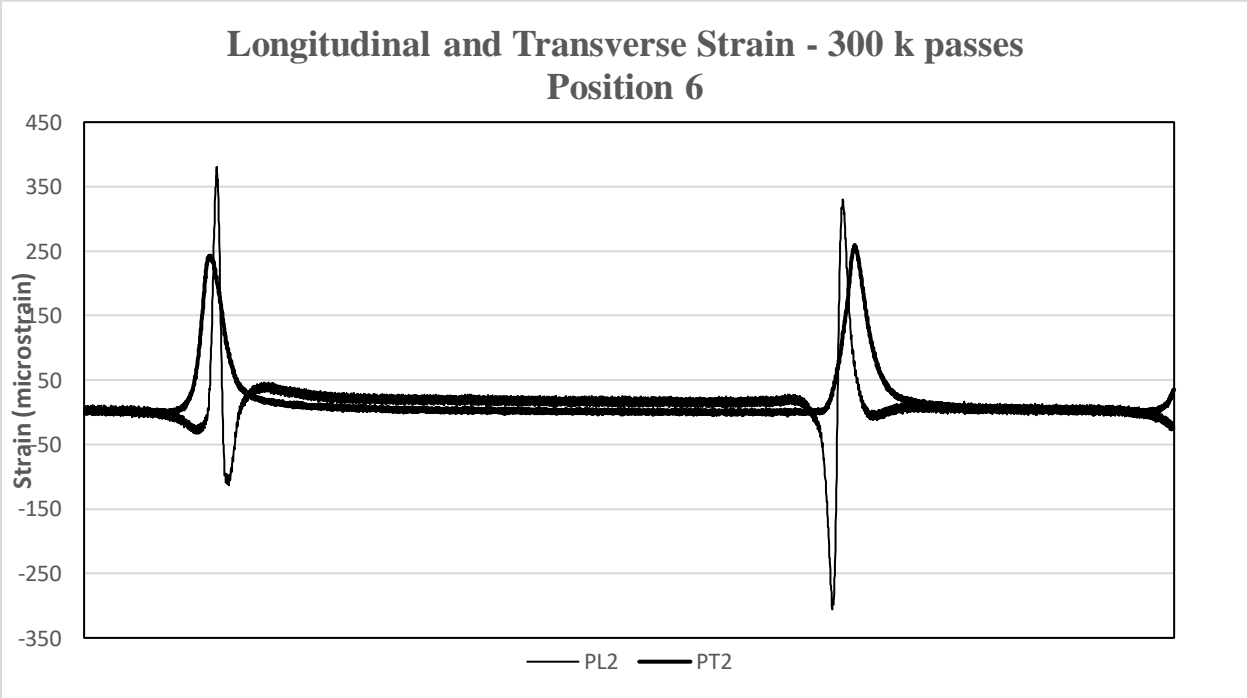


Figure D2-37 Strain Signals Recorded by PL2 and PT2 – 300,000 Passes

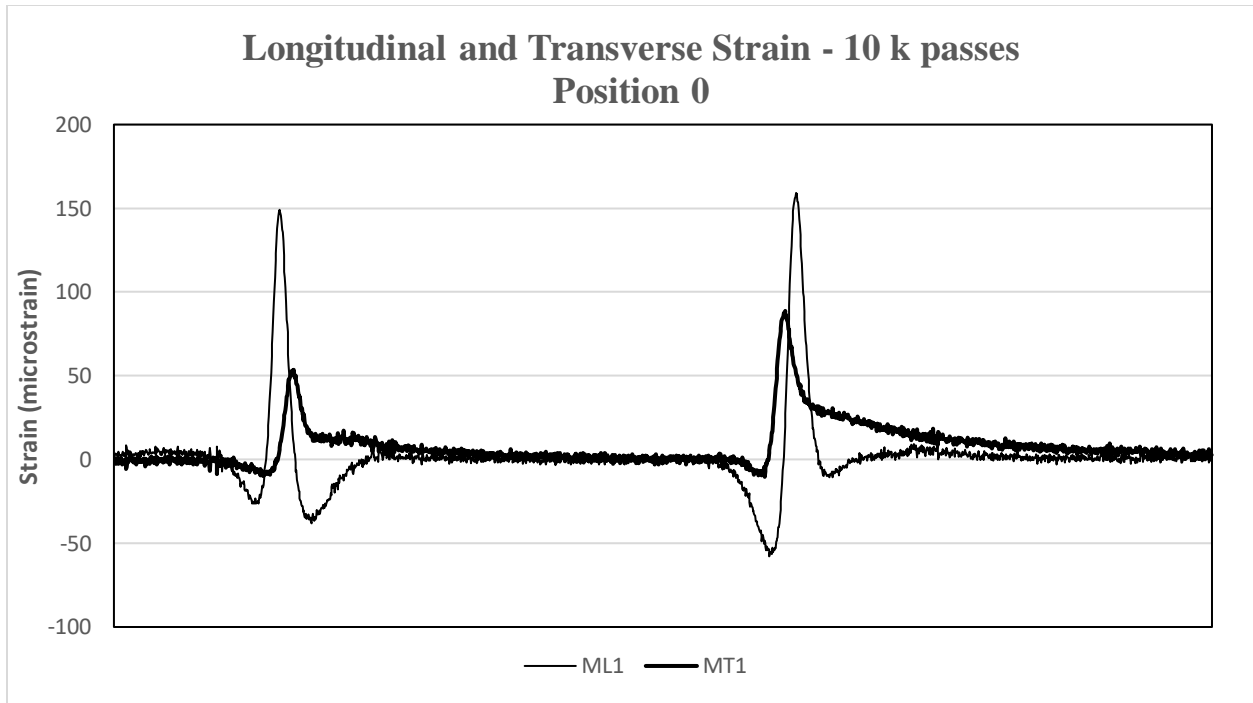


Figure D2-38 Strain Signals Recorded by ML1 and MT1 – 300,000 passes

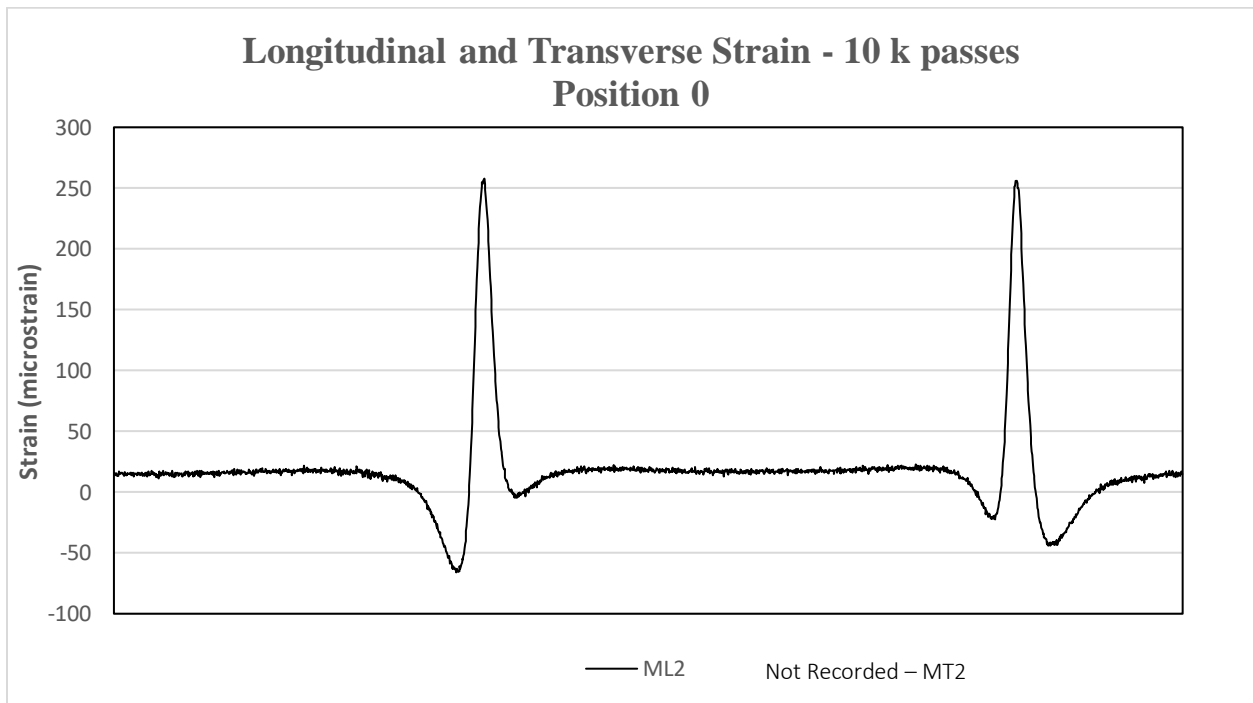


Figure D2-39 Strain Signals Recorded by ML2 – 10,000 passes

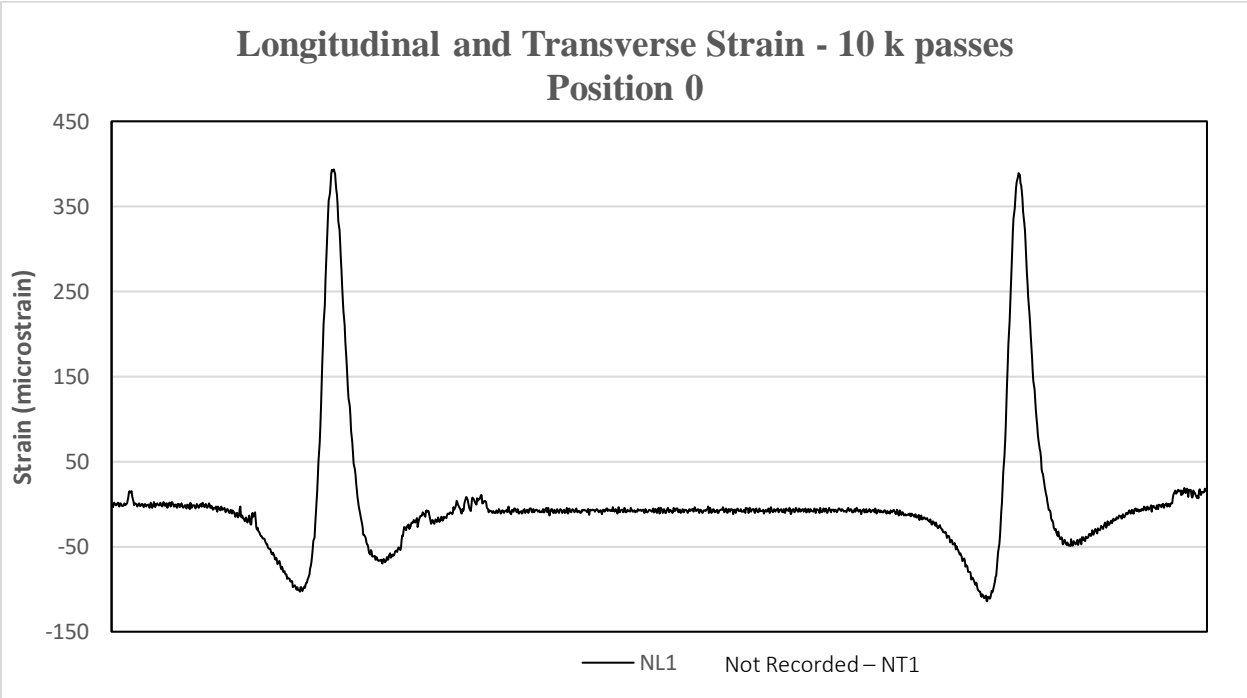


Figure D2-40 Strain Signals Recorded by NL1 – 10,000 passes

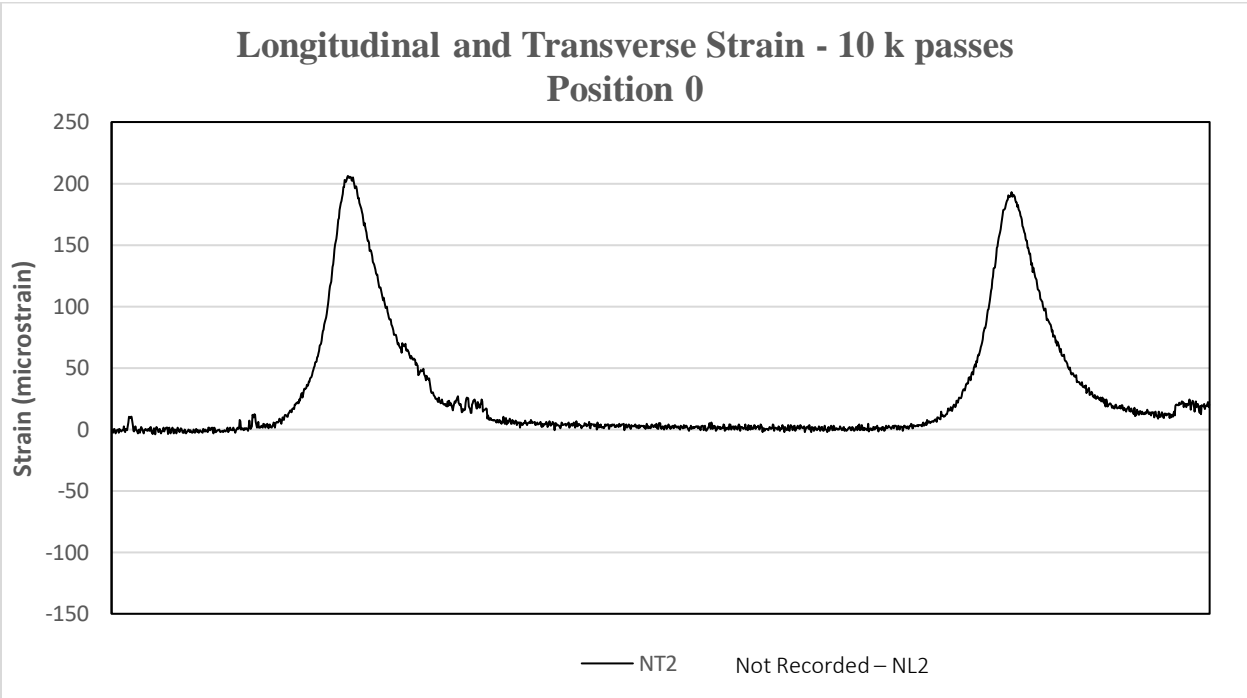


Figure D2-41 Strain Signals Recorded by NT2 – 10,000 passes

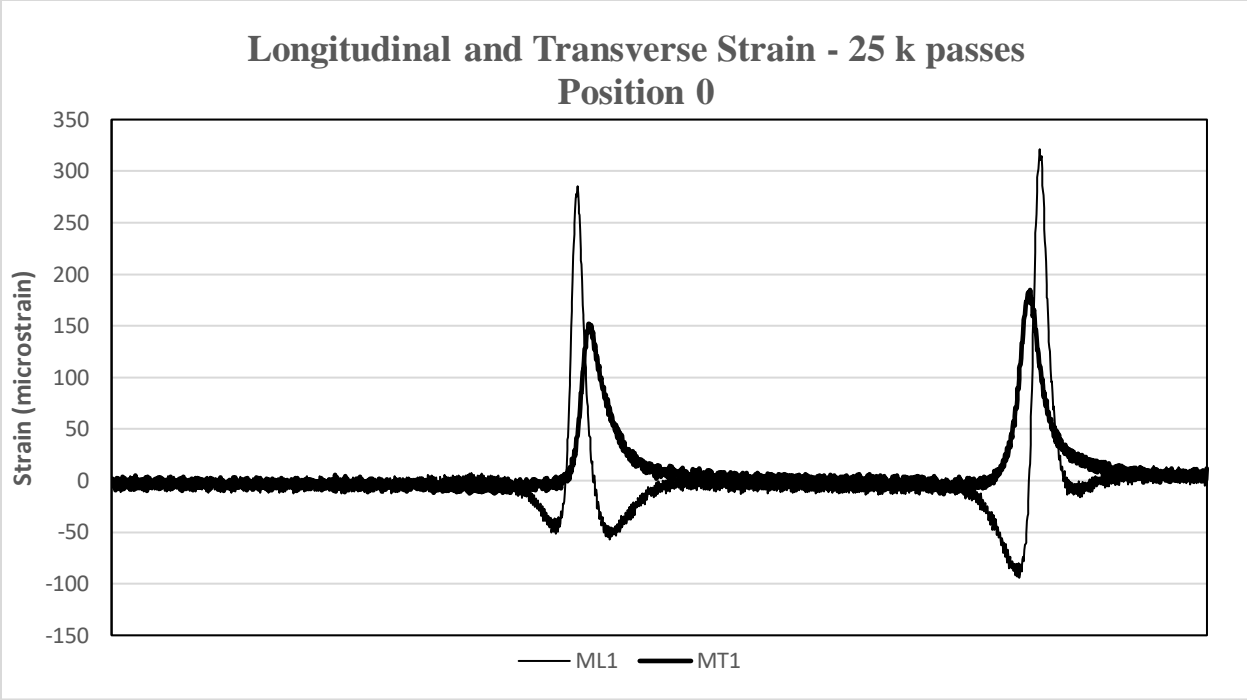


Figure D2-42 Strain Signals Recorded by ML1 and MT1 – 25,000 passes

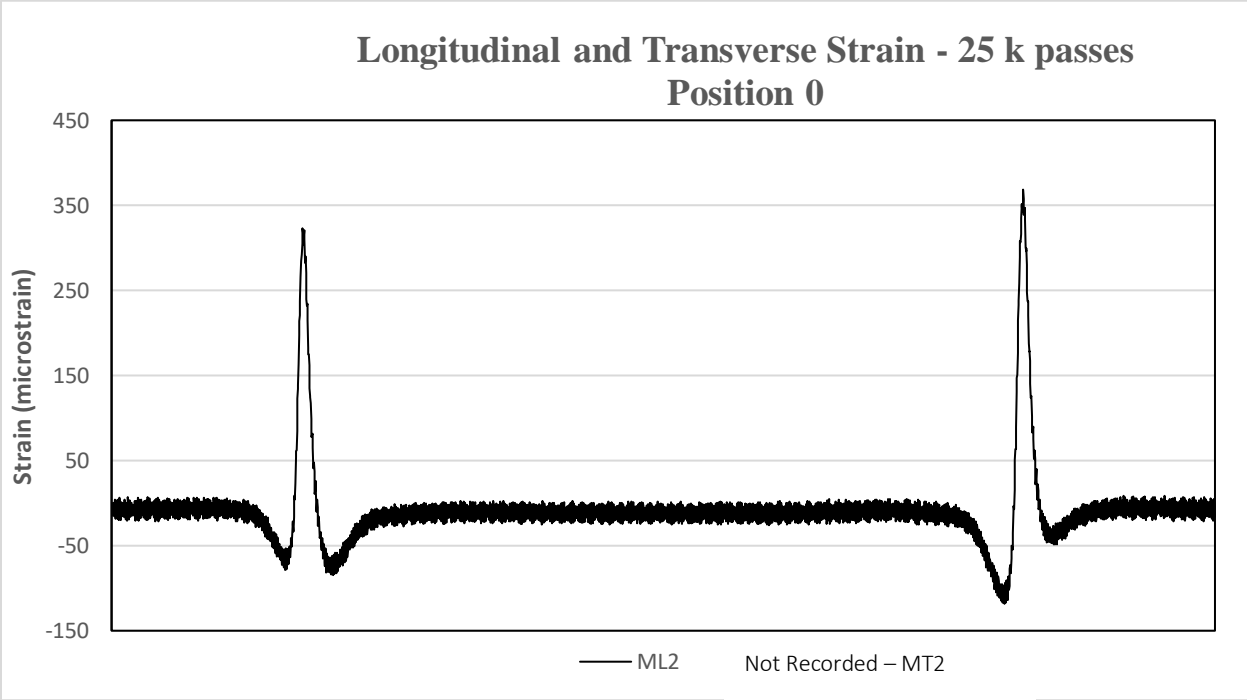


Figure D2-43 Strain Signals Recorded by ML2 – 25,000 passes

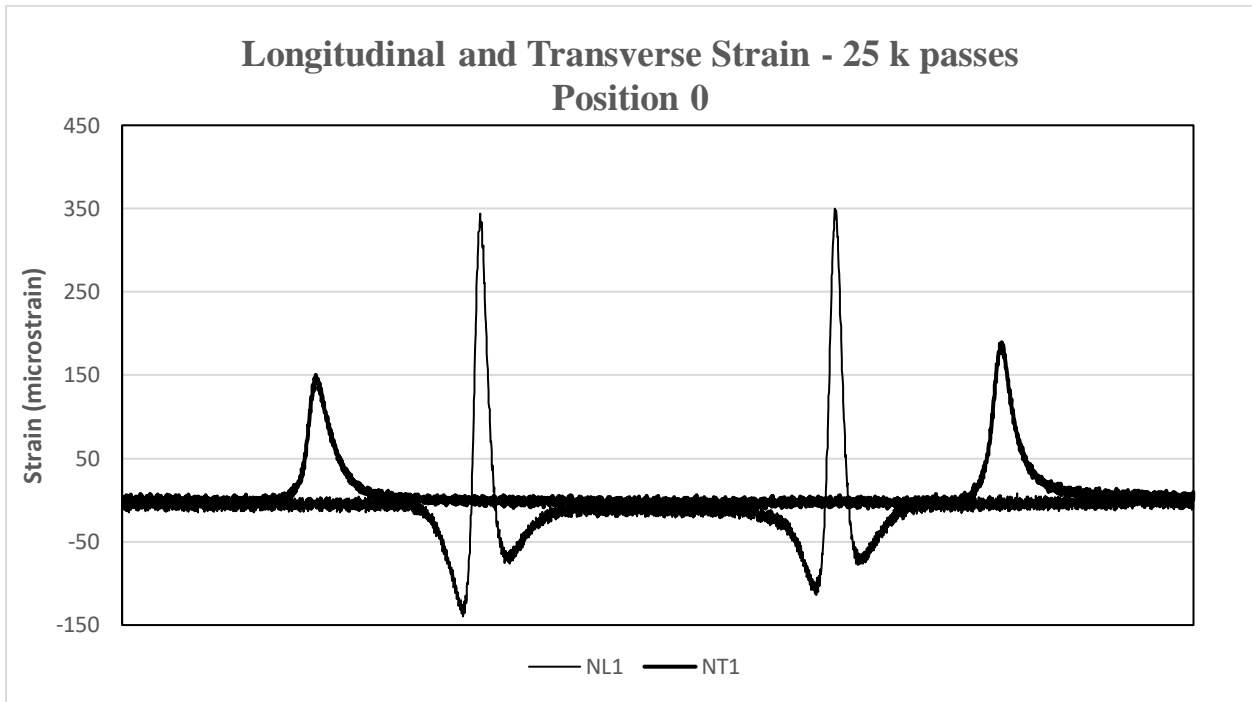


Figure D2-44 Strain Signals Recorded by NL1 and NT1 – 25,000 passes

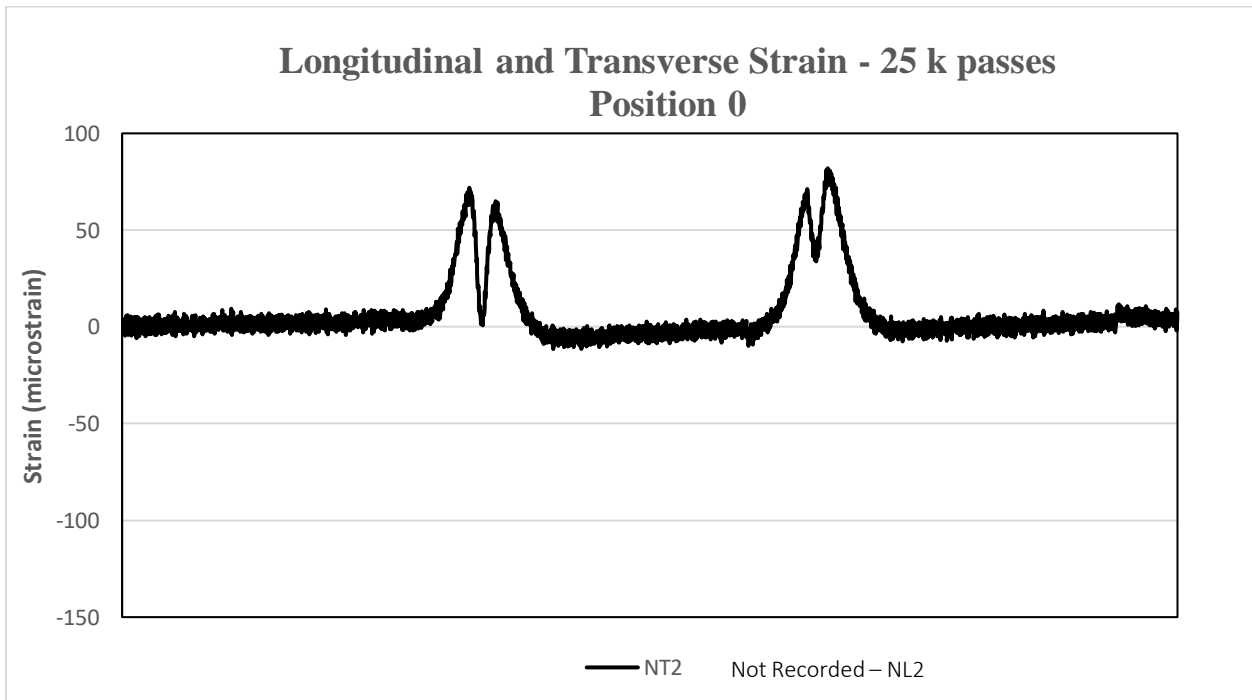


Figure D2-45 Strain Signals Recorded by NT2 – 25,000 passes

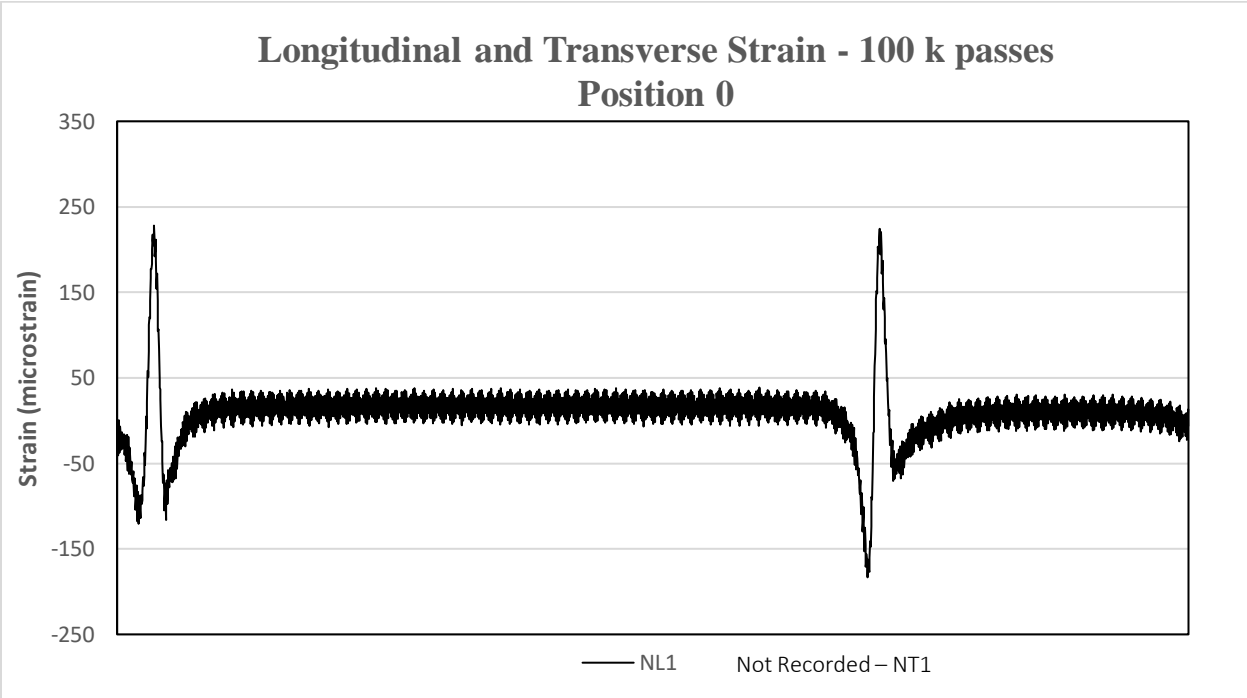


Figure D2-46 Strain Signals Recorded by NL1 – 100,000 passes

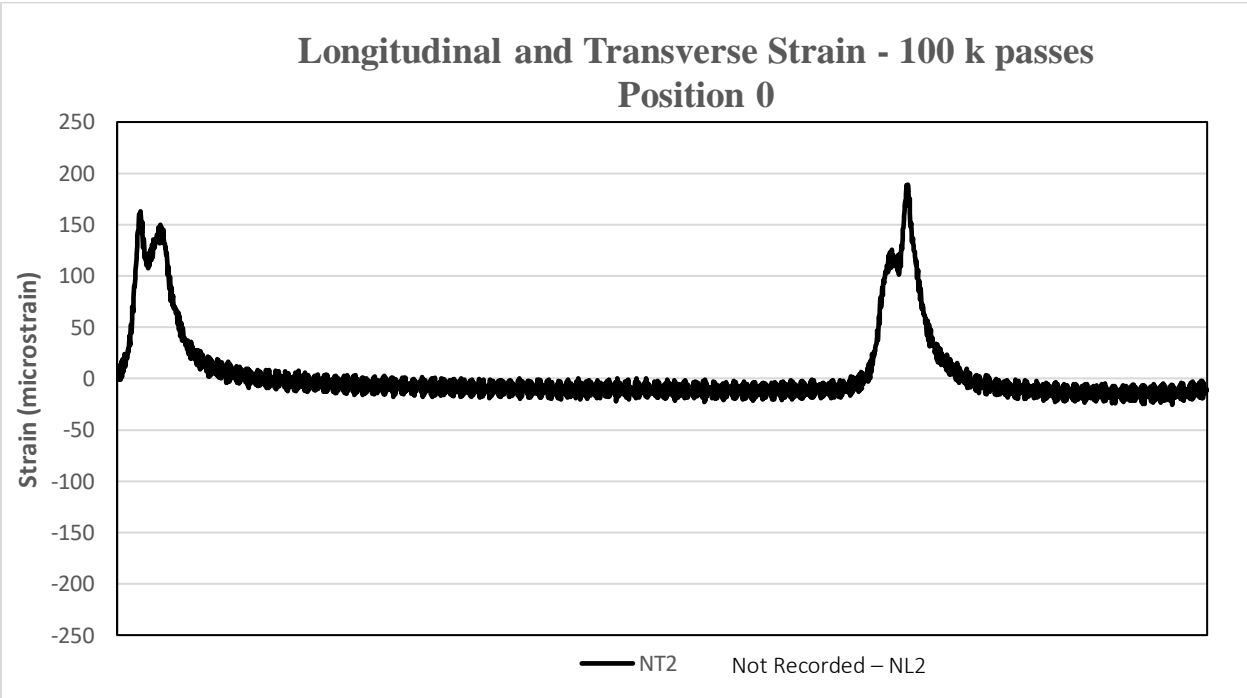


Figure D2-47 Strain Signals Recorded by NT2 – 100,000 passes

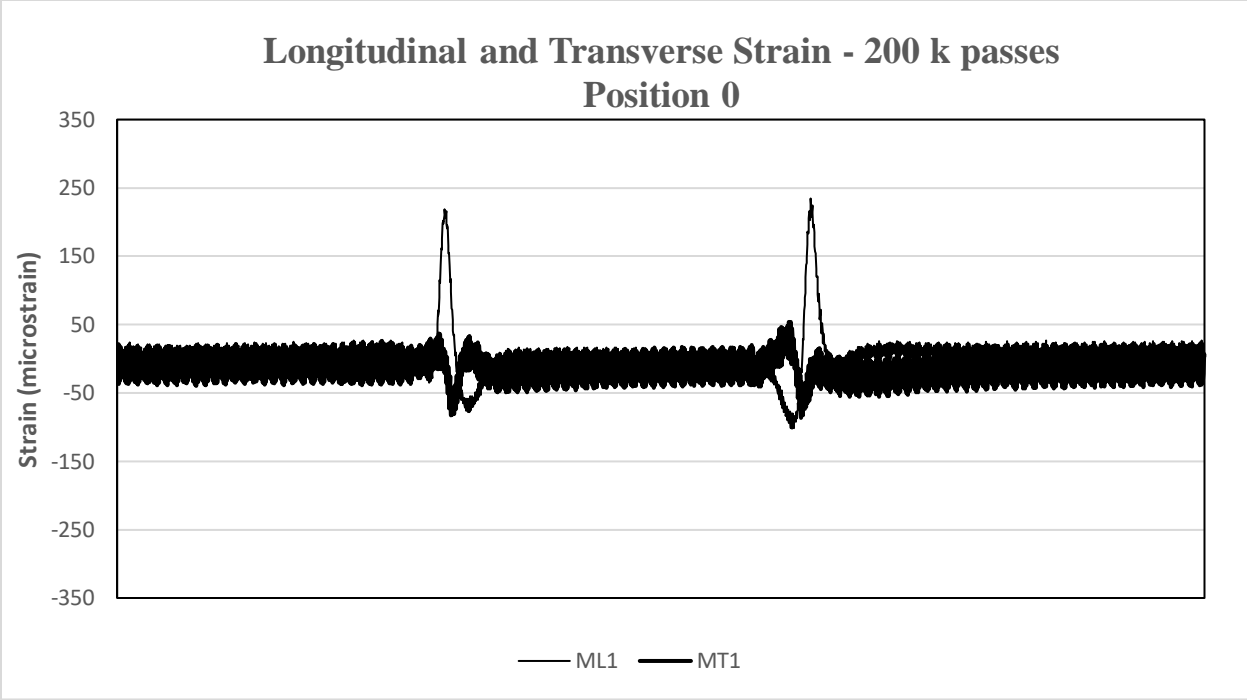


Figure D2-48 Strain Signals Recorded by ML1 and MT1 – 200,000 passes

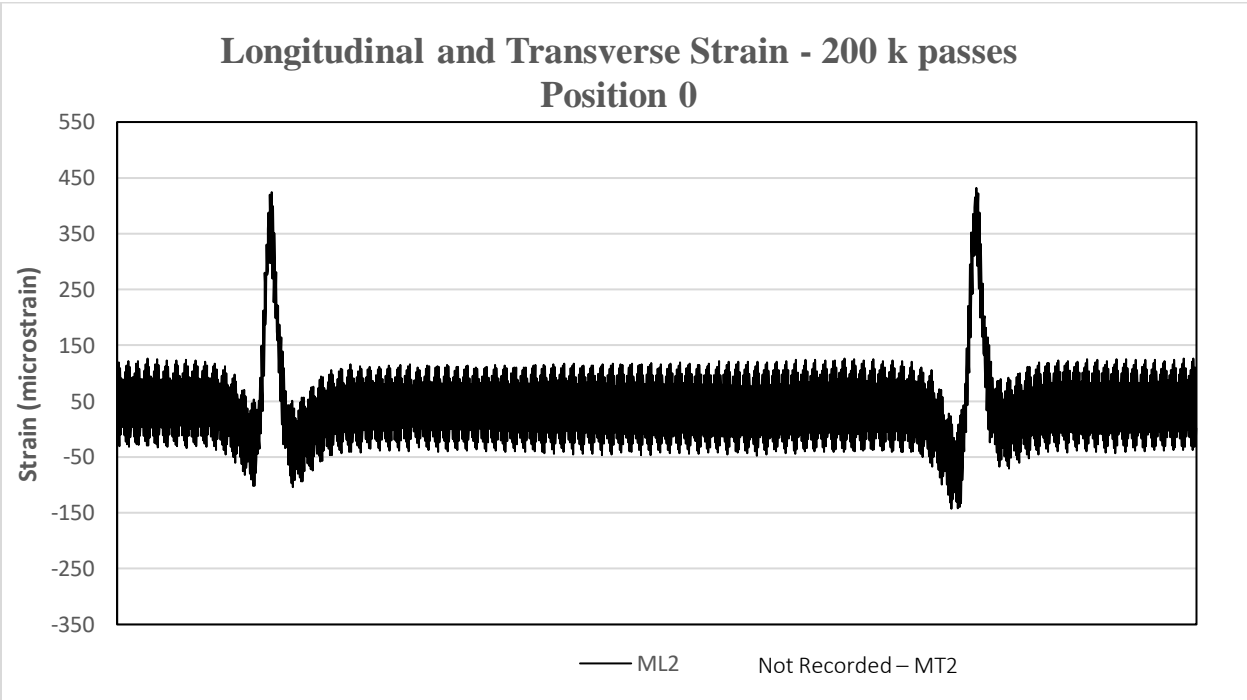


Figure D2-49 Strain Signals Recorded by ML2 – 200,000 passes

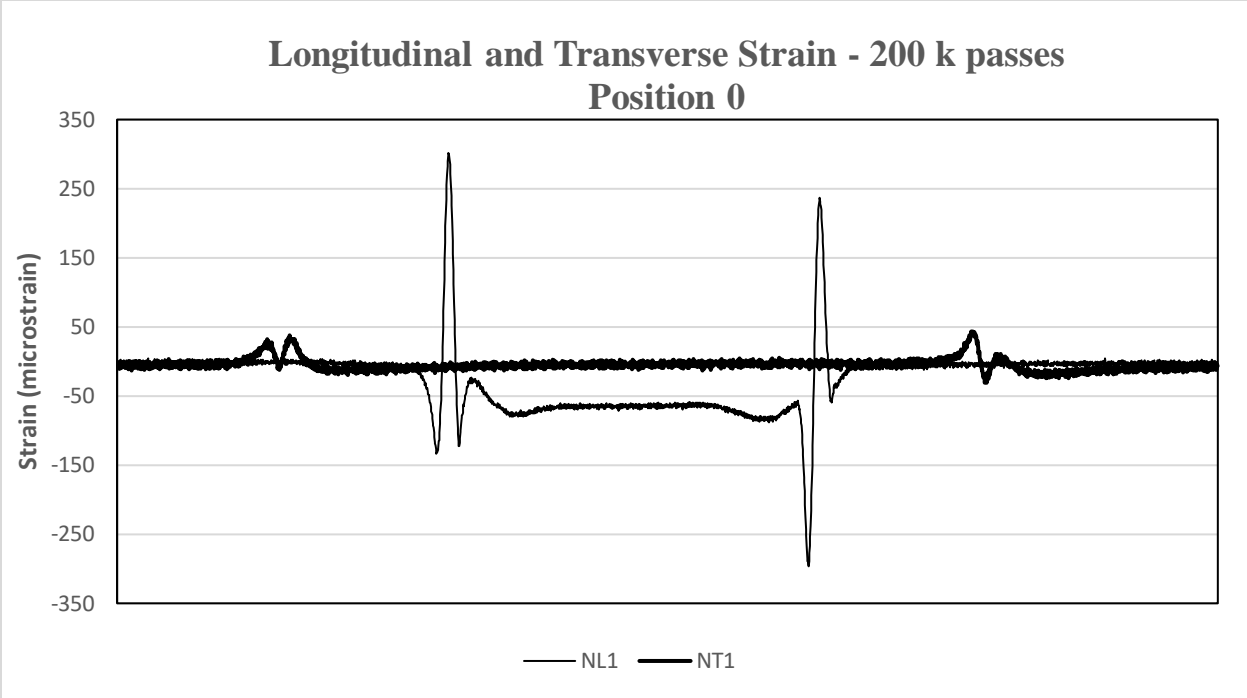


Figure D2-50 Strain Signals Recorded by NL1 and NT1 – 200,000 passes

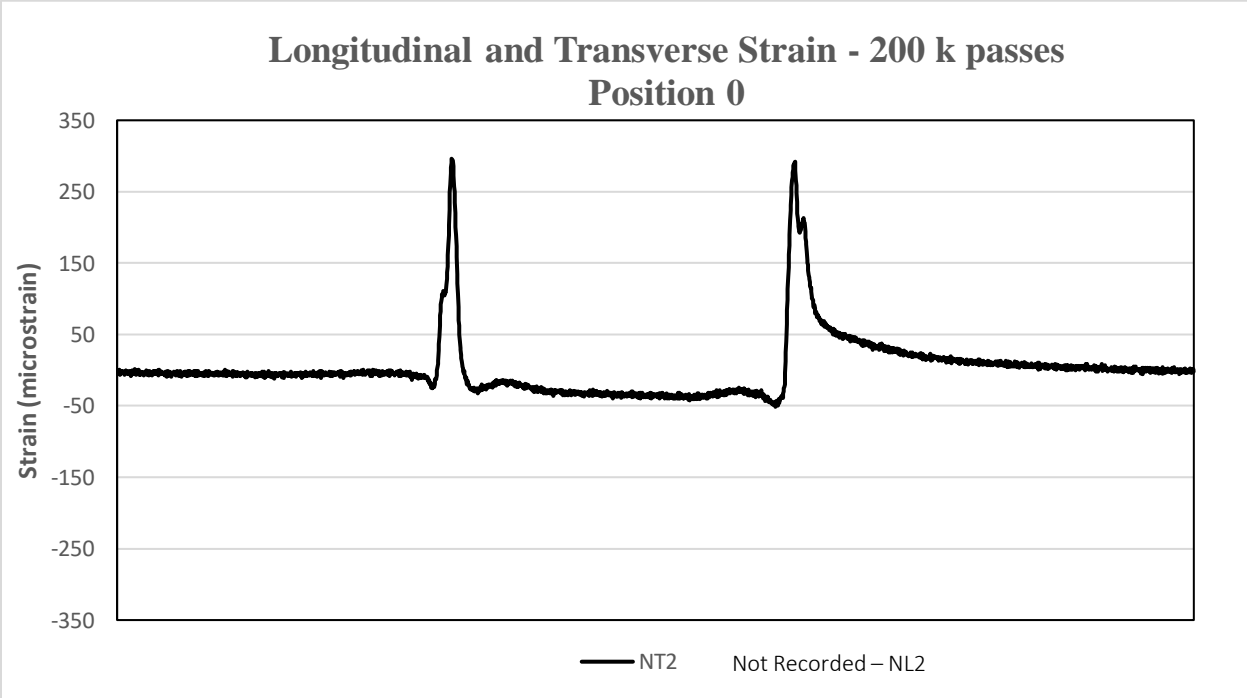


Figure D2-51 Strain Signals Recorded by NT2 – 200,000 passes

APPENDIX E

Hamburg Wheel Tracker Test Results

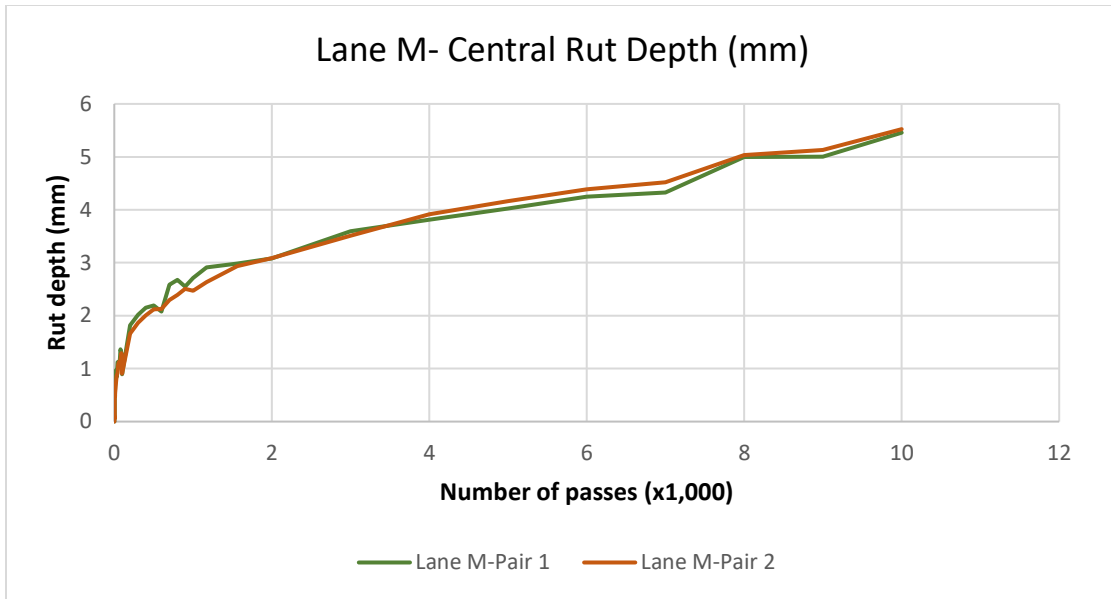


Figure E1. Central rut depth - Lane M&Q

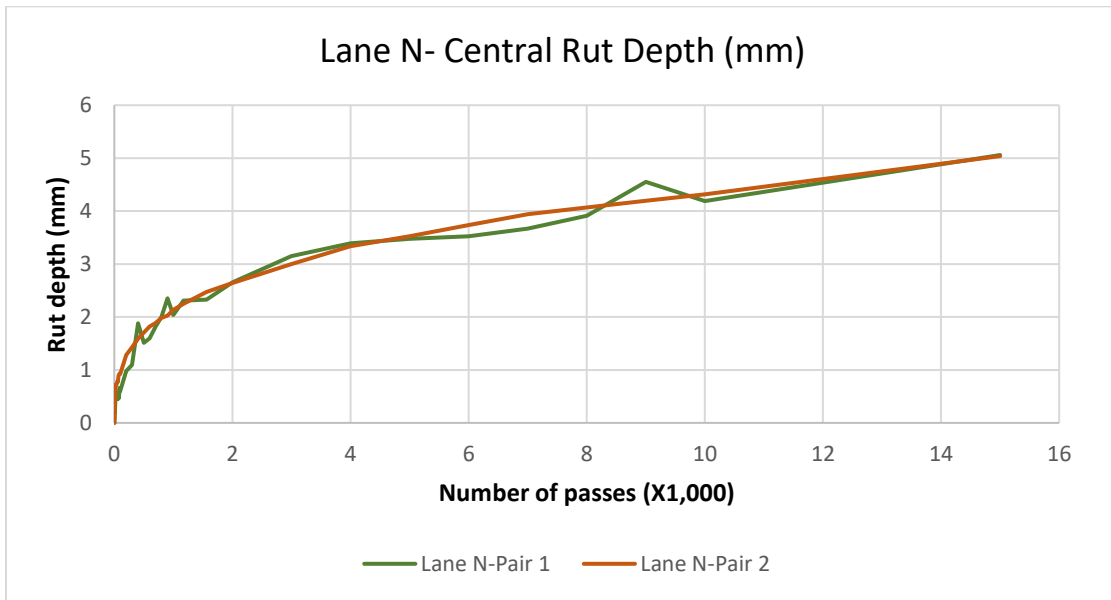


Figure E2. Central rut depth - Lane N

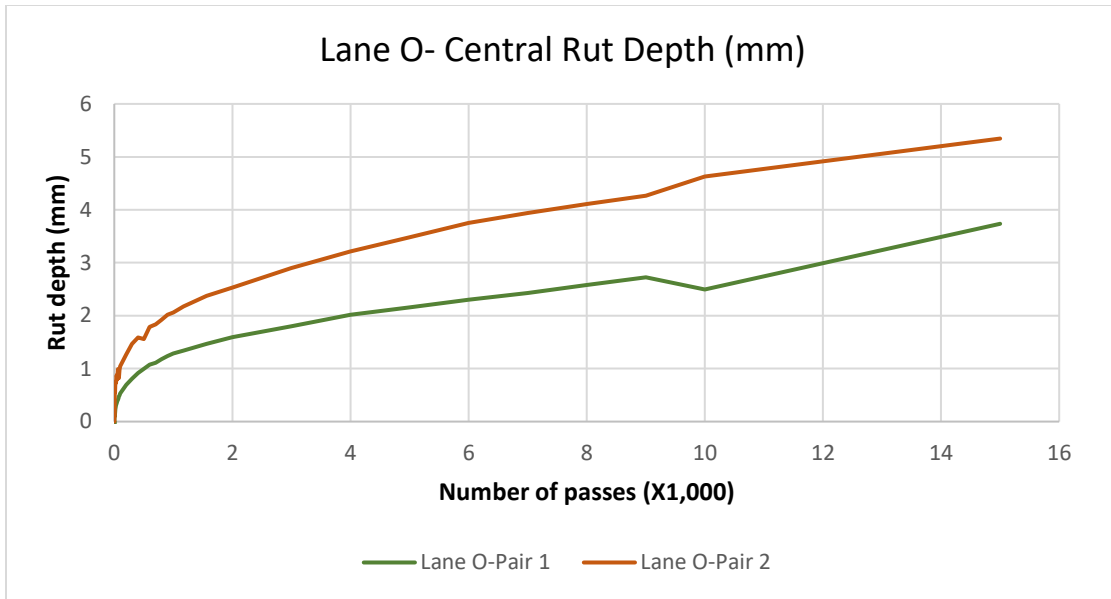


Figure E3. Central rut depth - Lane O

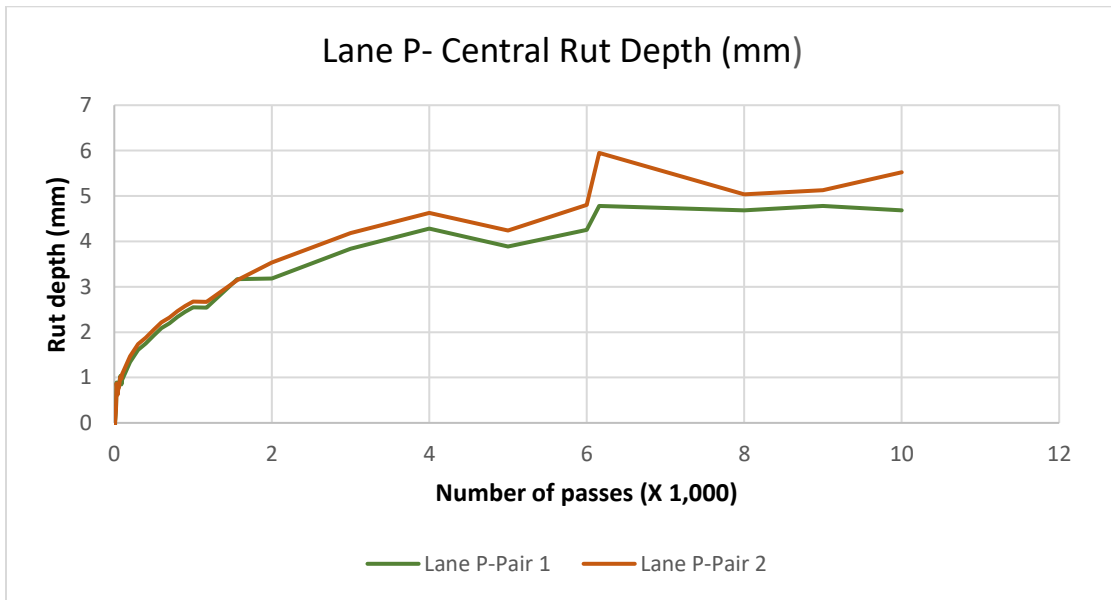


Figure E4. Central rut depth - Lane P

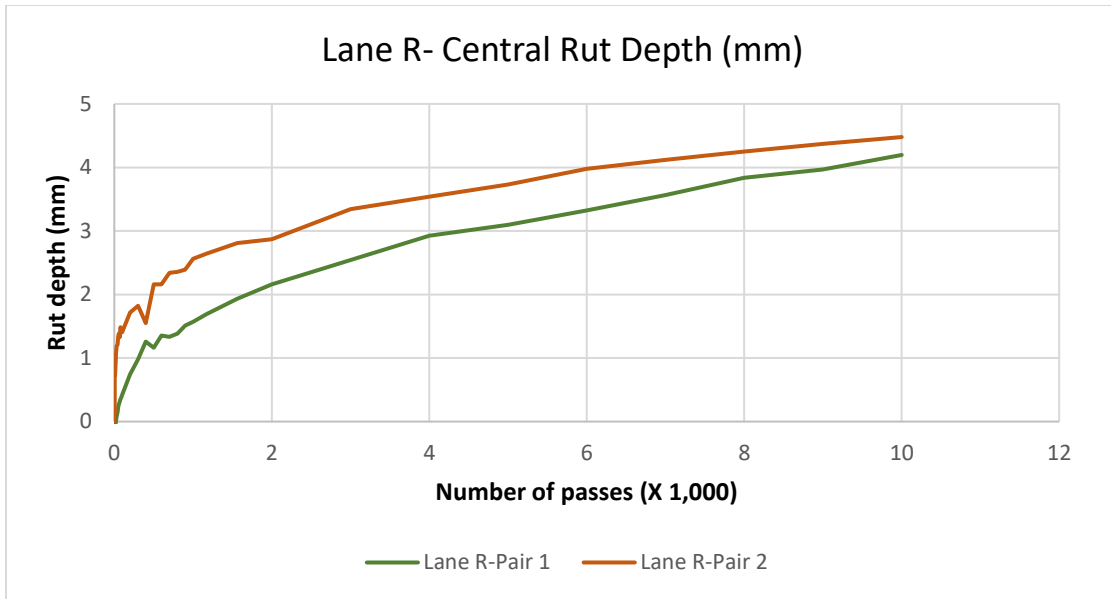


Figure E5. Central rut depth - Lane R

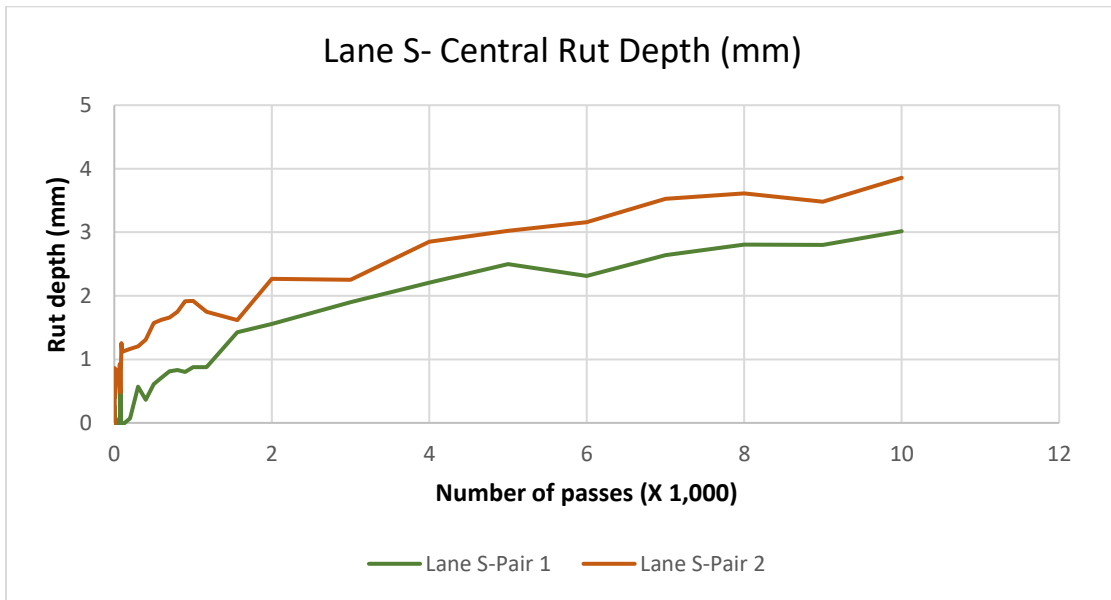


Figure E6. Central rut depth - Lane S

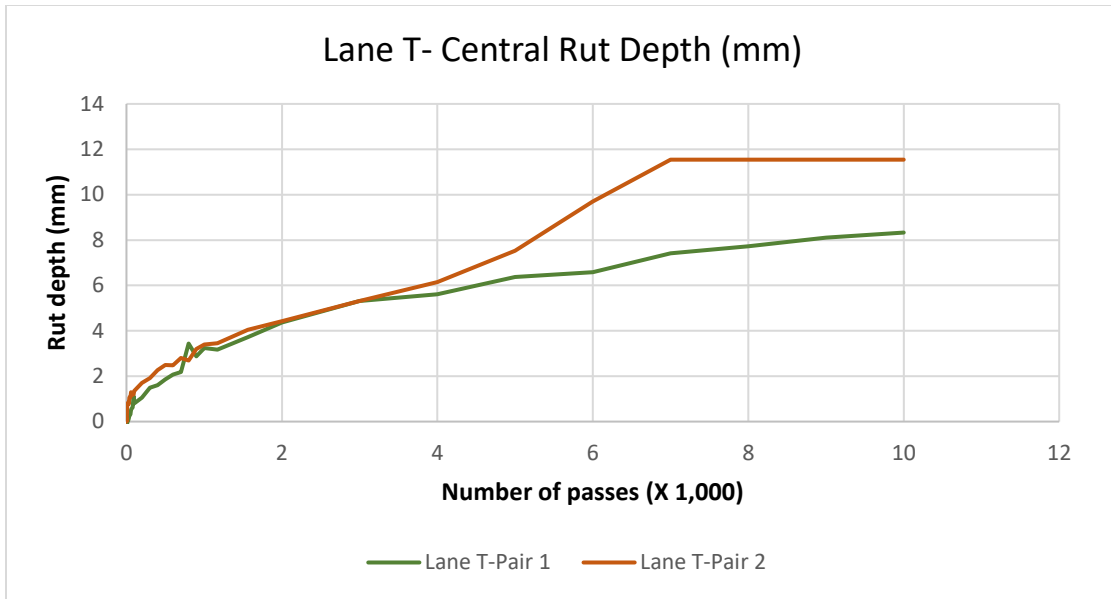


Figure E7. Central rut depth - Lane T

APPENDIX F

Dynamic Modulus Test Results

Table F1. Dynamic Modulus Results (MPa) – Lane M

Temp., C	Sample	Air Voids, %	25 Hz	20 Hz	10 Hz	5 Hz	2 Hz	1 Hz	0.5 Hz	0.2 Hz	0.1 Hz
15	M1	3.81	4289	13480	12004	10671	9027	7918	6862	5545	4727
	M2	3.89	15416	18788	16375	13725	11030	9442	8260	6806	5937
	M3	3.78	29401	16585	14720	12985	10980	9609	8404	6900	5938
20	M1	3.81	18800	12583	10747	9211	7484	6354	5437	4405	3771
	M2	3.89	25001	15085	12400	10256	8157	7013	6005	4750	4026
	M3	3.78	3260	12888	11208	9864	8166	7048	6001	4697	3841
25	M1	3.81	11972	10041	8305	7096	5649	4767	3901	2983	2431
	M2	3.89	14100	9014	7617	6405	5020	4226	3796	3540	3071
	M3	3.78	2399	12498	10975	9347	7442	6329	5344	4110	3342

Table F2. Phase Angle (Degrees) – Lane M

Temp., C	Sample	Air Voids, %	25 Hz	20 Hz	10 Hz	5 Hz	2 Hz	1 Hz	0.5 Hz	0.2 Hz	0.1 Hz
15	M1	3.81	37.3	18.23	18.4	18.82	20.04	21.19	22.31	23.83	24.77
	M2	3.89	28.05	30.73	29.48	26.78	24.95	24.9	26.5	28.56	29.6
	M3	3.78	79.19	18.6	19.4	19.71	20.62	21.22	22.2	23.72	24.44
20	M1	3.81	86.4	25.57	23.47	23.52	24.82	25.78	26.47	27.51	28.13
	M2	3.89	34.01	37.31	35	33.24	32.61	33.33	34.24	35.63	37.12
	M3	3.78	40.16	21.38	22.15	22.22	23.67	24.1	25.13	26.9	27.88
25	M1	3.81	65.11	31.64	29.51	28.86	29.81	30.93	31.88	32.71	33.51
	M2	3.89	42.74	26.27	27.93	28.3	28.62	29.6	32.79	35.9	32.83
	M3	3.78	8.63	28	33.3	32.78	30.72	32.74	33.76	33.92	34.1

Table F3. Dynamic Modulus Results (MPa) – Lane N

Temp., C	Sample	Air Voids, %	25 Hz	20 Hz	10 Hz	5 Hz	2 Hz	1 Hz	0.5 Hz	0.2 Hz	0.1 Hz
15	N1	2.81	5023	20369	18728	16315	13555	11771	10280	8253	7041
	N2	3.08	68182	20349	17006	14262	11394	10066	8843	7210	6025
	N3	2.99	40077	19273	17500	15410	12936	11343	9514	7652	6468
20	N1	2.81	17072.00	13665	11895	10330	8431	7367	6281	4839	4077
	N2	3.08	15390	14669	12840	11149	8953	7320	6306	10494	30787
	N3	2.99	70047	16054	13752	11802	9519	8017	6698	5190	4886
25	N1	2.81	1856	17688	14651	11224	8820	7194	5913	4736	3756
	N2	3.08	569.2	11957	8817	7566	5936	4849	3832	2722	2072
	N3	2.99	3833.3	15931	11185	9193	7238	6010	4893	3573	2803

Table F4. Phase Angle (Degrees) – Lane N

Temp., C	Sample	Air Voids, %	25 Hz	20 Hz	10 Hz	5 Hz	2 Hz	1 Hz	0.5 Hz	0.2 Hz	0.1 Hz
15	N1	2.81	47.8	27.32	27.94	26.75	26.07	26.32	27.93	29.35	30.33
	N2	3.08	47.16	30.43	27.62	24.99	24.22	25.26	26.72	27.43	28.62
	N3	2.99	23.68	23.79	26.01	26.37	27.12	28.62	29.83	31.26	32.66
20	N1	2.81	38.66	23.9	24.16	25.33	27.25	28.32	29.64	31.04	33.1
	N2	3.08	87.99	29.54	27.63	27.3	28.72	28.99	30.57	24.49	24.5
	N3	2.99	33.45	33.95	31.78	31.68	32.94	35.92	15.63	3.75	4.71
25	N1	2.81	5.82	4.95	11.69	44.15	42.37	40.56	41.27	45.39	44.09
	N2	3.08	14.91	92.76	26.16	26.35	27.1	27.76	29	30.06	30.73
	N3	2.99	0.98	42.6	38.42	36.58	36.14	35.96	36.2	35.5	37.01

Table F7 Dynamic Modulus Results (MPa) – Lane P

Temp., C	Sample	Air Voids, %	25 Hz	20 Hz	10 Hz	5 Hz	2 Hz	1 Hz	0.5 Hz	0.2 Hz	0.1 Hz
15	P1	3.97267696	7921.00	16887	15133	13117	11009	9398	8066	6060	5072
	P2	3.62	13227	14569	12787	11089	9057	7870	6738	5423	4502
	P3	3.98	9286	13232	11703	10285	8466	7245	6277	4997	4106
20	P1	3.97267696	18520.00	11859	10159	8702	6953	5843	4862	3769	3240
	P2	3.62	13227	14569	12787	11089	9057	7870	6738	5423	4502
	P3	3.98	9242	9589	8682	7359	5894	4935	4012	2987	2370
25	P1	3.97	4789	9017	7639	6409	5016	4108	3250	2379	1877
	P2	3.62	3753	7261	6088	5040	3920	3178	2456	1760	1371
	P3	3.98	7293	7283	6205	5097	3896	3117	2359	1648	1247

Table F8 Phase Angle (Degrees) – Lane O

Temp., C	Sample	Air Voids, %	25 Hz	20 Hz	10 Hz	5 Hz	2 Hz	1 Hz	0.5 Hz	0.2 Hz	0.1 Hz
15	P1	3.97	29.73	23.12	25.63	25.24	25.29	26.17	27.7	28.62	30.79
	P2	3.62	22.6	25.69	28.05	29.55	29.28	30.01	30.62	33.27	33.72
	P3	3.98	46.64	24.36	23.81	23.64	24.34	24.62	25.9	27.97	28.61
20	P1	3.97267696	21.77	25.52	25.03	25.61	26.92	27.63	28.57	30.13	32.27
	P2	3.62	22.6	25.69	28.05	29.55	29.28	30.01	30.62	33.27	33.72
	P3	3.98	132.51	25.59	25.91	26.05	27.17	28.01	28.92	30.08	30.42
25	P1	3.97	64.35	32.2	30.98	29.91	30.06	30.29	30.75	30.62	30.41
	P2	3.62	31.31	30.78	30.99	30.6	30.89	31.3	32.03	32.48	32.77
	P3	3.98	37.67	29.86	28.87	28.87	29.04	29.49	30.24	30.57	30.47

Table F9 Dynamic Modulus Results (MPa) – Lane R

Temp., C	Sample	Air Voids, %	25 Hz	20 Hz	10 Hz	5 Hz	2 Hz	1 Hz	0.5 Hz	0.2 Hz	0.1 Hz
15	R1	2.79	31947	17521	15642	13625	12090	10311	8991	7295	6313
	R2	2.51	3410	19383	17517	15671	12962	11337	9634	7892	6883
	R3	2.88	4410	13967	12540	11280	9755	9086	8256	7087	6437
20	R1	2.79	19626	14423	12078	10466	8633	7629	6496	5065	4262
	R2	2.51	16703	13468	11303	9651	7952	6852	5895	4757	4112
	R3	2.88	16244	12666	11597	10274	8653	7548	6523	5237	4427
25	R1	2.79	4429	13956	12150	10199	8141	6799	5699	4373	3677
	R2	2.51	12483	11659	9969	8466	6856	5798	4809	3701	3033
	R3	2.88	2901	11925	10122	8853	7197	6165	5136	4031	3345

Table F10 Phase Angle (Degrees) – Lane R

Temp., C	Sample	Air Voids, %	25 Hz	20 Hz	10 Hz	5 Hz	2 Hz	1 Hz	0.5 Hz	0.2 Hz	0.1 Hz
15	R1	2.79	57.12	26.91	20.88	20.77	20.67	22.42	23.93	25.59	26.61
	R2	2.51	47.97	21.95	21.72	20.66	14.84	20.35	22.12	24.5	26.12
	R3	2.88	21.92	20.74	20.6	20.08	20.77	21.49	22.84	25.06	26.61
20	R1	2.79	34.33	27.74	24.25	23.74	24.97	26.24	26.53	27.83	28.5
	R2	2.51	64.02	26.55	22.88	21.9	22.55	23.61	25.09	27.14	28.25
	R3	2.88	37.13	26.15	25.15	24.68	25.56	26.35	27.19	28.95	30.09
25	R1	2.79	7.65	38.13	36.39	36.53	36.75	36.9	38.28	40.96	42.28
	R2	2.51	11.6	22.08	23.13	24.23	25.44	26.38	27.44	29.27	29.95
	R3	2.88	61.01	38.26	32.58	32.7	34.37	35.2	36.34	37.37	37.92

Table F11 Dynamic Modulus Results (MPa) – Lane S

Temp., C	Sample	Air Voids, %	25 Hz	20 Hz	10 Hz	5 Hz	2 Hz	1 Hz	0.5 Hz	0.2 Hz	0.1 Hz
15	S1	3.27	25966	16255	14483	12827	10848	9501	8275	6849	6066
	S2	3.50	15240	14489	13569	12475	10895	9931	8907	7499	6657
	S3	3.29	13436	14407	12731	11402	9832	8827	7722	6602	5828
20	S1	3.27	2297	13697	12709	11319	9443	8415	7487	6090	5096
	S2	3.50	12670	12856	11938	10807	9151	8024	6962	5700	4908
	S3	3.29	15991	14237	12337	10925	9397	8435	7480	6162	5363
25	S1	3.27	2197	11081	9754	8502	7028	6089	5220	4139	3428
	S2	3.50	13412	12146	9900	8249	6718	5767	4868	3929	3358
	S3	3.29	10589	11947	10087	8397	6928	6021	5055	4055	3475

Table F12 Phase Angle (Degrees) – Lane S

Temp., C	Sample	Air Voids, %	25 Hz	20 Hz	10 Hz	5 Hz	2 Hz	1 Hz	0.5 Hz	0.2 Hz	0.1 Hz
15	S1	3.27	29.93	17.89	17.68	17.84	18.74	19.66	20.56	22.13	23.04
	S2	3.50	20.02	17.06	17.18	17.42	17.87	18.65	19.66	21.32	22.51
	S3	3.29	15.73	16.75	15.88	16.25	17.53	18.52	20.74	20.17	26.05
20	S1	3.27	34.82	22.39	27.32	27.95	29.48	30.87	32.93	34.97	35.67
	S2	3.50	20.68	18.98	19.18	19.62	21.03	22.11	23.18	24.52	25.43
	S3	3.29	26.83	22.65	21.77	20.85	20.78	21.23	22.24	23.81	24.77
25	S1	3.27	60.99	29.03	30.28	30.1	30.72	31.11	32.01	33.48	34.89
	S2	3.50	42.79	36.9	34.5	31.7	31.56	32.43	33.16	34.22	35.05
	S3	3.29	36.69	42.73	44.35	40.86	40.76	40	38.82	40.39	40.97

Table F13 Dynamic Modulus Results (MPa) – Lane T

Temp., C	Sample	Air Voids, %	25 Hz	20 Hz	10 Hz	5 Hz	2 Hz	1 Hz	0.5 Hz	0.2 Hz	0.1 Hz
15	T1	4.43	17115	12311	10255	8668	7129	6232	5437	4381	3748
	T2	4.31	1638	11570	10316	8731	7393	6345	5457	4271	3609
	T3	4.33	4095	15061	12642	10757	8550	7169	6023	4694	3948
20	T1	4.43	11024	10645	9138	7885	6380	5513	4694	3863	3357
	T2	4.31	13660	8329	7136	6072	4842	4055	3327	2551	2086
	T3	4.33	10164	11657	9658	8125	6629	5560	4705	3719	3072
25	T1	4.43	4160	7103	5875	4939	4086	3473	2873	2309	1946
	T2	4.31	9042	5898	4754	3918	3041	2484	2019	1545	1266
	T3	4.33	12831	8238	7154	6155	4924	4125	3365	2625	2019

Table F14 Phase Angle (Degrees) – Lane T

Temp., C	Sample	Air Voids, %	25 Hz	20 Hz	10 Hz	5 Hz	2 Hz	1 Hz	0.5 Hz	0.2 Hz	0.1 Hz
15	T1	4.43	49.54	37.84	34.98	32.92	33	33.79	35.45	38.43	40.37
	T2	4.31	21.68	26.93	31.97	31.72	32.1	33.22	34.09	36.1	37.92
	T3	4.33	18.25	28.06	27.13	26.34	26.09	25.12	27.96	30.07	31.49
20	T1	4.43	22.04	23.31	23.65	24.33	25.09	25.93	26.08	27.5	27.65
	T2	4.31	70.14	26.07	25.86	26.32	27.21	27.6	28.18	28.96	29.6
	T3	4.33	129.91	27.09	27.99	27.73	28.87	28.73	29.44	30.78	30.91
25	T1	4.43	59.39	37.33	35.65	33.14	34.4	34.55	35.69	37.78	38.86
	T2	4.31	2.87	33.19	32.12	32.8	33.64	34.16	34.33	35.05	35.36
	T3	4.33	63.21	28.06	29.02	28.84	28.62	28.55	29.26	30.25	30.15

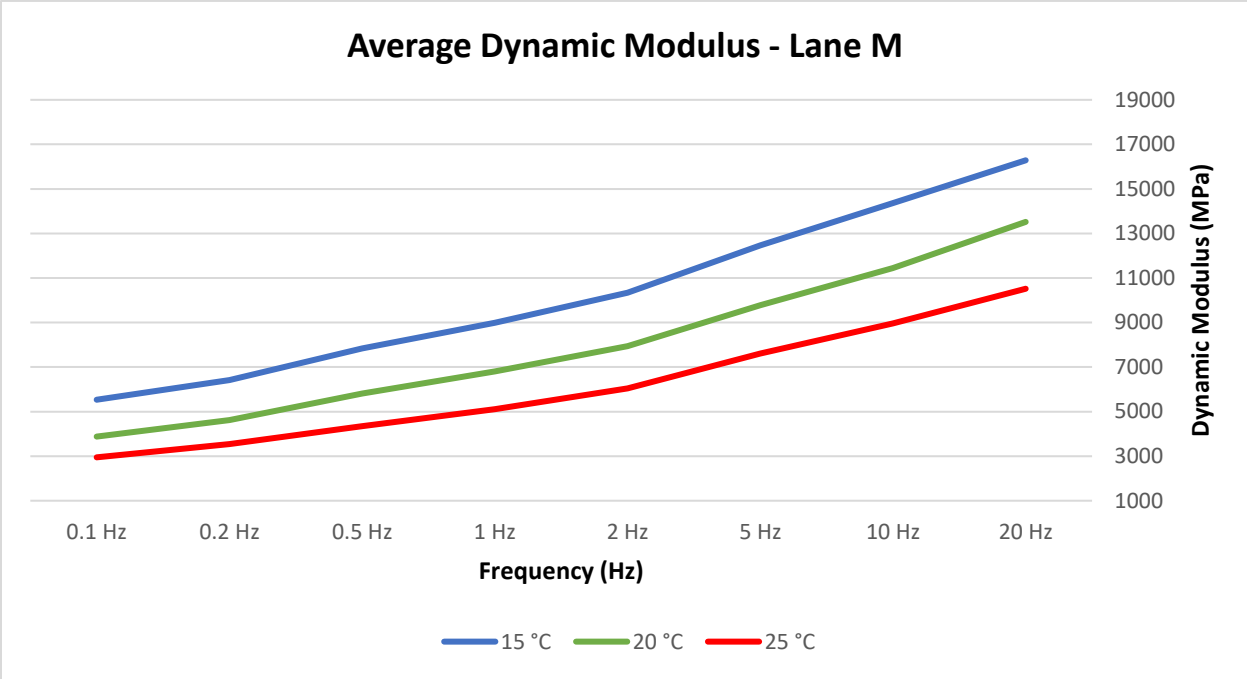


Figure F1. Dynamic Modulus -Lane M

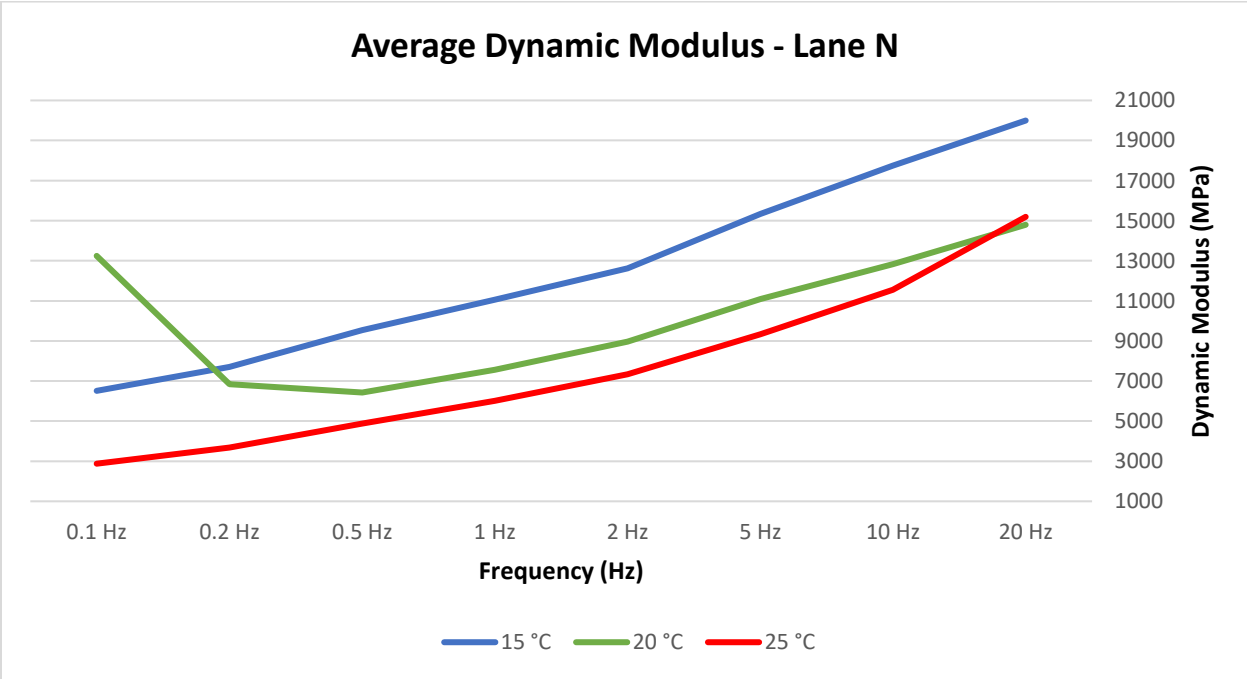


Figure F2. Dynamic Modulus -Lane N

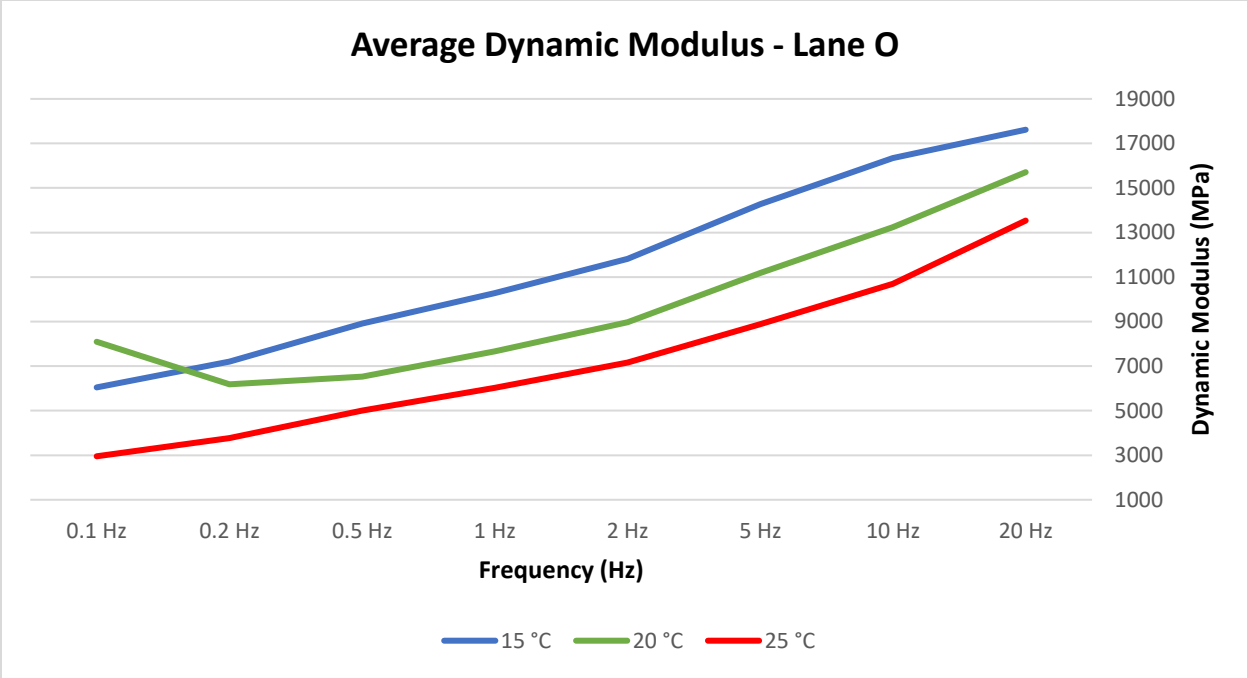


Figure F3. Dynamic Modulus -Lane O

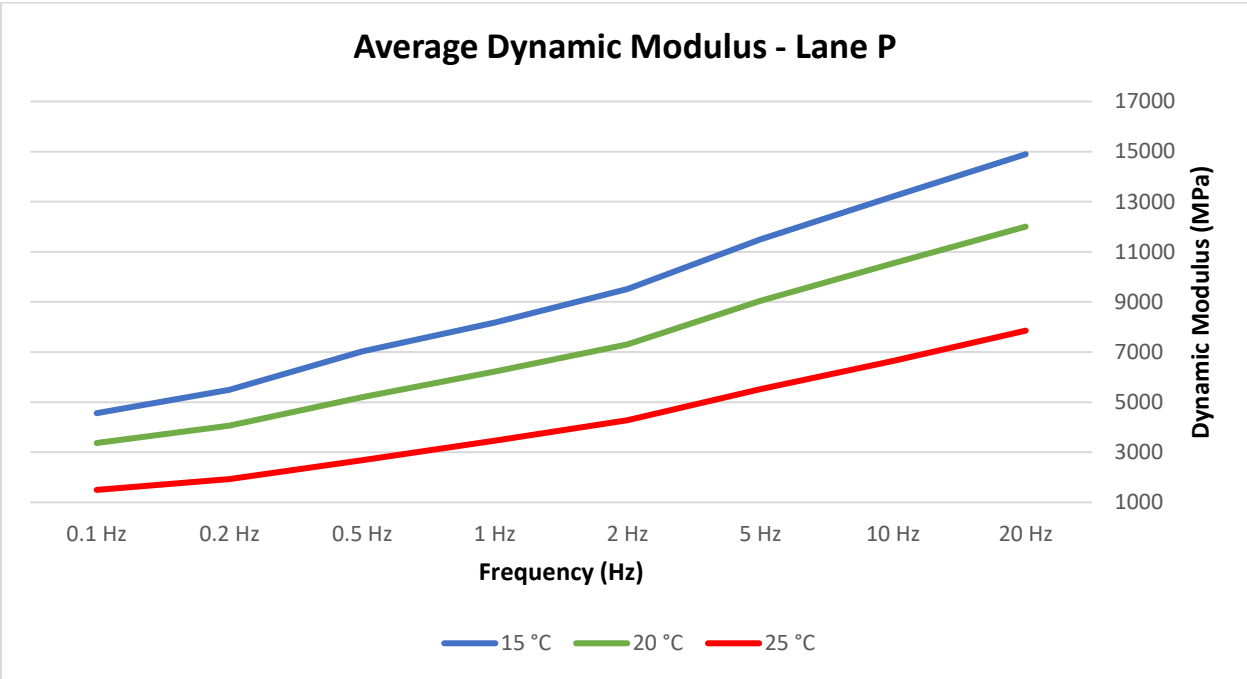


Figure F4. Dynamic Modulus -Lane P

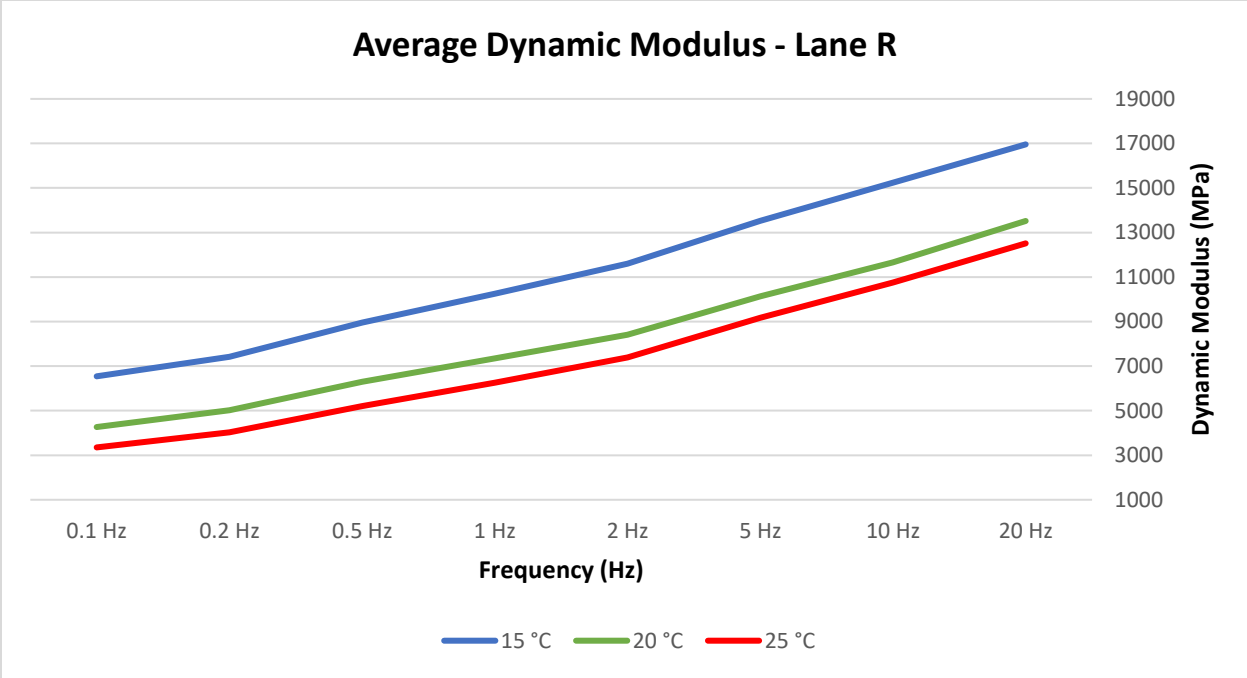


Figure F5. Dynamic Modulus -Lane R

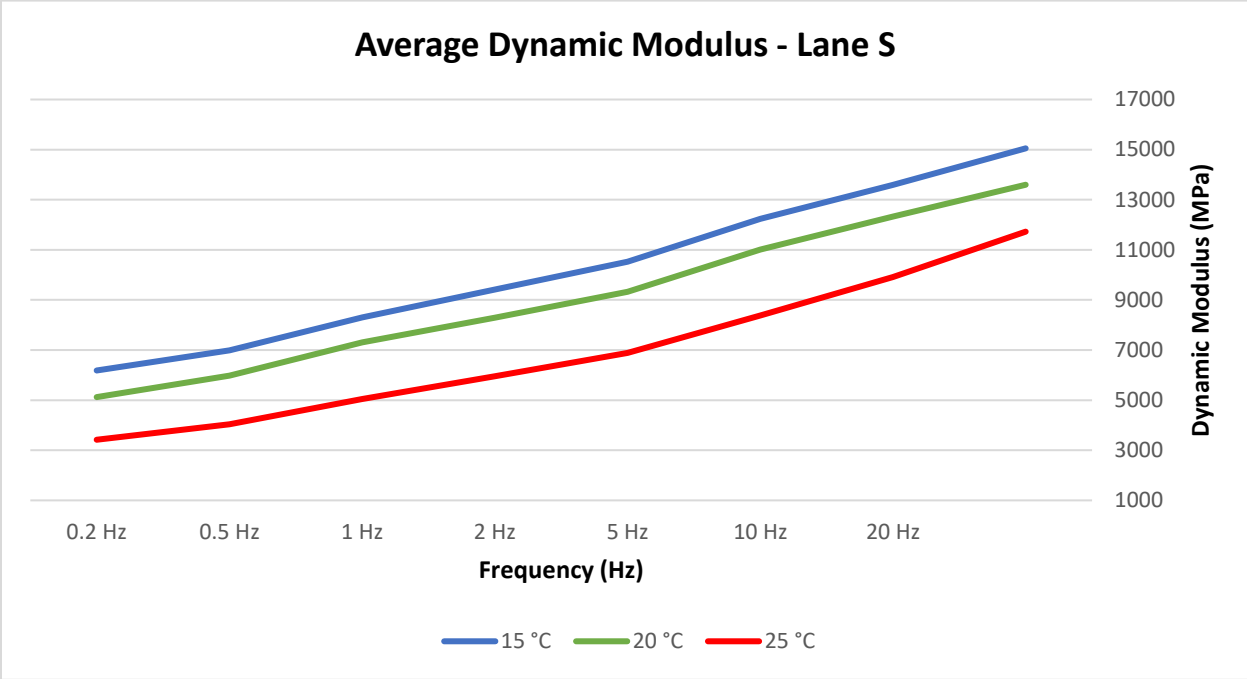


Figure F6. Dynamic Modulus -Lane S

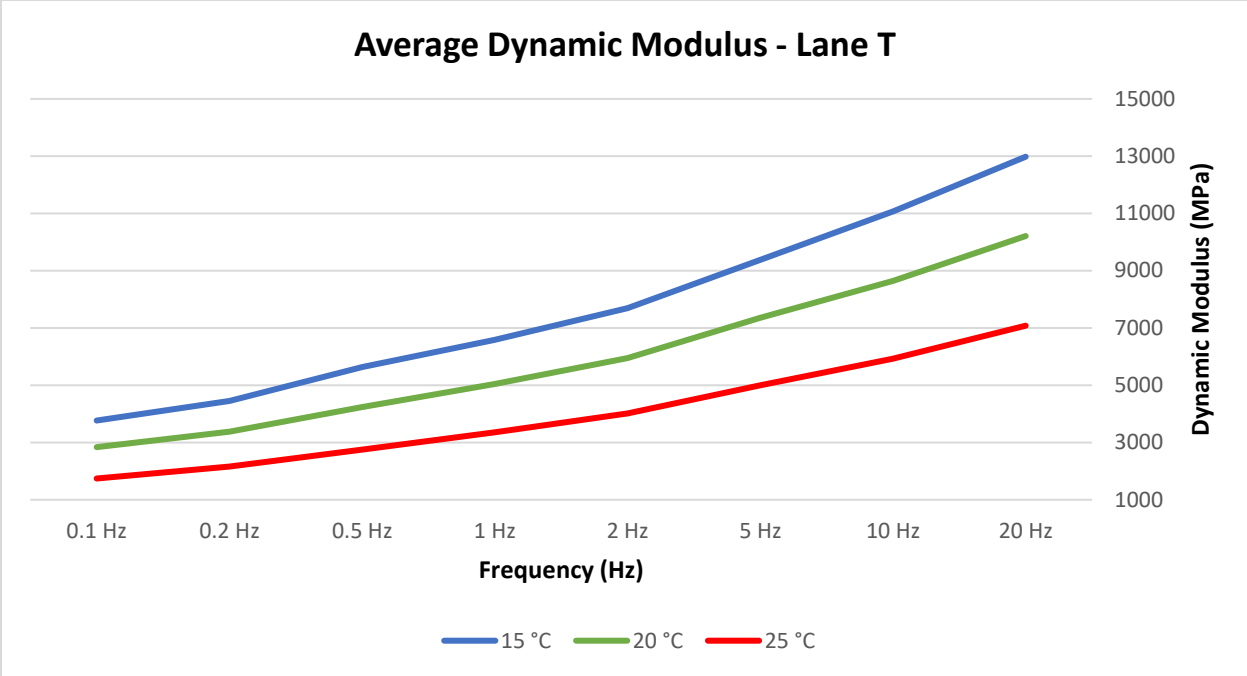


Figure F7. Dynamic Modulus -Lane T

APPENDIX G

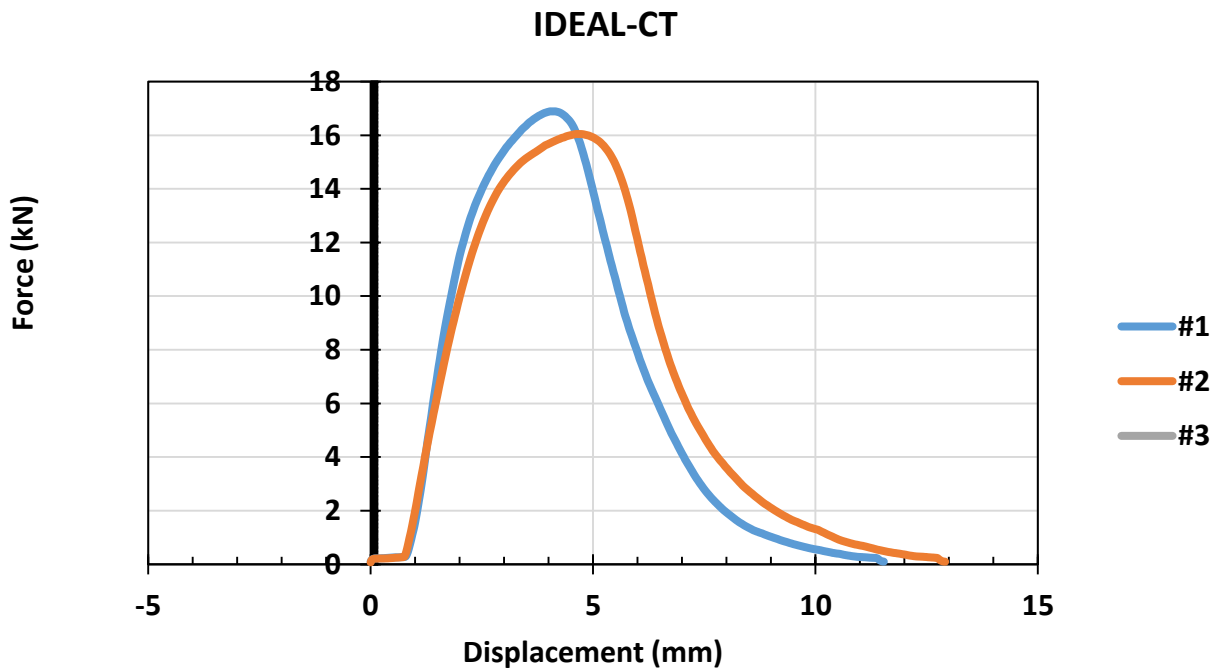
IDEAL CT Results

IDEAL-CT: Proposed Cracking Test

Project Name: Lane M	Institution: UTA
Mix Type: PG 64-22 15%RAP+2%RAS	Date Tested: 8/27/2021
Test Temperature: 75F	Technician: Ana Maria Coca

Specimen ID	1	2	3	Average	Standard Deviation	COV (%)
Air Voids (%)	4.9	5.9		5.4	0.7	13.0
Thickness (mm)	64.7	61.0		62.9	2.6	4.2
Diameter (mm)	151.6	151.4		151.5	0.1	0.1
Peak Load (kN)	16.9	16.0		16.5	0.6	3.6
Displacement (L), mm	5.2	6.0		5.6	0.6	10.4
Tensile Strength (kPa)	1096.2	1106.0		1101.1	6.9	0.6
Fracture Energy (LLD) (Gf) (J/m ²)	7706.2	9163.1		8434.7	1030.2	12.2
Slope (S)	6.61	7.01		6.81	0.28	4.2
Gf/S	1165.3	1306.3		1235.8	99.7	8.1
(Gf/S)*(L/D)	39.8	51.8		45.8	8.5	18.5
(Gf/S)*(L/D) ²	1.4	2.1		1.7	0.5	28.7

(Gf/S)*(L/D)	45.8	PASS
Minimum (Gf/S)*(L/D) Criteria		

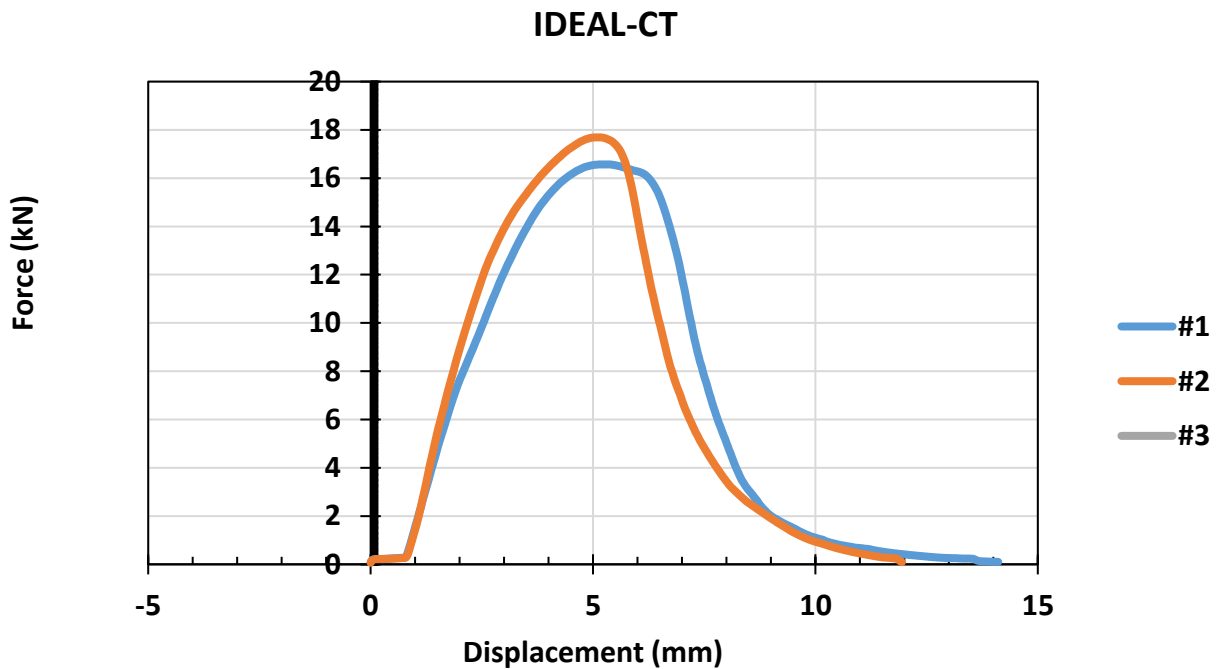


IDEAL-CT: Proposed Cracking Test

Project Name: Lane M	Institution: UTA
Mix Type: PH-64-22 (15%RAP +2%RAS)	Date Tested: 8/27/2021
Test Temperature: 75F	Technician: Ana Maria Coca

Specimen ID	1	2	3	Average	Standard Deviation	COV (%)
Air Voids (%)	6.0	4.2		5.1	1.3	24.6
Thickness (mm)	65.6	64.7		65.2	0.6	1.0
Diameter (mm)	150.7	151.5		151.1	0.6	0.4
Peak Load (kN)	16.6	17.7		17.1	0.8	4.6
Displacement (L), mm	6.9	6.1		6.5	0.6	8.8
TensileStrength(kPa)	1066.9	1148.9		1107.9	57.9	5.2
Fracture Energy (LLD) (Gf) (J/m ²)	9189.0	8849.5		9019.2	240.1	2.7
Slope (S)	8.09	9.48		8.78	0.98	11.2
Gf/S	1135.7	933.7		1034.7	142.8	13.8
(Gf/S)*(L/D)	52.3	37.7		45.0	10.3	22.9
(Gf/S)*(L/D) ²	2.4	1.5		2.0	0.6	31.8

(Gf/S)*(L/D)	45.0	PASS
Minimum (Gf/S)*(L/D) Criteria		

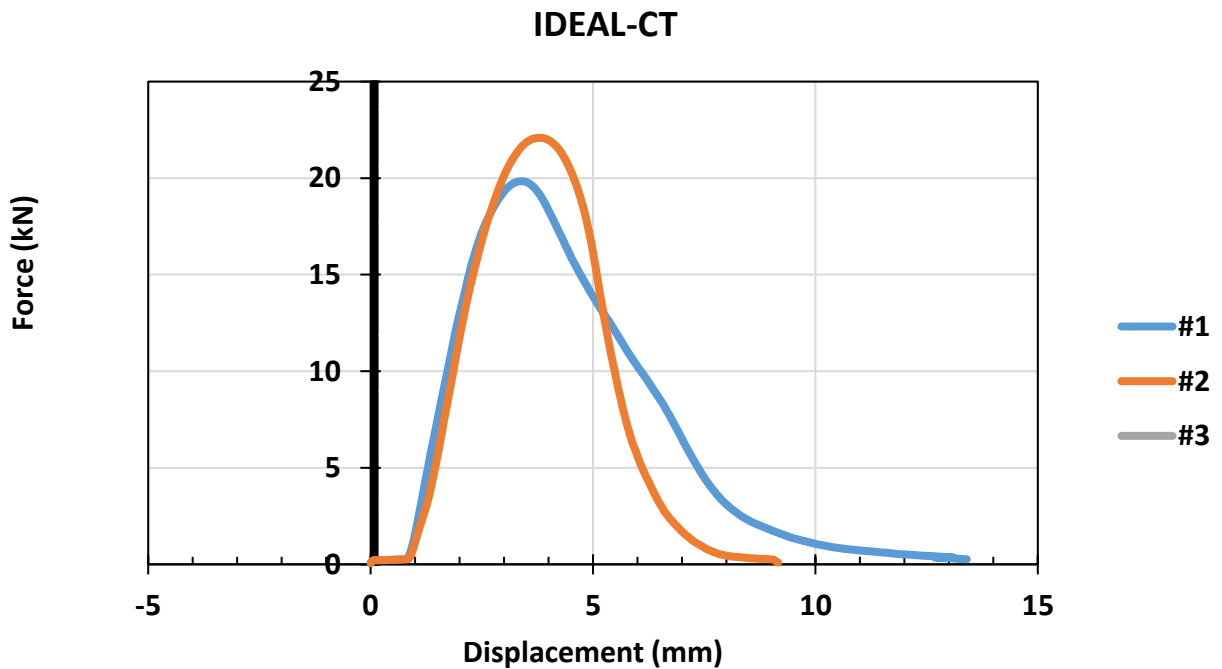


IDEAL-CT: Proposed Cracking Test

Project Name: Lane N	Institution: UTA
Mix Type: PG 70-22 (no RAP or RAS)	Date Tested: 8/27/2021
Test Temperature: 75F	Technician: Ana Maria Coca

Specimen ID	1	2	3	Average	Standard Deviation	COV (%)
Air Voids (%)	6.3	5.9		6.1	0.3	4.8
Thickness (mm)	64.5	64.8		64.7	0.2	0.3
Diameter (mm)	152.2	152.0		152.1	0.1	0.1
Peak Load (kN)	19.8	22.1		21.0	1.6	7.6
Displacement (L), mm	4.8	5.0		4.9	0.1	3.0
TensileStrength(kPa)	1286.5	1427.5		1357.0	99.7	7.3
Fracture Energy (LLD) (Gf) (J/m ²)	9261.1	8021.8		8641.5	876.3	10.1
Slope (S)	4.12	11.58		7.85	5.28	67.2
Gf/S	2249.7	692.8		1471.3	1100.9	74.8
(Gf/S)*(L/D)	70.3	22.6		46.5	33.7	72.6
(Gf/S)*(L/D) ²	2.2	0.7		1.5	1.0	70.3

(Gf/S)*(L/D)	46.5	PASS
Minimum (Gf/S)*(L/D) Criteria		



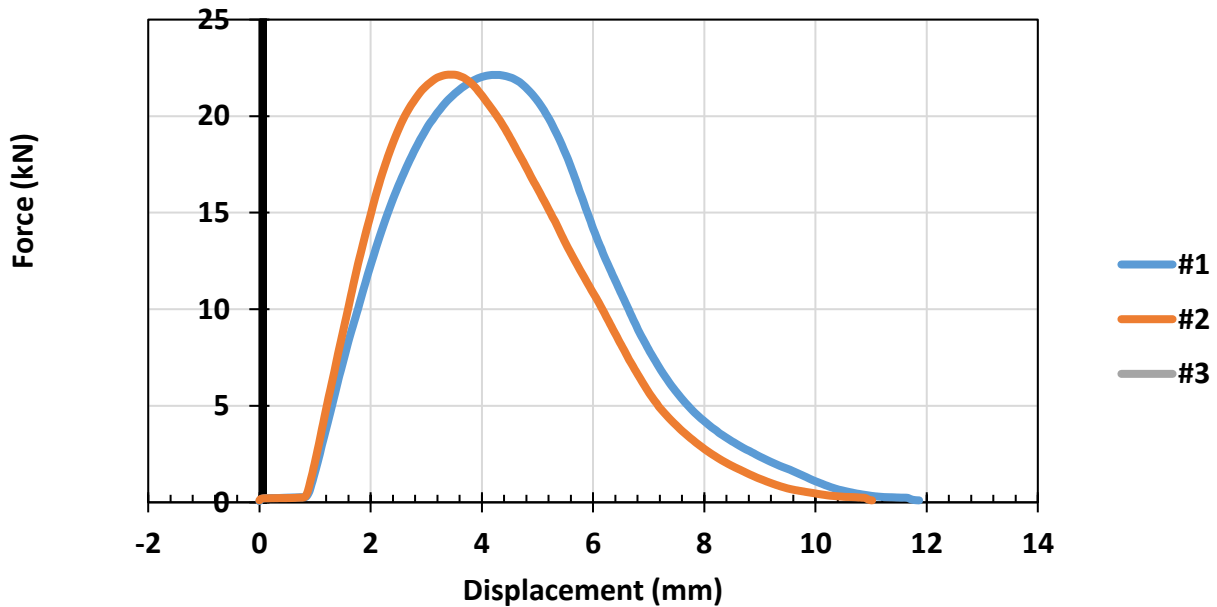
IDEAL-CT: Proposed Cracking Test

Project Name: Lane N	Institution: UTA
Mix Type: PG 70-22 (no RAP or RAS)	Date Tested: 8/27/2021
Test Temperature: 75F	Technician: Ana Maria Coca

Specimen ID	1	2	3	Average	Standard Deviation	COV (%)
Air Voids (%)	4.7	6.1		5.4	1.0	19.3
Thickness (mm)	65.5	64.0		64.8	1.1	1.6
Diameter (mm)	152.1	151.9		152.0	0.1	0.1
Peak Load (kN)	22.1	22.1		22.1	0.0	0.0
Displacement (L), mm	5.7	4.9		5.3	0.5	10.2
TensileStrength(kPa)	1414.3	1450.4		1432.3	25.5	1.8
Fracture Energy (LLD) (Gf) (J/m2)	10720.7	10031.8		10376.2	487.1	4.7
Slope (S)	7.71	5.37		6.54	1.65	25.3
Gf/S	1389.8	1866.4		1628.1	337.0	20.7
(Gf/S)*(L/D)	52.1	60.7		56.4	6.1	10.7
(Gf/S)*(L/D)^2	2.0	2.0		2.0	0.0	0.7

(Gf/S)*(L/D)	56.4	PASS
Minimum (Gf/S)*(L/D) Criteria		

IDEAL-CT



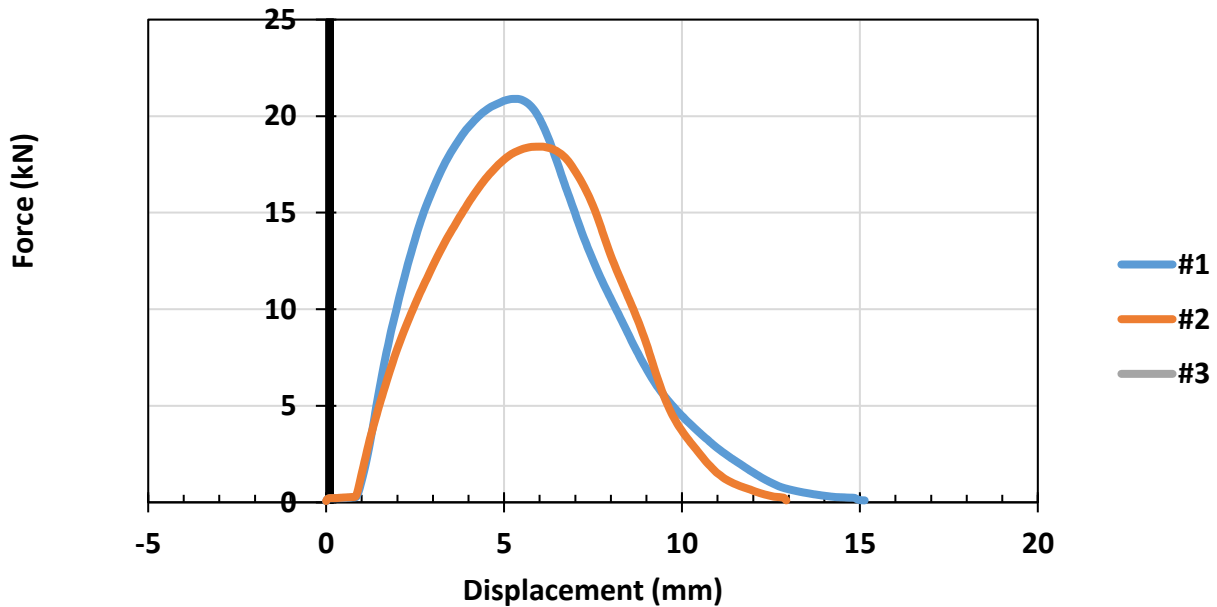
IDEAL-CT: Proposed Cracking Test

Project Name: Lane O	Institution: UTA
Mix Type: PG 70-22 (15%RAP)	Date Tested: 8/27/2021
Test Temperature: 75F	Technician: Ana Maria Coca

Specimen ID	1	2	3	Average	Standard Deviation	COV (%)
Air Voids (%)	4.2	3.9		4.1	0.2	5.9
Thickness (mm)	63.4	65.2		64.3	1.3	2.0
Diameter (mm)	152.5	152.0		152.3	0.4	0.2
Peak Load (kN)	20.9	18.4		19.7	1.7	8.9
Displacement (L), mm	6.9	7.8		7.3	0.7	9.2
TensileStrength(kPa)	1375.7	1183.2		1279.5	136.1	10.6
Fracture Energy (LLD) (Gf) (J/m2)	13489.1	11876.3		12682.7	1140.4	9.0
Slope (S)	5.21	5.10		5.16	0.08	1.5
Gf/S	2588.8	2328.7		2458.7	184.0	7.5
(Gf/S)*(L/D)	116.4	119.6		118.0	2.3	1.9
(Gf/S)*(L/D)^2	5.2	6.1		5.7	0.6	11.3

(Gf/S)*(L/D)	118.0	PASS
Minimum (Gf/S)*(L/D) Criteria		

IDEAL-CT

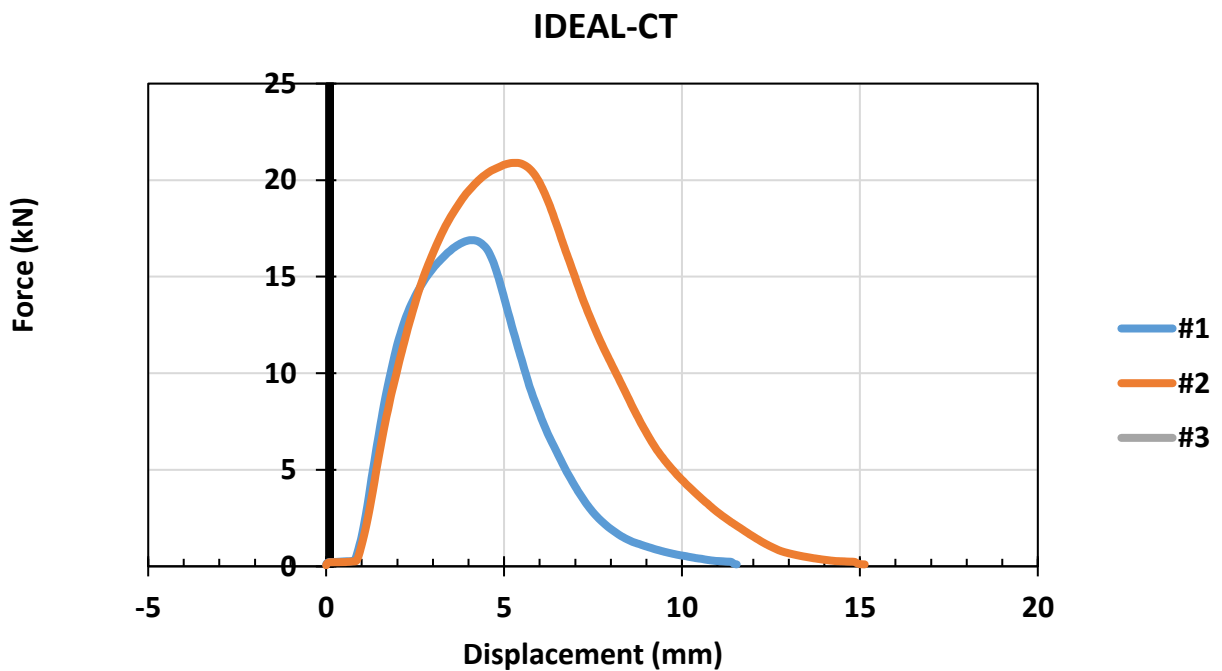


IDEAL-CT: Proposed Cracking Test

Project Name: Lane O	Institution: UTA
Mix Type: PG 70-22 (15%RAP)	Date Tested: 8/27/2021
Test Temperature: 75F	Technician: Ana Maria Coca

Specimen ID	1	2	3	Average	Standard Deviation	COV (%)
Air Voids (%)	4.5	3.6		4.1	0.6	14.5
Thickness (mm)	65.8	66.0		65.9	0.1	0.2
Diameter (mm)	152.2	152.1		152.2	0.1	0.0
Peak Load (kN)	16.9	20.9		18.9	2.8	15.0
Displacement (L), mm	5.2	6.9		6.0	1.2	19.7
TensileStrength(kPa)	1073.7	1324.8		1199.2	177.6	14.8
Fracture Energy (LLD) (Gf) (J/m2)	7547.5	12990.0		10268.8	3848.5	37.5
Slope (S)	6.61	5.21		5.91	0.99	16.8
Gf/S	1141.3	2493.1		1817.2	955.8	52.6
(Gf/S)*(L/D)	38.8	112.3		75.6	52.0	68.8
(Gf/S)*(L/D)^2	1.3	5.1		3.2	2.6	82.9

(Gf/S)*(L/D)	75.6	PASS
Minimum (Gf/S)*(L/D) Criteria		

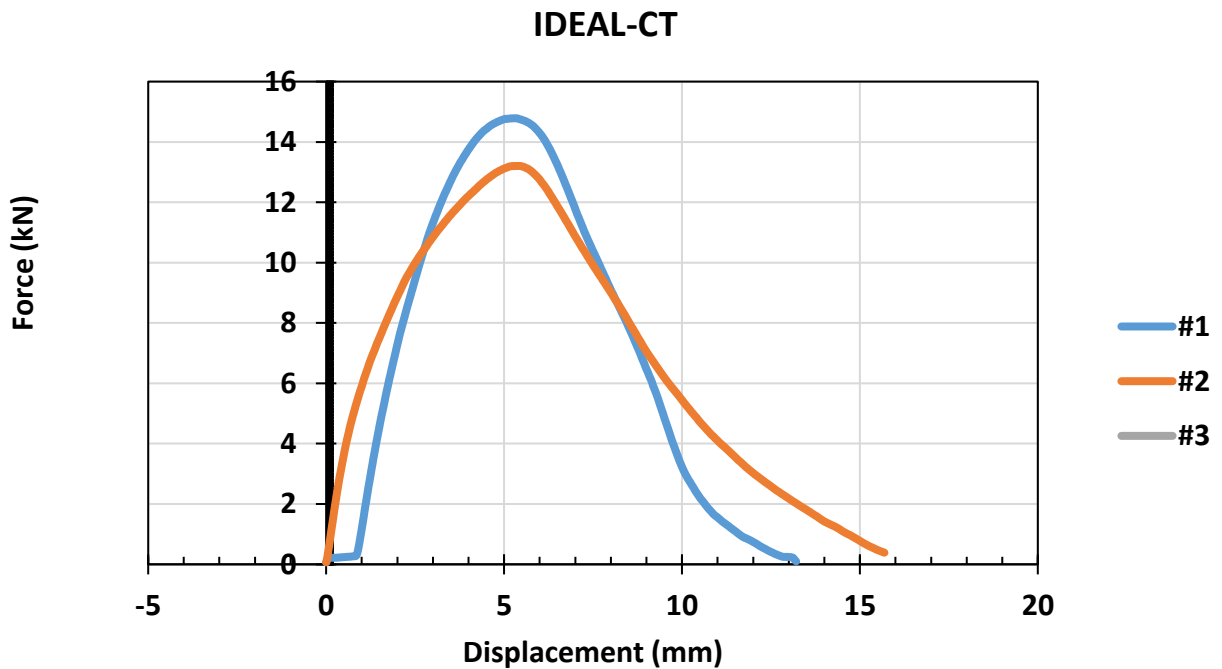


IDEAL-CT: Proposed Cracking Test

Project Name: Lane P	Institution: UTA
Mix Type: PG 64-28 (15%RAP+BMD)	Date Tested: 8/27/2021
Test Temperature: 75F	Technician: Ana Maria Coca

Specimen ID	1	2	3	Average	Standard Deviation	COV (%)
Air Voids (%)	3.6	3.5		3.5	0.0	1.4
Thickness (mm)	67.5	66.2		66.9	0.9	1.4
Diameter (mm)	149.6	149.6		149.6	0.0	0.0
Peak Load (kN)	14.8	13.2		14.0	1.1	8.0
Displacement (L), mm	7.2	7.5		7.4	0.2	2.7
TensileStrength(kPa)	932.0	848.7		890.4	58.9	6.6
Fracture Energy (LLD) (Gf) (J/m2)	9504.8	10947.4		10226.1	1020.1	10.0
Slope (S)	2.78	1.87		2.32	0.65	27.8
Gf/S	3418.7	5864.6		4641.6	1729.5	37.3
(Gf/S)*(L/D)	165.2	294.4		229.8	91.4	39.7
(Gf/S)*(L/D)^2	8.0	14.8		11.4	4.8	42.2

(Gf/S)*(L/D)	229.8	PASS
Minimum (Gf/S)*(L/D) Criteria		

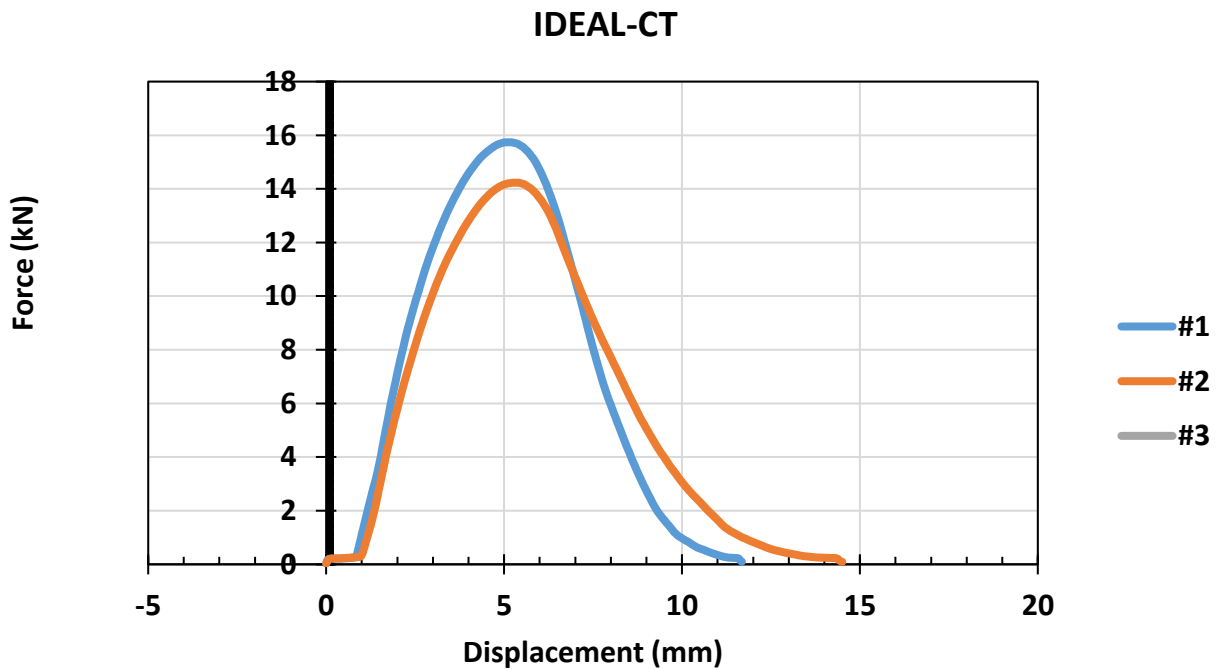


IDEAL-CT: Proposed Cracking Test

Project Name: Lane P	Institution: UTA
Mix Type: PG 64-28 (15%RAP+BMD)	Date Tested: 8/27/2021
Test Temperature: 75F	Technician: Ana Maria Coca

Specimen ID	1	2	3	Average	Standard Deviation	COV (%)
Air Voids (%)	3.6	2.4		3.0	0.8	27.1
Thickness (mm)	65.0	64.0		64.5	0.7	1.1
Diameter (mm)	149.8	149.9		149.9	0.1	0.0
Peak Load (kN)	15.7	14.2		15.0	1.1	7.1
Displacement (L), mm	6.7	7.0		6.9	0.2	2.7
TensileStrength(kPa)	1028.5	943.9		986.2	59.8	6.1
Fracture Energy (LLD) (Gf) (J/m2)	8805.7	9056.0		8930.8	177.0	2.0
Slope (S)	4.72	3.25		3.99	1.04	26.1
Gf/S	1864.7	2785.4		2325.0	651.0	28.0
(Gf/S)*(L/D)	84.0	130.2		107.1	32.7	30.5
(Gf/S)*(L/D)^2	3.8	6.1		4.9	1.6	33.0

(Gf/S)*(L/D)	107.1	PASS
Minimum (Gf/S)*(L/D) Criteria		

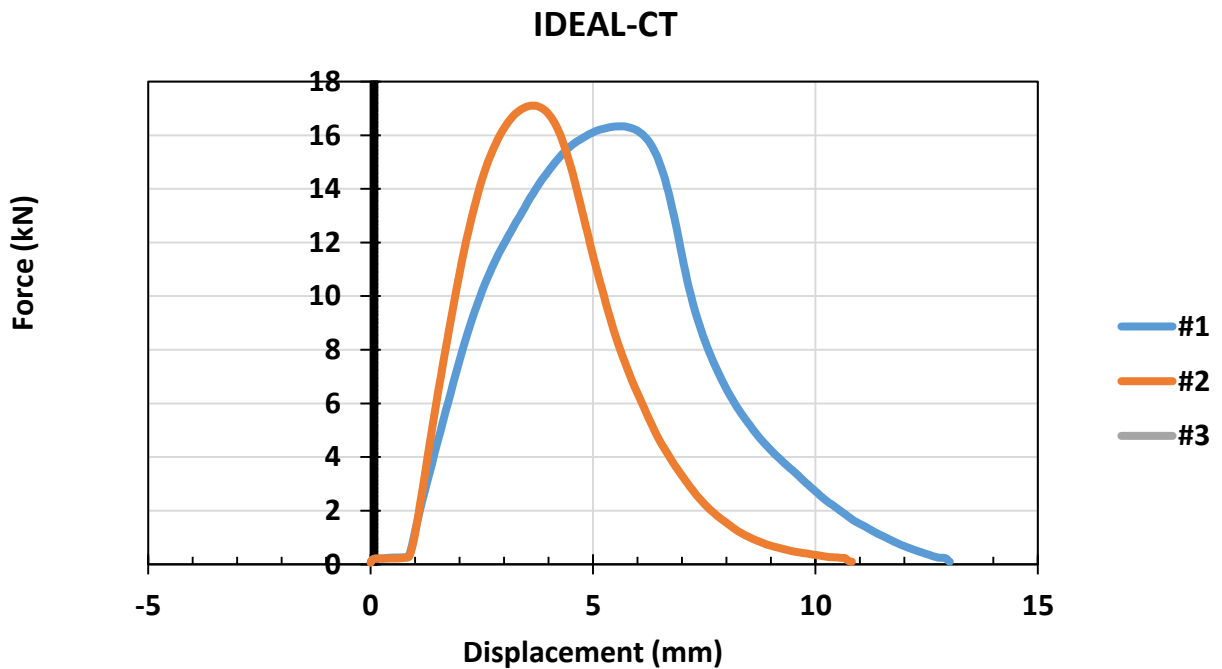


IDEAL-CT: Proposed Cracking Test

Project Name: Lane Q	Institution: UTA
Mix Type: PG 64-22 15% RAP+2%RAS	Date Tested: 8/27/2021
Test Temperature: 75F	Technician: Ana Maria Coca

Specimen ID	1	2	3	Average	Standard Deviation	COV (%)
Air Voids (%)	5.0	5.8		5.4	0.6	10.2
Thickness (mm)	64.4	63.8		64.1	0.4	0.7
Diameter (mm)	152.4	152.7		152.6	0.2	0.1
Peak Load (kN)	16.3	17.1		16.7	0.5	3.3
Displacement (L), mm	6.9	4.8		5.9	1.5	25.4
Tensile Strength (kPa)	1059.4	1117.6		1088.5	41.2	3.8
Fracture Energy (LLD) (Gf) (J/m2)	9728.7	7126.4		8427.6	1840.1	21.8
Slope (S)	7.95	6.72		7.34	0.87	11.8
Gf/S	1223.8	1059.9		1141.9	115.9	10.2
(Gf/S)*(L/D)	55.5	33.4		44.4	15.7	35.2
(Gf/S)*(L/D)^2	2.5	1.0		1.8	1.0	58.2

(Gf/S)*(L/D)	44.4	PASS
Minimum (Gf/S)*(L/D) Criteria		

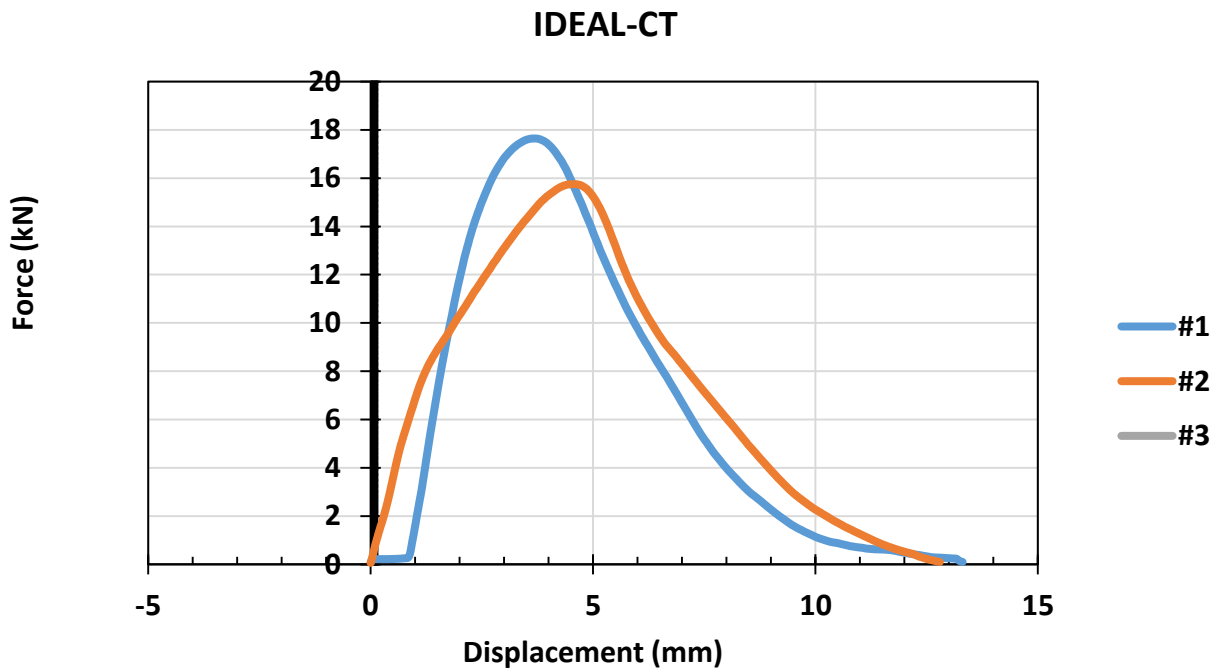


IDEAL-CT: Proposed Cracking Test

Project Name: Lane Q	Institution: UTA
Mix Type: PG 64-22 15% RAP+2%RAS	Date Tested: 8/27/2021
Test Temperature: 75F	Technician: Ana Maria Coca

Specimen ID	3	4	Average	Standard Deviation	COV (%)
Air Voids (%)	3.4	4.8	4.1	1.0	24.8
Thickness (mm)	65.5	66.5	66.0	0.7	1.1
Diameter (mm)	152.9	152.6	152.8	0.2	0.1
Peak Load (kN)	17.6	15.7	16.7	1.3	8.0
Displacement (L), mm	5.1	5.8	5.4	0.5	8.7
Tensile Strength (kPa)	1121.5	988.0	1054.7	94.4	8.9
Fracture Energy (LLD) (Gf) (J/m ²)	8692.5	9322.7	9007.6	445.6	4.9
Slope (S)	4.44	4.08	4.26	0.25	6.0
Gf/S	1958.9	2285.8	2122.4	231.2	10.9
(Gf/S)*(L/D)	65.5	86.6	76.1	15.0	19.7
(Gf/S)*(L/D) ²	2.2	3.3	2.7	0.8	28.3

(Gf/S)*(L/D)	76.1	PASS
Minimum (Gf/S)*(L/D) Criteria		

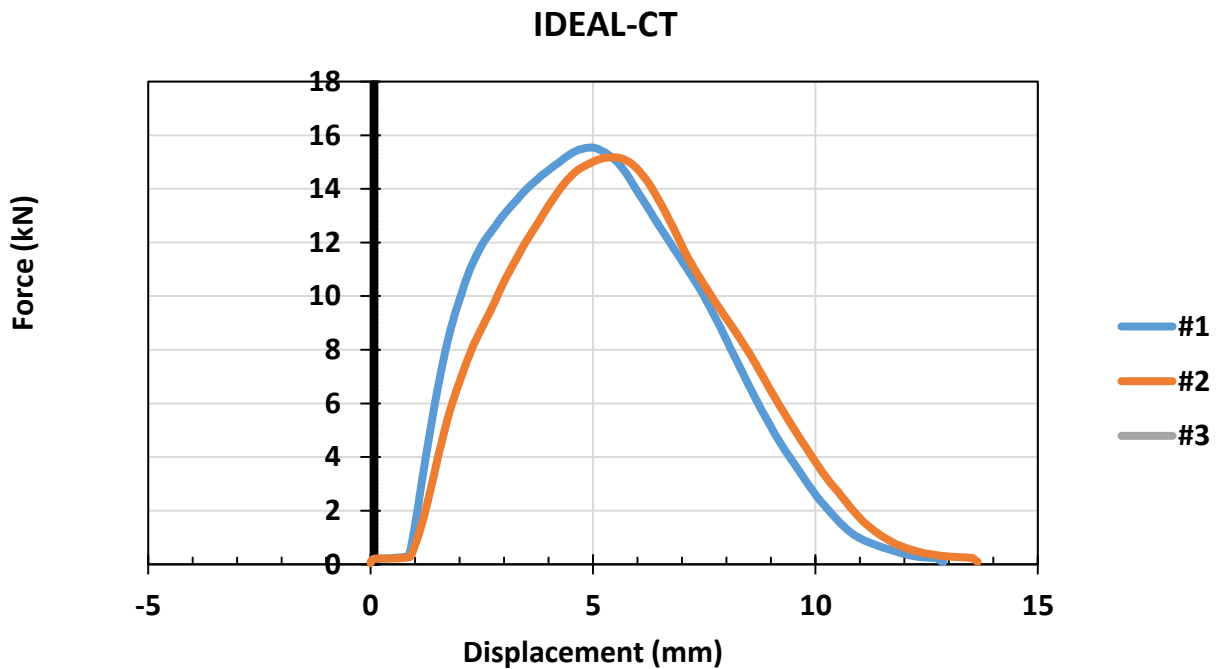


IDEAL-CT: Proposed Cracking Test

Project Name: Lane R	Institution: UTA
Mix Type: PG 64-22 25% RAP+BMD	Date Tested: 8/27/2021
Test Temperature: 75F	Technician: Ana Maria Coca

Specimen ID	1	2	5	Average	Standard Deviation	COV (%)
Air Voids (%)	3.9	4.6		4.3	0.5	11.1
Thickness (mm)	65.0	64.5		64.8	0.4	0.5
Diameter (mm)	153.5	153.0		153.3	0.4	0.2
Peak Load (kN)	15.5	15.2		15.4	0.3	1.7
Displacement (L), mm	6.9	7.2		7.0	0.2	3.0
Tensile Strength (kPa)	991.6	978.8		985.2	9.0	0.9
Fracture Energy (LLD) (Gf) (J/m ²)	9822.4	9684.5		9753.5	97.5	1.0
Slope (S)	2.57	2.97		2.77	0.29	10.3
Gf/S	3824.8	3257.3		3541.0	401.3	11.3
(Gf/S)*(L/D)	171.0	152.4		161.7	13.2	8.1
(Gf/S)*(L/D) ²	7.6	7.1		7.4	0.4	4.9

(Gf/S)*(L/D)	161.7	PASS
Minimum (Gf/S)*(L/D) Criteria		

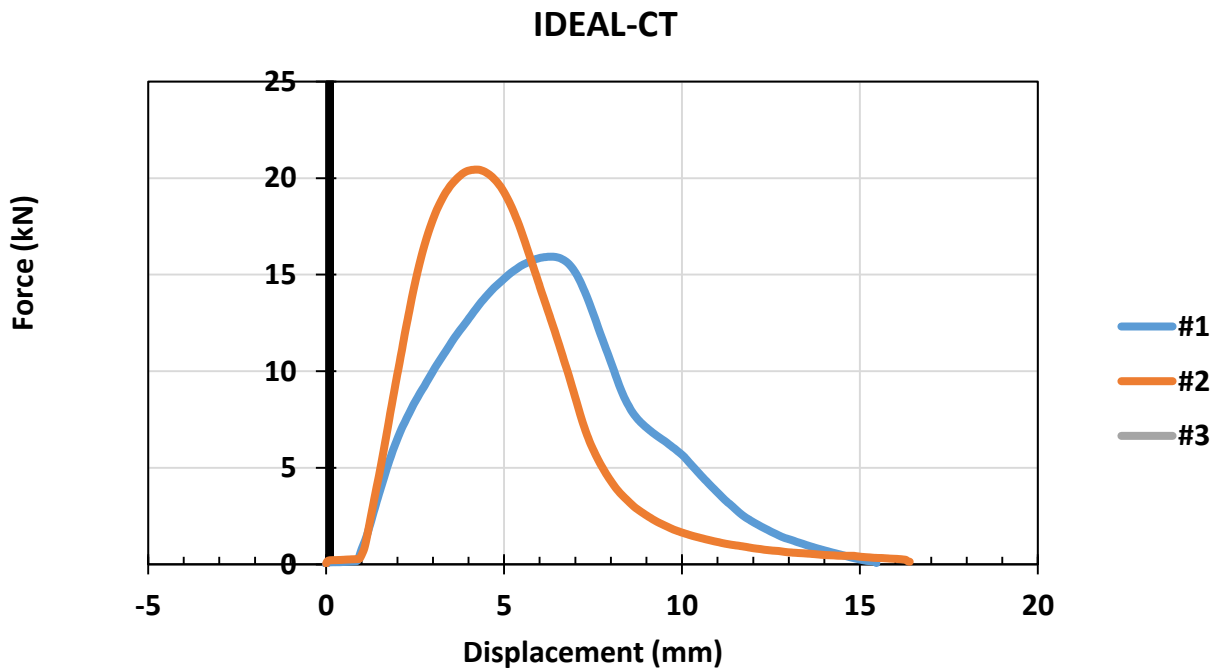


IDEAL-CT: Proposed Cracking Test

Project Name: Lane R	Institution: UTA
Mix Type: PG 64-22 25% RAP+BMD	Date Tested: 8/27/2021
Test Temperature: 75F	Technician: Ana Maria Coca

Specimen ID	1	2	5	Average	Standard Deviation	COV (%)
Air Voids (%)	3.1	4.5		3.8	1.0	25.5
Thickness (mm)	63.2	65.0		64.1	1.3	2.0
Diameter (mm)	152.8	152.7		152.8	0.1	0.0
Peak Load (kN)	15.9	20.4		18.2	3.2	17.5
Displacement (L), mm	7.7	5.8		6.8	1.3	19.7
Tensile Strength (kPa)	1050.3	1311.2		1180.7	184.5	15.6
Fracture Energy (LLD) (Gf) (J/m ²)	11103.0	10445.8		10774.4	464.8	4.3
Slope (S)	5.07	5.52		5.29	0.32	6.1
Gf/S	2192.1	1892.6		2042.3	211.8	10.4
(Gf/S)*(L/D)	110.6	72.2		91.4	27.1	29.7
(Gf/S)*(L/D) ²	5.6	2.8		4.2	2.0	47.9

(Gf/S)*(L/D)	91.4	PASS
Minimum (Gf/S)*(L/D) Criteria		

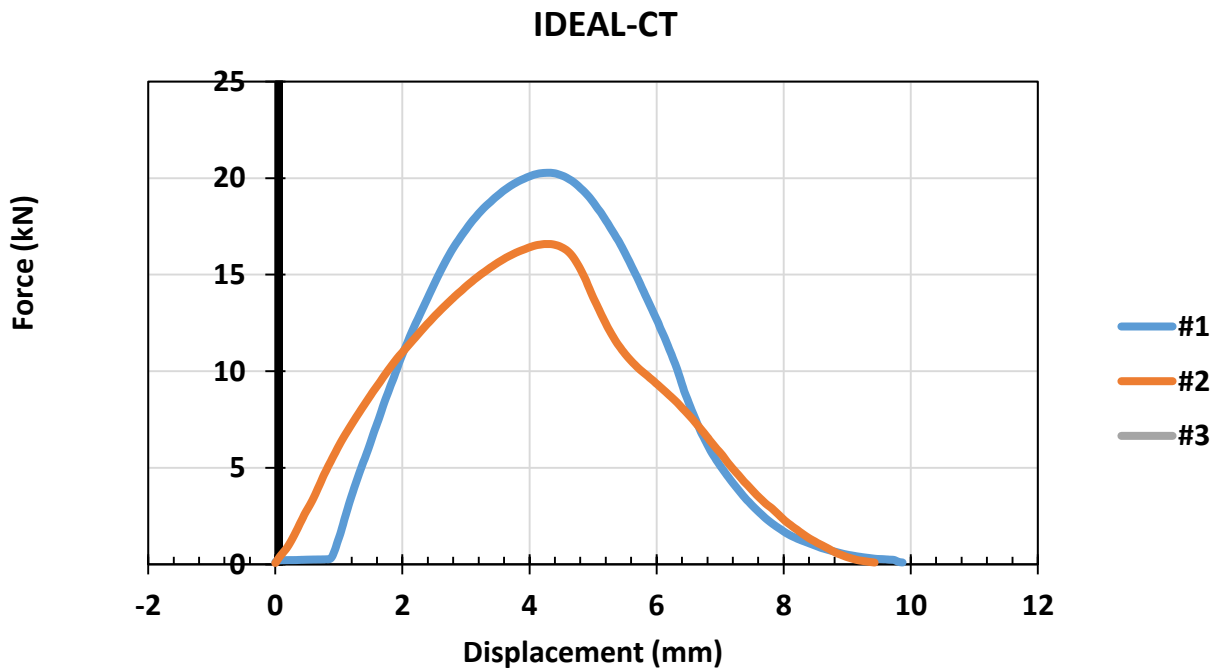


IDEAL-CT: Proposed Cracking Test

Project Name: Lane S	Institution: UTA
Mix Type: PG 64-22 15%RAP+2%RAS+BMD	Date Tested: 8/27/2021
Test Temperature: 75F	Technician: Ana Maria Coca

Specimen ID	1	2	3	Average	Standard Deviation	COV (%)
Air Voids (%)	4.6	5.3		4.9	0.5	11.0
Thickness (mm)	65.1	64.5		64.8	0.4	0.7
Diameter (mm)	151.7	151.9		151.8	0.1	0.1
Peak Load (kN)	20.3	16.6		18.4	2.6	14.2
Displacement (L), mm	5.6	5.2		5.4	0.3	5.6
Tensile Strength (kPa)	1307.1	1077.8		1192.4	162.2	13.6
Fracture Energy (LLD) (Gf) (J/m2)	9006.3	8164.9		8585.6	594.9	6.9
Slope (S)	6.62	5.90		6.26	0.51	8.2
Gf/S	1359.8	1384.9		1372.4	17.7	1.3
(Gf/S)*(L/D)	50.6	47.5		49.0	2.2	4.4
(Gf/S)*(L/D)^2	1.9	1.6		1.8	0.2	10.2

(Gf/S)*(L/D)	49.0	PASS
Minimum (Gf/S)*(L/D) Criteria		

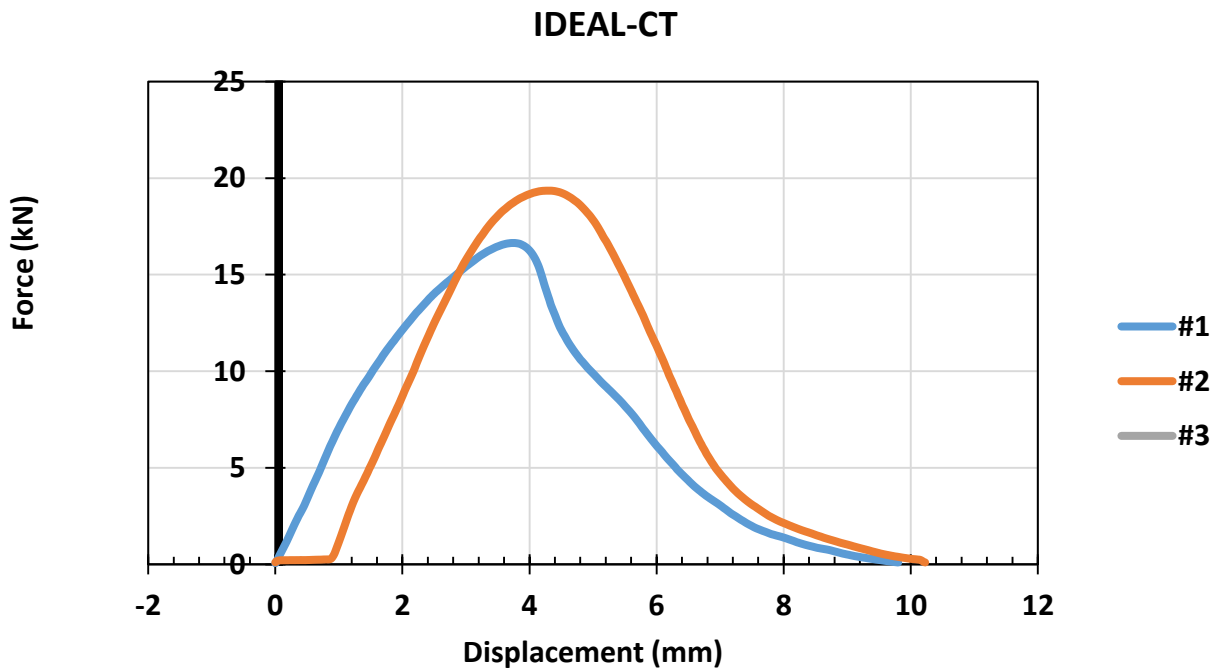


IDEAL-CT: Proposed Cracking Test

Project Name: Lane S	Institution: UTA
Mix Type: PG 64-22 15% RAP+2%RAS+BMD	Date Tested: 8/27/2021
Test Temperature: 75F	Technician: Ana Maria Coca

Specimen ID	1	2	5	Average	Standard Deviation	COV (%)
Air Voids (%)	4.6	4.5		4.6	0.1	1.6
Thickness (mm)	63.5	65.5		64.5	1.4	2.2
Diameter (mm)	152.0	152.3		152.2	0.2	0.1
Peak Load (kN)	16.6	19.4		18.0	1.9	10.6
Displacement (L), mm	4.4	5.5		5.0	0.8	15.7
Tensile Strength (kPa)	1097.6	1234.9		1166.3	97.1	8.3
Fracture Energy (LLD) (Gf) (J/m2)	7439.7	8267.1		7853.4	585.1	7.4
Slope (S)	6.66	6.74		6.70	0.05	0.8
Gf/S	1116.6	1226.7		1171.6	77.9	6.6
(Gf/S)*(L/D)	32.6	44.7		38.7	8.5	22.1
(Gf/S)*(L/D)^2	1.0	1.6		1.3	0.5	36.9

(Gf/S)*(L/D)	38.7	PASS
Minimum (Gf/S)*(L/D) Criteria		

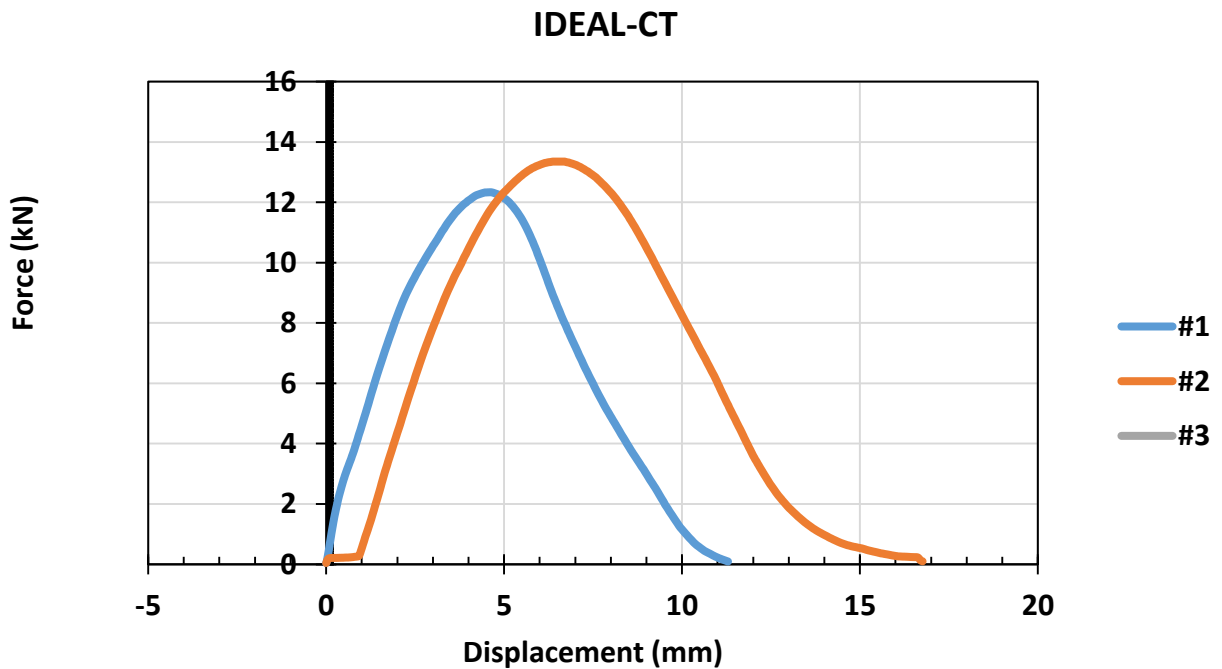


IDEAL-CT: Proposed Cracking Test

Project Name: Lane T	Institution: UTA
Mix Type: PG 64-22 15%RAP+2%RAS+BMD+Rejuvenator	Date Tested: 8/27/2021
Test Temperature: 75F	Technician: Ana Maria Coca

Specimen ID	1	2	3	Average	Standard Deviation	COV (%)
Air Voids (%)	3.5	4.5		4.0	0.7	17.5
Thickness (mm)	65.7	65.8		65.8	0.1	0.1
Diameter (mm)	149.4	150.0		149.7	0.4	0.3
Peak Load (kN)	12.3	13.3		12.8	0.7	5.6
Displacement (L), mm	6.3	9.2		7.7	2.1	27.1
Tensile Strength (kPa)	799.9	861.0		830.4	43.2	5.2
Fracture Energy (LLD) (Gf) (J/m ²)	7622.4	10811.9		9217.1	2255.4	24.5
Slope (S)	3.08	2.21		2.64	0.62	23.4
Gf/S	2475.6	4902.4		3689.0	1716.0	46.5
(Gf/S)*(L/D)	103.7	301.6		202.7	139.9	69.0
(Gf/S)*(L/D)^2	4.3	18.6		11.5	10.0	87.7

(Gf/S)*(L/D)	202.7	PASS
Minimum (Gf/S)*(L/D) Criteria		

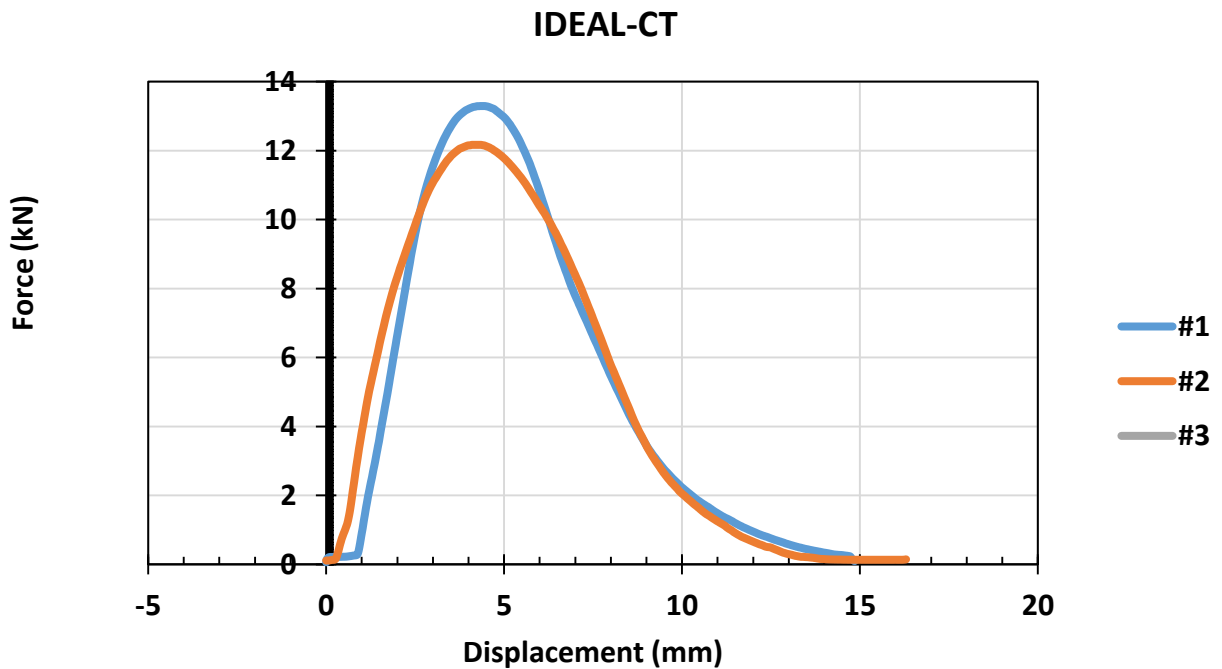


IDEAL-CT: Proposed Cracking Test

Project Name: Lane T	Institution: UTA
Mix Type: PG 64-22 15%RAP+2%RAS+BMD+Rejuvenator	Date Tested: 8/27/2021
Test Temperature: 75F	Technician: Ana Maria Coca

Specimen ID	1	2	3	Average	Standard Deviation	COV (%)
Air Voids (%)	3.3	4.1		3.7	0.6	16.8
Thickness (mm)	64.7	64.3		64.5	0.3	0.4
Diameter (mm)	150.3	149.8		150.1	0.4	0.2
Peak Load (kN)	13.3	12.2		12.7	0.8	6.2
Displacement (L), mm	6.3	6.7		6.5	0.3	4.7
Tensile Strength (kPa)	870.1	804.1		837.1	46.7	5.6
Fracture Energy (LLD) (Gf) (J/m2)	8099.4	8273.5		8186.5	123.1	1.5
Slope (S)	3.18	2.10		2.64	0.77	29.0
Gf/S	2545.6	3941.1		3243.4	986.8	30.4
(Gf/S)*(L/D)	106.0	176.0		141.0	49.5	35.1
(Gf/S)*(L/D)^2	4.4	7.9		6.1	2.4	39.7

(Gf/S)*(L/D)	141.0	PASS
Minimum (Gf/S)*(L/D) Criteria		



APPENDIX H

SCB Results

AASHTO TP 124

Standard Method of Test for Determining the Fracture Potential of Asphalt Mixtures Using Semicircular Bend Geometry (SCB) at Intermediate Temperature

Project Name: APT

Mix Type: PG 64-22 15% RAP +2% RAS

Test Temperature: 70

Institution: UTA

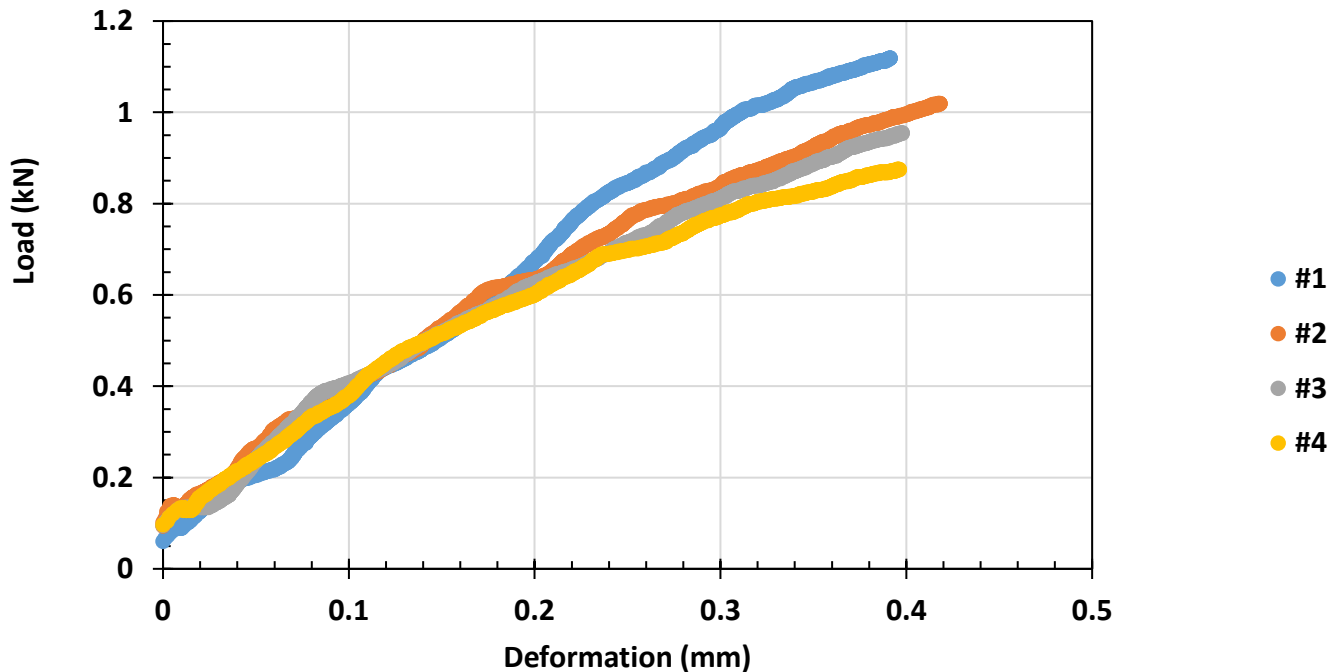
Date Tested: 08/27/21

Technician: Ana Coca

Specimen ID	1	2	3	4	Average	Standard Deviation	COV (%)
Air Voids (%)	5.3	5.3	5.0	5.0	5.2	0.2	3.4
Thickness (mm)	60.19	61.23	61.10	61.56	61.0	0.6	1.0
Ligament Length (mm)	24.12	23.78	25.14	23.78	24.2	0.6	2.7
Max Load (kN)	1.21	1.13	1.13	1.01	1.1	0.1	7.4
Fracture Energy, G_f (J/m ²)	610.4	552.0	556.9	714.5	608.5	75.5	12.4
Slope (kN/mm)	-0.69	-0.99	-1.23	-0.49	-0.85	0.33	38.5
Flexibility Index (FI)	8.84	5.57	4.51	14.56	8.4	4.5	54.0

Flexibility Index (FI)	8.37	PASS
Minimum Flexibility Index (FI) Criteria		

SCB Flexibility Index



AASHTO TP 124

Standard Method of Test for Determining the Fracture Potential of Asphalt Mixtures Using Semicircular Bend Geometry (SCB) at Intermediate Temperature

Project Name: Lane N

Mix Type: PG 70-22 no RAP or RAS

Test Temperature: 75F

Institution: UTA

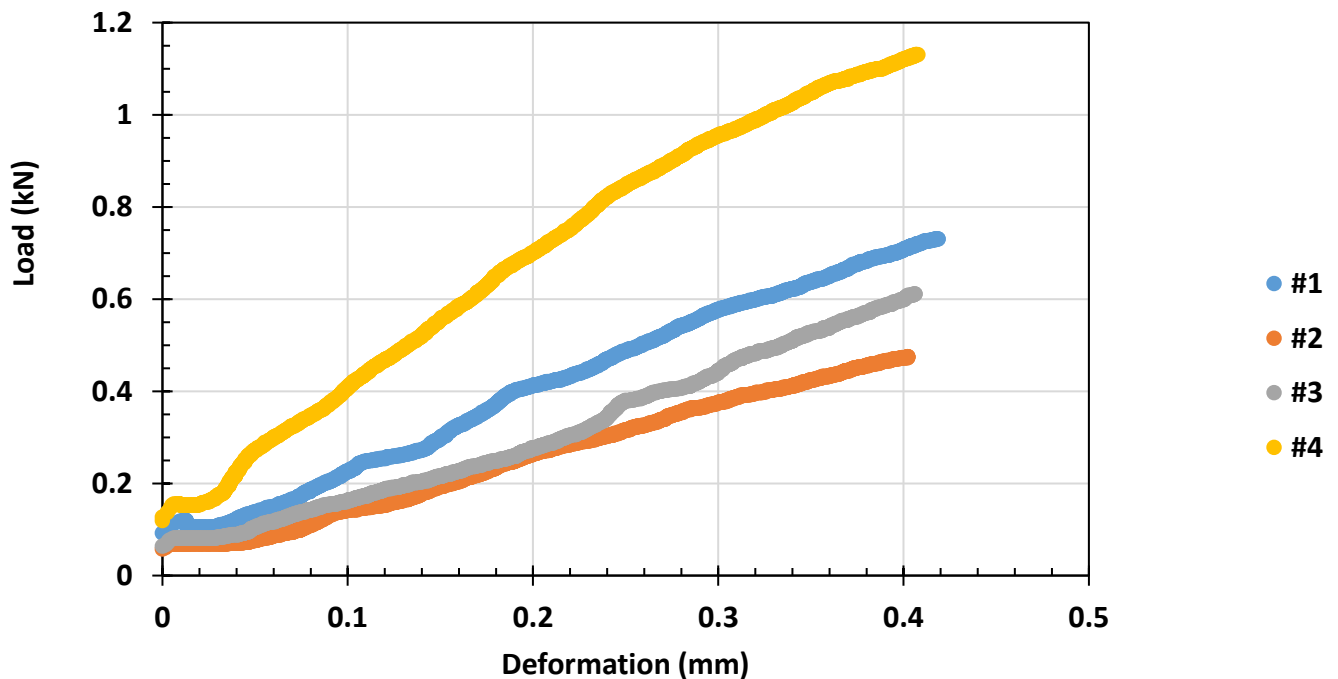
Date Tested: 08/27/21

Technician: Ana Maria Coca

Specimen ID	N1-1	N1-2	N2-1	N2-2	Average	Standard Deviation	COV (%)
Air Voids (%)	3.9	3.9	7.9	7.9	5.9	2.3	39.2
Thickness (mm)	59.90	59.60	60.77	60.78	60.3	0.6	1.0
Ligament Length (mm)	22.14	23.98	24.12	26.18	24.1	1.7	6.9
Max Load (kN)	1.03	0.86	1.22	1.26	1.1	0.2	16.8
Fracture Energy, G_f (J/m ²)	860.8	822.0	693.0	637.3	753.3	105.4	14.0
Slope (kN/mm)	-0.77	-0.56	-1.27	-1.70	-1.08	0.51	47.6
Flexibility Index (FI)	11.14	14.74	5.44	3.75	8.8	5.1	58.0

Flexibility Index (FI)	8.77	PASS
Minimum Flexibility Index (FI) Criteria		

SCB Flexibility Index



AASHTO TP 124

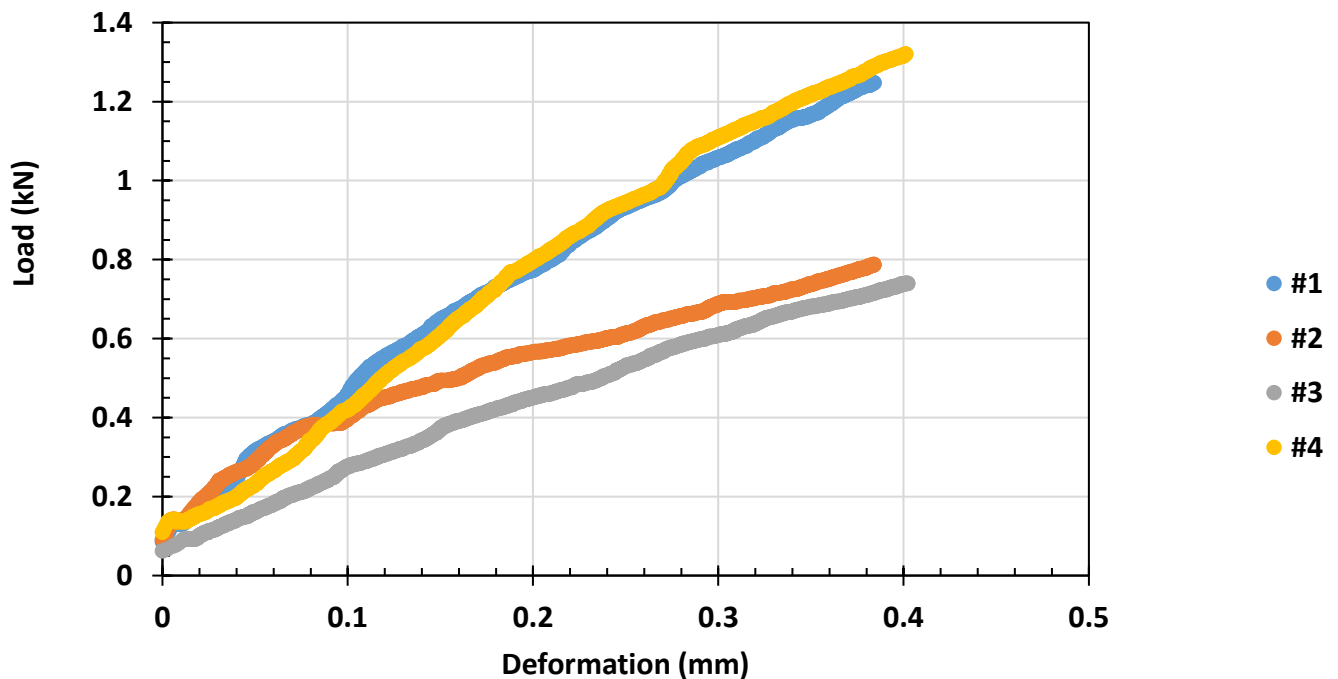
Standard Method of Test for Determining the Fracture Potential of Asphalt Mixtures Using Semicircular Bend Geometry (SCB) at Intermediate Temperature

Project Name: LANE O Mix Type: PG 70-22 15%RAP Test Temperature: 75F	Institution: UTA Date Tested: 08/27/21 Technician: Ana Maria Coca
---	--

Specimen ID	O1-1	O1-2	O2-1	O2-2	Average	Standard Deviation	COV (%)
Air Voids (%)	4.6	4.6	4.0	4.0	4.3	0.4	8.6
Thickness (mm)	58.60	60.06	58.90	58.88	59.1	0.6	1.1
Ligament Length (mm)	23.78	24.96	23.78	23.45	24.0	0.7	2.8
Max Load (kN)	1.55	1.00	1.18	1.54	1.3	0.3	20.9
Fracture Energy, G_f (J/m ²)	1065.5	635.3	1134.7	948.5	946.0	220.9	23.4
Slope (kN/mm)	-1.30	-0.88	-0.65	-1.36	-1.04	0.34	32.4
Flexibility Index (FI)	8.23	7.24	17.47	7.00	10.0	5.0	50.3

Flexibility Index (FI)	9.98	PASS
Minimum Flexibility Index (FI) Criteria		

SCB Flexibility Index



AASHTO TP 124

Standard Method of Test for Determining the Fracture Potential of Asphalt Mixtures Using Semicircular Bend Geometry (SCB) at Intermediate Temperature

Project Name: Lane P

Mix Type: PG 64-28 15%RAP+BMD

Test Temperature: 75F

Institution: UTA

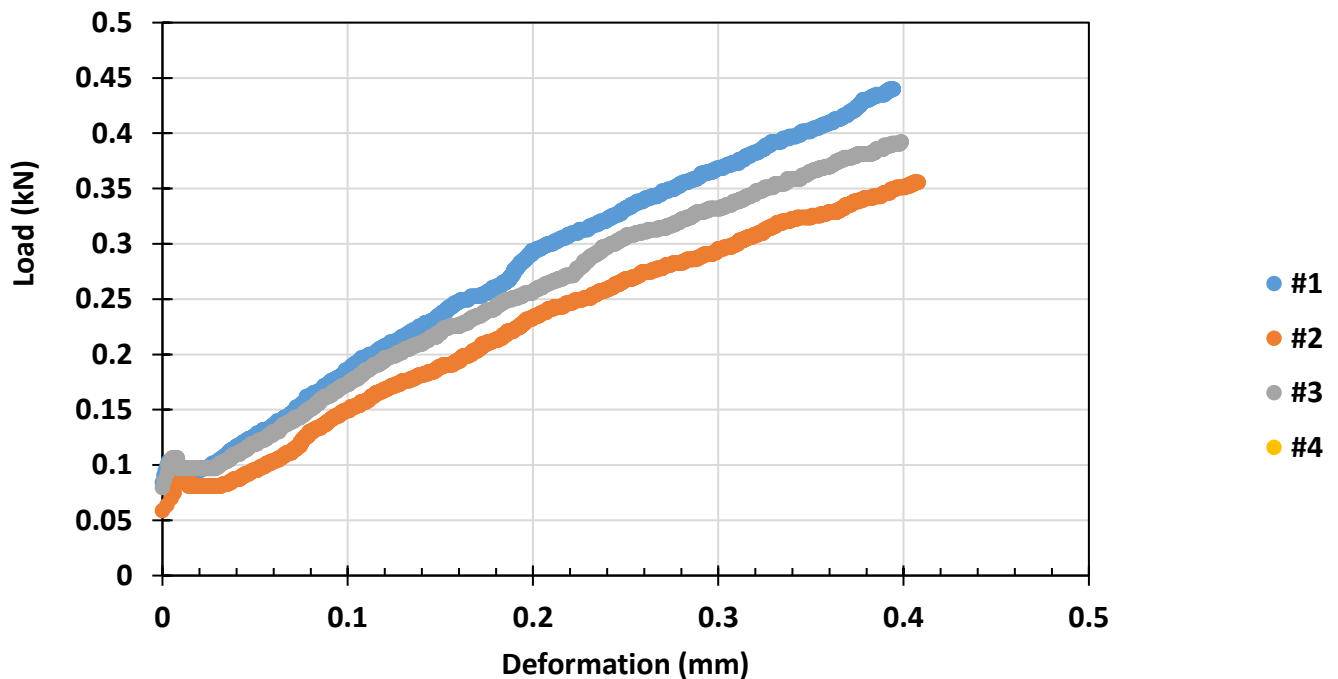
Date Tested: 08/27/21

Technician:

Specimen ID	P1-2	P2-1	P2-2		Average	Standard Deviation	COV (%)
Air Voids (%)	3.4	3.6	3.6		3.5	0.1	2.0
Thickness (mm)	58.89	57.54	58.27		58.2	0.7	1.2
Ligament Length (mm)	26.12	27.45	25.12		26.2	1.2	4.5
Max Load (kN)	0.68	0.54	0.57		0.6	0.1	12.8
Fracture Energy, G_f (J/m ²)	691.6	535.9	737.8		655.1	105.7	16.1
Slope (kN/mm)	-0.37	-0.19	-0.22		-0.26	0.10	37.7
Flexibility Index (FI)	18.60	28.16	33.95		26.9	7.8	28.8

Flexibility Index (FI)	26.90	PASS
Minimum Flexibility Index (FI) Criteria		

SCB Flexibility Index



AASHTO TP 124

Standard Method of Test for Determining the Fracture Potential of Asphalt Mixtures Using Semicircular Bend Geometry (SCB) at Intermediate Temperature

Project Name: Lane R

Mix Type: PG 64-22 25%RAP+BMD

Test Temperature: 75F

Institution: UTA

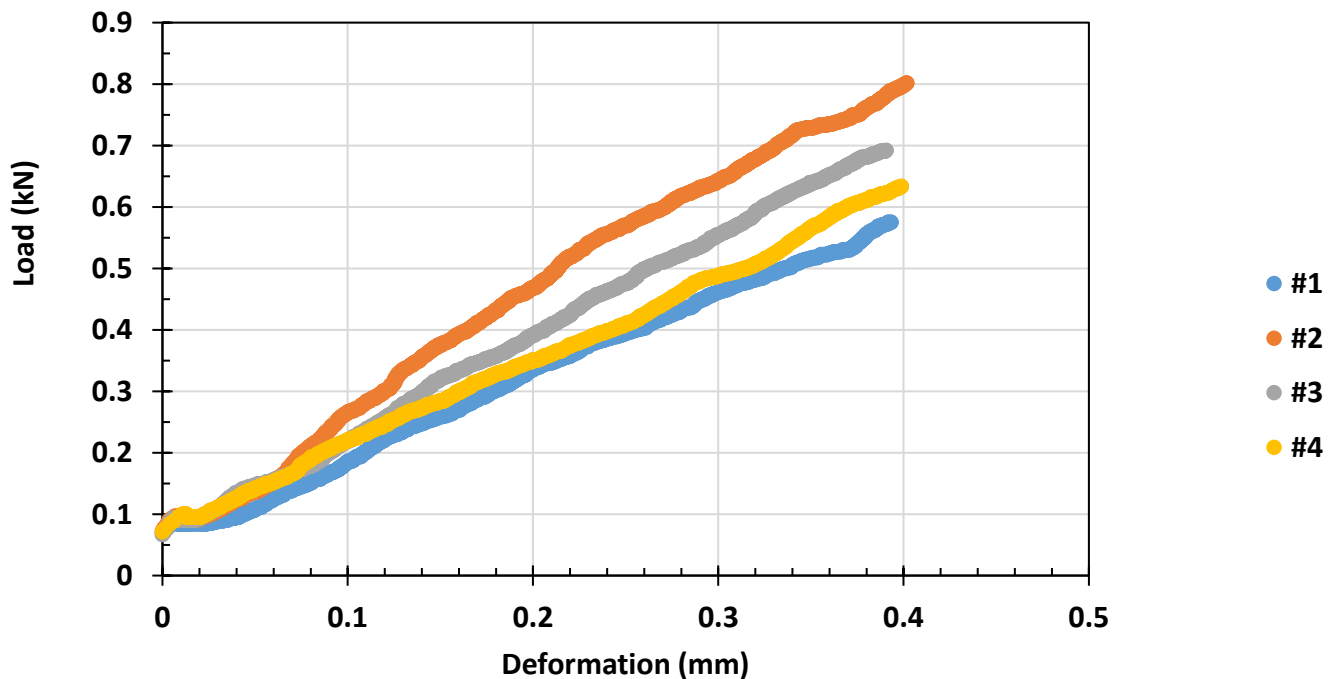
Date Tested: 08/27/21

Technician: Ana Maria Coca

Specimen ID	R1-1	R1-2	R2-1	R2-2	Average	Standard Deviation	COV (%)
Air Voids (%)	3.5	3.5	3.1	3.1	3.3	0.2	6.0
Thickness (mm)	59.62	59.86	57.91	58.16	58.9	1.0	1.7
Ligament Length (mm)	23.78	24.56	24.96	25.12	24.6	0.6	2.4
Max Load (kN)	0.97	1.16	1.10	1.10	1.1	0.1	7.2
Fracture Energy, G_f (J/m ²)	827.2	753.0	757.8	779.3	779.3	33.9	4.3
Slope (kN/mm)	-0.73	-0.85	-1.15	-0.75	-0.87	0.19	22.1
Flexibility Index (FI)	11.30	8.88	6.61	10.40	9.3	2.0	22.0

Flexibility Index (FI)	9.30	PASS
Minimum Flexibility Index (FI) Criteria		

SCB Flexibility Index



AASHTO TP 124

Standard Method of Test for Determining the Fracture Potential of Asphalt Mixtures Using Semicircular Bend Geometry (SCB) at Intermediate Temperature

Project Name: Lane S

Mix Type: PG 64-22 15%RAP+2%RAS+BMD

Test Temperature: 75F

Institution: UTA

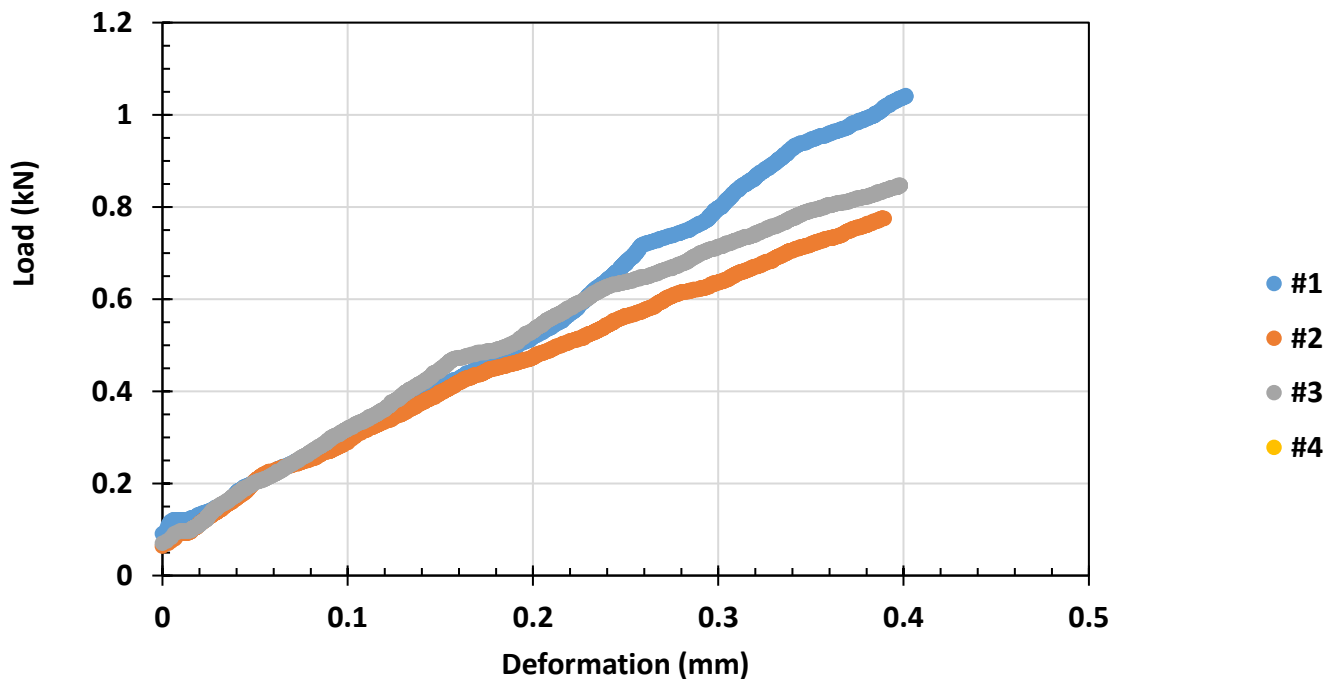
Date Tested: 08/23/21

Technician: Ana Maria Coca

Specimen ID	S1-1	S2-1	S2-2		Average	Standard Deviation	COV (%)
Air Voids (%)	5.6	4.9	4.9		5.1	0.4	8.4
Thickness (mm)	59.56	58.68	58.68		59.0	0.5	0.9
Ligament Length (mm)	23.87	23.95	24.78		24.2	0.5	2.1
Max Load (kN)	1.28	0.99	1.13		1.1	0.1	13.2
Fracture Energy, G_f (J/m ²)	648.1	466.7	613.9		576.2	96.4	16.7
Slope (kN/mm)	-1.36	-1.71	-1.44		-1.50	0.18	12.0
Flexibility Index (FI)	4.75	2.73	4.26		3.9	1.1	26.9

Flexibility Index (FI)	3.91	PASS
Minimum Flexibility Index (FI) Criteria		

SCB Flexibility Index



AASHTO TP 124

Standard Method of Test for Determining the Fracture Potential of Asphalt Mixtures Using Semicircular Bend Geometry (SCB) at Intermediate Temperature

Project Name: Lane T

Mix Type: PG 64-22 15%RAP+2%RAS+BMD+Rejuvenator

Test Temperature: 75F

Institution: UTA

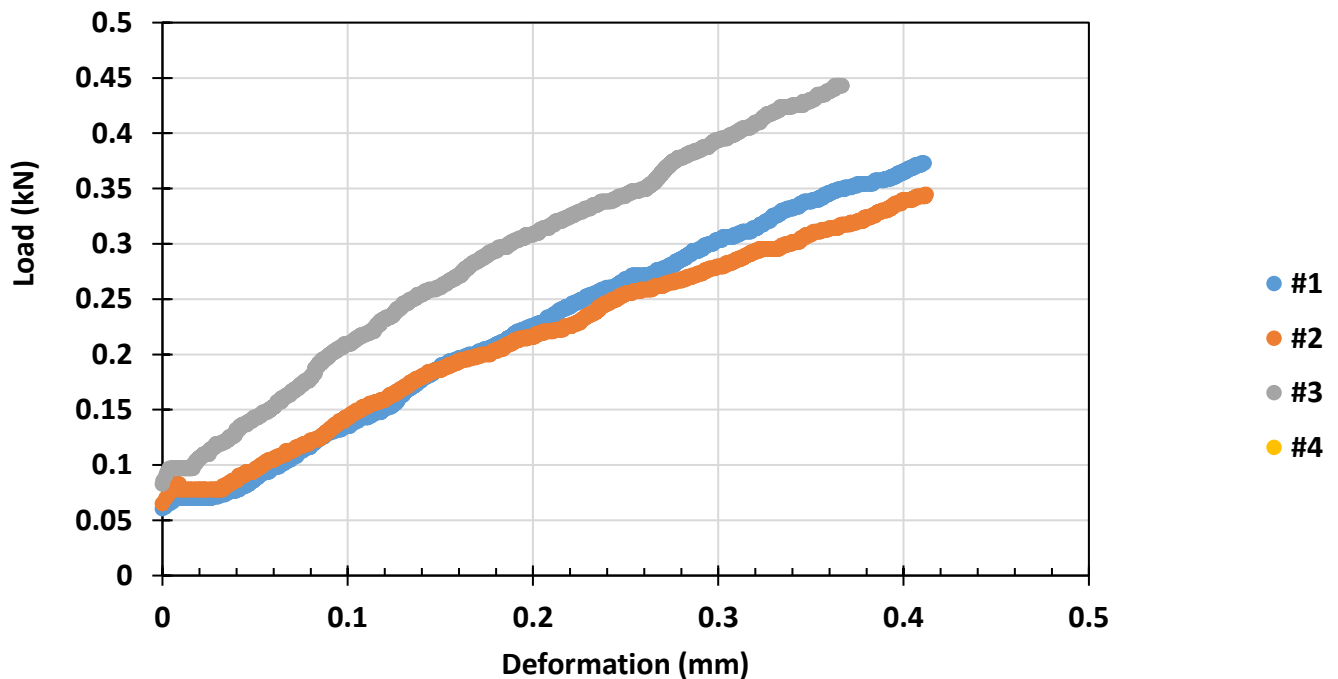
Date Tested: 08/27/21

Technician: Ana Maria Coca

Specimen ID	T1-1	T1-2	T2-1		Average	Standard Deviation	COV (%)
Air Voids (%)	4.2	4.2	3.5		4.0	0.4	11.2
Thickness (mm)	59.47	59.43	59.77		59.6	0.2	0.3
Ligament Length (mm)	26.12	24.78	22.89		24.6	1.6	6.6
Max Load (kN)	0.64	0.63	0.68		0.6	0.0	4.5
Fracture Energy, G_f (J/m ²)	492.3	623.6	638.6		584.8	80.5	13.8
Slope (kN/mm)	-0.47	-0.37	-0.51		-0.45	0.08	16.9
Flexibility Index (FI)	10.57	17.05	12.41		13.3	3.3	25.0

Flexibility Index (FI)	13.34	PASS
Minimum Flexibility Index (FI) Criteria		

SCB Flexibility Index



APPENDIX I

FPS21-Mechanistic Design Check

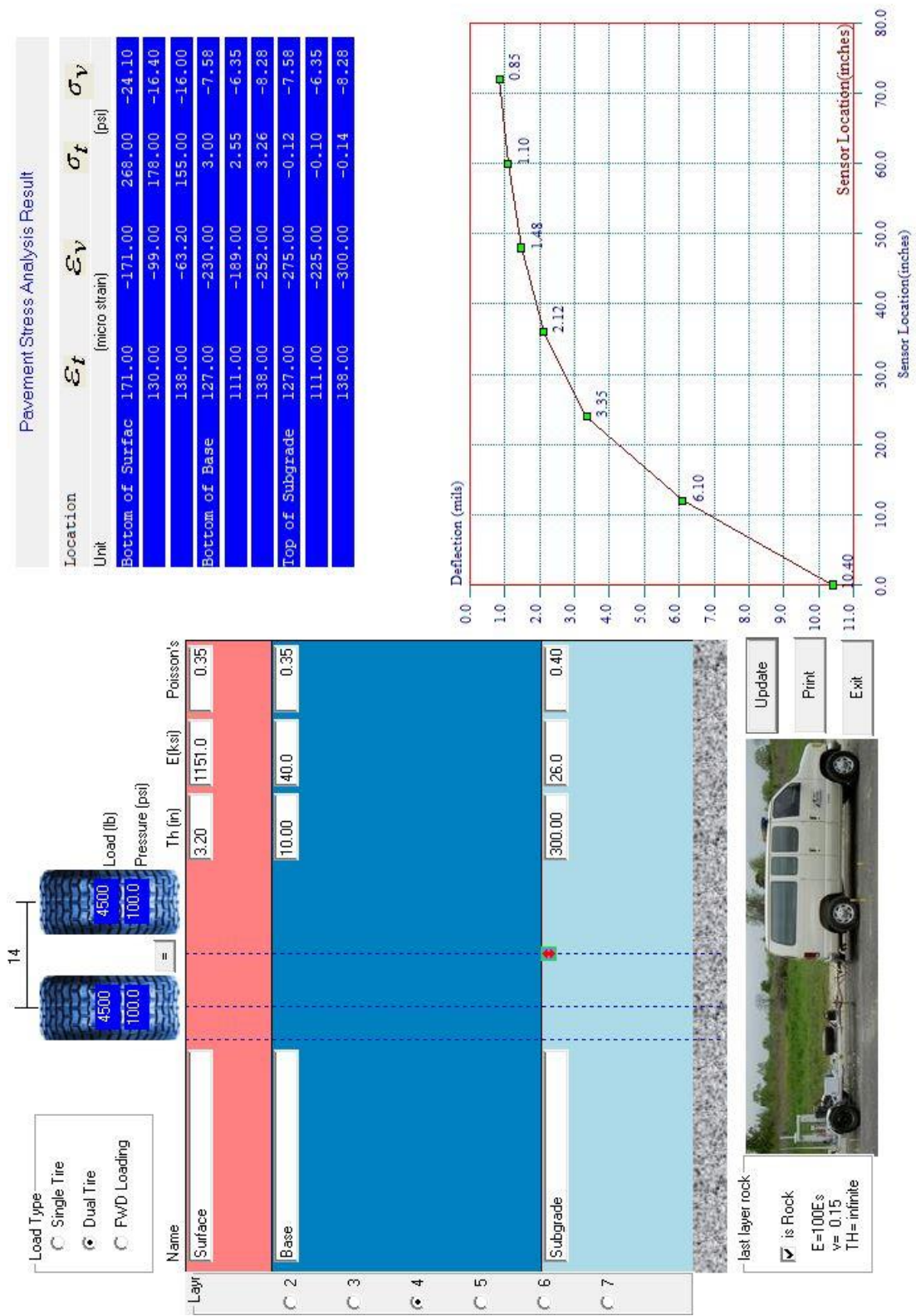


Figure I-1 Mechanistic design check -Lane M

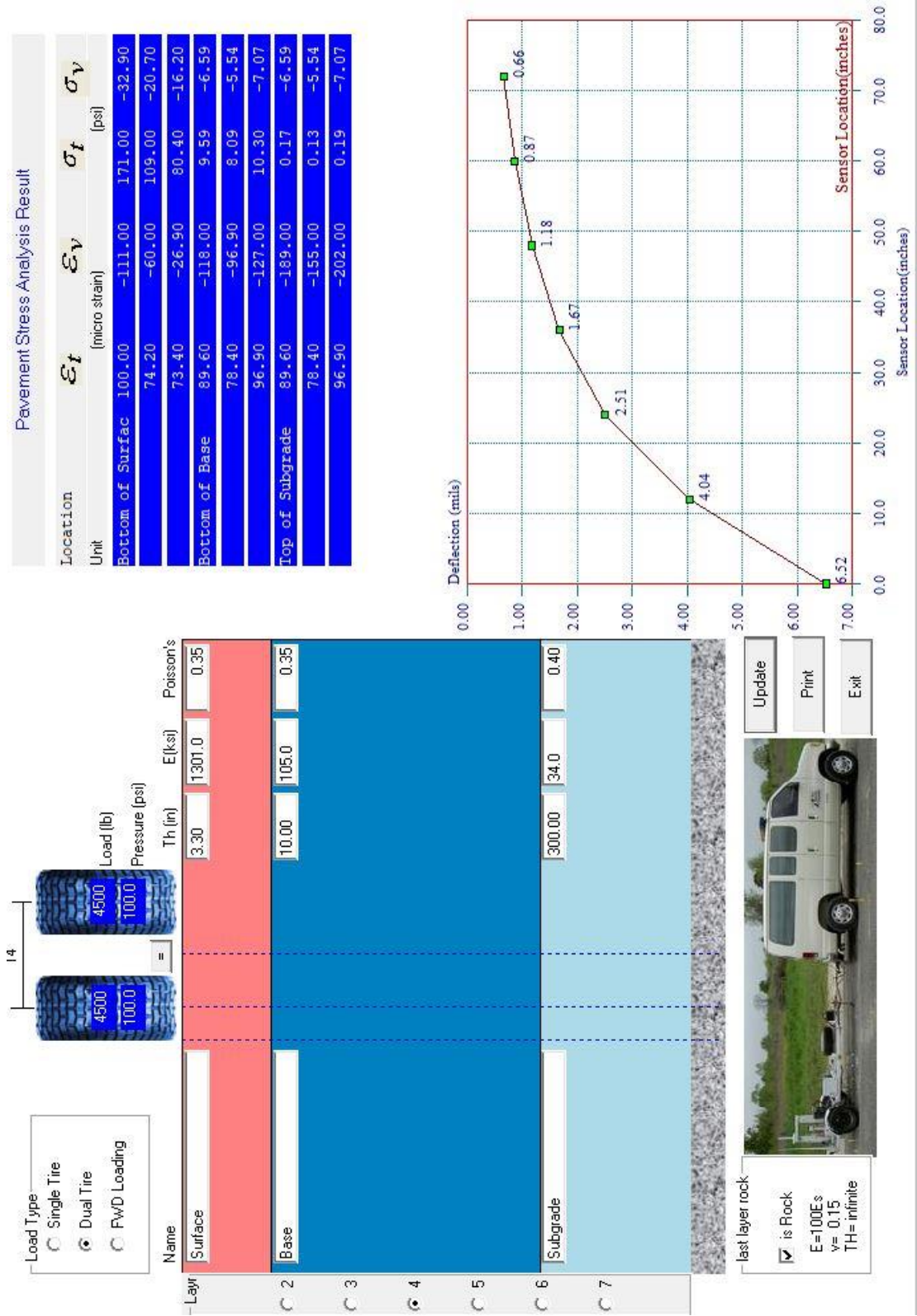


Figure I-2 Mechanistic design check -Lane N

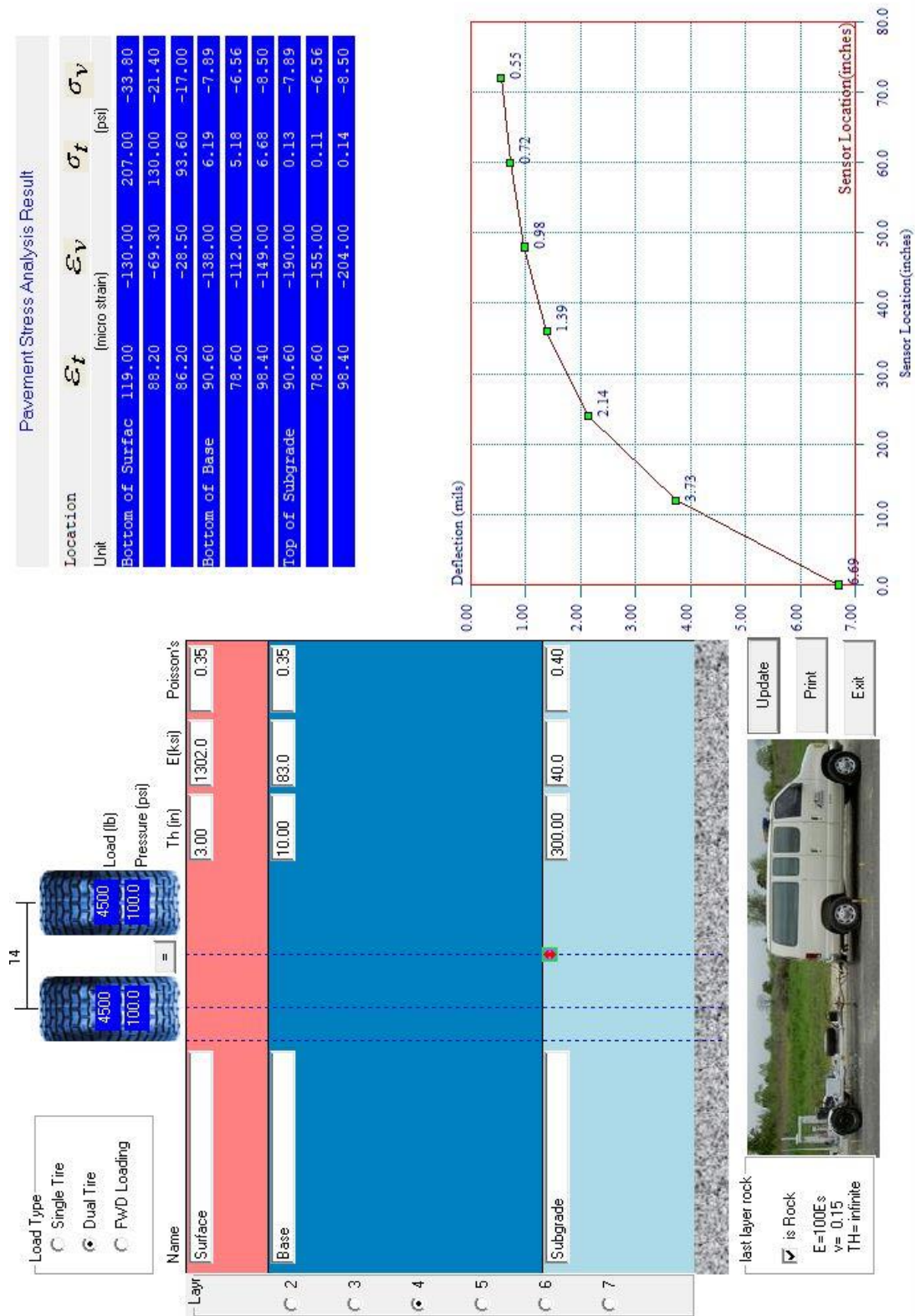


Figure I-3 Mechanistic design check -Lane O

Pavement Stress Analysis Result

Location	ϵ_t	ϵ_v	σ_t	σ_v
Unit	(micro strain)		(psi)	
Bottom of Surface	159.00	-161.00	248.00	-24.70
	121.00	-93.70	166.00	-16.50
	128.00	-60.60	145.00	-15.30
Bottom of Base	161.00	-221.00	7.80	-6.05
	142.00	-183.00	6.66	-5.15
	174.00	-240.00	8.46	-6.56
Top of Subgrade	161.00	-344.00	0.08	-6.05
	142.00	-287.00	0.06	-5.15
	174.00	-374.00	0.09	-6.56

Load Type

Single Tire

Dual Tire

FwD Loading

Load (lb)

Pressure (psi)

Th (in)

E(k/ksi)

Poisson's

Layer	Name	Th (in)	E(k/ksi)	Poisson's
C 2	Surface	3.30	1151.0	0.35
C 3	Base	10.00	49.0	0.35
C 4				
C 5	Subgrade	300.00	17.0	0.40
C 6				
C 7	last layer rock			

is Rock

E=100E\$

v= 0.15

TH= infinite

Update

Print

Exit

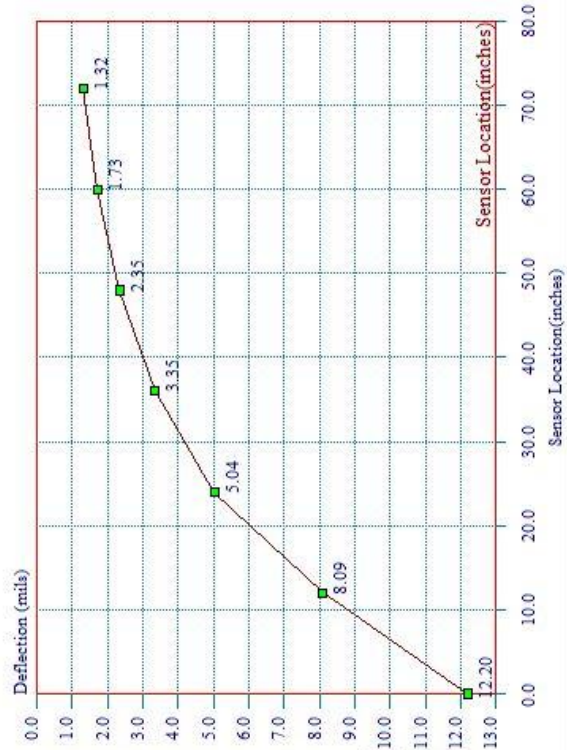


Figure I-4 Mechanistic design check -Lane Q

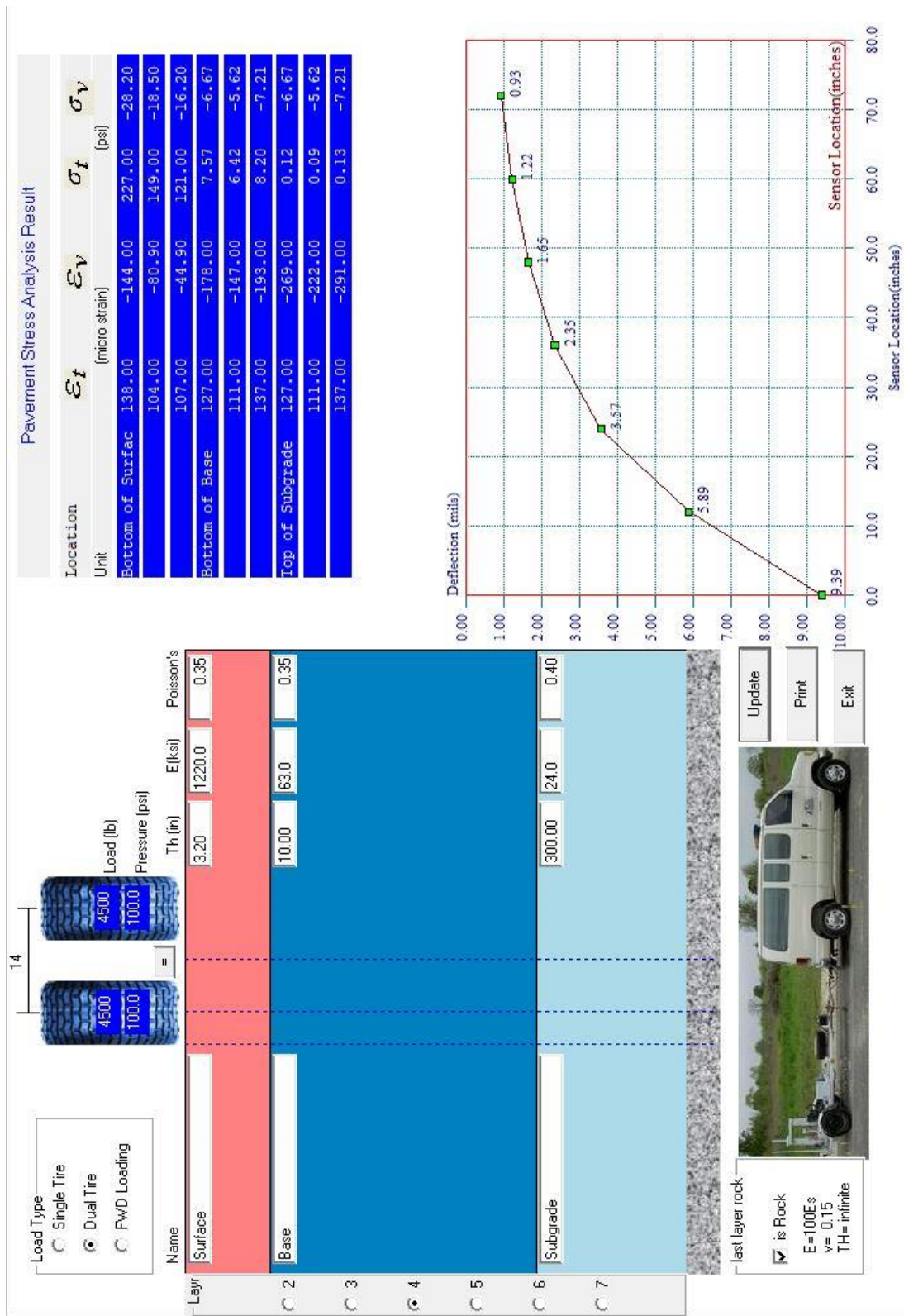


Figure I-5 Mechanistic design check -Lane R

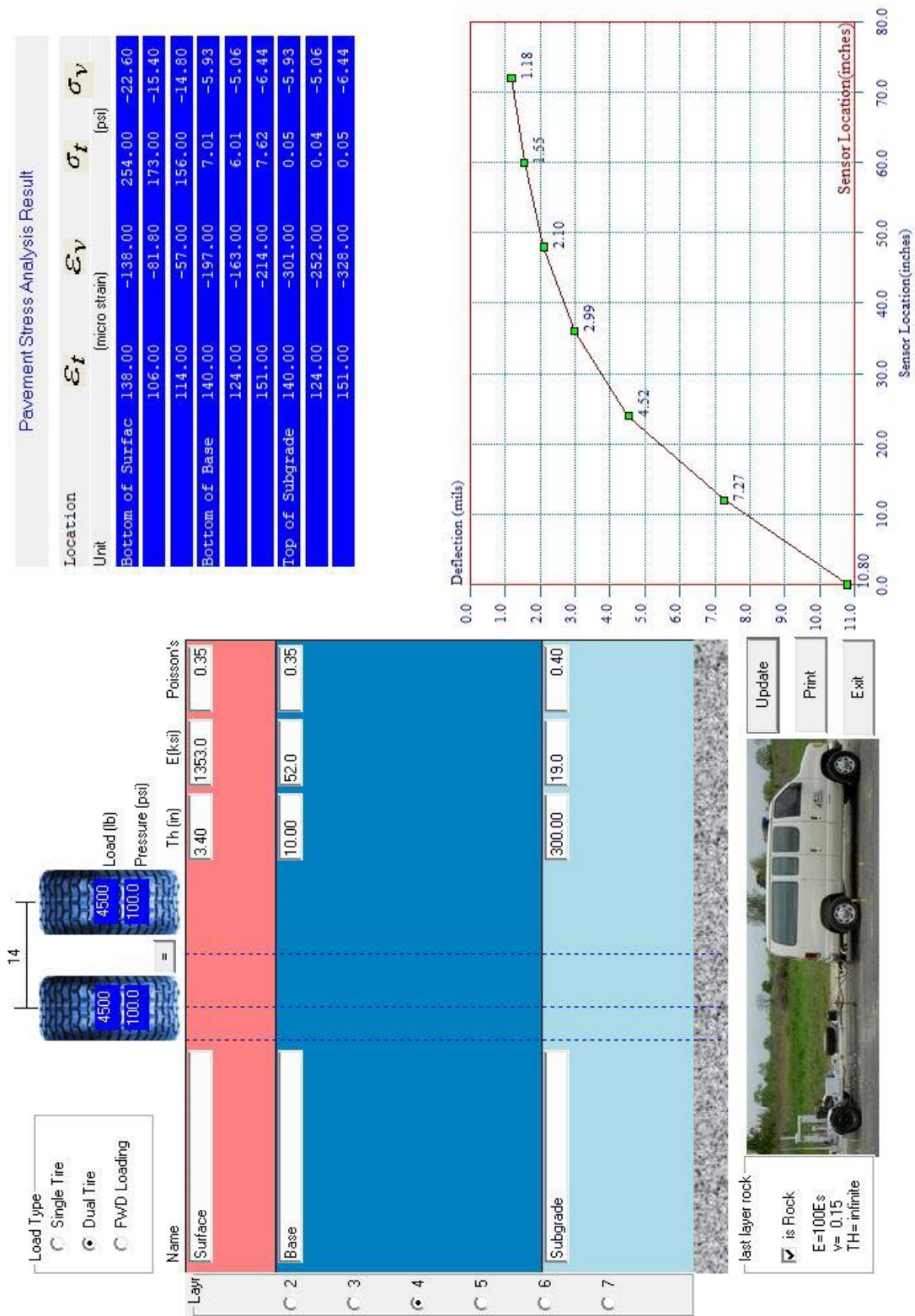


Figure I-6 Mechanistic design check -Lane S

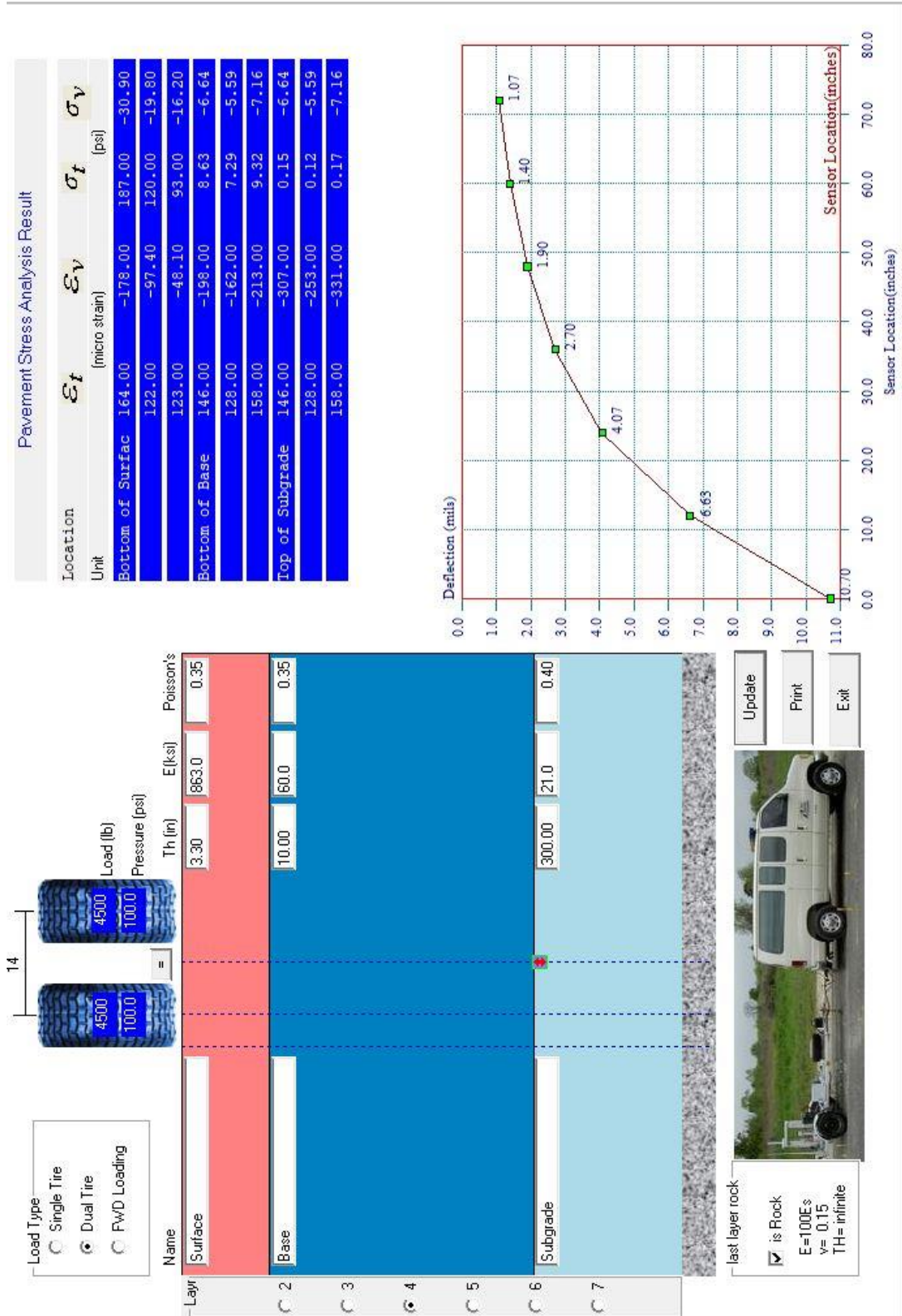


Figure I-7 Mechanistic design check -Lane T